



UNIVERSITY OF
PLYMOUTH



School of Biological and Marine Sciences Theses
Faculty of Science and Engineering Theses

2023

The Role of Circadian Entrainment in Rice Blast Disease

Ciaran Griffin

Let us know how access to this document benefits you



This work is licensed under a [Creative Commons Attribution-Share Alike 4.0 International License](https://creativecommons.org/licenses/by-sa/4.0/).

General rights

All content in PEARL is protected by copyright law. Author manuscripts are made available in accordance with publisher policies. Please cite only the published version using the details provided on the item record or document. In the absence of an open licence (e.g. Creative Commons), permissions for further reuse of content should be sought from the publisher or author.

Take down policy

If you believe that this document breaches copyright please [contact the library](#) providing details, and we will remove access to the work immediately and investigate your claim.

Follow this and additional works at: <https://pearl.plymouth.ac.uk/bms-theses>

Recommended Citation

Griffin, C. (2023) *The Role of Circadian Entrainment in Rice Blast Disease*. Thesis. University of Plymouth. Retrieved from <https://pearl.plymouth.ac.uk/bms-theses/55>

This Thesis is brought to you for free and open access by the Faculty of Science and Engineering Theses at PEARL. It has been accepted for inclusion in School of Biological and Marine Sciences Theses by an authorized administrator of PEARL. For more information, please contact openresearch@plymouth.ac.uk.



UNIVERSITY OF
PLYMOUTH

PEARL

PHD

The Role of Circadian Entrainment in Rice Blast Disease

Griffin, Ciaran

Award date:
2023

Awarding institution:
University of Plymouth

[Link to publication in PEARL](#)

All content in PEARL is protected by copyright law.

The author assigns certain rights to the University of Plymouth including the right to make the thesis accessible and discoverable via the British Library's Electronic Thesis Online Service (EThOS) and the University research repository (PEARL), and to undertake activities to migrate, preserve and maintain the medium, format and integrity of the deposited file for future discovery and use.

Copyright and Moral rights arising from original work in this thesis and (where relevant), any accompanying data, rests with the Author unless stated otherwise*.

Re-use of the work is allowed under fair dealing exceptions outlined in the Copyright, Designs and Patents Act 1988 (amended), and the terms of the copyright licence assigned to the thesis by the Author.

In practice, and unless the copyright licence assigned by the author allows for more permissive use, this means,

That any content or accompanying data cannot be extensively quoted, reproduced or changed without the written permission of the author / rights holder

That the work in whole or part may not be sold commercially in any format or medium without the written permission of the author / rights holder

* Any third-party copyright material in this thesis remains the property of the original owner. Such third-party copyright work included in the thesis will be clearly marked and attributed, and the original licence under which it was released will be specified. This material is not covered by the licence or terms assigned to the wider thesis and must be used in accordance with the original licence; or separate permission must be sought from the copyright holder.

Copyright statement

This copy of the thesis has been supplied on condition that anyone who consults it is understood to recognise that its copyright rests with its author and that no quotation from the thesis and no information derived from it may be published without the author's prior consent.



**UNIVERSITY OF
PLYMOUTH**

The Role of Circadian Entrainment in Rice Blast Disease

by

Ciarán Griffin

A thesis submitted to the University of Plymouth

in partial fulfilment for the degree of

DOCTOR OF PHILOSOPHY

School of Biological and Marine Sciences

September 2022

Acknowledgements

To begin with, I'd like to give a massive amount of thanks to my supervisory team:

George Littlejohn, Anne Plessis, Mick Hanley, and Nick Talbot for the incredible amount of support, guidance, and recommendations throughout my time as a student.

I would like to especially thank Anne for her enthusiasm and encouragement in pursuing a PhD during my undergraduate years – I wouldn't be here without you.

Thank you so much. Further, without you I wouldn't have fallen into the wonderful rabbit hole that is image analysis and the automation of data acquisition and analyses, which has made many parts of my PhD manageable (looking after Avril the cat was a wonderful bonus). To Mick, your insightful comments (occasionally over a well-needed pint!) and passion towards science is infectious and has kept me going throughout this long journey. Nick, your expertise, interest, and keen eye for avenues of research to focus on was pivotal in many aspects of this work and has provided me with a real appreciation for the scientific process. I would also like to thank Andy Foster, for his help and practical guidance in the CRISPR process, and Dan Maclean for his work on the development of Redpatch. Last, but in no way least: George. It has been an absolute pleasure working with you over the past few years, and I genuinely couldn't have asked for a better supervisor. The consistent conversations we have had about science, research, and pretty much anything else have been wonderful, and I will cherish my time working alongside you. Your expertise, enthusiasm, encouragement, and patience (it's been a long one!) have instilled in me a true passion for research, and the explorative and inventive approaches we have used in this work have been a lot of fun.

To the rest of the Littlejohn lab group (past and present), Naofel, Angela, and Trupti, it has been a pleasure working with you all, and your insightful comments and

encouragement has been wonderful. I would also like to give a big thanks to the technician team at UoP; to Sarah for her help with all things media related – I know I had a lot of questions to begin with! To Will, for his help with all things molecular: your advice and recommendations made everything much, much easier. Andy, I had an absolute blast climbing with you and Will (even when I ended up in the drink!). I would also like to mention and thank Li-An Stanley for her hard work and contribution during her undergraduate placement in the 'mystery metabolite' project. And to Matt, my go-to for basically everything and anything electronic and micro-related, your support has been nothing short of wonderful, both in and out of the lab. I'm glad to have you as such a good friend. Thanks to you all.

To my other wonderful friends that I've made over my time here, thank you. For listening to me lament about time course experiments, repeated failed experiments, and general moaning; but more importantly for your hilarious, interesting, insightful and fun company, both in and out of university. To My friends and family back home – thank you for the unending support and words of encouragement, I couldn't have done it without you. And to Mum and Dad, your support throughout my PhD means an incredible amount, thanks so much for everything, especially during my write up at home – you both mean the world to me.

Author's declaration

At no time during the registration for the degree of *Doctor of Philosophy* has the author been registered for any other University award without prior agreement of the Doctoral College Quality Sub-Committee.

Work submitted for this research degree at the University of Plymouth has not formed part of any other degree either at the University of Plymouth or at another establishment.

This study was financed with the aid of a studentship form the *University of Plymouth*

A programme of advanced study was undertaken, which included *BIO5131: Postgraduate Research Skills & Methods*

The Following external institutions were visited for research and consultation purposes: *The Sainsbury Laboratory*, Norwich, UK

Publications:

- Diurnal, Circadian, and Photomorphogenic Analyses in *Magnaporthe oryzae*, in: *Magnaporthe oryzae* Methods and Protocols (2021), doi: 10.1007/978-1-0716-1613-0_13.

Presentations at conferences:

- Plastid Preview (2018): 'Characterisation of chloroplast behaviour during rice blast disease progression'
- GARNet advances in plant imaging (2019): 'The use of image analysis in Rice Blast Disease'
- ISMPMI (2019): 'The role of circadian entrainment in the outcome of Rice Blast infection'
- Magnafest (2019): 'The *Magnaporthe oryzae* circadian clock functions in determining Rice Blast Pathogenicity'
- MBPP (2019): 'The role of circadian entrainment in Rice Blast Disease'
- PEPG (2019): 'The role of circadian entrainment in the Rice Blast pathosystem'
- Plastid Preview (2019): 'The use of image analysis in characterising Rice Blast disease'

Word count of main body of thesis: 78,596

Signed: Ciarán Griffin

Date: 2022.09.06

The Role of Circadian Entrainment in Rice Blast Disease

Abstract

A circadian clock is present in some capacity in almost all forms of life, and is useful for a wide array of traits, but crucially allows organisms to predict future conditions and adapt their behaviour to synchronise with, and thrive under, their dynamic environment. Accordingly, plant environmental stress responses are gated in a circadian manner, including that for pathogenic defence and immunity. Comparatively less work has been carried out on the plant pathogens, but there are increasing reports of pathogens capable of rhythmically altering their behaviour and virulence-related traits. *Magnaporthe oryzae*, the fungal pathogen responsible for the destruction of enough rice to feed at least 60 M people annually, has been shown to possess some circadian clock components, and based on bioinformatic analyses, likely contains all the core, accessory, and circadian-associated genes. *M. oryzae* displays a conidial banding pattern, reminiscent of the model clock species, *N. crassa*, and (after sufficient entrainment) this pattern can continue to occur under free running conditions for a number of days, with a period of approximately 24 h. This rhythm is also presented on a range of nutrient-rich and poor media, suggesting a nutritionally-compensated circadian rhythm in *M. oryzae*. This onset of conidial banding is partially determined by the presence of secreted metabolites, the sensation of which is facilitated by the circadian clock, predominantly via WC2. The entraining light

conditions that *M. oryzae* is exposed to can significantly alter its vegetative growth, conidiation and conidial development, and even pathogenicity. Further, inoculation timing (dawn or dusk) plays a role in both the virulence of *M. oryzae*, and in the susceptibility of the plant host, seemingly in a species-by-species manner, where rice is most susceptible at dawn, and barley most susceptible at dusk. For *M. oryzae*, pre-inoculation entrainment to darkness predominantly favours dawn inoculations, and those exposed to prolonged periods of light prefer dusk inoculation. Upon mutation of the core clock genes, WC2 and FRQ, vegetative growth, conidiation and conidial development, photoadaptation, and pathogenicity were all significantly altered compared to the wild type, suggesting an important role of the clock in the general fitness of *M. oryzae*. This work discusses how entraining light cycles and the circadian clock impacts the growth, development, conidiation, virulence, and ultimate severity in the economically important rice blast disease.

Contents

Copyright statement	1
The Role of Circadian Entrainment in Rice Blast Disease	2
Acknowledgements.....	3
Author’s declaration	5
Abstract.....	6
Contents.....	8
List of Figures	14
List of tables.....	19
Abbreviations.....	21
1 General introduction.....	23
1.1 The current status of global food security.....	23
1.2 The socioeconomic status of rice.....	27
1.3 The socioeconomic impact of rice blast disease.....	31
1.4 <i>Magnaporthe oryzae</i> : rice blast disease.....	33
1.5 The plant immune system.....	37
1.6 Circadian rhythms	38
1.7 Circadian rhythms in fungi	41
1.8 Circadian rhythms in plant pathology.....	43
1.9 Time of day-dependent infection in rice blast disease.....	44
2 Materials and methods.....	49
2.1 Fungal growth, maintenance, and storage	49
2.2 Plant growth, maintenance, and storage	53
2.3 Fungal colony growth and banding analysis	54
2.4 Pre-banding latency period assay	54
2.5 Conidial tip mucilage analysis	55
2.6 Conidial development analysis	56
2.7 Cytorrhysis analysis.....	58
2.8 Pathogenicity and infection assays.....	58
2.8.1 Spray inoculations.....	58
2.8.2 Leaf sheath inoculations	59
2.8.3 Chlorophyll fluorescence imaging system for leaf health analyses	60
2.9 Timing and localisation of clock gene expression analysis	61
2.10 CRISPR Cas9 genetic engineering design	62
2.11 Mutant confirmation and primer design	63
2.12 <i>M. oryzae</i> CRISPR transformation process	64

2.13	DNA extraction.....	70
2.14	Polymerase chain reaction (PCR).....	70
2.15	DNA restriction enzyme digest	71
2.16	Agarose gel electrophoresis.....	71
2.17	Sequencing.....	73
2.18	Statistical analyses	74
3	Image analysis toolkit development	76
3.1	Introduction	76
3.1.1	Digital image acquisition.....	77
3.1.2	Image processing and analysis.....	80
3.2	Results.....	88
3.2.1	Fungal colony area and conidial banding analysis	88
3.2.2	Conidial counts.....	96
3.2.3	Appressorial cytorrhysis analysis	99
3.2.4	Automated conidial development time course acquisition.....	102
3.2.5	Automated leaf segmentation and pre-processing	105
3.2.6	Leaf infection severity analysis: Redpatch	109
3.2.7	Chlorophyll fluorescence leaf health and pre-symptomatic disease analysis ..	116
3.2.8	Confocal ratiometric and intensity analysis.....	121
3.3	Discussion.....	124
4	Diurnal and circadian growth, development, and pathogenicity of <i>Magnaporthe oryzae</i>	125
4.1	Introduction	125
4.1.1	Environmental time signals: Zeitgebers.....	125
4.1.2	Plant circadian rhythms	131
4.1.3	Circadian rhythms in plant pathology.....	133
4.2	Results.....	135
4.2.1	Identification of core clock components and photoreceptors in <i>M. oryzae</i>	135
4.2.2	<i>M. oryzae</i> displays diurnal rhythmic conidiation under white, blue, and green light	138
4.2.3	<i>M. oryzae</i> has a nutritionally compensated circadian conidial banding phenotype.....	140
4.2.4	<i>M. oryzae</i> produces metabolite(s) responsible for the switch to conidial banding.....	145
4.2.5	Environmental entrainment conditions affect conidiation and conidial development	155
4.2.6	Time of day and pre-inoculation entrainment affects <i>M. oryzae</i> virulence and plant susceptibility	163

4.3	Discussion.....	173
5	WC2 plays a role in the growth, conidiation, and pathogenicity of <i>Magnaporthe oryzae</i>	189
5.1	Introduction	189
5.1.1	The WHITE COLLAR COMPLEX keeps the clock ticking	189
5.1.2	The WHITE COLLAR COMPLEX is multifunctional and acts as a photoreceptor	199
5.1.3	The WCC plays a role in fungal pathogenicity.....	201
5.1.4	Clock component mutants in <i>M. oryzae</i> show altered growth, development, and pathogenicity	204
5.2	Results.....	207
5.2.1	Generation and screening of Δ WC2.....	207
5.2.2	<i>M. oryzae</i> Δ WC2 displays an arrhythmic conidial banding phenotype	212
5.2.2.1	Δ WC2 does not present conidial banding under any light conditions.....	212
5.2.2.2	Δ WC2 produces, but does not respond to, the conidial banding metabolite(s).....	215
5.2.3	WC2 plays a role in photoadaptation and growth rates.....	217
5.2.4	WC2 functions in light-dependent conidiation repression.....	219
5.2.5	WC2 has a role in conidial germination, development, and appressorial stability	221
5.2.5.1	Δ WC2 conidia germinate and develop quicker than the wild type	221
5.2.5.2	WC2 has a role in conidial size.....	224
5.2.5.3	Δ WC2 appressoria undergo cytorrhysis more readily	226
5.2.6	WC2 plays a role in the early stages of pathogenesis.....	229
5.2.6.1	Δ WC2 is less able to penetrate the host cuticle	229
5.2.6.2	Δ WC2 displays reduced <i>in planta</i> cell to cell movement.....	231
5.2.7	WC2 functions in host pathogenicity	233
5.2.7.1	Δ WC2 produces fewer but larger lesion regions in rice.....	233
5.2.7.2	Prolonged light exposures favouring dusk inoculation is maintained in Δ WC2-rice infections.....	236
5.2.7.3	Prolonged light exposure inhibits dawn pathogenicity in Δ WC2-rice interactions	238
5.2.7.4	Under high inoculum densities on detached leaves, Δ WC2 is unable to overwhelm the host defences	240
5.2.8	WC2 has a profound impact on non-host pathogenicity.....	242
5.2.8.1	Δ WC2 produces fewer and smaller lesions than the wild type in barley infections.....	242
5.2.8.2	Time of day has less of an effect on disease severity in Δ WC2	246

5.2.8.3	Prolonged light exposure inhibits dawn pathogenicity in Δ WC2 regardless of host species.....	249
5.2.9	Δ WC2 infections show an optimal leaf area, but this phenomenon is dampened compared to the wild type.....	251
5.3	Discussion.....	253
6	FRQ determines periodicity, conidiation, and conidial development	267
6.1	Introduction	267
6.1.1	FREQUENCY's daily journey	273
6.1.2	FRQ stability: phosphorylation and FRH	277
6.1.3	Non-core clock control of FRQ.....	283
6.1.3.1	Antisense frq: qrf	283
6.1.3.2	VIVID.....	284
6.1.3.3	Methylation and chromatin remodelling.....	287
6.1.3.4	SWitch/Sucrose NonFermentable.....	289
6.1.3.5	frq is alternatively spliced	290
6.1.3.6	Multiple FRQs.....	299
6.1.3.7	FRQ-less rhythms	301
6.1.3.8	Which came first, FLOs or FWOs?.....	305
6.1.4	FRQ functions in plant-fungal pathogenesis.....	306
6.2	Results.....	312
6.2.1	Finding the <i>M. oryzae</i> FRQ gene	312
6.2.1.1	MGG_17345 and MGG_17344 map to either end of the <i>N. crassa</i> FRQ gene.....	312
6.2.1.2	Predicting the <i>M. oryzae</i> FRQ sequence	313
6.2.1.3	The predicted <i>M. oryzae</i> FRQ sequence contains numerous phosphorylation sites.....	317
6.2.1.4	<i>M. oryzae</i> FRQ contains PEST domains for ubiquitination	320
6.2.1.5	<i>M. oryzae</i> FRQ contains a coiled-coil domain for FRQ dimerization	322
6.2.1.6	<i>M. oryzae</i> FRQ contains motifs indicative of nuclear and cytoplasmic localisation	324
6.2.1.7	The predicted <i>M. oryzae</i> FRQ shows intrinsically disordered motifs	328
6.2.1.8	<i>M. oryzae</i> predicted FRQ shows conservation of the FRQ-FRH interaction domain.....	329
6.2.1.9	<i>M. oryzae</i> FRQ contains several (S/T)PXX sites, suggesting transcriptional regulation capability	331
6.2.2	Generating an FRQ mutant in <i>M. oryzae</i>	331
6.2.3	FRQ ^{NIN} maintains conidial banding, but has an altered period.....	338
6.2.3.1	FRQ ^{NIN} shows conidial banding, but its latency period prior to banding is lengthened.....	338

6.2.3.2	FRQ ^{NIN} displays circadian conidial banding, but its period is shortened under constant light	341
6.2.4	FRQ ^{NIN} shows environmentally-dependent vegetative growth differences	343
6.2.5	FRQ ^{NIN} mutation affects conidiation and conidial development	345
6.2.5.1	FRQ ^{NIN} mutation causes a profound reduction in conidiation	345
6.2.5.2	The FRQ ^{NIN} mutant conidia are less likely to germinate	347
6.2.5.3	FRQ ^{NIN} produces smaller conidia.....	349
6.2.5.4	FRQ ^{NIN} appressoria generate higher turgor pressure	351
6.2.6	Penetration and early <i>in planta</i> cell-cell movement is not affected by FRQ ^{NIN} mutation	353
6.2.7	Asynchronous FRQ ^{NIN} inoculations reduce rice-specific virulence	357
6.2.7.1	Antiphase-entrained FRQ ^{NIN} is less virulent than the wild type in rice at dawn (subjective dusk)	357
6.2.7.2	Constant darkness-entrained colonies favour dawn inoculations in FRQ ^{NIN}	359
6.2.7.3	Pre-inoculation treatment affects FRQ ^{NIN} virulence in rice	361
6.2.8	FRQ ^{NIN} and non-host interactions	363
6.2.8.1	Antiphase-entrained FRQ ^{NIN} inoculations reduce barley-specific virulence	363
6.2.8.2	FRQ ^{NIN} does not display time of day-dependent non-host virulence	365
6.2.8.3	Antiphase entrainment reduces dawn pathogenicity in FRQ ^{NIN}	367
6.2.9	FRQ ^{NIN} maintains optimal leaf size in rice infections	369
6.2.10	Δ WC2 mutation has a more severe impact on pathogenicity than FRQ ^{NIN}	371
6.2.10.1	Δ WC2 is less pathogenic than FRQ ^{NIN} in rice inoculations after LD entrainment	371
6.2.10.2	Δ WC2 is less pathogenic than FRQ ^{NIN} towards barley under all pre-inoculation treatments and times, except after antiphase entrainment at dawn	373
6.3	Discussion.....	376
7	General discussion	388
7.1	Context.....	388
7.2	Study aims.....	389
7.3	Key findings	390
7.3.1	<i>M. oryzae</i> has a functional, nutritionally compensated circadian conidial banding phenotype.....	390
7.3.2	WC2 is necessary for conidial banding	391
7.3.3	FRQ is not required for conidial banding, but affects the period of the clock	391
7.3.4	Conidiation, conidial banding, and conidial development is controlled by nutritional status and secreted metabolite(s)	392
7.3.5	FRQ and WC2 have roles in nutritional sensation	393
7.3.6	Circadian entrainment and function plays a role in vegetative growth	394
7.3.7	The circadian clock functions in conidiation	395

7.3.8	Pre-harvest entrainment and the circadian clock influences conidial development	397
7.3.9	The circadian clock affects early-stage pathogenicity	398
7.3.10	Timing, entrainment, and circadian function influences disease severity in host- and non-host <i>M. oryzae</i> -plant interactions	399
7.4	The role of the circadian clock in rice blast disease.....	401
7.5	Future research.....	402
8	References	404
9	Supplementary material	447
9.1	FIJI macro code	447
9.1.1	Colony area and conidial banding.....	447
9.1.2	Conidial counts.....	453
9.1.3	Appressorial cytorrhysis location.....	454
9.1.4	Leaf segmentation and pre-processing.....	455
9.1.5	Chlorophyll fluorescence	457
9.1.6	Confocal ratiometric and intensity analysis.....	467
9.2	Automated conidial development time course acquisition.....	469

List of Figures

- 2.1 The disease cycle of *Magnaporthe oryzae*.
- 2.2 LED wavelength emission spectra of the blue, green, red, and white LEDs used in this study.
- 2.3 Conidial developmental stages
 - 3.1 Overview of the fungal colony area and banding analysis macro
 - 3.2 Overview of the conidial counting and analysis macro
 - 3.3 Overview of the appressorial counter and analysis macro
 - 3.4 Openflexure conidial time course acquisition setup
 - 3.5 Overview of the leaf segmentation pre-processing macro
 - 3.6 Redpatch segmentation approach and interface
 - 3.7 Chlorophyll fluorescence image analysis approach
 - 3.8 Example output results file from the confocal analysis macro
- 4.1 Diurnal and circadian outputs
 - 4.2 *M. oryzae* exhibits diurnal conidial banding, which is chiefly controlled by blue light
 - 4.3 *M. oryzae* displays circadian conidial banding after sufficient entrainment
 - 4.4 *M. oryzae* growth rate is affected by photoperiod
 - 4.5 Media composition affects *M. oryzae* growth rate and latency period, but not circadian periodicity
 - 4.6 Nutritional scarcity and media pH does not cause the switch to conidial banding
 - 4.7 Spent media metabolite(s) are responsible for the conidial banding switch
 - 4.8 The conidial banding metabolite is dose-dependent and is affected by colony aeration
 - 4.9 Mobile *M. oryzae* metabolite(s) can inhibit early conidiation
 - 4.10 The conidial banding metabolite is predominantly produced just prior to banding

- 4.11 *V. dahliae* does not produce, and is insensitive to, the conidial banding metabolite(s)
- 4.12 Despite showing altered latency periods on different media, *M. oryzae* maintains a conidial banding period of ~24 h under constant conditions
- 4.13 Light conditions and media composition affect conidiation in *M. oryzae*
- 4.14 *M. oryzae* appressorial development is reduced under prolonged light and darkness
- 4.15 High doses of *M. oryzae* SM inhibit conidial development
- 4.16 Larger conidia adhere to hydrophobic surfaces better than smaller conidia
- 4.17 Appressorial turgor pressure is not significantly affected by pre-harvest light treatment
- 4.18 Synchronous- and dark-entrained *M. oryzae* is more virulent in rice at dawn and light-entrained *M. oryzae* is more virulent at dusk
- 4.19 Barley is more susceptible to *M. oryzae* penetration at dusk
- 4.20 Pre-inoculation treatment has a greater impact in *M. oryzae* infections at rice subjective dawn
- 4.21 Pre-inoculation entrainment of *M. oryzae* has a reduced effect in barley
- 4.22 Susceptibility to *M. oryzae* is highest in middle-aged leaves
- 5.1 A simplified WCC-centric view of the circadian clock
- 5.2 Potential *M. oryzae* WC2 target sites
- 5.3 Δ WC2 mutant screening and confirmation
- 5.4 *M. oryzae* Δ WC2 does not display conidial banding
- 5.5 WC2::GFP complementation rescues the conidial banding phenotype
- 5.6 Δ WC2 produces, but is insensitive to, the conidial banding metabolite(s)
- 5.7 WC2 affects photoadaptation in vegetative growth

- 5.8 WC2 plays a role in photoadaptation and conidiation
- 5.9 Pre-inoculation treatment has a reduced effect on Δ WC2 germination and development, but Δ WC2 develop quicker than the wild type
- 5.10 WC2 plays a role in conidial size
- 5.11 WC2 plays a role in appressorial stability
- 5.12 WC2 has a function in host plant penetration
- 5.13 WC2 affects *in planta* cell to cell movement and invasive growth
- 5.14 WC2 plays a role in lesion formation and lesion size in rice
- 5.15 Prolonged light exposure favours dusk inoculations in Δ WC2
- 5.16 Pre-inoculation light treatment affects Δ WC2 pathogenicity in rice
- 5.17 Δ WC2 displays significantly reduced pathogenicity in rice under high inoculation densities and disease-conducive conditions
- 5.18 WC2 plays a profound role in non-host pathogenicity on barley
- 5.19 Time of day has less of an effect on Δ WC2 pathogenicity in barley
- 5.20 Prolonged light exposure consistently reduces dawn pathogenicity in Δ WC2
- 5.21 Δ WC2 displays dampened leaf maturity-dependent infection severity
- 6.1 FRQ function in the positive and negative arm is dependent on time of day, phosphorylation status, and subcellular location
- 6.2 A simplified FRQ-centric map and model of the *N. crassa* circadian clock
- 6.3 Predicted FRQ motifs in the uncharacterised *C. kikuchii* protein CKM354_001184500
- 6.4 Predicted MGG_17345 – MGG_17344 open reading frames
- 6.5 The predicted *M. oryzae* FRQ is likely to have a high capacity for phosphorylation
- 6.6 The *M. oryzae* predicted amino acid sequence shows a C-terminal enrichment of PEST domains

- 6.7 The *M. oryzae* predicted FRQ AA sequence contains an N-terminally located coiled-coil domain
- 6.8 The predicted *M. oryzae* FRQ protein has motifs indicative of nuclear and cytoplasmic localisation
- 6.9 *M. oryzae* FRQ is likely a disordered protein
- 6.10 Pairwise Emboss Needle alignment of the *N. crassa* FFD to the predicted *M. oryzae* FRQ sequence
- 6.11 Potential MGG_17345 Cas9 target sequences
- 6.12 MGG_17345-targeting Cas9 mutation facilitated a large insertion
- 6.13 The MGG_17345 insertion is likely generated through (semi-) homology directed repair
- 6.14 FRQ plays a role in the conidial banding latency period
- 6.15 FRQ plays a role in the circadian periodicity of *M. oryzae*
- 6.16 FRQ^{NIN} shows light-dependent altered vegetative growth rates
- 6.17 FRQ plays an important role in conidiation
- 6.18 FRQ^{NIN} conidia are less likely to germinate, but those that do are more likely to produce appressoria
- 6.19 Circadian machinery plays a role in conidial size
- 6.20 FRQ^{NIN} generates higher appressorial turgor pressure or appressoria are more resistant to osmotic stress
- 6.21 FRQ^{NIN} does not show altered penetration or cell-cell movement 24 hours post-inoculation
- 6.22 FRQ^{NIN} strains show no significant difference in penetration and cell-cell movement 48 hours post-inoculation

- 6.23 The FRQ^{NIN} strain is less pathogenic than the wild type after antiphase entrainment at dawn towards rice
- 6.24 Prolonged darkness-entrained FRQ^{NIN} strains prefer dawn in rice inoculations
- 6.25 Pre-inoculation treatment plays a role in dawn virulence in FRQ^{NIN} mutants
- 6.26 FRQ^{NIN} mutants display reduced antiphase-entrained pathogenicity
- 6.27 Pre-inoculation entrainment has little effect on time of day-dependent infection severity in FRQ^{NIN}-barley inoculations
- 6.28 Antiphase entrainment to the host in FRQ^{NIN} reduces disease severity
- 6.29 FRQ^{NIN} displays smaller optimal leaf areas
- 6.30 The WC2 mutants are less pathogenic than FRQ^{NIN} towards rice
- 6.31 FRQ^{NIN} mutant strains are more virulent than their WC2 counterpart towards barley

List of tables

- 1.1 Predicted (BlastP) and confirmed clock gene homologues in *M. oryzae*
- 2.1 Complete media recipe (1 L)
- 2.2 Minimal media recipe (1 L)
- 2.3 20x nitrate salts recipe (1 L)
- 2.4 1000x trace elements recipe (100 ml)
- 2.5 1000x vitamin solution recipe (100 ml)
- 2.6 1000x penicillin-streptomycin stock (10 ml)
- 2.7 OM buffer recipe (150 ml)
- 2.8 STC buffer recipe (500 ml)
- 2.9 Tris-HCl buffer recipe (1 L, 1 M)
- 2.10 PTC buffer recipe (100 ml)
- 2.11 10x TE buffer recipe (1 L)
- 2.12 50x TAE buffer recipe (1 L)
- 3.1 A selected summary of a range of plant pathology-related image analysis toolkits
- 3.2 Comparative manual vs automated colony band and diameter analysis
- 3.3 Accuracy of the spore conidia counter macro
- 3.4 Accuracy of the appressoria finder
- 3.5 Accuracy of Redpatch
- 4.1 Putative and confirmed *M. oryzae* clock and photoreceptor genes
- 5.1 Fungal circadian-related mutant phenotypes
- 5.2 Δ WC2 donor DNA and diagnostic primers
- 5.3 Δ WC2 diagnostic amplicon restriction digest
- 6.1 A selected summary of FRQ mutations

6.2 Homologues of non-core clock machinery that influences FRQ expression and activity are present in *M. oryzae*

6.3 MGG_17345 – MGG_17344 ORF 1 + 3 predicted protein homology to sordariomycete FRQ

6.4 Δ FRQ donor DNA and diagnostic primers

6.5 Common and divergent phenotypes between a range of reported FRQ mutants and FRQ^{NIN}

Abbreviations

AM	Arbuscular Mycorrhizal
BIC	Biotrophic Interfacial Complex
BLAST	Basic Local Alignment Search Tool
C-box	Clock box
CCA1	Circadian Clock Associated 1
CCG	Clock Controlled Gene
CK1	Caesin Kinase 1
CLAHE	Contrast Limited Adaptive Histogram Equalisation
CM	Complete Media
CRISPR-Cas	Clustered Regularly Interspaced Short Palindromic Repeat- associated protein
CTCF	Corrected Total Cell Fluorescence
DAMP	Damage-Associated Molecular Pattern
DD	Constant Dark
ddH ₂ O	Double Distilled water
DDT	Dithiothreitol
DL	Dark-Light
DMF	Dimethylformamide
DPI	Days Post Inoculation
DPI	Dots Per Inch
dsDNA	Double Stranded DNA
EIHM	Extra-Invasive Hyphal Membrane
ETI	Effector-Triggered Immunity
FCD	FRQ-CK1 interaction domain
FFC	FRQ-FRH-CK1 complex
FIJI	FIJI Is Just ImageJ
FLO	Frequency-Less Oscillator
FRH	FRQ-interacting RNA Helicase
FRQ	Frequency
F_v/F_M	Variable / Maximum Fluorescence
FWD1	F-box/WD-40 Domain-containing protein 1
FWO	FFC-WCC Oscillator
GFP	Green Fluorescent Protein
GO	Gene Ontology
GOI	Gene Of Interest
HDR	Homology Directed Repair
HPI	Hours Post Inoculation
HR	Hypersensitive Response
HSB	Hue*Saturation*Brightness
Indel	Insertion/deletion
JA	Jasmonic Acid
LD	Light-Dark
LD-DD	Light-Dark-constant Dark
LD-LL	Light-Dark-constant Light
LED	Light Emitting Diode
LL	constant Light
LOV	Light-Oxygen-Voltage
LUX	LUX arrhythmia
MAMP	Microbial-Associated Molecular Pattern
MM	Minimal Media

NAMP	Nematode-Associated Molecular Pattern
NB-LRR	Nucleotide-Binding Leucine-Rich Repeat
NDVI	Normalised Difference Vegetation Index
NHEJ	Non-homologous End Joining
NHR	Non-Host Resistance
NLS	Nuclear Localisation Signal
NOP1	(Neurospora) Opsin 1
OCM	Osmotically stable CM
Oligo	Oligonucleotide
ORF	Open Reading Frame
PAM	Protospacer-Adjacent Motif
PAMP	Pathogen-Associated Molecular Pattern
PAS	PER (Period circadian protein)-ARNT (Aryl hydrocarbon Receptor Nuclear Translocator protein)-SIM (Single-Minded Protein)
PCD	Programmed Cell Death
PCR	Polymerase Chain Reaction
PEG	Polyethylene Glycol
PEST domain	Regions rich in Proline (P) glutamic acid (E) serine (S) and Threonine (T)
Phy1	Phytochrome 1
PLA	Polylactic Acid
PLRE	Proximal Light Regulatory Element
PRR	Pattern Recognition Receptor
PRR	Pseudo-Response Regulator
PSII	Photosystem II
PTC	Premature Termination Codon
PTI	Pattern-Triggered Immunity
px	Pixel
QTL	Quantitative trait loci
R gene	Resistance gene
R protein	Resistance protein
RFP	Red Fluorescence Protein
RNP	Ribonucleoprotein
ROI	Region Of Interest
ROS	Reactive Oxygen Species
RVE	Reveille
SA	Salicylic Acid
SAR	Systemic Acquired Resistance
SDI1	Succinate Dehydrogenase Iron subunit 1
sgRNA	Single Guide RNA
SM	Spent Media
TTFL	Transcriptional-Translational Feedback Loop
TWL	Twilight
UTR	Untranslated Region
UV	Ultra-Violet
VVD	Vivid/Envoy
WC1	White Collar 1
WC2	White Collar 2
WCC	White Collar Complex
WC-FLO	White Collar Frequency-Less Oscillator
Zt	Zeitgeber

1 General introduction

1.1 The current status of global food security

As the global human population continues to climb, from its current value of 7.8 billion as of 2021, to projected populations of 8.5 billion by 2030, 9.7 billion by 2050, and 10.4 billion by 2100 (1), the need to produce sufficient food to meet demands is now more pertinent than ever. Food insecurity occurs when people are unable to access safe and nutritious food on a reliable basis, in a quantity and quality that meets their dietary needs and food preferences required for an active and healthy lifestyle (2), and this lack of security can be due to physical, societal, economic, or political factors (3). Indeed, there are a multitude of causes, with links to the increases in violence and war, extreme weather and natural disaster, inequality of wealth and its distribution, and agricultural pests and diseases being predominant (3–5). Countries like Afghanistan, Syria, and Nigeria, which have unfortunately observed significant conflict and civil upheaval in recent years have experienced destruction of infrastructure and roads, subsequently affecting food markets and imports/exports (6).

Food insecurity has increased globally, in part due to climate crises and conflict; Ukraine, for example, is one of the world's largest producers of several key crops and produced 3.4% of global wheat, 5.2% of barley, 6.1% potatoes, 1.2% tomatoes, 5.1% sugar beet, 3.7% rapeseed oil, and a staggering 27.3% sunflower seed in 2018 (4,7). Due to the ongoing conflict with Russia, there are now significant supply chain issues arising, creating further knock-on effects. As a result, in Africa food and fuel prices are rising sharply, compounded by inflation and financial instability (8). A lack of access to safe and reliable work as a result of conflict then creates an inability (whether

financial or otherwise) to attain sufficient amounts of nutritious food (4,6), which can then further impact mental and physical wellbeing, as well as access to work, creating a viscous feedback loop.

All organisms are in some way adapted to their environment, and as the global climate continues to change so, too, does the need for organisms to either adapt to these changes or perish (9). With drastic temperature events like heatwaves becoming more commonplace, a crop species may begin to suffer and produce a lower yield, impacting both the farmers and their income, as well as the consumers who may be unable to afford the resulting price hikes (10,11). Additionally, an agricultural pest or disease's ecological range may be altered with climate change: increased temperature or humidity could facilitate faster pathogen growth, spread, and virulence, severely reducing global crop production (12,13). For example, phoma stem canker outbreaks are most severe in Mediterranean climates where oilseed rape is grown, but the disease has long been present in the UK (14). Here, the baseline severity of phoma stem canker at harvest from the 1960s – 90s had a maximal 'severity value' of 1.7 in a pocket in the southwest of England, whereas the predicted maximal severity value for 2050 is 2.3 and may cover a large region of the UK, both in the south (ranging from Wales down to the southeast of England) and in Western Scotland (14). If climate change trends continue their trajectory, events such as these could rapidly occur elsewhere.

14 crop species provide the majority of food for human consumption, all of which are susceptible to pre- and post-harvest disease (15). *Phytophthora infestans*, the causative agent of the potato famine of 1840s Ireland, has spread significantly, showing a vast presence across the globe, with epidemics in North America,

Southwest India, and Tunisia, amongst other locations, resulting in severe crop damage and economic losses surpassing \$6 billion (16–18). Further, since monoculture crop practices are common in the agricultural industry, the perfect breeding ground for plant pathogens is created: the pathogen is surrounded by genetically uniform hosts, allowing it to quickly adapt, propagate and effectively devastate a population of crops, unless fungicides and other control methods are used (19,20).

Fungicides are used with varying efficacy based on geographic location, fungal pathotype, and dosage (21), with broad-spectrum fungicides commonly used (21,22). Fungicides, however, can be expensive (sometimes over \$70 per hectare), and inability to afford fungicide was reported to be one of the main reasons for limited rice blast disease control in Tanzanian smallholder farms, for example (23). Further, much like antibiotic resistance in human and animal disease, plant pathogens are becoming increasingly resistant to pesticides (24,25). *Botrytis cinerea*, the grey mould fungus capable of infecting a wide range of important plant species, causes significant pre- and post-harvest crop losses and has developed resistance to a range of fungicides resulting from excessive spraying (24). *B. cinerea* displays high levels of resistance to the Benzimidazoles, Anilinopyrimidines, QoIs/strobilurins, and Hydroxyanilides, and this resistance can evolve rapidly, as the Hydroxyanilides were first used in 2004 (24). Further, since these staple crops are often grown far from their ancestral origin, they are (a) exposed to novel pathogens to which they do not have resistance, and (b) could quickly become susceptible to the pathogens present at their origin, as they are no longer co-evolving (15,26). It is therefore imperative that

control practices are maintained, and research carried out on plant pathogens, given their devastating effect on yield, the economy, and food security.

Finally, as the global population continues to rise, this will inevitably put more pressure on countries to produce (and trade) more food to maintain any level of food security and diversity they have. If food production cannot meet the demands of a growing population, prices may rise, potentially leaving only the wealthy with the purchasing power necessary for a sufficient and nutritious diet. This could lead to an increased wealth gap, along with tension and potential conflict between economically disparate sub-populations. Indeed, so-called 'food deserts' are already a common phenomenon, where low- and moderate-income communities have reduced access to nutritious food compared to richer areas (27). Thus, unless food production is increased and distributed fairly, this food insecurity cycle may continue. These factors, while interlinked, can be treated (at least in some capacity) as individual problems to address. Research in the plant sciences, crop protection, and production is one such approach that could significantly contribute towards attaining global food security.

1.2 The socioeconomic status of rice

Rice is a core component of over 50% of the world's diet, and more than 2 billion people obtain as much as 70% of their caloric intake from it (28–31). Rice demand is on the rise in Europe, the Americas, and especially sub-Saharan Africa, where consumption grew by over 50% in a 20-year period (31–33). Catering to this demand was largely facilitated by the 'Green Revolution', where intensification of farming practices and the introduction of new crop varieties, fertilisers, and irrigation techniques allowed for a massive boom in rice yield; Vietnam, for example, doubled its yearly rice production from 1.7 M tonnes in 1989 to 3.6 M tonnes in 2000 (29,31). Likewise, the International Rice Research Institute (IRRI) is part of a task force set out to increase rice productivity in spite of climate change, garner investment in rural and smallholder agriculture, and scale up food security programs targeting health, nutrition, and education (34). Further, the New Rice for Africa (NERICA) project aims to increase food security in Africa, through donations of basic 'foundation' seeds and supervision or provision of farming practices, production and processing equipment, storage and product marketing facilities, and post-harvest storage and processing equipment (35)

Keeping up with the increases in demand still has its difficulties, and rice production is just barely above consumption levels (3,29,36). As such, yield increases have slowed considerably over the past few years, with the 2017-2018 season seeing only a 0.6% increase on the previous year, causing localised shortages and increased prices, significantly impacting poorer income groups (3,4,29,36). Accordingly, the global population increase from 2017 – 2018 was 1.3%, double that of rice (1,3). This demand is expected to rise by a further 26% (an extra 116 M tonnes), from 439 M in 2010 to 555 M by 2035 (37). However, as traditionally rice-growing countries such as China and India

become more economically prosperous, there is a trend of diversification in diets towards a more 'Western' one, consisting of a wider range of meat, dairy, and vegetables, so perhaps this reduced pressure can allow for rice production to continue to match global consumption rates (32). If diversification does not continue or does not continue fast enough, though, exporters and growers may be unable to provide for the overall growing demand for rice in other regions of the world (32).

Throughout the 1990s, global rice trade grew an average of 7% each year, principally due to the actions of developing countries' increasing demand and production (28,29). Further, international rice trade has nearly quadrupled over a period of 50 years, from 7.5 M to 29.5 M tonnes traded annually, with developing countries responsible for ~83% of global exports (Thailand, Vietnam, China, India, and the United States alone contribute three quarters of the exports), and ~86% of the imports (3,28,37–39). In developing countries of South-East Asia, agricultural exports, particularly rice, finance a large portion of domestic income from the global market (38). However, only 7% of total global rice crop is actually exported, suggesting a heavy domestic reliance on rice in these developing nations (37). Accordingly, many governments, such as Indonesia, have developed practices to maintain food security, including the creation of a minimum rice stockhold, standardised purchasing prices for rice, and intervention on a local level to supervise production practices (30,33,38). This again supports the intrinsic value of rice as both a domestic and international commodity.

While global production of rice is still growing over the years, there are several imminent threats towards maintaining this increase to match demand (3,4). Firstly, due to the geographic concentration of rice predominantly in Asia, any localised natural disaster,

extreme weather, phytopathogenic outbreak, or market disruption will have a compound effect on the overall production and exportation of rice, negatively affecting international trade due to the increased predicted costs of rice resulting from its scarcity and supply chain issues (38). These same countries would then have to import a larger volume of rice from other countries, further increasing prices and depleting rice availability on the global market (33).

As climate change remains an ever-present and ever-growing threat elsewhere, so too, is it an increasing issue in rice production (29). In 2013, for example, drought was responsible for the destruction of approximately \$200 M's worth of rice in eastern India, north-eastern Thailand, and China(37). If drought incidences and temperature increases continue their current trajectory, it is estimated that rice production could fall by as much as 14% in the next 30 years (29).

Asia as a whole is also subjected to regular flooding and soil salination of 26 M hectares of farmland (37). Accordingly, as global temperature rises, so will sea levels, causing an influx of salt water inland, creating more saline soils which will again affect the large amount of coastal-grown rice, as well as reduce the remaining available land for rice harvest (40,41). It is estimated that some regions of Bangladesh could suffer yield losses of up to 15.6% by 2050 if soil salinity surpasses 4 dS/m (40,41). In 2018 alone, several Asian countries witnessed a reduced rice yield due to floods or droughts during the main crop cycles, the US gathered its smallest rice crop in 21 years, and production in Africa fell below that of 2016 due to irregular rainfall (3). More directly, rising temperatures will also negatively affect grain filling and thus gross yield: with a 1 °C increase above the current mean temperature, yield reductions could be as much as 10% (37). Finally, since rice is grown on

over 144 M farms, most of which are smaller than one hectare, it can be particularly difficult to disseminate growth practices to alleviate and control for these increasingly erratic environmental conditions (37).

Whilst abiotic stresses play a key role in rice productivity, their biotic stresses are just as pertinent. Since monoculture rice growth is commonplace, genetic erosion often occurs, creating a hotbed for phytopathogenic infection to become pandemic (31,42,43). In India, for example, pests are responsible for 30-40% of annual rice losses (44,45). Climate change will inevitably impact pest prevalence, too; the altered temperature and weather patterns could increase the number and range of hospitable environments for plant pathogens, alter pest reproduction rates, and increase plant susceptibility, as temperature is known to influence immunity and defence responses (46–49).

Due to their short generation time and large populations, plant pathogens are considered to be the first agriculturally relevant organisms to show the effects of climate change (37,46,50). For these same reasons, it is also possible that plant pathogens will also adapt to altered conditions first, allowing them to exploit the new environmental conditions for pathogenesis (46,51,52).

The vast majority of rice growers in the world make use of varieties that have been improved in some way by crop scientists (29,37). Researchers have produced rice with increased yield, resistance to biotic and abiotic stresses, and even increased nutritional value (33,37,53,54). Taking the current pressures on rice production into account, with the increasing issues of climate change, conflict, urban expansion, supply chain uncertainty, and population increase, it is essential that research into rice production and the effects of

both biotic and abiotic stresses on crops, and implementations of their findings is both necessary and time dependent to maintain food security in these uncertain times.

1.3 The socioeconomic impact of rice blast disease

Rice Blast disease, caused by the fungal pathogen *M. oryzae*, is considered the principal disease in rice (55,56), and is responsible for the destruction of 10-30% of rice crop, or enough to feed ~60 M people annually (22,57–59). This can cause global rice price spikes as a result of its scarcity, potentially making this staple food crop unattainable for the world's poorest (22). The damage caused by *M. oryzae* is expected to increase in the coming years and is a great threat towards sufficient rice production, as monoculture cropping systems, climate change, and intensification of farming for the growing population can provide avenues for a wider ecological range and greater virulence of the pathogen (22,46,59). Rice blast outbreaks are in no way new, and are exemplified by the repeated epidemics in Korea of the late 1970s and early 80s (60), and the great yield losses of up to 50% in Central-South USA (22). In the US alone, Nalley and colleagues (22) estimated that if rice blast were to be eradicated, an additional 1 M people annually could be fed, and a further \$63.4 M generated on an annual basis.

Currently, the most effective practice used to combat the threat of rice blast disease is in marker-assisted breeding (22,60). To date, over 80 resistance (R) genes and 350 quantitative trait loci (QTLs) linked to resistance in rice and its wild counterparts have been found, giving hope for continued development of cultivars tolerant and productive in spite of rice blast disease (59). However, this breeding process can take up to 10 years to develop a resistant cultivar (61), and the newly resistant plants often cannot remain so for prolonged periods of time (22,60). The rice blast fungus is often genetically diverse in the

field, and so efficacy of these R genes is dependent on geographical location and specific *M. oryzae* pathovars (59). This diversity and potential for overcoming host resistance in *M. oryzae* can then be confounded by import and export of infected plant material (62). Further, given the comparatively short life cycle and generation time of *M. oryzae* (and plant pathogens in general), researchers often find the fungus overcoming these R genes, and the new cultivars can lose their resistance in as little as 2 years - sustained defence against rice blast disease therefore remains a pertinent issue (22,57,59,63).

Due to the lengthy period taken to develop a resistant rice cultivar, and their short-term efficacy, there is unsurprisingly an increasing push in the scientific community to utilise alternative genetic techniques, such as genome engineering, in crop production (22,64–69). Here, resistance genes or motifs are located in rice with otherwise undesirable traits (such as those in their wild ancestors), or in closely related species and transferred into higher-yielding, commercially grown crops (65,66,70). Alternatively, if only small changes are needed to increase resistance, then the requirement for transgenes, for example, is completely removed; CRISPR-Cas based technology creates highly targeted double stranded DNA breaks in the transfected organism, creating small indels (insertions/deletions of a small number of nucleotides) or facilitating homology directed repair (HDR), and can be utilised to alter plant traits in a minimally invasive way (66,70–74). Indeed, Wang and colleagues demonstrated increased resistance to *M. oryzae* in their C-ERF922 (ethylene responsive factor) mutants, which displayed no significant difference in other desirable agronomic traits (67). Reports such as these point towards a more promising future for global food security, as these cultivars could decrease the environmental impact from intensive farming (reduced fossil fuel and fungicide usage would decrease carbon emissions, ecotoxicological damage, eutrophication, etc.), as well

as increase rice's global availability brought about by the higher productivity (22). However, governments have been hesitant to allow the production or consumption of transformed rice: transgenic, cisgenic, genome edited, or otherwise (22). This leaves growers with relatively few options for combating rice blast disease.

Since a tonne of rice can fetch as high as \$952, and with its ever-increasing price volatility on the international market, *M. oryzae* can have a large impact on the cost of rice at both a local and global scale (22,75,76). It is, therefore, of the utmost importance that rice blast disease pathosystem research continues.

1.4 *Magnaporthe oryzae*: rice blast disease

M. oryzae is a filamentous ascomycete fungus and hemibiotrophic pathogen (displaying biotrophic and necrotrophic stages), capable of infecting more than 50 species of grass, and it is the causative agent of rice blast disease (56,77–79). The fungus is present to some extent in six of the seven continents, particularly in the rice-growing regions of the world, with a concentration in Asia, given its hospitable environment (80). Accordingly, Saleh and colleagues (63) reported that a region spanning south China, northern Thailand, and western Nepal is the centre of origin of *M. oryzae*.

The fungal pathogen first grows biotrophically and asymptotically within the cells of plants, between the plasma membrane and cell wall, actively suppressing the immune system, before switching to a necrotrophic phase (the necrotrophic switch), where toxins are secreted *in planta*, causing cell death (77–79,81). *M. oryzae* propagates by releasing 3-celled spores (conidia) from aerial hyphae (conidiophores) that have erupted from the plant tissue lesions (78,79,82). Conidia are usually released and spread via wind and dewdrop in the early morning, prior to dawn (79,82,83). Upon landing on hydrophobic

surfaces such as foliar tissue, conidia produce apical spore tip mucilage, a sticky mucous-like compound, which enables them to adhere to the plant tissue surface, where they soon germinate and a germ tube then grows from the conidium along the leaf surface (84,85).

By 8 hours post-inoculation (HPI), the germ tubes have become swollen at the tip, and a bulbous infection structure may be produced: the appressorium (58,77,78,85). This process is facilitated by a switch in cellular growth directionality, from the polar, forward growth of the germ tube to the radial, isotropic growth of the appressoria (85,86). The dome-shaped, melanin-lined appressorium allows for glycerol to build up, acting as an osmoticum, which increases turgor pressure substantially (58,87). At this point, the 3-celled conidium undergoes autophagy, and the cell constituents are translocated to the appressorium, since the conidium is no longer needed (58). Turgor pressure within the appressorium allows a penetration peg to rupture and penetrate the host cuticle, beginning at approximately 24 HPI (55,78,88).

As *M. oryzae* enters the plant with its penetration peg and subsequent primary invasive hypha, it invaginates the host cell membrane, and the fungus grows apoplastically (89). The thin primary hypha initially grows in a biotrophic manner and utilises the plasmodesmata network for movement ~36 h after invasion at the primary infection site (58,89–92). At this point, primary hyphae differentiate into larger invasive hyphae, facilitating cell-cell movement and ultimate tissue colonisation (59,93,94). The membrane surrounding the invasive hypha is known as the extra-invasive hyphal membrane (EIHM), produced by the plant host cell, but facilitated by *M. oryzae* (93,95). The EIHM acts as a barrier between the fungus and plant, and the main means of interaction between host and pathogen is at the biotrophic interfacial complex (BIC) (58,96). Here, *M. oryzae* secretes effectors such as

Pathogenicity toward weeping lovegrass (Pw12), which moves into surrounding host cells prior to hyphal invasion and suppresses the plant defence response to create a more hospitable host environment (85,93,95,97–100). After this biotrophic growth phase of about 4 d, *M. oryzae* then undergoes its necrotrophic switch, where the invasive hyphae can cause tissue death, and aerial hyphae emerge from diamond-shaped lesions, followed by conidiophore formation as early as 6-7 days post-inoculation for the eventual propagation and spread of *M. oryzae*, where the disease cycle begins anew (58,78,85) (fig. 1.1).

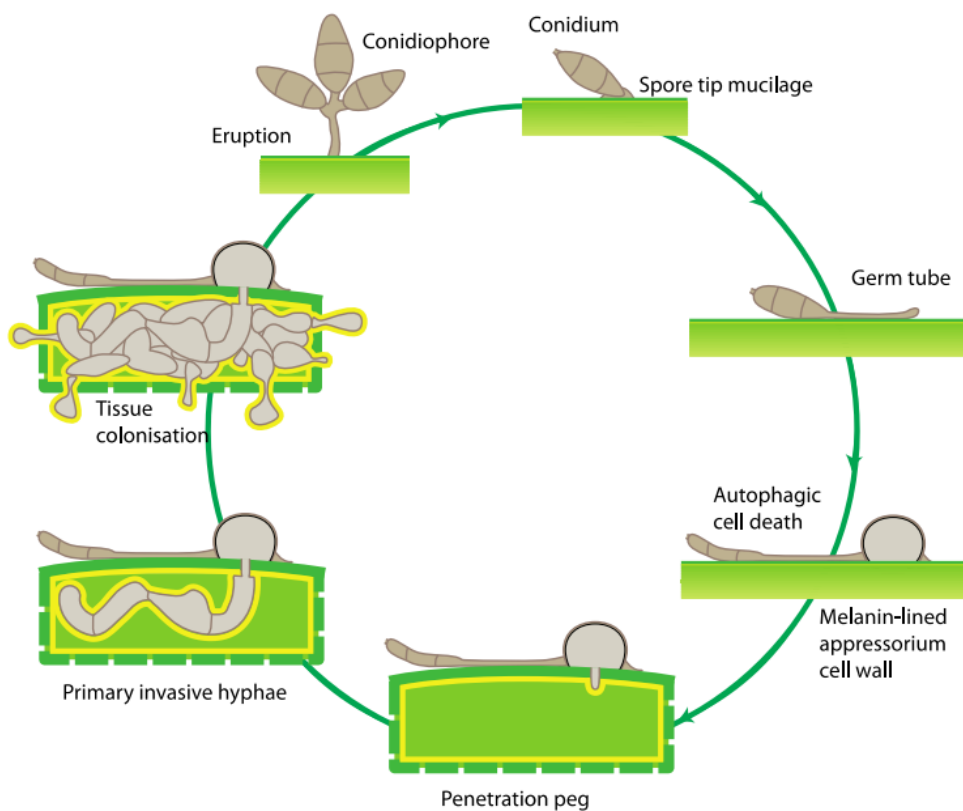


Figure 1.1: The disease cycle of *Magnaporthe oryzae*. Image prepared by Assoc. Prof. George Littlejohn

There are three crucial factors (known as the 'disease triangle') needed for successful progression of disease in plants; (a) a susceptible host, (b) a virulent pathogen, and (c) a disease-conducive environment (101–105). Grain yield, being the most important factor in rice crop production is, in part, dependent on which rice variety is grown (and its subsequent susceptibility to rice blast), the extent of infection and amount of inoculum, and efficacy of control measures such as fungicides (22). In the wet season, when days are warm and humid, *M. oryzae* can thrive and eradicate massive areas of rice crop (12,55). *M. oryzae* could, therefore, be more or less virulent at certain times of day or year due to a plethora of environmental factors, notably light intensity and length of exposure (i.e., photoperiod, or day length), wavelength composition (red wavelengths are comparatively abundant at sunrise and sunset compared to blue, for example), temperature, humidity, windspeed, and so on (46,104). Indeed, it has been observed that light exposure, day length, light quality, and 'photoperiodic stress' can impact both pathogen virulence and plant resistance/susceptibility to disease (82,106–111,111–115).

If a disease-causing species could predict and prepare for these disease-conducive environments, it would benefit their propagation and allow them to conserve and spend the available resources at times most beneficial (108,116–119). Alternatively, if a host can predict when a pathogen will be most virulent or abundant, then it can be better prepared to defend itself, utilising the energetically expensive defence mechanisms at times most critical for survival (120–122). A progression of knowledge in the rice blast pathosystem may subsequently inform new control strategies and their implementation, allowing for combat against this globally devastating plant pathogen, thus increasing food security from a local to global level, ensuring that rice production increases are maintained for a stabilisation of the cost and abundance of rice on the global market

1.5 The plant immune system

A plant's first line of defence against invading pathogens is the cuticle, providing a physical barrier between the intercellular contents and the outside world, coupled with antimicrobial compounds and enzyme inhibitors (106,123–126). Once this barrier is breached (through stomatal or wound entry, cell-wall degrading enzymes, or appressoria-mediated penetration), plants then utilise two facets of the innate immune system; one method detects microbial-, pathogen-, nematode-, or damage-associated molecular patterns (MAMPs, PAMPs, NAMPs, and DAMPs, respectively) via cell plasma membrane-localised pattern recognition receptors (PRRs) and responds accordingly with pattern-triggered immunity (PTI) (124–128). An important differentiation here is made between microbe and pathogen associated molecular patterns, as many non-pathogenic microorganisms will present the same conserved motifs as their pathogenic counterparts, whereas PAMPs are microbial patterns specific to pathogens: indeed, all PAMPs are technically MAMPs, but not all MAMPs are PAMPs (123). The other main avenue for immunity acts predominantly intracellularly, making use of NB-LRR (nucleotide-binding leucine-rich repeat) proteins, which are the products of some resistance (R) genes (124–126,128). These proteins serve to detect microbe-derived effectors (which target a range of cellular components, such as the chloroplasts, and can act to suppress the PTI system) and facilitates a signalling cascade for the subsequent effector-triggered immunity (ETI) – ETI is essentially an 'accelerated and amplified' version of PTI (123–125,129). Consequently, the current depiction of the plant immune system is based on the canonical 'zigzag' model, where the well-conserved molecular motifs (such as flagellin or chitin) associated with microbes are first recognised by PRRs, triggering PTI, and when the pathogen successfully avoids, suppresses, or survives this PTI with the use of effectors, ETI is then activated, which elicits a more severe reaction in the plant and makes use of R proteins (123–125). The term 'zigzag' is

used to denote progression from PTI to ETI, both of which cause the 'amplitude of defence' to fluctuate over time (124).

Pattern-triggered immunity induces an influx of calcium (used as a secondary messenger for defence responses), produces large amounts of reactive oxygen species (ROS) via the ROS burst, causes tissue to undergo callose deposition and alters the structure of the cell wall, and upregulates defence gene expression (124,125,127,130–132), all of which serve to destroy or block the invading pathogen. Effector triggered immunity makes use of calcium signalling, nitric oxide and ROS, altered membrane trafficking and defence gene upregulation and, distinctly, leads to a type of programmed cell death: the hypersensitive response (123–125,127,128,133).

Following ETI, a third component of plant immunity is activated: systemic acquired resistance (SAR) (124–126,133,134). As a result of the hypersensitive response, long-distance, plant-wide signalling is employed to prime the defences of unaffected tissue against further pathogenic attack, both in the short and long-term, ranging from weeks to entire seasons (125,126,133,134). Chloroplast-derived phytohormones are also employed here (importantly Salicylic acid and Jasmonic acid), performing a range of different functions in defence and signalling (126,133,134). Since plants are able to prime their immune system for future pathogenic attack based on previous infection so, too, are they able to regulate their immune system based on environmental factors, such as light, temperature, and even time of day (103,109,111,114,115,120,128,135–160).

1.6 Circadian rhythms

The earth rotates every 24 hours and tilts on its axis annually. As a result, most parts of the world experience reliable cycles in light and temperature, giving rise to diurnal light-dark cycles (day and night) and seasonal changes throughout the year. As several environmental

inputs including light, temperature, and humidity fluctuate on a daily and yearly basis, so too, can an organism's metabolism, physiology, and behaviour as a result of having evolved in this alternating, but predictable environment (139,161–165). Accordingly, biological rhythms are common in nature, where these outputs are cyclically regulated with varying timescales, from a second-by-second basis with the rhythmic beating of the heart, to seasonal or annual rhythms, like those shown in deciduous trees (164–166). Many organisms can measure time, anticipate the daily 24 h period, and adjust these aspects accordingly (167,168). This internal daily anticipation is termed the 'circadian rhythm', stemming from the Latin 'circa' (about) 'dies' (day) (169), where one cycle of the clock occurs approximately every 24 h. Likewise, biological rhythms with periods shorter than 24 h are termed ultradian, and those longer are infradian rhythms (164,170). A circadian rhythm is generated endogenously and can be maintained under constant conditions within physiologically relevant parameters (such as temperature, pH, or nutritional status), where there are no external diurnal or temporal cues such as light to input, reset, and entrain the circadian clock (104,169,171–173). Accordingly, whilst changes in temperature can entrain the circadian clock, the periodicity (i.e. the time taken to complete one circadian cycle) remains relatively uniform over a range of temperatures (167,174,175). Implicating the importance of the circadian clock, it has been reported in several studies on a range of organisms that a third or more of an organism's genome is expressed and regulated in a rhythmic fashion, which suggests that there is an adaptive advantage and/or heavy reliance on the clock for a number of different outputs (176–178).

If an organism can predict the future environmental conditions based on past experience, it could subsequently optimise its metabolic function, physiology, or behaviour to buffer against any future challenges or display phenotypes most beneficial to these changes.

These time of day-dependent changes, or clock outputs, are wide ranging in their functions and include the rhythmic control of biotic stress and immune responses (120,122,142), response to abiotic (e.g. osmotic) stresses (104,179), and even virulence (104,117,122,150,177,180). Importantly, these rhythmic changes in the organism continue to occur for a time even when in constant conditions (161): a diurnal process is based solely on external cues such as light's presence or absence (e.g., photosynthesis), whereas a circadian process is one in which there is a reliable rhythmic process (of approximately 24 h), independent of, but entrained (or reset) by, these diurnal cues.

A circadian rhythm can be adjusted, and the phase shifted by external signals, such as light or temperature, to facilitate synchronicity with the environment (171). In the lab, if the light phase of the photoperiod is adjusted by 2 h from 8 am – 8 pm to 10 am – 10 pm, then the circadian rhythm (and thus, circadian outputs, such as stomatal closure) will soon adapt by 2 h to reflect this change (104). These temporal signals, or Zeitgebers, can therefore be said to entrain the internal circadian rhythm to the external oscillation of day and night, allowing for optimal timing of physiological, metabolic, and behavioural phenomena (104,169). Signals at dawn and dusk are important entrainment cues (162); dawn providing light after a long period of darkness, and dusk providing relief from this light, both of which are signals to the photoreceptors that feed into the clock (106,150,180–182).

Most described circadian oscillators heavily rely on a network of integrated transcriptional-translational feedback loops (TTFLs) (117,148,160,177,183–185). At its core, there is generally (at least) a positive and negative arm of the network (161,186). Here, the (usually) transcription factor-based positive arm initiates the transcription of the negative arm, which, when translated, begins to suppress the action of the positive arm, thereby

repressing its own transcription (161). Over time, the negative arm protein(s) are then modified and inactivated, often through phosphorylation or ubiquitination, leading to eventual protein turnover in the proteasome (161,179,187). The cycle can then begin again after approximately 24 h, once the negative arm is no longer actively suppressing the positive arm.

Whilst the ticking of the clock is predominantly dictated by the two main entrainment signals of light and temperature, there are several further integrated feedback loops (179,181,184,185,188–192). For example, a number of nitrogen assimilation genes are driven by Circadian Clock Associated 1 (CCA1, a component of the plant clock), and the addition of nitrogen causes the phase of CCA1 to be shifted slightly (162,179). This suggests that the circadian clock is interconnected with different signalling systems in order to integrate an accurate representation of the world around it, and is not just a closed system as was previously thought (179).

1.7 Circadian rhythms in fungi

The circadian clock has been well described in the Sordariomycete (of which *M. oryzae* is a member of), *Neurospora crassa*. Accordingly, fungal circadian rhythms are chiefly maintained by autoregulatory positive and negative feedback loops dictated by the Frequency (FRQ) – FRQ-interacting RNA Helicase (FRH) – Caesin Kinase 1 (CK1) complex (FFC), which acts predominantly in the negative arm, and the White Collar Complex (WCC): White Collar 1 (which also acts as a blue light photoreceptor) and White Collar 2, contributing to the positive arm (101,104,116,119,161,177,183,185,193,194,194–215,215–226). Altogether, the FFC-WCC machinery forms the FFC-WCC oscillator (FWO) (discussed in detail in results chapters 5 and 6).

Late in the circadian evening, the WCC binds to the *frq* clock-box promoter region: *frq* transcript levels then peak in the early morning and FRQ protein peaks several hours later (181,192,201,227). FRQ then dimerises and binds with FRH (which acts to stabilise the protein) and CK1, to create the FFC (161,178,222,228–234). The FFC then enters the nucleus and rapidly phosphorylates the WCC, repressing its *frq*-activating function (161,178,222). Concurrently, cytoplasmic FRQ acts to transcriptionally upregulate *wc2* and stabilise WC1, acting in the positive arm (210,221,222,225,229). FRQ is gradually phosphorylated throughout the circadian day, which reduces its activity in both the positive and negative arm and is eventually rendered 'invisible' in the circadian system (161,178,193,195,221,232,235,236). When FRQ is inactivated, the circadian cycle can begin anew, and hyperphosphorylated FRQ is ubiquitinated and turned over at the proteasome via its interaction with FWD1 (161,177,178,181,195,210). Indeed, inactive or low levels of FRQ then allows the WCC to begin to upregulate *frq* expression again (177,178,181,189,210,229). This core clock is upstream of several other gene pathways, causing daily, rhythmic oscillations in gene expression, and thus controls many physiological outputs in a time-dependent manner (84,104,171,171,237,238). In essence, the negative clock gene, *frq*, is transcribed (facilitated by the WCC), the protein levels increase and nuclear-localised FRQ acts to repress its own transcription; the mRNA levels decline, followed by inactivation of FRQ via phosphorylation, which allows the positive arm to transcribe and translate *frq* again (161,178,186,190,193).

The ubiquitous nature of circadian rhythms (161,167) suggest that it brings a significant fitness advantage (117,176,179,239). One interesting example of a fungal advantage from circadian rhythmicity is in the bioluminescent mushroom *Neonothopanus garneri*, where luminous protein levels peak at night, causing the fungus to glow a pale green colour; this

attracts insects which disperse the spores in favour of wind, as the Brazilian forests that they inhabit are subject to low air flow as a result of the thick canopy (174). Importantly, once transferred to constant conditions after sufficient entrainment, the mushroom continues to brighten and darken approximately every 24 h (174). Further, it has been suggested in both *N. crassa* and *M. oryzae* that spore production occurs predominantly overnight, peaking just before dawn (82,101,161,177,181,192). At this time, temperatures are low, and humidity is high, which could allow for optimal spore dispersal by wind and dew drop (12,82,84,177). A circadian clock may also benefit above-ground fungi, as they can adapt to and expect light-induced stresses (such as DNA and oxidative damage) at dawn (104,240), which could potentially be one of the stressors influencing the evolution of melanin production in fungal species (such as *M. oryzae*), given its protective function against UV radiation and its role in pathogenesis (241). Benefits such as these, brought about by the maintenance of an energetically expensive circadian rhythm, suggests a worthwhile balancing of cost and return in fungal species.

1.8 Circadian rhythms in plant pathology

Circadian rhythms can also benefit plants, as they are able to anticipate timing of infection and alter their expression of defence genes accordingly (107,120–122,136,140–142,144,148,148,150,152,159,160,163,173,182,242–254). Bhardwaj and colleagues showed that *Arabidopsis* exhibits circadian variation in susceptibility to the bacterial pathogen *Pseudomonas syringae*, being least susceptible in the morning, and they suggest that there is a cyclic regulation of PTI (243). Further, *Arabidopsis* also shows time of day-dependent susceptibility to *B. cinerea*, where successful infections are also least likely at dawn compared to other times of day (120), and there is temporally gated opening of guard cells in plants that need to defend against stomata-infecting pathogens (122,255). When

core clock genes were knocked out in Arabidopsis, producing an arrhythmic line, there was no difference in disease outcome, regardless of subjective inoculation time, suggesting that Arabidopsis upregulates its defence response at dawn (243). Jasmonate-mediated defence and wound healing in Arabidopsis also displays circadian rhythmicity, aiding to prevent insect herbivory at certain times of day (163). Hevia and colleagues suggest that the severity of the disease outcome is not solely dependent on the plant clock, but rather a combination between the fungal and plant clock: the 'pathogen circadian system' (117). Indeed, clock disruption in *B. cinerea*, through mutation, overexpression or constant light exposure showed that the fungal clock holds the main role in disease outcome in Arabidopsis, and the clock is required to maximise (or repress) virulence at certain times of day (117). Ultimately, plants may ready their defences at times when it is anticipating attack based on their current and previous environmental cues, and fungi may release their spores, germinate, and attack plants when the fungi are most virulent and/or plants most susceptible. Due, in part, to the limited availability of resources in both members of the pathosystem (nutritionally or otherwise), the timing of infection is an important factor, where both virulence and defence must be balanced against growth and survival (103,148,228,256,257). These factors suggest a critical need to understand the circadian clock in terms of plant defence, fungal virulence, and subsequent disease outcome – understanding the clock could ultimately help improve crop production for the expanding human population in spite of mitigating factors such as climate change.

1.9 Time of day-dependent infection in rice blast disease

In *M. oryzae* and rice, like other pathosystems, it is possible that circadian rhythmicity and time of day could play a substantial role in determining the outcome of disease. Firstly, bioinformatic analyses show there are many homologous clock and clock-related genes in

M. oryzae (Table 1.1, and chapters 4.2.1, 5.1.1, and 6.1.3) (82,84,101,117,177,257–259). There are several different aspects of pathogenicity that could be time of day-dependent and temporally gated, and fungal effector production or secretion could depend on external signals such as light intensity and quality, humidity, hydrophobic surface contact, or temperature, and may be controlled by the clock (260). Twilight (TWL) protein production, for example, is influenced by the light-dark boundary (dawn and dusk) and peaks at night, showing rhythmic expression under light-dark (LD) and constant dark (DD) conditions (84). TWL is important for asexual development and conidiation, and plays a role in the pathogenicity of *M. oryzae* (84). Interruption of the clock, therefore, should negatively affect *M. oryzae*'s ability to infect crop species and successfully propagate. Indeed, select studies (82,101,258,259) show that (a) knocking out the MoWC1 gene causes blue light insensitivity, a lack of light-dependent aerial hyphae production, reduced conidial release, and the loss of light-dependent disease suppression (82,101); (b) MoFwd1 KO mutants displayed reduced vegetative growth and loss of conidial banding, produced fewer conidia, delayed conidial germination and reduced appressorial formation (259); and (c) mutations in the MoFRQ gene can cause slowed vegetative growth, reduced conidiation, delayed germination, decreased appressorial formation, irregular conidial morphology, and reduced virulence (258,259).

Table 1.1: Predicted (BlastP) and confirmed clock gene homologues in *M. oryzae*

<i>N. crassa</i> clock gene	Function	<i>M. oryzae</i> homologue	Reference
frq	Core clock component, forms the FFC, promotes WCC stability, represses WCC activity	MGG_17345 – MGG_17344 (Mgfrq/Mofrq, see chapter 6.2.1)	(84,101,258,259)
wc1	Blue light photoreceptor, core clock component, forms the WCC	MGG_03538 (MGWC1)	(82,84,101,257)
wc2	Core clock component, forms the WCC	MGG_04521 (MGWC2)	(84)
frh	Core clock component, forms the FFC	MGG_03931	NA
fwd1	Facilitates ubiquitination-mediated FRQ turnover	MGG_09696 (MoFwd1)	(259)
ck1	Core clock component, forms the FFC	MGG_02829	NA
vvd	Blue light photoreceptor, photoadaptation	MGG_01041 (ENVOY)	(82,101)
phy1	Red light photoreceptor	MGG_12377 (PHYTOCHROME 1)	(82,101)
nop1	Green light photoreceptor	MGG_09015 (hypothetical protein)	NA

Wang and colleagues have observed a rhythmic expression in components of PAMP-triggered immunity (PTI) and effector-triggered immunity (ETI) in Arabidopsis, thereby affecting their responses to certain diseases (173). Indeed, it has been shown that *M. oryzae* infections are more severe in old Arabidopsis leaves compared to younger leaves at dusk, a phenomena not seen at dawn (253). However, Yamauchi and colleagues (253) did not state the photoperiodic regime for the fungus prior to inoculation, which could contribute towards virulence. *M. oryzae* has also shown that conidiation and conidial release peaks between midnight and dawn, when conidia are most likely to be successfully transported by dewdrop and wind, further implicating time of day and the circadian clock in virulence-related traits (46,82,261).

The recognition of the pathogen or microbe-associated molecular patterns, or secreted effector molecules associated with disease causes Arabidopsis to upregulate its immune response through PTI and ETI, respectively (91). It is therefore reasonable to assume that there may be a circadian regulation of PTI and ETI common to plants, including in rice, allowing for anticipation and response to infection. So, it seems the pathogen-host interaction is more complex than previously assumed, and depends on the plant as well as fungal circadian clock, integrating all manner of environmental cues. Altogether, there may be a temporal effect on the susceptibility to, spread of, and subsequent success of rice blast disease.

Plants and pathogens live in a predictable, but dynamic environment. For plants, one such change is the presence of certain pathogens. Evidence for a role of intrinsic circadian clocks in the outcome of diseases is growing, and it is likely that these clocks have a function in the virulence of fungal pathogens (such as *M. oryzae*) and in the defence against these

pathogens in plants. Whilst some studies have been conducted on the role of circadian clocks in abiotic stress resistance, such as drought in rice (262), comparatively little research has been conducted on biotic stresses like rice blast disease, and the interaction between the two partners of the pathosystem. However, interest in the interactions between the (perception of) time of day, environmental conditions, and circadian rhythmicity in plants and their pathogens, such as in rice blast disease, is growing (82,84,101,177,259).

As new information comes to light, signalling the importance of circadian rhythms in plant pathology, it is all the more important to research time of day-specific outcomes of infection, and the effects of clock disruption on pathogenicity and defence, especially in economically important pathosystems like rice blast disease. This work reports on the role of timing, entrainment, and circadian machinery on the growth, development, and pathogenicity of *M. oryzae* in rice and barley plants. This information could eventually inform on better pathogen management programs to improve crop productivity: an ever-increasing necessity.

2 Materials and methods

2.1 Fungal growth, maintenance, and storage

M. oryzae isolates used in this study were initially provided by the Talbot laboratory (Exeter University, UK and The Sainsbury Laboratory, UK), then stored, used, and transformed in the Littlejohn laboratory (University of Plymouth, UK). WC2::\DeltaWC2 and FRQ::NIN complementation strains (see chapters 5 and 6, respectively) were generated by Dr. Xia Yan (Talbot laboratory, The Sainsbury Laboratory, UK). For long-term storage, small pieces of sterilised Whatmann filter paper (~1 cm²) were placed on complete media (CM, Table 2.1) (79) petri dishes (9 cm diameter), inoculated with *M. oryzae*, and the mycelia allowed to grow into and penetrate the filter paper for 10-12 d. The paper was then removed with sterile forceps and dried in a bell jar with desiccant for 7 d. The filter paper was placed in sterile glassine bags and stored at -20 °C in a sealed box with desiccant.

Fungal strains were typically grown on CM petri dishes, in incubators (Metritherm, Phillip Harris Ltd / Gallankampf) at 25 ± 1 °C with a 12 h light – 12 h dark cycle (LD) (white, red, green, or blue LED light, spectra shown in fig. 2.1), in phase with the plant growth chambers light cycle (i.e. lights on / 'dawn' and lights off / 'dusk' are synchronous between the two), unless stated otherwise, for up to 14 d.

Table 2.1: Complete media recipe (1 L)

Reagent	Amount	Concentration
20x Nitrate salts	50 ml	1X
1000X trace elements	1 ml	1X
D-glucose	10 g	56 mM
Peptone	2 g	8 mM
Yeast extract	1 g	~ 3 mM
Casamino acids	1 g	2 mM
1000X vitamin solution	1 ml	1X
Dissolve fully in ddH ₂ O. Adjust pH to 6.5 with NaOH and dilute to 1 L with ddH ₂ O. Autoclave and store at room temperature. For solid media, add 15 g Agar (45 mM)		

Table 2.2: Minimal media recipe (1 L)

Reagent	Amount	Concentration
20X Nitrate salts	50 ml	1X
D-glucose	10 g	56 mM
1000X trace elements	1 ml	1X
Thiamine (1% W/V)	1ml	38 μM
Biotin (0.05% W/V)	50 μl	1 μM
Dissolve fully in ddH ₂ O. Adjust pH to 6.5 with NaOH and dilute to 1 L with ddH ₂ O. Autoclave and store at room temperature. For solid media, add 15 g Agar (45 mM)		

Table 2.3: 20x Nitrate salts recipe (1 L)

Reagent	Mass (g)	Molarity
NaNO ₃	120	1.4 M
KCl	10.4	0.14 M
MgSO ₄ *7H ₂ O	10.4	42 mM
KH ₂ PO ₄	30.4	0.22 M
Dissolve fully in ddH ₂ O. Dilute to 1 L with ddH ₂ O. Autoclave and store at 4 °C		

Table 2.4: 1000x trace elements recipe (100 ml)

Reagent	Mass (g)	Molarity
ZnSO ₄	2.2	0.14 M
H ₃ BO ₃	1.1	0.18 M
MnCl ₂ *4H ₂ O	0.5	25 mM
FeSO ₄ *7H ₂ O	0.5	18 mM
CoCl ₂ *6H ₂ O	0.17	13 mM
CuSO ₄ *5H ₂ O	0.16	6.4 mM
Na ₂ MoO ₄ *2H ₂ O	0.15	6.2 mM
Na ₄ EDTA	5	0.13 M
Add reagents in order, to ddH ₂ O and boil in a microwave to dissolve. Cool to 60 °C and adjust to pH 6.5 with KOH. Allow reagents to cool and dilute to 100 ml with ddH ₂ O. Autoclave and store at 4 °C		

Table 2.5: 1000x vitamin solution recipe (100 ml)

Reagent	Mass (g)	Molarity (mM)
Biotin	0.01	0.41
Pyridoxine	0.01	0.59
Thiamine	0.01	0.38
Riboflavin	0.01	0.27
p-aminobenzoic acid (PABA)	0.01	0.73
Nicotinic acid	0.01	0.81
Dilute to 100 ml with ddH ₂ O, filter sterilise, and store in a glass bottle at 4 °C		

Table 2.6: 1000x penicillin-streptomycin stock (10 ml)

Reagent	Mass (g)	Molarity
Penicillin sodium salt	0.5	0.14
Streptomycin sulphate salt	0.5	0.068
Dilute to 10ml with ddH ₂ O, filter sterilise, and aliquot to 500 µl measures		

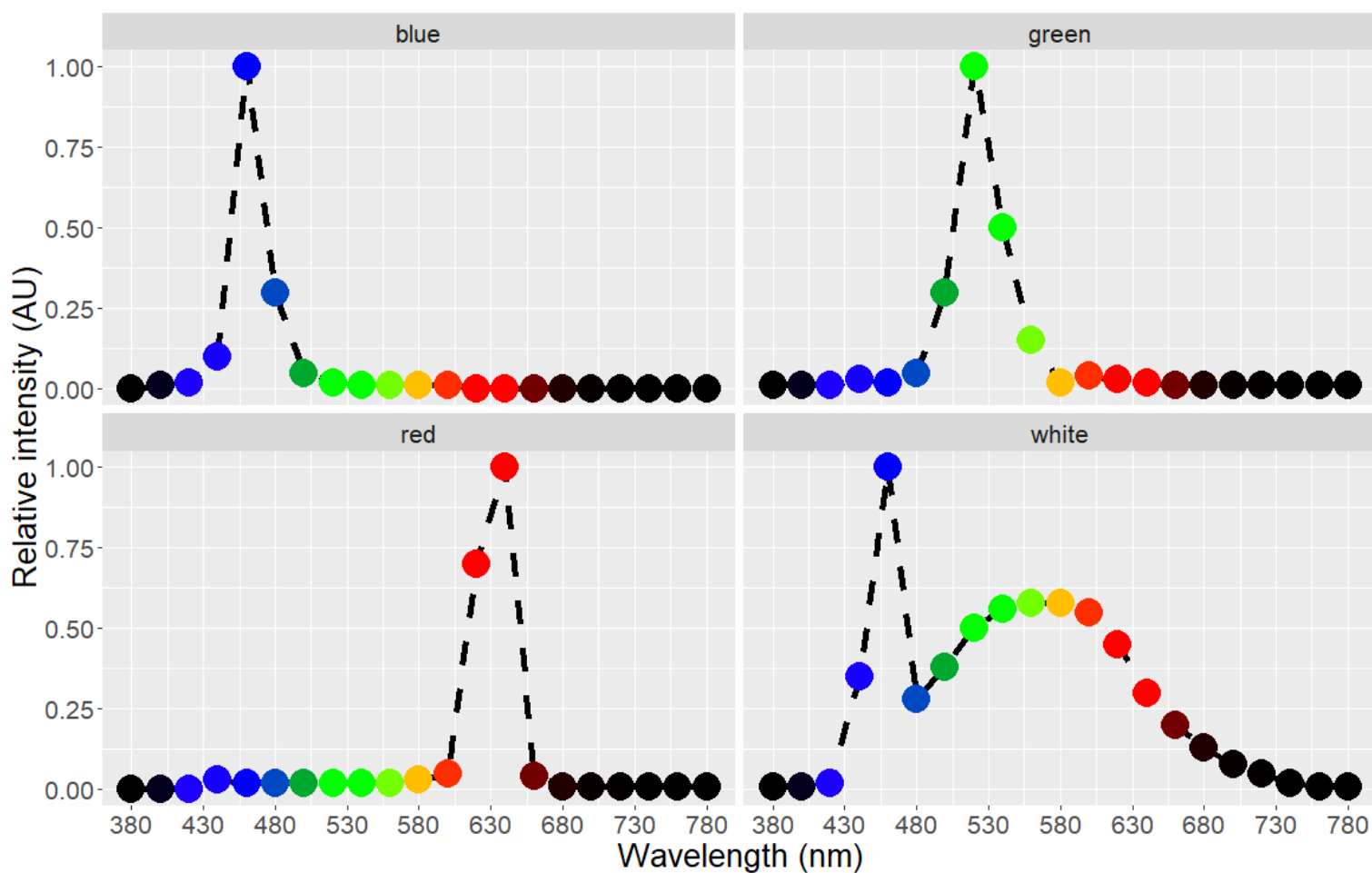


Figure 2.1: LED wavelength emission spectra of the blue, green, red, and white LEDs used in this study.

For shaking cultures, fungal strains were typically grown in liquid CM in a shaking incubator (Grant-bio orbital shaker-incubator ES-80) under ambient light conditions at 25 °C and 130 RPM for 10-12 d until the cultures were fully melanised and a dark black colour, unless otherwise stated. For inoculation of shaking cultures, the leading hyphal edge (non-melanised) of 8-10 d old *M. oryzae* cultures were removed with sterile scalpels and homogenised in a small amount of liquid CM, then introduced to the liquid media with a sterile spatula. 100 ml media was inoculated with *M. oryzae* in 250 ml sterile flasks with bungs to allow for sufficient aeration.

To make e.g., 50% spent media, complete media was made up as above, but diluted to a final volume of 500 ml instead of 1 L, creating a 2x CM concentrate. This 2x CM concentrate was then diluted to a 1x concentration using spent media from shaking cultures instead of water, creating a 1x CM with 50% SM. Considering the concentration of media components were at least 1x (there may have been residual nutrients from the spent media), nutrients were considered to be in excess.

2.2 Plant growth, maintenance, and storage

Rice CO-39 (initially provided by the Talbot laboratory, Exeter University, UK, then bulked seeds from the greenhouse were used) and Barley Golden Promise (provided by Simpsons Malt, McCreath Simpson & Prentice agriculture) were used throughout. Seeds were sterilised in 70% ethanol for 5 min and washed three times with double distilled water (ddH₂O) for 5 min each. They were then placed on damp paper towel in plastic boxes for 3-5 d in growth chambers (Snijders Scientific Economic Lux Chamber) to allow for germination. Growth chambers had 12/12 h light/dark cycles ($\sim 100 \mu\text{Mol m}^{-2} \text{s}^{-1}$) at 25 °C, in phase with fungal growth chambers unless otherwise stated, i.e., lights in fungal incubators and plant growth chambers switched on and off at the same time every day.

Once germinated, 5 seeds were transferred to 7 cm x 7 cm square pots filled with soil (John Innes no. 2) and 20% (v/v) profile greens (Rigby Taylor Ltd.). Once transferred to pots, plants were watered once with 4 ml/L Nitrogen feed (Baby Bio), ~ 3 g/L sequestered iron (Vitax), and 4 ml micronutrients Vitalink A and 4ml Vitalink B /L (VitaLink). Plants were subsequently watered three times per week with tap water (Plymouth, UK).

To bulk and expand seed stocks, plants were grown in 10 cm diameter circular pots, and fed weekly with nitrogen feed and micronutrients, and monthly with sequestered iron as above,

but in greenhouses (Plymouth, UK) at ~25 °C with supplementary light. Rice and barley plants were inoculated with *M. oryzae* at 3-4 weeks old.

2.3 Fungal colony growth and banding analysis

To analyse diurnal and circadian growth and development on petri dishes, CM plates (unless otherwise stated) were inoculated with *M. oryzae* filter stocks (see above) and placed in a 25 °C incubator. Lighting conditions were as follows: 12 h light/dark (LD, in phase with the plant growth chambers), 12 h dark/light (DL, directly out of phase with the plant growth chambers), constant light (LL), constant dark (DD), 12 h light/dark followed by transfer to constant light (LD-LL), or 12 h light/dark followed by transfer to constant dark (LD-DD). During the light period, fungal colonies were grown under white LEDs (unless otherwise stated) (spectra shown in Fig. 2.1). To image the growth and development of fungal colonies, petri dishes were placed lid down on a light box and photographed (Canon EOS rebel SL1 camera) from above, usually after 10, 12, or 14 d of growth (unless otherwise stated; time lapse photography was also implemented, unless colonies were in constant darkness). The images were subsequently analysed using a FIJI-based macro (FIJI is just imageJ, a 'batteries included' version of imageJ with many useful plugins pre-installed (263), see 3.2.1).

2.4 Pre-banding latency period assay

To determine when conidial banding first appears, and how nutritional composition might affect the latency period, fungal strains were grown on different types of media and (usually) imaged daily for at least 10 d. Colonies were grown on complete media, minimal media, complete media without penicillin/streptomycin stocks and complete media of different pH (pH adjusted using either 1 M NaOH or HCl to 5, 6, 6.5, 7, and 8). Colonies were also grown on CM plates containing spent media (SM) from shaking cultures.

Shaking cultures were grown as above for ~10 d until dark and melanised, the spent media (SM) filtered through one layer of Miracloth and the mycelium discarded. The SM was then autoclaved and stored in sealed bottles and refrigerated until needed. Double strength complete media (2x CM – see above) was made and diluted with either SM or water to produce a range of spent media concentrations, while the final concentration of CM remained ~1x (e.g., to make up 1 L 10% SM, mix 500 ml 2xCM, 400 ml ddH₂O, and 100 ml SM).

To prevent melanisation, fungal cultures were grown at a slower shaking speed (70 RPM as opposed to 130 RPM) or increased volumes of CM in the same 250 ml sized flask. To sequester metabolites, 0.1% (w/v) activated charcoal was added to spent media, autoclaved, shaken vigorously, and placed in the fridge for at least 24 h prior to use.

2.5 Conidial tip mucilage analysis

This method is an adapted version of a previously established adhesion assay on polystyrene (264). *M. oryzae* conidia were harvested from 10-12 d old plates by first adding 3 ml double distilled water and scraped with a sterile plate spreader to knock off the conidia until the colonies no longer look grey and fluffy. The resulting conidial suspension was then pipetted into Eppendorf tubes and filtered through one layer of sterile Miracloth (Milipore). Conidial suspensions were then centrifuged at 3000 g for 3 min and water was carefully removed without disturbing the conidial pellet. Conidia were then resuspended in 1 ml of ddH₂O. For strains that produce low conidial counts (i.e., FRQ, see 6.2.5), conidia from several colonies were pooled at this stage. Conidial concentrations were then determined with a haemocytometer and conidial suspensions were diluted to 4x10⁵ conidia / ml, then left to incubate in Eppendorf tubes for 15 min. 200 µl conidial suspension was then transferred to 55 mm polystyrene petri dishes, and a line drawn around the droplet in permanent marker to

denote where the conidia had settled. The petri dishes were then incubated at room temperature for 1 h to allow conidia to settle and adhere to the dishes. 5 ml sterile double distilled water was then added to the dishes and 3 images of the conidial suspension were captured under a light microscope with a camera adaptor (Canon EOS rebel SL1 camera with a t-ring microscope adaptor, Kyowa Medilux-12 light microscope). The petri dishes were sealed with parafilm and transferred to a shaking incubator for 100 s at 200 RPM. A further 3 images were captured within the marked area and percent conidia remaining was determined using a FIJI-based macro (see 3.2.2).

2.6 Conidial development analysis

Conidia were harvested as above and diluted to a concentration of 1×10^5 /ml (manual coverslip assay) or 5×10^5 /ml (time-lapse microscopy assay). Once diluted to the correct concentration, 50 μ l droplets of conidial suspension were pipetted onto glass hydrophobic coverslips and placed on damp paper towel in glass trays (covered with saran wrap) in a 25 °C growth chamber. Conidial germination and development was then monitored regularly every 2 h for 24 h, using at least two cover slips per time point. At least 100 spores per time point and cover slip were scored for their developmental stage (Fig. 2.2). For the automated microscope time course, a 50 μ l droplet of conidial suspension was pipetted onto a 30 mm polystyrene petri dish and 3 ml ddH₂O pipetted onto the edges of the dish, so as not to disturb the conidial droplet while maintaining humidity, then placed under a 3D-printed Openflexure microscope (265) with a raspberry pi running a small python script that captures images every 30 minutes for 24h or until prompted to stop (see 3.2.4). The 3D-printed microscope was left on the benchtop at room temperature to avoid temperature increases from the raspberry pi. The conidia present on the microscope images were scored for developmental stage as above at a later date (see 3.2.4).

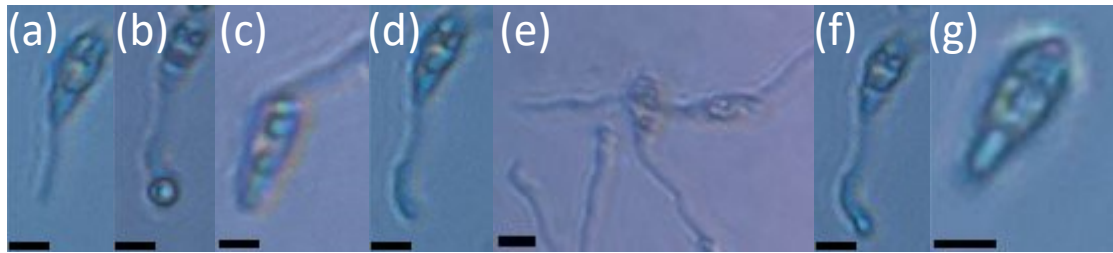


Figure 2.2: Conidial developmental stages: (a) not germinated, (b) apical germ tube only, (c) basal germ tube only, (d) multiple germ tubes (horizontal conidia) and elongated germ tube (central, vertical conidia), (e) hooking, (f) tip swelling, and (g) appressoria. Images captured with the Openflexure microscope. Scale bar = 10 μm .

2.7 Cytorrhysis analysis

Conidia were harvested as above and diluted to a concentration of 1×10^5 /ml. 50 μ l droplets were pipetted onto hydrophobic glass cover slips and placed on damp paper towel in a glass, saran wrap-covered tray in a 25 °C growth chamber and allowed to develop for 8, 10, and 12 h. At these time points, the water from the conidial droplets was wicked away by holding lens tissue against them. The ddH₂O was then replaced with fresh water, or with increasing glycerol concentrations. The conidia were incubated for 30 min before imaging under a light microscope (Kyowa Medilux-12 with a camera attachment). Appressorial collapse as a result of the glycerol solution was scored as a percentage of total spores (at least 100 spores counted per time point and treatment). Additionally, conidial suspensions (5×10^5 /ml) were pipetted onto 30 mm polystyrene petri dishes and incubated, then replaced with glycerol solutions as above. Petri dishes were then placed under 3D-printed microscopes (see above) and, using a small Python script, imaged every 5 min (until prompted to stop) to determine the timing of collapse at a higher temporal resolution, as well as the required glycerol concentration for appressorial collapse.

2.8 Pathogenicity and infection assays

2.8.1 Spray inoculations

Plants were grown for 3-4 weeks in a 12/12 LD growth chamber as above. *M. oryzae* colonies were always grown for 12 d at 25 °C, in incubators with differing light cycles (LD, DL, LL, DD, LD-LL, LD-DD; 10 d LD – 2 d constant light or darkness for LD-LL and LD-DD). *M. oryzae* conidia were harvested as above at either subjective dawn relative to plants (Zt 0) or subjective dusk (Zt 12), and plants were inoculated as soon as possible thereafter. Prior to inoculation, plants were placed in transparent plastic boxes with water at the

base and wet paper towel along the side of the boxes and acclimated for at least 15 min. Conidial suspensions were diluted to a final concentration of 1×10^5 /ml, and tween 80 and gelatine were added to a final concentration of 0.1% (v/v) and 0.1% (w/v), respectively. 2 ml of ddH₂O was sprayed, using an artist's airbrush (Harder & Steenbeck), into the boxes containing plants to increase the local humidity, then 2 ml of conidial suspension per plant pot was sprayed into the boxes. One plastic box was used per inoculation treatment and fungal strain (i.e., LD, DL, LL, DD, LD-LL, LD-DD, guy11, Δ WC2, and FRQ^{NIN}), and the artist's airbrush was cleaned by spraying 70% ethanol through, followed by 2 washes with ddH₂O to prevent contamination of other strains/pre-inoculation treatment conditions. Once inoculated, plastic boxes with plants were placed into a 25 °C 12/12 LD growth chamber and plastic lids were kept on the boxes for 2 d. Lids were then removed, and inoculated plants were incubated for a further 4 d (6 d total).

6 days post-inoculation (DPI), all the leaves were removed from the plants and taped (using white masking tape) adaxial side down onto a flatbed scanner (so the tops of the leaves are facing the camera sensor) and images acquired as 800 DPI .tif files. Images were separated based on plant species, fungal strain, and pre-inoculation conditions. Leaf images were then pre-processed using a FIJI-based macro (see 3.2.5) to create individual leaf images and fed into the image analysis pipeline, Redpatch (3.2.6).

2.8.2 Leaf sheath inoculations

Plants were grown for ~4 weeks in a 12/12 LD growth chamber as above. *M. oryzae* was grown at 25 °C in incubators with 12/12 LD lighting conditions for 12 d. Conidia were harvested at subjective dawn (as above) and diluted to 3×10^5 conidia/ml. No tween or gelatine was used. 100 μ l of conidial suspension was pipetted into attached (to the plant) or detached, excised leaf sheaths. For detached leaf sheaths, sheaths were peeled away

from the central stem, and a ~6 cm long section trimmed using a razor blade (266). A small plug of Vaseline was placed at the end of the sheaths and 100 μ l conidial suspension injected into the sheaths. Sheaths were then secured on a bed of taped 200 μ l pipette tips on damp paper towel in glass dishes and sealed with saran wrap (266). For attached leaf sheaths, they were peeled away from the centre stem, laid on their side in a transparent plastic box with damp paper towel, and a plug of Vaseline placed at the end of the sheaths, just above the soil. 100 μ l conidial suspension was pipetted into the leaf sheaths. Leaf sheaths were left for 24 and 48 h in a 25 °C 12/12 LD growth chamber before penetration and cell-cell movement was assayed. For microscopic analysis, leaf sheaths were sectioned and trimmed with a razor blade as follows: the top of the leaf sheath was trimmed off, leaving the boat-shaped cross section of the sheath, followed by trimming off the base of the leaf sheath, leaving a thin section to be viewed under a light or confocal microscope (for fluorescently labelled strains) (266)).

At 24 HPI, leaf sheaths were analysed and scored under a light microscope (Kyowa Medilux-12) as either: appressoria only (no penetration), penetration, confined to the primary penetrated cell, or cell to cell movement. At 48 HPI, leaf sheaths were scored as appressoria only (no penetration), penetration, confined to the primary penetrated cell, movement into one neighbouring cell, 2 neighbouring cells, or 3 or more neighbouring cells. At least 100 conidia were counted and scored at each time point for each strain.

2.8.3 Chlorophyll fluorescence imaging system for leaf health analyses

A chlorophyll fluorescence imaging system (PSI, Open Fluorcam, here) is a camera setup with specific LEDs used to determine F_v/F_M (a measure of photosystem II efficiency (267)) and NDVI (Normalised Difference Vegetation Index, a measure of the difference between visible and near-infrared light reflected by vegetation as a common marker for plant

health (268)). Plants were grown for ~4 weeks and spray inoculated as above. Each day, infected leaves were then removed from the plants and stapled to a piece of black craft foam (black paper or card was insufficient because of their reflective properties). Leaves were left for at least 30 min to dark adapt prior to imaging. F_V/F_M values above 0.79 were considered 'healthy', as were values above 0.6 for NDVI. The output images were displayed as false colour heatmaps for F_V/F_M and NDVI using lookup tables, with warmer colours (reds, oranges) denoting high values and cooler colours (blues, greens) denoting lower values. Since the output images were false colour heatmaps, the scales for F_V/F_M and NDVI were kept uniform for image analysis. Output images were then sent through a short semi-automated FIJI-based macro to determine percent healthy tissue per inoculated leaf (see 3.2.7).

2.9 Timing and localisation of clock gene expression analysis

M. oryzae conidia and hyphae clock genes (WC2 and FRQ) may be expressed, active, and localised in the cell in a time of day-dependent manner (178,181). WC2::GFP and FRQ::GFP strains were grown as above for 12 d LD prior to imaging (unless otherwise stated). For conidial expression and localisation, conidia were harvested as above and diluted to a concentration of $\sim 5 \times 10^5$ /ml. 50 μ l droplets were pipetted onto hydrophobic glass coverslips and placed onto damp paper towel in a sealed glass dish in a 25 °C incubator with a 12/12 LD lighting regime. Suspensions were incubated for a number of (specified) hours and imaged under a confocal microscope (Zeiss LSM800 Airyscan) (confocal settings: 8 bit, EGFP, aperture diameter: 4.4, filter method: average, filter mode: line, sampling number: 4, Lsm tube lens focal distance: 150, scan lense focal distance: 52.5, tube lense focal distance standard: 164.5, objective: C-Apochromat 40x/1.2 W Korr FCS M27, pixel period: 4×10^{-6} , Rt binning: 1, Rt line period: 3×10^{-5} , Laser:

Argon Remote (488 nm), laser power: 0.0225, filter: MBS 488/561, camera integration time: 4.096×10^{-6} , amplifier gain: 3.7). Images were then analysed using a Fiji-based macro (see 3.2.8)

For hyphal clock gene expression and localisation, colonies were grown on CM petri dishes for 12 d under a range of diurnal and circadian conditions (LD, DL, LL, and LD-LL). Prior to the dark period (for treatments that had a dark period), all petri dishes were wrapped in tin foil and only used once for harvesting the hyphae, to reduce resetting of the clock from light reception during the dark period. The leading edge of the colonies were then sectioned and placed onto a coverslip. The media with the growing hyphae were then squashed with a glass slide and imaged under the confocal as above approximately every 5 h for ~26 h.

2.10 CRISPR Cas9 genetic engineering design

M. oryzae CRISPR Cas9 editing follows the Foster and colleagues approach (269), whereby hyphal protoplasts are co-transformed with two Cas9 ribonucleoproteins (RNPs) targeting a gene of interest (GOI) alongside the SDI1 gene (269). With a single base edit to the SDI1 gene, carboxin (a fungicidal compound) resistance can be introduced to successfully transformed colonies. This co-editing theoretically increases the likelihood of finding a GOI mutant, as all colonies that grow on the carboxin-laden selection media have taken in the Cas9 ribonucleoprotein (RNP) and donor DNA for the SDI1 gene and therefore are more likely to also have been transformed for the GOI.

M. oryzae target genes were determined based on protein and nucleotide homology to the model fungal clock species, *N. crassa* (see tables 1.1, 4.1, 5.1, and 6.2). *M. oryzae* gene sequences were submitted to e-CRISP (270) to determine potential target sequences. Settings were selected as follows: Strict application (NGG only protospacer-

adjacent motif (PAM)), ignore non-intronic regions for the purpose of a knockout (UTRs excluded), 20 bp guide RNA length excluding PAM, gene annotation filtering (hits outside the gene, overlapping genes, non-exon hits, and hits outside the coding sequence were all ignored), and guide RNAs (sgRNAs) with off-target sequences were ignored. The potential target sequences were selected if there were nearby in frame codons that could have a single base edited to create a premature termination codon (e.g., GAG to TAG). Once target sequences were selected, they were submitted to the NeBio EnGen sgRNA design tool (271) to determine the sgRNA-coding DNA template to be used with the sgRNA synthesis kit (see below). The corresponding sgRNA-coding template oligo was synthesised (Eurofins, Germany) and transcribed into the appropriate sgRNA that binds to the Cas9 protein using the sgRNA synthesis kit (EnGen sgRNA synthesis kit, *S. pyogenes*). Longmer donor DNA oligos (80bp) were synthesised (Eurofins, Germany) for homology directed repair containing the single base pair edit required for a premature termination codon in the gene of interest.

2.11 Mutant confirmation and primer design

When selecting the edit site, donor sequences were checked for the removal or introduction of a restriction enzyme site for screening purposes using Restriction Mapper (272). To screen for successful targeted CRISPR-generated mutations, primers for amplicons of ~200-250 bp were designed that flanked either side of the CRISPR target sequence and edit site. The desired ~200-250 bp amplicon was submitted to Primer3 (273), and primer pairs were selected to have a GC content of ~50% and melting temperature (T_m) between 55-60 °C, with no more than 2 °C difference between the pairs. When these amplicons were run on an agarose gel after restriction digest (see below), the mutant with the correct codon edit showed one band compared to the wild

type two bands (or vice versa). Amplicons were designed to show asymmetrical sizes after digestion (e.g., 100 and 150 bp) for gel-based visualisation, and primers were synthesised by Eurofins (Eurofins Genomics, Germany).

2.12 *M. oryzae* CRISPR transformation process

M. oryzae cultures were grown on CM petri dishes for 8-12 d, and the leading, non-pigmented edge of the colony was cut out and homogenised in liquid CM, then transferred to 100 ml liquid CM and grown for 2-3 d at 70 RPM and 30 °C. After shaking incubation, sgRNA synthesis (for both GOI edit and SDI1 carboxin resistance) was carried out using the NeBio sgRNA synthesis kit, following the manufacturer's instructions. All reagents and tubes were nuclease-free and reactions were assembled in microfuge tubes. The EnGen 2x sgRNA reaction mix, *S. pyogenes*, 0.1 M DDT and sgRNA-coding DNA oligo (1 µM) were all thawed on ice and briefly centrifuged. The reaction mix was assembled at room temperature in order without the use of master mixes: 2 µl nuclease-free water, 10 µl EnGen 2x sgRNA reaction mix (*S. pyogenes*) was briefly centrifuged, then 5 µl sgRNA-coding DNA oligo was added (1 µM) and the mix briefly centrifuged, followed by the addition of 1 µl DDT (0.1 M) and 2 µl EnGen sgRNA enzyme mix to a total volume of 20 µl. The solution was mixed thoroughly by flicking or tapping the microfuge tube, then briefly centrifuged. The reaction was subsequently incubated at 37 °C for at least 30 min (1 h in our laboratory), then transferred to ice for 5 min. For DNase treatment, the reaction volume was brought to 50 µl with nuclease free water and 2 µl DNaseI (RNase-free) added, tubes were mixed by gently flicking or tapping, briefly centrifuged, and then incubated for a further 30 min at 37 °C.

sgRNA mixes were purified and concentrated using a spin-column based kit (Zymo clean and concentrator kit). Buffer preparation: 48 ml 100% ethanol added to the 12 ml RNA

wash buffer concentrate prior to use. All steps were performed at room temperature and centrifugation carried out at 16,000 g for 30 s unless otherwise stated. 104 µl RNA binding buffer was added to the 52 µl sgRNA sample (156 µl total) and flicked to mix. After 1 min, 1 volume of 100% ethanol (156 µl) was added and mixed. After 2 min, the sample was transferred to the Zymo-Spin IICR column in a collection tube and centrifuged. After discarding the flow-through, 400 µl RNA wash buffer was added to the column. After centrifugation and removal of the flow-through, the DNaseI reaction mix was prepared in an RNase-free tube: 5 µl DNaseI and 75 µl DNA digestion buffer was mixed by gentle inversion. The DNaseI reaction mix (80 µl) was added directly into the column matrix and incubated at room temperature for 15 min. 400 µl RNA prep buffer was added to the column and centrifuged. The flow-through was then discarded. 700 µl RNA wash buffer was added to the column and centrifuged, followed by discarding of the flow-through. 400 µl RNA wash buffer was added to the column and centrifuged for 1 min to ensure complete removal of the wash buffer. The column was then transferred to an RNase-free tube and 60 µl DNase/RNase-free water was added and centrifuged. sgRNA concentration was determined with a Nanodrop; 2 µl nucleotide-free water was placed on the nanodrop as a blank, followed by 2 µl sample and read, with a desired concentration of 1.5 µg/µl. sgRNA was stored at -80 °C for later use, if needed.

OM buffer was prepared (Table 2.7) and glucanex/lysing enzyme added (Sigma, 1.8 g/150 ml). *M. oryzae* growing in liquid CM was filtered through one layer of miracloth, allowing as much of the liquid to drain off as possible. The spent medium was discarded, leaving just the mycelium, which was non-melanised due to the slow shaking speed and high temperature. The mycelium was then split into two sterile falcon tubes with 25 ml OM buffer/lysing enzyme and incubated for 4-6 h (30 °C, 70 RPM).

Table 2.7: OM buffer recipe (150 ml)

Reagent	Amount	Molarity
MgSO ₄ *7H ₂ O	44.4 g	1.2 M (MgSO ₄)
NaPO ₄ (1 M, pH 5.8, 1:1 molar ratio of mono- and di-basic)	1.5 ml	10 mM
Dissolve fully in ddH ₂ O and Filter sterilise		

Cas9 ribonucleoproteins (RNPs) were then prepared: 6 µg Cas9 NLS (EnGen Spy Cas9 NLS (nuclear localisation signal added) - NEB) was complexed with 1.5 µg sgRNA and prepared in 10x nuclease buffer, e.g., 1.8 µl Cas9, 1 µl sgRNA (1.5 µg/µl), 0.311 µl nuclease buffer, total volume 3.11 µl), then left for 10 min at room temperature to form the Cas9-sgRNA complex. This was performed twice; once for the GOI edit, and once for the SDI1 carboxin resistance edit.

Double stranded donor DNA oligos were then prepared. Oligos were diluted to 100 pMol/µl for both the top and bottom strand. 5 µl each of both top and bottom strand was mixed by gentle flicking and then briefly centrifuged. Donor mixes were transferred to a heat block at 95 °C for 4 min and then cooled to room temperature on the bench top for 2 min to allow for annealing. Annealed dsDNA Donor oligos were then briefly centrifuged. This process was performed for both the GOI and the SDI1 edit. At this point, there were two tubes of donor dsDNA oligos (GOI and SDI1) and two tubes of Cas9 RNP complexes (GOI and SDI1). These were introduced to the protoplasts.

The protoplasts in OM buffer/lysing enzyme mix were filtered through one layer of miracloth into new falcon tubes; protoplasts should move through the miracloth, and any undigested mycelium remain in the miracloth. The undigested mycelium was discarded and the falcon tubes with digested protoplasts were centrifuged at 2000 RPM with minimal acceleration and deceleration for 20 min at 10 °C and a beige pellet of

protoplasts at the bottom of the tube was formed. The supernatant was discarded, and the protoplast pellets resuspended in 40 ml ice cold STC (Table 2.8, 2.9) by gentle swirling and inversion (this can take up to 10 min). Protoplasts in STC were centrifuged again at 2000 RPM with minimal acceleration and deceleration at 10 °C. The supernatant was discarded, and protoplasts resuspended in 1 ml ice cold STC again by gentle mixing. Protoplast concentrations were determined with a haemocytometer and diluted to $\sim 1 \times 10^8$ /ml.

Table 2.8: STC buffer recipe (500 ml)

Reagent	Amount	Molarity
Sorbitol	109.32 g	1.2 M
Tris-HCl buffer (1 M), pH 7.5	5 ml	10 mM
CaCl ₂ (1 M)	5 ml	10 mM
Dissolve fully in ddH ₂ O and autoclave		

Table 2.9: Tris-HCl buffer recipe (1 L, 1 M)

Reagent	Amount	Molarity
Trizma base	121.1 g	1 M
Add concentrated HCl until pH 7.5 is reached, then dilute to 1 L with ddH ₂ O		

To a control Eppendorf tube, 150 μ l protoplast solution was added (1×10^8 /ml). For the transformation tubes: 150 μ l protoplast solution (1×10^8 /ml), 2 μ l SDI1 donor dsDNA, 2 μ l GOI dsDNA, all of the SDI1 RNP mix (Cas9/sgRNA complex for carboxin resistance), and all of the GOI RNP (cas9/sgRNA complex for GOI edit) mix was combined. The total volume added to the protoplast solution was kept to a minimum and ideally less than 15 μ l. Tubes were gently flicked to mix, then wrapped in tin foil, as protoplasts are UV sensitive. Protoplasts were incubated at room temperature for 30 min in the dark. 1 ml PTC buffer (Table 2.11) was added to both control and transformation tubes and mixed by inverting

tubes ~5 times (otherwise PTC does not mix well due to its viscosity) to aid in transfection.

Tubes were incubated at room temperature for 20 min in the dark.

Table 2.10: PTC buffer recipe (100 ml)

Reagent	Amount	Molarity
Polyethylene glycol (PEG)-4000	60 g	~0.15 M (60% w/v)
Tris-HCl (1 M), pH 7.5	1 ml	10 mM
CaCl ₂ (1 M)	5 ml	10 mM
Dissolve fully in pre-heated ddH ₂ O (~70 °C) and autoclave		

Protoplast solutions were added to 50 ml falcon tubes with 5 ml liquid OCM (osmotically stable CM - [0.8M] sucrose in either solid or liquid CM); one for the control tubes and one for the transformation tubes. Falcon tubes were wrapped in tin foil to keep dark and incubated at 25 °C and 70 RPM overnight. At least 600 ml solid OCM (100 ml for control protoplasts and 500 ml for transformed protoplast) was then melted and kept molten overnight.

After overnight incubation, protoplast solutions in OCM were collected and the molten OCM allowed to cool to ~40 °C in a water bath. Penicillin/streptomycin stocks (100 µl/100 ml) were added to the OCM to avoid contamination. Protoplast solutions were then added to the OCM; 100 ml OCM for the control protoplasts and 500 ml for the transformed protoplasts. Protoplasts were mixed in the OCM by rolling the bottle of OCM back and forth. A thin layer of OCM containing the protoplasts was poured into petri dishes (40-50 petri dishes for the transformed protoplasts and ~10 petri dishes for the control protoplasts). The protoplast-laden OCM was allowed to dry without any condensation (preferably with the lids off in a CL2 hood). Plates were wrapped in tin foil (protoplasts are still UV sensitive while regenerating) and incubated at 25 °C overnight.

At least 600 ml CM was melted (100 ml for control protoplasts and 500 ml for transformed protoplasts) and kept molten at ~45 °C overnight.

After overnight incubation, the molten CM was collected and allowed to cool to ~40 °C in a water bath. Penicillin/streptomycin stock was added to the CM (as above, 100 µl/100 ml). Half of the control, non-transformed plates and 1 or 2 transformed plates were overlaid with the CM to determine protoplast regeneration.

To the remaining CM, 100 µl/100 ml Carboxin (Sigma) solution (Fully dissolved 40 mg of carboxin in 1 ml Dimethylformamide (DMF)) was added and mixed well by rolling the bottle. The remaining half of the control, non-transformed plates, and all the remaining transformed plates were overlaid with the carboxin-CM, covering the entirety of the OCM base with a thin layer of the selection media. The control plates were used to show that protoplasts regenerate properly (when no carboxin is present) and will not grow in carboxin-laden media unless transformed. The two transformed plates that were not given selection media were used to check that the Cas9 RNPs and donor DNAs have not destroyed the protoplasts, as Cas9 can be cytotoxic to *M. oryzae* (269). The petri dishes were wrapped in tin foil again and placed in an incubator at 25 °C in the dark for 5-10 d, while protoplasts regenerated and began to grow through the selection media. Colonies were visually checked briefly after 5 d in the dark.

While the protoplasts were regenerating, at least 5 L selection media (CM with carboxin and penicillin/streptomycin) was made. The selection media was poured into ~200 plates and a few pieces of sterile filter paper was placed on each plate for generation of freezer stocks (see 2.1). After 5 d, transformed colonies growing up through the selection media were subcultured onto the new selection media plates, both to isolate individual colonies and ensure transformation for carboxin resistance is conferred. Individual colonies were

subcultured onto at least 200 plates and incubated in a 25 °C incubator for at least 5 d or until all filter paper pieces have been penetrated by the mycelium. The filter paper stocks were peeled off for storage and DNA extraction for mutant confirmation.

2.13 DNA extraction

Due to the large number of prospective mutant samples for the gene of interest edit, a quick filter stock DNA extraction method was followed (274). Single pieces of filter stocks from each individual colony were placed in Eppendorf tubes (nuclease-free) with 100 µl 10x TE buffer (Table 2.11). Samples were then heated to 95 °C on a heat block or thermocycler for 10 min followed by centrifugation at 3000 RPM for 1 min. 50 µl of supernatant was then transferred to a new microfuge or Eppendorf tube and placed in the freezer until use.

Table 2.11: 10x TE buffer recipe (1 L)

Reagent	Amount	Molarity
Tris-HCl (1 M), pH 8	100 ml	0.1 M
EDTA (0.5 M)	20 ml	10 mM
Dilute to 1 L with ddH ₂ O and autoclave		

2.14 Polymerase chain reaction (PCR)

Reactions were carried out in a thermocycler and Primer solutions were diluted to working concentrations of 10 pMol/µl from a stock solution of 100 pMol/µl. Primers, RedTaq (Cambio), and MilliQ water, were all thawed and stored on ice prior to use, followed by brief centrifugation. Master mixes for 12.5 µl reactions were then produced to amplify regions of interest; for each sample, 6.3 µl 2x RedTaq, 4.2 µl MilliQ water, 0.5 µl forward primer, and 0.5 µl reverse primer were mixed. 11.5 µl of mastermix was added to each microfuge tube prior to addition of 1 µl extracted DNA in 10x TE buffer (see above). Routine PCR protocol was as follows: lid at 100 °C, initial denaturation step of 95

°C for 1 min followed by 30 cycles of: denaturation at 95 °C for 15 s, annealing at 55-60 °C for 15 s, and extension at 72 °C for 15 s, and a final extension step for 1 min at 72 °C. Samples were then cooled to 10 °C until use in agarose gel electrophoresis or restriction enzyme digestion.

2.15 DNA restriction enzyme digest

Restriction enzymes were obtained from NEBio (Sacl) and Fisher Scientific (BsPMI). For Sacl restriction digests, 2 µl PCR product was mixed with 1 µl 10x NEBuffer 1.1, 6.5 µl nuclease free water, and 0.5 µl Sacl (10 µl total volume) and incubated for 2 h at 37 °C. For BsPMI digestion, 2 µl PCR product was mixed with 1 µl buffer O, 0.2 µl 50x oligonucleotide, 0.5 µl BsPMI, and 6.3 µl nuclease free water and incubated at 37 °C for 2 h. Digests were held at 10 °C until use. Agarose gel electrophoresis was used to fractionate the digested amplicons.

2.16 Agarose gel electrophoresis

Due to the small size amplicon (200-250 bp) and digested products used, a 3% agarose gel was made by adding 2.7 g low EEO agarose (Sigma) to 90 ml 1x TAE buffer (Table 2.12).

Table 2.12: 50x TAE buffer recipe (1 L)

Reagent	Amount	Molarity
Tris base	242 g	2
Glacial acetic acid	57.1 ml	1
EDTA (0.5 M)	100 ml	0.05
Dilute to 1 L with ddH ₂ O and autoclave, pH ~8		

The agarose-TAE solution was boiled for ~2 min (in 30 s periods) in a microwave to dissolve agarose until completely clear. The gel was then allowed to cool to ~50 °C and poured slowly into a gel cast, avoiding bubbles. Gel comb(s) were added to the gel, and

allowed to set for ~20 min. No DNA stain was added to the gel (see below). 1x TAE buffer was poured into the tank until the gel was just submerged.

0.6 μl of 10,000x GelRed nucleic acid stain (Cambio) was added to 1 ml 6x loading buffer and dye (NeBio) to give a final concentration of 6x loading buffer + dye + GelRed. Rather than adding 9 μl 10,000x GelRed to each 90 ml agarose gel (allowing for a total of 111 gels to be produced from that 1 ml GelRed), 1 ml of GelRed can be used in up to 1.666 L of loading buffer. Assuming 12 μl samples are added to each well in a gel, and 2 lanes of 16 samples per gel (32 samples per gel total), 1 ml GelRed could be theoretically used in up to 26,031 gels (0.6 μl GelRed added to 1 ml loading buffer = 999.6 μl added to 1.666 L loading buffer giving a final 6x concentration. 2 μl loading buffer is used per sample = 833,000 potential samples. 32 samples per gel = 26,031 gels), which is approximately 225x cheaper than conventional methods. DNA fragments that were stained in this way showed no discernible difference on a gel when compared to the conventional method. Further, there was reduced background emission from the gel when imaging, because only the DNA samples were stained.

Once the loading buffer had been made, samples were prepared as follows in microfuge tubes: DNA ladder (ultra-low range or 100 bp ladder, NeBio): 1 μl ladder, 2 μl loading buffer + GelRed, and 9 μl nuclease-free H_2O ; PCR product: 1 μl PCR product, 2 μl loading buffer + GelRed, and 9 μl nuclease-free H_2O ; restriction digest product: 10 μl restriction digest mix, 2 μl loading buffer + GelRed. Samples were mixed by pipetting up and down (avoiding cross contamination – single microfuge tubes are better than strips, here) and then briefly centrifuged. 12 μl samples were loaded (with ladders at either end of the lanes and negative water-only controls for both PCR and digest products) into each well of the gel.

Samples were run at 40 V for 5 min, then 80 V for 45 min or until fragments were well separated and the dye nearly run into the lower lanes. Gels were imaged on a UV gel dock and analysed visually or using FIJI. For successful HDR- or NHEJ-based CRISPR edits, the introduction/removal of a restriction enzyme site (i.e., from 1 to 2 bands or vice versa) or amplicon size shift were screened for on the gels. Prospective mutant PCR products were then re-amplified and digested to confirm, then cleaned and sent off for sequencing (see below)

2.17 Sequencing

Primer pairs used for sequencing were the same as above for gel electrophoresis and restriction digest-based putative mutant screening. For each putative mutant (and a control wild type), DNA extracts were re-amplified as above and cleaned using a QIAquick column-based PCR purification kit following manufacturer's instructions.

100% ethanol was first added to buffer PE. All centrifugation steps were carried out at 17,900 g in a microfuge at room temperature. 1:250 volume pH indicator I was added to buffer BP. 5 volumes of buffer PB was added to 1 volume of PCR sample and mixed by gentle flicking, the mixture should be yellow, indicating pH is <7.5. if the mixture was orange or violet, 10 µl 3 M sodium acetate, pH5 was added and the samples mixed. The sample was applied to the QIAquick column in a 2 ml collection tube, centrifuged for 60 s and the flowthrough discarded. 750 µl buffer PE was added to the QIAquick column, centrifuged for 60 s and the flowthrough discarded. The column was centrifuged for an additional 1 min. The column was then placed in a new nuclease-free Eppendorf tube. To elute DNA, 30 µl buffer EB (10 mM Tris-Cl, pH 8.5) was added directly onto the membrane, the column incubated for 1 min at room temperature, then centrifuged for 1 min. The flow-through containing the DNA was stored at -20 °C until further use.

DNA was sequenced by Eurofins' GATC Lightrun Tubeseq service and DNA and primers were prepared according to Lightrun Tubeseq guidelines. Purified PCR product DNA concentration was determined using a Nanodrop and diluted to ~ 2 ng/ μ l using nuclease-free water. 5 μ l diluted PCR product was mixed with 5 μ l primer [5 pMol/ μ l], tubes were then sealed with parafilm and sent for sequencing. Sequences were manually annotated from the .abi sequence file to account for any automated misannotations. Sequences were then submitted to a Blastn (NCBI) to confirm the sequences map well to the target gene in *M. oryzae*. Putative mutant sequences were also aligned against the wild type sequences to determine base edits and indels.

2.18 Statistical analyses

All statistical and data analyses were performed on R studio with a number of common libraries/plugins (275–289) and graphs were generated using ggplot (278). Box plots are displayed with the interquartile ranges and median lines, with the 'whiskers' displaying the range of data up to 1.5x the interquartile range. Dots/crosses and numbers within boxplots display the mean (if specified). Line graphs were plotted using the 'Loess' method and the grey shading denotes the standard error.

For statistical significance, a p value < 0.05 was considered significant, and graphs display statistical significance as stars (*), with increasing stars denoting lower p values (* < 0.05 , ** < 0.01 , *** < 0.001 , and **** < 0.0001). 'ns' denotes no statistical significance (p > 0.05), and a p value of ~ 1 when capitalised (NS). With pairwise comparisons, analysis of variance (ANOVA) was performed, and the individual groups being compared may be denoted with bars and */'ns' above. In larger comparisons, Tukey's HSD was typically performed, and letters are shown above each group in graphs, where each different letter represents a statistically independent collection of groups. For multiple

comparisons in leaf infection experiments, Dunn's multiple comparisons test was applied if there was significance ($p < 0.05$, Bonferonni adjustment) following rejected a Kruskal-Wallace one way ANOVA test.

For fungal colony growth and development experiments, images captured of colonies growing under identical conditions between experiments were pooled, e.g. many experiments used the wild type guy11 grown on CM petri dishes under L/D conditions at 25 C as a control and thus explain larger sample sizes. Further, experiments were performed in the same set of incubators under the same LED bulbs, temperatures were consistent to ± 1 C, and timings of lights on/off were identical.

3 Image analysis toolkit development

3.1 Introduction

Computer-based image analysis helps to eliminate the purely descriptive nature of imaging, be that microscopy, photography, or hyperspectral. Importantly, it reduces the inherent human bias applied when analysing biological samples (290–301). Computers, unlike humans, do not introduce any further bias beyond that which is initially implemented in the source code or data acquisition stage (290,297,300,302). Further, a computer does not get tired, can run continuously until a user prompts it to stop, will approach each input file in exactly the same way, and will not introduce any exogenous factors (290,297,300,302). In essence, image analysis is a type of bioinformatics that uses computers to interpret and acquire meaningful biological data from images to help answer questions that would otherwise require significant time, effort, expertise, or be impossible to process manually (301,303–305).

Most image analysis pipelines consist of several constituent steps: image acquisition, pre-processing, background exclusion, filtering, and segmentation/region of interest (ROI) location (290,292,293,293,295,298,306–312). This is then subsequently followed by the quantification and analysis stage, including (but in no way limited to) counting, classification, and colour or shape description (306). Ideally, image analysis pipelines should not require expertise to execute the code, should run near-continuously, and (generally) be faster and more accurate than manual methods (293,295,296,300,301,303,305–308,310,313).

3.1.1 Digital image acquisition

Before image analysis can take place, the imaging setup must be considered, as the way in which an image is acquired can significantly alter the design, reliability, and accuracy of the proposed algorithm (305,314). Generally, a computer does not understand or interpret images in the same way a human does; as with any digital file, all computers 'see' is an array of binary values: ones and zeroes. The human brain, on the other hand, has the ability to recognise patterns which, without artificial intelligence or bespoke pattern recognition algorithms, a computer cannot (292,294,298,302,315,316).

When capturing an image, there are many factors that can affect the information contained within, and thus how it will eventually be analysed, such as noise, background features, shadow, reflectance, illumination, light clipping (where values falling above or below a sensor's dynamic range are displayed as white and black, respectively), and exposure time can all change what information is included in the resulting image (290,301,306,308,310,314,315,317). Further, there can often be a trade-off between the optimal acquisition of images and optimal treatment of (biological) samples (309,314,318). In confocal microscopy, for example, laser intensity and scanning time can both positively and negatively affect image quality; at times, the longer or more intense a laser is used for, the better signal and background can be differentiated, but this also increases the likelihood of photobleaching (the process by which fluorescent molecules in a sample are destroyed by overexcitation) and subsequent sample damage occurring (309,319). This then decreases the signal to noise ratio of an image and, in turn, reduces image and downstream data quality (319). In this way, before image analysis pipelines are constructed, researchers need to be aware of what and how they are going to capture the phenomena of interest. An ideal image would therefore have an object in the

foreground that is well focussed with a high pixel density, a clear, matte background to allow for simple segmentation, uniform lighting and minimal reflectance, little image noise, and few artifacts: just the region(s) of interest (290,293,295,296,301,302,306,307,309,313,315,316,318,320–325). This is, however, very difficult to produce, given the complex nature of biological imaging.

A digital image is a computer-based representation of a real-world object, which can be gathered in a number of ways, most simply by using a light-based sensor, such as that found in a conventional camera. However, images can also be created by the use of sound (i.e., with an ultrasound scanner), laser light (such as with a confocal microscope), invisible light (using hyperspectral imaging systems, like chlorophyll fluorescence imaging), and even pressure and texture with an atomic force microscope, creating images with the use of a physical scanning probe, much like the needle of a record player (301,302,309,310,315,318,322,325–327). Despite the fact that images can be created with a variety of techniques, many of which do not use light, computers treat them all in the same way: a sensor interpolates an analogue input into a digital output, which is just an array of numbers (292,294,298,302,315,316). This digital output then subsequently becomes an input for image analysis pipelines to interact with.

Image noise is considered to be exogenous, unwanted data generally produced by the image acquisition process (292,298,302,310,315). Noise can occur as a result of low-resolution images, diffraction/reflection of light, or compression of images and subsequent data loss (293,315,325). Because of this, it can be difficult to discern what is image noise and what is important ROI information; observers and researchers need to know what they are looking at to determine these differences, which a computer is

unable to do (290,296,311,315,328,329). Accordingly, noise reduction is one of the first operations performed during image processing (310,315). In a standard digital camera, for example, the silicon sensor may have sections that are 'dead' and thus not recording signal or have sections in the sensor that are erroneously sending a signal continuously (330). These sections will give rise to regions of pure white (255) and pure black (0), respectively, in the final image and is aptly named 'salt-and-pepper' noise.

Digital colour images generally consist of 3 separate greyscale channels (one for red, green, and blue, respectively) with intensity ranges from e.g., 0-255 and these values make up pixels. Since a computer cannot innately interpret an image based on regions of pixels and their respective values, processing must be employed to make sense of an image and gather useful data from them, as there is no inherent relationship or interaction between pixels and their values in an image (292,296,308,309,315,331). Further, a computer has no way to draw on previously learnt and disparate real-world information like humans do (unless specifically trained using artificial intelligence, for example) (290,293,295,296,302,307,311,314,315,332–334). Indeed, humans rely on all manner of implicit visual cues, such as size and scale, colour, shape, texture, edges, contours, and even real-world location to determine what is in front of them. Essentially, humans can contextualise an image in a way computers cannot. Programmers, therefore, must provide computers with the assumptions humans naturally use when determining the image subject, and must be provided with specific instructions to process, transform, and manipulate an input file/image: an algorithm (315).

3.1.2 Image processing and analysis

Whilst image quality can be heavily affected by noise, there are many filter-based approaches to reduce and minimise its impact (290,292,315,322,328,331). Rather than focussing on individual pixels, filters often take into account a pixel's neighbour(s), usually as a kernel (300,324,330). kernels can differ in size drastically, and are typically 3x3 px or larger, as filters are often centred around a core pixel (300,324,330). In the case of a median filter, for example, the kernel is sent across the whole image from left to right, one pixel line at a time, and at each pixel position, the e.g., 9 (3x3) pixel intensity values are ordered, and the central number applied to the central pixel position (298,328,330,331). This essentially clips out erroneously high or low pixel values created through salt and pepper noise (318). This, as is the case with all filters, does not determine the true pixel value and merely approximates its value based on the surrounding neighbours (330). Whilst noise can be a significant issue under certain conditions, it can often be ignored if image acquisition setups are carefully designed: if the sensor quality is high, lighting is uniform, and file compression is minimal, then the noise might be so minor that it may not be worthwhile to approach.

Once a sufficiently clear, in focus, and noise-free image of a sample has been produced, data can then be gathered with biological relevance (306). Generally, an image will consist of a region(s) of interest (ROI) to the researcher, with the rest of the image being additional unnecessary information (310). In this way, the image can be considered to have a 'foreground' containing ROIs and a 'background' containing exogenous information (306). The goal of image processing is to ultimately separate the foreground from the background to allow for subsequent quantification and characterisation of a range of parameters, such as size or shape of the ROI(s), to generate accurate, high-

throughput, and quantitative data from (biological) images (293,302,306,307,309,313). This separation of foreground from background can be achieved using a process called 'segmentation', of which there are a vast number of approaches, most simply pixel thresholding, where any pixels above a given value are considered foreground, and any below are considered background (or vice versa) (293,302,306,308,310,325).

The introduction of scale to an image can also help to answer biological questions (307). Many commercially available digital microscopes include metadata dictating the number of pixels occupying a given unit of area, and flatbed scanners, for example, can translate real world spatial data into their digital counterpart by dictating the number of pixels generated from imaging objects in a known area (such as A4 paper size), commonly termed DPI (dots per inch – the number of pixels occupying an inch on the scanning area). Scale can also be determined in a more complex fashion, by way of imaging an object with known dimensions: a 'scale card'. Here, if the object of known dimensions can be located on an image and the number of pixels it occupies calculated, then that information can be extrapolated or scaled to the rest of the image and subsequent real-world data can be gained (290,296,308,323,335–337).

Whilst there is a plethora of software, plug-ins, and image analysis pipelines available to researchers in plant pathology and related fields (see Table 3.1 and quantitative-plant.org, a website that collates a wide variety of plant and plant-related research software), these are often produced for specific model systems, lack automation, require significant user input on a per-image basis, or require customised setups. Unfortunately, due to a range of reasons (funding, time, or otherwise), many of these toolkits are also not maintained or available in the years following publication; in the case of web-based

tools especially, that cannot be downloaded or utilised locally, this may force researchers to change analysis techniques between (or within) studies. Indeed, software such as HPGA (338), ACA (339), Grow Map-Leaf (340), Growscreen (341), Leaf-GUI (342), Leaf Processor (343), Leaf Growth (344), and Phenotic (345) are all no longer supported or available to download (Table 3.1).

In Fiji specifically, given its opensource and freeware approach to image processing and analyses, 'Macros' are essentially the automated execution of pre-written functions/plugins previously developed by other researchers and computer scientists (346–351). The 'IJM' language follows a similar syntax and format to JavaScript and can be used for complex mathematics, dataframe creation/manipulation, and image processing. Implemented functions and previously written code in this work include, but are not limited to: colour segmentation, CLAHE, get date and time, and subtract background (346–351) (see 9.1).

This chapter, therefore, presents a range of (semi-) automated image analysis pipelines that can utilise lab-standard or inexpensive equipment (with the exception of confocal microscopy), namely light microscopes, cameras, and flatbed scanners, that can be used 'as-is' or altered based on user requirements. The toolkits presented here were designed to aid in the research of plant-pathogen interactions and fungal morphology. Macro- (leaf infection severity analyses, chlorophyll fluorescence, and fungal growth on petri dishes) and micro-scale (conidial counts and development, and protein expression and localisation) analysis toolkits are shown, which produce high-throughput, reliable, and accurate data. These image analysis pipelines introduce techniques used to advance the understanding of the importance of time of day and circadian entrainment in the

outcome of rice blast disease. The tools can help answer whether *M. oryzae* (a) colonies alter their conidial banding phenotypes under different environmental conditions; (b) lighting regimes, harvest time, or circadian mutation alters conidial size, shape, and mucilage production; (c) conidial germination and developmental rates are affected by time of day, lighting regime, or mutation; (d) appressorial turgor pressure is altered in circadian mutants; (e) displays altered virulence at different times of day or after circadian entrainment; (f) clock genes (specifically FRQ and WC2) undergo rhythmic localisation and expression; and (g) whether rice and barley display altered susceptibility to *M. oryzae* at different times of day.

Table 3.1: A selected summary of a range of plant pathology-related image analysis toolkits (information gathered from literature and quantitative-plant.org)

Tool name	Function	Subject	Software	Licencing	Source	Reference
Rhizotrak	Manual time series annotation of root growth; visualisation of root growth	Plant minirhizotrons	Fiji/ImageJ plugin; R package integration for analysis	Opensource	https://prbio-hub.github.io/rhizoTrak/pages/installation.html	(312)
HTPheno	High throughput plant phenotyping; height, width, projected shoot area	Plants	Fiji/ImageJ plugin	Opensource	http://htpheno.ipk-gatersleben.de/index.html	(308)
Image Harvest	High throughput plant image processing and analysis; height, width, leaf area	Plants	Python package. High performance computing integration	Opensource	http://cropstressgenomics.org/data/html/index.html	(310)
PYM	Customisable Raspberry pi-based plant phenotyping; in-field leaf area analysis	Plants	Python package	Opensource	https://github.com/bevalle/pym	(305)
Hyphatracker	Early spore germination and development; germination, germ tube growth rate	Fungi	Fiji/ImageJ plugin	Opensource	https://pols.phys.strath.ac.uk/research/super-resolution/software/	(328)
Leaf doctor	Plant leaf disease severity estimation; total leaf area, diseased leaf area	Plant disease	Fiji/ImageJ plugin; IOS App	Freeware	https://apps.apple.com/us/app/leaf-doctor/id874509900?ls=1	(304,352)
None given	Disease severity estimation: disease severity (utilises Plantvillage image as a training dataset)	Apple black rot	Imagenet pre-trained model	Opensource	Unavailable / not maintained	(300)
None given	Morphology of pelleted and dispersed growth of liquid cultured fungi; culture heterogeneity, fungal structure	Fungi	Fiji/ImageJ plugin	Opensource	Supplementary file 4 in original paper (DOI: 10.1186/s13068-019-1473-0)	(303)

	parameterisation (diameter, aspect ratio, area, solidity)					
None given	Quantification of actively released conidia; location and measurement of sporulation zones on petri dishes, quantification of microscopic conidial images	Fungi	Fiji/ImageJ plugin	Opensource	Unavailable / not maintained	(294)
Fungal feature tracker	Quantitative characterisation of filamentous fungi morphology; conidial quantification, morphology, length measurement, hyphal tip quantification, mycelium area	Fungi	Mathmatica tool	Opensource	https://github.com/hsueh-lab/FFT	(324)
ACA	Rosette measurement; leaf area, colour, senescence measurements	Plants	R	Opensource	Unavailable / not maintained	(339)
None given	Stomata detection and pore measurement; machine learning and automatic stomatal quantification, pore area	Grapevine	Matlab	Not provided	Unavailable / not maintained	(333)
BioimageXD	3D phenotyping; area, length, width, 3D volume, colour metrics	Multipurpose	Standalones software	Opensource	http://www.bioimagexd.net/	(353)
Balloon	Cell wall segmentation and cell separation; cell quantification, cell size and shape descriptors	Plants / fungi	Fiji/ImageJ plugin	Opensource	https://imagej.net/plugins/balloon	(354)
Bioleaf	Leaf damage identification; insect herbivory determination and quantification	Plants	Android app	Freeware	https://play.google.com/store/apps/details?id=upvision.bioleaf&hl=en	(355)
Black spot	Leaf area estimation	Plants	Standalones software	Opensource	https://www.ncbs.res.in/blackspot	(356)
Compu-eye	Leaf area estimation; herbivory determination	Plants	Standalones software	Opensource	https://www.ehabsoft.com/CompuEye/LeafSArea/	(357)
Deep plant phenotyping	General plant phenotyping; machine learning based	Arabidopsis	Python package	Opensource	https://github.com/p2irc/deeplantphenomics	(358)

	parameterisation of Arabidopsis phenotypes					
Easy leaf area	Leaf area measurements	Plants	Python package, Android app	Opensource	https://github.com/heaslon/Easy-Leaf-Area	(335)
Endrov	Length, width, surface area, 3D structure parameterisation	Any	Standalone software	Opensource	http://www.endrov.net/	(359)
Grow map-leaf	Leaf growth and development rate	Plants	Standalone software	Licensed	Unavailable / not maintained	(340)
Growscreen	Leaf surface area; plant shoot surface area and growth rate analysis	Plants	Standalones software	Licensed	Unavailable / not maintained	(341)
HPGA	leaf surface area, leaf counts, growth rate; high throughput plant phenotyping	Arabidopsis	Standalone software	Freeware	https://phenomics.uky.edu/HPGA/index.html	(338)
Lamina	Leaf shape determination; width, surface area, length, disease presence	Plants	Standalone software	Freeware	http://lamina.sourceforge.net/index.shtml	(360)
Lamina2shape	Leaf length, surface, shape	Monocots	Matlab	Freeware	https://www.researchgate.net/publication/329514733_Matlab_code_for_Lamina2shape_An_image_processing_tool_for_an_explicit_description_of_lamina_shape_in_grasses	(361)
Leaf colour segmentation	Leaf quantification and area	Arabidopsis	Matlab	Freeware	https://www.helmholtz-munich.de/dig/working-groups/systems-thinking/projects/environmental-research/color-based-classification/	(362)
Leaf angle distribution toolbox	3D leaf structure and parameterisation; canopy reconstruction	Plants	Matlab	Freeware – academic use only	Available from authors upon request	(363)
Leaf-GUI	Macroscopic structure of leaf veins; size, shape, descriptive statics	Plants	Matlab	Freeware	Unavailable / not maintained	(342)

Leaf processor	Leaf geometry evaluation; size, shape, descriptive statistics	Plants	Matlab	Licensed	Unavailable / not maintained	(343)
Leaf growth	3D Leaf growth rate analysis; size, shape, descriptive statistics	Plants	Matlab	Freeware	Unavailable / not maintained	(344)
Leafanalyser	Leaf shape data acquisition, collation, and analysis	Plants	Standalone software	Freeware	https://sourceforge.net/projects/leafanalyser/files/	(337)
Leaf recognition	Leaf identification on woody plants; quantification and area measurements	Woody trees	Webtool	Freeware	http://leaves.utia.cas.cz/index	(364)
Leafsnap	Tree species identification based on leaf parameters	Trees	IOS app	Freeware	http://leafsnap.com/	(365)
Leafbyte	Leaf surface area, damage quantification, percent affected	Plants	IOS app	Freeware	https://zoegp.science/leafbyte	(336)
Leafscan	Leaf surface area	Plants	IOS and Android app	Freeware	https://www.leafscanapp.com/	(366)
Leafj	Leaf shape analysis; length, width, surface area	Plants	ImageJ/FIJI plugin	Opensource	https://bitbucket.org/jnmaloof/leafj/wiki/Home	(367)
Phenotic	Chlorophyll fluorescence analysis, F_v/F_M	Plants	R	Opensource	Unavailable / not maintained	(345)
Plantix	Pest, disease, and nutritional treatment recommendation; identification of plant disease, pest damage, or nutritional deficiency	Plants	Android app	Freeware	https://plantix.net/en/	(368)
WinDIAS	Leaf disease detection and quantification; leaf area, diseased/pest effected area, percent effected area	Plants	Standalone software	Licensed	https://delta-t.co.uk/product/wd3/	(369)

3.2 Results

3.2.1 Fungal colony area and conidial banding analysis

Many fungal species grow (relatively) radially from an inoculation point on petri dishes, and produce rhythmic, circadian conidial banding patterns on a daily basis (after a latency period prior to banding) (84,108,119,194,247,256,370–373). Fungal growth rates can also be altered by numerous environmental factors, such as temperature, lighting conditions and photoperiod, pH, and media composition (108,110,116,119,181,189,251,371,374–377). Colony diameter / radius and number of bands can be determined using manual measurements, but total colony area, maximum diameter / radius, distance between bands (a proxy for periodicity), and band amplitude are difficult or impossible to determine without image processing techniques. Additionally, since many fungal species do not grow in a truly radial fashion, the mean number of bands, radius, etc. may be utilised as opposed to taking a single measurement from the colony centre.

Banding and growth rate analysis can be used to determine how different environmental conditions and mutants (e.g., a those with a dysfunctional circadian clock) affect fungal development. Here, a semi- and fully automated FIJI-based tool is shown that determines colony area, average radius, and maximum diameter (Feret diameter), and plots inverted pixel intensity across the colony radius (in real world units or as a percentage across the colony), which shows the number of bands, distance between bands, and band amplitude. Most analyses for circadian fungal growth utilises race tubes and thus colonies are growing in a linear instead of radial fashion, and these analysis techniques are typically performed manually (traditionally under red safety light, which may alter

virulence related traits in *M. oryzae*) and thus not amenable to the techniques used here (82,104,110,119,181,184,215,256,257,371,378,379).

All colony images were captured using a digital camera (Canon EOS Rebel SL1) and petri dishes were placed lid down (so that the camera was imaging from the base of the dish) on a light box to better increase the contrast between the bands. Images were captured from directly above the plates with the optional inclusion of a black 5 cm² calibration square. Images were then transferred to a computer and processed using the FIJI pipeline as described.

First, the file details are called and stored (file name, file type, image width and height, and input folder). An output subfolder is then created (if not already present) in the input folder for results tables and plots to be saved.

Next, the petri dish or calibration card is located on the image (depending on which version is used): a Canny edge detection algorithm is employed to segment the petri dish and a binary image is created (Fig 3.1). The 'Analyze particles' function is then called, disregarding any objects (objects here, referring to a region of conjoined binary pixels, also known as a superpixel) smaller than 10% of the image and with a circularity of 0.2 or above. Circularity is calculated with the following equation:

$$\text{Circularity} = 4\pi * \frac{\text{Object area}}{\text{Perimeter}^2}$$

For the calibration card location, a colour threshold segmentation step is carried out instead of Canny Edge detection to pick out the darkest pixel regions (i.e., the black calibration card) that has a lower circularity and area of at least 1% of the original image size.

Once the petri dish or calibration card has been located, the image is cropped to that size and the width and height of the new image is called. The real-world units are calculated by determining the number of pixels occupying a region of known area, for the petri dish:

$$\text{pixels per cm} = \left(\frac{(\text{cropped image height}) + (\text{cropped image width})}{2} \right) / 9$$

and for the calibration card:

$$\text{pixels per cm} = \left(\frac{(\text{cropped image height}) + (\text{cropped image width})}{2} \right) / 5.$$

The bounding box of the calibration card (if present) is then removed from the original image and the petri dish located as above and cropped (Fig 3.1). The calibration card version is useful if the petri dish edges are poorly differentiated from background due to e.g., longer exposure times, as the location of the petri dish can be skipped and just the colony region thresholded, since the pixels / cm have already been determined. The image pixel values are subsequently inverted (dark regions become light and vice versa), and colony area is segmented with either pre-defined Hue*Saturation*Brightness (HSB) values (fully automated version), or by prompting the user to manually and interactively select HSB ranges. A binary image of the colony is then produced (Fig 3.1).

Once the image has been thresholded, the colony is segmented and located using the analyse particles function: the selected object/superpixel (the colony) must fall between 5 – 62 cm². This ignores any background noise, pen marks, etc. on the petri dish and does not select the petri dish (which has an area of ~63.6 cm²). The colony area (cm²) and perimeter (cm) are calculated based on the assumption of circularity:

$$\text{Circular radius} = \sqrt{\frac{\text{area}}{\pi}}.$$

Additionally, the Feret diameter (and subsequent radius) is computed, which is the longest distance between any 2 points of the colony superpixel, and this is used as the colony diameter in following calculations. The colony centroid coordinates are also determined, which is the average of the x and y coordinates of all the pixels in the colony superpixel. These colony metrics are saved as a .csv file in the output folder with the file name corresponding to the original input image.

The 'colony offset' is then calculated, which is the x, y coordinate difference between the image centre and the colony superpixel centre:

$$X \text{ offset} = \text{plate } X \text{ centre} - \text{colony } X \text{ centre}$$

$$Y \text{ offset} = \text{plate } Y \text{ centre} - \text{colony } Y \text{ centre}$$

The image contrast is then increased using a Contrast Limited Adaptive Histogram Equalisation (CLAHE) function with a block size of 1mm (variable pixel size depending on the image) followed by a Gaussian blur with a sigma variance of 3 to smooth the jagged edges as a result of the CLAHE. After increasing the contrast and smoothing, the colony centre is translated to the image centre by artificially moving the image by X offset, Y offset (Fig. 3.1)

Once the new image centre corresponds with the colony superpixel centroid, a rectangle is drawn from the centre point with a width of the colony radius (calculated by determining the ferret diameter as above) and height of 10 pixels. The X, Y pixel values across this selection are then stored and the image is rotated about the centre point by a user-defined number of degrees (that must be divisible by 360) and the process is repeated for n rotations;

$$\text{number of rotations} = \frac{\text{rotational angle}}{360}$$

The Y pixel intensity values for each rotation are tabulated, along with their respective X location. The X location is also converted from the distance from the centre point (cm) to % colony radius:

$$\% \text{ colony radius} = \frac{x \text{ position (cm)}}{\text{colony radius (cm)}} * 100$$

An empty plot is created with an X axis of distance from colony centre (cm) or % colony radius, depending on user preference. The plot is subsequently filled with the segment values for each rotation (Fig 3.1). Next, the sum and average of the segment pixel intensity for each row (X position) is calculated, and the mean value for each X position plotted and saved (Fig. 3.1). Another plot is created and saved, showing just the mean pixel intensity at each X position (Fig. 3.1). Finally, the standard deviation and standard error of the mean are calculated for each X position:

Standard deviation of pixel intensity =

$$\sqrt{\frac{1}{\text{rotations}} \sum_{\text{rotation } x}^{\text{rotations}} (\text{rotation } x - \text{rotational mean})^2}$$

Standard error = $\frac{\text{standard deviation}}{\sqrt{\text{rotations}}}$

The results table is appended with the square difference to the mean for each rotational segment, along with the sum of square differences to the mean, standard deviation, and standard error of the mean. This second results table is then saved as a .csv file to the output folder. Finally, the log file for the analysed image is saved as a .txt file, which shows the analysis start date and time, input/output folder, input file name, input file

width/height, minimum plate area (10% of the image area), plate width/height/radius/diameter (in px and cm), plate centre X, Y coordinates, colony radius/diameter (px and cm), colony centre X, Y coordinates, colony centre X, Y offset, rotational angle, number of rotations, the number of X point samples (results length), and the titles of the saved images/plots/log file.

Table 3.2: Comparative manual vs automated colony band and diameter analysis

Image	Manual bands	Automated bands	Manual diameter	Automated diameter (Feret)	% Accuracy
1	4	4	5.8	5.9	98.3
2	6	6	6.7	6.8	98.5
3	0	0	5.8	5.9	98.3
4	7	7	6.7	6.9	97.1
5	4	4	5.4	5.8	93.1

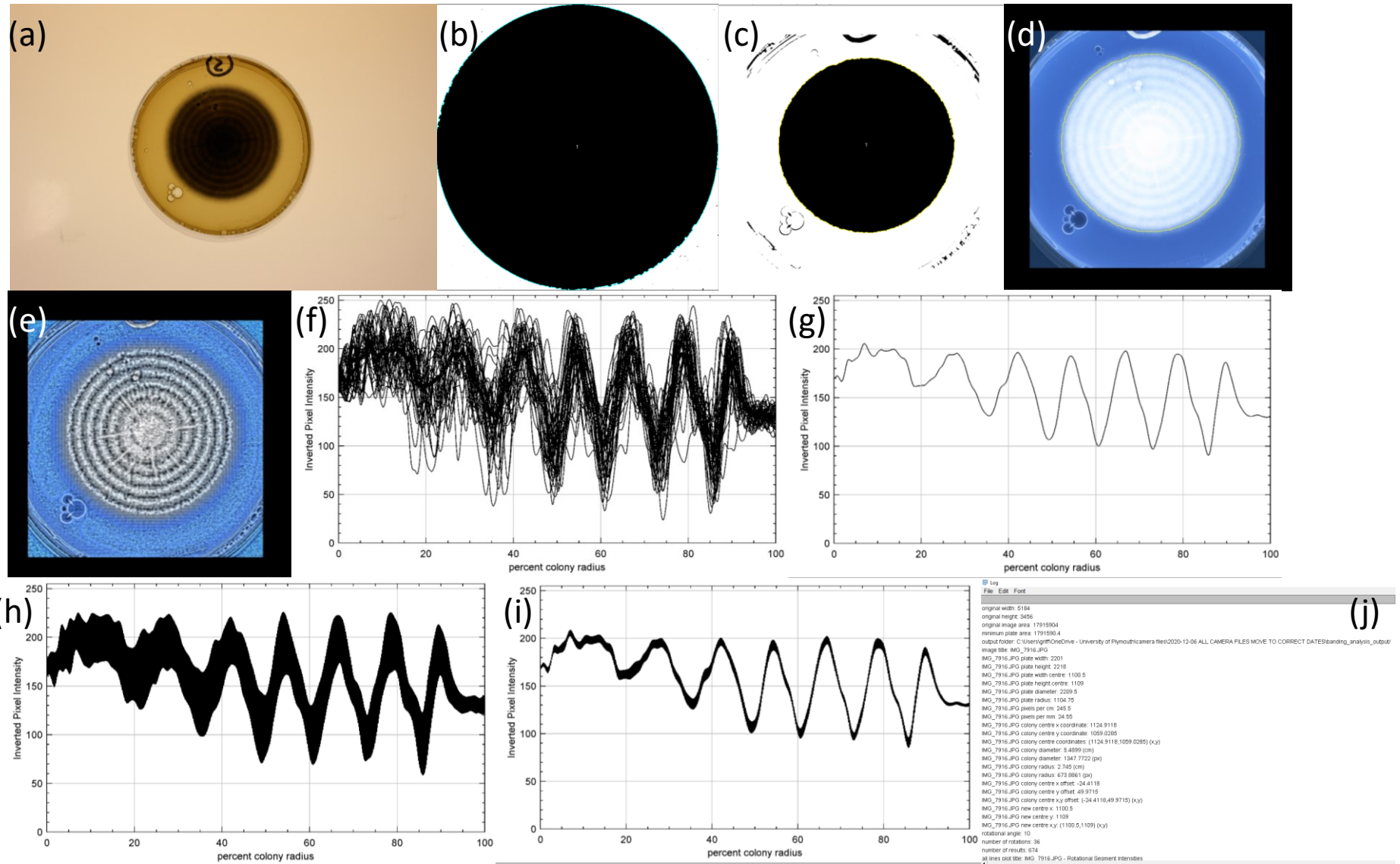


Figure 3.1: Overview of the fungal colony area and banding analysis macro. (a) an input image without a scale card, (b) automated location and cropping of the petri dish, (c) automated thresholding for the fungal colony, (d) inverting the pixel intensity, locating the colony and cropping the edges of the petri dish, (e) enhancing contrast, smoothing the edges, and transforming the colony centre to the image centre. Output plots showing (f) all segmented intensities, (g) the mean intensity, (h) standard deviation of the intensities, (i) SEM of intensities, and (j) the macro log file.

3.2.2 Conidial counts

Since *M. oryzae* produces conidia in a rhythmic fashion during the dark period (82), conidial counts may differ depending on time of day, environmental conditions, photoperiod, and circadian function. Additionally, *M. oryzae* conidia tend to be released just before dawn and are spread by wind and dewdrop (82). When conidia land on a hydrophobic surface, such as foliar tissue in nature, or glass coverslips and polystyrene petri dishes in the lab, they soon begin to produce a sticky substance called spore tip mucilage, used to adhere to plant tissue (78). To determine adherence and spore tip mucilage production of conidia grown under different lighting conditions or circadian mutants, conidia are located and counted microscopically, then the conidial suspension is agitated (see materials and methods). Conidia are then imaged and counted again to determine percent adherence. *M. oryzae* conidia have melanised cell walls, which presents contrast ideal for segmentation against the bright background in light microscope images. Using a semi- and fully automated image analysis pipeline presented here, conidial counts, size, and shape can be estimated. The Fungal Feature Tracker toolkit was considered for use (324), but the pipeline presented here was produced prior to its publication (2019), and much experimental data was collected prior to FFT's release. Additionally, it is a semi-automated pipeline, and presented here is a method specific and bespoke for the imaging setup in UoP.

First, the input folder, image dimensions, and image title is retained, then an output subfolder is then created (if not already present). The central 75 % of the image is selected and cropped to remove the characteristic 'halo' effect, where the periphery of the image is darker than the centre, generated by a square sensor (the camera) capturing light from the circular aperture of the microscope (380). A minimum intensity filter

followed by a Gaussian blur is applied to the image to increase contrast and homogenise conidia and background. HSB colour thresholding is then used (either automatically or user-prompted) to segment conidia from the background and a binary image is created (Fig. 3.2). The binary image is then dilated, holes are filled, and eroded to reduce background noise and false counts. Particles are analysed, with a user-defined area (e.g., 300 – 1000 px) and a circularity of 0.5 – 0.8. These selections are then applied to the original, non-binary image, counted, and measured. Area, perimeter, circularity, and mean grey value for each particle (conidia) is shown in the results table, and a summary table is created showing the total count, mean size, etc. for the image. This allows for comparison of conidial size, shape, and pixel intensity between different treatments or strains.

For manual confirmation, the selected particles are drawn in blue onto the original image to determine false positives/negatives and the annotated image is saved to the output subfolder. The macro then loops onto the next image in the folder and repeats for all image files in the input folder. For each image, the counts and measurements are appended to the results and summary tables, including the original input file title. Once all images have been processed in the input folder, the results and summary files can be saved as .csv files for ease of downstream statistical analyses. The accuracy of the macro is presented in table 3.3.

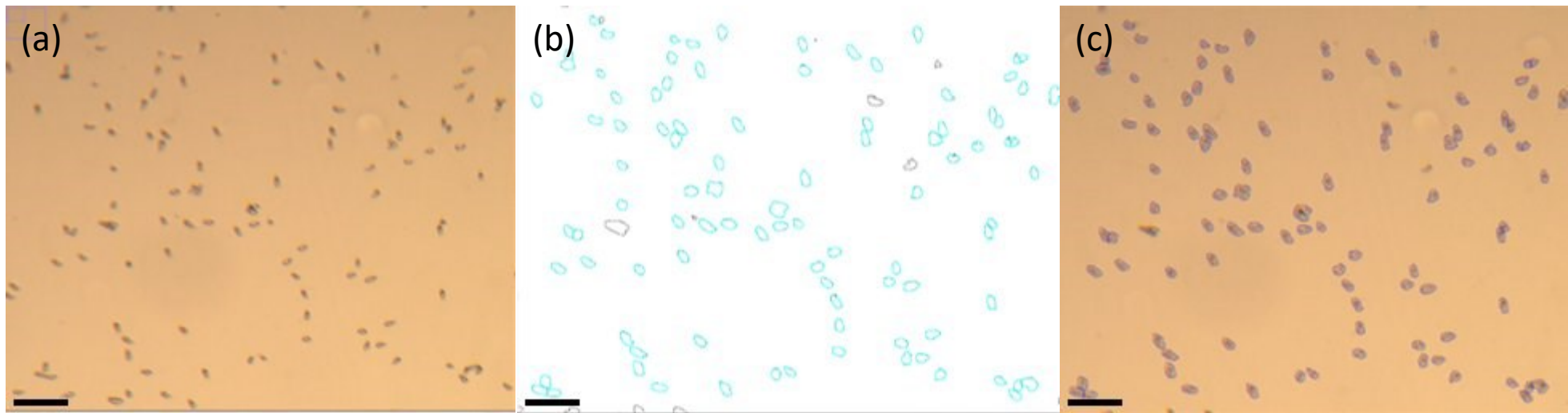


Figure 3.2: Overview of the conidial counting and analysis macro. (a) cropped input image of melanised conidia under a light microscope, (b) outlines of successfully segmented and counted conidia (blue) and ignored particles (black), and (c) output image of segmented and outlined conidia for manual confirmation. Scale bar = 100 μm .

Table 3.3: Accuracy of the conidia counter macro

Manual count	spore	Automated count	spore	% Accuracy	Manual average area	Automated average area (px)
153		123		80.39	NA	664.9
212		167		78.77	NA	664.5
217		191		88.02	NA	682.7

3.2.3 Appressorial cytorrhysis analysis

Once conidia land on and adhere to a hydrophobic surface, they soon germinate and after ~8 h produce a melanised, dome-shaped infection structure called an appressoria (78). The appressoria subsequently generates an enormous amount of turgor pressure, which allows it to punch its way through the plant cuticle (78). Exposing these appressoria to increasing concentrations of glycerol can cause them to collapse (indicated by a faint line through the appressoria) due to the loss of internal positive pressure, through a process called cytorrhysis (381–383). By gradually increasing the concentration of glycerol, the approximate internal turgor pressure of the appressoria can be determined.

A cytorrhysis assay was performed on *M. oryzae* conidia (see 2.2.7). Conidial suspensions were imaged after a 30 min incubation in the glycerol solution under a light microscope with a camera adaptor (Canon EOS Rebel SL1 camera with a t-ring microscope adaptor, Kyowa Medilux-12 light microscope). A short FIJI-based macro was developed to locate, count, measure, and save individual appressorial images for manual scoring of collapse. Automated scoring of appressorial collapse was attempted, but the number of false negatives was unacceptably high. To date, no fully-automated image analysis pipelines have been reported to count and describe appressorial characteristics whilst differentiating (and ignoring) conidia.

First, the input folder, image file name, and image dimensions are called, and an output folder is created (if not already present). The central 75 % of the image is selected to account for the halo effect, as with the conidia counter, and the image is cropped (Fig. 3.3). The image is then converted into an 8-bit format and the background subtracted,

followed by application of a minimum pixel intensity filter to differentiate the dark edges of the melanised appressoria from the background.

The darkest regions of the image are segmented by a pixel intensity threshold and a binary image is created. The binary image is then dilated, eroded, and holes filled to remove background noise and create homogenous dark sections, which denote conidia and appressoria. A watershed filter is applied to separate any appressoria or conidia that are overlapping. Particles are then analysed based on a user-supplied size threshold (e.g., between 1000 and 3000 px, depending on the camera and image quality), and only particles with a circularity greater than 0.7 are considered as true, which should exclude the less-rounded conidia, leaving just the appressoria (Fig. 3.3).

The 'true' particle (appressoria) locations are then redirected from the binary image to the original image, counted and measured (size, shape, perimeter, mean pixel intensity). The appressoria are then outlined in blue for manual conformation of appressoria and to manually determine if they are collapsed or intact. The annotated output image and results file are then saved in the output subfolder for confirmation and statistical manipulation. There is the additional option included to save the annotated appressoria as individual files for manual processing. The accuracy of the macro is presented in table 3.4.

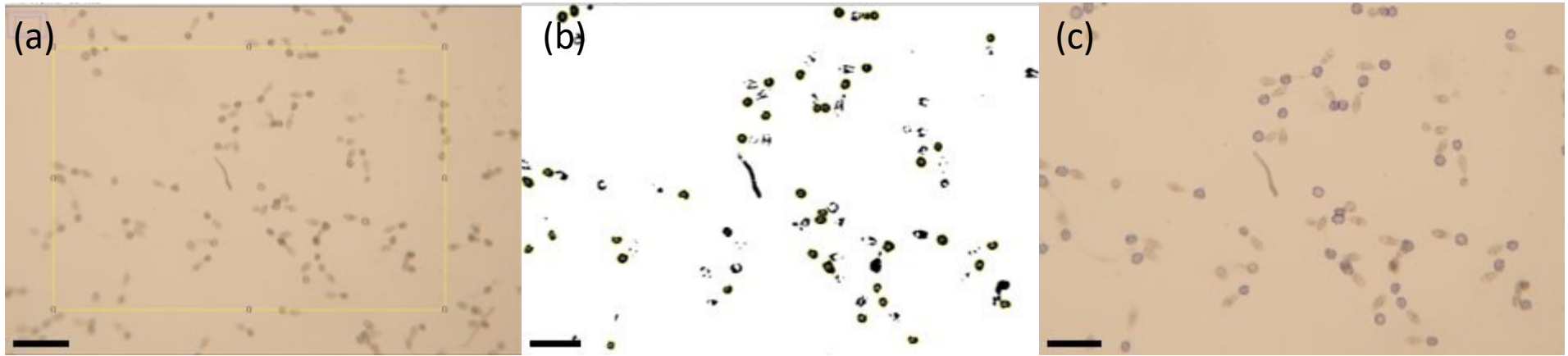


Figure 3.3: Overview of the appressorial counting and analysis macro. (a) input image showing the central 75 % selection, (b) segmented appressoria and ignored conidia, (c) annotated output image, where the successfully segmented appressoria are outlined in blue. Scale bar = 100 μm .

Table 3.4: Accuracy of the appressoria finder

Manual appressoria	Automated appressoria	% Accuracy	False positives
30	35	85.7	1
52	57	91.22	2
54	40	74.07	0

3.2.4 Automated conidial development time course acquisition

Conidial germination and development may differ between *M. oryzae* strains and is known to be affected by a number of environmental conditions, such as presence of a hydrophobic surface, pH, nutritional availability, light intensity (78,259,384), and potentially circadian clock function (259). To gather temporally relevant data in conidial germination and development, it is necessary to characterise the conidial developmental stage at several different time points over a period of (up to) 2 d. This would require many long hours of operation and analysis for researchers, shift work, or expensive microscopy equipment.

The Openflexure microscope (265,385) is an open-source 3D-printable microscope that utilises the flexibility of a commonly used printing material, polylactic acid (PLA) to move a stage in the X, Y, and Z axes with adequate control at a fraction of the price of conventional microscopes (Fig. 3.4). Once the components have been printed, all that is required is a lens, camera, and computer interface, coming to a total approximate cost of £80-100. Additionally, 3D printers can be acquired for less than £300, facilitating a cost-effective method for timelapse microscopy.

Raspberry Pis are inexpensive computers that have a plethora of uses in prototyping and simple computing applications, including camera and Openflexure integration. A small piece of python code was written that imports a PiCamera package and presents the live view of the microscope so that conidia can be located and focussed. A second script was written that displays the live view in a small subwindow and saves images to a user-defined folder every x number of seconds, typically every 30 min, or 1800 s (386) (Fig. 3.4). The output file includes an increasing counter to indicate the imaging time point.

Additionally, live-streaming capability was implemented so that the microscope image (with the current time and number of images captured displayed in the bottom right corner of the screen) could be viewed remotely via an internet connection to check for X, Y, or Z axis drift and sample drying. Live streaming was implemented using the Motion home surveillance software (387). Losing focus is an occasional issue due to gravity acting on the Openflexure system, and the heat from the raspberry pi computer located underneath the sample can cause the water droplet to evaporate. If this happens, then the user can check the remote feed, readjust the stage position, add more water to the sample, or disregard the images.

The code continues to run and capture images every X seconds, until the user prompts it to stop, and images can be transferred to an external drive and manually scored for developmental stage at leisure.

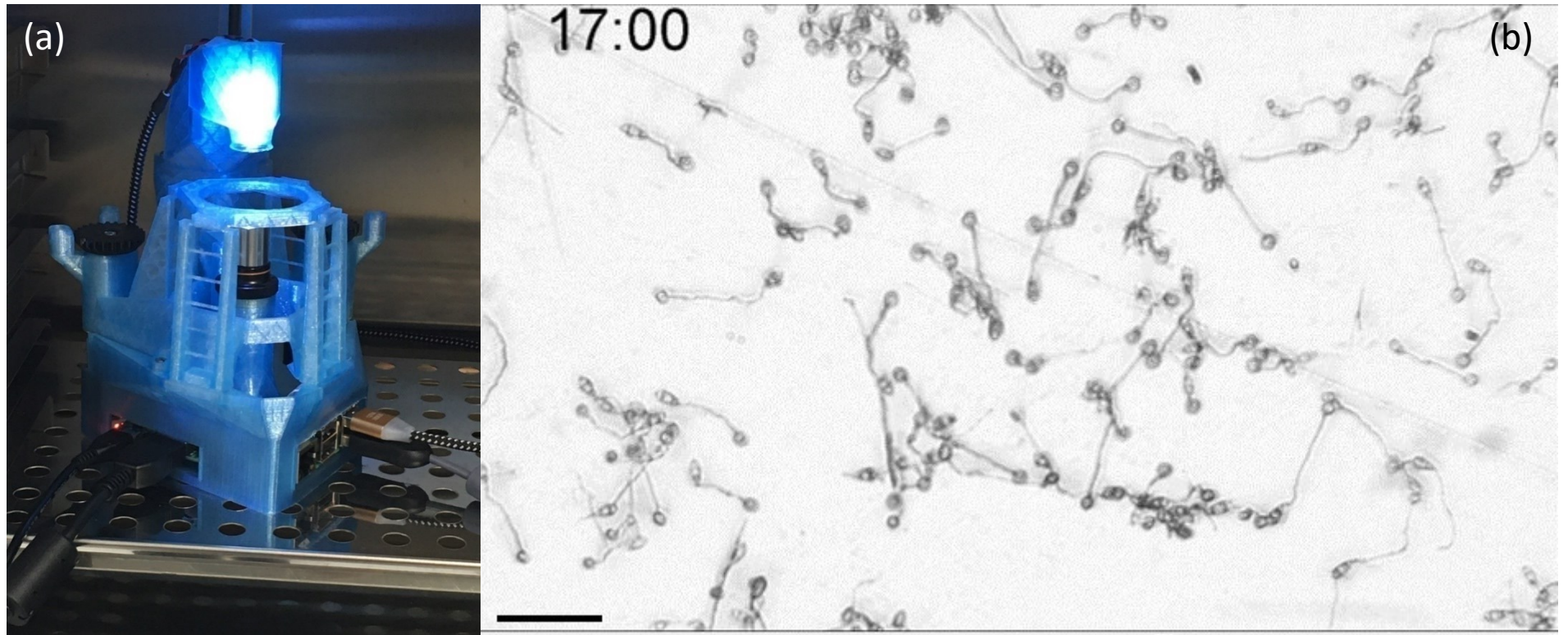


Figure 3.4: Openflexure conidial timecourse acquisition setup. (a) Openflexure microscope, (b) example output image of developing conidia at 17 hours post inoculation. Scale bar = 100 μm .

3.2.5 Automated leaf segmentation and pre-processing

Images that contain multiple regions of interest can often make image processing and subsequent analysis difficult due to the increased complexity of the image. An analysis pipeline can be applied to an entire image, considering all of the segmented regions as one continuous object rather than discrete individual objects that need to be analysed independently from one another. Taking this into account, researchers can either (a) change the imaging setup and image one ROI/object at a time, which can significantly increase acquisition time and labour costs, or (b) alternatively, the algorithm can be applied individually to each object/ROI within an image. This increases computational resource use and processing time, though, due to the requirement to individually segment out ROIs and apply the code to individual objects. A final option is to introduce a pre-processing step, to split the objects in the original image into multiple files to be fed into the analysis pipeline individually.

Infected leaf images were scanned using a flatbed scanner (Perfection V39 Photo and Document Scanner) 6 days post-inoculation by placing them adaxial side down towards the scanner using white masking tape to match the matte white background of the scanner lid. Leaves on masking tape were laid as close as possible to one another without overlapping and scanned at a resolution of 800 DPI (315 px/cm). A colour balance card was placed in the corner of the scanner to ensure images were captured with uniform and comparative colour values (Fig. 3.5). Leaves were scanned together based on plant species, fungal strain, and pre-inoculation treatment (i.e., rice and barley were scanned separately, and wild type and mutant infections were scanned separately). .tiff images were automatically saved with the acquisition date (YYY.MM.DD) and an incrementally increasing 3-digit counter, e.g., "2020.02.07 – 002.tiff". A key .txt file was manually

produced which describes the infection conditions of the scanned leaf images, and this key was used in downstream data manipulation, annotation, and analyses for the Redpatch output data (see 3.2.6). Images were then fed into a short macro in FIJI to segment, measure, and save individual leaves from the original multi-leaf image. Other software was considered to count, measure, and save the images of leaves (see table 3.1), but were either semi-automated, required different imaging setups, or produced files in formats that were incompatible with Redpatch (see 3.2.6)

First, the image file name and image dimensions are stored, the scale is set (all images were captured at 800 DPI) to 315 px/cm, and the colour calibration card cleared from the image. Next, a simple colour threshold filter is applied to the image to remove the matte white background, leaving just the darker (predominantly green) regions, i.e., the leaves. a binary image is created, and the holes are filled to account for any bright/yellowed sections of leaves that could be erroneously missed and considered background (Fig. 3.5).

The analyse particles function is then executed, which excludes any superpixels smaller than 0.1 cm² (such as debris or dirt), and the objects are added to the ROI manager. Individual object selections are then applied to the original image, cropped, and duplicated, leaving an individual leaf on a clear, white background (Fig. 3.5). This process loops over the ROI list and the individual leaves are saved in a .tiff format to a user-defined output folder.

Individual leaves are saved to the output folder with the file name convention: “individual leaf – “[original image name]” – n”, where n is an individual ROI. The next image in the user-defined input folder is then opened and the process repeated for all the images in the folder. Results and summary files are generated, which can be saved (if desired) and

displays the number of leaves in each image, their individual, total, mean area, and mean grey value (Fig. 3.5).

An adapted version of this macro works for images with unknown pixel densities. Leaves are placed on a white background, such as a sheet of paper, and a bright pink 5 cm² calibration card (in contrast to the white background and green leaves) is used as the ground truth for pixel density. An additional colour threshold segmentation step is applied to locate and crop to the card. The width and height of the cropped calibration card image is then called and averaged (to account for rotation of the card):

$$\text{Pixels per cm} = \frac{\text{calibration card width (px)} + \text{calibration card height (px)}}{2} / 5$$

Once the variable pixel density has been determined and set, the macro continues in the same way as the flatbed scanner version. For a series of 500 multi-leaf images, 22 output images were incorrectly produced due to over/under segmentation or misannotation (a 95.6% accuracy).

The individual leaf files are then fed into Redpatch (see 3.2.6) for disease severity analysis.

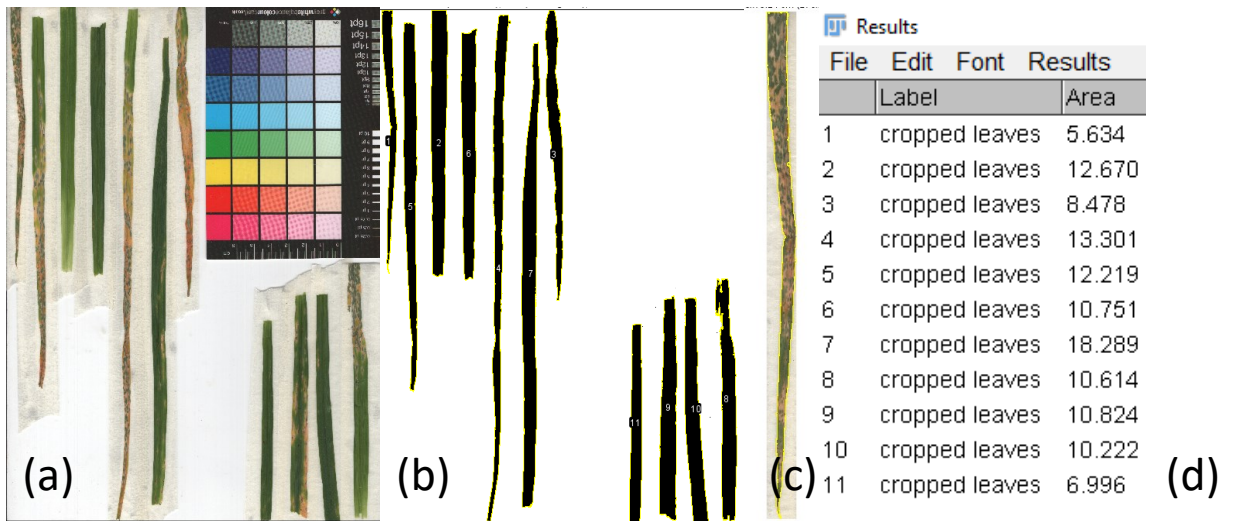


Figure 3.5: Overview of the leaf segmentation pre-processing macro. (a) input multi-leaf image, (b) multiple individually segmented leaves, (c) an individual output leaf, and (d) a results file showing the individual leaf areas.

3.2.6 Leaf infection severity analysis: Redpatch

Many pathogenic infections of foliar tissue display characteristic disease symptoms (78,110,122,150,381,388,389). In rice blast infections, brown, diamond-shaped lesions are formed on leaves (78,381). These typical disease symptoms can be screened for, and disease severity approximated in an automated fashion. The developmental goal for this toolkit was to ultimately infer how infection severity of rice blast disease differs due to a range of pre-inoculation treatments (such as constant light vs constant dark), time of day, plant host, and fungal strain.

Disease symptom severity is usually scored by a researcher manually, according to a numbered severity scale (26,77,101,304,311,326,381,388,390–394). This assessment is often done in person and requires significant expertise and experience to discern severity. Further, leaves may need to be preserved by drying and flattening onto index cards (393) or photographed to be manually scored at a later date. Manual analysis inherently introduces bias to the measurements, as individuals will score leaves differently, and researchers may be tired or inexperienced, which makes it difficult to determine the ‘true’ disease severity. Additionally, since the traditional severity scale technique bins the severity into discrete categories (e.g., 1 out of 5, or 30 – 50%), which can be difficult to distinguish by eye, there is significant data lost, turning what should be a continuous scale into a discrete, categorical one.

Researchers are interested in a wide array of disease-related metrics, such as total leaf area, healthy and diseased area, lesion size, shape, and counts. These metrics can be used to determine % diseased area, % area covered by lesions, lesions per leaf cm², maximum/minimum/mean lesion area, and so on. Semi- and fully automated leaf disease

severity can provide most, if not all, of these metrics, but there are several processing problems to contend with. One of the most important of these issues are the inter-object relationships; all healthy, diseased, and lesion areas are found within a single object. There is, therefore, a requirement to carry out subsequent thresholding and segmentation steps which exclude different regions within the central object: the leaf. On the other hand, if a pipeline can successfully locate a leaf (which is usually overwhelmingly green and has significantly different pixel characteristics from the background), the algorithm can ensure that the ROIs must be contained within the given leaf bounding coordinates and it can essentially ignore the rest of the image. This step of ignoring pixel values outside of the leaf coordinates can reduce computational requirements, runtime, and erroneous results: a true lesion cannot exist outside of leaf tissue, for example.

Initially, a FIJI-based macro specific to the rice blast pathosystem was developed, but this was later ported and improved (in collaboration with Prof. Dan Maclean, The Sainsbury Laboratory), and a python-based toolkit called Redpatch was produced. Redpatch (<https://github.com/TeamMacLean/redpatch/>) is a fully automated, customisable, web- and local-based image analysis pipeline devised to measure total leaf area, diseased leaf area, count lesion regions (which includes coalescing lesions), and lesion centres (individual lesions) and provide lesion shape statistics. Other semi- and fully automated disease analysis pipelines exist, but they often focus on a single pathosystem such as in *Z. tritici* leaf blotch (395,396), place infection severity into bins similar to a manual scale (e.g. healthy, early, middle infection, etc.), are unsupported, unavailable, or depreciated, or focus on % coverage only (Table 3.1).

Redpatch presents raw counts of leaves (if multiple are present in the input image), healthy area, lesion regions, and lesion centres (individual lesions and their 'parent' lesion region if coalescing) on a per sub-image (leaf) basis. Area measurements are also presented for the above metrics of each sub-image. The output of Redpatch is the area metrics, area type, input image title, image parent region, and long:short axis (aspect) ratio for lesions. This information is presented in a .csv format, and a report .html file which logs the analysis start date/time, filter settings, and images processed; the input and output images are also called and shown in the html report document (Fig. 3.6). Annotated output sub-images are also produced, showing 'healthy', 'lesion', and 'centre' locations, with the pixel dimensions shown (Fig. 3.6). These output images are saved to the user-defined output folder.

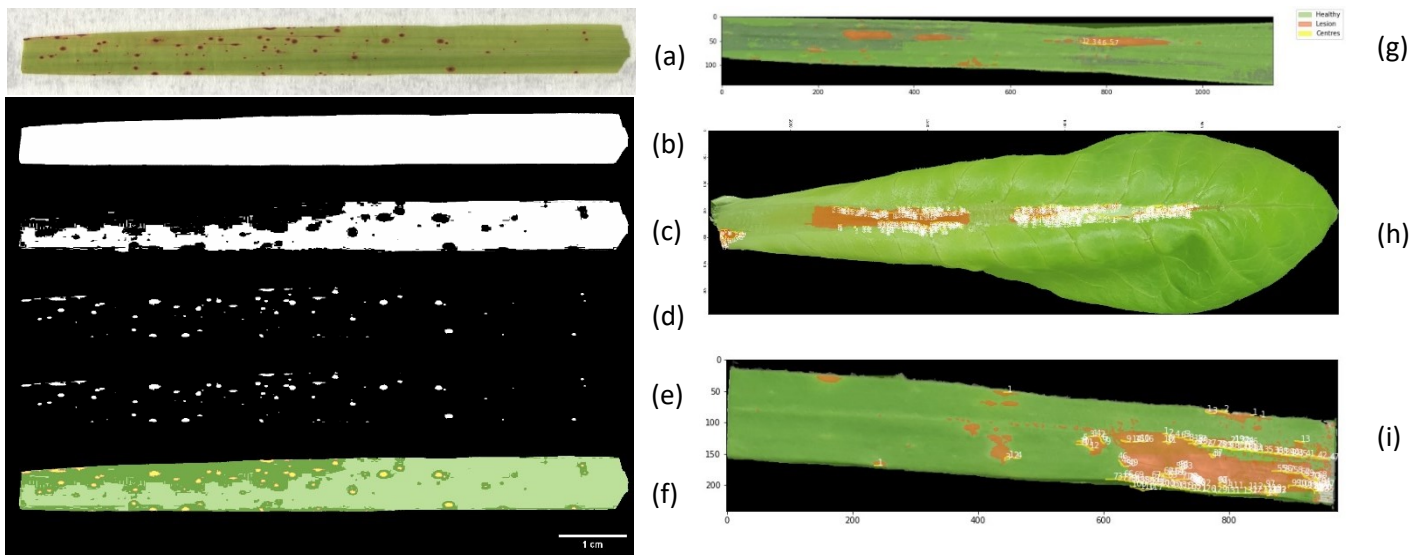
To define filter settings for multiple image processing, images can be uploaded to the Redpatch webapp (<http://redpatch.tsl.ac.uk/>) and the interactive HSV sliders moved to cover scale cards (if present), leaf area, and lesion area (Fig 3.6). The config file (containing the filter settings) generated here can be downloaded and used to process images locally (interactively, on a per-image basis in Jupyter Notebook, or in a batch process), or the config file can be uploaded to the webapp to analyse images remotely with the same settings. To run in batch mode, users must define the input folder, output folder (which is created if not already present), and a YAML config filter setting file (a default setting file can be created locally and the HSV settings altered in a text editor). For use in high-throughput experiments with thousands of leaf images, the core methods are included in a Python package that can be implemented and expanded into local data-gathering pipelines, for example using Redpatch on a high-performance computer or in-situ analysis.

Redpatch can be installed locally using 'pip install redpatch' and relies on Shapely ('conda install shapely'), a python package for set-theoretic analysis and manipulation of planar features (397). The Redpatch python package also allows for optional arguments to be called (defined in the -help function), which includes the scale card length in real world units (if present), the px/cm scale (if known), the option to run Redpatch on a server as opposed to locally, the scale image file name (if present), minimum lesion area to be considered true (in real world units or pixels), the maximum length to width ratio a lesion centre can have (the shape of a lesion centre), the minimum lesion centre size (in real world units or pixels), and the proportion of lesion width the lesion centres must exceed to be within to be included (counted from either side). These parameters allow for Redpatch to better differentiate different area types in the image. The webapp processes images remotely with a more user-friendly graphical user interface but does not have the same flexibility or options to alter the lesion parameters. For local installation and user guides, see <https://github.com/TeamMacLean/redpatch/>.

Redpatch initially determines the scale of the image, which can be none (i.e. no scale card or px/cm provided), a user-defined px/cm, or can rely on a user-defined scale card image with a known area. The scale is then subsequently applied globally to all images in the input folder. The input image is then segmented independently, multiple times to produce a series of leaf sub-images (if multiple are present), followed by the healthy regions, lesion regions, and lesion centres within each sub-image. To create leaf sub-images, once leaf area has been segmented, bounding boxes are created around the objects, and the subsequent thresholding steps are applied independently to those leaves. To detect lesion centres, a Canny edge detection step is applied post-

thresholding. The thresholded binary regions of interest are then quantified and measured.

Once an empty dataframe has been created, Redpatch appends the leaf, healthy, lesion region, and lesion centre metrics to the dataframe for each sub-image, before moving onto the next image in the input folder. A run-time log is shown in the active window displaying Redpatch's progress through the input folder. The resulting .csv file can then be manipulated with statistical processing software. The accuracy of Redpatch is shown in Table 3.5



Instructions

1. Select the HSV values to isolate the different regions in the test image. The white areas in the preview indicate the regions that will be selected.
2. If you have selected a scale card please remember to add the side length in centimetres.
3. Click "Process all images" to apply the settings.
4. If want to save the settings to use them again or in other versions of Redpatch select "Download config".
5. If you have previously saved settings, upload them using "Upload config"



Figure 3.6: Redpatch segmentation approach and interface. (a) Rice blast-infected rice leaf input image, HSV thresholding for (b) leaf location and area, (c) healthy area, (d) lesion-affected area, (e) lesion centres. (f) Demonstrative composite image of segmented areas; green: total leaf area, light green: healthy area, brown: lesion-affected area, yellow: lesion centres, scale bar = 1cm. (g), (h), and (i) show annotated and scaled (by pixels) output images of *Septoria tritici* blotch-infected wheat, bacterial blight-infected lettuce and powdery mildew-infected barley, respectively. This process can be performed using the Redpatch webapp interface (j) – here, showing rice blast-infected barley

Table 3.5: Accuracy of Redpatch

Image file	Area (cm ²)							% coverage		Lesion counts per cm leaf tissue		Lesion shape descriptors			
	Leaf	Healthy	Mean lesion region	Max lesion region	Mean lesion centre	Max lesion centre	Total lesion occupation	Healthy area	Area occupied by lesions	Lesion regions	Lesion centres	Mean lesion region ratio	Max lesion region ratio	Mean lesion centre ratio	Max lesion region ratio
Leaf_A_manual.tif	6.02	3.95	NA	NA	NA	NA	NA	65.65	NA	11.96	15.28	NA	NA	NA	NA
Leaf_A_redpatch.tif	6.07	4.20	0.0067	0.073	0.0008	0.0055	0.5692	69.20	9.38	12.02	15.16	2.58	16.75	3.38	9.72
Leaf_B_manual.tif	7.88	6.52	NA	NA	NA	NA	NA	82.76	NA	6.72	11.04	NA	NA	NA	NA
Leaf_B_redpatch.tif	7.93	6.53	0.0187	0.3506	0.0004	0.0071	0.8507	82.3	10.73	5.42	11.85	2.61	12.51	4.59	9.93
Leaf_C_manual.tif	4.16	3.07	NA	NA	NA	NA	NA	73.88	NA	28.39	44.26	NA	NA	NA	NA
Leaf_C_redpatch.tif	4.22	2.70	0.0041	0.2477	0.0003	0.0022	0.5666	63.94	13.42	30.56	33.17	2.89	10.54	4.69	9.77

3.2.7 Chlorophyll fluorescence leaf health and pre-symptomatic disease analysis

Due to pathogenic infection, many plants develop characteristic discolouration of foliar tissue, coupled with altered photosynthetic efficiency (78,110,122,150,381,388,389). A chlorophyll fluorescence imager is a camera and filter-based system that can determine plant health through measuring and quantifying normalised difference vegetative index (NDVI) and chlorophyll fluorescence (F_V/F_M) (106,115,149,249,251,267,290,293,295,301,305,311,326,345). Chlorophyll in plant cells absorb large amounts of visible light for use in photosynthesis and reflect infrared light (infrared light is not used on photosynthesis and can cause unwanted temperature rises) and researchers can use these leaf characteristics to locate plant tissue and approximate plant health (295,301,305,311,326). NDVI is calculated from these reflection and absorption characteristics:

$$NDVI = \frac{\textit{near infrared light} - \textit{red light}}{\textit{near infrared light} + \textit{red light}}$$

Due to the ratiometric nature of NDVI, values always fall between 0 and 1, with values above 0.6 generally considered 'healthy'.

F_V/F_M is used to determine if a plant's photosystem II is affected by stress when dark-adapted (traditionally plants are placed in the dark for at least 30 min). F_V/F_M determines the maximum quantum efficiency of photosystem II by measuring the difference between the minimum fluorescence value (F_0 , pre-photosynthetic fluence rate), captured using a light pulse too low of an intensity to drive photosynthesis, and the maximum fluorescence value (fluorescence rate after a brief, intense, and saturating light pulse) (267). This difference is the variable fluorescence, F_V , and determining the ratio between

the variance and maximum fluorescence gives a robust indication of the PSII yield (267). The more stressed or unhealthy a plant, the lower the F_V/F_M due to a reduction in photosynthetic capability. F_V/F_M is calculated by:

$$\frac{F_V}{F_M} = \frac{\text{Maximum fluorescence} - \text{minimum fluorescence}}{\text{maximum fluorescence}}$$

There is much debate regarding whether arbitrary classification values in NDVI and F_V/F_M should be used to determine 'healthy' or 'stressed', in favour of more quantitative approaches, utilising continuous data. For the purpose of this analysis, determining the presence and developmental rate of pathogenic infection in plant leaves, NDVI values above 0.6 and F_V/F_M values above 0.79 are considered healthy.

Presented here is a semi-automated FIJI-based macro that determines leaf area, healthy area, unhealthy area, and dead area according to NDVI and F_V/F_M images of infected plant tissue. Percent healthy, unhealthy, and dead areas can be calculated from the results table, and drawings of the area classes are produced for manual confirmation.

Leaves were placed on a black matte, non-reflective material and dark adapted for at least 30 minutes prior to imaging in an Open Fluorcam (PSI). Data was interpolated by the proprietary Fluorcam software and images created according to lookup tables with a range of 0.3-1 for NDVI images and 0.5-0.85 for F_V/F_M images (these values can be altered, but the threshold ranges need to be changed to reflect this). Since the pipeline analyses the image data output from the fluorimager software, as opposed to the raw numerical data, all images need to have the same lookup table range, or the code will not perform as designed.

Users are prompted to draw a bounding box around the leaf of interest in the NDVI image (which better shows the leaf area). This selection is reapplied to the F_V/F_M image since they have the same pixel density and location, and both images are cropped to the selected area (Fig. 3.7). A simple HSV colour threshold step is applied to the NDVI image to select the noisy grey background, which is then subsequently removed from the original image, leaving the leaf on a clear black background (Fig. 3.7). This selection is also applied and removed from the F_V/F_M image as the leaves in the NDVI image generally give a true leaf area reading since the images are not dependent on a functional PSII (if there is no photosynthetic activity, there will be no signal captured by the fluorimager for F_V/F_V measurements).

Two blank canvases are then created with the same dimensions as the user-selected leaf-bounding box, which will be subsequently filled with the classified NDVI and F_V/F_M drawings (Fig. 3.7). Once the background has been removed from the two images, three rounds of colour threshold segmentations are applied for each area type: first for total leaf area, then for healthy area, and unhealthy area. The areas in pixels for each respective area type are measured for NDVI and F_V/F_M images and drawings are created for each on the blank canvases; green fill for total leaf area, red fill for healthy area, blue outline for unhealthy area, and any black pixels in the F_V/F_M drawing shows dead/non-photosynthetic regions (Fig. 3.7). Once the drawings have been created, the percentage healthy and unhealthy areas are calculated for the NDVI and F_V/F_M images and percent dead tissue calculated:

$$\% \text{ dead tissue} = \frac{\text{total NDVI leaf area} - \text{total } \frac{F_V}{F_M} \text{ area}}{\text{total NDVI leaf area}} * 100$$

The % area types are appended to the results file and output results and leaf drawings can then be saved to a user-prompted location (Fig. 3.7).

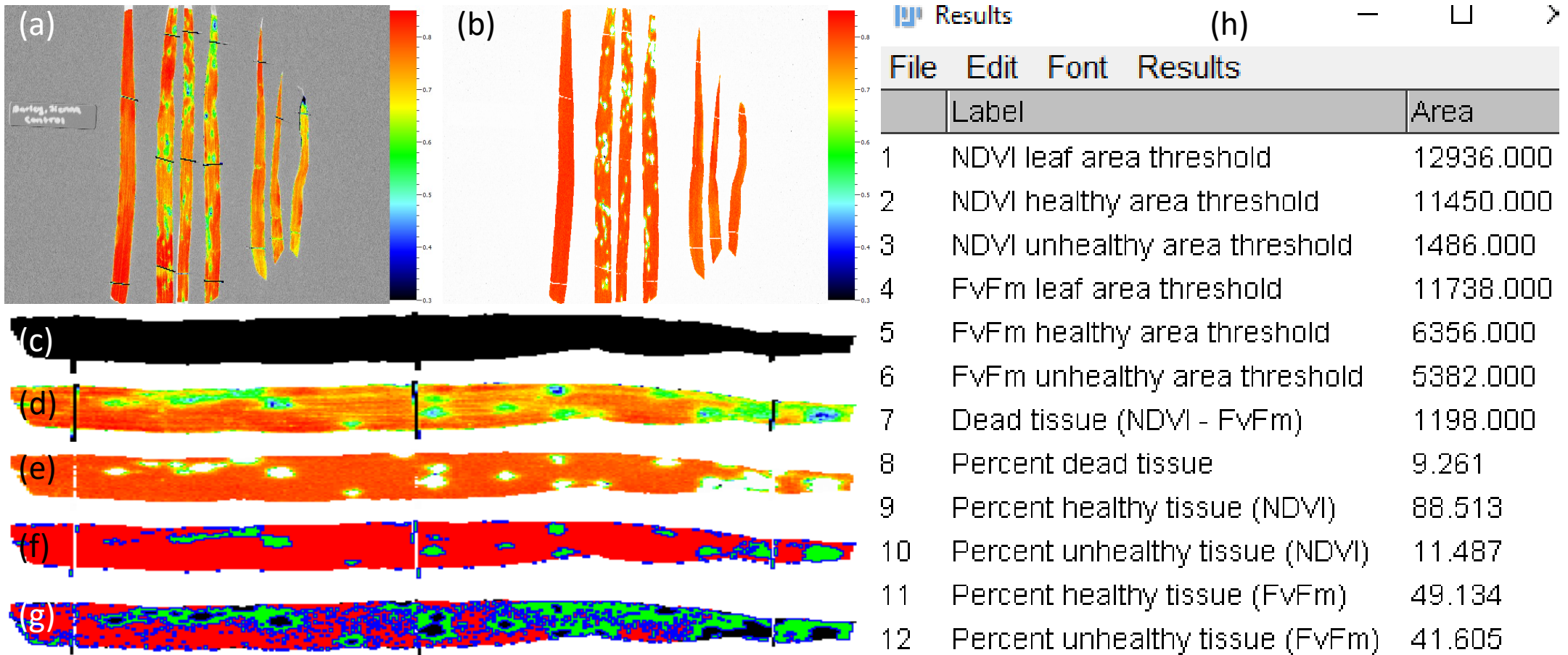


Figure 3.7: Chlorophyll fluorescence image analysis approach. (a) input NDVI image, (b) input F_v/F_m image, (c) segmented total leaf area based on NDVI image, (d) background-removed NDVI leaf, (e) background-removed F_v/F_m image, and (f, g) drawings of classified regions for NDVI and F_v/F_m , respectively (green denotes total leaf area, red healthy area, blue outline for unhealthy area, and black, if present, denotes dead/non-photosynthetic tissue). (g) output results file giving area and percentage statistics for the selected leaf.

3.2.8 Confocal ratiometric and intensity analysis

Fluorescent protein tags such as green fluorescent protein (GFP) and red fluorescent protein (RFP) can be attached to (or replace) genes of interest through genetic engineering (259,398,399). When GFP is exposed to a blue laser, it emits a bright green light which can be used to determine the expression levels, timing, and localisation of the tagged protein (259,398,399). Some gene products, such as FRQ are rhythmically expressed and active, and can move into and out of the nucleus throughout the day (181). Accordingly, *M. oryzae* GFP-tagged FRQ and WC2 complementation mutants (produced by Dr. Xia Yan, TSL) were generated, in part, to elucidate the circadian expression and localisation of clock genes throughout the day. Considering some clock protein function depends on phosphorylation status, localisation, and interaction with its accessory proteins, the relative intensity of GFP present in the nucleus compared to the cytoplasm may give an approximation of subjective circadian time. In this way, it might be possible to see the clock 'ticking' in real time.

M. oryzae WC2- and FRQ-tagged lines were grown under different circadian conditions (see materials and methods). Conidia were harvested (as described in materials and methods) and the leading edge of the colony hyphae were collected with a sterile scalpel and squashed onto a glass microscope slide prior to imaging under a Zeiss LSM800 Airyscan confocal microscope. Samples were imaged approximately every 5-6 h for 24 h to gain a time course displaying a range of intensities and localisations of the tagged clock genes.

2-channel (GFP and brightfield) Z stacks were generated (see materials and methods) and imported into FIJI. A short semi-automated macro was developed to determine mean

pixel intensity (fluorescence) in the GFP channel at different times and locations intracellularly. The macro first calls the image title, width, height, depth, and channels of the hyperstack. Text prompts ask the user to first click on the brightfield channel, followed by the GFP channel, which are both duplicated into individual stacks for downstream processing.

Users are then prompted to scroll through and set the first and last Z slices of the stack to be analysed, followed by drawing boxes inside the vacuole, nucleus, and cytoplasm of a given cell. The vacuole and cytoplasm can be located using the brightfield channel, and the nucleus with the GFP channel. The X and Y coordinates, along with the width and height of the drawn boxes (for the vacuole, nucleus, and cytoplasm, respectively) are then stored in the active memory. The vacuole box selection is then applied to the start slice and the GFP channel pixel intensity is measured and mean grey value of the selection placed in the results table. This iterates over every selected slice (starting from the first) in the Z stack for the calculated number of slices:

$$\textit{number of slices to analyse} = \textit{final z slice} - \textit{first z slice}$$

The mean (of the mean) pixel intensity for the selection is calculated by first determining the sum of the mean grey values for the slices analysed divided by the number of slices. The mean (of the mean) grey value is then stored for the vacuole and the results window cleared. This process is repeated for the nuclear and cytoplasmic selections. Next, the normalised grey values are calculated; since the vacuole should not contain any GFP-tagged clock proteins, it acts as a baseline GFP autofluorescence/noise marker. The vacuolar mean grey value is removed from the nuclear and cytoplasmic grey values and

the new values placed in the results table. The nuclear:cytoplasmic ratio is then determined:

$$\text{nuclear: cytoplasmic ratio} = \frac{\text{nuclear mean grey value} - \text{vacuolar mean grey value}}{\text{cytoplasmic mean grey value} - \text{vacuolar mean grey value}}$$

Finally, the nuclear and cytoplasmic variance is divided by the mean grey value of nuclear and cytoplasmic pixel intensity (a measurement similar to F_V/F_M):

variance: mean grey value

$$= \frac{(\text{nuclear} - \text{vacuolar mean grey value}) - (\text{cytoplasmic} - \text{vacuolar mean grey value})}{((\text{nuclear} - \text{vacuolar mean grey value}) + (\text{cytoplasmic} - \text{vacuolar mean grey value})) / 2}$$

Vacuolar-normalised ratiometric values are used instead of background values to account for inter-image differences in autofluorescence, background noise, interference, and laser reflection as a result of the growth media etc. This process could be expanded further to determine corrected total cell fluorescence (CTCF) but could continue to utilise the intracellular vacuole as a background:

$$\text{CTCF} = \text{integrated density} - (\text{volume of selection} \\ * \text{mean fluorescence of vacuolar selection})$$

Where integrated density is the sum pixel intensity of the selection in n slices (the total fluorescence within the measured volume) (400,401).

No filters or processing techniques are applied to these images, and the macro does not iterate over images in a folder because of the heavy reliance on manual inputs.

A new results table is then constructed, showing the mean grey values for the vacuole, nucleus, and cytoplasm, along with the vacuole-normalised nucleus and cytoplasm mean

intensity, the nuclear:cytoplasmic ratio, and the variance:mean grey value, which can be saved to a user-defined file location for further analysis (Fig. 3.8).

Results

	Label	Mean grey value
1	vacuolar	1.276
2	nuclear	5.002
3	cytoplasmic	1.807
4	nuclear - vacuolar	3.726
5	cytoplasmic - vacuolar	0.531
6	nuclear:cytoplasmic	7.016
7	$(\text{nuclear-cytoplasmic variance})/((\text{nuclear+cytoplasmic})/2)$	1.501

Figure 3.8: Example output results file from the confocal analysis macro. Results here suggest that the GFP signal is comparatively higher in the nucleus than the cytoplasm.

3.3 Discussion

This chapter has discussed current and previous approaches to biological imaging and image analysis, and has introduced novel approaches to morphological and phenotypic analyses in fungi and plant-pathogen interactions, both on the micro- and macro-scale. All of the tools here could benefit researchers with their standardised and (semi-) automated processing, giving rise to reliable and consistent results in a manner much faster than manual methods.

The tools presented here were used regularly for data acquisition and analyses presented in chapters 4, 5, and 6. All FIJI-based macros are included in the supplementary materials and are commented for clarity, indicating regions to be altered for independent use (such as the HSB thresholding parameters).

4 Diurnal and circadian growth, development, and pathogenicity of *Magnaporthe oryzae*

4.1 Introduction

4.1.1 Environmental time signals: Zeitgebers

Most organisms live in a dynamic environment, where light quality and quantity, temperature, humidity, and nutritional availability are under a constant state of flux (181,212). On a daily basis, dawn brings increased light and temperature alongside a decrease in humidity, and dusk is associated with cooler temperatures, reduced light levels, and increased humidity. Further, time of day often correlates with certain stressors (201,402) like in the middle of the day, when temperature and light levels are highest, both UV and desiccation stresses are common issues for an organism to overcome (107,181,192). An ability to anticipate these environmental changes, and alter growth, behaviour, and physiology, can consequently confer increased fitness, survival, and reproduction (82,139,181). Indeed, most, if not all, organisms can adapt to a changing environment in some capacity (139,403,404). When plants are exposed to salt stress, for example, where sodium accumulates to toxic levels, they actively regulate ion homeostasis and alter their cytoskeletal dynamics and cell wall composition to buffer against the damage caused by the increased salt content (113,405). Circadian reprogramming of responses, which may subsequently include plant salt stress responses (113), is fundamentally different from longer-term, chronic adaptations, in that these changes occur on a daily basis and, importantly, in a transient manner (140,208,239,245,406–410). In order to adapt to a changing environment, however, organisms must first sense these dynamic conditions (212,411–413).

Light (or lack, thereof) is one of the most important environmental cues to organisms, as it denotes time of day and correlates with other potential stressors such as increased temperature, desiccation, UV stress, and reduced humidity (139,180,191,248,377,414). Signals at dawn and dusk are especially important environmental cues; dawn provides light after a long period of darkness, and dusk subsequently removes this signal. Light and temporal cues to photoreceptors are then interpolated and ultimately affect an organism's behaviour, metabolism, growth and development (181,182,388,415–417).

The evolution of photoreceptors allows for the perception of light wavelengths and intensity, and photoreceptors are, therefore, well conserved across phyla and bring numerous benefits (108,113,259,415). Accordingly, different Classes of photoreceptors are found in nature: phytochromes are responsible for red and far-red light sensation, rhodopsins green, and cryptochromes, phototropins, and Light Oxygen Voltage (LOV - an amino acid motif associated with circadian rhythmicity and molecular signalling) photoreceptors sense blue and UV-A light, with UVR8 sensing UV-B light (113,142,418–422). Together, the sensation of intensity, quality and ratio of light determined by these photoreceptors can provide important environmental, temporal, and spatial information, as certain wavelengths and fluence rates are associated with specific times or stressors, as mentioned above (109,150,180,181). For example, at dawn and dusk there is relatively high red compared to blue light (due to blue light being scattered by the atmosphere when sunlight has a longer path to travel at these times), which is why we experience orange/red skies at either end of the day; indeed, the ratiometric abundance of different light wavelengths can vary significantly throughout the day and year (discussed in detail by (423) and also covered by (215,422,424–429)).

Other environmental sensation mechanisms also exist, such as those for temperature, humidity, and nutritional status, which act in tandem to provide further contextual information to the organism sensing these cues (82,139,182,191,248,259). There are also more nuanced and indirect cues for time of day, such as the intercellular reactive oxygen species (ROS) content; a timekeeping and photoreceptor protein complex in *Neurospora crassa*, the White Collar Complex (WCC) may be able to sense the cellular redox state of the cell due to the presence of the PAS (PER (Period circadian protein) - ARNT (Aryl hydrocarbon receptor nuclear translocator protein) - SIM (Single-minded protein)) and LOV domains, which may subsequently feed into the timekeeping mechanism of the fungus (184). This is unsurprising, given that redox states of cells fluctuate on a daily basis, both independently and as a result of environmental stressors (109,113,430). High energy UV light, for example, can generate ROS and cause cellular damage, but also acts as a proxy for time of day, where high UV (and subsequently ROS) levels are associated with mid-day (431,432).

Many organisms can anticipate potential future challenges in their surroundings based on previous environmental conditions and life history through a process called entrainment (122,422,433). This anticipation of fluctuating changes in the environment can facilitate increased fitness and survival in the outside world, as organisms can alter their physiology, behaviour, growth, and development in advance, to better match their environment (82,139,411). Entrainment is the process by which an organism synchronises these parameters and subsequently sets its endogenous clock to align with its external, rhythmic environment; it may then continue to run in an asynchronous or continuous environment, such as constant light or darkness (182,184). At its core, diurnal rhythms are those which are synchronous, but entirely dependent on environmental

cues, whereas circadian rhythms also synchronise, but can continue to run (for some time) without these inputs, at least after a period of entrainment (103,144,231) (Fig. 4.1). Circadian rhythms are also temperature and/or nutritionally compensated and can continue to occur under a range of physiologically relevant temperatures or nutritional states (181). Diurnal rhythms, on the other hand, will cease to occur in free-running conditions and are dependent entirely on current environmental conditions (117,183,434). Indeed, Circadian rhythms are endogenous timekeeping mechanisms that can allow an organism to regulate its growth, development, physiology, behaviour, and metabolic state in an arrhythmic environment but are principally important in fine tuning the organism's response to a constantly changing, but (somewhat) predictable environment, and are particularly useful in adapting to e.g. seasonal changes where day length can be significantly longer or shorter (113,181,249). It is important to note here that the asynchronous and constant conditions that organisms are submitted to in the laboratory would rarely, if ever, be experienced in the wild: several days of completely constant conditions (light, temperature, pH, nutritional status etc.) is a near impossibility in the real world. Summarily, circadian clocks rely on sensory mechanisms (predominantly light, temperature, and nutritional status) as an input, and a central oscillating transcriptional-translational feedback loop (TTFL) that alters the circadian output parameters: growth and development, behaviour, physiology, and metabolic state, which change based on circadian time over a roughly 24 h period (181). Circadian rhythms are, therefore, defined as having a period of approximately 24 h that can persist in free running conditions under physiologically relevant temperatures and nutritional states. Circadian rhythms in some form are found across almost all genera of life and are essential to many (144,181,435,436).

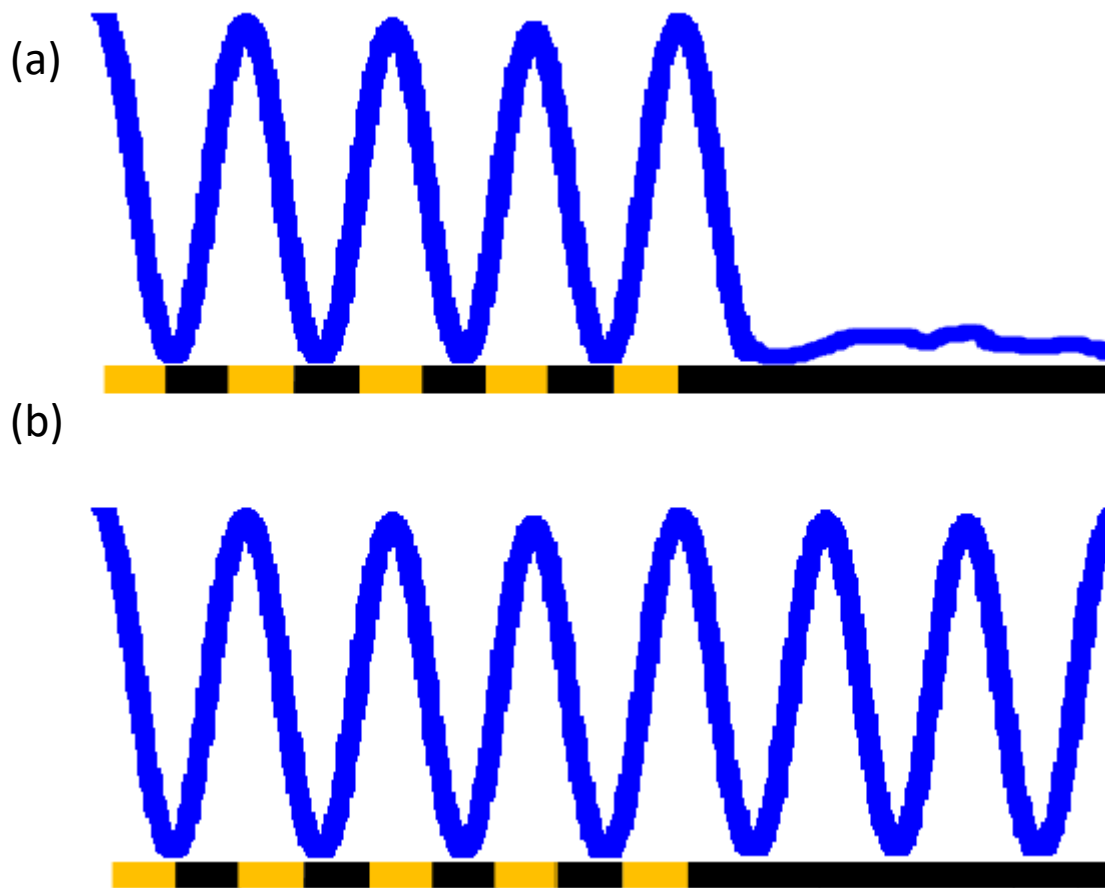


Figure 4.1: Diurnal and circadian outputs. (a) Diurnal outputs are wholly dependent on environmental conditions and do not display rhythmicity under constant conditions, whereas (b) circadian rhythms can continue to occur roughly every 24 h, even in free-running conditions, such as constant light or darkness.

4.1.1 Fungal circadian rhythms

In fungi, the TTFL generally consists of a positive arm which promotes the transcription and translation of the negative arm; the negative arm components then repress the activity of the positive arm – a process that takes approximately 24 h to complete (161,178,193,234). For *Neurospora crassa*, the model fungal species for circadian studies (and member of the Sordariomycetes, like *M. oryzae*), the clock machinery predominantly relies on two core protein complexes: the FFC and WCC (228,231). Briefly, early in the circadian morning, Frequency (FRQ) is promoted by the White Collar Complex (WCC), which is a multiplex of White Collar 1 (WC1) and White Collar 2 (WC2) (231,437). As FRQ protein is produced, it dimerises and interacts with FRH (FREQUENCY INTERACTING RNA HELICASE) and Casein Kinase 1 (CK1) to become the FFC (161,177,222). Nuclear-localised FFC phosphorylates the WCC, preventing its DNA-binding capability, and thus FRQ represses its own transcription by preventing the WCC from acting as a transcription factor for *frq* – this is the negative arm of the clock (161,228). Concurrently, FRQ stabilises functional WC-1 and upregulates *wc-2* transcript, acting in the positive arm (178,216,221,222). When FRQ is rendered inactive due to hyperphosphorylation and is eventually turned over by the proteasome, the WCC can again interact with the *frq* promoter (161). This fine-tuned transcription, translation, phosphorylation, and localisation of the core circadian clock components causes activity levels to rise and fall at certain times of the day to ensure a cyclical ~24 h loop (for a comprehensive description of the WCC and FFC, see chapters 5 and 6, respectively, and (178,181,190,221,257)). The fungal circadian clock influences many essential components of growth and development, and has been implicated in: cellular metabolic potential, sexual and asexual development and conidiation, cellular osmotic regulation,

melanisation, cellular redox state, growth rate, and virulence of pathogens (177,178,181,184,190,192,194,217,377,438,439). Considering that approximately 40% of the *Neurospora* genome is clock controlled, there are undoubtedly more circadian outputs to be discovered (181).

When grown on petri dishes or 'race tubes' (long tubes with a thin layer of media on the base), *N. crassa* and many other fungal species including *M. oryzae* produce characteristic pigmented bands of conidia during the dark period of the day-night cycle (82,181,259,378). When transferred from cycling conditions into free running light or dark, rhythmic conidiation may continue for a number of circadian cycles, and as such is an excellent visual indicator of a functional circadian clock (181). In some fungal species, such as *Verticillium dahliae*, this conidiation pattern is not circadian, merely diurnal (434). Importantly, a lack of a visual circadian phenotype, such as conidial banding, does not necessarily mean that the organism has no functional circadian machinery, as there are clear molecular rhythms displayed without a banding pattern present in some fungi like *Aspergillus nidulans* (191). While there are many conserved clock components throughout the fungal kingdom, there is still much research required to fully elucidate the role and presence of circadian rhythms in fungi (82,84,101,112,117,122,171,174,177,178,181,188,189,191,194,198,212,225,228,230,232,240,257,258,370,392,404,408,412,415,418,430,434,438,440–459).

4.1.2 Plant circadian rhythms

In plants, the circadian system operates in a similar manner, utilising interlinked TTFLs (172). For *Arabidopsis*, the most commonly-studied circadian plant model, there are three main transcriptional-translational feedback loops that are expressed throughout

the circadian day, with specific morning and evening oscillators (169,172). TOC1 (Timing of CAB expression 1), a PRR (Pseudo-Response Regulator) gene, closes one loop, three TOC1 paralogs, PRR5, PRR7, and PRR9 close a second loop, and LUX (LUX ARRHTHMO), a Myb transcription factor, closes the third loop (169,172). In the morning oscillatory pathway, CCA1 (Circadian Clock-Controlled 1) and LHY (Late Elongated Hypocotyl) repress the afternoon-expressed TOC1, PRR5 (Pseudo-Response Regulator 5), PRR7, and PRR9 (139,169,172). TOC1 and the PRR proteins repress CCA1 and LHY expression in a comparable fashion to FRQ in the fungal clock (139,169,172). CCA1 and LHY also interact with the evening complex, consisting of ELF3 (Early Flowering 3), ELF, and LUX (139). Positive regulators of clock genes play a significant role in the fine tuning of subjective time throughout the circadian day: afternoon-expressed MYB-like transcription factors REVEILLE4 (RVE4), RVE6, and RVE8 promote the expression of several clock genes including TOC1 and PRR5, which then feed into the other clock feedback loops (139). As relative expression levels of morning, afternoon, and evening complexes rise and fall due to overlaps in promotion and repression, the subjective time of the plant is fine-tuned to synchronise with the external environment, based on inputs of the clock such as light and temperature as mentioned above (139,169,172).

Essentially, circadian rhythms allow for synchronisation, responsiveness and priming of organisms to predictable environmentally favourable (for growth, development, and fitness) or stressful conditions (404). Indeed, the plant clock goes on to control several outputs; increased responsiveness to light during the day, hormonal signalling and regulation, regulation of photosynthesis and respiration, growth, development and flowering, and even abiotic and, crucially, biotic stress responses are all gated in a circadian manner (122,139,144,146,249,411).

4.1.3 Circadian rhythms in plant pathology

The virulence of plant pathogens and concurrent susceptibility of plants to those pathogens is, in some species, dependent on time of day and circadian status (82,101,103,109,112,121,122,137,139,140,144,144,149,150,152,158,180,228,244,253, 257,414,419,430,456,460). Many fungal species, as mentioned above, produce and release conidia during the dark period under light-dark (LD) cycles and thus the conidia may have functional clocks to gate their germination and development to best utilise environmentally favourable conditions for successful pathogenesis (82,101,104,111,117,177,257,422). Likewise, if there are certain times of day when pathogens are likely to be present in a plant's vicinity, they, too, may gate an immune response to anticipate pathogenic attack (103,120,136,142,144,152,159,160,163,173,251,419,461). The maintenance of an immune system in plants is energetically expensive, so restricting the activity of the immune system to coincide with certain times of day associated with high pathogenic load would allow plants to divert their resources to other important processes, such as growth and development (115,141,257,460).

The entry mechanism of a pathogen into the host plant may be a temporal and circadian factor influencing timing of virulence traits. To this end, pathogens that enter through the stomata are only able to infect the host when the stomata are open, whereas pathogens that have evolved penetration structures such as appressoria, or produce lytic enzymes to degrade the host cuticle, do not face the same constraints (101,103,111,122,144,145,149,152,158–160,212,255,257,404,422). Further, it has been reported that stomatal pore size is a rhythmic output, where they generally begin to open just prior to dawn, remain open throughout the day, and begin to close as the dark period

(where photosynthesis cannot occur) draws near (255) . It is therefore possible that stomatal plant pathogens may be physically restricted by the plant to only infect between dawn and dusk, whereas other pathogens with specialised modes of entry could potentially infect at any time of day, perhaps gating their virulence for times more amenable to infection (122,158,422,462). Indeed, *P. syringae*, a stomatal-infecting pathogen is 'primed' by the dark period, where they begin to express virulence traits just prior to dawn (422). Additionally, *M. oryzae* (which utilises appressoria) has been observed to show altered pathogenicity at certain times of day and after exposure to light; *M. oryzae*-infected rice plants exposed to light shortly after inoculation display reduced disease severity compared to those placed in the darkness (101), and Arabidopsis infections also show that *M. oryzae* is able to penetrate older leaves at dusk better than younger leaves, a difference not observed at dawn (253). This surprising result may be due to tissue-specific alterations in the clock, as it has been reported that vascular and mesophyll clocks run asymmetrically, and the root clock can act as a slave oscillator to above-ground foliar tissue (145,253,463–465). Neither of these articles considered (or at least did not disclose) the pre-inoculation entrainment conditions of *M. oryzae*, which may have an important role in the outcome of disease, as is the case in *B. cinerea* (117).

There have been multiple reports of *M. oryzae* having some functional photoreceptors and core clock genes homologous to *N. crassa*, with a potentially functional circadian clock (82,101,259,457), however their role in pathogenesis is yet to be fully elucidated. This chapter describes the circadian and diurnal behaviour of *M. oryzae*, and the effect of pre-inoculation entrainment and timing of infection on the virulence of the pathogen and susceptibility of the host plant is investigated. *M. oryzae* colonies were submitted to

different light cycles and nutritional conditions to determine how light and media composition affects growth, development, conidiation, and conidial behaviour ex-planta, and how these pre-inoculation conditions ultimately determine severity of infection in rice (*Oryza sativa* cv. CO-39) and barley (*Hordeum vulgare* cv. Golden Promise).

4.2 Results

4.2.1 Identification of core clock components and photoreceptors in *M. oryzae*

There have been several reports in the literature of conserved genes coding for photoreceptors and circadian machinery across diverse members of the fungal kingdom (84,101,104,108,110,116,137,161,178,181,190,194,212,228,235,240,371,377,420,434,437,438,442,448,451,452,457,459,466–468) and a select number of publications that have implicated the presence of these same genes in *M. oryzae* (82,84,101,194,206,259,373,469), however a collated view of prospective *M. oryzae* photoreceptors and circadian genes has yet to be discussed.

A comprehensive literature review of *M. oryzae* photoreceptor and clock machinery was performed and Protein BLAST (470) analysis was carried out to determine homologous proteins (and subsequent genes) between *N. crassa* and *M. oryzae*, followed by a comparison of the (predicted) protein motifs (based on the Ensembl Fungi protein domains and features (471,472), which includes a wide range of databases, such as Pfam, PROSITE, SMART) between the two species to further infer the presence of a functional circadian clock (Table 1.1, 4.1, and 6.2 discussing accessory and core clock genes). Based on the available literature and comparative protein sequences, there is likely a functional circadian clock in *M. oryzae*. Of particular note in the literature is the rhythmic expression of a light-responsive gene, TWILIGHT, (84) and FRQ under light-dark (LD) and constant

dark (DD) conditions (259), the specific timing of conidial release (82,101), and the comparative genomics for putative photoreceptors (104), all of which are convincing evidence of a functional circadian oscillator in *M. oryzae*.

Table 4.1: Putative and confirmed *M. oryzae* clock and photoreceptor genes

<i>N. crassa</i> gene	<i>M. oryzae</i> gene	Function	% Cover (BlastP)	% Identity (BlastP)	Common domains and features (Ensembl Fungi)	References
PHY-1	MGG_12377	Red light photoreceptor	84	64.58	C-terminal histidine kinase, phytochrome domain	(82,104)
VVD	MGG_01041	Blue light photoreceptor	72	52.69	PAS/LOV domain	(82,101,104)
NOP-1	MGG_09015	Green light photoreceptor	82	32.53	Archaeal/bacterial/fungal rhodopsin domain	NA
WC-1	MGG_03538	Blue light photoreceptor, forms the WCC (positive clock element)	87	54.72	PAS domains, GATA-type zinc finger transcription factor	(82,101,104,457)
WC-2	MGG_04521	Forms the WCC (positive clock element)	64	61.77	PAS domain, GATA-type zinc finger transcription factor	(82,457) (see chapter 5)
FRQ	MGG_17345 – MGG_17344 (misannotation; NCBI predicted ORF finder)	Forms the FFC (negative clock element) (see chapter 6)	78	41.1	6 potential SPXX sites, 3 potential cAMP and cGMP-dependent protein kinase phosphorylation sequences, 4 potential PEST domains, N-terminal coiled-coil domain, disordered domain, and 7 predicted helix regions	(82,258,259,457) (see chapter 6)
FRH	MGG_03931	Forms the FFC (negative clock element)	91	70	ATP-dependent RNA helicase Ski2, C-terminal, DEAD/DEAH box helicase domain, Helicase superfamily 1/2, ATP-binding domain, Helicase, C-terminal, P-loop containing nucleoside triphosphate hydrolase, rRNA-processing arch domain	(178,457)
CK1	MGG_02829	Forms the FFC (negative clock element)	100	89.23	Protein kinase domain, ATP binding site	NA
FWD1	MGG_09696	Interacts with ubiquitylated FRQ for turnover in the proteasome	70	55.34	F-box domain, WD40 repeats	(259,457)

4.2.2 *M. oryzae* displays diurnal rhythmic conidiation under white, blue, and green light

In a similar fashion to *N. crassa*, *M. oryzae* exhibits alternating light and dark bands denoting different developmental phases when grown under environments with a light-dark (LD) cycle (Fig. 4.2). Each dark band is produced at subjective night-time, when *M. oryzae* conidia melanise (215) and the concentric rings are formed approximately every 24 h. Freezer stocks of *M. oryzae* wild type Guy11 were placed on petri dishes with complete media (CM) and exposed to 12 h – 12 h light-dark cycles under white, blue, green, or red LED light (iLC colour changing light bulb) with peak wavelength emissions at 460nm, 520nm, and 630nm, respectively) (see 2.1). Under LD conditions, there was no significant effect of light quality on *M. oryzae* growth rate (data not shown), but red light consistently produced fewer/no conidial bands after 6 – 8 d of growth, in contrast to colonies grown under blue, green, or white light (Fig. 4.2). This is in agreement with several articles, where red light has little effect on conidial banding, and blue light is the chief entrainer of the clock (82,110,184,191,194,256,257,371,379,434,473,474). It is important to consider here that a lack of conidial banding does not necessarily imply that the circadian clock or red light photoreception is non-functional, as many fungal species can detect and respond to red light (82,104).

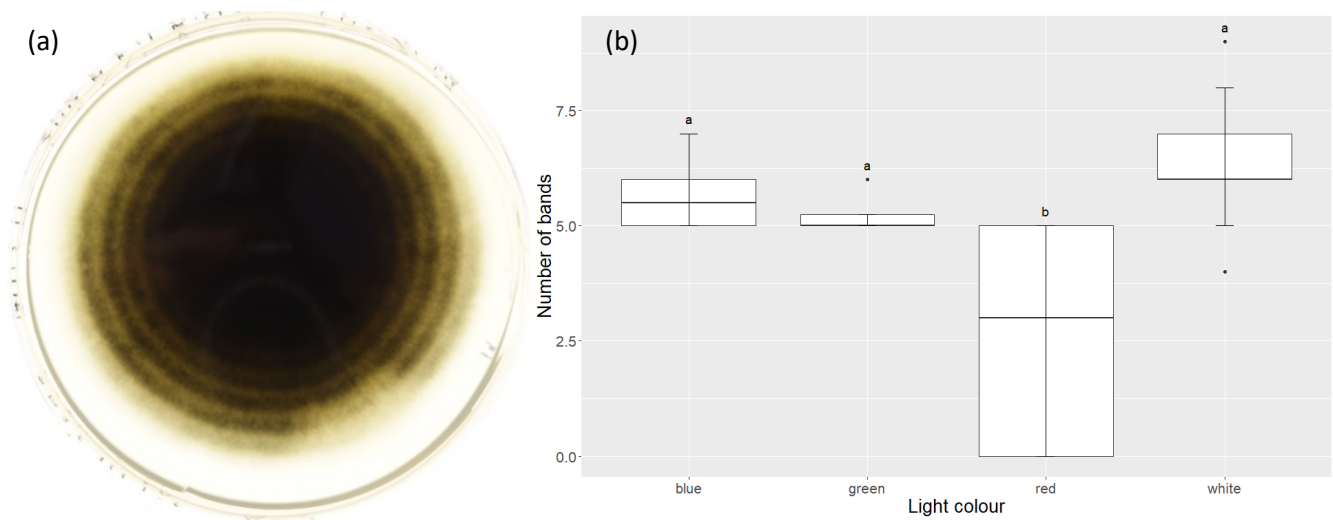


Figure 4.2: *M. oryzae* exhibits diurnal conidial banding, which is chiefly controlled by blue light. (a) *M. oryzae* colonies grown on petri dishes display light and dark bands of melanised conidia that occur on a daily basis, (b) colonies grown for 14 d on CM under red light/dark (L/D, 12 h) cycles display significantly fewer bands than those grown under blue, green, or white L/D cycles. (6 individual colonies were examined for each light treatment n =24). Letters describe statistically significant differences between groups (p < 0.05, Tukey's HSD).

4.2.3 *M. oryzae* has a nutritionally compensated circadian conidial banding phenotype

M. oryzae does not display any conidial banding when grown for 14 d under constant light or constant darkness and as such, periods of light and dark are important entraining signals for this rhythmic output (Fig. 4.3). However, if a sufficient period of entrainment under LD conditions occurs, *M. oryzae* can continue to produce conidial bands for a number of circadian cycles after transfer to both constant light (LD-LL) and dark (LD-DD) (Fig. 4.3). Once entrained, there is little effect of the length of time spent in constant conditions: there is no significant difference in the number of conidial bands produced by 14 d old colonies after 2, 4, or 7 d in constant conditions, suggesting that the output is circadian, as colonies grown for a shorter period of time in constant conditions would otherwise produce more conidial bands (Fig. 4.3). To further study circadian rhythmicity, serological pipettes with a thin layer of CM were produced, acting as race tubes for long term growth under differing conditions. Colonies were grown for 12 d under LD conditions, then transferred from LD cycling conditions to constant conditions for 10 d. Conidial banding continued for several days under these free running conditions (Fig. 4.3). Intriguingly, the intensity and clarity of conidial bands when moved back into cycling LD conditions is much greater than before, which could be the result of a build-up (or lack) of photoactivatable proteins – in *N. crassa*, for example, VVD levels fall rapidly and remain low under constant darkness, which causes a subsequent increase in photosensitivity (see 5.1 and 6.1 (214,475)). In addition to *M. oryzae* requiring an entraining signal for conidial banding, the fungus also shows a significant ‘latency’ period of 6 – 8 d, where colonies do not undergo conidial banding, and instead show continuous melanised growth, giving rise to a dark ‘bullseye’ phenotype at the centre of the colony (Fig. 4.3)

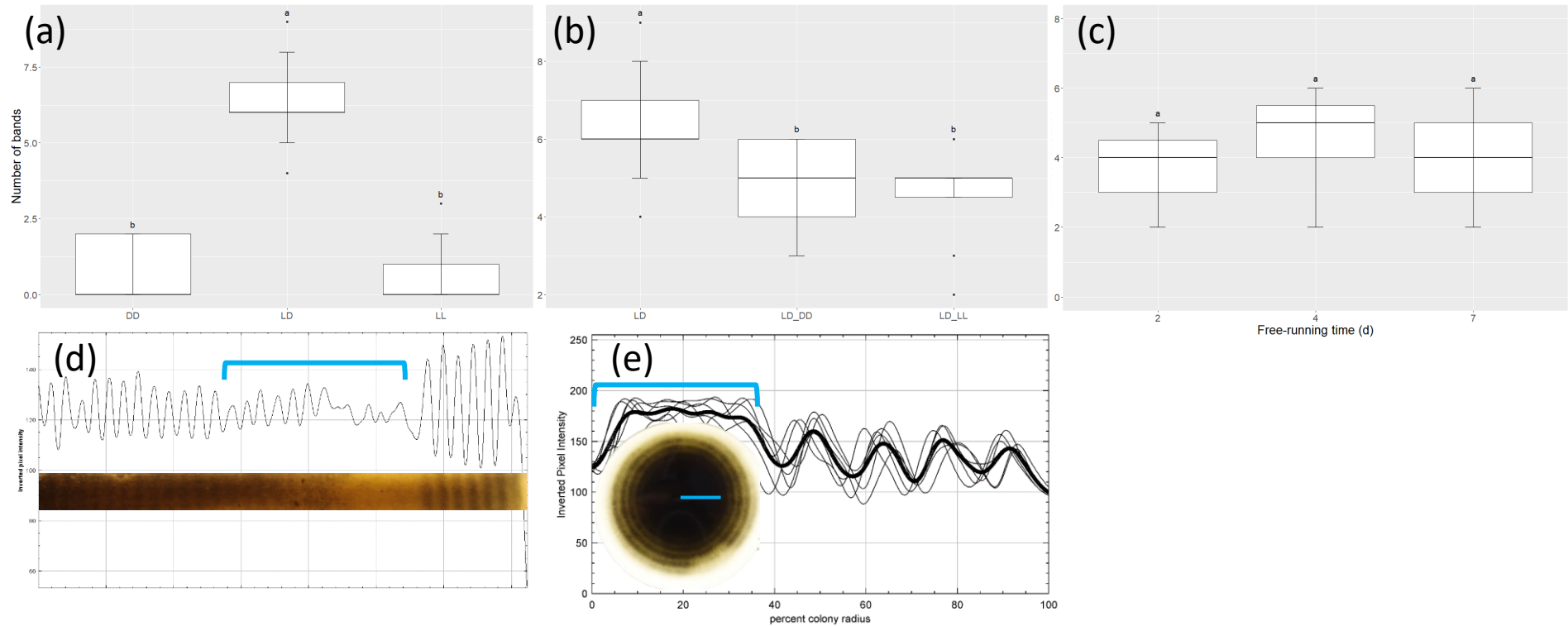


Figure 4.3: *M. oryzae* displays circadian conidial banding after sufficient entrainment. (a) *M. oryzae* requires light dark cycles for conidial banding, even after 14 d growth (16 DD colonies, 18 LL colonies, 23 LD colonies, $n = 57$), (b) conidial banding can continue to occur when transferred to constant conditions ($n = 23$ LD, $n = 15$ LD-DD, $n = 15$ LD-LL), (c) and can occur after 7 d of entrainment (11 2-day free-run colonies, 8 4-day free-run colonies, 5 7-day free-run colonies, $n = 18s$), (d) upon returning to LD cycling conditions, the conidial banding amplitude is increased (the blue line denotes 10 d of growth under constant conditions), (e) a latency period of approximately 6 – 8 d exists, prior to which conidial banding does not occur (blue bands denote the latency period). Letters describe statistically significant differences between groups ($p < 0.05$, Tukey's HSD).

As well as entraining the conidial banding, LD cycles also reduce the average radial colony growth rate; those grown under constant conditions tend to grow slightly quicker on average than those under cycling conditions (Fig. 4.4). However, once colonies begin to produce conidial bands, the average growth rate increases significantly, beyond the rate of those grown in constant conditions, suggesting that, after the latency period has ended, the gating of conidiation and vegetative growth allows for increased fitness (Fig. 4.4).

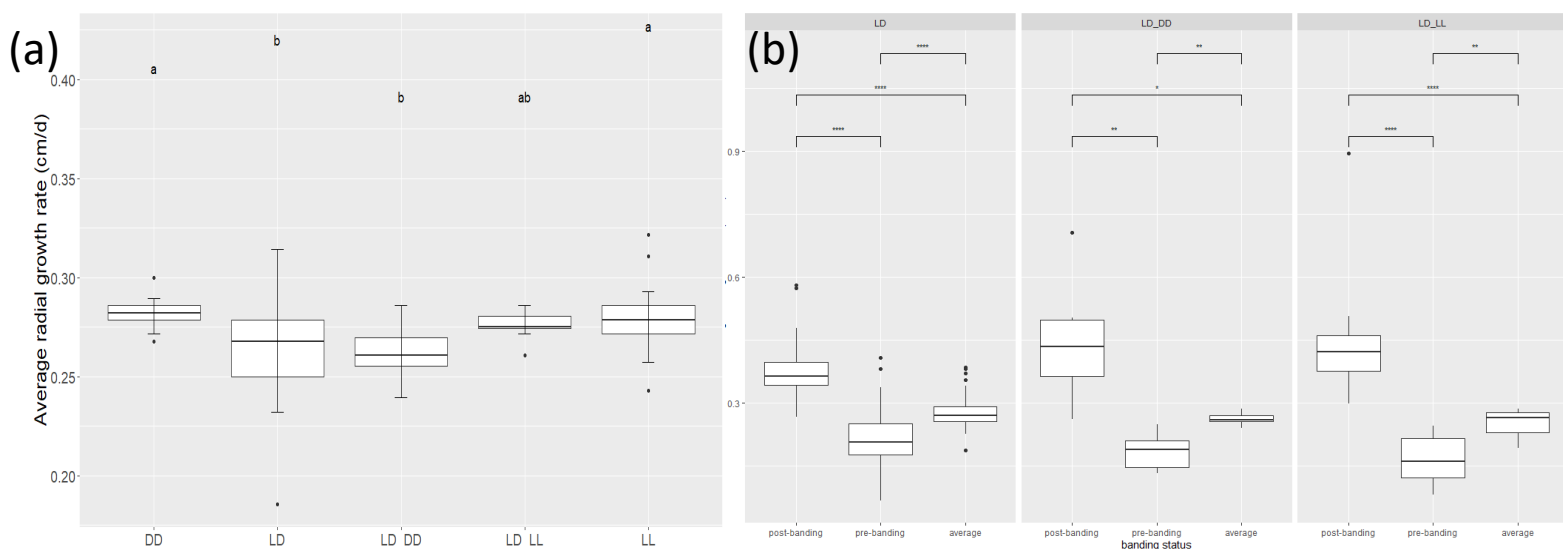


Figure 4.4: *M. oryzae* growth rate is affected by the photoperiod. (a) Over a period of 14 d, average colony radial growth rates are higher under constant conditions, but (b) growth rates are increased once the latency period ends, and conidial banding begins (n = 16 DD, n = 20 LD, n = 15 LD-DD, n = 13 LD-LL, n = 19 LL). Letters describe statistically significant differences between groups (p < 0.05, Tukey's HSD), bars with stars atop denote statistically significant differences (p < 0.05, ANOVA).

Once the average post-latency growth rate has determined, it is possible to approximate the period (in h) between each conidial band:

$$Period (h) = \frac{\text{average distance between bands (cm)}}{\text{post-latency growth rate (cm/d)}} \times 24$$

In a similar fashion to many fungal species, when transferred to constant conditions, the period of the *M. oryzae* clock is slightly shorter than those grown under cycling LD conditions, but, importantly, the period is still close to 24 h, which is further evidence of a functional circadian clock (Fig. 4.5). The continuation of conidial banding in constant conditions is also conserved across a range of nutritional statuses, whilst the growth rate and the latency period are significantly affected by the media on which *M. oryzae* is grown. Once banding does occur, the calculated period is still very close to 24 h (Fig. 4.5).

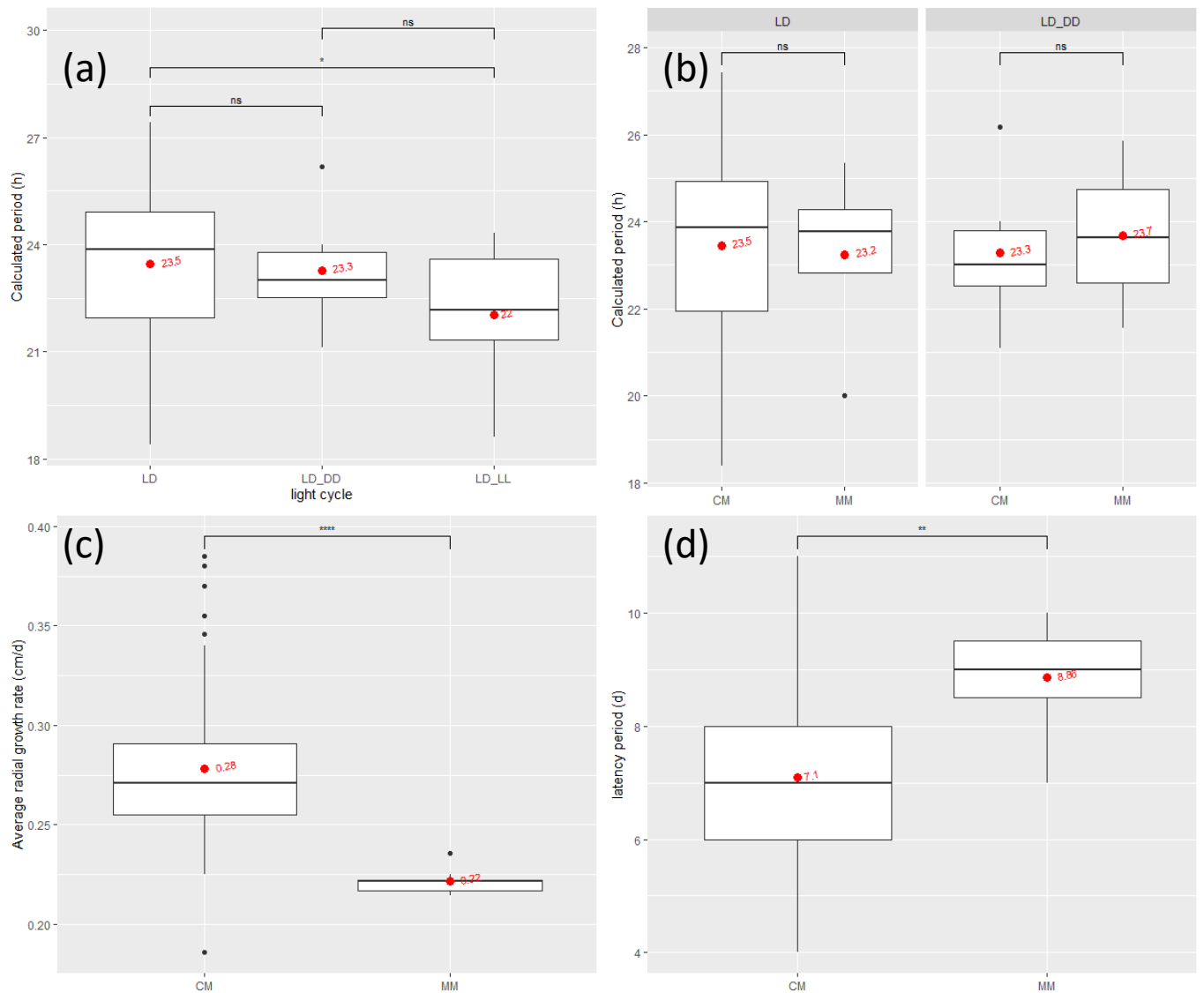


Figure 4.5: Media composition affects *M. oryzae* growth rate and latency period, but not circadian periodicity. (a) like many fungal species, the innate period of the clock is slightly faster than 24 h ($n = 23$ LD, $n = 15$ LD-DD, $n = 15$ LD-LL), and (b) the ~ 24 h period of the circadian clock is maintained under different growth media ($n = 23$ LD CM, $n = 5$ LD MM, $n = 13$ LD-DD CM, $n = 5$ LD-DD MM). Reduced nutritional content (c) slows the colony growth rate, and (d) increases the latency period ($n = 23$ LD CM, $n = 5$ LD MM). Bars with stars atop denote statistically significant differences ($p < 0.05$, ANOVA), red points and text show the mean values for each group.

4.2.4 *M. oryzae* produces metabolite(s) responsible for the switch to conidial banding

Having observed that the latency period can be altered depending on nutritional status, attempts were made to determine what was responsible for the switch to diurnal conidial banding. First, it was considered that the switch could be due to the consumption and subsequent lack of specific nutrients: under minimal media and half strength CM (where all constituent nutrients are half as concentrated), the latency period either increased or remained within the usual 6-8 d period, suggesting that nutritional scarcity does not cause the switch to conidial banding (Fig. 4.6). Since the optimal media pH often differs depending on composition and fungal species (and can subsequently change as the colony grows), the effect of pH on latency period was tested. *M. oryzae* was grown on CM petri dishes with pH (adjusted with either NaOH or HCl) ranges between 5 and 8: all colonies began to band between 6-8 d as usual (Fig. 4.6).

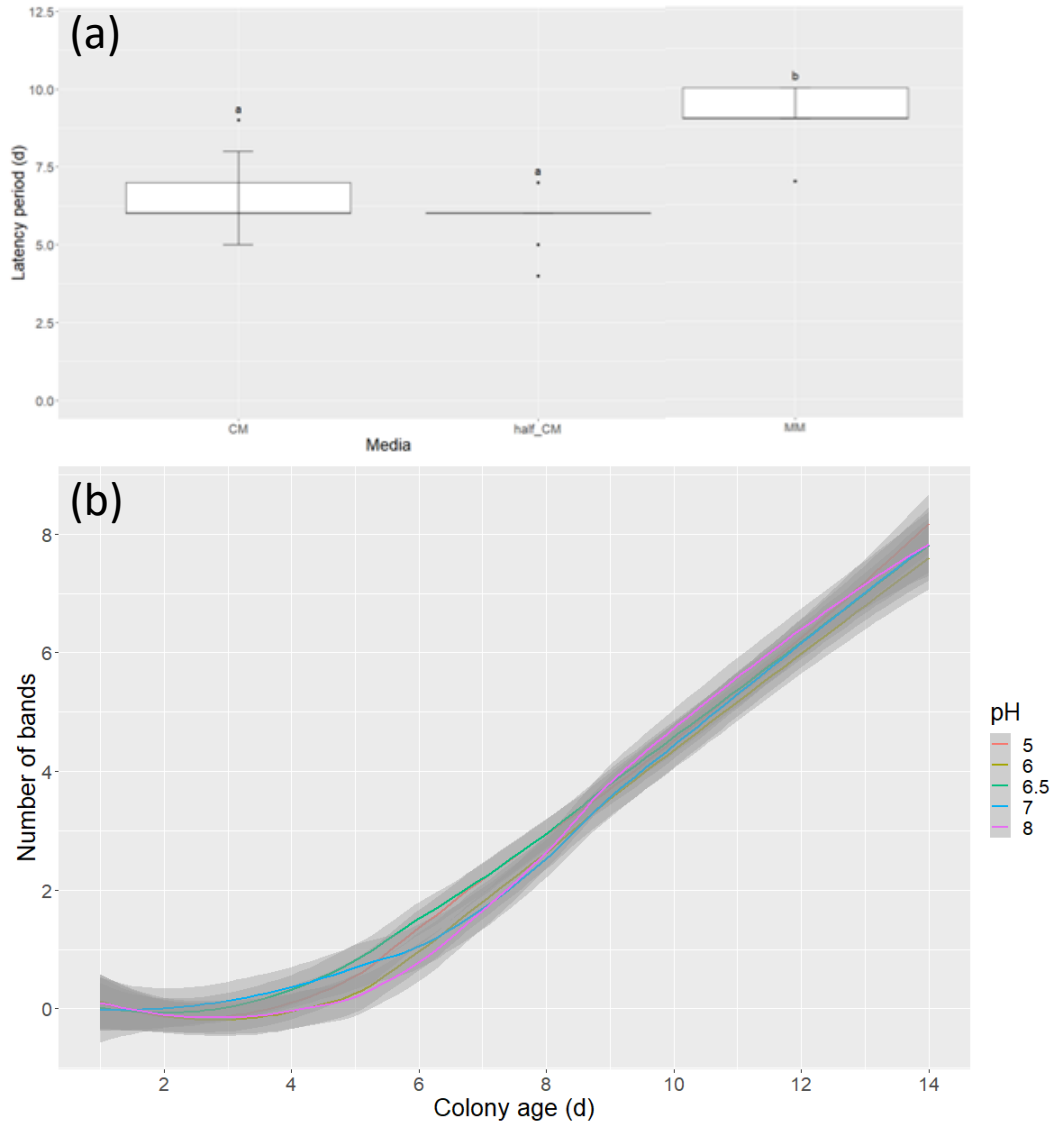


Figure 4.6: Nutritional scarcity and media pH does not cause the switch to conidial banding. (a) colonies grown on nutrient-poor media do not band earlier than those grown on nutrient-rich media ($n = 23$ CM, $n = 10$ strength half CM, $n = 5$ MM), and (b) physiologically relevant pH levels do not significantly alter the latency period ($n = 5$ for each pH treatment, grey shading denotes the standard error). Letters describe statistically significant differences between groups ($p < 0.05$, Tukey's HSD)

Finally, the possibility of a build-up of waste products/secreted metabolite(s) over time was proposed, which could be responsible for the switch to conidial banding. To address this, *M. oryzae* was grown in shaking cultures for at least 7 d (the average latency period) until they were melanised (see materials and methods). 2x CM was then diluted with the spent media (SM) to create a 1x CM with 50% v/v SM content (see materials and methods). Remarkably, the latency period in the SM plates was consistently reduced by 2 d, and the average growth rate was increased (Fig. 4.7). The increase in average growth rate was unsurprising considering that *M. oryzae* grows faster post-conidial banding (Fig. 4.4)

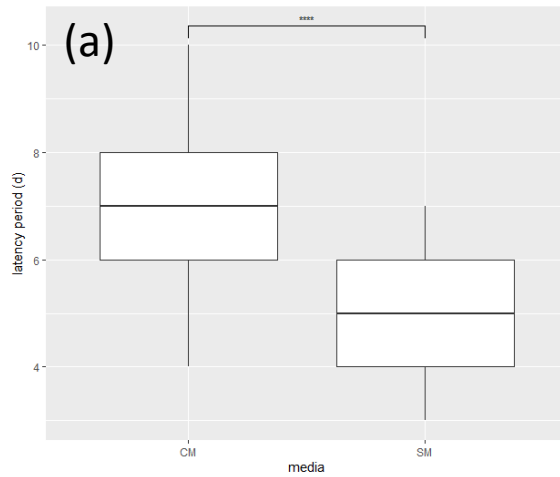
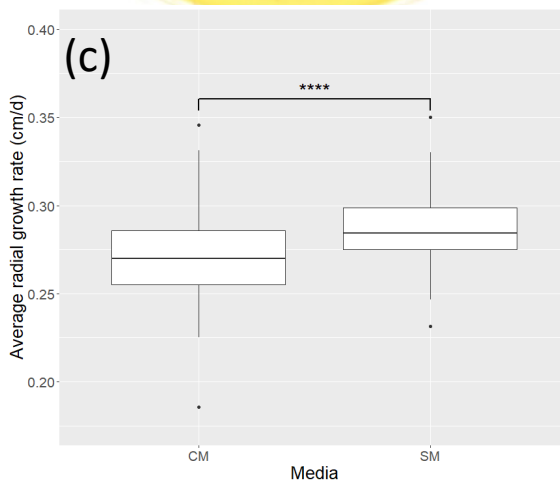
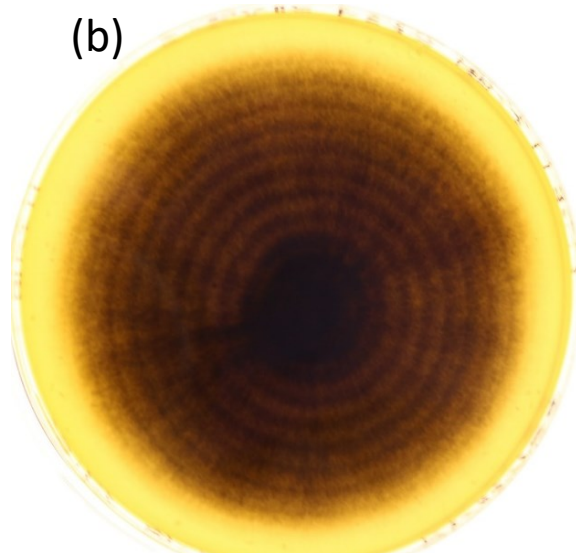


Figure 4.7: Spent media metabolite(s) are responsible for the conidial banding switch. (a, b) The addition of SM to the growth medium reduces the latency period by approximately 2 d, and (c) the addition of SM or the early conidial banding facilitates an increased growth rate in *M. oryzae* (wild type guy11). Stars represent increasing statistical significance (ANOVA, n=23 CM, n = 17 SM).



To confirm that the latency reduction and growth rate increase was not due to an excess of nutrients, *M. oryzae* colonies were grown on double concentrated CM plates: the latency period was consistently between 6-8 d (data not shown), while the growth rate was not significantly altered. A series of dilutions of SM prior to adding it to double concentrated CM was then performed (ensuring that the final nutrient concentration was still at least 1x CM). Relatively high concentrations of SM are required to produce the early banding phenotype, but there may be a dose-dependent effect on the latency period (Fig. 4.8). Further, when shaking cultures were grown under slower speeds or increased media volume (which both serve to reduce colony aeration), the subsequent cultures were non-melanised and the effect of SM on the latency period was dampened, further suggesting that secreted product(s) or metabolite(s) are responsible for the conidial banding switch (Fig. 4.8).

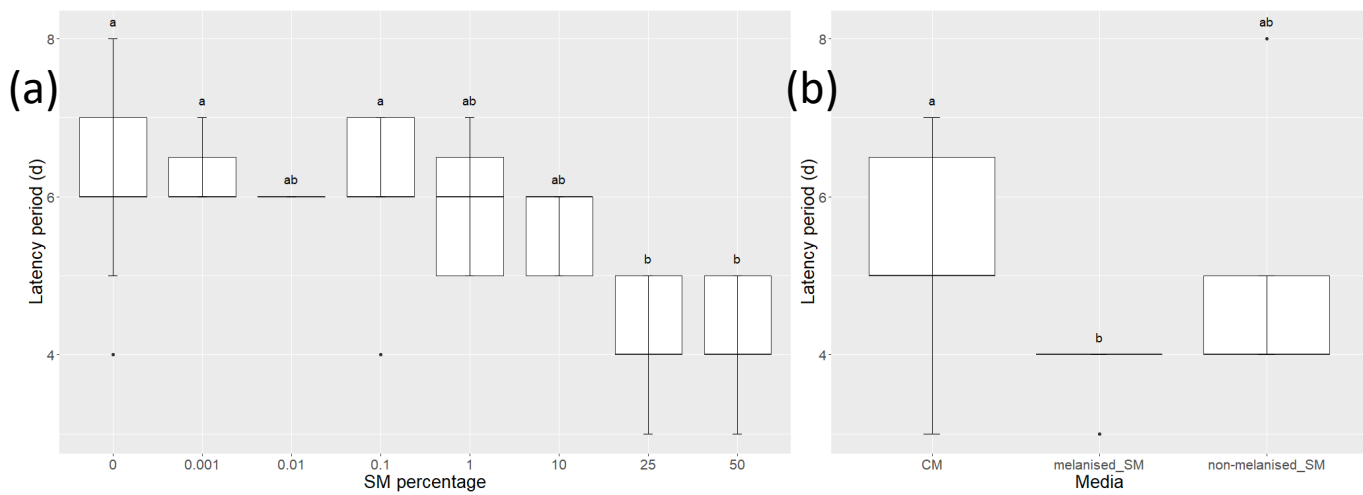


Figure 4.8: The conidial banding metabolite is dose-dependent and is affected by colony aeration. (a) SM is effective at high concentrations (colonies grown for 10 d under LD conditions; n = 25 0%, n = 3 0.001%, n = 3 0.01%, n = 9 0.1%, n = 7 1%, n = 6 10%, n = 14 25%, n = 23 50%), and (b) shaking culture aeration and subsequent melanisation affects the potency of the spent media (n = 10 per treatment). Letters describe statistically significant differences between groups ($p < 0.05$, Tukey's HSD)

To further elucidate if secreted metabolite(s) alter the latency period, *M. oryzae* was grown for 10 d on cellophane discs that were placed on top of CM. The cellophane was subsequently peeled off along with the growing colony, and fresh CM was poured on top of the thin layer of spent solid media underneath to produce two layers of media. These plates were then inoculated with a new colony. As opposed to producing melanised conidia for the first several days post inoculation, as is typical for colonies grown on CM, there was significant inhibition of melanised biomass, and a light-coloured 'halo' of vegetative growth surrounded the inoculation point, suggesting that high concentrations of *M. oryzae* metabolites inhibit conidiation (Fig. 4.9). Further, the metabolite(s) must be relatively mobile due to this observation occurring on the additional media layer.

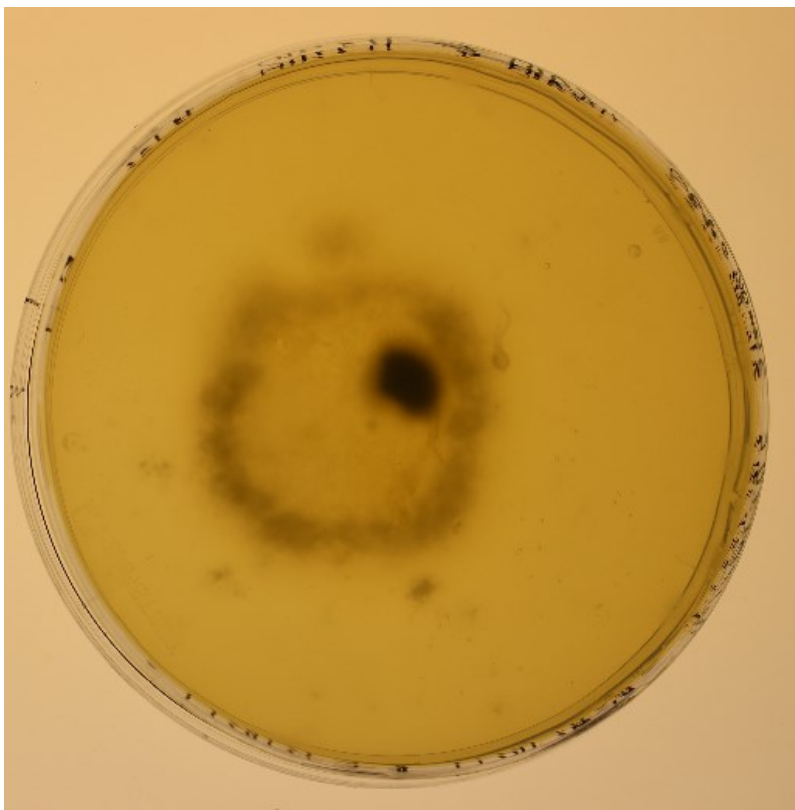


Figure 4.9: Mobile *M. oryzae* metabolite(s) can inhibit early conidiation. Spent media from previous *M. oryzae* colonies underneath a layer of fresh complete media can almost completely arrest melanisation for several days.

Specific timing of the metabolite(s) production was then considered. A 3D-printed autoclavable nylon 'raft' with a honeycomb-shaped mesh was produced that a cellophane disc could be placed atop, allowing for liquid media to be introduced (and removed) underneath (Fig. 4.10). The holes allow for media to reach the growing fungal colony whilst the cellophane disc kept it separate from the liquid media below. When grown in liquid cultures, the metabolite(s) are secreted into the media in a cumulative fashion, making it difficult to determine the timing of production. Here, the raft allowed for the liquid media beneath to be siphoned off and replaced with fresh media every 2 d for 10 d. The spent media temporal fractions were then tested for the conidial banding switch by adding the SM to double concentrated CM as above. Interestingly, the early banding phenotype was most pronounced with media harvested from the 4–6-day old colony, i.e., just before the switch to diurnal banding on conventionally-grown solid CM colonies (Fig. 4.10). Banding differences in *M. oryzae* were unable to be determined on the cellophane disc due to atypical colony growth.

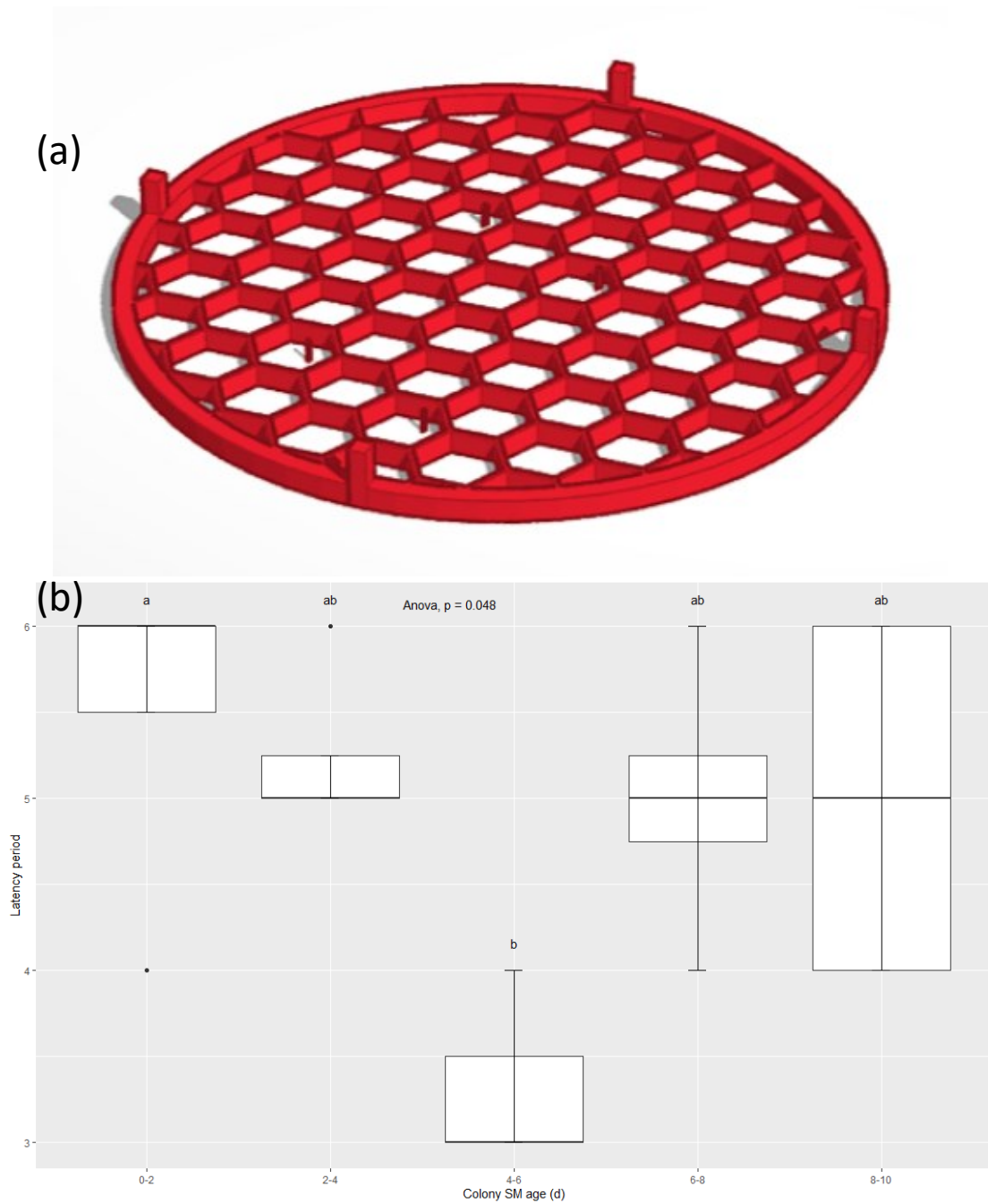


Figure 4.10: The conidial banding metabolite is predominantly produced just prior to banding. (a) a 3D-printable nylon raft that fits in a 9 cm petri dish, containing liquid media below, (b) the banding metabolite is likely produced just prior to the switch to conidial banding ($n = 3$ per treatment). Letters describe statistically significant differences between groups ($p < 0.05$, Tukey's HSD).

Finally, to determine if the conidial banding metabolite(s) was common to other plant pathogenic species that display similar phenotypes, *Verticillium dahliae* shaking cultures were grown under the same conditions as *M. oryzae*. *V. dahliae* neither produces nor is sensitive to the metabolite(s) responsible for the conidial banding switch in *M. oryzae*, as colonies began to band at roughly the same age on both 50% SM plates and CM plates (Fig. 4.11). Further, *V. dahliae* SM did not cause an early banding phenotype in *M. oryzae* (Fig. 4.11). This data, along with the fact that the SM is still effective after filtration (media tests were also conducted after filtration through 0.45 μm filter syringes and 10 kD pore size centrifuge filters), long-term refrigerated storage, and autoclaving, suggests that there are non-protein secreted metabolite(s) responsible for the switch to conidial banding and vegetative hyphal growth.

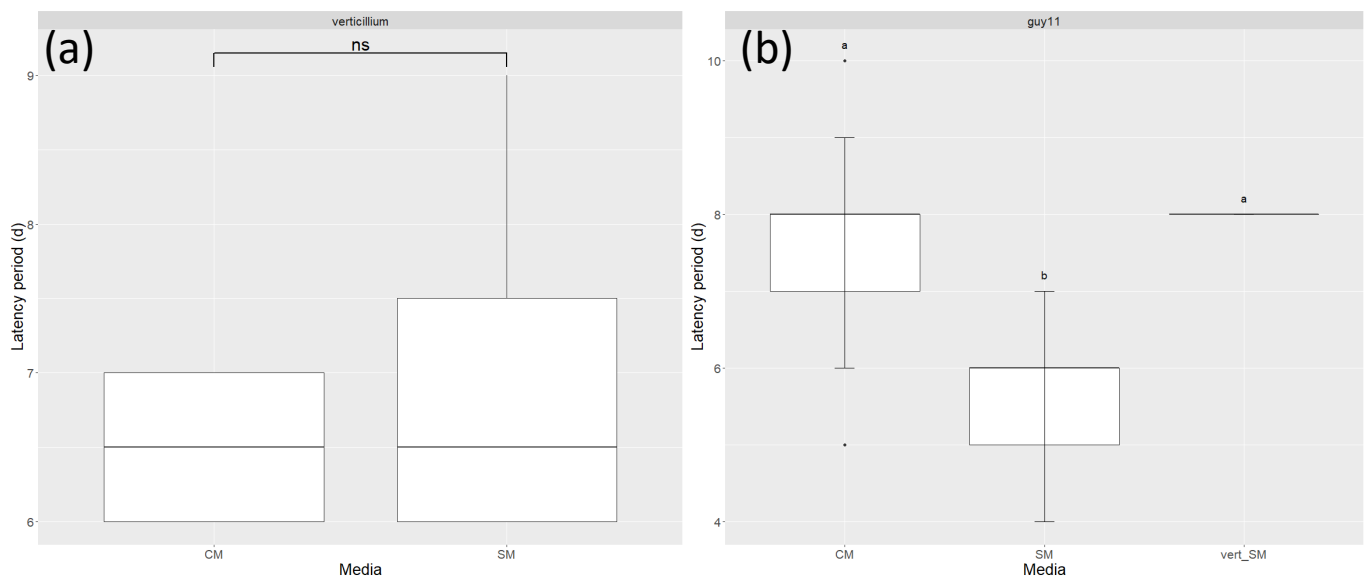


Figure 4.11: *V. dahliae* does not produce, and is insensitive to, the conidial banding metabolite(s). (a) *V. dahliae* does not display early conidial banding when grown on *M. oryzae* SM (n = 4 per treatment), and (b) *M. oryzae* colonies grown on 50% *V. dahliae* SM do not display early conidial banding (n = 23CM, n = 17 SM, n = 3 *V. dahliae* SM). Letters describe statistically significant differences between groups (p < 0.05, Tukey's HSD).

In summary, whilst different media can affect the latency of the conidial banding phenotype, the circadian period (h) when in free running conditions is maintained at roughly 24 h after sufficient entrainment and as such *M. oryzae* has a nutritionally compensated circadian conidiation rhythm (Fig. 4.12).

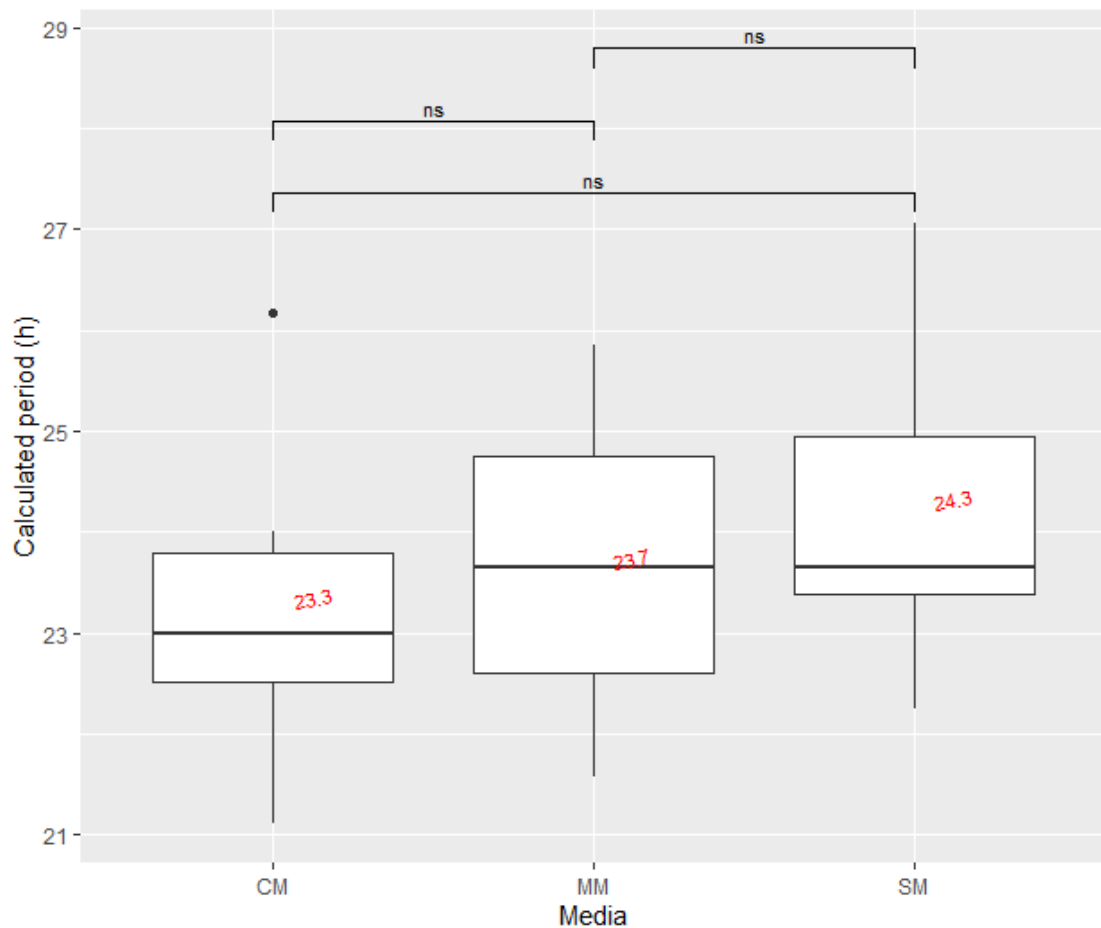


Figure 4.12: Despite showing altered latency periods on different media, *M. oryzae* maintains a conidial banding period of ~24 h under constant conditions. (n = 23 CM, n = 6 MM, n = 17 SM, bars show individual ANOVA comparisons, 'ns' denotes no significant difference between groups, and red text denotes mean values)

4.2.5 Environmental entrainment conditions affect conidiation and conidial development

There have been many reports in the literature about how environmental light conditions and circadian rhythmicity can affect conidiation in fungal species (82,101,108,110,150,181,184,257,259,404,413,418,442,452,476–479). The subsequent observation of a conidial banding phenotype in *M. oryzae* grown under cycling light-dark conditions suggested a possible role of light conditions and entrainment in conidiation and conidial development.

The *M. oryzae* wild type strain Guy11 was grown under constant conditions (DD or LL), 12 h LD, or LD followed by constant conditions (LD-DD or LD-LL) as described above. Conidia were then harvested (as described in materials and methods) and conidial counts were determined using a haemocytometer. Constant conditions with or without entrainment significantly reduces conidiation compared to colonies grown under LD cycling conditions (Fig. 4.13). Further, there is no significant difference in conidiation between colonies harvested at dawn as opposed to dusk, suggesting that conidia may be produced at night-time the previous day (data not shown). There was no time of day effect on conidiation within any of the pre-harvest entrainment conditions, which is surprising, but the fact that time of day had no effect under any circumstances likely means that it takes more than 12 h for *M. oryzae* to produce mature conidia. Finally, in contrast to the increased growth rate and early banding phenotype on 50% SM plates, conidiation is actually lower than the plates CM plates (Fig. 4.13).

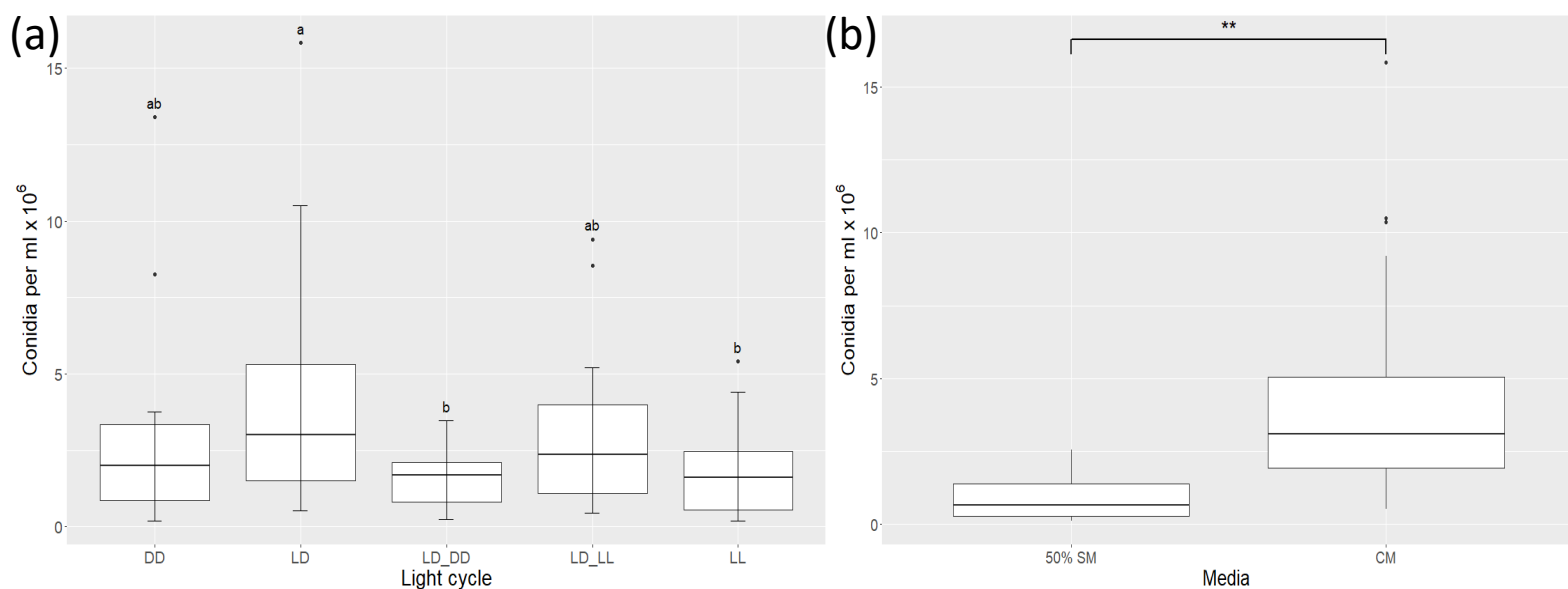


Figure 4.13: Light conditions and media composition affect conidiation in *M. oryzae*. Conidiation is reduced by (a) constant light and dark conditions (n = 10 DD, n = 56 LD, n = 14 LD-DD, n = 11 LD-LL, n = 13 LL), and (b) high levels of spent media (n = 56 LD, n = 6). Bars with stars atop denote statistically significant differences (p < 0.05, ANOVA), Letters describe statistically significant differences between groups (p < 0.05, Tukey's HSD).

For conidial development assays, petri dishes were harvested at dawn or dusk after 12 d growth in constant conditions (DD or LL), LD, or 10d LD followed by 2 d constant conditions (LD-DD or LD-LL). Conidial development was then tracked using an OpenFlexure RPi system (see 3.2.4). In a similar fashion to conidiation, conidial germination and development is not affected by harvest time (data not shown), suggesting that once conidia are produced and land on a hydrophobic surface, they germinate at a relatively consistent rate. However, whilst pre-harvest treatment has no effect on conidial germination, by 8 h post inoculation (HPI), conidia grown under constant conditions (LL or DD) showed significantly reduced appressorial development compared to those grown under LD cycling conditions (Fig. 4.14). Appressorial developmental rate is not significantly reduced in LD-DD or LD-LL treatments, which could

suggest that circadian entrainment to LD conditions partially aids in appressorial development.

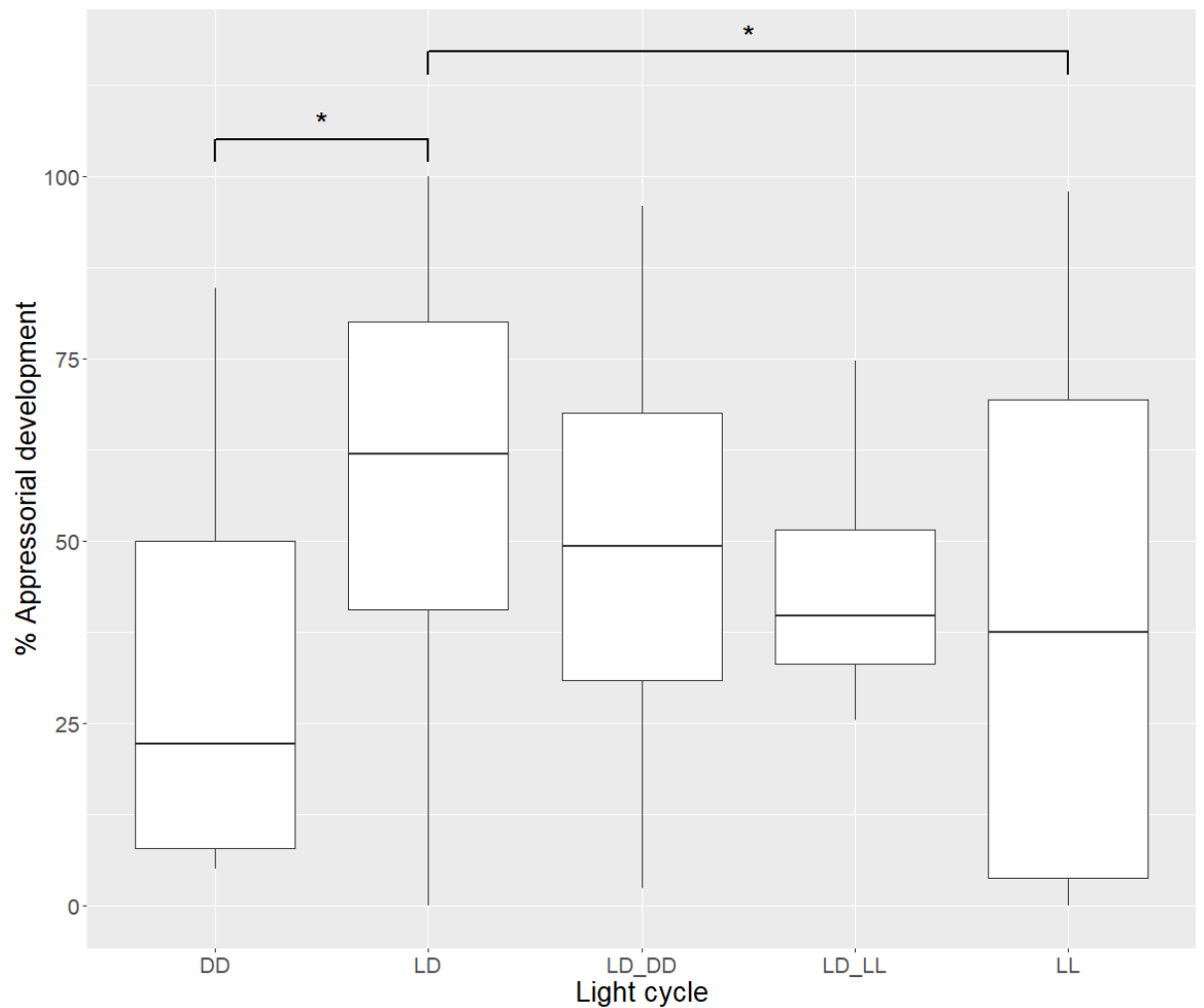


Figure 4.14: *M. oryzae* appressorial development is reduced under prolonged light and darkness. n = 4 DD, n = 23 LD, n = 5 LD-DD, n = 3 LD-DD, n = 6 LL; at least 40 spores were counted per sample. Bars with stars atop denote statistically significant differences ($p < 0.05$, ANOVA).

Intriguingly, high doses of spent media also have a significant inhibitory effect on conidial germination and development. Conidia were harvested as above, centrifuged, and the supernatant replaced with increasing concentrations of *M. oryzae* SM. By 4 HPI, ~50% of conidia had germinated when incubated with 10% spent media, and only ~10% germinated with 50% SM (Fig. 4.15). Further, appressorial development was almost completely arrested in conidia incubated in 50% SM, suggesting waste products or secreted metabolite(s) inhibit conidial development (Fig. 4.15).

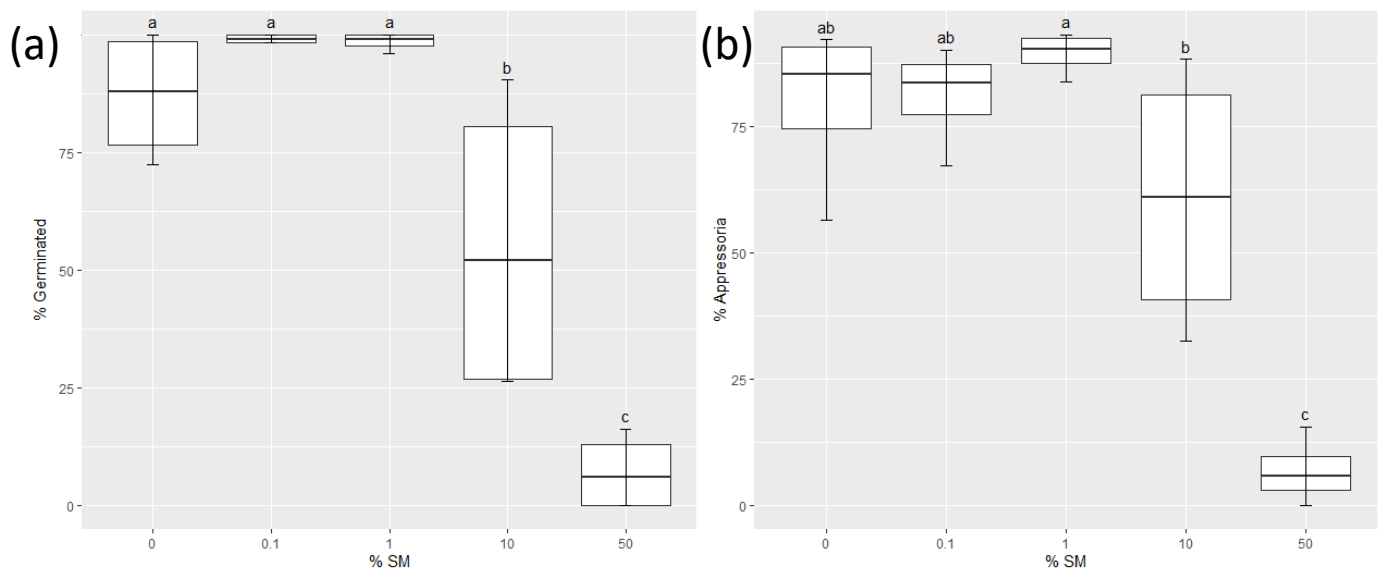


Figure 4.15: High doses of *M. oryzae* SM inhibit conidial development. (a) By 4 HPI, high concentrations (>10%) significantly inhibited conidial germination, and (b) by 8HPI, appressorial development was either reduced or completely arrested (n = 3 per treatment, at least 100 conidia counted per treatment). Letters describe statistically significant differences between groups (p < 0.05, Tukey's HSD)

Considering *M. oryzae* produces conidia during the dark period and actively releases them just prior to dawn (82), the effect of time of day on conidial adherence was considered. Spore tip mucilage is a sticky mucous-like substance that conidia use to adhere to hydrophobic surfaces such as plant leaves, cover slips, and petri dishes. Conidia were harvested as above at Zt 2, 6, 10, 14, and 22, photographed after 15 min, then shaken vigorously (200 RPM for 100 s) and imaged again to determine % conidia remaining (see materials and methods 2.5). There was no observed effect of harvest time on conidial adherence (data not shown), as all timepoints had ~40% of conidia remaining. This is consistent with the lack of dawn vs dusk differences in conidiation and conidial development. Interestingly, though, the conidia remaining after agitation were significantly larger (~10%) than the average prior to agitation, perhaps due to either increased weight or resources available for mucilage production (Fig. 4.16).

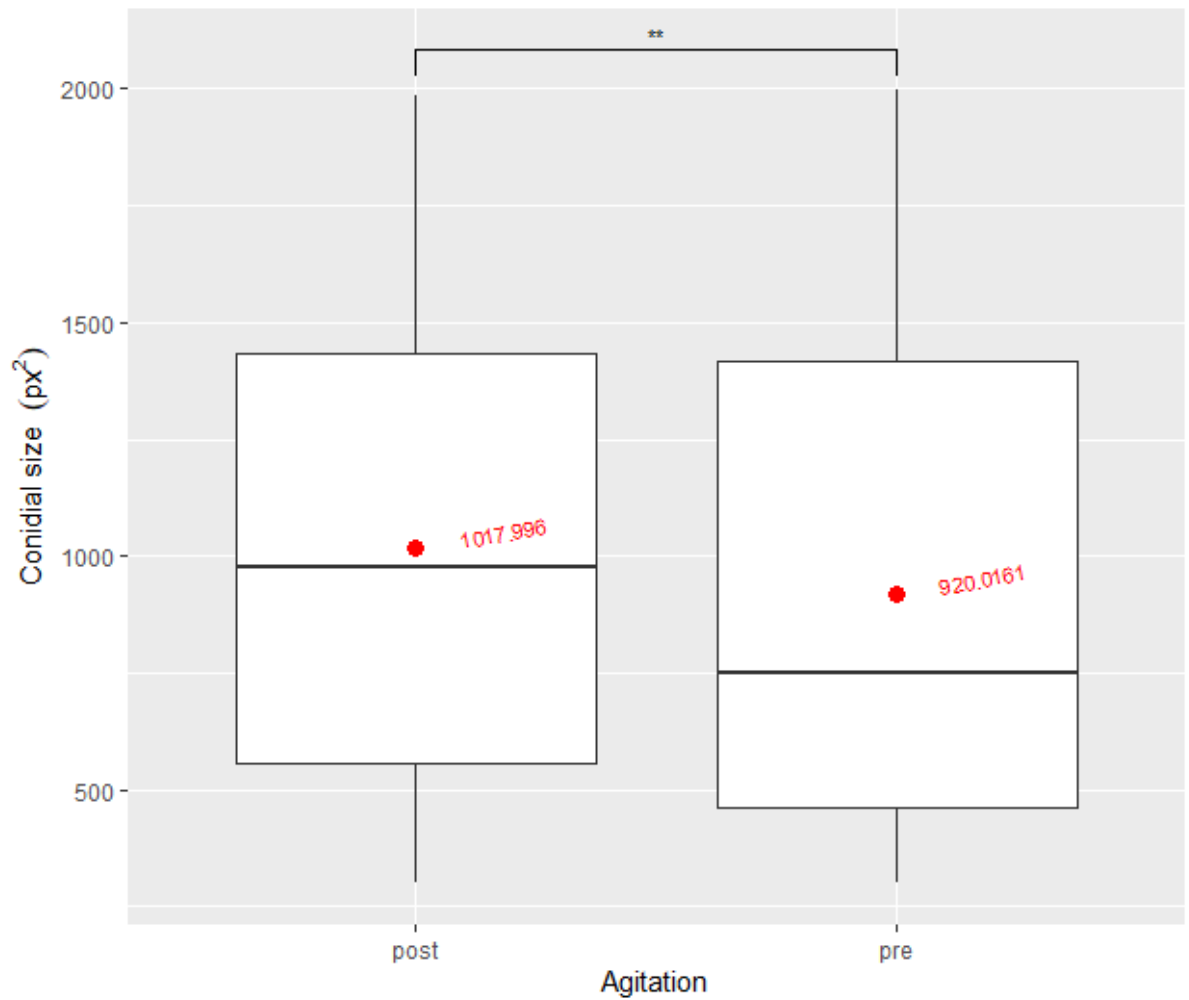


Figure 4.16: Larger conidia adhere to hydrophobic surfaces better than smaller conidia. After agitation, the conidia remaining were, on average, larger than those prior to shaking. $n = 3$, at least 100 conidia were counted per observation. Stars represent increasing statistical significance (ANOVA). Red points and text show the mean values for each group.

There was also no significant effect of pre-harvest light treatment on appressorial cytorrhysis (collapse of the appressoria resulting from osmotic stress caused by increased glycerol content in the solution); appressoria began to collapse at a relatively uniform rate from 0.5 M to 2 M glycerol. Over 70% of appressoria had collapsed at 2 M glycerol, regardless of pre-treatment (Fig. 4.17). Further, the appressorial maturity had no significant impact on cytorrhysis, as the same results were seen when glycerol solutions were added to conidial suspensions at 8, 9, 10, 11, and 12 HPI. These data suggests that once appressoria have been successfully produced, they generate approximately the same amount of turgor pressure.

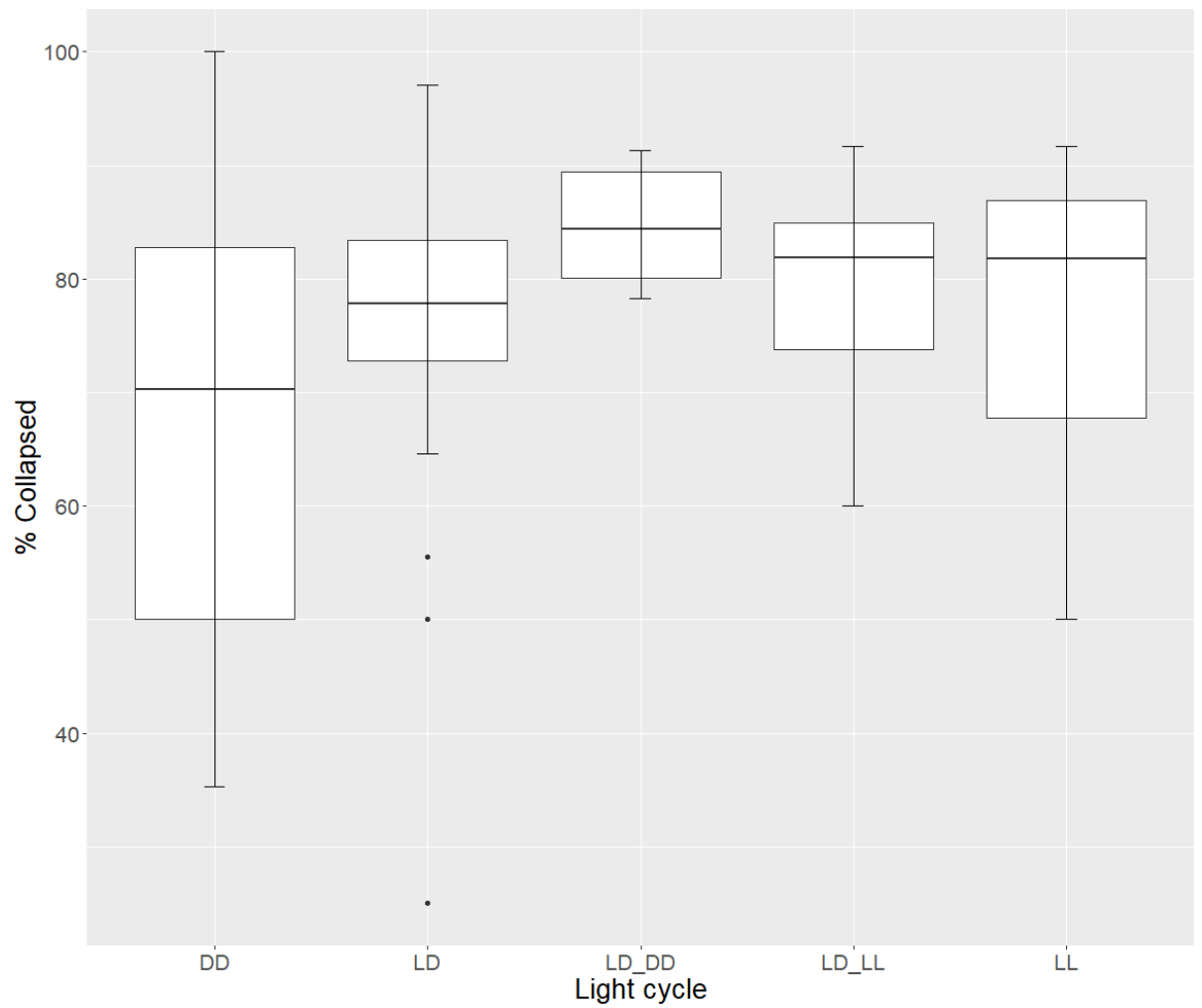


Figure 4.17: Appressorial turgor pressure is not significantly affected by pre-harvest light treatment. There was no significant effect of pre-harvest light cycles on appressorial collapse. $n = 3$ DD, $n = 12$ LD, $n = 3$ LD-DD, $n = 3$ LD-LL, $n = 3$ LL. At least 100 spores were counted per sample.

4.2.6 Time of day and pre-inoculation entrainment affects *M. oryzae* virulence and plant susceptibility

Time of day, light, and circadian rhythms play an important role in the outcome of several plant-pathogen interactions; plants can gate their immune system towards different types of attack depending on the time of day, and pathogens or herbivores can be more virulent in a similar manner (103,107,117,120–122,136,140–142,144,148,150,152,159,160,160,173,228,242–248,250–254,256,257). To this end, after observing the diurnal and circadian behaviour of *M. oryzae* growth *ex planta*, experiments were performed to determine if there was an effect of pre-inoculation entrainment of *M. oryzae* in the outcome of rice blast disease in two economically important cereal crops: rice (*Oryza sativa* cv. Co39) and barley (*Hordeum vulgare* cv. Golden promise). All rice blast inoculations were performed on 3-4 week old plants (grown under 12 h LD conditions) at either dawn or dusk, with 12 d old *M. oryzae* that were entrained prior to infection under constant conditions (LL or DD), 12 h LD (synchronised to the plant growth conditions or 12 h out of phase, DL), or 10 d LD followed by 2 d constant light (LD-LL) (see and 2.1.1, 2.1.2, and 2.8.1).

In rice, *M. oryzae* grown under synchronous LD conditions gave rise larger lesions at dawn compared to dusk, whereas under LD-LL conditions, lesions are larger at dusk compared to dawn. Under constant conditions, DD-grown *M. oryzae* produce larger lesions at dawn and LL-grown colonies produce larger lesions at dusk. Further, DD colonies cause a higher percentage lesion region cover at dawn compared to dusk, and LD-LL and LL colonies cause greater cover at dusk compared to dawn, suggesting that in rice-*M. oryzae* interactions, constant dark and synchronous inoculations favour dawn inoculations whereas elongated light treatment (LD-LL and LL) favour dusk inoculations (Fig. 4.18).

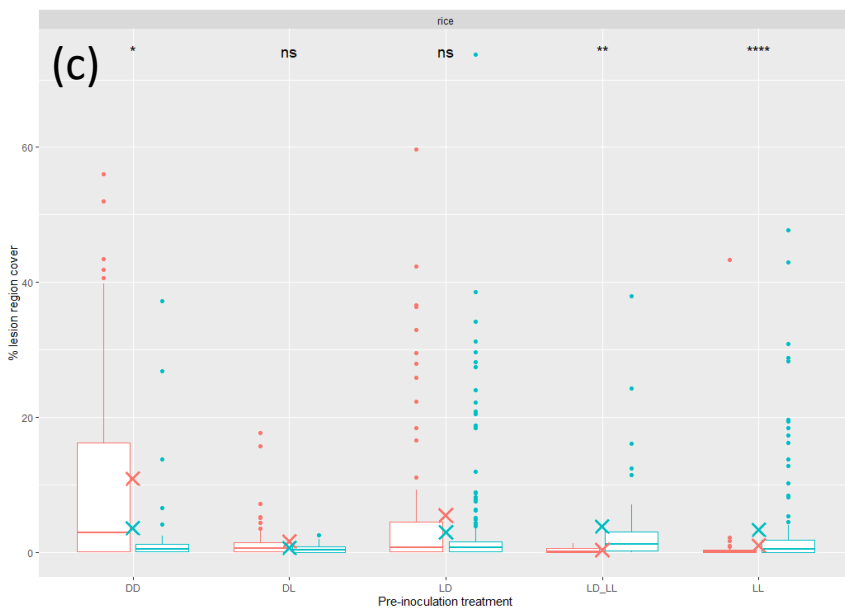
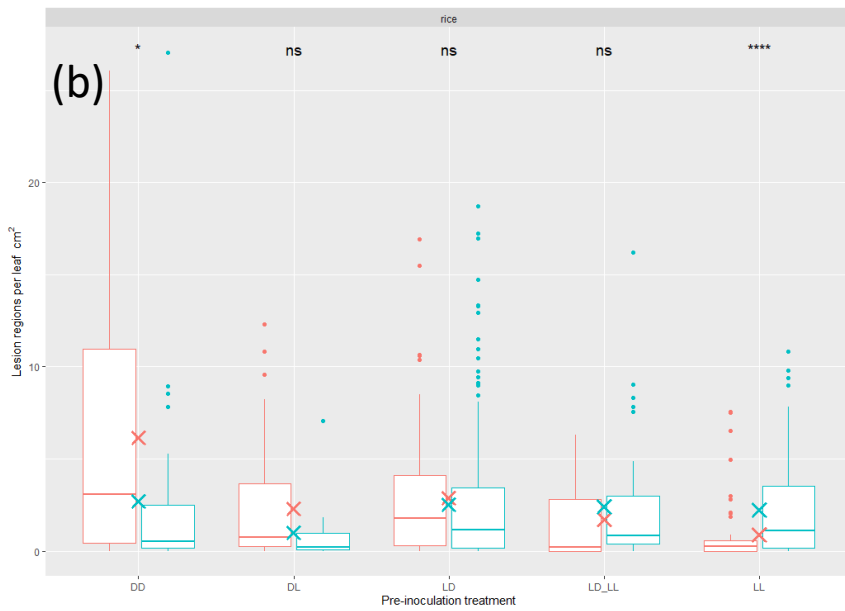
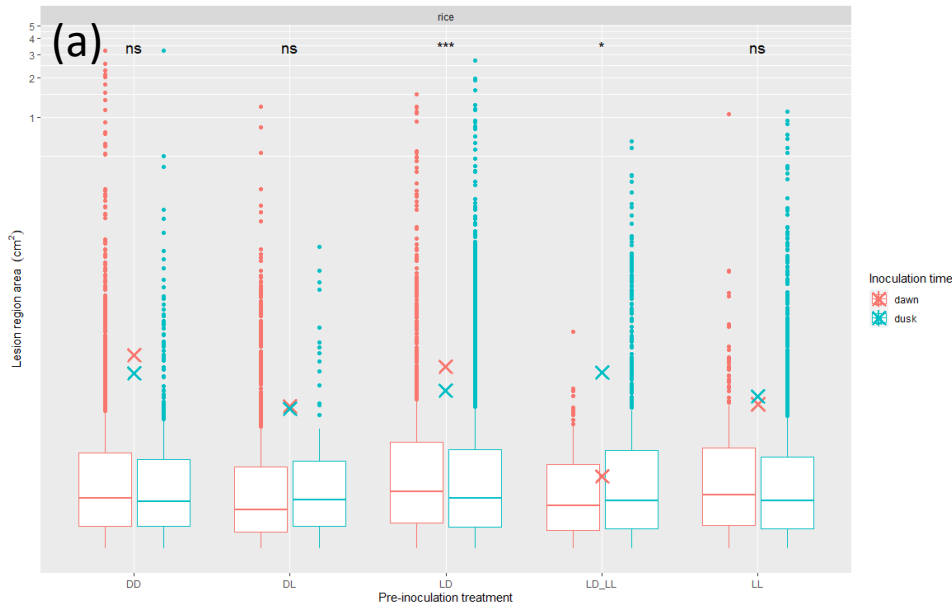


Figure 4.18: Synchronous- and dark-entrained *M. oryzae* is more virulent in rice at dawn and light-entrained *M. oryzae* is more virulent at dusk. In rice-*M. oryzae* interactions, (a) Lesions are larger at dawn from LD-entrained colonies and larger at dusk in LD-LL (n = 2358 lesions) DD dawn, n = 1303 DL dawn, n = 1565 LD dawn, n = 178 LD-LL dawn, n = 330 LL dawn, n = 601 DD dusk, n = 93 DL dusk, n = 6098 LD dusk, n = 705 LD-LL dusk, n = 2382 LL dusk), (b) lesions are more numerous at dawn after DD entrainment and at dusk after LL entrainment, and (c) lesion coverage is greater at dawn after DD entrainment and greater at dusk after LD-LL and LL entrainment (n = 55 leaves DD dawn, n = 63 DL dawn, n = 87 LD dawn, n = 13 LD-LL dawn, n = 58 LL dawn, n = 28 DD dusk, n = 12 DL dusk, n = 224 LD dusk, n = 41 LD-LL dusk, n = 128 LL dusk). Stars represent increasing statistical significance (Dunn's test, p < 0.05) and crosses mean values.

Similarly, in barley, LD-grown *M. oryzae* gave rise to larger lesions at dawn compared to dusk. Antiphase inoculations also showed a larger average lesion size at dawn (relative to the plant – dusk for the fungus), but a higher median area at dusk, perhaps implicating both the plant and fungal clock in disease severity, as is the case in *B. cinerea* (117). Interestingly, LD-LL colonies show an opposite phenotype to DL, where lesion regions are larger on average at dusk, but the median is higher at dawn. Constant-light grown *M. oryzae* also produce larger lesions at dawn (mean and median), perhaps suggesting that synchronicity with barley host plants or light exposure prior to inoculations favour dawn infections (Fig. 4.19).

The majority of pre-inoculation treatments caused a higher lesion region density at dusk in barley, however, with LD, LD-LL, and LL-treated *M. oryzae* showing more lesion regions per leaf cm² compared to their dawn counterparts. Prolonged light-treated *M. oryzae* (LD-LL and LL) also showed higher percent lesion region coverage at dusk compared to dawn, in a similar manner to rice. Barley may, therefore, be more susceptible to penetration at dusk (Fig. 4.19).

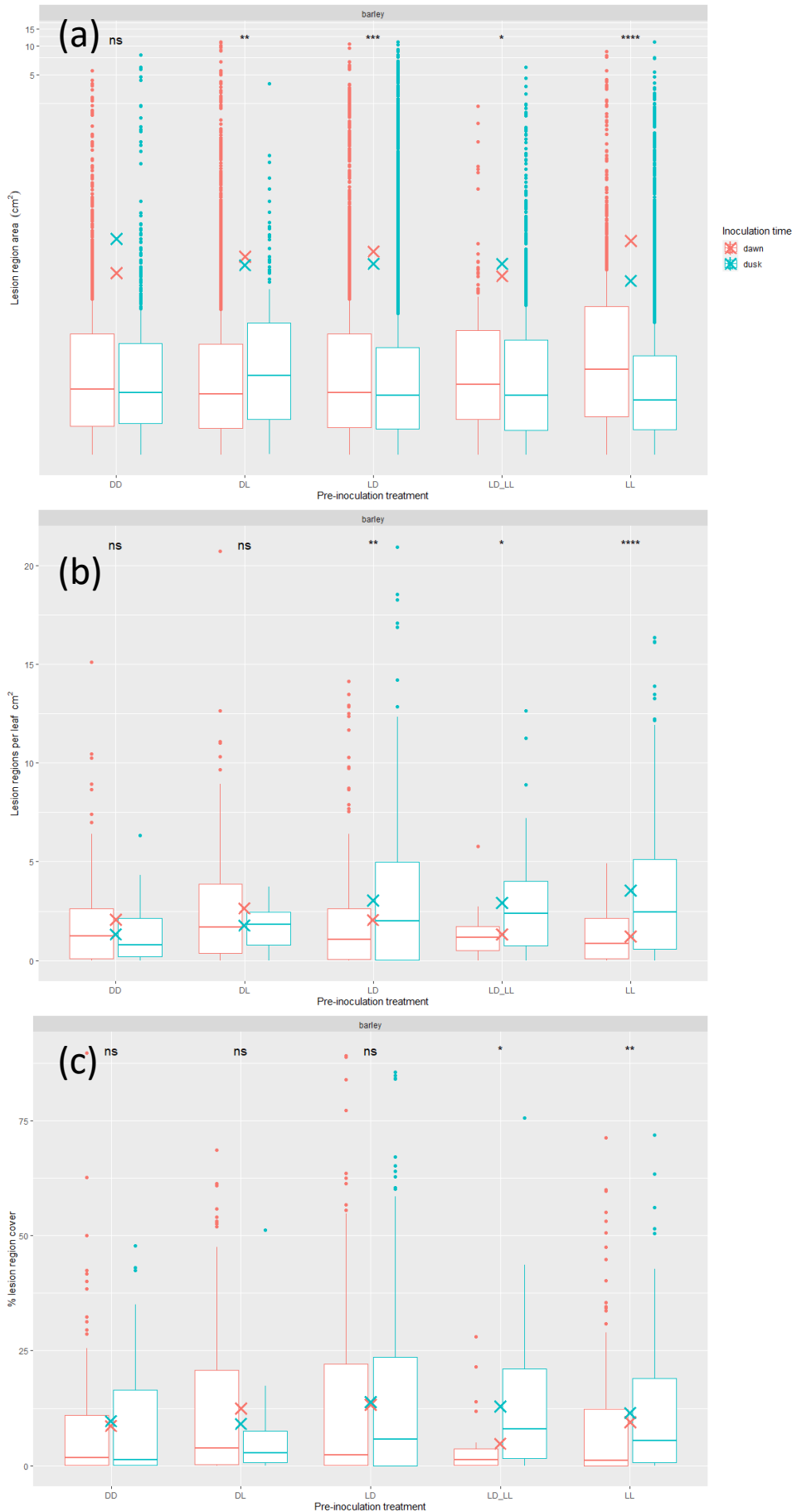


Figure 4.19: Barley is more susceptible to *M. oryzae* penetration at dusk. In barley-*M. oryzae* interactions, (a) Lesions are larger at dawn compared to dusk after LD, LD-LL, and LL treatment (n = 2100 lesions dawn DD, n = 4183 DL dawn, n = 3267 LD dawn, n = 218 LD-LL dawn, n = 1221 LL dawn, n = 508 DD dusk, n = 172 DL dusk, n = 11215 LD dusk, n = 1171 LD-LL dusk, n = 6349 LL dusk), but (b) lesions are more numerous at dusk after these same entraining conditions, and (c) lesion coverage is reduced at dawn after LD-LL and LL entrainment (n = 97 leaves DD dawn, n = 151 DL dawn, n = 196 LD dawn, n = 19 LD-LL dawn, n = 107 LL dawn, n = 39 DD dusk, n = 10 DL dusk, n = 374 LD dusk, n = 54 LD-LL dusk, n = 176 LL dusk). Stars represent increasing statistical significance (Dunn's test, $p < 0.05$) and crosses mean values.

Summarily, pre-inoculation treatment of *M. oryzae* and timing of inoculation displays a profound effect in the rice blast pathosystem in both barley and rice; a period of dark prior to inoculation primarily favours dawn pathogenicity and a period of light prior to inoculation favours dusk inoculations. Whilst fungal pre-inoculation entrainment clearly plays a role in virulence, it is important to note that the majority of inoculations cause a higher disease incidence at dawn in rice, but dusk in barley, so perhaps the host clock is more important than the pathogen clock.

Comparing treatments at dawn and dusk to the base means paints a different story, however. In dawn inoculations of rice, synchronous LD-grown *M. oryzae* colonies gave rise to larger lesions, and antiphase and LD-LL colonies caused smaller lesions (Fig. 4.20). There is no significant effect of pre-inoculation treatment on lesion region size at dusk in rice, suggesting that the rice clock is the key determinant of disease outcome (Fig. 4.20). In agreement with the time-of-day comparisons, constant dark-grown *M. oryzae* created larger lesions and constant light-grown colonies produced smaller lesions at dawn. Constant dark-treated colonies also give rise to a higher lesion region coverage of rice leaves and LL and LD-LL treatments have a lower coverage at dawn. Antiphase inoculations create fewer lesion regions than any other treatments at dusk. Antiphase inoculations also cause a lower percent coverage at dusk compared to other treatments. These results suggest that synchronicity with the host clock is perhaps more important than the inoculation timing (Fig. 4.20).

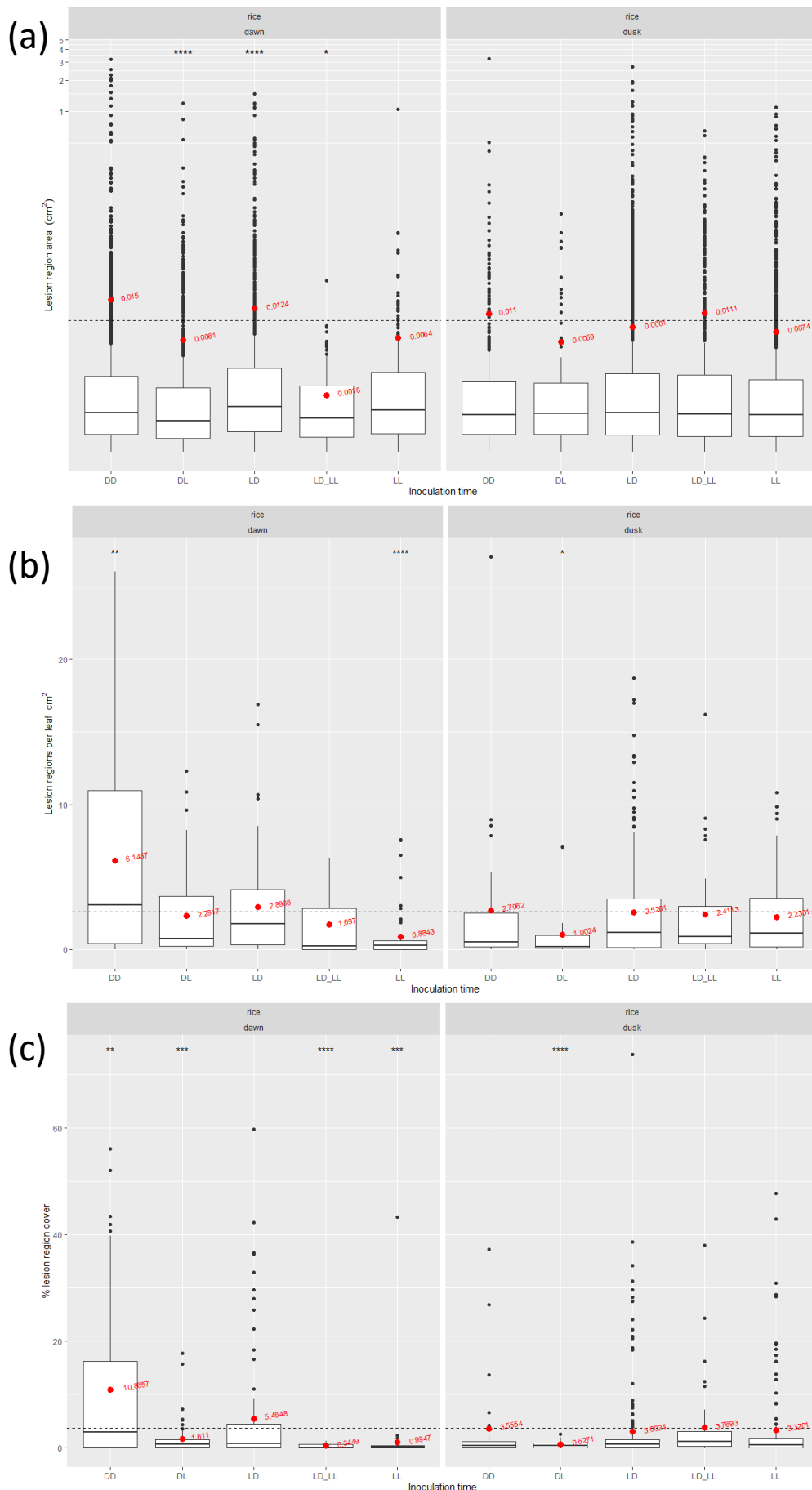


Figure 4.20: Pre-inoculation treatment has a greater impact in *M. oryzae* infections at rice subjective dawn. (a) Synchronous LD-entrained *M. oryzae* colonies produced larger lesions at dawn, and DL- and LD-LL entrained colonies produced smaller lesions (n = 2358 lesions DD dawn, n = 1303 DL dawn, n = 1565 LD dawn, n = 178 LD-LL dawn, n = 330 LL dawn, n = 601 DD dusk, n = 93 DL dusk, n = 6098 LD dusk, n = 705 LD-LL dusk, n = 2382 LL dusk), (b) DD- and LL-entrained conidia were more (DD) or less (LL) likely to successfully produce lesions at dawn, respectively, and (c) DD- and LD-entrained conidia showed increased lesion coverage at dawn, whereas DL-, LD-LL-, and LL-entrained colonies covered a smaller proportion of leaves at this time. Pre-inoculation treatment had little effect on lesion size, density, or coverage at dusk in rice (n = 55 leaves DD dawn, n = 63 DL dawn, n = 87 LD dawn, n = 13 LD-LL dawn, n = 58 LL dawn, n = 28 DD dusk, n = 12 DL dusk, n = 224 LD dusk, n = 41 LD-LL dusk, n = 128 LL dusk). Stars represent increasing statistical significance (Dunn's test, p < 0.05), red points and text show the mean values for each group.

In contrast, *M. oryzae* pre-inoculation treatment had less of an effect in barley inoculations. Lesion regions were larger on average (but had a lower median) at dawn after antiphase or constant light treatment suggesting that light exposure prior to barley infections favour barley subjective dawn (Fig. 4.21). However, antiphase treatments also gave rise to larger lesion regions at dusk in barley, and constant light caused smaller lesions (Fig. 4.21). Further, antiphase treatments showed a higher lesion region density at dawn and constant dark-treated colonies showed decreased lesion densities at dusk. Pre-inoculation treatment has a small effect on percent coverage in barley compared to the base mean, with only LD-LL treatments causing a decrease in dawn inoculations. Altogether, pre-inoculation entrainment of *M. oryzae* seems to have a greater effect on disease severity in its natural host, rice.

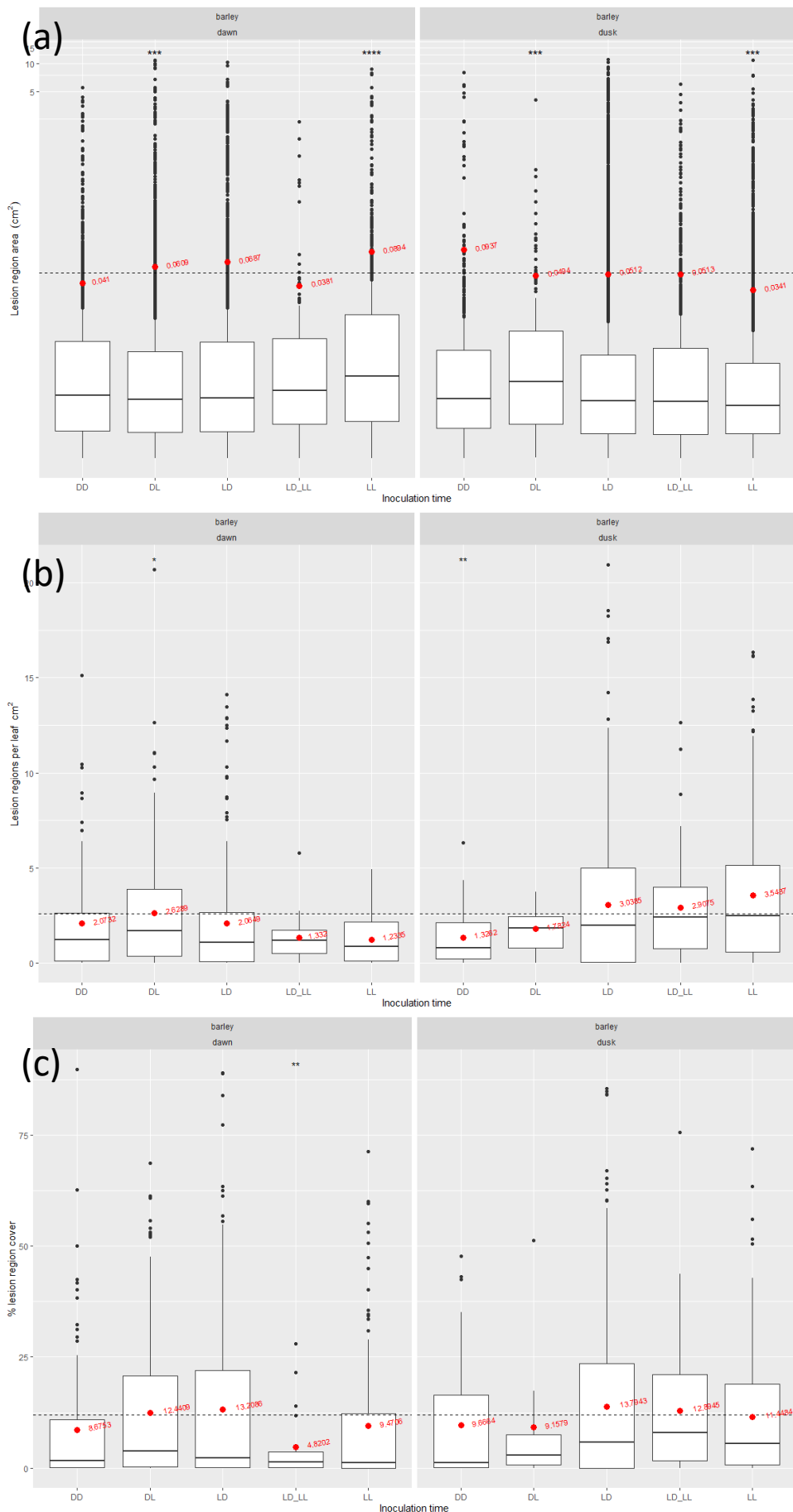


Figure 4.21: Pre-inoculation entrainment of *M. oryzae* has a reduced effect in barley. (a) Both DL- and LL-entrained *M. oryzae* produce larger lesions on average at dawn and smaller lesions at dusk (n = 2100 lesions dawn DD, n = 4183 DL dawn, n = 3267 LD dawn, n = 218 LD-LL dawn, n = 1221 LL dawn, n = 508 DD dusk, n = 172 DL dusk, n = 11215 LD dusk, n = 1171 LD-LL dusk, n = 6349 LL dusk), (b) DL treatments also caused an increased lesion density at dawn, whereas DD entrainment reduced lesion density at dusk, (c) pre-inoculation entrainment had little effect on lesion coverage in barley, except after LD-LL where coverage was significantly reduced compared to the base mean (n = 97 leaves DD dawn, n = 151 DL dawn, n = 196 LD dawn, n = 19 LD-LL dawn, n = 107 LL dawn, n = 39 DD dusk, n = 10 DL dusk, n = 374 LD dusk, n = 54 LD-LL dusk, n = 176 LL dusk). Stars represent increasing statistical significance (Dunn's test, p < 0.05), red points and text show the mean values for each group.

Interestingly, when there is also an effect of the total leaf area on lesion density (number of lesion regions per leaf cm^2) in both rice and barley; there are maximal lesion densities in the smallest leaves and those $\sim 10\text{-}15 \text{ cm}^2$, suggesting that larger leaves (which can be used as a proxy, in some capacity, for age/maturity) are less susceptible to *M. oryzae* infection. In rice, there is also a decrease in lesion density in leaves $\sim 5 \text{ cm}^2$ (Fig. 4.22). Further, when accounting for inoculation timing, there appear to be altered optimal leaf sizes for lesion density and subsequent infection severity. In rice at dawn and dusk, leaves that are $\sim 3\text{-}8 \text{ cm}^2$ show the lowest lesion density, suggesting increased resistance, and maximal lesion density in the smallest (youngest) leaves and those approximately $10\text{-}15 \text{ cm}^2$. Likewise, barley displays higher lesion densities after dusk inoculation, but as leaf area increases, lesion densities decrease in a near-linear fashion, which is not shown at dawn, where lesion densities are highest in leaves $\sim 10 \text{ cm}^2$. Further, after dawn inoculations, rice infections do not display a decrease in lesion density as leaf area increases past 15 cm^2 , perhaps suggesting increased susceptibility at dawn. These observations contrast those reported in *Arabidopsis-M. oryzae* infections, where increased entry rates were observed at dusk only (253). However, as noted previously, *M. oryzae* utilises different infection mechanisms in rice and *Arabidopsis*, and potentially barley, too (480). Together, leaf size, developmental stage, or the maturity of the leaves may play a role in the outcome of disease. Indeed, it has been reported that leaf age is a determining factor in infection severity, rice blast pathosystem included (149,253,260,390,414,460).

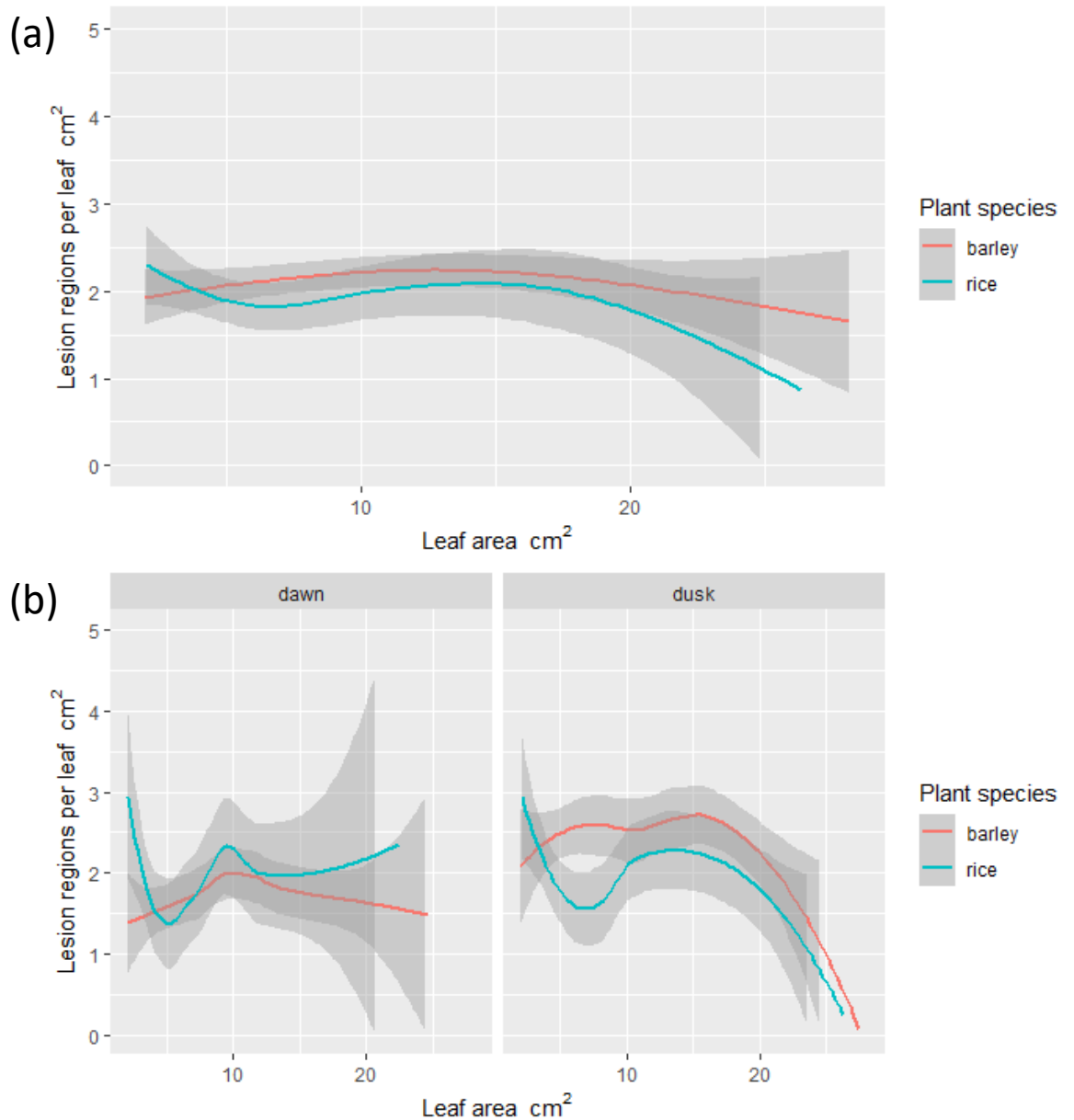


Figure 4.22: Susceptibility to *M. oryzae* is highest in adolescent leaves. (a) When ignoring inoculation time, leaf area (which can be an indicator of leaf age and plant developmental stage) correlates with lesion density, showing maximal lesion densities $\sim 10\text{-}15\text{ cm}^2$ (b) The subsequent effect of leaf area on lesion density when separating by inoculation timing shows that there are optimal leaf sizes for infection and that after dawn inoculation, lesion density remains higher than dusk inoculations in rice. Dusk inoculations in barley also display a higher maximal lesion density, and as leaf area increases, lesion density decreases, suggesting species-dependent susceptibility to *M. oryzae* at different times of day (n = 570 leaves barley dawn / n = 653 dusk, n = 276 rice dawn / n = 433 dusk, data displayed using Loess smoothed conditional means, grey shading denotes standard error).

4.3 Discussion

This chapter has indicated that *M. oryzae* contains confirmed and putative genes for photoreceptors and core circadian machinery, based on literature, BlastP and protein motif comparisons (82,101,178,258,259,457). To this end, *M. oryzae* displays conidial banding in response to blue, white, and green light, with a reduced response to red light. Red 'safe light' is commonly used in fungal manipulation due to the lessened effect on conidial banding and fungal development in comparison to white or blue light (82,104,110,119,184,191,194,215,256,370,379,434,473,474). Likewise, this study has shown that red light is insufficient to induce robust and diurnal conidial banding, let alone entrain the circadian clock. However, there have been many studies suggesting that *M. oryzae* and other fungal species do respond to red light (82,104,116,119,180,215,371,415,452,477,481–483), so treating red light as essentially dark is a practice difficult to justify.

On a daily basis, the intensity, quality, and ratio of certain wavelengths of light dynamically change. At dawn and dusk, longer wavelengths of light like red and far-red are present to a higher degree than blue or green wavelengths, giving rise to the orange-red skies early in the morning and later in the evening. Further, for pathogenic fungal conidia spread by wind and dew-drop etc., upon landing on plant foliar tissue, the relative ratio of green light to other wavelengths will increase significantly due to the absorption of red and blue light and reflectance and/or transmission of green and far-red by the plant (104). Bieszke and colleagues (418,474) reported that the *N. crassa* opsin gene *nop-1* is regulated and repressed by the circadian WC2, and that *nop-1* is highly expressed during the formative stages of conidiation and shortly after conidial release, and may act to regulate conidial development alongside the blue light receptor pathway. If the *M.*

oryzae NOP-1 (MGG_09015) acts in a similar way to its *N. crassa* counterpart, it could provide a signal to the pathogen that it has landed on e.g., a leaf. Some excellent evidence of the importance of green light reception in virulence is that green light photoreceptors and rhodopsins are enriched and mostly found in plant pathogenic and plant-associated fungi (473). This includes *N. crassa*, which was recently found to have the capability to act as a phytopathogen towards Scots pine (484). Lyu and colleagues (420) have also shown that the opsin homolog Sop1 in the plant pathogen *Sclerotinia sclerotiorum* plays a role during infection and sclerotial development: knockout strains showed reduced virulence and increased sensitivity to salt and osmotic stress. Interestingly, the Sop1 mutants were more tolerant to oxidative stress (420), and so the plant pathogen green light photoreceptor may play a role in sensing plant presence and priming the fungal redox state in preparation for attack. These reports could therefore be interpreted to mean that it is not only the presence of a certain wavelength of light that is important to a fungal pathogen, but rather the relative ratio and intensities of light that could give important temporal (i.e. high red, low blue correlating with dawn and dusk) and spatial cues (i.e. high green and far-red, low blue and red correlating with plant presence), as well as the previous perception of light; increasing amounts of red and blue sensed after a long period of dark correlates with dawn and decreasing amounts of blue light after a long period of light perception correlates with dusk. The technical complexity of performing experiments and analysing the effects of relative wavelengths, ratios, intensities, and timing of light, however, may prove very difficult to perform and is likely why most experiments are performed in a lights on-lights off or monochromatic fashion, as presented here.

Unlike *N. crassa*, the model fungal circadian species, *M. oryzae* shows a significant latency period of ~6-8 d before switching to the diurnal conidial banding phenotype. Prior to banding, *M. oryzae* constantly displays dark, melanised growth which is a phenotype consistent with constant light or darkness. This phenomenon has been briefly mentioned in the literature (370), but is clearly visible on many fungal species including, but not limited to, *Botrytis cinerea*, *Cercospora kikuchii*, and *Aureobasidium pullulans* (116,194,370,434). This latency period is also nutrient- and metabolically dependent. In nutrient-poor environments, such as minimal media, *M. oryzae* takes 8 d or more of entrainment before showing the conidial banding phenotype, whereas on media with *M. oryzae* spent media included, the latency period can be reduced to ~4 d. This switch from constant melanised growth to the repression of conidiation during the day could be beneficial to the fungus, as once the colonies have made this switch to diurnal conidiation, the colonies grow significantly faster than those that were grown in constant conditions and as such did not display banding. No work to date has been done to discern what causes the switch to diurnal banding. Here, fungal metabolite(s) that are produced by *M. oryzae* have been shown to inhibit conidiation during the day; spent media added to CM plates can cause an early banding phenotype and at high doses can inhibit melanised growth and conidiation almost entirely. Further, the metabolite(s) is predominantly synthesised just prior to the switch to diurnal banding.

Once *M. oryzae* does display the conidial banding phenotype, it can then be transferred into constant light or darkness and still rhythmically conidiate for several days with a period of approximately 24 h, which is suggestive of a functional circadian clock. To be a truly circadian output, the *M. oryzae* circadian clock needs to be temperature and/or nutritionally compensated over a physiologically relevant range

(174,178,183,189,228,230,257,404,459,476,485). *M. oryzae* colonies grown on CM, MM, and 50% SM (containing the crude spent media from *M. oryzae* shaking cultures) show a continuation of the conidial banding pattern with a period of ~24h for a number of days in constant conditions. This data, the presence of circadian clock and photoreceptor genes, and the convincing evidence of rhythmic expression of twilight (84), a gene that partially controls phototropism and nutrient and redox homeostasis, and the core clock gene, FRQ (259), suggests that *M. oryzae* has a fully-functional nutritionally-compensated circadian rhythm.

Having established that *M. oryzae* has an entrainable circadian phenotype for rhythmic conidial banding, attempts were made to elucidate what, if any, effect these entrainment conditions have on conidiation and conidial development. In agreement with several studies in other fungi, *M. oryzae* exhibits reduced conidiation under constant light (150,194,224,257,371,376,379) and constant darkness (84,222,434) and colonies grown under an LD light cycle are most conducive for conidiation (247). Surprisingly, after entrainment sufficient to continue banding under constant conditions, the colonies transferred from LD to constant light or darkness (LD-LL or LD-DD, respectively), showed the same degree of conidiation reduction as the constant dark or constant light grown colonies. As opposed to conidiation being a circadian response, this could be an acute response to the drastic changes in their respective environment, and as such, regardless of circadian time, constant light (or lack thereof) represses the quantity of conidia produced. There have been no other reports about the inhibition of conidiation in response to constant conditions after entrainment under light dark cycles in *M. oryzae*. Interestingly, rapid changes in photoperiods act as stressors to several plant species and are termed 'photoperiodic stress'; RNA-seq analysis suggests that photoperiod stress as

a result of prolonged light exposure induced several ROS-related transcripts and that the transcriptomic response to photoperiodic stress in plants were reminiscent of ozone stress and pathogen attack (113), so the observations in *M. oryzae* might be similar to acute photoperiodic stress responses upon transfer to constant conditions.

12 d old colonies were harvested at dawn and dusk on the same day after being grown under LD, constant conditions (DD or LL), or circadian conditions (LD-DD or LD-LL). Despite constant conditions inhibiting conidiation, there was no significant time of day-dependent effect of harvest time, which is surprising since constant conditions cannot entrain the clock, and thus a linear increase in conidia over time could be expected. The fact that there was no effect of harvest time on colonies under any diurnal or circadian conditions suggests that conidia may have been made the previous subjective 'night' and that conidiation was repressed during the subjective day, even in the absence of environmental light cues, as is the case with LD-LL and LD-DD. This could be interpreted to mean that, even though constant conditions repress conidiation, the fact that there is no effect of harvest time means that the LD-DD and LD-LL colonies were successfully entrained to inhibit daytime conidiation. Alternatively, a simpler explanation could be that *M. oryzae* requires more than 12 h to produce mature conidia, regardless of subjective time of day.

When grown on 50% spent media plates, an early conidial banding phenotype is observed. SM still allows for continued banding upon transfer to constant conditions, but the degree of conidiation (i.e., number of conidia produced per colony) is significantly reduced in comparison to growth on CM plates. There are several reports of low-nutrient media giving rise to fewer conidia, and media composition being closely linked to the

circadian clock and conidiation (110,201,201,257,442). These reports include *M. oryzae*, where the Flb3p transcription factor is implicated in the response to nutrient limitation, causing altered aerial mycelium formation and melanin biosynthesis, both of which are associated with the circadian clock (194,486). However, in the SM plates presented here, nutrients were in excess, and at least the same concentration as 1x CM. Mathias and colleagues (486) report that colonies grown on low nutrient content media (e.g., MM, or CM with olive oil as a carbon source) show very low conidial densities and that a minimum amount of biomass must be accumulated before conidiation begins, since conidiation occurs much later on low the nutrient media. Taking this, and the data on spent media experiments presented here, showing reduced conidiation but early conidial banding, it could be possible that, rather than low nutrient composition, it is the build-up of secreted metabolite(s) or waste products (usually produced as a result of low nutrient composition or high fungal biomass) that cause the switch to conidiation in a quorum-sensing, dose-dependent fashion. Further, the same spent media significantly inhibits conidial germination and development, which suggests that the metabolite(s) may function to inhibit conidiation (especially during the day) and conidial development, perhaps as a signal that the current environment is either (a) low in nutrients, since *M. oryzae* needs to first produce the metabolite(s) to a high concentration or (b) the current environment has a large population of *M. oryzae* cells. The spent media metabolite(s) could function to reduce competition from new colonies growing from nearby conidia. These compound(s), therefore, may have significant implications as a novel fungicide.

Regarding conidial development, in a similar manner to conidial production, harvest time (dawn or dusk) had no significant effect on conidial germination and appressorial development, suggesting that regardless of time of day, once conidia sense a

hydrophobic surface, they will germinate and develop at a relatively uniform rate, mostly forming appressoria by 8 HPI. This is in agreement with Yamauchi and colleagues (253), who reported that conidia from *M. oryzae* showed no difference in germination rates and appressorial development when harvested at either dawn or dusk. Interestingly, while harvest time has no effect on germination and appressorial development, the results presented here showed that *M. oryzae* conidia grown under constant conditions (DD or LL) showed reduced appressorial development in comparison to those grown under LD cycling conditions. Aver'yanov and Shimizu (384,460) both reported that light can inhibit conidial development, but these light treatments were applied post-harvest. Considering that LD-DD and LD-LL entrainment conditions did not significantly reduce appressorial development, it is possible that an entrained and functional circadian clock allows for conidial development to occur at the correct rate. To support this point, there have been some studies where circadian clock genes in *M. oryzae* (MoFwd1 and MoFRQ) have been knocked out, resulting in reduced conidiation and conidial development (259). Finally, it is important to consider that in the conidial development assays presented here, conidia were imaged under constant light from the microscope LED, and thus the conidia may have experienced acute light inhibition in a similar manner to those shown by Aver'yanov (384) and Shimizu (460). This effect may have masked more subtle differences in development caused by pre-harvest entrainment conditions. However, even if the lights were switched on only during image acquisition time points, it may have a similar effect to constant light, as skeleton photoperiods can entrain the circadian clock in some species (487). Therefore, it would be impossible to assess the same conidia as they develop over time. Indeed, fluorescent or bioluminescent reporter mutants require and produce light, respectively.

There was no effect of harvest time on conidial adherence, which again suggests that once conidia are produced and successfully entrained, harvest time has little effect on conidial development. Interestingly, the average size (μm^2) of conidia remaining after agitation were $\sim 10\%$ larger than the population prior to agitation. This could be due to the fact that larger conidia likely weigh more, and thus require more force to be shaken away, they could have a higher surface area allowing for greater adherence to the petri dish, or the larger conidia may be able to allocate more resources into producing spore tip mucilage. Further evidence that pre-harvest environmental conditions had little effect on conidial development were that appressorial cytorrhysis was not affected by pre-harvest conditions and as such mature appressoria will produce similar turgor pressure regardless of entrainment conditions. Kim and colleagues (101) showed that knocking out the *M. oryzae* WC1 gene had no effect on osmotic stress responses, which further suggests that the circadian clock has little role in appressorial stability.

Finally, attempts were made to discern if there were any effects of pre-inoculation entraining conditions of *M. oryzae* in plant inoculations and what, if any, role time of day has in the outcome of infection. In rice, the majority of inoculations were more favourable for the pathogen at dawn; lesions were generally larger, more numerous, and covered a larger proportion of the leaves compared to their dusk counterpart. In barley, however, the reverse was true. Primarily, this suggests that the plant clock may be more important than the fungal clock, as the fungal colonies were entrained by the same range of treatments. Two main explanations come to mind when comparing the plants. Firstly, barley exhibits nonhost resistance (NHR) to *M. oryzae*, as barley has not evolved alongside the pathogen for most of its life history, and may explain why in the experiments presented here, disease severity was greater in barley. Yamauchi and

Shimizu (253,460) report that there is a time of day- and photoperiod-dependent inoculation effect on *M. oryzae*-*Arabidopsis thaliana* interactions, another non-host plant. Here, they show that dawn-inoculated *M. oryzae* conidia were less able to penetrate the epidermis of the *Arabidopsis* leaves compared to those inoculated at dusk and as such these experiments may show a similar outcome in Barley. It should be noted that there is no mention of pre-inoculation entrainment of *M. oryzae* in either of these articles. Additionally, *Arabidopsis* is also more susceptible to the necrotrophic fungal pathogen *Botrytis cinerea* at dusk compared to dawn (117). In great support of the difference between host and non-host resistance *M. oryzae*-plant interactions, Park and colleagues (480) show that *M. oryzae* infects *Arabidopsis* via a mechanism distinct from that of rice: while in both interactions, the appressoria is utilised to penetrate the host cuticle, three fungal genes necessary for pathogenicity in rice had limited roles in *Arabidopsis*. Park and colleagues went on to say that *M. oryzae* acted in a necrotrophic manner, as opposed to hemibiotrophic. Necrotrophic pathogens traditionally elicit the Jasmonic acid (JA) defence pathway whereas biotrophs (and hemibiotrophs) elicit the Salicylic acid (SA) pathway, both of which are clock-regulated – JA accumulates at midday and SA at midnight (antiphase to one another) in *Arabidopsis* (103,152,163,251,419). These could explain why *Arabidopsis* is more susceptible to *M. oryzae* inoculations at dusk and may provide a similar explanation for the dusk-favoured inoculations in these barley experiments (253,460). *M. oryzae* conidia have also been shown to produce and secrete abscisic acid compounds that act antagonistically towards the host SA signalling pathway (488). Rice-*Cochliobolus miyabeanus* interactions (previously known as *Helminthosporium oryzae*, a necrotrophic pathogen and causative agent of brown leaf spot) display greater disease severity when inoculations occurred very late at night and

just prior to dawn, with disease severity falling as dusk draws nearer before picking up again later in the evening, significantly after dusk (388,389). This rice susceptibility at dawn may be reminiscent of the dawn effect observed in the *M. oryzae* interactions presented here; indeed, *C. miyabeanus* penetrates the host epidermis by using penetration pegs erupting from appressoria in a very similar fashion to *M. oryzae* (389). Taking into account the timing of appressorial development and penetration in *M. oryzae*, dawn inoculations may correspond to penetration occurring late at night or just prior to dawn, coinciding well with *C. miyabeanus* optimal infection time (388).

Arabidopsis is also reported to respond to different pathogens and inoculation methods in a time dependent-manner (212). *P. syringae* spray inoculations carried out at dawn give rise to more severe outcomes when compared to dusk (158,159); pressure-infiltrated inoculations show the opposite effect, though, suggesting that the main barrier for the pathogen is making its way into the plant, as pressure-infiltrated *P. syringae* bypass the circadian-regulated stomatal defence (212). These results, suggest that it is not only the plant clock that is important, but also the pathogen clock, since, depending on the mode of pathogen entry, both partners may gate their defence responses and virulence, respectively (247). On a mechanistic level, pathogens that rely on physical or lytic enzyme-mediated penetration (such as *M. oryzae* and *Blumeria graminis*, respectively) may be optimised for infection times that correspond to night-time and stomatal-independent infection; it is important to consider that dawn inoculations do not necessarily correspond to dawn penetration/infection, as mentioned earlier.

Alternatively, there are reports that the day length at which flowering occurs in plants may affect the timing and expression of defence-related genes and signalling processes;

day length is known to affect pathogen susceptibility (489), and the accumulation of salicylic acid (SA) and Jasmonic acid (JA) is clock regulated, see above (103,152,419). High SA levels are associated with increased resistance to *M. oryzae* in Arabidopsis (488) and for this non-host plant, SA levels would be relatively increased just as *M. oryzae* begins to penetrate the plant cuticle under dawn inoculations (~8 h to produce the appressoria, with most penetrations having occurred by 24 HPI, i.e. late at night, shortly before dawn). Biotrophic pathogens are known to induce the SA defence pathway, whereas necrotrophs and herbivores induce the JA pathway (103). Additionally, Sarris and colleagues (490) report that pathogen effectors target WRKY transcription factors, some of which are known to be involved in, and regulated by, the circadian machinery and subsequent clock-controlled ROS status. Further, there have been studies suggesting that plant pathogens are capable of targeting and even manipulating the plant host circadian machinery, which would include SA and JA timing and regulation, a tactic which may be common to a wide range of pathogens (102,103,173,491). Genes responsible for ROS breakdown in *N. crassa* (now known to be a facultative plant pathogen) for example, are controlled by the circadian clock (413). If a pathogen is expecting increased ROS levels at certain times of day as a result of breaching the plant host, then it may be better equipped to handle the ROS attack at infection-conducive times.

Clock genes can be expressed differentially depending on day length, and circadian clock mutants can give rise to exceptionally early flowering, as is the case with LUX ARRHYTHMO (245,492). Fascinatingly Izawa and colleagues, (493) reported that rice and Arabidopsis have orthologous clock genes (FT in Arabidopsis and Hd3a in rice) that are expressed in antiphase to one another: FT is expressed at dusk in Arabidopsis but Hd3a is expressed at dawn in rice. Further, it has been reported (494) that clock mutants of

paralogous genes of Arabidopsis in rice showed different expression patterns, further suggesting that the timing of clock-controlled genes and downstream processes may differ between species and perhaps more generally between long- and short-day flowering plants. Considering many defence signalling pathways are clock controlled, it could be possible that short- and long-day plants may have their defence response(s) set to different times, and subsequently are susceptible to the same pathogens at altered times of day. This could partly explain why the experiments presented here have shown dusk inoculation-favoured infection outcomes in barley (a long-day plant) and dawn inoculation-favoured infection outcomes in rice (a short-day plant).

It is difficult to discern whether the LD-LL pre-inoculation treatment effects are a result of circadian entrainment as opposed to acute light responses or fungal photoperiodic stress. For example, Santamaría-Hernando and colleagues (422) report that even as little as 10 minutes of light exposure can significantly inhibit virulence prior to inoculation. This begs the question that each and every plant inoculation in the lab may be affected by this phenomenon. Researchers need to be able to see the colonies that they are harvesting conidia from and the plants that they are inoculating – it is virtually impossible to carry out these experiments in the dark, and almost all inoculations, harvesting etc. take significantly longer than 10 minutes. As mentioned above, even using red safety light may have an impact on the research being carried out, and red light has been shown to affect plant resistance to a number of pathogens (113–115,144,150,180,257,419,422,495–497). Therefore, it may be best to supplement laboratory-based work with environment and ecological studies where plants can be infected in the complete absence of light. In *M. oryzae*, specifically, Kim and colleagues (101) reported that illumination at early stages of rice-*M. oryzae* interactions reduced disease severity, which could account for the

overall reduced severity in LL and LD-LL inoculations observed in this work, but does not explain the increased virulence in dawn LD inoculations. Kim and colleagues did not mention entrainment of their *M. oryzae* colonies before inoculation, though, and as such the inhibitory effect of light may be a more acute environmental effect instead of a circadian one (101).

This work shows a profound effect of pre-inoculation entrainment conditions to the extent that time of day-dependent disease severity can be altered by the conditions under which *M. oryzae* is grown. Unsurprisingly, synchronicity with the plant host generally aids in *M. oryzae* infection, with LD-grown colonies usually giving rise to larger and more numerous lesions than those grown under constant or circadian-entrained conditions. LL and LD-LL pre-treatment favours dusk inoculations, perhaps because pre-illumination stimulates superoxide production in *M. oryzae*; if conidia have had a long exposure to light, then they may be better equipped to handle any ROS bursts *in planta* (384,473,498). However, whilst light exposure stimulates antioxidant production, *M. oryzae* also requires the generation of its own ROS burst to successfully make its appressoria and enter the plant, so gating the production of both reactive oxygen species and antioxidants to a time most conducive for disease would provide a significant advantage to *M. oryzae* (499,500). Alternatively, perhaps dawn inoculated conidia benefit from having most of the day (where they are exposed to light as they germinate and grow along the plant host prior to appressorial generation) to utilise this light to generate the necessary ROS and superoxide enzymes (473,498). There have been several reports showing a link between the fungal circadian clock and antioxidant regulation, as well as ROS production and antioxidant homeostasis associated with pathogenic virulence, suggesting that the correct timing of both of these antagonistic processes is essential for

successful infection (116,184,384,413,479). Aver'yanov and colleagues (384) reported that long periods of light exposure (4 h or more) inhibited conidial germination of *M. oryzae* (perhaps through a similar mechanism to that observed in the conidial development assays reported here, where appressorial development is reduced in the LL-entrained conidia), but that this same light treatment stimulated the production of superoxide, which could potentially be used for the fungal ROS burst *in planta*. Further, they show that light-treated conidia were more tolerant to exogenous addition of ROS (such as hydrogen peroxide or superoxide), which would be beneficial when faced with the plant ROS burst (384). The findings reported here in the pre-inoculation treatment experiments complement Aver'yanov (384) and colleague's observations well: firstly, LL and LD-LL entrained *M. oryzae*, while poorer overall at causing disease, have a heavy skew towards increased pathogenicity at dusk, perhaps because they have been preconditioned to be tolerant to ROS, and produce ROS to both attack and defend against the plant host. Dawn inoculations after LD-LL and LL entrainment (i.e., more exposure to light throughout the subsequent day) would provide little benefit beyond the pre-inoculation light exposure. Further, these experiments showed that LL-entrained conidia germinated and developed slightly quicker (although not significantly) than those entrained under LD, LD-LL, and DD. As mentioned earlier, though, these experiments would ideally be repeated without any conidial exposure to light to discern the true effects of pre-inoculation entrainment. Secondly, dark-entrained colonies have greater success with dawn inoculations, perhaps because they will be (a) penetrating the (rice) plant at the optimal time, just prior to dawn, and (b) they will have received a light treatment throughout the day while growing along the plant tissue prior to penetration. Aver'yanov and colleagues (384) also observed that with low inoculation density (similar

to the concentrations used here), light exposure rescued the darkness-incubated inoculum and perhaps could explain why dusk inoculated DD-entrained *M. oryzae* performs so much worse than their dawn-inoculated DD-entrained counterpart: there was not a sufficient light exposure to rescue the dark-induced 'weak symptoms'.

Finally, in the experiments discussed here, there seems to be a correlation between leaf area and lesion density, with the highest densities observed in middle-sized (~10-15 cm²) leaves in rice and barley. Chen and colleagues (390) reported that differently aged rice shows altered susceptibility to *M. oryzae*, with rice plants being more susceptible at the younger V1-V4 stage, and that susceptibility was reduced from V5 onwards, with enhanced resistance at later growth stages. Whilst this study ignored the leaf area, it is a fair assumption to make that increasing leaf area corresponds with increased maturity of the plant, and so it seems that 'adolescent' rice leaves are most susceptible to *M. oryzae* infections, as there were lower lesion densities in 'younger' (smaller) and 'older' (larger) leaves.

To conclude, this chapter has shown that (a) *M. oryzae* contains many genes homologous to core clock components and photoreceptors found in *N. crassa*, (b) *M. oryzae* displays conidial banding predominantly in response to white, blue, and green light, (c) entrainment to a rhythmic environment (LD, LD-DD, and LD-LL) is generally conducive to increased fitness in *M. oryzae* growth and development, (d) *M. oryzae* conidial banding is a nutritionally-compensated circadian output that requires sufficient entrainment, (e) the switch to conidial banding after the latency period is caused by some sort of secreted metabolite(s) that inhibits conidiation and melanised growth during the day, (f) time of day has little effect on conidial germination and development, and (g) pre-inoculation

treatment, time of day, and host species all have a profound impact on the outcome of rice blast disease. Importantly, these time of day-dependent differences in disease outcome between host plants have yet to be discussed in the rice blast pathosystem and, as such, presents a novel direction for research in *M. oryzae*-host interactions.

5 WC2 plays a role in the growth, conidiation, and pathogenicity of *Magnaporthe oryzae*

5.1 Introduction

5.1.1 The WHITE COLLAR COMPLEX keeps the clock ticking

Most circadian clocks combine an input pathway, circadian machinery, and an output pathway, giving rise to daily and rhythmic behavioural, metabolic, growth, and developmental processes (184). The fungal circadian machinery generally consists of a transcriptional-translational feedback loop(s) (TTFL), where the timing, transcription, translation, post-translational modification, and localisation of clock genes/proteins interact with and feedback on one another depending on the time of day (183–185,228). In *N. crassa*, this machinery is predominantly made up of FREQUENCY (FRQ), WHITE COLLAR 1 (WC1) and WHITE COLLAR 2 (WC2); WC1 and WC2 interact with one another through their PAS domain(s) to form the WHITE COLLAR COMPLEX (WCC), and together with FRQ, these proteins create the FRQ/WCC oscillator (FWO) (Fig. 5.1) (178,184,192,233,501). Late at night/early in the circadian day, *frq* mRNA and FRQ protein are at their lowest (178,192). At this time the WCC, acting as a transcriptional activator, binds to the clock box motif (Cbox) of the FRQ promoter region, increasing *frq* expression (181,184,192,227). The abundance of the WCC also increases the levels of the (as yet unknown) repressor of WC2, causing *wc2* transcription to fall (216). 4-5 h later, as *frq* mRNA levels peak (178,192), FRQ protein accumulates and some homodimerizes and enters the nucleus, associating with FRQ-RNA-Helicase (FRH) and casein kinase 1 (CK1) to form the FRQ-FRH complex (FFC) (178,178,192,200,212,222,228,233).

The FFC then interacts with, and phosphorylates the nuclear WCC, inactivating it and causing it to be exported to the cytoplasm, thus preventing the WCC from promoting *frq* expression for the rest of the circadian day (178,192,202,212,222,228,452,502). When FRQ levels are high (and thus WCC activity comparatively low), there is little repression of *wc2* transcription, allowing WC2 levels to begin to rise again (216). Concurrently, FRQ in the FFC becomes increasingly phosphorylated throughout the day, which progressively reduces its ability to interact with the WCC, closing the negative arm of the feedback loop (178,192,228).

By the late circadian afternoon, *frq* expression (and subsequent FRQ synthesis) is declining due to its inactivation of WCC-mediated *frq* transcription, and the remaining hyperphosphorylated FRQ protein interacts with FWD1 (F-box/WD-40 repeat-containing protein), which leads to its eventual ubiquitination and turnover by the proteasome, causing FRQ levels to fall further (161,178,191). As FRQ levels decline or are rendered 'invisible' to the circadian system because of increasing phosphorylation, the WCC can begin to perform its *frq*-promoting function again, and thus a new circadian cycle commences (178,192,228).

Cytosolic FRQ also post-transcriptionally upregulates WC1, contributing to a WC1 peak at approximately circadian midnight (178,192,216,221), however WC2 must be present to allow for this upregulation to occur (221). FRQ is additionally shown to increase *wc2* transcript levels through its interaction with the WCC, which indirectly inhibits WC2 (178,191,192,201,216). WC1 also negatively regulates *wc2* transcription independently of FRQ, forming an external feedback loop (199,216). FRQ and WC1 protein activity therefore run antiphase to one another, whilst the relative abundance of FRQ and WC2

remain comparatively constant (178). The stable WC2 abundance is, in part, achieved by a transcriptional activator independent of the WCC, suggesting that a basal level of *wc2* transcript and/or WC2 protein is important in maintaining the relative WC1:WC2 ratio (216). However, the phosphorylation status of WC2 is rhythmic and subsequently regulates the DNA-binding capability of the WCC (178). FRH and WC2 cellular localisation can also vary throughout the circadian day due to their phosphorylation status and interaction with FRQ and WC1, respectively (178,503). In this way, the circadian clock is more than just a rhythmic expression of genes; it is the complicated interaction between interconnected transcriptional, translational, and post-translational control that, alongside protein localisation, facilitates circadian function. A simplified WCC-centric view of the *Neurospora* clock is represented in Fig. 5.1

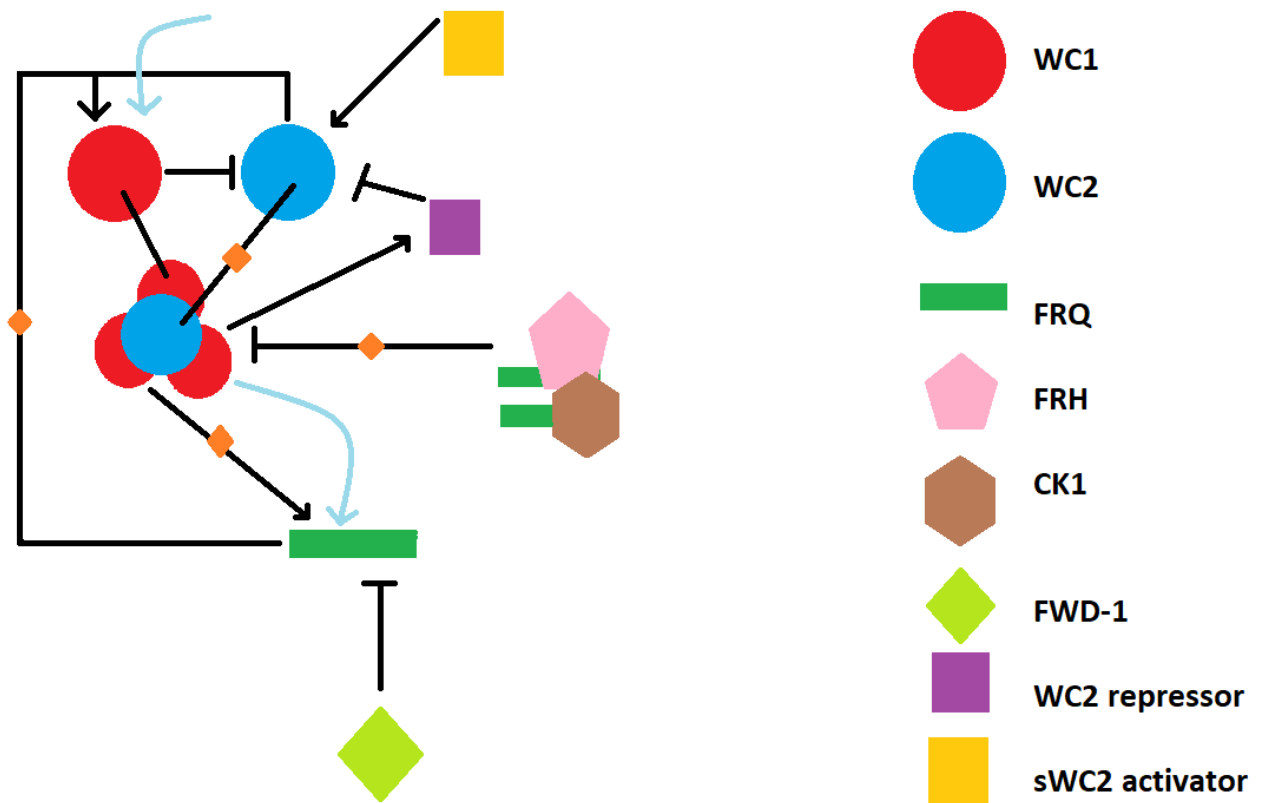


Figure 5.1: A simplified WCC-centric view of the circadian clock. Arrows represent activation and lines with bars on denote repression. Blue lines show the light-dependent PLRE activation of FRQ and orange boxes are phosphorylation status-dependant activation/repression.

The clock then goes on to rhythmically influence the expression and regulation of a plethora of clock-controlled genes (CCGs) (192,231,504), which ultimately determine a wide range of processes. Clock-controlled processes in *N. crassa* include cell division, sexual and asexual reproduction, cell signalling/communication, cell/cytoskeleton structure, cell defence, development, gene regulation, metabolism, protein processing and synthesis, glycolysis, and ROS homeostasis (192). Indeed, several non-functional and semi-functional clock mutants have been reported in fungi, displaying a wide variety of phenotypes which have profound effects on fitness. Table 5.1 shows a range of clock- and clock-associated mutant phenotypes displayed by *N. crassa* and other fungal species.

Table 5.1 – Fungal circadian-related mutant phenotypes

Fungal species	Gene	Mutation type	Phenotype	References
<i>A. fumigatus</i>	LreA	Null	Blue light blindness Reduced conidial germination in darkness Light-dependent cell wall instability	(371)
<i>A. nidulans</i>	WC1	Null	Light-independent increased conidiation Blue light blindness	(452,505)
<i>A. nidulans</i>	WC2	Null	Light-independent increased conidiation	(452)
<i>A. nidulans</i>	WC1/WC2-fphA double/triple mutant	Null	Reduced conidiation	(452)
<i>A. nidulans</i>	fphA	Null	Far-red light insensitivity	(118,118,481,483)
<i>A. nidulans</i>	velA	Null	Impaired sexual fruiting body formation Altered secondary metabolism	(506)
<i>A. nidulans</i>	velB	Null	Impaired sexual fruiting body formation Altered secondary metabolism	(506)
<i>B. cinerea</i>	BcCRY2	Null	Early conidiation Increased conidiation Increased melanisation	(108)
<i>B. cinerea</i>	BcCRY2	Overexpression	Decreased vegetative growth rate Reduced conidiation Decreased melanisation Increased aerial mycelium Exclusive aerial mycelia after 5d	(108)
<i>B. cinerea</i>	BcCRY1	Null	Reduced conidial UV tolerance	(108)
<i>B. cinerea</i>	BcCRY1	Overexpression	Increased UV tolerance	(108)
<i>B. cinerea</i>	BcWC1	Null	Reduced conidial UV tolerance Persistent conidiation Reduced growth rates under LL Pronounced conidial banding Light insensitivity Increased ROS susceptibility	(108,116,117,448)

			Reduced virulence (light treatment and host species-dependent) Loss of time-dependent gating of virulence	
<i>B. cinerea</i>	BcWC1	Overexpression	Increased aerial hyphae Reduced conidiation Increased ROS tolerance	(116)
<i>B. cinerea</i>	BcWC2	Null	Altered cell fusion Altered filament formation UV hyper-sensitivity Increased ROS susceptibility	(448)
<i>B. cinerea</i>	BcWC2	overexpression	Increased aerial hyphae Reduced conidiation Increased ROS tolerance	(116)
<i>B. cinerea</i>	BcFRQ	Null	Decreased macroconidiation Enhanced sclerotia formation Impaired virulence Pronounced media-dependent phenotypes Loss of time-dependent gating of virulence	(117)
<i>B. cinerea</i>	BcLTF1	Null	Light-dependent decreased growth rate Blue light blindness Reduced aerial hyphae Increased conidiation Increased ROS accumulation Reduced virulence	(119)
<i>B. cinerea</i>	BcLTF1	Overexpression	Increased aerial hyphae Decreased conidiation 'fluffy' phenotype	(119)
<i>C. militaris</i>	CmWC1	Null	Thicker aerial hyphae Disordered fruiting body development Reduced conidiation	(430)

			Reduced carotenoid biosynthesis Reduced cordycepin production	
<i>C. neoformans</i>	WC1	Null	Increased UV sensitivity Decreased virulence	(412,448)
<i>C. neoformans</i>	WC2	Null	Increased UV sensitivity Decreased virulence No light repression of mating, cell fusion and filament formation	(118,412,448,467)
<i>F. fujikuroi</i>	CarO	Null	Increased virulence	(473)
<i>F. oxysporum</i>	WC1	Null	Reduced aerial hyphae Impaired surface hydrophobicity Impaired light-induced carotenogenesis Impaired post-UV treatment photoreactivation Reduced virulence	(456)
<i>M. oryzae</i>	MoFwd1	'Null'	Reduced lesion diameter Fewer lesions Reduced appressorial penetration Reduced vegetative growth reduced conidiation Reduced conidiophore differentiation Delayed conidial germination Reduced appressorium formation No conidial banding	(259)
<i>M. oryzae</i>	MoFRQ	'Null'	Reduced vegetative growth Reduced conidiation Altered conidial morphology Delayed conidial germination Decreased appressorial formation Reduced virulence	(258,259) see chapter 6
<i>M. oryzae</i>	MgWC1	Null	No blue light specific repression of asexual development	(82,101)

			Constitutive asexual development in LL and DD Constitutive aerial hyphae development Reduced conidial release Reduced conidiation No light-dependent disease suppression	
<i>M. oryzae</i>	TWL	Null	Altered light-dependent carbon source utilisation Reduced conidiation Reduced light-dependent aerial hyphae formation Reduced conidiophore formation Reduced pathogenicity Impaired penetration and <i>in planta</i> cell-cell movement Reduced ROS suppression/tolerance Increased ROS sensitivity	(84)
<i>N. crassa</i>	WC1	Null	Arrhythmic conidiation Arrhythmic antioxidant regulation Blue light blindness Temperature insensitivity Reduced protoperithecia formation Reduced conidiation No conidial banding Altered ROS homeostasis	(177,184,199,201,202,437,485,507,508)
<i>N. crassa</i>	WC2	Null	Arrhythmic conidiation Arrhythmic antioxidant regulation Reduced conidiation Blue light blindness Temperature insensitivity Reduced protoperithecia formation No conidial banding Altered ROS homeostasis	(177,184,202,227,227,234,379,437,476,485,507,508)
<i>N. crassa</i>	WC1-WC2	Double Null	Rhythmic conidiation under lipid-deficient conditions	(509)

			Light insensitivity	
<i>N. crassa</i>	FRQ	Null	Arrhythmic conidiation Reduced conidiation Altered ROS homeostasis	(184,379,502,510,511) see chapter 6
<i>N. crassa</i>	SET-2	Null	Arrhythmic frq expression and conidiation	(512)
<i>N. crassa</i>	VVD	Null	Rhythmic conidiation under constant light Fast conidiation period	(513)
<i>S. sclerotiorum</i>	Sop1	Null	Increased salt sensitivity Increased fungicide sensitivity Increased osmotic stress sensitivity Increased ROS tolerance Reduced growth rate Altered sclerotial development	(420)
<i>V. dahliae</i>	FRQ	Null	Light-independent slowed colony growth Altered secondary metabolism Reduced pathogenicity	(434)
<i>Z. tritici</i>	MVE1	Null	Reduced growth rate Increased stress sensitivity Reduced melanisation Light-independent aerial hyphae formation	(215)
<i>Z. tritici</i>	ZtWco-1	Null	Reduced hyphal development Reduced melanisation Reduced virulence and delayed disease symptoms Altered pycnidiospore development Increased vegetative growth (under DD and LL) Increased micropycnidiospore production (relative to pycnidium production)	(392)

5.1.2 The WHITE COLLAR COMPLEX is multifunctional and acts as a photoreceptor

WC1 also has a function as a blue light photoreceptor, mediated by its LOV domain, and is often considered the principal photoreceptor in *N. crassa* (181,199,211,234,511,514,515). WC2 possesses no such photoreceptor ability due to its lack of a LOV domain (178), but its close association with WC1 means its function and location is indirectly associated with light, and therefore non-functional WC1 and/or WC2 often present similar phenotypes and light insensitivity (227,479,509). Upon detection of light, the WCC goes on to interact with a second component of the FRQ promoter region, the proximal light regulatory element (PLRE), which is located downstream of the C-box and is close to the transcriptional start site (178,181,192,224). PLRE activation causes an acute induction of *frq* transcript and thus resets the clock to ensure a synchronous intercellular phase with the environment (Fig. 5.1, blue arrows) (178,181,192,224,516). Indeed, the WCC actually exists in two forms: a smaller WC1/2 heterodimer that strongly binds to the FRQ C-box promoter in the dark (for circadian function), and a larger light-dependent complex consisting of a single WC2 bound to several WC1 proteins that rapidly regulates light responses through the PLRE (178,184,191,199,202,208,211,476). During prolonged exposure to light, the PLRE-based activation of FRQ does not constantly occur (214), as the photoactivated WCC also highly induces the expression and activity of VIVID (VVD), which inactivates the WCC by competitively forming WCC-VVD heterodimers, causing available WCC levels to quickly fall back to their pre-light activated stage (198,214,517). In this way, the light activation of the WCC (and subsequent regulation of FRQ) is transient and undergoes photoadaptation (198,214,517).

Wang and colleagues (234) reported that light induction of *frq* by the WCC utilises the WC2 DNA binding capability and does not use any part of the WC1 DNA binding regions,

suggesting that WC1 senses the light, but WC2 acts to upregulate FRQ expression at the PLRE. For circadian regulation, though, both WC1 and WC2 DNA binding is required (234). Since WC2 is essential in both circadian and light regulation of FRQ, there have been suggestions that WC2 is perhaps the key player in the WCC, despite its inability to directly sense light (227,437).

In addition to the WCC existing in two isoforms, WC2 itself exists in two forms: the full length WC2, and an N-terminally truncated, shorter WC2 (sWC2) (216). To this end, WC2 contains a second in-frame internal promoter and transcriptional start site on its second exon, which gives rise to sWC2 (216). A similar alternative splicing phenomenon is observed in FRQ (see 6.1.3.5). WC2 and sWC2 are expressed antagonistically, with sWC2 expressed to a much smaller degree, independently of WC1 and FRQ repression/activation (Fig. 5.1) (216). sWC2 can still interact with WC1, though, and potentially acts to supplement WC2, ensuring that basal (s)WC2 levels are maintained above a functionally critical minimal threshold (216). In support of this, it has also been reported that WC2 is in excess in the circadian system; low levels of WC2 protein can still support sufficient FRQ expression, suggesting that WC1 is the defining component of the WCC (191,202,221,510,518). Neiss and colleagues (216) subsequently generated a *N. crassa* strain that expressed only sWC2 and the mutant maintained a robust, although lengthened, conidial banding period, implicating sWC2 in C-box circadian regulation of FRQ as opposed to PLRE light regulation. Overexpression of sWC2 also showed a robust rhythm under constant darkness, further suggesting that WC1 is the limiting factor in the WCC (216). Perhaps, then, the N-terminal region missing in sWC2 facilitates the recruitment of several WC1 proteins, allowing for light activation of FRQ.

5.1.3 The WCC plays a role in fungal pathogenicity

The effect of time of day, circadian machinery, and photoreception on fungal virulence is becoming increasingly well studied in certain species, most of all the necrotrophic *Botrytis cinerea* (108,116,180,392,392,478,495,519–521). *B. cinerea* contains homologues for WC1, WC2 and FRQ, implicating a functional circadian clock (116). In a similar fashion to *N. crassa*, the WCC in *B. cinerea* plays a role in conidiation, growth and development, and oxidative stress responses (116). Whilst there are many similarities between the two species, Canessa and colleagues (116) reported that the *bcwcl1* knockout actually showed a clearer conidial banding phenotype under LD compared to the wild type, although the period did not correspond to a band once per day, implicating the conidial banding phenotype in *B. cinerea* as a WCC- and FRQ-less oscillator (see 6.1.3.7). They suggested that the enhanced phenotype may be due to the altered intracellular ROS status, which is known to cycle back into the circadian clock (116,184). This phenotype suggests that there may be an alternative role of the clock and/or WCC in *B. cinerea* conidiation and development compared to *N. crassa*, where most non-functional WCC mutants do not present conidial banding. In support of altered or additional clock function in certain species, FRQ has an additional role in microconidia and sclerotial production in *B. cinerea* depending on the culture medium, which has not been observed in *N. crassa* (117,257).

Two WCC-regulated genes responsible for black/near-UV light sensing (BcCRY1 and BcCRY2) have functions in *B. cinerea* photoprotection and conidiation, respectively (108). The WCC mediates the expression of both of these genes upon exposure to light, and WC1 mutant conidia are less tolerant to UV stress due to misregulation of BcCRY1 (108,116). Overexpression of BcCRY2 gives rise to reduced conidiation, suggesting that

BcCRY2 represses conidiation during the day, which is mediated by the WCC through its photoreception ability (108). bcVEL1 is a VELVET gene that also has a function in light-dependent differentiation and virulence in *B. cinerea*, and is likely a downstream target of the WCC, as a bcVEL1 null strain showed light-independent conidiation (a common phenotype in WCC mutants), an inability to produce sclerotia and oxalic acid (which aids in pathogenic invasion), and reduced virulence towards a range of different host species (478,520).

In a comprehensive study conducted by Hevia and colleagues (117), *Arabidopsis* plants were infected with *B. cinerea* at dawn and dusk, using clock mutants in both the host plant and pathogen. Here, they showed that the wild type *Arabidopsis* was more susceptible to infection at dusk, but crucially, also observed the same time of day difference in clock-deficient *Arabidopsis* strains, implicating the fungal clock in pathogenicity. To prove that the fungal clock had a function in pathogenicity, arrhythmic WC1 strains of *B. cinerea* were used to infect wild type plants and they saw no significant effect of inoculation timing on *B. cinerea* infection severity (117). Further, an *frq* overexpression strain was generated, which again showed no time of day-dependent differences in pathogenicity, but also produced smaller lesions than the wild type fungus, implicating the fungal clock in the outcome of disease (117). Finally, *B. cinerea* was also grown in antiphase to the plant host (DL: dawn for plants is dusk for the pathogen) prior to infection and the results were reversed: dawn inoculations gave rise to larger lesions (117). These results suggest that (at least in *B. cinerea*-*Arabidopsis* interactions), the fungal clock plays a significant, and perhaps dominant role in the outcome of disease. There have also been reports of time of day-dependent outcomes and roles of photoreceptors in other plant pathogenic species (as is discussed in chapter 4), but

considerably less work has been done on the role of circadian machinery in the outcome of fungal disease.

Beyond *B. cinerea*, the WCC has a significant effect on the virulence of *Cryptococcus neoformans*, the casual fungus of meningitis in humans; light inhibits mating and haploid fruiting in *C. neoformans* through the WCC, and mutations in either component (WC1 or WC2) are less virulent in mice, with spores more susceptible to UV irradiation, a phenotype similar to the CRY mutants observed in *B. cinerea* (108,116,412,448). WC2 mutation in *C. neoformans* also caused the pathogen to lose its light-dependent repression in mating, cell fusion, and subsequent filament formation, which are phenotypes reminiscent of *N. crassa* clock mutants, and have significant implications in pathogenicity (118,448). A recent report by Tiley and colleagues (392) also showed that WC1 knockout mutants in *Zyoseptoria tritici* grew faster than the wild type under constant conditions (DD and LL), WC1 is required for light perception (mutants displayed no significant differences in vegetative growth rates between DD and LL, unlike the wild type) and hyphal growth in liquid culture. Importantly, the *Z. tritici* Δ WC1 strain also showed reduced and delayed pathogenesis towards wheat, where the onset of necrosis and chlorosis symptoms occurred 2-4 d later than the wild type, and sporulation was reduced ,both *in-* and *ex-planta* (392). Summarily, there is increasing research implicating the clock in the virulence of pathogenic fungi, showing (at times) species-specific roles of clock components in growth, development, and pathogenicity. For further reading, the current scope and importance of circadian rhythmicity in fungal pathogenesis and host defence is covered in an excellent review by Larrondo and Canessa (257), and a summary of select clock- and clock-associated mutant fungal strains with a focus on fungal pathogens is displayed in Table 5.1.

5.1.4 Clock component mutants in *M. oryzae* show altered growth, development, and pathogenicity

In *M. oryzae*, there have been a small number of studies implicating the role of circadian machinery in the outcome of rice blast disease (82,101,259). Shi and colleagues (259) show that FWD1 (which is responsible for the turnover of hyperphosphorylated FRQ in *N. crassa*) regulates transcription and stability of FRQ, and (when knocked out) FWD1 mutants gave rise to fewer lesions compared to the wild type. Further, FWD1 null strains had a reduced vegetative growth rate (by approximately 10%) on CM plates compared to the wild type Guy11 and a ~90% reduction in conidiation and germination rate by 4 HPI (259). The FWD1 null strain also showed a 90% reduction in appressorium formation, in agreement with the reduced germination (259). Shi and colleagues reasoned that the deletion of FWD1 could cause FRQ levels to increase as a result of reduced FWD1-dependent FRQ repression or turnover (259). The increased FRQ levels could then suppress the WCC and consequently prevent light-induced transcription of FRQ, causing altered photosensitivity. To (partially) confirm this, they determined that degradation of FRQ::GFP was impaired in the FWD1 null strain (259). However, the addition of a GFP tag on FRQ may also have altered its structure and/or functional capability. Further, whilst FWD1 is chiefly responsible for the degradation of FRQ, it is not responsible for its circadian function, as FWD1 predominantly facilitates the turnover of hyperphosphorylated FRQ, which is already inactive in the circadian system (see 6.1.1).

WC1 null strains generated by Lee and colleagues (82) showed a blindness to blue light and they lost the conidial banding phenotype, in contrast to *B. cinerea* and reminiscent of the *N. crassa* mutants (see table 5.1). Accordingly, WC1 mutant aerial hyphae development was similar under constant light and constant darkness, exhibiting

constitutive asexual development, suggesting that blue light and WC1 in tandem control the asexual development and photoadaptation of *M. oryzae* (82). These mutants also showed a slight decrease in conidial production and did not show a time-dependent release of conidia, implicating WC1 in the release of conidia during the dark period, where conidial release peaks just before dawn (82). Thus, non-functional WC1 could significantly affect pathogenicity in the field, as optimal timing of conidial release would not occur (82,101).

Kim and colleagues (101) expanded on the WC1 experiments by Lee (82), showing that WC1 complementation restored conidial banding and that functional WC1 allows for photo-induction of FRQ in *M. oryzae*, in a similar fashion to the *N. crassa* PLRE-dependent activation. *wc1* mRNA transcript levels were also observed to be highly enriched in conidia compared to mycelia, suggesting that the clock and/or photoreception is important for conidial-specific and thus potentially virulence function (101). Indeed, it has been reported that circadian periodicity and function can differ depending on tissue type in plants, so perhaps a similar phenomenon is presented in this study (101,172,464,465). Due to the WC1 *M. oryzae* mutant being insensitive to blue light, the degree of light-dependent disease suppression was reduced, where the wild type showed decreased pathogenicity upon post-inoculation light exposure, but the mutant did not. These pathogenicity experiments did not mention pre-inoculation entrainment of *M. oryzae*, however, and as such this effect may be a result of the WC1 mutant's inability to undergo PLRE-based light induction of FRQ as opposed to a circadian effect, a potential example of a diurnal vs circadian output (101). This study also showed that *vvd* transcript (a WCC-ccg (white collar complex clock-controlled gene) and blue light photoreceptor in

N. crassa) followed a similar pattern in *M. oryzae* as in *N. crassa* upon transfer to constant darkness, where vvd levels fell rapidly.

Finally, Deng and colleagues (84) showed that TWILIGHT (TWL, a circadian-controlled gene) plays a role in light-induced asexual development and pathogenicity in *M. oryzae*. TWL mutants had reduced asexual reproduction, nutrient utilisation, signal perception, and pathogenicity, whereby invasive hyphae were unable to cross the host cell wall from the primary penetrated cell (84). This lack of cell-cell movement may be a result of the TWL mutant's reduced ability to suppress and/or tolerate the high levels of ROS found within the host, since exogenous addition of the antioxidant glutathione restored the mutant's invasive capability (84). As mentioned previously, ROS regulation is a well-documented circadian output (84,116,119,184,192,420,448). Deng and colleagues concluded that TWL is not a member of the core clock machinery but is essential in light- and nutrient-responsive events (especially conidiation and pathogenesis), both of which are influenced by the WCC in a rhythmic and light-dependent manner. To date, there have been no reports on the biological role of WC2 in *M. oryzae*, despite its essential function in the WCC and clock of *N. crassa*. This chapter therefore focusses on WC2 and its role in growth, conidiation, conidial development, and pathogenicity in host- (rice) and non-host (barley) plant species.

5.2 Results

5.2.1 Generation and screening of Δ WC2

A CRISPR Cas9-mediated knockout in *M. oryzae* WC2 (MGG_04521) was generated through homology-directed repair (HDR) using an 80 bp double stranded donor DNA template containing a single base edit that corresponds to a premature termination codon. Concurrently, co-editing of SDI-1 was implemented, which gives rise to carboxin resistance, the rationale being that transformants showing carboxin resistance had been successfully edited at the SDI-1 locus so would be more likely to have taken up the second ribonucleoprotein and donor DNA targeting WC2 (for full details, see 2.10 and (269)).

Potential WC2 sgRNA target sequences were determined using E-CRISP and a target sequence present on the second exon was selected for DNA cleavage and HDR (Fig. 5.2).

The second exon could potentially contain an in-frame sequence for a hypothetical sWC2 (as is the case in *N. crassa*) and thus the first exon may house the N-terminally truncated section absent in sWC2, so a target sequence in the centre of exon 2 was a good choice.

A codon 10 bases upstream of the WC2 target PAM site, coding for Glutamine (GAG), was selected for editing due, in part, to its proximity to the PAM site and the requirement for a single base edit conferring a premature termination codon (PTC): GAG → TAG. Donor sequences with base edits are shown in table 5.2. In addition to creating a PTC with the donor DNA, the TAG edit also removes a SacI restriction enzyme recognition site (gagctc), allowing for faster screening of putative mutants (see 2.10, 2.11, and 2.15). A 224bp amplicon (based on compatible primers, chosen using Primer3web) centred around the edit site was used for screening (primers in table 5.2).

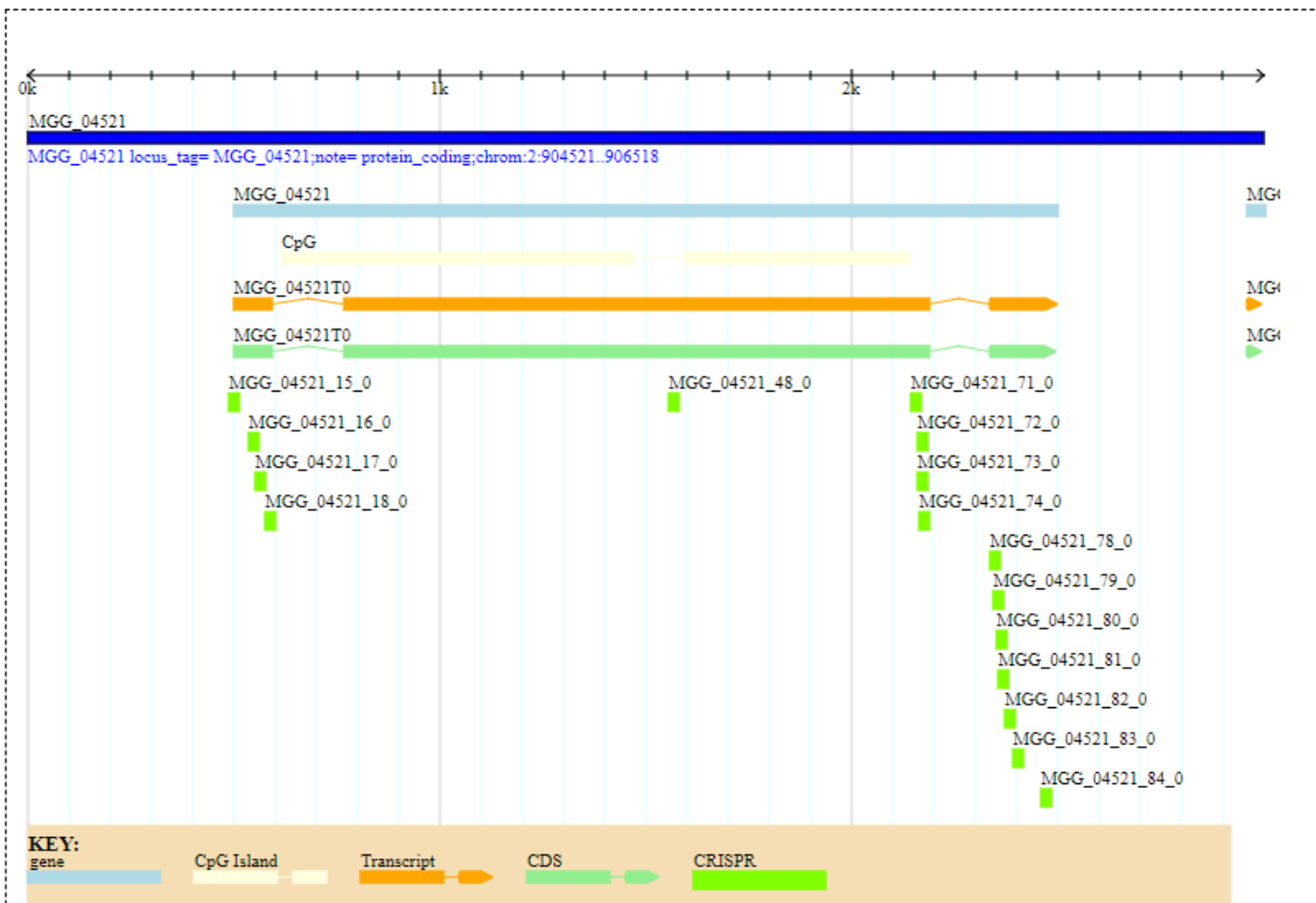


Figure 5.2: Potential *M. oryzae* WC2 target sites. E-Crisp predicted Cas9 target sites on the *M. oryzae* WC2 (MGG_04521).

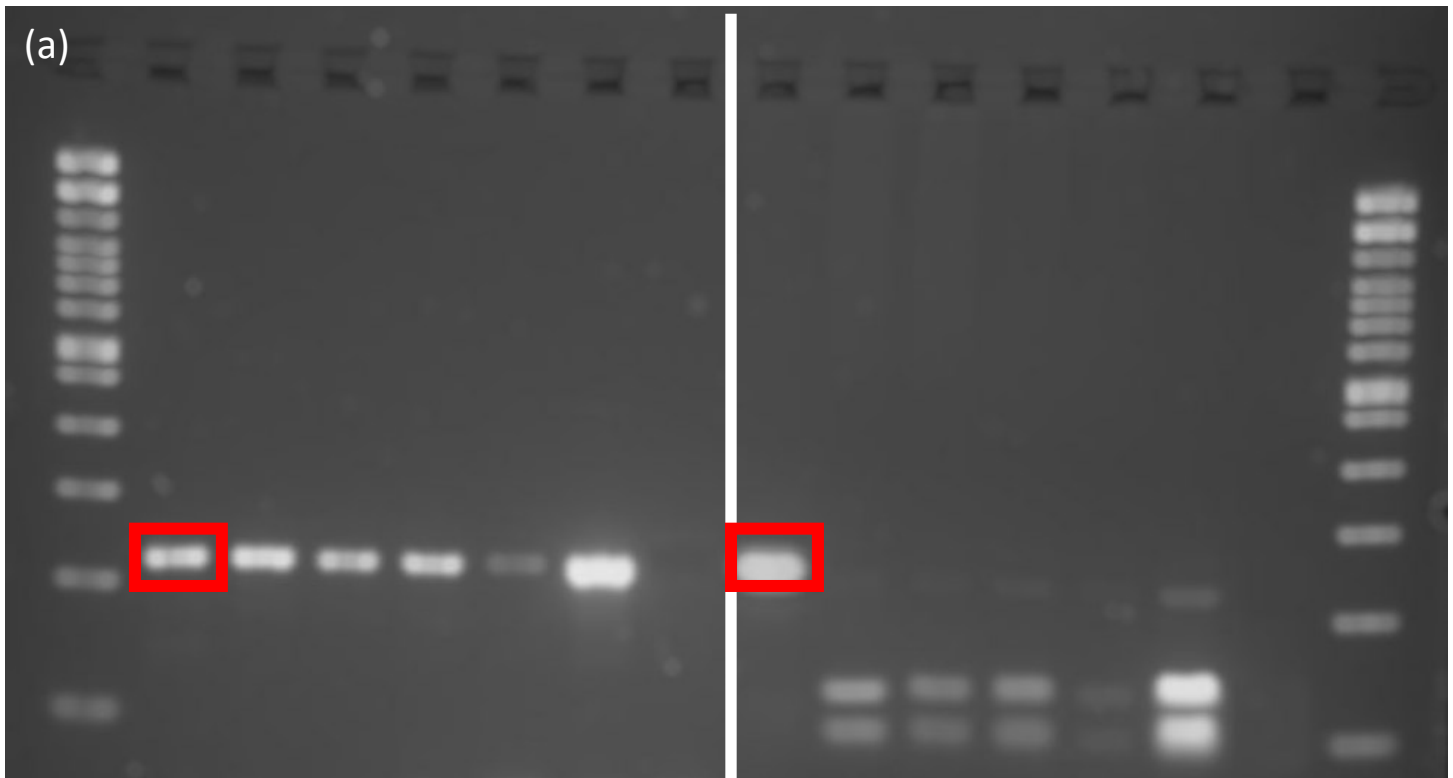
Table 5.2: Δ WC2 donor DNA and diagnostic primers

Δ WC2 donor template top strand (5'-3')	AAATTGAGAACGAGCGCTTGCCTCGTAGGATAGCAT <u>TAG</u> CTCCGAAAGGAGGAATATGAAGACGGGGGCGAGGATGCGCA
Δ WC2 donor template bottom strand	TGCGCATCCTCGCCCCGTTCATATTCCTCCTTCGGAG <u>CTA</u> TGCTATCCTACGACGCAAGCGCTCGTTCTCAATTT
WC2 diagnostic forward primer (5'-3')	ACCAATCACATTTCCGCCAG (Tm 57.3)
WC2 diagnostic reverse primer (5'-3')	AGATACTGTTGCATCCTCGGA (Tm 57.9)

In the wild type, the 224 bp amplicon contains a single *SacI* restriction enzyme site, which would correspond to a 130 bp and 94 bp fragment (Table 5.3) (virtual digests were carried out using RestrictionMapper V3). Restriction enzyme edit sites and primer locations were selected, in part, to ensure that any fragments would be asymmetrical and thus could be resolved on an agarose gel. Upon gel electrophoresis, the only WC2 amplicons showing a single band must have an edit at the directed site. As expected, a putative WC2 mutant was generated that did not cut after *SacI* digestion (Fig. 5.3). Full length (224 bp wild type and putative mutant) amplicons were then sequenced (Eurofins Sanger sequencing), confirming this edit (Fig. 5.3). Interestingly, the WC2 mutant also showed an off-target mutation 3 bases upstream of the PTC edit, changing GCA (Alanine) to ACA (Threonine) (Fig. 5.3). Indels located very close to the prospective cut site are not uncommon in successfully Cas-transfected cells, however. Regardless, the observed phenotype clearly suggests a non-functional WC2 strain (discussed below). WC2::GFP complementation strains were kindly generated and provided by Dr. Xia Yan (Prof. Nick Talbot lab - TSL) using a split marker gene replacement approach.

Table 5.3: Δ WC2 diagnostic amplicon restriction digest

Strain	Length	5' Enzyme	5' Base	3' Enzyme	3' Base	Sequence
Wild type	130	None	1	SacI	130	ACCAATCACATTTCCGCCAGGCCGTTTTCTTATGTTCGAG ACCCTAGCCAACGAAGAACGCCGA ACTACTAGACTCATT TTGGAGCACAAAATTGAGAACGAGCGCTTTCGTCGTAGG ATAGCAGAGCT
	94	SacI	131	None	224	CCGAAAGGAGGAATATGAAGACGGGGGCGAGGATGCGC AGAGGAACTGGCCTGACGGTCGGTCAGAGATGACATCCG AGGATGCAACAGTATCT
Δ WC2	224	SacI does not digest this sequence				



WC2_WT_FP

Sequence ID: Query_37381 Length: 177 Number of Matches: 1

(b)

Range 1: 1 to 177 [Graphics](#)

▼ [Next Match](#) ▲ [Pre](#)

Score	Expect	Identities	Gaps	Strand
316 bits(171)	1e-91	175/177(99%)	0/177(0%)	Plus/Plus
Query 3	CCAACGAAGAACGCCGA	ACTACTAGACTCATTCTTGGAGCACAAAATTGAGAACGAGCGC	62	
Sbjct 1	CCAACGAAGAACGCCGA	ACTACTAGACTCATTCTTGGAGCACAAAATTGAGAACGAGCGC	60	
Query 63	TTGCGTCGTAGGATAAC	ATAGCTCCGAAAGGAGGAATATGAAGACGGGGGCGAGGATGCG	122	
Sbjct 61	TTGCGTCGTAGGATAGC	AGAGCTCCGAAAGGAGGAATATGAAGACGGGGGCGAGGATGCG	120	
Query 123	CAGAGGAACTGGCCTG	ACGGTCGGTCAGAGATGACATCCGAGGATGCAACAGTATCT	179	
Sbjct 121	CAGAGGAACTGGCCTG	ACGGTCGGTCAGAGATGACATCCGAGGATGCAACAGTATCT	177	

Figure 5.3: ΔWC2 mutant screening and confirmation. (a) Gel electrophoresis (3% agarose) separation of 224 bp WC2 amplicon. Left side of the gel (lanes 2-8) are PCR products of Cbx-resistant transformants. Right side (lanes 10-16) are the same digested PCR products (expected 130 + 94 bp for non-edited, 224 bp for edited mutants) of lanes 2-8. The red box surrounds the putative mutant to be sequenced. Lanes 8 and 15 are no-sample controls, where water was used in place of extracted DNA in the PCR. Lanes 1 and 16 are 100 bp ladders (NEBio). (b) Sequence comparison (Blastn) of the putative mutant (query) from (a) and a randomly selected wild type (digestible) sample (sbjct), showing the expected GAG → TAG edit, as well as off-target GCA → ACA

5.2.2 *M. oryzae* Δ WC2 displays an arrhythmic conidial banding phenotype

5.2.2.1 Δ WC2 does not present conidial banding under any light conditions

Wild type Guy11 and Δ WC2 strains were grown under a range of different light conditions (as in chapter 4), and Δ WC2 showed no conidial banding under any entraining conditions, including light-dark (LD) cycling conditions: a phenotype common to WCC knockouts of many fungal species (Fig. 5.4, Table 5.1). The *M. oryzae* guy11 wild type does not produce conidial bands without proper entrainment (see 4.2.2), and thus WC2 must be (partly) responsible for the entrainment of the circadian clock. Further, the conidial banding returned in the WC2::GFP complement strain and continued in free-running conditions after a period of entrainment, suggesting that WC2 is absolutely essential for circadian conidial banding in *M. oryzae* (Fig. 5.5). However, the latency period in WC2::GFP is slightly longer than the wild type, which may result from an altered conformational shape from the additional GFP tag.

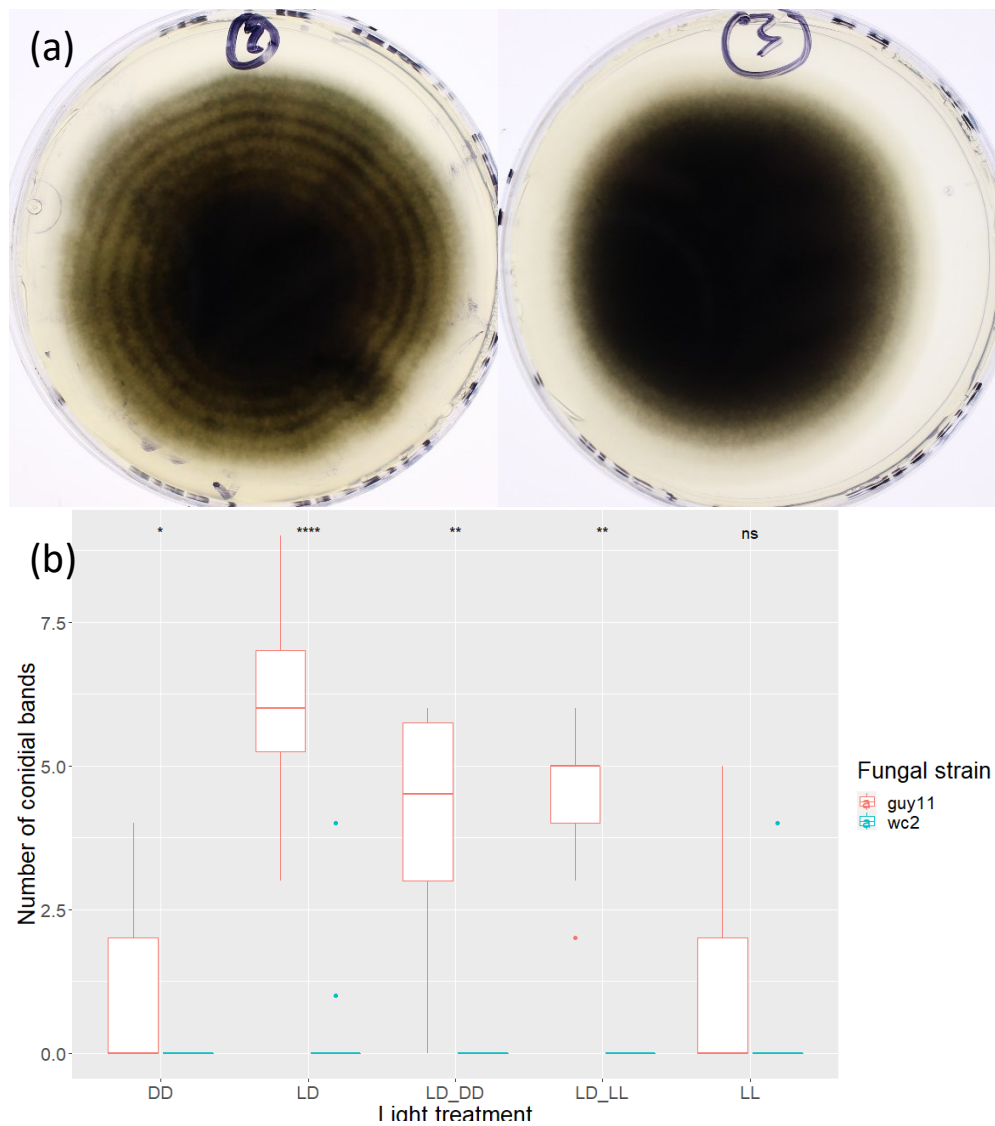


Figure 5.4: *M. oryzae* Δ WC2 does not display conidial banding. (a) demonstrative image of wild type Guy11 and Δ WC2 strains grown on complete media (CM) under LD conditions. (b) Δ WC2 were grown on CM alongside wild type Guy11 under a range of different light treatments and did not show any conidial banding over a period of 12 d. n = 16 guy11 DD, n = 8 Δ WC2 DD, n = 23 guy11 LD, n = 16 Δ WC2 LD, n = 15 guy11 LD-DD, n = 8 Δ WC2 LD-DD, n = 13 guy11 LD-LL, n = 5 Δ WC2 LD-LL, n = 19 guy11 LL, n = 15 guy11 LL. Stars show increasing statistical significance within treatments (ANOVA, p < 0.05).

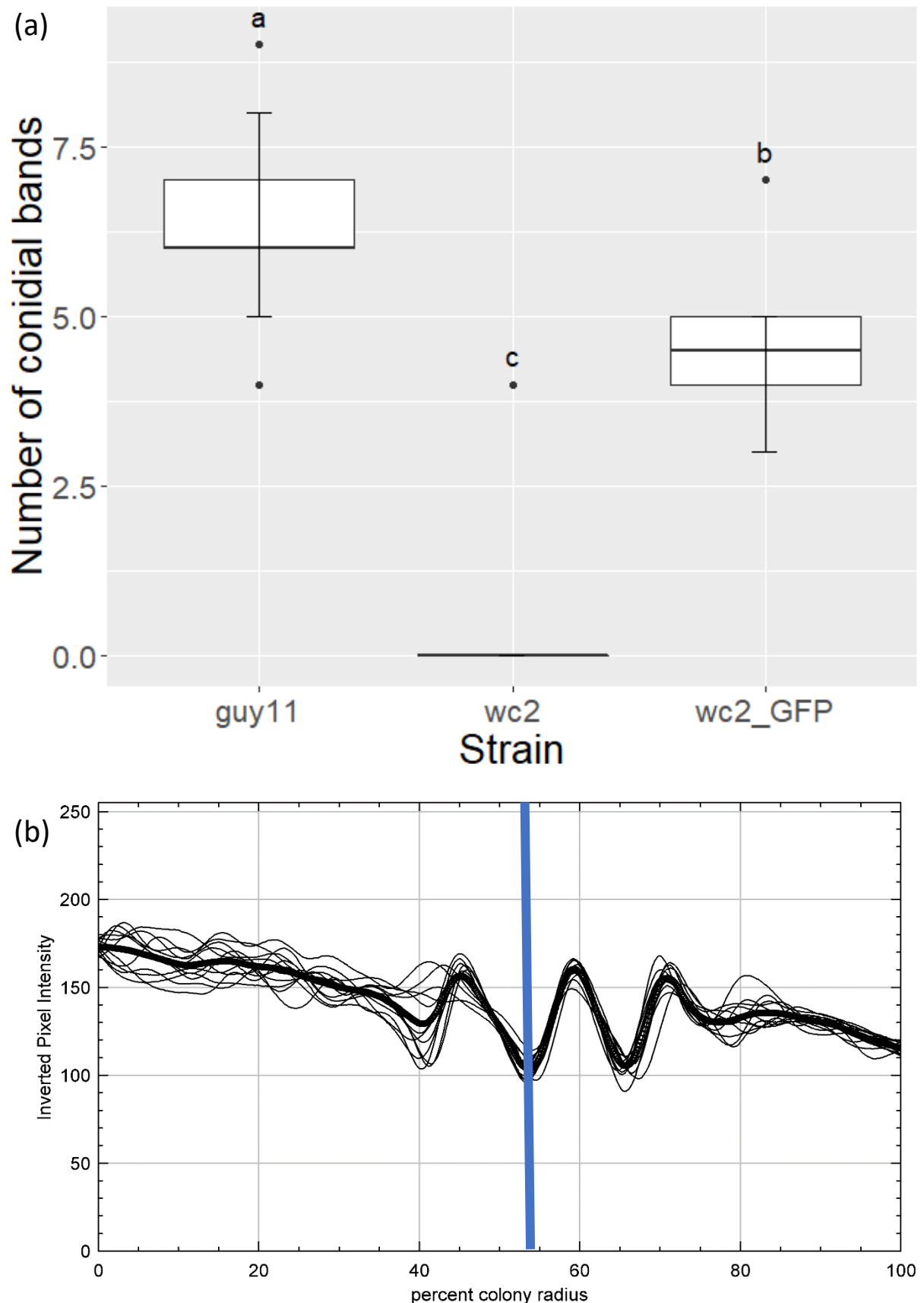


Figure 5.5: WC2::GFP complementation rescues the conidial banding phenotype. (a) WC2::GFP complement strains display conidial banding phenotype, but the latency period is increased ($n = 23$ LD, $n = 11$ WC2, $n = 9$ WC2::GFP). Letters describe statistically significant differences between groups ($p < 0.05$, Tukey's HSD). (b) Conidial banding continues to occur under free running conditions in WC2::GFP after entrainment to LD. The blue line denotes the point at which the WC2::GFP strain was transferred to constant light.

5.2.2.2 Δ WC2 produces, but does not respond to, the conidial banding metabolite(s)

To determine if the lack of conidial banding in Δ WC2 was due to its inability to produce or respond to the spent media (SM) metabolite(s) responsible for the latency period (see 4.2.4), wild type and Δ WC2 strains were grown in shaking cultures for 10 d and used to dilute 2x CM (see 2.2.1 and 2.2.4). Wild type and Δ WC2 were then grown in a reciprocal manner on either CM, 50% wild type SM, or 50% Δ WC2 SM plates (Fig. 5.6). Δ WC2 failed to band on any of the media types, whereas wild type *guy11* showed early conidial banding (~4 d) on both WT SM and Δ WC2 SM. This suggests that Δ WC2 produces, but is insensitive to, the conidial banding metabolite(s), and thus WC2 is responsible for its sensation and eventual conidial banding.

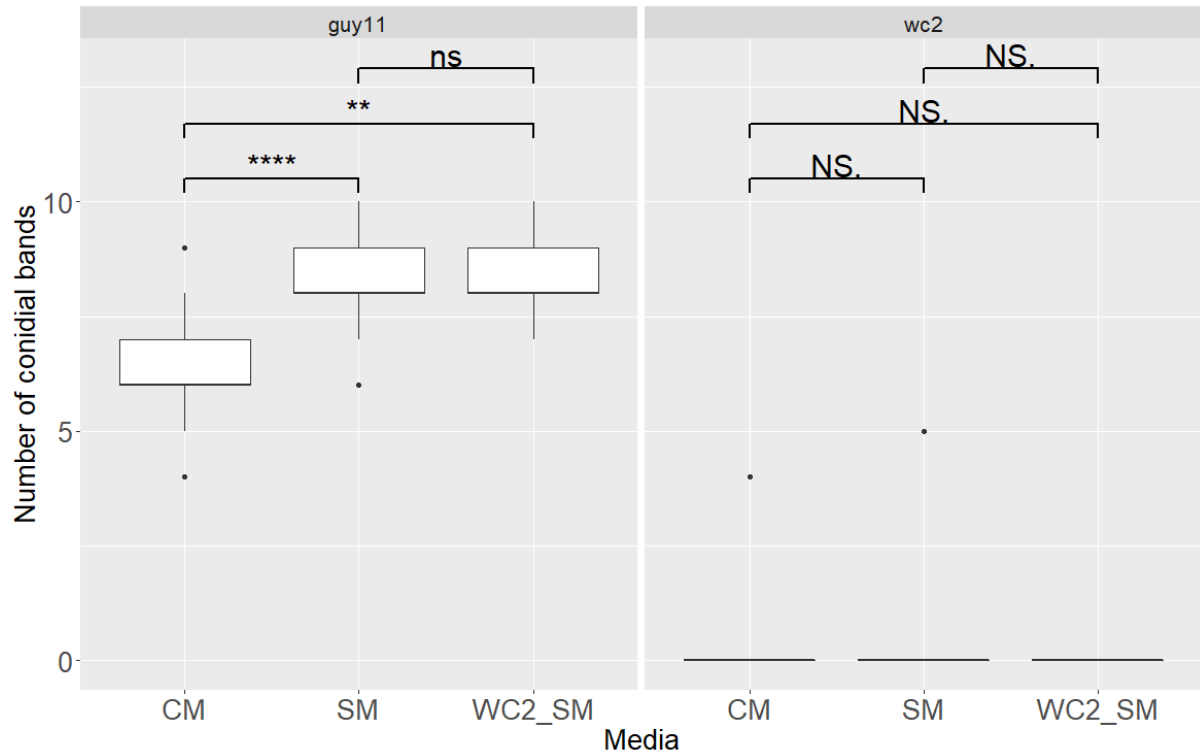


Figure 5.6: Δ WC2 produces, but is insensitive to, the conidial banding metabolite(s). Wild type *guy11* (left) and Δ WC2 strains (right) were grown on complete media (CM), 50% wild type spent media (SM), and Δ WC2 SM (WC2_SM) (v/v) for 14 d under LD conditions. Wild type colonies grown on either SM plates showed earlier banding, suggesting that Δ WC2 can still produce the mystery metabolite(s) ('ns' denotes a p value above 0.05, and 'NS.' Shows a p value of ~ 1). n = 23 *guy11* CM, n = 17 *guy11* SM, n = 6 *guy11* WC2_SM, n = 11 WC2 CM, n = 8 WC2 SM, n = 3 WC2 WC2_SM.

5.2.3 WC2 plays a role in photoadaptation and growth rates

Interestingly, despite light cycles having no effect on conidial banding in *M. oryzae* Δ WC2 strains, growth rates under LL treatments were comparatively higher than colonies grown under LD-LL and LD (Fig. 5.7); all other treatments with dark periods (DD, LD, LD-DD) fell between LL and LD-LL (Fig. 5.7). This result implies that there may still be functional photoreception (or sensation of darkness) in Δ WC2. In comparison, the wild type displays increased growth rates under both constant light and darkness. In this way, WC2 may play a role in dark adaptation, like its partner protein, WC1 (82,101).

In support of this, there is no significant difference between wild type and Δ WC2 growth rates when grown under LD-DD or LL, whereas Δ WC2 grows slower than the wild type under DD, LD, and LD-LL (Fig. 5.7). Therefore, it is possible that Δ WC2 may be able to sense cycling diurnal conditions but cannot undergo dark adaptation. It is important to consider here that the wild type showed an increase in growth rate once conidial banding began to occur, a phenotype not displayed in Δ WC2. These data suggest that, alongside WC1, WC2 is likely responsible for photoadaptation in *M. oryzae* (82,101).

This reduced growth rate under LD conditions is not restored in the WC2 complement mutant, and it is slower growing than Δ WC2, perhaps as a result of the additional energetic expenditure on GFP production (Fig. 5.7). Alternatively, the tagging of a GFP to the end of the WC2 protein may cause altered protein-protein interactions or DNA binding, perhaps due to a conformational shape change, which may lead to the reduced growth rates.

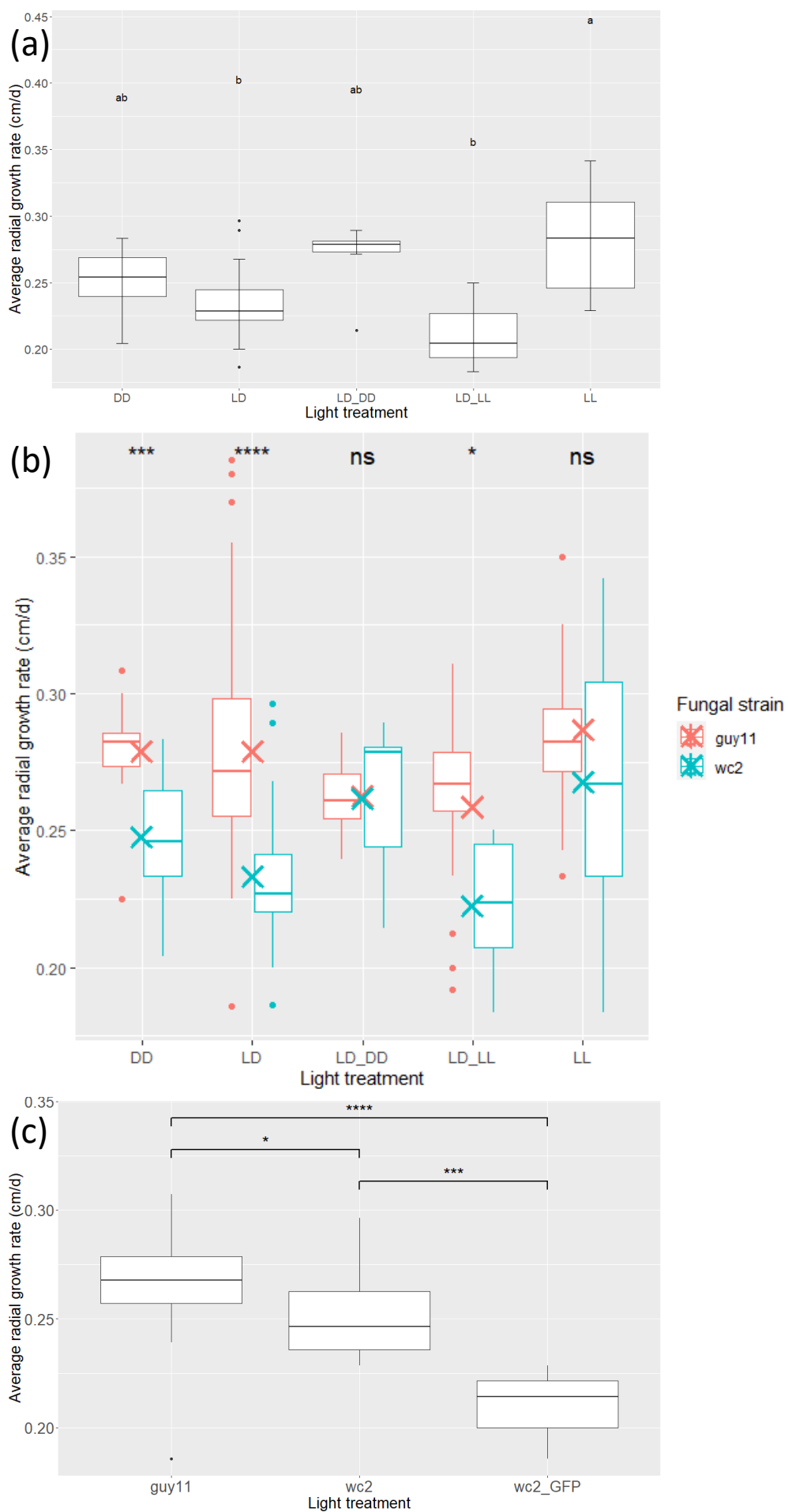


Figure 5.7: WC2 affects photoadaptation in vegetative growth. (a) constant light-grown Δ WC2 grows significantly faster than LD and LD-LL grown Δ WC2 colonies but does not display dark adaptation to prolonged darkness. (b) Δ WC2 grows significantly slower than the wild type except under LD-DD and LL, further suggesting an inability to sense/adapt to darkness. (c) the WC2::GFP complementation strain grows even slower than Δ WC2 (n = 8 WC2 DD, n = 11 WC2 LD, n = 8 WC2 LD-DD, n = 6 WC2 LD-LL, n = 15 WC2 LL, n = 16 guy11 DD, n = 23 guy11 LD, n = 15 guy11 LD-DD, n = 13 guy11 LD-LL, n = 19 guy11 LL, n = 9 WC2::GFP LD). Letters describe statistically significant differences between groups (p < 0.05, Tukey's HSD), Bars with stars atop denote statistically significant differences (p < 0.05, ANOVA), and crosses mean values.

5.2.4 WC2 functions in light-dependent conidiation repression

Despite the observations that prolonged light exposure increased growth rates in Δ WC2, LL and LD-LL conditions had little effect on the number of conidia produced in Δ WC2 colonies (Fig. 5.8). Instead, DD and LD-DD conditions in Δ WC2 showed a significant reduction in conidiation compared to LD cycling conditions (which is most conducive for conidiation in both wild type and Δ WC2), with LD-LL and LL falling between the two groups (Fig. 5.8). This further suggests that WC2 plays a role in light/dark adaptation in *M. oryzae*. Harvest time (dawn or dusk) again had no impact on conidiation, agreeing with the notion that it takes more than 12 h to produce mature conidia, as is the case in the wild type (see 4.2.5).

In comparison to the wild type, where LD conditions are most conducive for conidiation compared to all other treatments, the fact that LD-LL and LL treatments do not cause as significant a reduction in conidiation implies that WC2 plays a role in light-dependent repression of conidiation or prolonged darkness adaptation. Δ WC2 produces fewer conidia than the wild type under DD, LD, and LD-DD (Fig. 5.8), further suggesting either a lack of light sensitivity and/or an inability to dark adapt in the mutant (Fig. 5.8). In support of WC2 playing a role in photoadaptation and conidiation, a common phenotype in fungal WCC mutants is observed, where light exposure has less of an effect on conidial production (see table 5.1). Finally, despite its reduced growth rate, the conidiation reduction under LD conditions in Δ WC2 is restored in the WC2::GFP complementation (Fig. 5.8), showing that WC2 is responsible for the reduced conidiation phenotype.

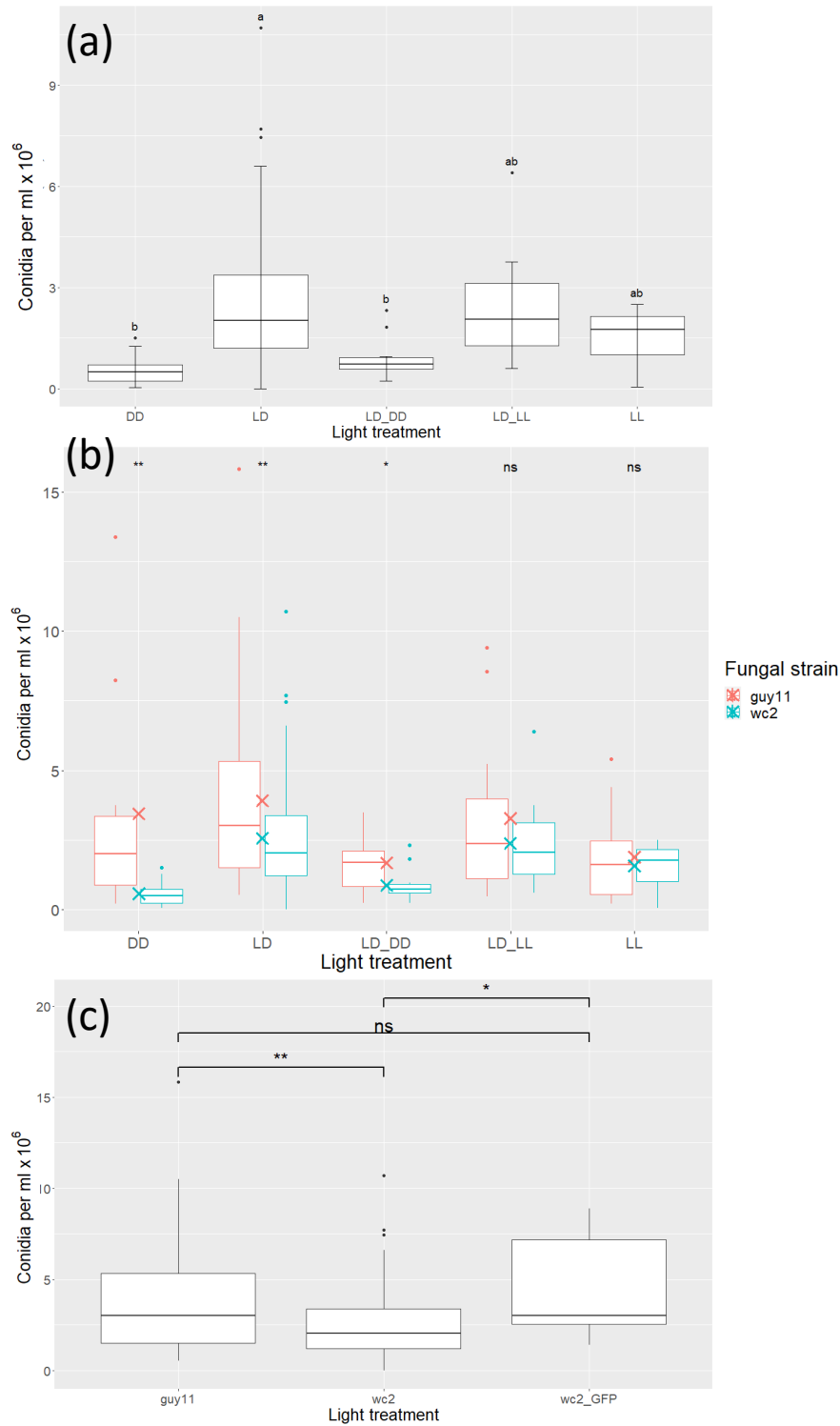


Figure 5.8: WC2 plays a role in photoadaptation and conidiation. (a) 12-day old $\Delta WC2$ DD and LD-DD treatments produce less than half the number of conidia than those grown under LD conditions (n = 16 DD, n = 72 LD, n = 13 LD-DD, n = 20 LD-LL, n = 17 LL). (b) $\Delta WC2$ produces fewer conidia under prolonged darkness (DD and LD-DD) and cycling conditions (LD) compared to the wild type; prolonged light exposure shows no difference between the wild type and $\Delta WC2$ mutant (n = 15 DD *guy11*, n = 68 LD *guy11*, n = 17 LD-DD *guy11*, n = 18 LD-LL *guy11*, n = 16 *guy11* LL, n = 16 DD $\Delta WC2$, n = 72 LD $\Delta WC2$, n = 13 LD-DD $\Delta WC2$, n = 20 LD-LL $\Delta WC2$, n = 17 LD-LL $\Delta WC2$). (c) Reduced conidiation under LD cycling conditions is rescued in the *WC2::GFP* complementation (n = 56 *guy11*, n = 66 $\Delta WC2$, n = 8 *WC2::GFP*). Letters describe statistically significant differences between groups (p < 0.05, Tukey's HSD), Bars with stars atop denote statistically significant differences (p < 0.05, ANOVA), and crosses mean values.

5.2.5 WC2 has a role in conidial germination, development, and appressorial stability

5.2.5.1 Δ WC2 conidia germinate and develop quicker than the wild type

In a similar fashion to the wild type, pre-harvest entrainment conditions had no significant effect on conidial germination in Δ WC2; approximately 90% of conidia had germinated by 4 HPI under all treatment (Fig. 5.9). Unlike the wild type, however, constant conditions (LL or DD) did not reduce appressorial development (Fig 5.9). Further, Δ WC2 mutant conidia germinate and develop quicker than the wild type: 75% of Δ WC2 conidia had produced appressoria by 8 HPI under all entrainment conditions (Fig. 5.9).

By 4 HPI, more Δ WC2 had germinated than the wild type, and by 6 HPI, Δ WC2 showed increased numbers of appressoria compared to the wild type. This increased developmental rate compared to the wild type was not observed under LL and LD-LL conditions, however (Fig. 5.9). As such, prolonged light exposure prior to conidial harvest in the wild type may speed up the conidial developmental rate but reduce the likelihood of developing appressoria. Non-functional WC2 increases conidial developmental rates and displays a phenotype reminiscent of wild type grown under constant light, further implicating WC2 in light/dark adaptation. Together, these data suggest that Δ WC2 conidia develop faster, at a more uniform rate, and do not display prolonged dark- or light-dependent inhibition of appressorial development. Interestingly, there was a much higher variability in the developmental rate of Δ WC2 under LL compared to other conditions, so perhaps there are still light-dependent (but clock or WCC-independent) developmental processes occurring in Δ WC2.

Given that time of day has no effect on conidial development and that, under most conditions, Δ WC2 develops quicker than the wild type, perhaps the clock can function

not only as a way to approximate time to ensure synchronicity with the environment, but also as a means to measure the amount of time elapsed for biological functions that need to be performed within a given time limit. A functional clock may allow for the conidia to germinate and develop at the appropriate rate for increased fitness and pathogenicity based on previous and current environmental conditions. In support of this, *wc1* transcripts have been observed to be increased in conidia compared to other tissue types (101), so perhaps an increase in WC1 protein (known to be a rate-limiting factor in the circadian clock (518)) allows for the clock to cycle quicker than normal, thus speeding up (some) temporally controlled outputs, including conidial development. WC1 is also known to inhibit WC2 activity (199,216), so increased WC1 and decreased WC2 may display similar phenotypes, such as those observed in conidial development.

Alternatively, in the wild type, the constant light from the imaging system (see 2.2.6) may have an acute effect on the development of conidia. This may not occur in the Δ WC2 strain because of altered photoreception, and thus the light may be affecting wild type conidial development only.

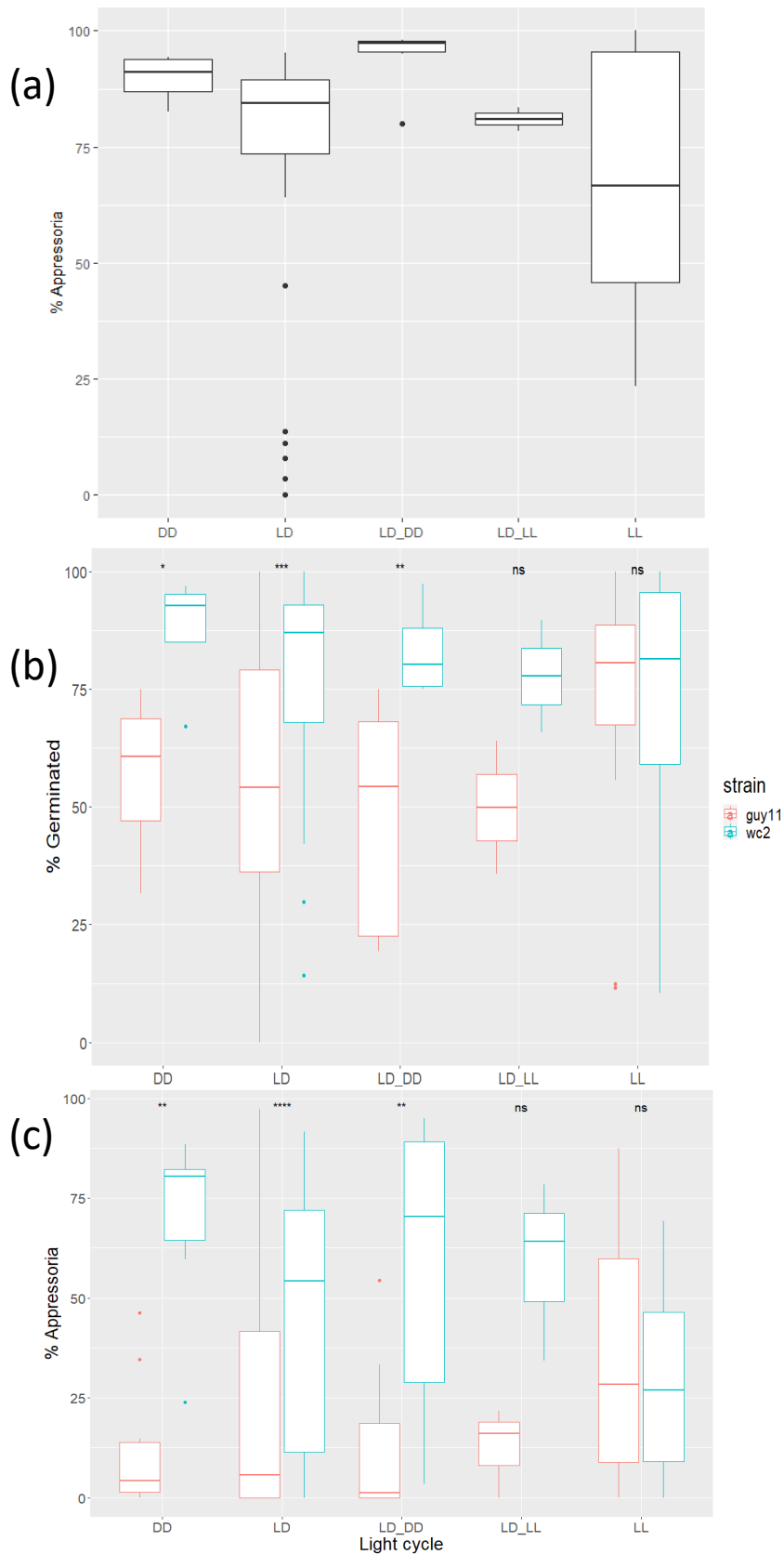


Figure 5.9: Pre-inoculation treatment has a reduced effect on $\Delta WC2$ germination and development, but $\Delta WC2$ conidia develop quicker than the wild type. (a) pre-inoculation light treatment has no significant effect on $\Delta WC2$ appressorial development by 8 HPI; (b) by 4HPI, $\Delta WC2$ showed increased conidial germination, and darkness did not slow germination; (c) $\Delta WC2$ produces appressoria faster than the wild type, and conidial developmental rate is not slowed by darkness (data shown at 6 HPI). $n = 3$ $\Delta WC2$ DD, $n = 14$ $\Delta WC2$ LD, $n = 3$ LD-DD $\Delta WC2$, $n = 3$ $\Delta WC2$ LD-LL, $n = 3$ LL, $n = 3$ guy11 DD, $n = 21$ guy11 LD, $n = 5$ guy11 LD-DD, $n = 3$ guy11 LD-LL, $n = 6$ guy11 LL. Stars represent increasing statistical significance (ANOVA). 'ns' denotes no significant difference between groups ($p > 0.05$), and crosses mean values.

5.2.5.2 WC2 has a role in conidial size

Under LD conditions, there were no observed differences between the wild type and Δ WC2 in terms of percent adherence to petri dishes, suggesting that WC2 is not responsible for spore tip mucilage production (data not shown). In contrast to the wild type, there were no differences in average conidial size before and after agitation in the Δ WC2 strain (Fig. 5.10). Indeed, In the wild type, the conidia remaining were ~10% larger on average than those observed before agitation, whereas there is only a ~2% (insignificant) size difference in Δ WC2. Interestingly, prior to agitation Δ WC2 conidia were larger on average than wild type, whereas they were smaller after agitation (Fig. 5.10). Together, these data suggest that WC2 is in part responsible for conidial size, where Δ WC2 only produce 'medium'-sized conidia, and perhaps Δ WC2 conidia germinate and develop quicker as a result of altered conidial size and, by proxy, resources.

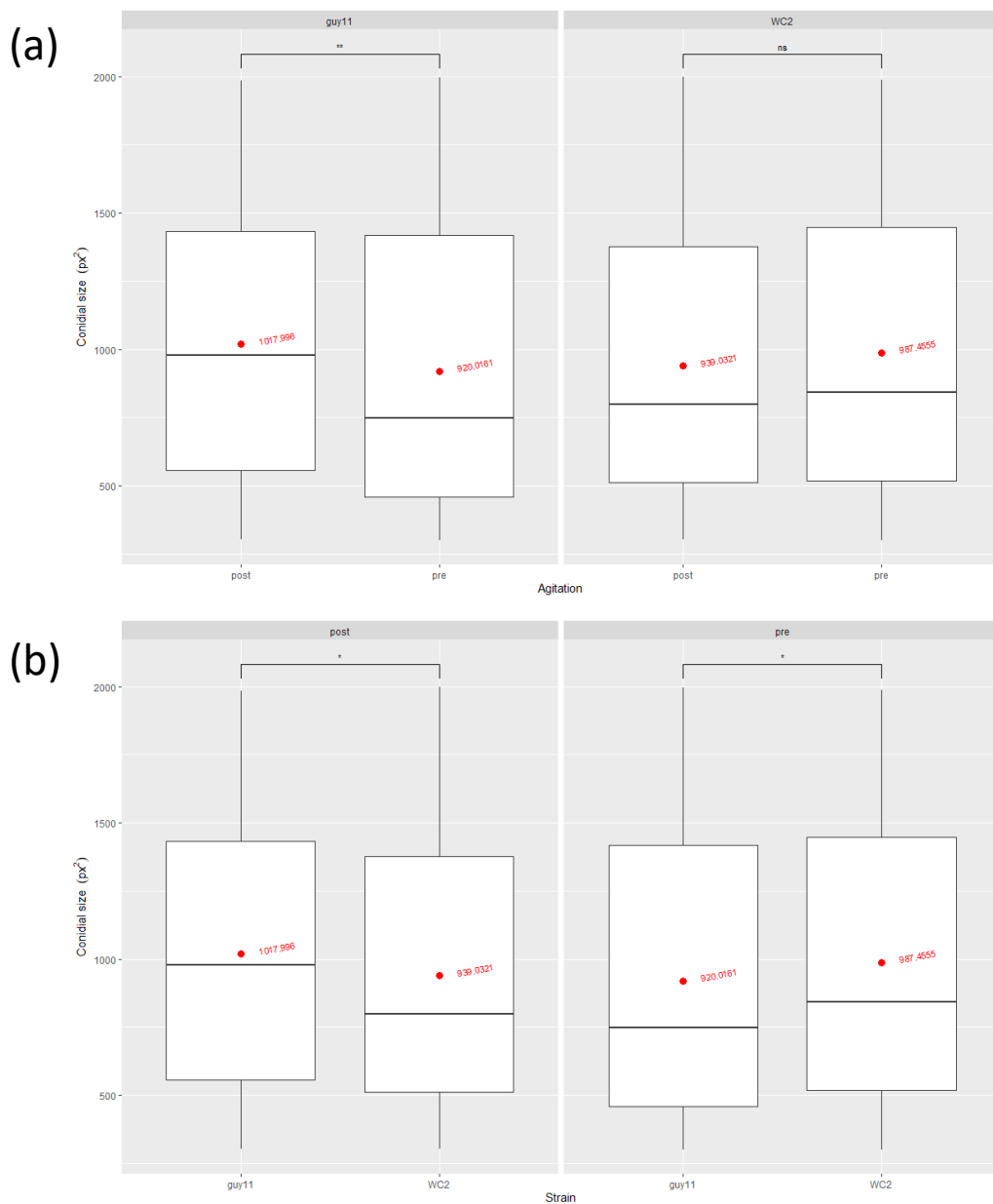


Figure 5.10: WC2 plays a role in conidial size. (a) The Δ WC2 strain does not show any significant size difference between pre- and post-agitation, whereas the remaining conidia post-agitation in the wild type are significantly larger. (b) Δ WC2 conidia are smaller than the wild type post-agitation, but larger pre-agitation. (n = 3 per treatment, at least 100 conidia counted per treatment). Stars represent increasing statistical significance (ANOVA, $p < 0.05$). Red points and text show the mean values for each group.

5.2.5.3 Δ WC2 appressoria undergo cytorrhysis more readily

Despite their increased appressorial development rate, Δ WC2 appressoria undergo cytorrhysis more readily than the wild type and thus may generate a lower turgor pressure (Fig. 5.11). Wild type and Δ WC2 appressoria were subjected to increasing glycerol concentrations in solution (see 2.2.7), and at 0.75 M glycerol, approximately 15% more Δ WC2 appressoria had collapsed than the wild type. This could be a result of an insufficient amount of time to accumulate solutes and/or melanin in the appressoria, or a lack of resources due to altered conidial size (Fig. 5.10). Melanin is known to play a structural role in *M. oryzae* appressoria, where it can also function to prevent solute efflux and function in turgor regulation (58,89,382). Further, melanisation has been shown to be under circadian and environmental control in some fungal species (101,104,177,194,370,384), so perhaps the lower turgor pressure generated in Δ WC2 is a result of compromised melanisation of the appressoria.

Surprisingly, unlike the wild type where pre-harvest light treatment had little effect on appressorial collapse (see chapter 4), constant conditions seem to have a protective role in the appressorial cytorrhysis of Δ WC2 (Fig. 5.11). This could be further evidence towards *M. oryzae* WC2 playing a role in photoadaptation. At 1 M glycerol, only ~40% of Δ WC2 appressoria grown under constant light or darkness collapsed, whereas ~70% or more had collapsed under LD, LD-DD, and LD-LL. This is surprising, as if there were a non-functional clock in Δ WC2, LD-DD and DD should present similar phenotypes, as should LD-LL and LL. Upon increasing the glycerol content further to 2 M, this effect remains to an extent, where DD and LL occupy one statistical group and LD another, with LD-DD and LD-LL falling between the two (Fig. 5.11). It is possible that many of the conidia harvested were produced during the cycling conditions prior to constant light/darkness and thus

could explain the difference in phenotype without discarding the loss of light/dark adaptation. In this way, perhaps the effect of environmental conditions on conidial germination and development (and maybe even pathogenicity) is terminated when conidia have fully matured. Ideally, in subsequent experiments, only conidia produced during the most recent two days of growth would be harvested, as they would not have been produced under cycling conditions in LD-LL and LD-DD. These experiments would prove difficult to perform, given the common association of reduced conidiation in circadian mutants (Fig. 5.8, table 5.1).

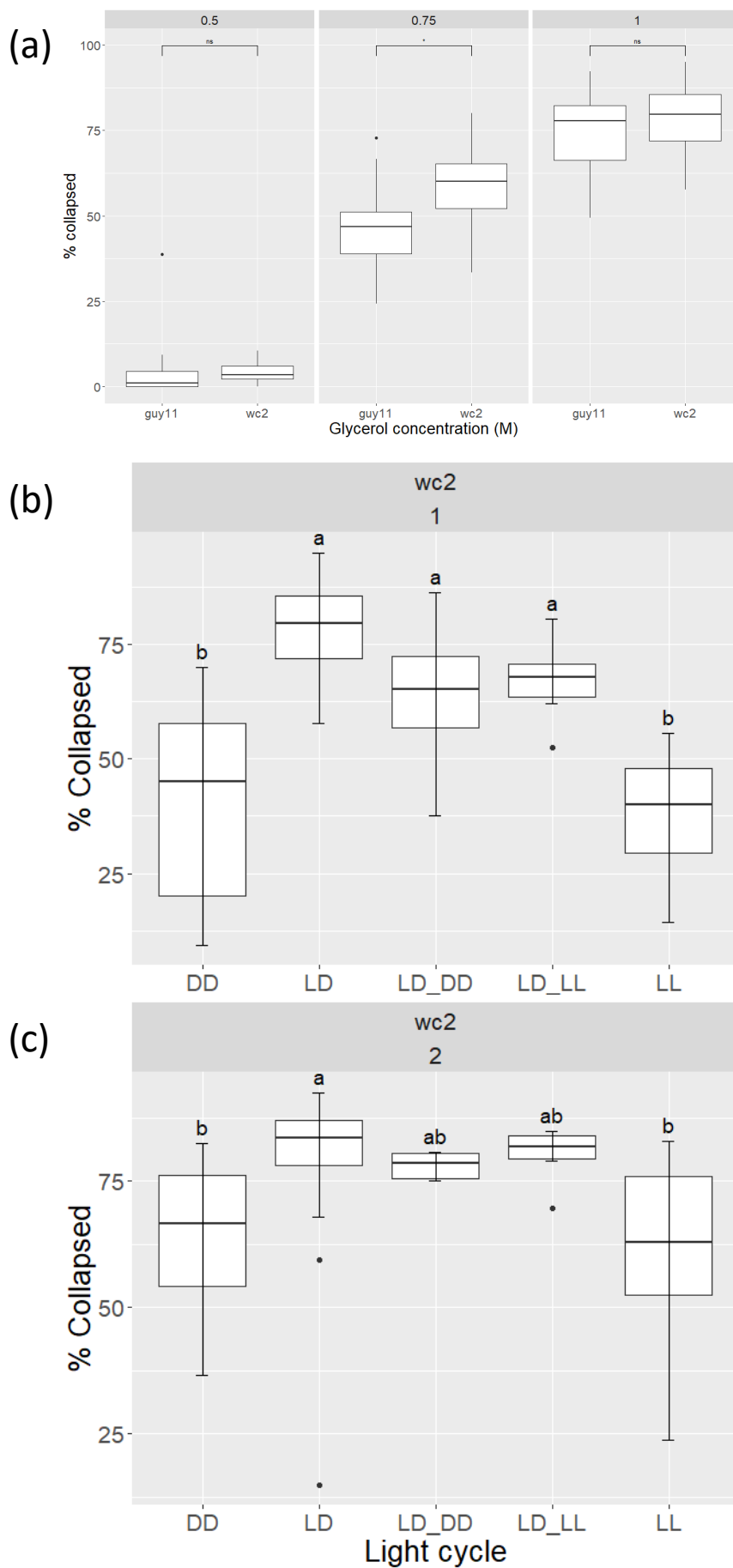


Figure 5.11: WC2 plays a role in appressorial stability. (a) Under LD conditions, Δ WC2 appressoria collapse more readily than the wild type ($n = 12$ [0.5 M] *guy11*, $n = 12$ [0.5 M] Δ WC2, $n = 5$ [0.75 M] *guy11*, $n = 5$ [0.75 M] Δ WC2, $n = 12$ [1 M] *guy11*, $n = 12$ [1 M] Δ WC2), (b) at 1 M glycerol, constant conditions play a protective role in appressorial stability for Δ WC2 ($n = 3$ DD, $n = 12$ LD, $n = 3$ LD-DD, $n = 3$ LD-LL, $n = 3$ LL). (c) The protective effect of constant conditions continues even at high glycerol concentrations (2 M) ($n = 3$ DD, $n = 12$ LD, $n = 3$ LD-DD, $n = 3$ LD-LL, $n = 3$ LL). Letters describe statistically significant differences between groups ($p < 0.05$, Tukey's HSD), Bars with stars atop denote statistically significant differences ($p < 0.05$, ANOVA).

5.2.6 WC2 plays a role in the early stages of pathogenesis

5.2.6.1 Δ WC2 is less able to penetrate the host cuticle

Rice leaf sheathe inoculations were performed using wild type and Δ WC2 strains (see 2.8.2), and scored for penetration and cell to cell movement. At 24 hours post-inoculation (HPI), Δ WC2 conidia were less able to penetrate the host cuticle, perhaps due to the reduced appressorial turgor pressure reported above (Fig. 5.11, 5.12). The GFP complementation strain fell between the wild type and Δ WC2 strain, suggesting partial rescue of penetration at 24 HPI. By 48 HPI, Δ WC2 maintained poorer penetration whereas WC2::GFP showed full complementation; there was no significant difference between wild type and WC2::GFP and approximately 10% fewer penetrations occurred in Δ WC2 (Fig. 5.12).

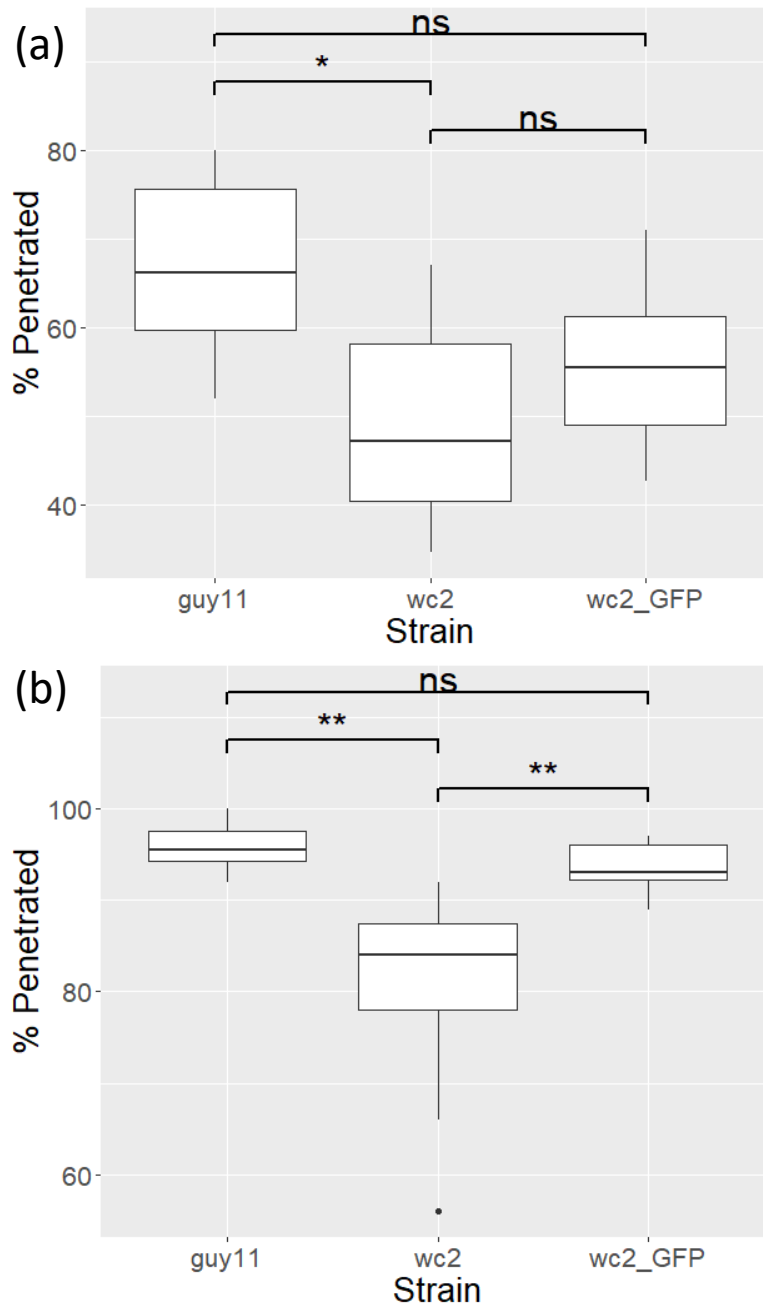


Figure 5.12: WC2 has a function in host plant penetration. (a) at 24 HPI, Δ WC2 shows a significant reduction in its ability to penetrate the host cuticle ($n = 6$ per strain, at least 100 conidia were counted per sample), and (b) by 48HPI, Δ WC2 shows reduced penetration compared to both the wild type and WC2::*GFP* complement strain ($n = 6$ per strain, at least 50 conidia were counted per sample). Bars with stars atop denote statistically significant differences ($p < 0.05$, ANOVA).

5.2.6.2 Δ WC2 displays reduced *in planta* cell to cell movement

There was relatively little (~10%) cell to cell movement at 24 HPI in all strains (data not shown), but by 48 HPI, Δ WC2 showed a large decrease in cell to cell movement, by almost 50% on average, compared to the wild type and WC2::GFP (Fig. 5.13). Interestingly, in a similar manner to the TWL mutants (84), Δ WC2 were often constrained *in planta* after penetration and initial invasion, showing a large amount of growth restricted entirely to the entry cell (Fig. 5.13). Given the complementary expression profile of the WCC components and TWL it is possible that WC2 is in control of TWL in a circadian manner, as the WCC is highly active late at night/just before dawn and TWL transcript peaks just before sunrise (84). In support of this, Δ WC2 and Δ TWL also display a comparable reduction in cell-to-cell movement (84). Thus, when knocked out WC2 may give rise to impaired cell movement *in planta* as a result of reduced TWL-mediated suppression and/or tolerance of reactive oxygen species (84). Δ TWL mutants still displayed conidial banding under LD conditions (84), so if the observed phenotype here is a result of impaired TWL expression, WC2 is likely upstream of TWL and has a wider biological function. In agreement with this, Deng and colleagues (84) also concluded that TWL is not involved in maintaining a circadian rhythm but plays a role in light-responsive events as a transcriptional regulator.

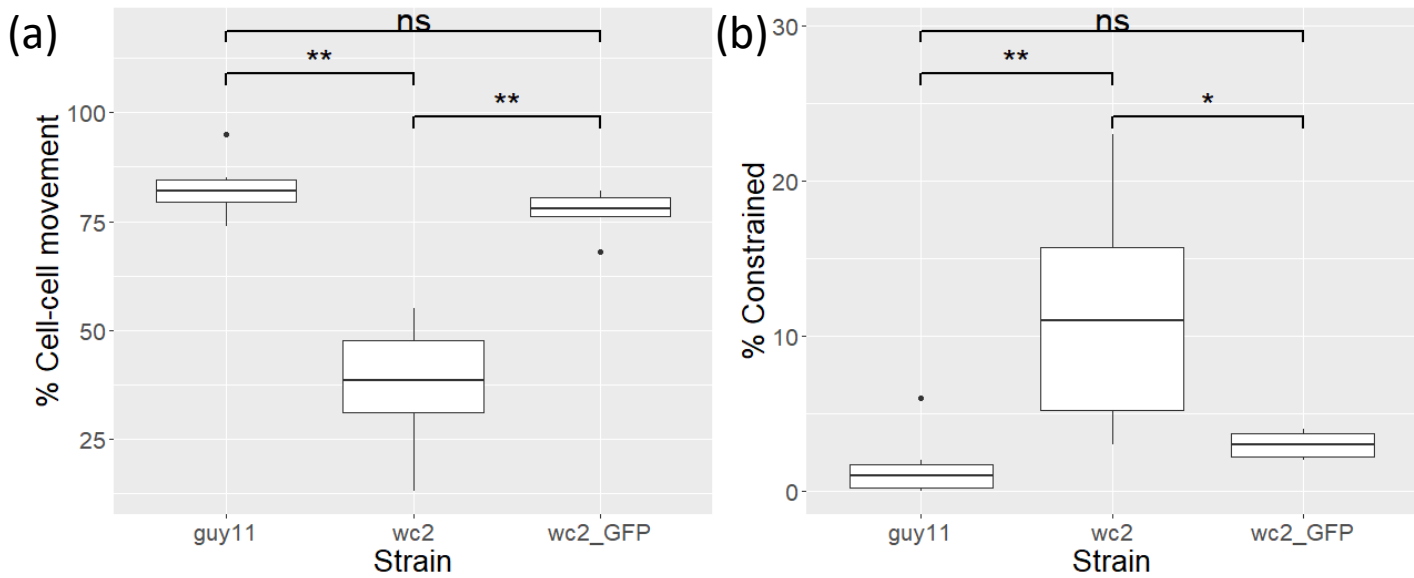


Figure 5.13: WC2 affects *in planta* cell to cell movement and invasive growth. (a) Δ WC2 displays reduced cell to cell movement compared to the wild type and complementation. (b) A significantly higher percentage of Δ WC2 invasive hyphae display excessive growth within the primary invasive cell and are unable to breach the plasmodesmata. (n = 6 per strain, at least 50 conidia were counted per sample). bars with stars atop denote statistically significant differences (p < 0.05, ANOVA).

5.2.7 WC2 functions in host pathogenicity

5.2.7.1 Δ WC2 produces fewer but larger lesion regions in rice

In agreement with the reduced penetration phenotype observed in rice, Δ WC2 gives rise to significantly fewer lesion regions per cm² of leaf tissue at dawn under antiphase, in-phase, and constant light conditions (Fig. 5.14). For dusk inoculations, though, there are no significant differences between the wild type and Δ WC2, except under constant light conditions, where Δ WC2 again produces fewer lesion regions (Fig. 5.14), suggesting that (at dusk), the rice clock is the more important determinant in disease severity.

Counterintuitively, Δ WC2 actually produces larger lesion regions on average in rice infections under DL, LD and LD-LL pre-inoculation treatments (Fig. 5.14) The wild type gives rise to larger lesion regions under DD and LL conditions at dawn, though, which further suggests that Δ WC2 may be unable to undergo light and/or dark adaptation. Further, Δ WC2 produces larger lesion regions at dusk under LD, LD-LL, and LL conditions in rice, so it seems that pre-inoculation light exposure favouring dusk inoculations is even more pronounced when *M. oryzae* has impaired clock function (Fig. 5.14).

Finally, in terms of percentage cover of lesion regions in rice, there is no significant difference between the wild type and Δ WC2 under any conditions or time, except at dawn after constant light pre-treatment, where the wild type covers a very low, although significantly higher proportion of infected leaves compared to Δ WC2 (Fig. 5.14). Together, these data suggest that even though Δ WC2 is less able to penetrate the rice leaf sheath cuticle and proliferate through the host tissue, those that are successful can develop *in planta* in the usual manner and under certain conditions can grow larger than

the wild type. This may be a result of reduced competition or perhaps 'slave' synchronicity with the plant host (181,183).

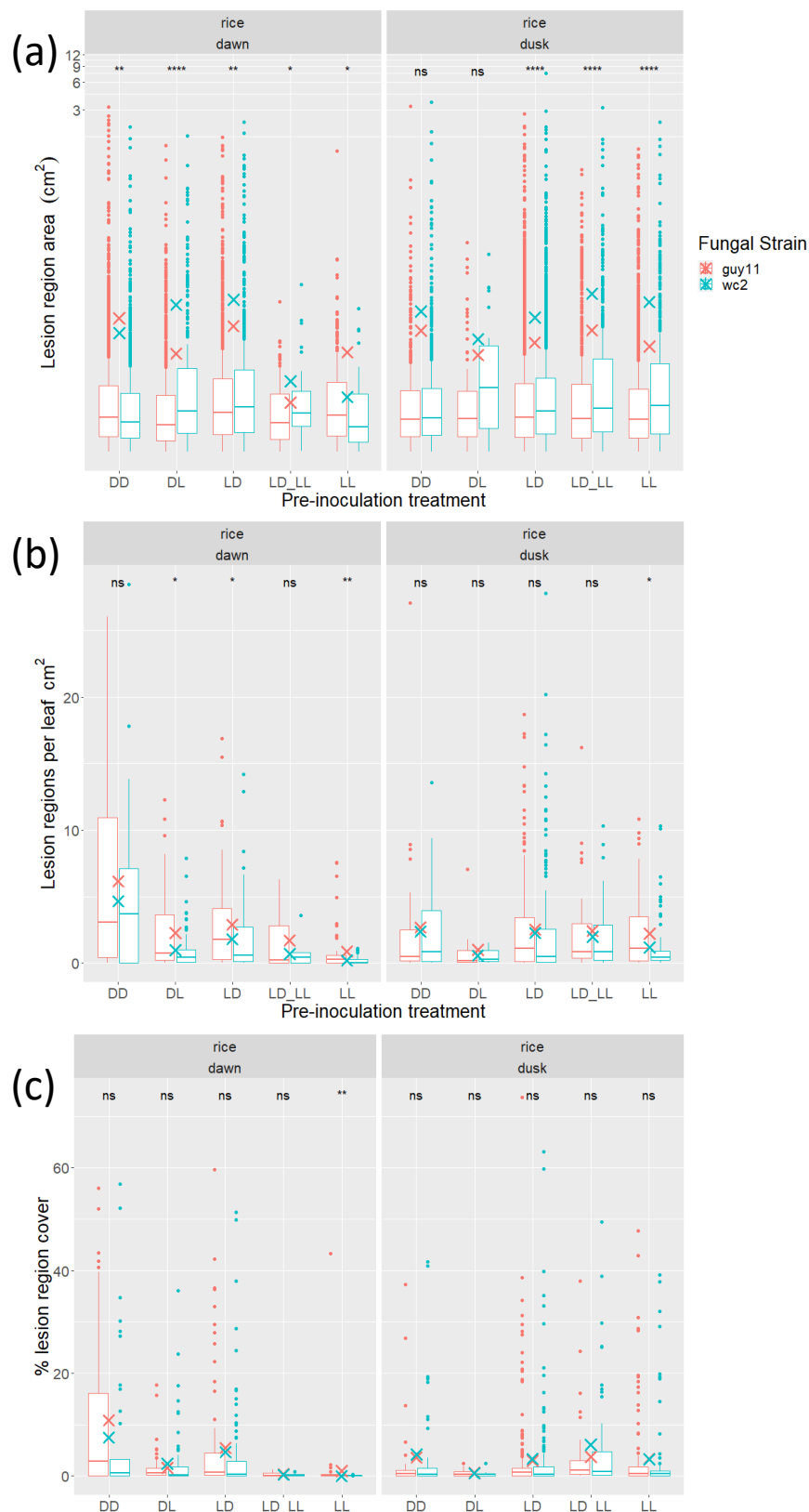


Figure 5.14: WC2 plays a role in lesion formation and lesion size in rice. (a) Δ WC2 produces larger lesions under DL conditions at dawn, LD conditions at dawn and dusk, LD-LL at dawn and dusk, and LL conditions at dusk. The Wild type produces larger lesions under DD and LL conditions at dawn (n = 2358 lesions guy11/ 1094 Δ WC2 DD dawn, n = 601 guy11/ 697 Δ WC2 DD dusk, n = 1303 guy11/ 358 Δ WC2 DL dawn, n = 93 guy11/ 29 Δ WC2 DL dusk, n = 1565 guy11/ 624 Δ WC2 LD dawn, n = 6098 guy11/ 2749 Δ WC2 LD dusk, n = 178 guy11/ 46 Δ WC2 LD-LL dawn, n = 705 guy11/ 502 Δ WC2 LD-LL dusk, n = 330 guy11/ 69 LL dawn, n = 2382 guy11/530 Δ WC2 LL dusk). (b) Δ WC2 causes fewer lesions at dawn under DL and LD conditions, and fewer lesions at both dawn and dusk under LL conditions. Under no pre-inoculation conditions does Δ WC2 give rise to more lesions than the wild type. (c) There are no significant differences between Δ WC2 and wild type in terms of % leaf coverage of lesions under any conditions or inoculation time, except LL at dawn, suggesting an interaction between lesion size and lesion density (n = 55 leaves guy11/ 41 Δ WC2 DD dawn, n = 28 guy11/ 45 Δ WC2 DD dusk, n = 63 guy11/75 Δ WC2 DL dawn, n = 12 guy11/ 9 Δ WC2 DL dusk, n = 87 guy11/ 83 Δ WC2 LD dawn, n = 224 guy11/ 177 Δ WC2 LD dusk, n = 13 guy11/10 Δ WC2 LD-LL dawn, n = 41 guy11/ 48 Δ WC2 LD-LL dusk, n = 58 guy11/46 Δ WC2 LL dawn, n = 128 guy11/ 81 Δ WC2 LL dusk). Stars represent increasing statistical significance (Dunn's test, p < 0.05), and crosses mean values.

5.2.7.2 Prolonged light exposures favouring dusk inoculation is maintained in Δ WC2-rice infections

When comparing inoculation timing in the Δ WC2 mutant, lesion regions are larger at dusk under constant conditions (DD and LL), but lesion regions are larger at dawn under synchronous conditions (Fig. 5.15). This suggests that Δ WC2 may have lost its dark adaptation in pathogenicity, as constant dark pre-inoculation treatment showed larger lesions at dawn in the wild type. There is little effect of inoculation timing on lesion density in Δ WC2, except under constant light pre-treatment, where dusk inoculations are favourable for *M. oryzae* (Fig. 5.15). Under LL and LD-LL conditions, Δ WC2 covers a higher percentage of leaf area at dusk in both conditions, suggesting that, in a similar manner to the wild type, after prolonged light exposure, dusk inoculations are more disease-conducive than dawn inoculations (Fig. 5.15). In this way, Δ WC2 may still have residual photoreception or prolonged light exposure may have caused a ROS priming effect in a similar manner reported by Aver'yanov and colleagues (384).

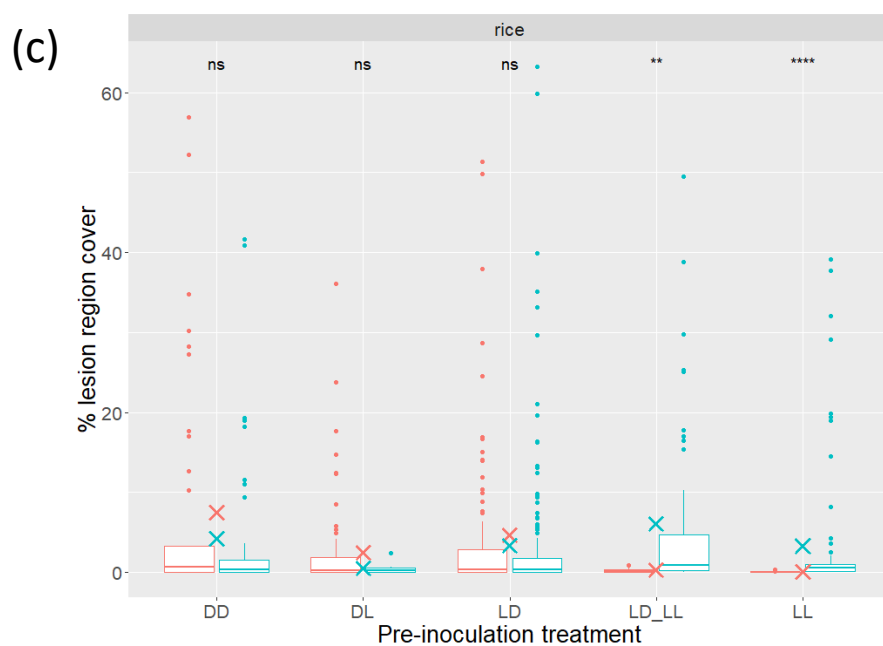
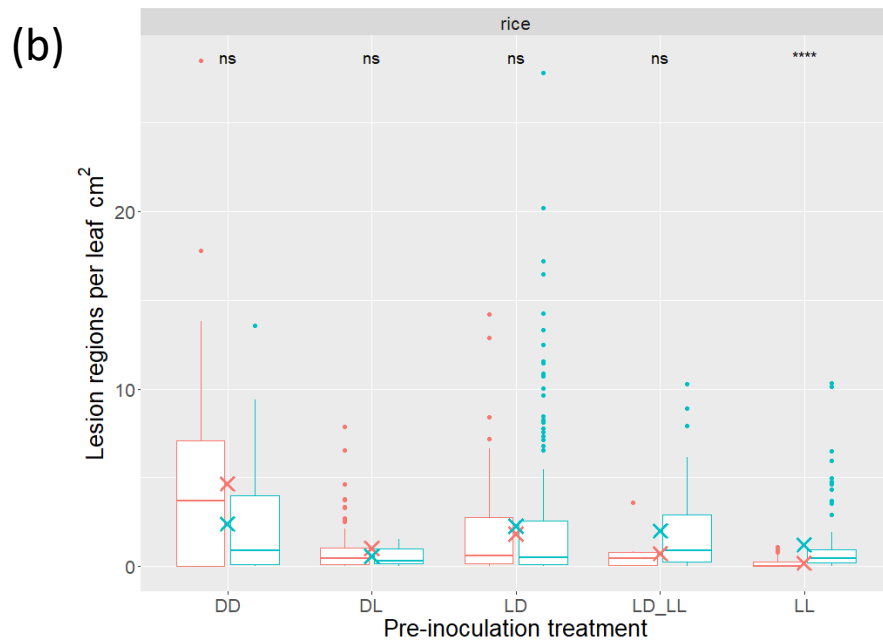
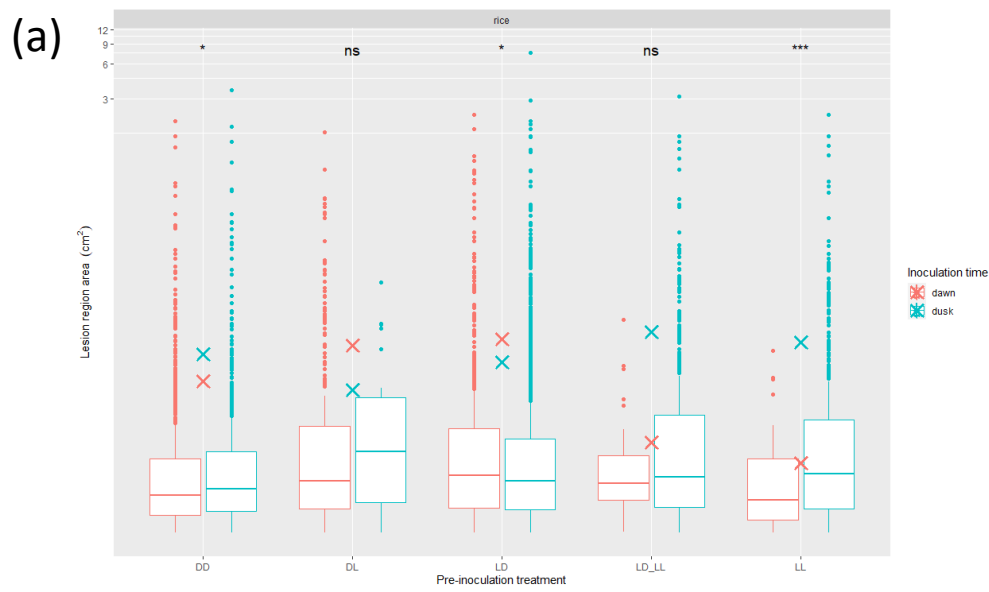


Figure 5.15: Prolonged light exposure favours dusk inoculations in $\Delta WC2$. (a) Constant pre-inoculation conditions in $\Delta WC2$ gave rise to increased lesion area at dusk in $\Delta WC2$, whereas synchronous LD conditions favoured dawn inoculations. Entrainment followed by constant conditions showed no time-of-day effect on lesion area in $\Delta WC2$ (n = 1094 lesions DD dawn, n = 697 DD dusk, n = 358 DL dawn, n = 29 DL dusk, n = 624 LD dawn, n = 2749 LD dusk, n = 46 LD-LL dawn, n = 502 LD-LL dusk, n = 69 LL dawn, n = 530 LL dusk). (b) Pre-inoculation conditions had little effect on $\Delta WC2$ lesion density, except constant light, which favoured dusk inoculations. (c) Overall, prolonged light-treated $\Delta WC2$ lesions covered an increased leaf area at dusk (n = 41 leaves DD dawn, n = 45 DD dusk, n = 75 DL dawn, n = 9 DL dusk, n = 83 LD dawn, n = 177 LD dusk, n = 10 LD-LL dawn, n = 48 LD-LL dusk, n = 46 LL dawn, n = 81 LL dusk). Stars represent increasing statistical significance (Dunn's test, $p < 0.05$), and crosses mean values.

5.2.7.3 Prolonged light exposure inhibits dawn pathogenicity in Δ WC2-rice interactions

In rice- Δ WC2 infections, compared to the base mean, constant dark pre-treated Δ WC2 caused a decrease in lesion area at dawn and dusk, but prolonged light (LL) exposure showed decreased lesion area at dawn and increased lesion region areas at dusk, as did LD-LL (Fig. 5.16). This suggests that Δ WC2 maintains light conditions favouring dusk inoculations and may have lost its dark-adapted virulence. Interestingly, both synchronous and asynchronous (LD and DL) pre-infection conditions showed increased lesion area at dawn in Δ WC2, implying that rice may be more susceptible at this time. Pre-inoculation entrainment had little effect on lesion density in Δ WC2, except at dawn where constant light exposure gave rise to fewer lesions per leaf cm² and constant darkness increased lesion density (Fig. 5.16). Prolonged light exposure (LD-LL and LL) also reduced % leaf coverage at dawn, and DL pre-treatment reduced lesion coverage at dusk (Fig. 5.16). These data suggest that instead of prolonged light exposure favouring dusk inoculations, it actually inhibits virulence at dawn in host rice plant interactions, and as such while the *M. oryzae* clock plays a role in its pathogenicity in host-pathogen interactions in rice blast disease, the environmental conditions at the time of infection and the plant clock may be more important than the pathogen clock. In the field, however, the clock and environmental status would be inextricably linked due to the reliable and cyclical nature of day and night. Together, in Host-*M. oryzae* infections, the fungal clock may instead be most important during pre- and early infection stages.

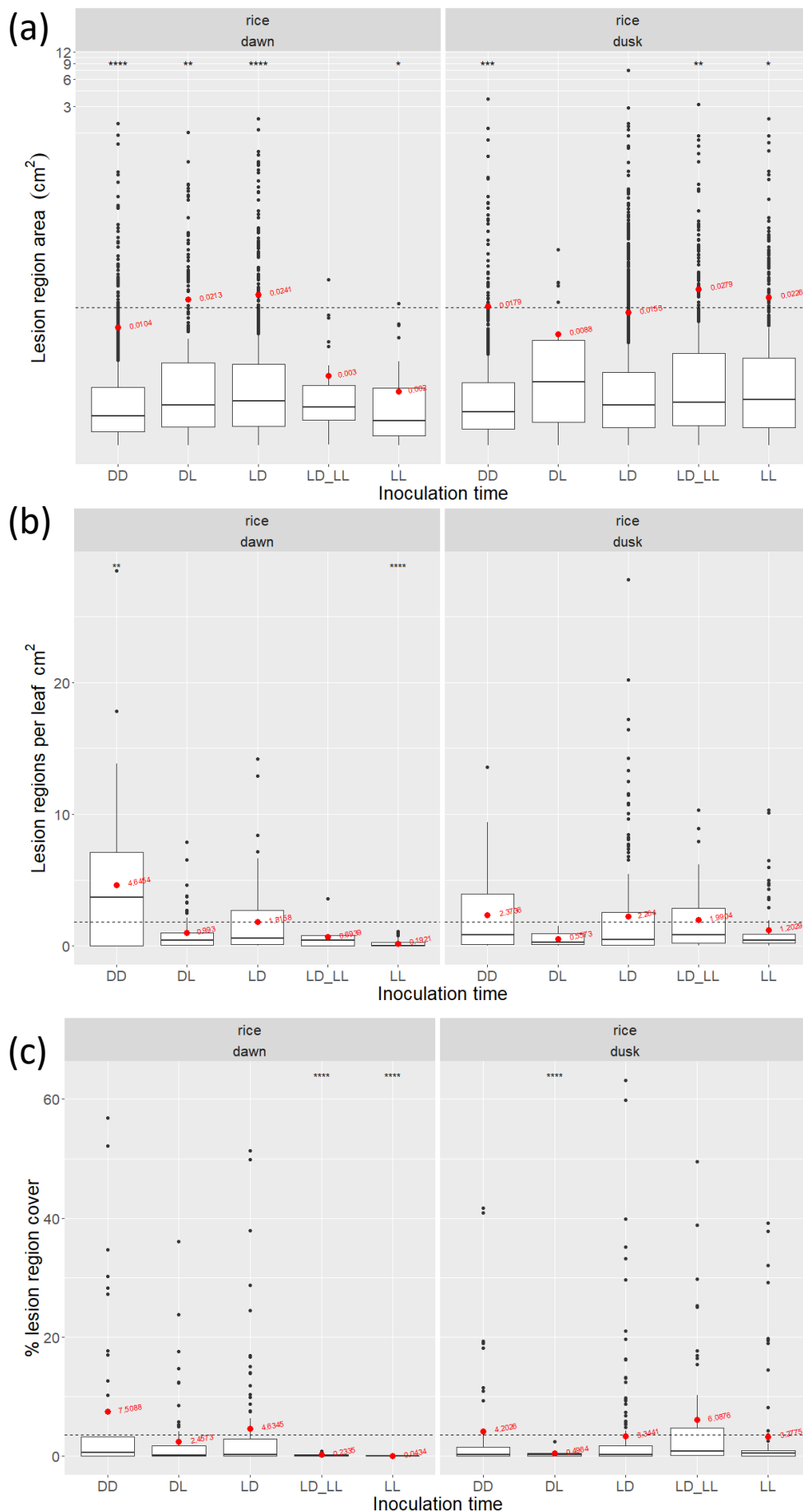


Figure 5.16: Pre-inoculation light treatment affects Δ WC2 pathogenicity in rice. (a) constant conditions reduce lesion area at dawn, and light-dark cycles (both LD and DL) show increased lesion size at dawn but decreased area at dusk (n = 1094 lesions DD dawn, n = 697 DD dusk, n = 358 DL dawn, n = 29 DL dusk, n = 624 LD dawn, n = 2749 LD dusk, n = 46 LD-LL dawn, n = 502 LD-LL dusk, n = 69 LL dawn, n = 530 LL dusk). (b) DD increases and LL decreases lesion density at dawn. Pre-inoculation light conditions have little effect on lesion density at dusk. (c) prolonged light exposure (LL and LD-LL) reduces overall lesion coverage at dawn, and antiphase conditions reduce coverage at dusk (n = 41 leaves DD dawn, n = 45 DD dusk, n = 75 DL dawn, n = 9 DL dusk, n = 83 LD dawn, n = 177 LD dusk, n = 10 LD-LL dawn, n = 48 LD-LL dusk, n = 46 LL dawn, n = 81 LL dusk). Stars represent increasing statistical significance (Dunn's test, $p < 0.05$), and red points and text denote mean values for each group.

5.2.7.4 Under high inoculum densities on detached leaves, Δ WC2 is unable to overwhelm the host defences

To determine if Δ WC2 could overwhelm the host defence system under high inoculum densities, detached rice leaf cuttings were spray inoculated with 100 μ l of 1×10^5 conidia (10,000 conidia per leaf cutting), placed into moist paper towel in sealed glass dishes and observed 7 days post inoculation. Under these high inoculum and disease-conducive conditions, where rice plant leaves had open wounds, Δ WC2 clearly is less virulent than the wild type. Wild type inoculations showed almost complete tissue death and necrosis, where lesion sporulation was beginning to occur. In Δ WC2 inoculations, infected leaves fared far better than the wild type, where large amounts of green, non-necrotic tissue remained (Fig. 5.17). Patches of dead tissue were observed, and some large lesions were present, but severity was vastly decreased in comparison to the wild type. This further suggests that the sub-optimal infection conditions observed in these experiments masked some of the pathogenicity effects in altered clock mutants.



Figure 5.17: Δ WC2 displays significantly reduced pathogenicity in rice under high inoculation densities and disease-conducive conditions. Left panel: wild type-inoculated rice leaves. Right panel: Δ WC2-inoculated leaves. Leaves were sprayed with the same volume and concentration of conidia from the respective *M. oryzae* strains and placed in sealed glass containers with damp paper towel.

5.2.8 WC2 has a profound impact on non-host pathogenicity

5.2.8.1 Δ WC2 produces fewer and smaller lesions than the wild type in barley infections

In non-host barley-*M. oryzae* interactions, Δ WC2 produces larger lesions than the wild type under DD pre-treatment at both dawn and dusk (although the median lesion size is larger at dusk in wild type inoculations, suggesting a greater number of larger lesions in the wild type) and larger lesions than the wild type when grown under LL at dusk (Fig. 5.18), again suggesting that Δ WC2 has altered photoadaptability. When entrained under cycling conditions (DL and LD), Δ WC2 gives rise to smaller lesions at both dawn and dusk compared to the wild type, implicating a benefit of synchronicity and virulence in wild type *M. oryzae*. Further, prolonged light exposure (LL only) produces smaller lesions at dawn, suggesting that cycling light conditions provides little benefit to Δ WC2, unlike the wild type and thus constant conditions have little inhibitory effect on a non-functional clock.

When comparing lesion density and lesion coverage, Δ WC2 gives rise to significantly fewer lesion regions per cm² than the wild type under all observed conditions at both dawn and dusk in barley, and those lesions also cover a smaller proportion of the leaf (Fig. 5.18). As observed in host-*M. oryzae* interactions (see 5.7.2), the Δ WC2 conidia that are able to successfully penetrate the host cuticle and breach the plasmodesmata between cells can continue to develop in a fashion similar (or even improved) compared to the wild type. This could explain the increased Δ WC2 lesion area under some circumstances, but consistently reduced lesion densities. Taken together, this data suggests that the role of the clock in *M. oryzae* pathogenicity is more important in non-host infections, where impaired clock function profoundly reduces pathogenicity.

Perhaps in host-*M. oryzae* interactions, where co-evolution has occurred between the plant and fungus, *M. oryzae* is able to utilise *in planta* signals from rice to supplement a non-functional clock (84). In non-host interactions, however, *M. oryzae* may be unable to make sense of or utilise time of day signals derived from barley and thus may need to rely more heavily on its internal timekeeping machinery.

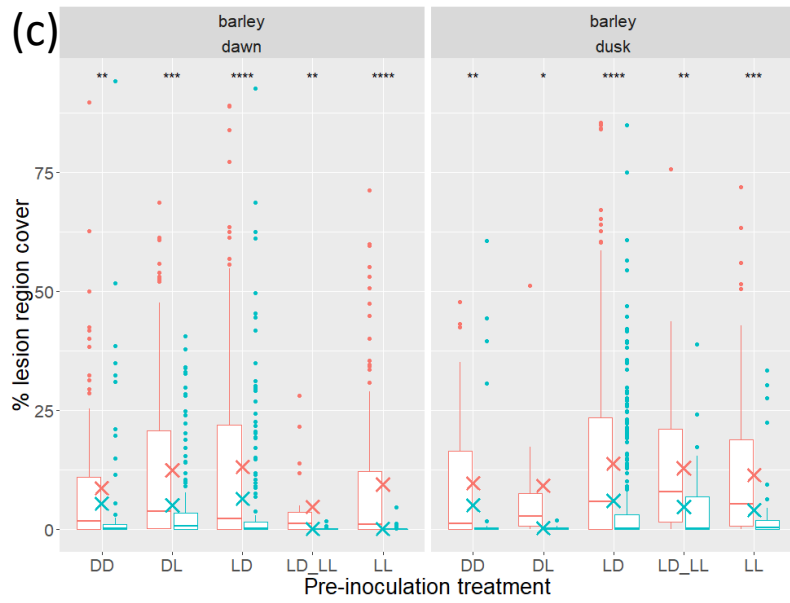
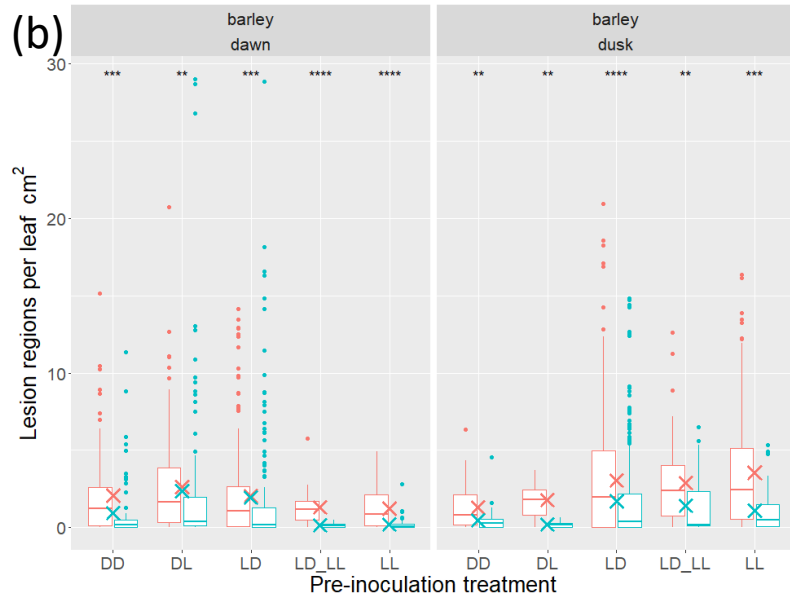
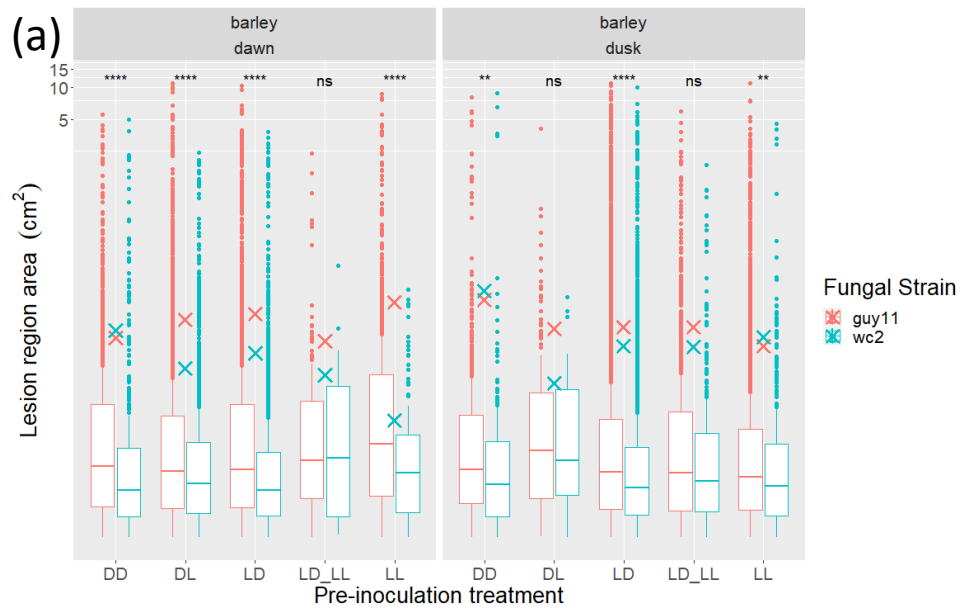


Figure 5.18: WC2 plays a profound role in non-host pathogenicity on barley. WC2 plays a profound role in non-host pathogenicity on barley. (a) Δ WC2 lesions are larger at dawn under DD pre-treatment and at dusk under LL conditions, whereas wild type lesions are larger at dawn after DL, LD, and LL treatment. Wild type lesions are also larger at dusk after synchronous LD pre-treatment (n = 2100 lesions guy11/ 567 Δ WC2 DD dawn, n = 508 guy11/ 206 Δ WC2 DD dusk, n = 4183 guy11/ 1991 Δ WC2 DL dawn, n = 172 guy11/ 24 DL dusk, n = 3276 guy11/ 2371 Δ WC2 LD dawn, n = 11215 guy11/ 5236 Δ WC2 LD dusk, n = 218 guy11/ 21 Δ WC2 LD-LL dawn, n = 1171 guy11/ 304 Δ WC2 LD-LL dusk, n = 1221 guy11/ 187 Δ WC2 LL dawn, n = 6349 guy11/ 466 Δ WC2 LL dusk). (b) Δ WC2 gives rise to fewer lesions per leaf cm² under all pre-treatment conditions at both dawn and dusk. (c) Wild type lesions also cover a larger proportion of inoculated leaves at both dawn and dusk under all pre-inoculation light treatments in barley. (n = 97 leaves guy11/ 70 Δ WC2 DD dawn, n = 39 guy11/ 35 Δ WC2 DD dusk, n = 151 guy11/ 119 Δ WC2 DL dawn, n = 10 guy11/ 13 Δ WC2 DL dusk, n = 196 guy11/ 158 Δ WC2 LD dawn, n = 374 guy11/ 279 Δ WC2 LD dusk, n = 19 guy11/ 17 Δ WC2 LD-LL dawn, n = 54 guy11/ 33 Δ WC2 LD-LL dusk, n = 107 guy11/ 94 Δ WC2 LL dawn, n = 176 guy11/ 37 Δ WC2 LL dusk). Stars represent increasing statistical significance (Dunn's test, p < 0.05), and crosses mean values.

5.2.8.2 Time of day has less of an effect on disease severity in Δ WC2

In barley- Δ WC2 inoculations, time of day had no effect on lesion region area, except in synchronous pre-inoculation treatment (LD), where dusk inoculations gave rise to slightly larger lesions, suggesting that WC2 plays a role in altering virulence toward non-host plant(s), since there is a clear time of day difference in wild type-barley inoculations (Fig. 5.19). Interestingly, antiphase (DL) pre-treated inoculations caused increased lesion densities at dawn compared to dusk, which suggests that Δ WC2 strains may be more virulent in barley at their subjective dusk and may still have residual environmental reception and/or clock function. Perhaps then, Δ WC2 can display (some) diurnal, but not circadian outputs. Constant light (LL) pre-treated Δ WC2 also presented fewer lesions at dawn, implying that in non-host interactions, light-dependent dawn disease suppression remains (Fig. 5.19). Finally, Δ WC2 lesions covered an increased proportion of leaves at dawn in DL treatments; under LD-LL and LL treatments, dusk inoculations increased lesion coverage, similar to the wild type (Fig. 5.19). Perhaps, then, residual clock function or diurnal output in Δ WC2 remains, where barley susceptibility is increased at dusk, but Δ WC2 is unable to re-entrain or act as an interspecies 'slave' oscillator to the plant clock (181,183).

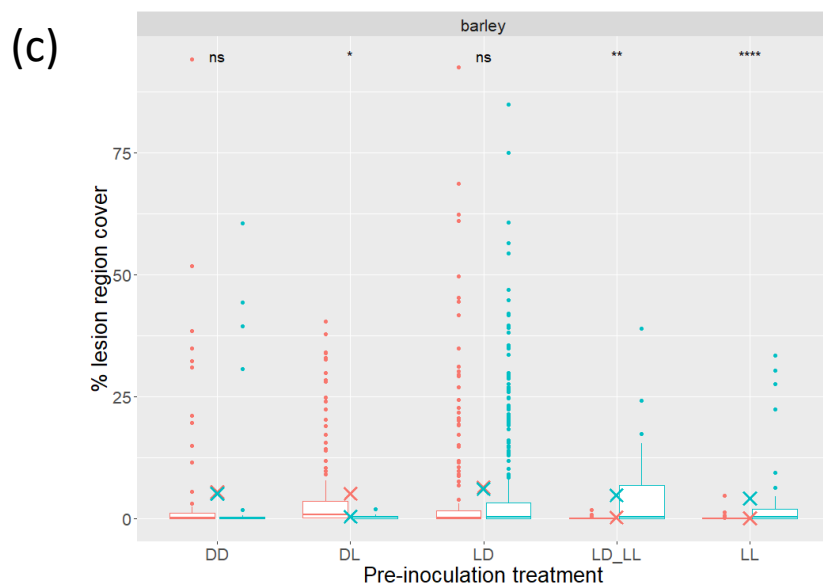
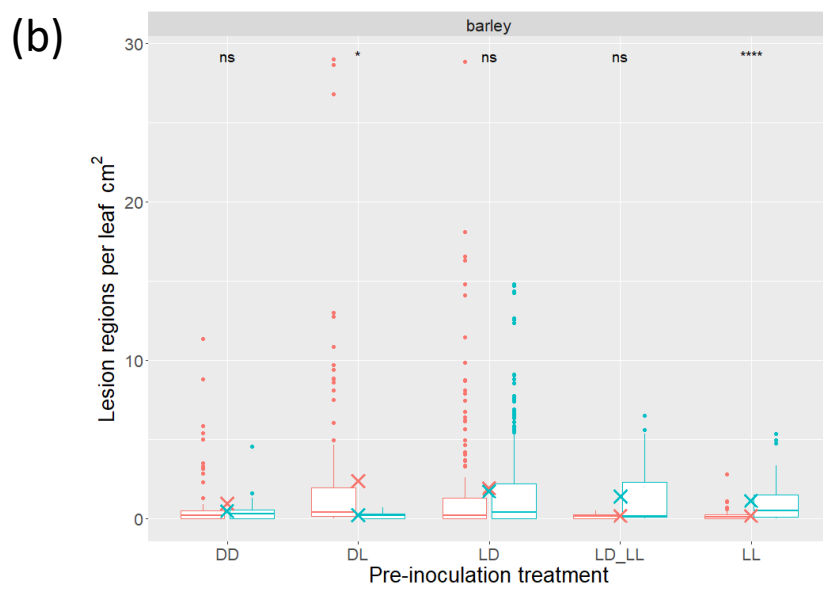
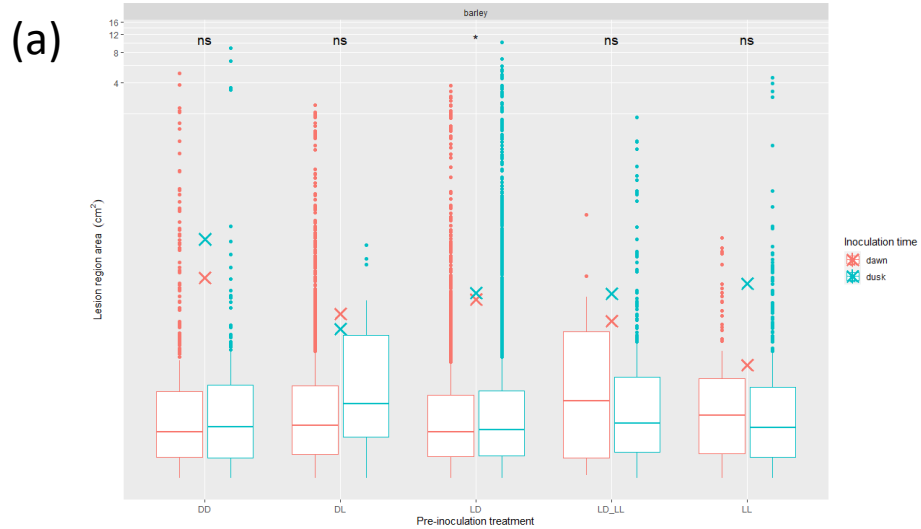


Figure 5.19: Time of day has less of an effect on Δ WC2 pathogenicity in barley. (a) Dusk inoculations give rise to larger lesion regions in Δ WC2 inoculations only after LD pre-inoculation treatment (n = 567 lesions DD dawn, n = 206 DD dusk, n = 1991 DL dawn, n = 24 DL dusk, n = 2371 LD dawn, n = 5236 LD dusk, n = 21 LD-LL dawn, n = 304 LD-LL dusk, n = 187 LL dawn, n = 466 LL dusk). (b) Antiphase entrainment conditions cause reduced lesion density at dusk (subjective Δ WC2 dawn) and constant light conditions give rise to fewer lesions at dawn. (c) Δ WC2 presents reduced lesion coverage at dusk under DL conditions and at dawn under LD-LL and LL pre-treatment (n = 70 leaves DD dawn, n = 35 DD dusk, n = 119 DL dawn, n = 13 DL dusk, n = 158 LD dawn, n = 279 LD dusk, n = 17 LD-LL dawn, n = 33 LD-LL dusk, n = 94 LL dawn, n = 37 LL dusk). Stars represent increasing statistical significance (Dunn's test, $p < 0.05$), and crosses mean values.

5.2.8.3 Prolonged light exposure inhibits dawn pathogenicity in Δ WC2 regardless of host species

When comparing pre-inoculation treatments to the base mean, treatment has no effect on Δ WC2 lesion region size at dusk, whereas light cycling conditions (LD and DL) and constant light (LL) reduce the average lesion area in barley dawn infections (Fig. 5.20), suggesting the plant clock is the main determinant in dusk inoculations. Further, LL conditions reduce the number of lesions per cm² leaf tissue at dawn, but DL inoculations increase the lesion density at dawn in spite of their reduced area (Fig. 5.20). In this way, perhaps the increased number of successful penetrations in Δ WC2 under DL conditions gives rise to reduced lesion area due to increased fungal competition, in a similar manner to that observed in rice, where increased lesion density can negatively correlate with lesion area. Again, pre-inoculation treatment has no significant effect on lesion density in dusk inoculations.

Prolonged light exposure (LL and LD-LL) also reduces the total lesion coverage per leaf at dawn, and only DL treatments show reduced lesion coverage at dusk. Interestingly, there are no pre-inoculation treatment conditions that improve pathogenicity compared to the base mean in barley infections, and so perhaps Δ WC2 has lost its ability to gate its virulence depending on environmental conditions, as differing entrainment can only act to dampen pathogenicity (Fig. 5.20). In support of this, the same phenomenon is seen in rice where, compared to the base mean, Δ WC2 shows no increase in pathogenicity between treatments at any time or pre-inoculation treatment. Taken together, pre-inoculation treatment seems to have less of an effect on Δ WC2 pathogenicity.

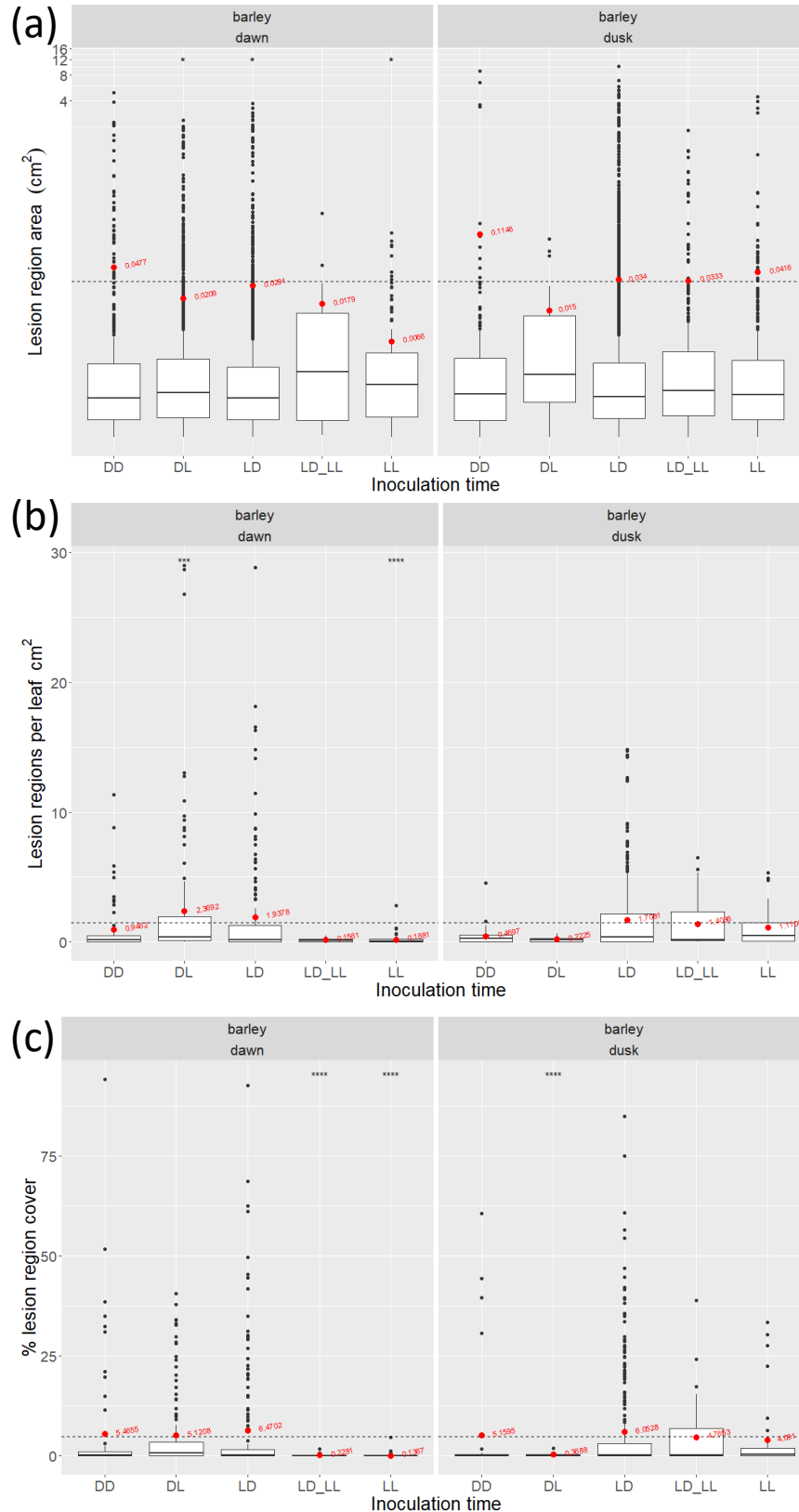


Figure 5.20: Prolonged light exposure consistently reduces dawn pathogenicity in $\Delta WC2$. (a) $\Delta WC2$ displays reduced lesion area under DL, LD, and LL at dawn. There is no significant effect of treatment on lesion area at dusk ($n = 567$ lesions DD dawn, $n = 206$ DD dusk, $n = 1991$ DL dawn, $n = 24$ DL dusk, $n = 2371$ LD dawn, $n = 5236$ LD dusk, $n = 21$ LD-LL dawn, $n = 304$ LD-LL dusk, $n = 187$ LL dawn, $n = 466$ LL dusk). (b) LL-treated $\Delta WC2$ produces fewer lesions at dawn, and antiphase treatments produce more lesions at dawn. Light treatment has no significant effect on lesion density at dusk. (c) Prolonged light treatments (LL and LD-LL) reduce the lesion coverage at dawn, whereas antiphase treatments reduce lesion coverage at dusk ($n = 70$ leaves DD dawn, $n = 35$ DD dusk, $n = 119$ DL dawn, $n = 13$ DL dusk, $n = 158$ LD dawn, $n = 279$ LD dusk, $n = 17$ LD-LL dawn, $n = 33$ LD-LL dusk, $n = 94$ LL dawn, $n = 37$ LL dusk). Stars represent increasing statistical significance (Dunn's test, $p < 0.05$), and red dots and text displays means for each group.

5.2.9 Δ WC2 infections show an optimal leaf area, but this phenomenon is dampened compared to the wild type

Wild type inoculations show that lesion densities are highest in rice and barley leaves that are ~10-15 cm² in area (see 4.2.6 and Fig. 5.21). This is not observed in Δ WC2 infections; Δ WC2 lesion densities are highest in newly formed leaves less than 5 cm², and densities steeply decline as leaf area and maturity increases (Fig. 5.21). As such, Δ WC2 may favour less mature leaves or may be unable to overcome the host defences in more mature leaves. It is interesting to note that infection severity profiles are very similar between wild type and Δ WC2 in the youngest of rice leaves, but the difference between the two strains increases with leaf area, further suggesting an inability to overcome the host defences.

When taking time of day into account in this observation, Δ WC2 also does not display an increase in lesion density with leaf area at dawn like in the wild type-rice interactions (Fig. 5.21). In contrast, Δ WC2 infections in barley show very similar, but dampened density profiles across the range of leaf areas (Fig. 5.21). Together, these data suggest that WC2 may have a host-dependent importance, leaf size/maturity plays a role in disease outcome, and that time of day day-dependent plant susceptibility may differ by species, with barley being more susceptible at dusk, like many other long day plants, and rice susceptibility greatest at dawn.

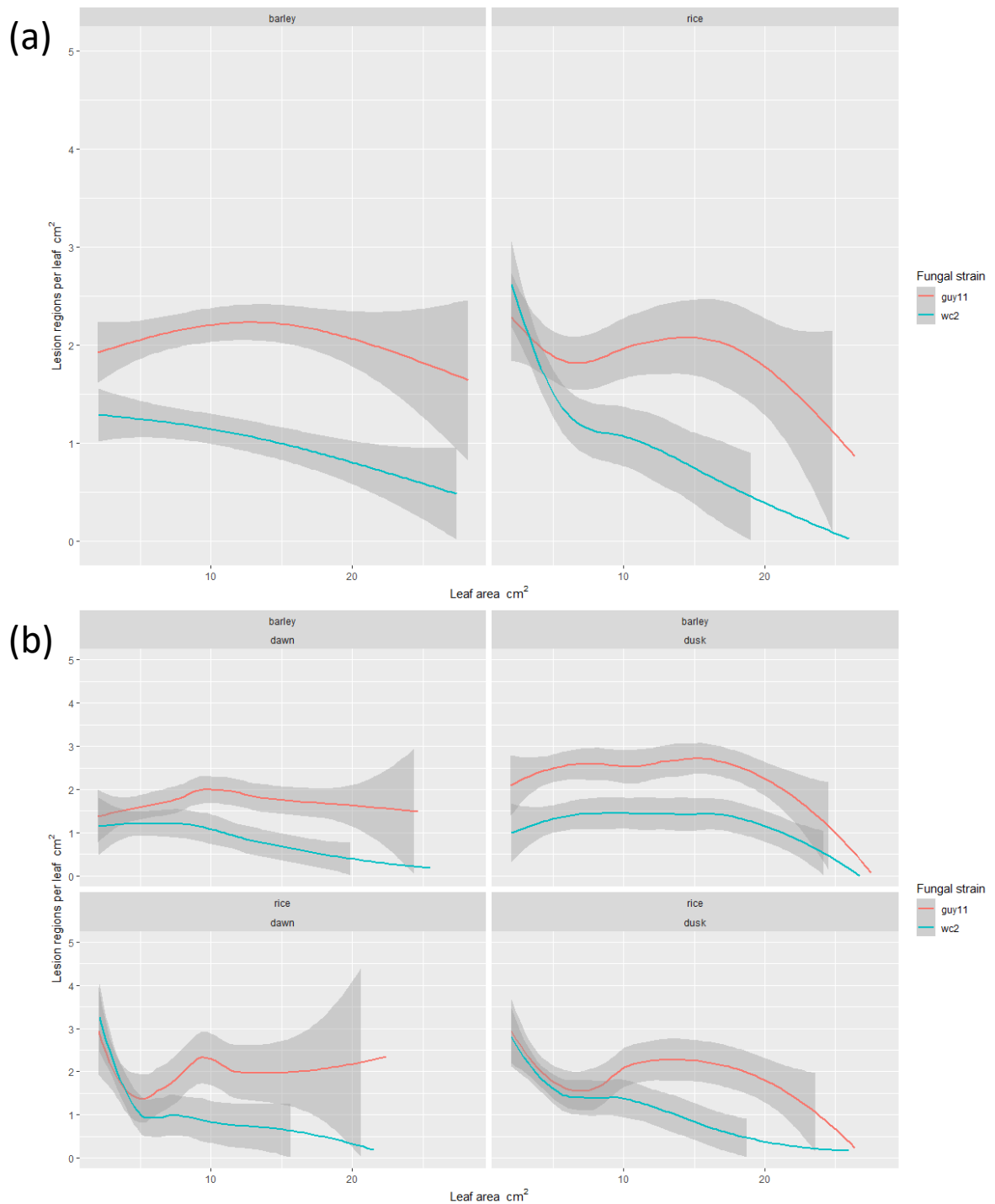


Figure 5.21: Δ WC2 displays dampened leaf maturity-dependent infection severity. (a) Unlike the wild type Δ WC2 inoculations do not show a preference for middle-aged leaves, and instead show highest lesion densities in the youngest leaves in both rice and barley. (b) Δ WC2 also does not display any time of day-dependent differences in lesion density in rice but displays similar (although dampened) infection profiles in barley at dusk, with a similar preference for middle-aged leaves ($n = 570$ leaves *guy11* / 458 Δ WC2 barley dawn, $n = 653$ *guy11* / 397 Δ WC2 barley dusk, $n = 276$ *guy11* / 255 Δ WC2 rice dawn, $n = 433$ *guy11* / 360 Δ WC2 rice dusk). Data displayed using Loess smoothed conditional means, grey shading denotes standard error.

5.3 Discussion

Here, WC2 has been shown to be essential in conidial banding, where Δ WC2 does not display this rhythmic output under any examined light cycles and instead shows a banding phenotype reminiscent of the wild type grown under constant light/dark conditions. This is not an unexpected outcome, as conidial banding is often arrested in the model clock species, *N. crassa*, when the White Collar Complex is non-functional (177,184,199,202,234,379,437,476,476,485,507,508,522). In *N. crassa* WC2 knockouts, *frq* transcript levels were very low and dark-synthesised FRQ protein showed no photoreponsiveness, giving rise to a 'blind' phenotype (227,476), in agreement with the results presented here. It is important to consider that a lack of rhythmic conidial banding does not necessarily mean that there is a lack of circadian regulation, as in some fungal species, core clock knockouts still show (altered) circadian rhythms (82,177,181,183–185,191,192,210,213,219,234,417,434,476,509), so Δ WC2 may still have residual clock function outside of the FRQ-WCC oscillator, despite its lack of conidial banding. This non-banding phenotype observed in Δ WC2 may also be the result of an inability to sense the conidial banding metabolite(s) (see 4.2.4). Considering that the wild type displayed early conidial banding when grown on Δ WC2 spent media, but Δ WC2 did not show conidial banding on wild type spent media, WC2 must be responsible for the sensation of the metabolite only.

Circadian mutants have often been observed to have altered vegetative growth rates (see table 5.1), and in *M. oryzae* specifically, mutations in the circadian-dependent TWL gene displayed compromised carbon source utilisation and increased ROS sensitivity (84). FWD1 and FRQ knockouts in *M. oryzae* also showed decreased vegetative growth rates compared to the wild type (259). None of these experiments performed growth rate

comparisons under a wide range of diurnal, constant, and circadian light cycles, however, so there may be subtle environmentally-dependent growth effects in these mutants, as described here. Whilst $\Delta WC2$ does not band under any environmental light conditions, it does display growth differences between treatments, where LL showed the fastest growth, and LD and LD-LL the slowest. This would suggest that light dark cycling conditions slow the growth rate of $\Delta WC2$, but LD-DD conditions do not inhibit growth to the same degree as LD and LD-LL. This instead implies that $\Delta WC2$ may have lost its dark adaptation, since LD and LD-DD conditions show the slowest average growth in the wild type, a phenotype not seen in $\Delta WC2$. Further, $\Delta WC2$ grows at a comparable rate to the wild type under LD-DD and LL conditions, but grows slower under DD, LD, and LD-LL. $\Delta WC2$ also no longer displays an increased growth rate under constant darkness, which is evidence that WC2 is responsible for photoadaptation, as in the wild type the average growth rate is fastest under constant darkness and constant light. These results could suggest that WC2 plays a role in both dark adaptation and the maintenance of circadian growth after sufficient entrainment in *M. oryzae*, as LD-LL and LL treatments are not significantly different to one another in the wild type. Alternatively, the similarity between $\Delta WC2$ and the wild type grown under prolonged light could mean $\Delta WC2$ displays an 'always light' phenotype, as may be the case in conidial development.

The presence of a functional clock may also grant an organism increased plasticity in response to altered environmental conditions, where gating of biological functions can occur under a wider range of physiologically relevant conditions. It is also important to consider that in the wild type, after conidial banding begins to occur, the average daily growth rate increases beyond that of the constant dark/light-grown colonies and as such, perhaps $\Delta WC2$ is constrained to grow in a manner similar to that observed during the

latency period of the wild type. This hypothesis aligns well with the fact that $\Delta WC2$ produces but is insensitive to the conidial banding metabolite.

$\Delta WC2$ displays reduced conidiation under prolonged darkness (DD and LD-DD) in a similar manner to the wild type and does not show any significant differences compared to the wild type under prolonged light exposure (LL and LD-LL). In contrast to the wild type, prolonged light exposure in $\Delta WC2$ does not significantly inhibit conidiation compared to LD, further implicating WC2 in a photoadaptive role. A lack of light repression on conidiation is a commonly observed phenotype in WCC mutants (see table 5.1) and is also seen in WC1 knockouts in *M. oryzae* (82,101), where WC1 mutants did not show any blue light-specific repression of conidiation. What differentiates WC1 from WC2 here, though, is that $\Delta WC2$ displays an additional conidiation repression under prolonged dark exposure. Together, the growth and conidiation differences observed in $\Delta WC2$ under constant light and constant darkness compared to those grown under cycling conditions suggests that WC2 plays a significant role in photoadaptation to light and/or darkness. Photoadaptation to light (light adaptation) may cause reduced conidiation, whereas photoadaptation to dark (dark adaptation) might subsequently increase conidiation (82,101). This hypothesis could explain why (assuming a lack of light/dark photoadaptation in $\Delta WC2$) prolonged light does not repress conidiation in $\Delta WC2$ to the same extent as prolonged darkness, where in the wild type there are no significant differences between prolonged light and prolonged dark exposure on conidiation.

In additional support of WC2 playing a role in light adaptation, $\Delta WC2$ conidia germinate and develop quicker than the wild type under all pre-harvest light treatments except under prolonged light exposure (LL and LD-LL), where there is no significant difference

between the two. Pre-harvest light conditions have little effect on Δ WC2 conidial development whereas constant light shows an increased developmental rate in the wild type. This is in agreement with Aver'yanov (384) who reported that light exposure increases 'aggressiveness' in *M. oryzae* conidia under low inoculation density, where they developed quicker than conidia that were not pre-treated with light.

Again, time of day had no effect on the rate of conidial development in Δ WC2. However, the fact that there is no difference does not necessarily mean that the clock is not important in conidial development. Since Δ WC2 conidia germinate and develop quicker than the wild type under most conditions, perhaps the circadian clock can also function as a 'stopwatch' or 'starting gun' in their development. In plants, for example, the circadian clock functions differently depending on the tissue type, where roots display a slave oscillator phenotype and do not have a fully functional circadian clock, relying instead on signals from the above-ground tissue (464,465), so perhaps the clock function in *M. oryzae* depends on the cell type. Likewise, A recent report indicated that *Z. tritici* WC1 affects melanisation differently in hyphae and pycnidia, where vegetative hyphal cells (but not pycnidia) displayed melanisation defects (392). Indeed, WC1 has been shown to be significantly upregulated in *M. oryzae* conidia compared to the mycelia (101) and as such may perform tissue-specific different functions.

Green light photoreception is well conserved in plant pathogenic fungi (474) and WC2 has been shown to act as a repressor of the *N. crassa* green light photoreceptor, NOP-1 (474). Since WC1 (which can act as a repressor of WC2) is upregulated in *M. oryzae* conidia (101), it is possible that green light photoreception could be an important influence on conidial development rate, as when conidial WC2 levels are low (as a result

of increased WC1 repression of WC2, or WC2 knockout), green light photoreception can occur to a much higher degree since NOP-1 is not being repressed. NOP1 expression in *N. crassa* is also highest during conidiation and remains high in conidia after their release (474), possibly as a result of the increased WC1 levels observed in conidia(101). Green light could therefore be an indicator to a conidium that it has successfully landed on a leaf and therefore should begin to germinate. This could also explain why prolonged white (i.e., containing green) light-exposed wild type conidia germinated and developed at a similar (and faster) rate to Δ WC2, which in some cases displays an 'always light' phenotype.

Since Δ WC2 undergoes cytorrhysis at lower glycerol concentrations than the wild type, the strain might generate a lower appressorial turgor pressure or may be less able to create a functional barrier to maintain turgor (381,523). The increased conidial developmental rate in Δ WC2 could also reduce the amount of time allocated for the accumulation of relevant osmolytes or develop a fully melanised appressorial cell wall. Accordingly, *M. oryzae* mutants that have a reduced ability to produce melanin have been shown to be less pathogenic and undergo cytorrhysis more readily (58,78,89,241,382,384,524). Melanisation is also known to be under circadian control in some fungal species, so perhaps the altered circadian phenotype in Δ WC2 has also caused an inability to produce fully melanised mature appressoria (101,108,177,181,194,215). In support of this, Kim and colleagues (101) reported that *M. oryzae* melanin biosynthetic genes were upregulated in response to a dark to light transition ('dawn'), of which the WCC is known to play a role in photoreception (see table 5.1). Interestingly, LD cycling conditions in Δ WC2 seem to have a negative effect on appressorial stability as they consistently collapsed to a greater degree compared to prolonged light- or dark-exposed

Δ WC2 conidia. Perhaps, then, the cycling conditions cause a misregulation of melanin biosynthetic genes as a result of non-functional WC2. This effect is not observed in the wild type, and further suggests a lack of photoadaptability in the mutant. Alternatively, wild type conidia are larger than Δ WC2 conidia after agitation, so perhaps the increased conidial size allows for a greater allocation of resources for proper appressorial generation.

Δ WC2 mutants further showed a reduced ability to penetrate the host plant cuticle in rice leaf sheathe inoculations, likely as a direct result of the reduced appressorial turgor pressure generated. Alternatively, the increased conidial developmental rate could lead to a mistiming of penetration, causing Δ WC2 to attempt to puncture the host cuticle at a point in which rice is less susceptible. Usually, *M. oryzae* plant penetration has begun by \sim 12 HPI (79), which would mean the pathogen is breaching the plant during the dark period. In faster-developing conidia, such as those of Δ WC2, the fungus may instead be penetrating the plant during the light or early-dark period, which may be less conducive for disease progression. After penetrating the host cuticle, these mutant invasive hyphae also showed a reduced ability to undergo cell-cell movement *in planta*, and were often constrained to the primary invaded cell, showing large amounts of hyphal growth within that cell. This could be due to Δ WC2 being unable to tolerate or dampen the host ROS response, as there are several similarities in phenotypes observed in Δ WC2 and Δ TWL, a circadian controlled gene mutant, where the addition of exogenous antioxidants restored Δ TWL cell-cell movement (84). Excess ROS has also been shown to prevent heterodimerisation of WC1 and WC2, lowering functional WCC (184). Altered intracellular ROS levels in TWL and WC2 mutants may then feed back into the clock, causing further mistiming of *M. oryzae* pathogenicity related processes. Δ TWL also

showed altered carbon source utilisation and ROS homeostasis, so in this way, perhaps TWL is downstream of the WCC and is partially responsible for nutritional sensation (potentially including the banding metabolite). Thus, when WC2 function is arrested, TWL function is, too. Δ TWL maintained the conidial banding phenotype, however, so WC2 is likely responsible for additional nutritional/metabolic sensation (84). This reduced penetration and cell-cell movement was also observed in the *M. oryzae* circadian FWD1 mutant (259), further implicating a role of the circadian clock in pre- and early pathogenesis.

Whilst Δ WC2 often showed a reduced lesion density, counterintuitively, Δ WC2 did not show significantly reduced pathogenicity (lesion region area and lesion coverage) in rice inoculations 6 DPI, which is surprising, given the reduced appressorial stability and early infection phenotypes observed. It is possible that Δ WC2 may be able to produce conventional lesions in host plant interactions as a result of communication with the host or interpretation of host signals. Δ WC2 may be able to progress in a similar manner to the wild type by synchronising its metabolism in a slave oscillator-like manner (181,183). Alternatively, biological rhythms can occur in the absence of the WCC or FRQ in (some) fungi, so perhaps there is residual clock function in Δ WC2 despite the non-functional core clock, allowing for continued host pathogenicity (181,183).

In support of this host-pathogen communication hypothesis, Deng and colleagues (84) reported that crude extract from rice plants grown under light were able to restore the reduced conidiation phenotype of TWL Δ better than extracts from dark-grown plants, and as such the accumulation of host nutrients may depend on the (circadian) time of day. Perhaps then, *M. oryzae* can entrain and set its clock to the host based on a number

of entraining signals from the plant (ROS, nutritional, hormonal status etc.) and extrapolate the time of day based on the plant clock status, even when its circadian rhythmicity is dampened *ex planta* (84). Deng and colleagues also showed that growing TWL mutants (which display reduced conidiation) on rice extract rescues the conidial reduction phenotype better than those grown on barley extract, suggesting different nutritional and signal utilisation in host- and non-host interactions. Accordingly, in non-host barley-*M. oryzae* interactions, $\Delta WC2$ shows a profound reduction in pathogenicity under all treatments at dawn and dusk compared to the wild type, which may be a result of an inability to discern any signals from the plant; it also cannot rely on its own clock because WC2 is non-functional. Barley- $\Delta WC2$ interactions did show some effect of pre-inoculation treatment on pathogenicity, suggesting an ability to sense environmental changes and perhaps alter its behaviour in a diurnal, environmentally-dependent, but clock-independent, manner.

It has been reported that in some symbiotic plant-fungi relationships, a mutually beneficial holobiont is formed, where the circadian rhythms between both partners are linked (212). In arbuscular mycorrhizal (AM) interactions, the underground (and thus dark-dwelling) fungi retain clock function but may have undergone selective pressure to favour plant-associated carbon-related and nutritional signals as Zeitgebers, so it is possible that *M. oryzae* may utilise non-canonical zeitgebers and clock machinery in a similar fashion (212). Perhaps *M. oryzae* prioritises different Zeitgebers depending on its environment; light and temperature might be most important *ex planta*, but chemical/nutritional/metabolic/ROS status might be more important entraining signals *in planta*, given the drastically different environmental challenges to face.

The nutrient-dependent clock of the AM fungi allows for synchronisation of important organismal processes despite their dark environment based on the plant-derived signals (212). This is also seen in the root tissue of plants, where the root clock is dependent on input from the foliar tissue clock (464,465). The observations in this chapter of maintained pathogenicity in the Δ WC2-host interactions, where the plant and pathogen have co-evolved may suggest that *M. oryzae* can utilise *in planta* environmental cues to entrain (and supplement) its clock even when clock function is arrested. *M. oryzae* may, therefore, establish what could be considered a 'pathogenic holobiont' (212). In non-host interactions, where there has not been co-evolution between the plant and fungus, *M. oryzae* may be unable to utilise the nutritional Zeitgebers, and therefore cannot synchronise cellular processes that benefit pathogenesis. Further, as a long-day plant, barley may express defence-related and perhaps even nutritional signals out of phase to rice, which is a short-day plant (see 4.3). Therefore, in this scenario where *M. oryzae* may interpret barley-derived signals, they could perhaps 'anti-entrain' or 'mis-entrain' *M. oryzae*, as the nutritional/ROS/metabolic status of rice cells that are beneficial to *M. oryzae* virulence may occur at different (or opposite) times of day in barley.

Shi and colleagues (259) showed that a non-functional circadian *Fwd1* gene reduced the average lesion size 5 days post-inoculation in detached barley leaf infections (using mycelial plugs or conidial droplets) - This is in direct agreement with the observations here (259). Further, upon rice spray inoculations, *Fwd1* and *FRQ* mutants showed a reduced number of lesions per leaf, in agreement with the Δ WC2-host interactions (259). Shi and colleagues did not report on infection timing, and lesion sizes or lesion cover in rice infections, however, so there may be more subtle differences in the host- and/or

non-host plant pathogen interactions in virulence, susceptibility, and circadian rhythms. They also used higher inoculation densities than those described here.

As observed in rice under high inoculation densities, perhaps a similar clock-dependent loss of virulence would be observed in host plant-pathogen interactions if the infection conditions were more favourable for the pathogen, i.e., higher inoculation densities, shorter time spent in solution prior to inoculation etc. These seemingly conflicting results in rice-*M. oryzae* interactions may be a result of the sub-optimal inoculation conditions. Briefly, in as short a period of time as possible after the incubator/growth chamber lights were switched on, multiple colonies from the different strains were harvested, their conidial concentrations determined and diluted to 1×10^5 /ml with 0.1% gelatine and Tween 80, plants were placed in plastic boxes with water to increase humidity, and then spray-inoculated with *M. oryzae* strains. The air brush used for inoculations also needed to be cleaned repeatedly between strains with water and 70% ethanol to ensure that there was no cross-contamination. Under 'true' dawn inoculations consistent with the field, conidia would be spread naturally by wind and dew drop prior to dawn, when conidia are actively being released (82,101), which is difficult or even impossible to achieve in the laboratory. Due to the fact that researcher-performed inoculations require sight, all conidia were harvested after subjective dawn, as removing fungal material prior to their subjective dawn may cause a PLRE-dependent FRQ resetting of the clock (see 5.1). *M. oryzae* conidia have also been shown to respond to red light (82), so inoculations could not be performed under red safety light.

To speed up inoculations, single strains could be harvested and used to inoculate plants on a daily basis allowing for infections to occur closer to dawn. However, if same-age

plants and *M. oryzae* strains were used there would need to be repeated sowing of seeds and inoculations of plates with fungi, which would take up significant lab time. This would also mean that different strains were not inoculated under identical conditions. Additionally, since $\Delta WC2$ produces significantly fewer conidia, more fungal material is required to generate the same amount of inoculum, so infections would inevitably occur later in $\Delta WC2$ than the wild type, as opposed to roughly the same time, since plants were inoculated with different strains within ~ 5 minutes of each other. The amount of time that conidia spent in solution post-harvest and pre-inoculation may also have affected pathogenicity since strains were harvested one at a time to minimise any chances of cross contamination. All of these confounding factors made it technically difficult or impossible to recreate 'true' dawn inoculations, so perhaps alternative methods of inoculation need to be considered for future research. For example, open petri dishes could be placed in plastic boxes with plants in the growth cabinet with a fan that would switch on automatically shortly before dawn, causing conidia to be spread in a more natural fashion by the wind generated. It would be almost impossible to control for conidial densities in this setup, however.

Unlike the wild type, $\Delta WC2$ did not show a preference for middle-aged leaves of 10-15 cm² and instead showed a general decrease in lesion density as leaf area increased, except under dusk inoculations in barley, where $\Delta WC2$ displays a slight increase in lesion densities at ~ 10 -20 cm² compared to both smaller (<5 cm²) and larger (>20 cm²) lesions. However, this effect is significantly dampened compared to wild type inoculations at dusk in barley. These results suggest that there may be times of day in which different plant species are most susceptible to infection (dawn in rice, dusk in barley). Further, instead of 'middle-aged' leaves being most susceptible to *M. oryzae* infection, these results instead

suggest that the pathogen circadian clock is, at least in part, responsible for overcoming the plant defences of these leaves, since $\Delta WC2$ infections generally show a decrease in lesion density as leaf area increases. WC2 may therefore be responsible for the sensation and subsequent response to plant defence mechanisms.

As discussed in chapter 4, plant developmental stage and susceptibility are linked; Chen and colleagues (390) show that rice-*M. oryzae* infections are most severe in younger plants (stages V1 to V3), and rice susceptibility rapidly decreases from stage V5 onwards, which could align well with the observations made here, since the largest leaves showed the lowest lesion densities (in both rice and barley, and in wild type and $\Delta WC2$). Chen and colleagues did not discuss leaf area and, by proxy, leaf age, though. Importantly, Chen and colleagues used different inoculum amounts at each growth stage to account for the increased amount of foliar tissue in older leaves. (15 ml 1×10^5 conidia for V1-V5 plants, and 30 ml for V6-V10), which may have masked some differences between inoculations. Yamauchi and colleagues (253) also showed that older *Arabidopsis* leaves are more susceptible to *M. oryzae* penetration at dusk compared to younger leaves, a phenotype which is not observed at dawn, where penetration was consistently lower in both young and old leaves. This phenotype is consistent with dusk inoculations in both rice and barley, where there is a clear peak in middle-aged leaves. In dawn wild type inoculations, however, this peak is not seen, where lesion densities increase with leaf area. The $\Delta WC2$ inoculations at dawn do not show this correlation. Together, these results perhaps suggest that *M. oryzae* is more pathogenic at dawn, plant susceptibility is species and time of day dependent, and that gating of virulence is, in part, dependent on the clock.

Interestingly, $\Delta WC2$ still showed reduced dawn pathogenicity after prolonged light exposure (LL and LD-LL). This could suggest that prolonged light exposure plays a role outside of clock function. Light is a known stressor and inducer of reactive oxygen species in fungi (106,109). ROS also plays a role in pathogenicity and susceptibility in both members of several plant-fungi pathosystems; in the necrotrophic *A. brassicicola*, for example, fungal-derived ROS mediates host cell death and encourages pathogenic growth, but ROS bursts are also associated with plant defence (106,149,152,460,525). Photoperiod, and thus length of time exposed to light, further influence disease severity in *B. juncea*-*A. brassicicola* interactions (149), so perhaps a clock-independent but ROS-dependent phenotype is observed after prolonged light exposure in *M. oryzae*. In support of this, Shimizu (460) showed that prolonged light exposure after dusk inoculations of Arabidopsis with *M. oryzae* increased plant resistance to penetration, and that prolonged dark exposure after inoculations at dawn suppressed this resistance to penetration. ROS-derived metabolite(s) also contributed to the photoperiod regulation of non-host resistance to *M. oryzae* in Arabidopsis (460). Since ROS homeostasis is under circadian control in both plants and fungi (106,113,152,184,249,479), perhaps the prolonged light exposure causing reduced pathogenicity in dawn infections is maintained in $\Delta WC2$ because it is exhibiting a 'constant light' phenotype, consistent with the increased conidial developmental rate observed in $\Delta WC2$ and prolonged light-entrained wild type conidia. Concurrently, while ROS homeostasis is in part a clock-regulated output, it also feeds back into the clock as an input signal, so the increased ROS levels due to prolonged light exposure may have caused the light-dependent conidial development and virulence phenotypes independently of clock function in the wild type (182,184).

This chapter has reported on the generation of a WC2 mutant via CRISPR Cas9-mediated HDR, displaying a phenotype indicative of a core clock knockout. Δ WC2 displays no banding under any of the light treatments, possibly as a result of its inability to sense the conidial banding metabolite. Δ WC2 still showed a light treatment-dependent vegetative growth phenotype, which has not been explored in many other plant pathogenic fungi, and could be a result of a loss of photoadaptation or other extra-circadian effects. Δ WC2 lost its light-dependent inhibition of conidiation and instead shows a prolonged darkness repression of conidiation; light-dark cycling conditions remain to be most conducive for conidiation. Δ WC2 also displayed increased conidial developmental rates, a phenotype similarly observed under prolonged light exposure in the wild type, suggesting an 'always light' phenotype. WC2 is partly responsible for host cuticle penetration, likely due to its reduced appressorial turgor pressure. Early infection cell-cell movement is also reduced in Δ WC2, potentially due to a reduced ability to tolerate or inhibit ROS production *in planta*. The *M. oryzae* core clock also plays a significant role in non-host pathogenicity, where Δ WC2 consistently showed a reduced disease severity under almost all pre-inoculation treatments and times compared to the wild type. And finally, *M. oryzae* may be able to interpret host plant-derived temporal signals to re-entrain or supplement its clock even in the absence of a fully functional circadian system to ensure virulence is gated in an optimal fashion. Summarily, WC2 plays a role in photoadaptation (to both light and darkness), chemical sensation, conidiation and conidial development, and pathogenicity.

6 FRQ determines periodicity, conidiation, and conidial development

6.1 Introduction

FRQ is one of the most well described genes in the fungal literature, and has been implicated in several functions, predominantly circadian rhythmicity and gene regulation (117,161,178,186,193,195,203,213,221,225,232,502,526,527). As such, throughout the circadian day, FRQ has been described to interact with a plethora of clock and clock-controlled genes (CCGs), ensuring that the endogenous rhythm is set and synchronised to the environment (178,181,193,257,438,439). Further, FRQ's function lies beyond just keeping time, as mutants have been observed to have altered vegetative growth, sexual and asexual reproduction, conidiation and conidial development, reactive oxygen species homeostasis, light- and temperature-sensitivity, nutritional utilisation, and even virulence. Table 6.1 describes published FRQ mutants and their respective phenotypes. Together, these reports show that FRQ is important for a wide range of growth, maintenance, developmental, and perceptive functions in fungi.

Table 6.1: A selected summary of FRQ mutations

Species	Mutation	Phenotype	Reference
<i>M. oryzae</i>	Partial deletion (see 6.2.1)	Slowed growth Reduced conidiation Delayed conidial germination Decreased appressorial formation Reduced virulence	(259)
<i>M. oryzae</i>	C-terminal Insertional knockout (see 6.2.1)	Irregular conidiophore morphology Wild type vegetative growth, conidial germination and appressorium formation	(258)
<i>N. crassa</i>	Null	Altered light-induced transcription of FRQ Altered ROS homeostasis No entrainment to LD or temperature cycles Light insensitivity Maintenance of temperature-dependent conidial banding (diurnal but not circadian) 'Arrhythmic' conidial banding under DD (unless grown on media supplemented with geraniol or farnesol, where temperature compensation is lost, and period is altered) 'conditionally' rhythmic Carbon source-dependent period Rhythmic conidiation after several days on long race tubes Increased but arrhythmic osmotic stress response gene expression (OS-2) Reduced temperature, pH, and nutritional compensation Reduced conidiation Reduced aerial hyphae Reduced WC1 RNA and protein levels Reduced WC2 RNA and protein levels	(183,184,191,192,200,210,213,408,437,439,485,502,509)

<i>N. crassa</i>	C-box deletion	Low level frq expression Dampened oscillation	(528)
<i>N. crassa</i>	Coiled-coil domain deletion	FRQ-FRQ dimerization inhibition Arrhythmic conidiation Inability to interact with the WCC	(510)
<i>N. crassa</i>	Phosphorylation site mutagenesis	Lengthened or shortened period (depending on site) Altered FRQ stability	(161,181,195)
<i>N. crassa</i>	C-terminal deletion	Hypophosphorylated FRQ Reduced FRQ stability Shortened rhythm 'Arrhythmic' conidial banding Reduced WC1 accumulation	(193,221)
<i>N. crassa</i>	PEST domain phosphorylation sites (amino acid change to negatively charged aspartate)	'Arrhythmic' conidial banding Reduced dark FRQ levels Accumulation of phosphorylated FRQ and WC1	(193)
<i>N. crassa</i>	PEST domain deletion	Reduced FRQ phosphorylation Stabilised FRQ levels Reduced WC1 expression 'Arrhythmic' conidiation under DD and LD	(161,221)
<i>N. crassa</i>	qrf (FRQ antisense transcript) elimination	Period increase 'Arrhythmicity' at low temperatures Earlier phase setting upon light to dark transfer	(178,526)
<i>N. crassa</i>	C-terminal point mutations	Shortened period	(178)

<i>N. crassa</i>	NLS deletion	Reduced nuclear FRQ Increased phosphorylated FRQ in the cytoplasm	(221)
<i>N. crassa</i>	Inducible overexpression	Reduced native frq mRNA expression	(221)
<i>N. crassa</i>	Exogenous inducible expression in a null mutant background	Increased negative feedback on FRQ Increased recovery time from negative feedback	(529)
<i>N. crassa</i>	Constitutive expression	'Arrhythmic' under DD Conidial banding under LD conditions Reduced carotenogenesis Reduced WC1 RNA levels Increased WC1 protein levels Increased WC2 protein levels Reduced native frq mRNA expression	(213,225,502)
<i>N. crassa</i>	Site-directed mutagenesis of codons S885 and/or S887; altered to aspartate (putative phosphorylation sites)	Increased accumulation of WC1 Unaltered WC2 levels 'Arrhythmic' FRQ RNA and protein levels 'Arrhythmic' conidial banding under DD Maintained conidial banding under LD Altered WC1 phase	(221)
<i>N. crassa</i>	FCD point mutation (FRQ-CK1 interaction domain)	Impaired CK1 interaction Hypophosphorylation of FRQ	(195)
<i>N. crassa</i>	C-terminal phosphorylation site mutations (Ser/Thr – Ala)	Shortened period Hypophosphorylated FRQ	(195)

<i>N. crassa</i>	FRQ codon optimisation	Arrhythmic conidiation Arrhythmic molecular circadian rhythm Increased FRQ levels Altered FRQ phosphorylation profile Reduced FRQ stability Altered FRQ structure (due to increased translation rate)	(527)
<i>N. crassa</i>	L-FRQ only	Shortened period	(203)
<i>N. crassa</i>	S-FRQ only	Longer period Dampened rhythms under higher temperatures	(203,530)
<i>B. cinerea</i>	Overexpression	Persistent inhibition of WCC 'Arrhythmic' conidial banding Inability to produce large dusk lesions Reduced dawn and dusk virulence Decreased endogenous frq expression	(117)
<i>B. cinerea</i>	Null	Media-dependent sexual development (microconidia and sclerotia production) in the light Decreased macroconidiation Enhanced sclerotia formation 'Arrhythmic' conidial banding Inability to produce large dusk lesions Increased conidial 'aggressiveness' at dawn and dusk, compared to the wild type	(117)

<i>V. dahliae</i>	Null	<p>Light-independent (but media-dependent) reduced growth rate</p> <p>Reduced pathogenicity (isolate-dependent)</p> <p>Maintenance of conidial banding under LD and temperature cycles</p> <p>Downregulation of FWD1, WC1, and WC2</p> <p>Upregulation of VVD</p> <p>Misexpression of secondary metabolite genes</p> <p>Upregulation of metabolic, translation, protein secretion and nucleotide metabolism genes; downregulation of redox process, haem oxidation, circadian rhythms, and glutamate biosynthesis genes (regardless of light condition) compared to wild type</p> <p>Light only downregulation of phosphate ion transport, nitrate assimilation transport, superoxide anion generation, one-carbon metabolic processes and pathogenesis</p>	(434)
<i>B. bassiana</i>	FRQ1 deletion (<i>B. bassiana</i> has two FRQ homologs)	<p>Delayed conidiation (undetectable conidia prior to 8 days of growth)</p> <p>Reduced conidiation</p> <p>Decreased conidiation with longer daylight hours</p> <p>Wild type growth rate</p>	(232)
<i>B. bassiana</i>	FRQ2 deletion (<i>B. bassiana</i> has two FRQ homologs)	<p>Delayed conidiation (undetectable conidia prior to 9 days of growth)</p> <p>Reduced conidiation</p> <p>Decreased conidiation with longer daylight hours</p> <p>Wild type growth rate</p>	(232)

6.1.1 FREQUENCY's daily journey

The circadian rhythm and subsequent regulation of clock-controlled genes in fungi are, in part, dependent on the expression, abundance, localisation, and phosphorylation status of FRQ (84,117,161,177,178,181,189,192,193,195,212,213,221,222,225,227–230,234–236,434,439,502,510,518,527,531,532). Early in the circadian day/late at night, frq transcription and translation occurs as a result of White Collar Complex (WCC)-dependent upregulation (for an in-depth description of the WCC activity in the clock, see 5.1) (201). The circadian clock ultimately relies on the spatiotemporal activation and repression of core clock components: the positive and negative arms, respectively (161,178,193,195,221,235,236,527) (Fig. 6.1).

FRQ also has several phosphorylation sites, which can ultimately affect its charge, shape, localisation, protein interaction and subsequent circadian function (161,178,181,193,195,210,221,225,228,229,231,233,235,236,259,404,527,532,533).

FRQ phosphorylation status and subsequent activity is controlled and fine-tuned by a number of proteins which phosphorylate and dephosphorylate the protein continuously throughout the day: phosphorylation is chiefly carried out by CK1, CAMK-1, CK-2, PKA, and PRD-4 (an ortholog of checkpoint kinase 2, not to be confused with casein kinase 2); and dephosphorylation is carried out by PP1, PP2A, and PP4, where mutations in many of these proteins (or their respective site(s) on FRQ) cause altered periodicity in *N. crassa* (178,181,193,195,210,221,225,228,229,229,231,233,236,259,404,532–539).

Once FRQ protein is produced, it follows two main routes: (a) rapid hypophosphorylation-dependent interaction with both FRQ-interacting RNA Helicase (FRH) and Casein Kinase 1 (CK1) to form the FRQ-FRH-CK1 complex (FFC) and nuclear localisation to carry out its

function in the negative arm; and (b) when retained or exported to the cytoplasm (via its interaction with FRH), FRQ serves to post-transcriptionally stabilise *wc2* mRNA and post-translationally upregulate WC1, performing its role in the positive arm (178,193,195,221,235,236,527) (Fig. 6.1). As a result of increasing phosphorylation throughout the day, FRQ gradually becomes less active in both the positive and negative arm and the cycle begins anew (195). Hyperphosphorylated FRQ is then targeted by FWD1 for ubiquitination and eventual turnover (178,181,189,195,210,259).

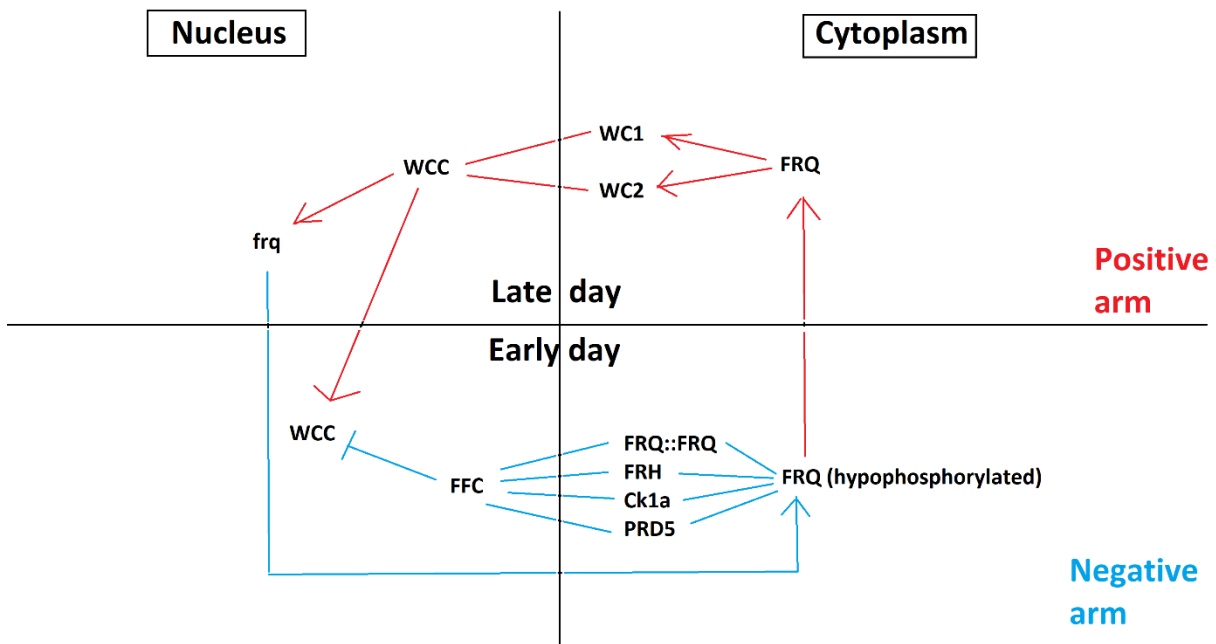


Figure 6.1: FRQ function in the positive and negative arm is dependent on time of day, phosphorylation status, and subcellular localisation. Red and blue lines denote positive and negative arm activity, respectively.

In its nuclear journey, newly formed, hypophosphorylated FRQ is in a closed/folded conformation as a result of differences in residue charge: the FRQ N-terminus is positively charged and the middle and C-terminal is negatively charged, which likely determines the proteins shape (178,236). This folding might also expose a central nuclear localisation signal (NLS), facilitating FFC localisation and activity in the nucleus (178,221,234,236), since the charge-dependent closed conformation is known to be required for CK1 recruitment and nuclear transport (236). Here, the hypophosphorylated FRQ proteins dimerise due to their coiled-coil domains, interact with FRH (which acts to stabilise FRQ, preventing turnover), and binds to CK1 at the FRQ/CK1 interacting domain (FCD), altogether forming the FFC (178,193,195,221,236).

Once inside the nucleus, the FFC-bound CK1 readily phosphorylates the WCC, which represses the WCC-mediated expression of frq and causes the WCC to be translocated

from the nucleus for turnover (178,195,212,221,222,228,235). This causes frq transcript levels to plateau and then fall, as the WCC is no longer functioning in the positive arm (192) (Fig. 6.1). Phosphorylated WCC on its way to the cytoplasm for turnover can be dephosphorylated by phosphatases such as PP2A, which act to prevent the degradation of the WCC, likely creating a baseline pool of WCC throughout the day (178,221,229). Interestingly, PP2A has also been shown to interact with FRQ, and thus may play a role in both the positive and negative arm (178,181,193). As a result of FFC phosphorylation-mediated WCC inactivation, when total FRQ protein levels are at their peak (approximately 6-8 h after initial frq transcription), frq mRNA levels are rapidly falling due to a lack of WCC-dependent frq transcription (178,181,192,212,221,225,437).

Nuclear FFC also represses the function of VVD, a photoreceptor known to sequester light-activated WCC that would ordinarily cause an acute increase of frq and subsequent light resetting of the circadian clock via PLRE-activated FRQ transcription: this process is termed light adaptation (see 5.1 and 6.1.3.2) (178,181,205,209,228,231,234). Here, FRQ may act to increase or supplement its own expression by limiting VVD sequestration of PLRE-targeting WCC and photoadaptation (192,201,227,227). Perhaps this inhibition of VVD acts to (somewhat) compensate for the rapidly falling levels of nuclear WCC (183,225,413). Alternatively, reduced levels of active VVD (due to FRQ-mediated inhibition) could serve to facilitate light resetting of the clock, since WCC could remain photoactivatable (178,181,189,191,192,209,476,513,540).

In addition to reducing WCC activity in the nucleus, CK1 also progressively phosphorylates the FFC-bound FRQ to eventually inactivate FRQ over the course of the circadian day (178,193,228,235,236). It is possible that FRQ in FFC can maintain its activity for a longer

period than the WCC due to its high capacity for phosphorylation, or because phosphorylation occurs preferentially at peptide locations that do not cause a loss of function (161,178,195,229,236,434,518,531,532). In this way, CK1 in the FFC rapidly inhibits WCC activity and progressively inactivates nuclear FRQ over the span of a circadian day, facilitating a tightly controlled oscillation of positive and negative regulators of core clock components and the subsequent clock controlled genes (178,193,228,231,236,532,533,541).

Cytoplasmic FRQ acts to stabilise WC2 mRNA and post-translationally upregulate WC1, allowing WCC to form and function in the nucleus, again facilitating its role in frq transcription (178,192,222,231,501). As the cytoplasmic (and nuclear) FRQ becomes increasingly phosphorylated, its function in the circadian system (both positive and negative regulation of WC1, WC2, and the WCC) is dampened and FRQ is eventually rendered 'invisible' to the other circadian machinery (178). Altogether, FRQ acts to both inhibit its own activator in the negative arm early in the circadian day and upregulate and stabilise the constituents of its activator (the WCC) throughout the day.

6.1.2 FRQ stability: phosphorylation and FRH

As well as acting to stabilise FRQ via its interaction at the C-terminus, FRH also serves to traffic FRQ to the cytoplasm where it performs its role in the positive arm and is eventually turned over (195). Whilst the majority of total of FRQ lies in the cytoplasm throughout the circadian cycle (195,221), it is important to consider how the relative concentration of nuclear vs cytoplasmic FRQ can play a role in circadian regulation. In budding yeast, for example, the nucleus occupies approximately 7% of the total cellular volume, and thus if the concentration (as opposed to total abundance) is the more

important determinant in circadian action, the nucleus would require less than 10x the amount of cytoplasmic FRQ to achieve a 1:1 nuclear:cytoplasmic concentration (542,543).

Accordingly, in a comprehensive study on the role of FRH and localisation of FRQ throughout the circadian cycle, Cha and colleagues (195) systematically studied a range of clock mutants. This work showed that relative nuclear enrichment of FRQ was similar throughout the circadian day and that nuclear-cytoplasmic shuttling did not change significantly (195). They also observed that decreased levels of FRH caused both an increase in *frq* transcript levels and decrease in overall FRQ protein levels in the cell, likely because of reduced WCC repression but increased FRQ instability (178,195,221,544).

Importantly, it was previously suggested that phosphorylation status dictated FRQ nucleocytoplasmic localisation, and that progressive phosphorylation removes FRQ from the nucleus (544). Cha and colleagues (195) instead showed that FRH is the key player in FRQ localisation; a lack of FRQ-FRH interaction increases relative nuclear FRQ, but decreases overall abundance of FRQ, suggesting that FRH plays a role in both the nuclear export and stabilisation of FRQ. Indeed, it has been shown that the majority of cellular FRQ is found in the cytoplasm (195,221). When considering circadian function, these two ideas in no way contradict one another: if FRH is absolutely required for FRQ stability, but FRH causes preferential localisation to the cytoplasm, then the majority of FRQ will be present in the cytoplasm, as was reported by Schafmeier and colleagues (221). However, FRQ is known to be turned over in the cytoplasm towards the end of the end of the circadian cycle when it is hyperphosphorylated, which understandably suggests a causal link between FRQ localisation and phosphorylation (195,221,544).

An FRQ strain harbouring amino acid substitutions at the FRQ-FRH interaction domain (FFD) (alanine replacements at aa positions 773 – 775) that was severely impaired in its FRH interaction still showed some FRQ in the cytoplasm, so FRH is not essential for cytoplasmic localisation (195,545,546). However, since FRH is important for FRQ stabilisation (FRQ levels were low in this mutant), FRH directly, through nuclear export, and indirectly, via stabilisation, facilitates the relative cytoplasmic abundance of FRQ (195,545,546). Further, an FRQ mutant strain with point mutations at the FRQ-CK1 interaction domain (FCD) caused persistent hypophosphorylation, but still showed normal nucleocytoplasmic abundance of FRQ, suggesting that low levels of phosphorylation do not cause nuclear localisation of FRQ (195). Likewise, mutants in PP1 and PP4 (two phosphatases that dephosphorylate FRQ) give rise to hyperphosphorylated FRQ and do not show altered FRQ localisation compared to the wild type, which implies that phosphorylation does not prevent FRH-FRQ interaction, nor dictate FRQ localisation (195).

This phosphorylation-dependent inactivation of nuclear FRQ facilitates the circadian cycle to begin anew, as nuclear FRQ is no longer inhibiting WCC function, and cytoplasmic FRQ eventually stops upregulating WC1 and WC2 due to increasing phosphorylation; both nuclear- and cytoplasmic-derived FRQ is then targeted by FWD1 (F-box/WD-40 -repeat-containing protein) for ubiquitination and turnover (161,178,181,191,193,195,229,235,259). It is important to consider here that while FWD1 is important to the circadian clock and facilitates the degradation of FRQ, the cycle is not reset when FRQ protein is degraded, but rather when the FRQ pool has become so hyperphosphorylated that it is unable to interact with the WCC (and upregulate its constituent parts) or function in the FFC (235,533). However, whilst FWD1 is not essential

for the circadian oscillation of FRQ, FWD1 knockout strains display increased levels of hyperphosphorylated FRQ, and the mutant colonies lose their conidial banding (235). This suggests that excessive (hyperphosphorylated) cytoplasmic FRQ may act to competitively inhibit the rhythmic conidiation phenotype and implicates FRQ in extra-circadian conidiation function (235,533). Accordingly, it would be interesting (if not experimentally difficult) to study how the relative concentration, localisation, and abundance of hypo- and hyperphosphorylated FRQ dynamics change throughout the circadian day. Perhaps the functionally inactive hyperphosphorylated FRQ acts in a competitive manner to the functionally active hypophosphorylated FRQ: FRH may be a limiting factor in the cell, and when available after FRQ phosphorylation and turnover could serve to stabilise newly synthesised hypophosphorylated FRQ. In this way, it is not the overall abundance of FRQ that is most important in circadian function, rather its localisation, relative concentration, and phosphorylation status, all of which affect its availability, activity, conformation, and charge (161,178,193,195,221,221,235,236,527).

In Summary, late at night/prior to dawn, WCC facilitates *frq* transcription, which is then translated, leading to a peak of FRQ protein at subjective midday ~6-8 h later (201). Light signals at dawn also cause an acute increase in PLRE-activated FRQ, facilitating a phase resetting and synchronisation with dawn (see 5.1.2) (178,181,183,184,192,213,214,225,227,234,437,516,526,528,547). As FRQ is made, a proportion is localised and active in the nucleus, acting to repress WCC activity and subsequently its own transcription via FFC-mediated inhibition (161,178,221,229,234,236). As the day progresses, cytoplasmic FRQ acts to upregulate WCC activity, but as FRQ becomes increasingly phosphorylated, it is then less able to perform its negative (nuclear WCC inhibition) and positive (cytoplasmic WCC activation)

functions, allowing for the circadian cycle to start again, where the WCC acts in the nucleus to transcriptionally upregulate *frq* (178,192,222,231,501). The remaining pool of hyperphosphorylated inactive FRQ is 'cleaned' from the cell by FWD1-mediated ubiquitination and turnover (161,178,181,191,193,195,229,235,259). A simplified overview of the FRQ-centric *N. crassa* clock is displayed in Fig. 6.2.

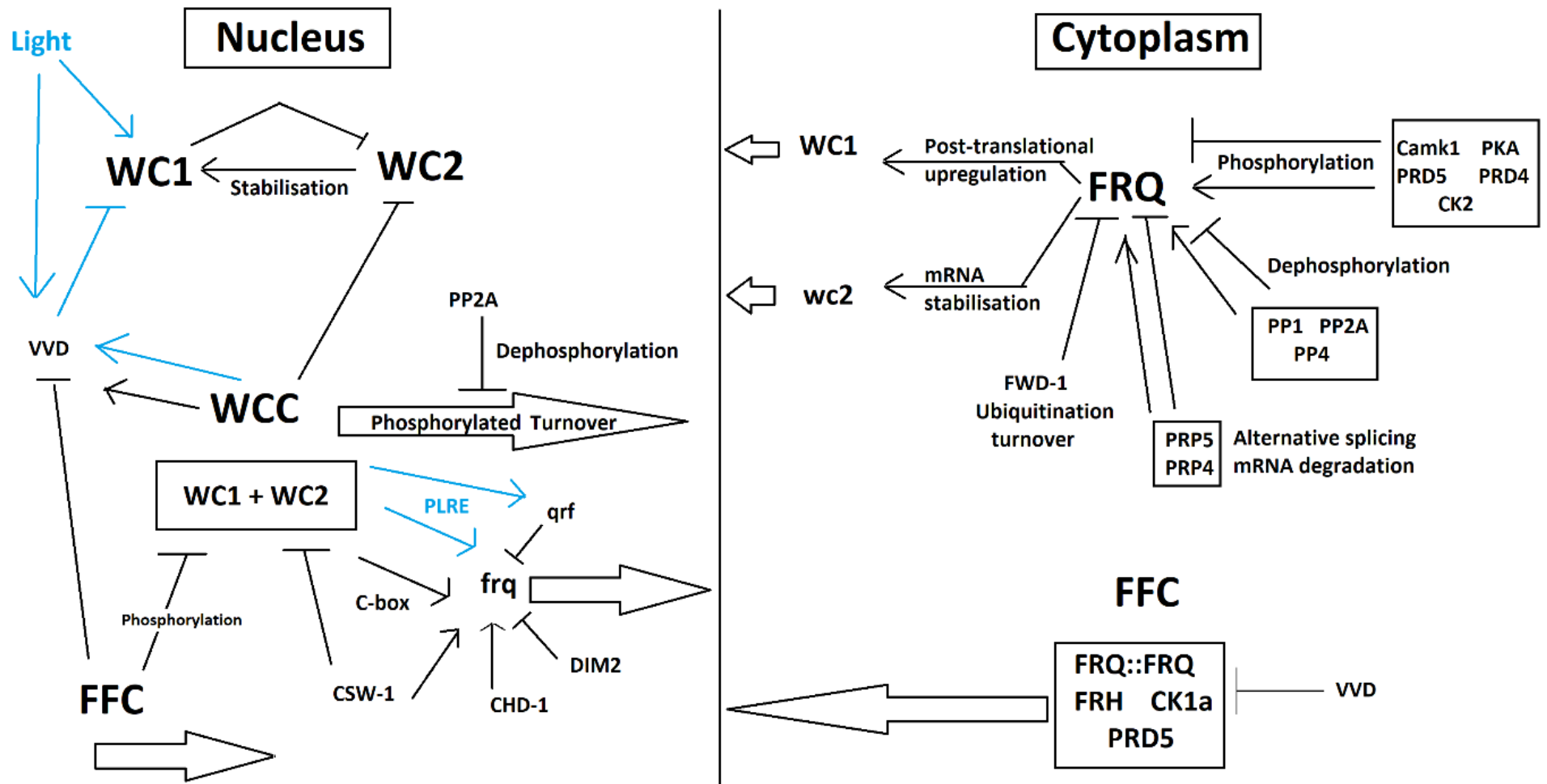


Figure 6.2: A simplified FRQ-centric map and model of the *N. crassa* circadian clock. Large open arrows denote transport, lines with bars show repression, lines with arrowheads denote activation, and blue coloured lines are light-dependent.

6.1.3 Non-core clock control of FRQ

6.1.3.1 Antisense frq: qrf

WCC-mediated frq transcription and translation is not only affected by nuclear FFC presence, but also by several accessory proteins and transcripts that act to fine tune its activity depending on environmental conditions and time of day (82,161,178,181,184,185,192,193,195,197,201,208–210,214,221,229,235,259,370,409,457,479,517,528,540,548). Firstly, the aptly named qrf is a long, non-coding transcript that runs the entire length of the main FRQ open reading frame, but in the reverse direction (526,528). After light exposure, the WCC binds to a promoter downstream of the FRQ coding region on the antisense strand (the qrf promoter), where qrf serves to dampen frq levels (178,181). Since light induced WCC causes an acute activation of both frq and qrf, it is thought that the inhibitory effect of qrf may lead to FRQ being produced in a pulsatile manner, rather than causing a chronic long-term upregulation of FRQ (181). This hypothesis is reminiscent of that proposed for the regulation of VVD, where VVD acts to sequester light-activated WCC (which would otherwise cause PLRE-dependent FRQ upregulation, see 6.1.3.2), creating a short-term burst of FRQ production for the light resetting and phase shift of the circadian clock, so, perhaps the two act in tandem (207,209,409,517,540). Additionally, Kramer and colleagues reported that after transition from dark to light, the phase of the qrf mutant *N. crassa* clock was set to an earlier subjective timepoint than the wild type, suggesting that qrf does act to sequester available frq transcript (526). As well as being rhythmically expressed via WCC activation, qrf has also been observed to be transcribed constantly (perhaps independently of the WCC) and in antiphase to frq, but at a low level, where it

serves to reduce background frq transcript levels, allowing for a more robust rhythm (526,528).

Elimination of qrf transcript causes rhythmicity to be lost at low temperatures in *N. crassa* and a slight period increase over a wide range of temperatures, perhaps as a result of increased levels of available frq transcript and thus FRQ protein (178,526). Interestingly, (as covered in 6.1.3.5), S-FRQ is predominantly produced (due to alternative splicing) at low temperatures, giving rise to a longer period, whereas L-FRQ is preferentially synthesised at higher temperatures and, concurrently, facilitates a shorter period (203,530). Together, this suggests that the qrf transcript can inhibit both L-FRQ and S-FRQ synthesis (203,226,378,518,549).

6.1.3.2 VIVID

VIVID (VVD) is a blue light photoreceptor (82,101,198,207,209,232,434,513,517), and is predominantly responsible for photoadaptation, where it negatively regulates WCC-based light activation of frq, amongst other light-induced genes (116,178,181,198,201,207,209,210,214,225,409,513,517,540,548). This repression of activity is facilitated by competitive binding between the WCC and VVD, forming a VVD-WCC multi-protein complex instead of the frq-activating WCC (178,207,214). Whilst this VVD-WCC complex acts to repress the light activation, VVD also stabilises the WCC, preventing its degradation and increasing its half-life compared to the volatile light-activated WCC (207,214). VVD, therefore, has both positive and negative functions on the WCC and subsequent regulation of FRQ.

The VVD-WCC complex is also transient and can dissociate over time (potentially as a result of photoadduct formation and subsequent degradation, or phosphorylation status)

(207), and thus facilitates a pool of both WCC and VVD during the day (207,214). Since VVD abundance correlates with light intensity and length of exposure, the VVD-dependent dampening of WCC activity can be applied to a wide range of fluence rates, preventing repeated light resetting of the clock while allowing for light reactivation (181,184,214). This facilitates a gated response to increased light intensity perception and subsequent light-intensity dependent responses over the course of the day, such as those caused by cloud cover or sunspots (181,184,214). Indeed, despite the fact that *frq* mRNA levels quickly decrease after its initial light induction, the *frq* transcript levels do not return to dark levels until the light source is removed, suggesting the presence of photoactivatable WCC whilst VVD is active during the daylight hours (409).

As VVD accumulates during the day due to light-dependent upregulation, it remains for several hours during the dark period and can function both as a molecular memory of the previous day and as a means to ignore the low, but detectable, light levels caused by moonlight (178,207,214). When VVD is non-functional, the WCC is sufficiently activated by moonlight (which has a ~1000x lower intensity than daylight), causing mistiming of *frq* upregulation, and thus *N. crassa* is unable to entrain to LD cycles when low intensity light is present (214). Further, in a VVD knockout strain generated by Schneider and colleagues, rhythmic conidiation occurs under constant light, unlike the wild type, implicating a role for VVD in both photoadaptation (and the perception of darkness) and the circadian input/output pathways, likely through its interaction with the WCC (513).

VVD in the dark has been shown to have a half-life of ~2.5 h (214), so if submitted to a 12/12 LD photoperiod, there would be approximately 0.4% of VVD remaining after the dark period, allowing for a large effect of light at dawn. Gin and colleagues (207) modelled

the interaction between VVD and light resetting during the dark period, where they compared the moonlight-insensitive wild type and moonlight-sensitive vvd mutant; they determined that a phase resetting response to moonlight (mediated by the WCC) would not occur until at least 6 h into the dark period, or almost 2.5 half-lives, where ~19% of VVD would remain. Further, dark WCC is significantly more stable than its light activated counterpart, so during the night, as the WCC continues to be expressed (and VVD-WCC disassociates), the WCC can accumulate in order to complete its dark c-box dependent upregulation of frq whilst also providing WCC amenable to light-dependent frq PLRE phase resetting of the clock (178,184,191,199,202,207,208,234,476). It is important to note that VVD is not a requirement for circadian function, as vvd mutants retain rhythmic conidiation amongst other molecular rhythms in the dark and light (207,475,513).

Intriguingly, as well as interacting with the WCC (and thus indirectly affecting frq transcription), VVD also interacts with FRH, the stabiliser of FRQ and member of the FFC (see 6.1), independently of both the WCC and FFC (209). Since VVD localises to both the nucleus and the cytoplasm, VVD may act to sequester components of both the positive arm (the WCC) and the negative arm via FRH (207,209). Altogether, VVD attenuates the acute light induction of FRQ, stabilises the WCC for subsequent re-activation and/or phase resetting after the dark period, and represses FFC-dependent WCC inactivation via its repression of FRH-FRQ interaction, therefore creating photoadaptation in both the positive and negative arms of the circadian system (178,181,184,207,209,214,409,475).

VVD's function lies beyond photoadaptation, sequestration of light-activated WCC, and inhibition of FRH, though, as it has been suggested that under dark conditions, accumulated VVD can undergo conformational changes depending on the intracellular

redox state (184). In the Superoxide Dismutase-1 (SOD-1) mutant, which displays higher ROS levels during the dark period, and NADPH oxidase (NOX-1) mutant, with lower dark ROS levels, *frq* showed increased and decreased light-induced expression, respectively (184), and so VVD may be partly responsible for ROS- and light induction of *frq*. Interestingly, high ROS levels often correlate with light intensity (or prolonged exposure) due to light stress, so VVD may act to interpolate both light and ROS signals and feed them into the clock (106,109,116,182,184,384,479). ROS levels are also known to oscillate in a circadian manner, so VVD may also aid in fine-tuning the light response depending on the circadian time of day (184). Indeed, the *sod-1* mutant was hypersensitive to light entrainment and had a shorter rhythmic conidiation period than the wild type (413).

Finally, Yoshida and colleagues (479) reported that a *sod-1:vvd* double mutant displayed an additive effect on light-inducible carotenoid generation in *N. crassa*, and suggested that ROS status (and thus VVD-mediated inhibition) affects the light signal transduction pathway through the white collar proteins. It is well documented that the intracellular chemical environment is both influenced by, and influences the clock itself, with ROS status being one of the most important factors in this process, suggesting that the clock is set by more than just light, temperature, and the canonical core clock machinery (84,103,116,119,149,160,182,184,192,242,413,430,479,550).

6.1.3.3 Methylation and chromatin remodelling

Clockswitch (CSW-1) reduces WCC-mediated *frq* transcription by altering the chromatin structure at the C-box promoter region, preventing WCC DNA binding (178,550). When CSW-1 is non-functional, a 4 h delay of peak *frq* expression is observed: *frq* transcript and

protein levels are also arrhythmic and found at significantly higher levels than the wild type, suggesting that CSW-1 is responsible for closing the positive arm of the circadian clock by reducing the effectivity of an activator (the WCC) and rate of *frq* transcription (550).

Chromodomain helicase DNA binding 1 (CHD-1) is also responsible for time of day-dependent chromatin remodelling, instead providing WCC access to the C-box and PLRE for subsequent expression in a rhythmic and light-responsive manner, respectively (406). *chd-1* knockout mutants show increased methylated regions in several light- and/or clock-regulated genes, including *frq*, and so CHD-1, in part, regulates the degree of DNA methylation throughout the circadian day (406). This altered *frq* and, therefore, *qrf* methylation is catalysed by the DNA methyltransferase DIM-2 (defective in methylation 2) (406). An *N. crassa* mutant with a lack of DIM-2 gave rise to a phase advance, where early onset of conidiation occurred, suggesting that CHD-1 and DIM-2 control the availability of *frq* to the WCC (406).

Chromatin modification and subsequent WCC-independent *frq* transcription is also partly controlled by SET-2, a histone H3K36 methyltransferase protein that interacts with phosphorylated RNA polymerase, playing a direct role in transcription (512,551). Loss of SET-2 function has been shown to allow *frq* to be transcribed in a WCC-dependent and independent manner (via elevated histone acetylation), suggesting that SET-2 inhibits this pathway (512). SET-2 was observed to be trafficked to the *frq* locus in a circadian manner, where it serves to methylate and subsequently reduce transcription factor access (512). Altogether, CSW-1, CHD-1, DIM-2, and SET-2 alter the structure and methylation status of the *frq* locus depending on the time of day to allow or prevent WCC access for rhythmic

and light-dependent transcription of *frq*. In a wider context, Fustin and colleagues have shown that methylation and circadian rhythms are closely linked in a wide range of eukaryotes, and this coupling between rhythmicity and methylation is believed to have been conserved for at least 2.5 billion years (446).

6.1.3.4 SWitch/Sucrose NonFermentable

In antagonism to CSW-1, the SW1-SNF (SWitch/Sucrose NonFermentable) complex interacts with the WCC and facilitates DNA bending near the *frq* gene, bringing the distal clock box (found ~1 kb upstream from the *frq* transcriptional start site) where circadian-acting WCC is bound, towards the beginning of the *frq* gene for rhythmic expression of *frq* in the dark period (224). SW1-SNF is not required for light-induced *frq* expression, suggesting that it only functions in the circadian/dark regulation (224). In this way, it is likely that the SW1-SNF complex is only able to interact with the smaller WCC (see 5.1.2), as one form of the WCC (consisting of a single WC2 bound to several WC1 units) interacts with the PLRE FRQ promoter, and another (consisting of a single WC1-WC2 heterodimer) interacts with the C-box of FRQ (178,184,191,199,202,208,234,476). Perhaps, then, the smaller WCC, with fewer WC2-bound WC1 subunits, allows for a conformational shape amenable to SW1-SNF interaction. When either component of the SW1-SNF complex was knocked out by Wang and colleagues (224), rhythmic conidiation was abolished, suggesting its essentiality for WCC clock activity. FRQ levels were measured early in the subjective circadian day (when FRQ levels are supposed to be at a maximum) and 12 h later, when inactive hyperphosphorylated FRQ is being degraded late in the subjective day; *frq* mRNA and protein levels were found to be significantly lower in the SW1 and SNF mutants compared to the wild type at both time points, as was WC1, which is ordinarily post-transcriptionally upregulated and stabilised by FRQ (224).

6.1.3.5 frq is alternatively spliced

As mentioned previously, there have been several observations of different isoforms of FRQ, that importantly give rise to long/large-FRQ and short/small -FRQ (L-FRQ, and S-FRQ, respectively) (203,226,378,518,549). Diernfellner (203) showed that these two isoforms are produced in different ratios because of the alternative splicing of an intron containing the L-FRQ start codon, which predominantly depends on temperature and displays circadian rhythmicity. The removal of this intronic region therefore causes S-FRQ to be produced instead of the full-length L-FRQ.

The ratio of L- to S-FRQ is altered by temperature and facilitates rhythmicity under physiologically relevant ranges; L:S-FRQ increases with temperature due to thermosensitive splicing of frq RNA, where (relatively) even levels of L- to S-FRQ levels are seen at 15 C, and much higher levels of L-FRQ are seen at temperatures of 25 C and above (178,203,549). However, in mutants expressing either L-FRQ or S-FRQ in isolation, both L- and S-FRQ levels were observed to increase with temperature, suggesting that higher temperatures promote FRQ expression regardless of isoform, but that L-FRQ is more readily produced under higher temperatures (203,549). Additionally, when only S-FRQ is present, a longer period is observed and rhythmicity is dampened under higher temperatures, whereas L-FRQ only gives rise to a shortened period but maintained rhythmicity under high temperatures (203,530). concurrently, it has been suggested that FRQ may also act independently of the clock as a temperature sensor mechanism due to the (L- and S-) FRQ-temperature correlation and splicing (217,549).

PRP5 (Pre-mRNA-processing ATP-dependent RNA helicase), RRP44 (RNase R, also known as Dis-3, a catalytic subunit of the exosome), PRMT5 (protein arginine methyl transferase

5), and U4-2 (U4 tri-snRNP associated protein 2, which is a subunit of the U4/U6/U5 tri-small nuclear ribonucleoprotein) all play a role in the alternative splicing of *frq* transcripts at the spliceosome/exosome complexes (226,378,513,552–555). PRP5 knockdown caused a reduced growth rate, aerial hyphae and conidiation reduction, and a dampening of molecular and conidiation rhythmicity, but rhythmic expression of *frq* in constant darkness was still observed, albeit with a period ~2 h shorter than the wild type suggesting a lack of S-FRQ (378). Further, *frq* and *wc2* transcript and protein levels were lower, and *wc1* transcript (but not protein) levels were higher than the wild type in the PRP5 mutant, cementing the role of FRQ role in positive and negative arm regulation, where it acts to stabilise *wc2* transcript, post-translationally upregulate WC1 and inactivate the WCC (161,178,193,195,221,235,236,378,527). Additionally, WC2 knockout mutants display increased abundance of PRP5, and *prp5* transcript rhythmicity is abolished in strains with non-functional FRQ, suggesting that PRP5 both influences, and is influenced by, the circadian clock (378,485,556). Supporting this, the PRP5 promoter region contains a putative C-box motif, PRP5 protein and mRNA levels oscillate, and cytosolic localisation is rhythmic (378).

Knockdown of RRP44 causes increased levels of S-FRQ and a subsequent increase in period length, suggesting that RRP44 negatively regulates the S-FRQ splicing machinery (226). This increased production of S-FRQ in the RRP44 knockdown mutant may be due to increased U4-2 activity, as the RRP44 knockdown has increased *u4-2* transcript levels, and in the U4-2 knockdown strain, L-FRQ is predominantly produced (226). RRP44 and U4-2 may therefore act antagonistically, increasing and decreasing the splicing of FRQ, respectively (226,378). PRMT5 knockdown strains also showed decreased levels of L-FRQ (which should give rise to a longer period, since S-FRQ will be ratiometrically higher), and

since RRP44 knockdown strains (which predominantly produces S-FRQ) caused increased levels of *prmt5* transcript levels, this suggests that RRP44 and PRMT5 act in tandem to increase the relative abundance of L-FRQ (or decrease the degree of FRQ alternative splicing), thereby shortening the period (161,210,226,378).

N. crassa cultures grown under constant light as opposed to darkness displayed reduced amounts of alternative splicing and thus predominantly produced L-FRQ, shortening the intrinsic period (203). The preference for L-FRQ production under constant light might be due an increase in FRQ transcription rate because of PLRE activation and the proportionally lower availability of splicing machinery (181,228,549,557). Supportingly, Vitalini and colleagues (439) show that the transcripts of ribosomal proteins are rhythmic and have a night-time peak (when FRQ production is low), and therefore ribosomal proteins may be a limiting factor for FRQ translation during the day. This may serve to further increase the L:S-FRQ ratio, as L-FRQ would be preferentially produced due to competitive use of translation machinery (192).

It has been suggested that the additional phosphorylation sites present on the 100 AAs of the N terminal on L-FRQ may facilitate the shorter period observed with higher concentrations of L-FRQ, even when S-FRQ is present (161,203). Phosphorylation adds negative charge to peptide sequences and these additional sites could serve to unfold the FRQ protein faster or produce weaker binding, since the N terminal is positively charged and attracted to the central negatively charged region (178,236,558). This premature unfolding and/or weaker folding interaction could cause the circadian machinery to cycle faster if the central NLS is inaccessible earlier or if there is reduced FRQ-CK1 interaction, which is known to depend on FRQ phosphorylation status and

charge (178,221,234,236). Concurrently, it has been shown that the FRQ isoforms have differential nucleocytoplasmic shuttling, with L-FRQ accumulating preferentially in the nucleus, suggesting that the premature and/or excessive phosphorylation of L-FRQ does not affect its nucleocytoplasmic localisation (378). Further (as discussed in 6.1.2), FRQ phosphorylation status has little effect on the localisation of FRQ, but does affect its activity, where increased phosphorylation of FRQ in the FFC reduces its nuclear and cytoplasmic circadian function (195). In this regard, it is likely that in L-FRQ, rather than the phosphorylation altering FRQ localisation, the sites instead facilitate a quicker inactivation of FRQ and subsequent repression of the WCC, removal from the circadian system, and eventual turnover in the cytoplasm (178,181,193,195,203,259,378).

It is possible that the high temperature-favoured L-FRQ is, in part, due to enzyme kinetics; higher temperatures can increase reaction rates for many enzymes (within their temperature tolerance), which could lead to an increase in transcription and translation, and a subsequent reduction in alternative splicing, since less time is spent producing each FRQ protein (559–561). Whilst few published studies on this phenomenon are available, *Arabidopsis* provides some interesting examples, as the plant showed that temperature-responsive transcript levels correlated with temperature increases due to elevated transcription rates relative to decay, and Sidaway-Lee and colleagues (561) report that *Arabidopsis* protein translation rates correlate with temperature increases (560,561). In support of temperature rates affecting transcription and translation in fungi, Colot and colleagues (549) also showed that L- and S-FRQ selection in *N. crassa* (which is temperature dependent) may rely on transcripts available for more efficient translation, i.e. the unspliced L-FRQ.

In *S. cerevisiae*, increased temperatures can lead to the inclusion and subsequent translation of the supposed 5' untranslated region of an open reading frame via the utilisation of upstream ORF frames (uORFs) and potential 'near cognate' start codons (those that differ from a start AUG codon by one base, such as UUG, ACG, or AUU) (559). These uORFs, especially those with the traditional AUG start codon, have an increased translational efficiency at higher temperatures, and perhaps a similar mechanism exists in the regulation of FRQ (559). Kulkarni and colleagues later suggest that the utilisation of such uORFs can alter the expression of the downstream 'main ORF' (mORF) through a range of processes, including nonsense mediated decay. In this way, FRQ may utilise a similar mechanism, where the uORF coding for L-FRQ is included preferentially under higher temperatures, as mentioned above, and that the increased amounts of this upstream open reading frame facilitates increased qrf-dependent nonsense-mediated decay and maintenance of rhythmicity (see 6.1.3.1) (559).

In support of temperature and light-dependent increased FRQ production rates correlating with a decreased period, a codon optimised FRQ mutant was produced by (527), in which FRQ production can occur more rapidly because of *N. crassa* codon bias. This strain showed increased levels of FRQ, but it also gave rise to altered FRQ protein conformation, phosphorylation status, protein stability, and, notably, arrhythmia. The wild type, non-optimal codon usage of FRQ, and reduced efficiency in translation is actually essential for circadian function, perhaps as a result of altered mRNA secondary structure, or the additional time allocated to wild type translation due to the reduced efficiency of non-optimal codons (527,562,563). In a follow-up study conducted by Zhou and colleagues (564), it was shown that transcriptional silencing occurs in some genes with non-optimal codon usage, such as FRQ, adding an additional layer of transcriptional

regulation. Indeed, Plotkin and Kudla, for example, posit an ‘efficiency and accuracy’ model, differentiating between the rate of polypeptide production vs a reduction in erroneous mistranslation as a result of codon adaptation (563,564). Fascinatingly, Le Nouën and colleagues (565) codon de-optimised two surface glycoproteins of the human respiratory syncytial virus and saw that the resulting proteins were more thermosensitive than the wild type, as is FRQ. Perhaps, then, codon ‘deoptimisation’ has a biological function (at both the transcriptional and translational level) in some circumstances, including circadian rhythmicity and temperature sensitivity (527,563–569).

From an ecological standpoint, increased temperatures are often associated with the longer day lengths (and shorter nights) during the summer months, so perhaps L-FRQ is produced to a relatively higher degree during this time of year to compensate for the overall increase in FRQ levels as a result of higher temperatures and light intensities or longer exposure: high levels of FRQ may usually cause the WCC activity to be dampened sooner, but if most of the FRQ produced during the warmer summer months is L-FRQ, then the additional phosphorylation sites on L-FRQ could facilitate a more transient WCC repression, acting (somewhat) as a buffer against the overall protein increase, and thus maintaining a circadian rhythm of ~24 h regardless of season, temperature, or light exposure (203). Altogether, higher temperatures reduce the removal of the FRQ region containing the sequence for L-FRQ, and this differential splicing both impacts, and is impacted by, an endogenous circadian rhythm that is altered by temperature and light to aid in the organism’s synchronicity with its environment (178,203,226,378).

Whilst the description of the clock presented here primarily focusses on *N. crassa*, several parallels and inferences can be drawn for the *M. oryzae* clock and circadian system, as

Blastp searches suggest the presence of core clock machinery (Tables 1.1 and 4.1), as well as all of the accessory machinery influencing the expression and activity of FRQ (Table 6.2).

Table 6.2: Homologues of non-core clock machinery that influences FRQ expression and activity are present in *M. oryzae*

<i>N. crassa</i> gene ID	<i>M. oryzae</i> gene ID	% Cover	% Identity	Relevant reference(s)
Clockswitch-1 (CSW-1)	Chromodomain helicase DNA binding protein 3 (MGG_09930)	78	54.72	(178,550)
Chromodomain helicase DNA binding 1 (CHD-1)	Chromodomain helicase DNA binding protein (MGG_04589)	95	68.85	(406)
DNA methyltransferase (DIM-2)	Modification methylase Ddel (MGG_00889)	73	45.71	(406)
Histone 36 H3K36 methyltransferase (SET-2)	Histone-lysine N-methyltransferase (MGG_01661)	79	53.61	(512,551)
SWI-2 (subunit of the SWItch/Sucrose NonFermentable complex)	SNF-2 family ATP-dependent chromatin-remodelling factor snf21 (MGG_06388)	94	69.65	(224,570,571)
SNF5 (subunit of the SWItch/Sucrose NonFermentable complex)	Transcription regulatory protein SNF5 (MGG_06315)	87	51.53	(224)
Pre-mRNA-processing ATP-dependent RNA helicase (PRP5)	Pre-mRNA processing ATP-dependent RNA helicase prp-5 (MGG_15532)	86	67.33	(226,378)
RNase R/Dis-3 (RRP44)	Mitotic control protein dis3 (MGG_00193)	99	80.93	(226)
Protein arginine methyltransferase 5 (PRMT5)	Protein arginine N-methyltransferase (MGG_03894)	98	62.64	(226)
U4 tri-snRNP associated protein 2 (U4-2)	U4/U6/U5 tri-snRNP-associated protein 2 (MGG_08169)	99	70.83	(226)
Calcium calmodulin dependent kinase 1 (CAMK-1)	CAMK/CAMK1 protein kinase (MGG_09912)	94	77.63	(538)
Casein kinase 2 subunit beta-2	Casein kinase 2 subunit beta-2 (MGG_05651)	79	85.46	(181,536,539)
cAMP dependent protein kinase A catalytic subunit (PKA)	AGC/PKA protein kinase (MGG_06368)	66	92.26	(181,536,539)
Serine/Threonine Checkpoint kinase 2 (PRD-4)	CAMK/RAD53 protein kinase (MGG_01596)	96	67.25	(161,181,534,572)
ATP-dependent RNA helicase DBP-2 (PRD-1)	ATP-dependent RNA helicase DBP2 (MGG_16901)	79	92.38	(185)

Serine/Threonine protein phosphatase 1 (PP1)	Serine/Threonine protein phosphatase PP1 (MGG_10195)	99.2	99.02	(161,178,534,573)
Serine/threonine Protein phosphatase 2a catalytic subunit (PP2A)	Serine/threonine protein phosphatase (MGG_01690)	100	94.06	(161,181,534,573)
Protein phosphatase 4 (PP4) (also known as calcineurin-like phosphoesterase)	Serine/Threonine protein phosphatase (MGG_01528)	100	76.07	(178,181,534,535)
UV-90 (NCU05950)	Uncharacterised protein (MGG_08335)	93	44.17	(213,574)

6.1.3.6 Multiple FRQs

F. oxysporum is believed to contain up to 10 FRQ-like proteins, which perhaps suggests either increased fitness or functional redundancy associated with FRQ (457). Surprisingly, little circadian research has been performed on *F. oxysporum*, but it has been reported that WC1 plays a role in aerial hyphae production, surface hydrophobicity, carotenogenesis, and UV sensitivity (reminiscent of *N. crassa*), and thus may have functional clock components (456). Ruiz-Roldan and colleagues also reported that WC1 was required for full virulence of *F. oxysporum* in mice, but was not necessary for tomato plant pathogenesis, suggesting that clock components (a) can (conditionally) play a role in pathogenicity, and (b) may have different roles depending on the host (as may be the case in *M. oryzae*, see Chapters 4 and 5 and (253)).

Recently, Tong and Colleagues (232) reported the presence of two FRQ genes in the entomopathogenic *B. bassiana* (amongst other circadian and circadian-related genes, such as WC1/2, VVD, and PHY). These FRQ genes are independent of the L- and S-FRQ regulation mentioned above; FRQ-1 is 964 AAs in length and FRQ-2 is 583 AAs long, and both have regions with high similarity to *N. crassa* FRQ (232). The expression of the two FRQ proteins actually run antiphase to one another, creating a near-steady state of cytoplasmic FRQ abundance and, perhaps, may be the reason why *B. bassiana* does not display rhythmic or diurnal conidiation (232). This report suggested that the constant expression of FRQ and subsequent constant conidiation may be evolutionarily advantageous to *B. bassiana* as a way to maximise conidiation. Further, the N-terminally located coiled-coil domain necessary for FRQ homodimerization and thought to be essential for nuclear localization (510) is absent in FRQ-2 in *B. bassiana*, so perhaps cytoplasmic FRQ plays the predominant role in rhythmic conidiation (232).

However, Tong and colleagues also observed that both FRQ-1 and FRQ-2 displayed time of day-dependent nuclear localization, so the coiled-coil domain-mediated FRQ dimerization may not be a necessary step in FFC interaction and subsequent nuclear trafficking as believed previously (510), or at least is not necessary in *B. bassiana*. Instead, FRH may be the determinant of FRQ localization in *B. bassiana*, as is the case in *N. crassa*, where FRQ by default localises to both the nucleus and the cytoplasm, but FRH serves to stabilise and traffic FRQ to the cytoplasm (see 6.1.2). Given the light-dependent antiphasic nuclear periodicity of FRQ-1 and FRQ-2 (and light-independent high levels of cytoplasmic FRQ-1/2), it is possible that FRQ-1 may show PLRE-dependent activation and FRQ-2 PLRE-dependent repression, or FRQ-1 may (directly or indirectly) inhibit FRQ-2 expression (232). As mentioned previously, cytoplasmic stability and abundance of FRQ does not necessarily ensure constant circadian action, since phosphorylation can render FRQ inactive in the circadian clock (178). However, the constant production of hypophosphorylated FRQ throughout the day as a result of antiphasic FRQ-1 and FRQ-2 expression would ensure an active pool of FRQ in *B. bassiana* for conidiation at all times under a range of photoperiods (232).

When either FRQ-1 or FRQ-2 was knocked out, conidiation began to occur much later than the wild type (increasing the latency period), and the conidial yield was greatly reduced, especially under prolonged darkness, but the vegetative growth rate showed little change (232). Together, both FRQ proteins seem to perform a similar function in *B. bassiana*, but their opposite rhythmic activity facilitates a constant phenotypic output and thus, despite an arrhythmic conidiation phenotype, the underlying molecular ticking of the clock still occurs (232). Finally, it has been reported that the Sordariomycete, *N.*

haematococca, has two FRQ genes (457), and these additional FRQs may have similar or alternative functions in circadian regulation, as reported in *B. bassiana* (232).

6.1.3.7 FRQ-less rhythms

Not all molecular and physiological rhythms are circadian or rely on the core FFC-WCC oscillatory (FWO) machinery, and comparatively few fungi actually possess FRQ (178,181,441,457). Oscillations such as these are called FRQ-less oscillators (FLOs) and can have periods ranging from less than one to over one hundred hours (178,181,257,575). Rhythms shorter than the circadian cycle, which can occur multiple times a day (such as the ~44 min cycling of septum formation in *S. pombe*), are termed ultradian, and those longer (such as sclerotial formation in *A. flavus*, with a period of ~33 h) are infradian rhythms (177,231,257,457,575). Whilst FLOs are not necessarily circadian, they can display circadian rhythmicity, and may even be under FFC-WCC circadian control and are thus 'slave' oscillators to the canonical core clock (178,181,183). When FWO function is arrested, these slave FLOs revert to their inherent rhythm, which can, in fact, be circadian-like (178,181). These FLOs are often more sensitive to temperatures than the canonical FWO, but can maintain rhythmicity regardless (175,189,213). An excellent example of a FLO slave oscillator in *N. crassa* is conidial banding, because under certain conditions (such as prolonged darkness, lipid-deficiency, or growth media supplemented with farnesol, geraniol, or menadione), mutants can still display rhythmic conidiation in the absence of functional FFC-WCC machinery, but the period can be drastically altered (178,184,191,210,485,509). In the *cog-1:frq*-null and *cog-1:WCC* null mutant backgrounds, for example, conidiation rhythms have been observed under constant light. Indeed, mutants such as these have been called 'conditionally rhythmic' (210).

ROS homeostasis is also influenced by both the FWO and FLO (184). Indeed, it has been suggested that oxidation-reduction cycles of peroxiredoxin proteins (an antioxidant enzyme family) could be treated as a 'universal marker' for circadian rhythmicity (444). Rhythmic oscillations of cellular ROS have been observed in *N. crassa* circadian clock mutant backgrounds (FRQ, WC1, and WC2), but the amplitude of the oscillation is much lower than the wild type (184). In this way, the FLO may act in support of the FWO and facilitate a basal oscillation that is amplified by the FFC-WCC machinery (184). As mentioned previously, the cellular ROS status can also influence the circadian machinery, creating a ROS feedback loop – Yoshida and colleagues (184) show exogenous application of H₂O₂ can mimic the effects of light, potentially causing an upregulation of FRQ, reminiscent of PLRE activation.

A subset of the FLOs is the WC-FLO, exemplified by the evening-peaking *ccg16* (clock-controlled gene 16) mRNA, which oscillates in a circadian manner (under constant light or darkness) in the absence of FRQ, but is dependent on functional WC1 and WC2, suggesting that FRQ is not essential for all circadian rhythms (175,188,457). Further, WC1 protein oscillates in a FLO-like manner, albeit with a significantly lower amplitude; WC1 protein levels are rhythmic in wild type strains under constant light, and in an FRQ-less strain under constant darkness (175). FRQ does, however, seem to control the alternative splicing of WC1, as an FRQ knockout strain predominantly produced a larger WC1 isoform (175). *ccg-16* does not control the WC-FLO rhythmicity, as WC1 protein levels displayed circadian rhythmicity in the *frq* null:*ccg-16* double mutant (175,178,181,184,409). When *ccg-16* is knocked out, the growth rate is decreased compared to the wild type, but circadian rhythmicity is maintained and periodicity is unaltered, cementing *ccg-16* as an output, rather than an input and output to the clock, like VVD (175,207,214).

The nuclear-localised PRD-1, on the other hand, is part of the non-WC-FLO machinery in *N. crassa* (185). PRD-1 mutation has been shown to lengthen the circadian period in a *frq* wild type, and when PRD-1 is disrupted in both *frq* and *wc-1* null strains, the FLO rhythm is abolished (185), implicating it as a core component of the FLO machinery that interacts with, and feeds into, the FWO. UV90, a member of the TOR (Target Of Rapamycin) nutrient-sensing pathway, has also been shown to be a member of the *N. crassa* FLO machinery that affects the FWO (213,574): mutations of UV90 in the 'FRQ-sufficient' background displayed a dampening of molecular circadian rhythmicity. Further, UV90 protein levels are not rhythmic (and thus may instead display rhythmic activity and/or phosphorylation status), but it is essential for nutrient sensing and growth (574). When UV90 is disrupted in a *frq*-null:*chol-1* background (which usually displays conidial rhythmicity on choline-deficient media), rhythmic conidiation was abolished under both choline-containing and choline-deficient media (213,574). Together, it seems that the WCC-FFC system chiefly controls and amplifies circadian rhythmicity in *N. crassa*, but the (WC-)FLO(s) act in tandem and support of the canonical FWO (210).

Cercospora kikuchii, a soybean blight pathogen, has been suggested to have a circadian FLO (194). It displays regions of melanised and hyaline hyphae, producing dark and light bands, respectively, when grown on petri dishes (194). Much like *N. crassa*, when transferred from cycling LD conditions to constant conditions, this banding pattern persists for several days under constant darkness (but not constant light) (194). Importantly, Bluhm and colleagues (194) were unable to identify an *frq* orthologue in *C. kikuchii*, despite several attempts and modifications of PCR cycling parameters and degenerate primers, and thus it was suggested that *C. kikuchii* circadian rhythmicity may be controlled by a FLO. At the time of publication (2010), the *C. kikuchii* genome was not

6.1.3.8 Which came first, FLOs or FWOs?

Much work has gone into disentangling the hierarchy of the rhythmicity in FWO and FLOs, where the FWO may drive the FLO and vice versa, or if they act in tandem or support of one another (178). It has been proposed that environmentally dependent diurnal oscillations in metabolic components and their subsequent interconnected feedback loops preceded circadian rhythmicity and facilitated the evolution of entrainment from synchronisation (453). Considering that the FRQ gene is not found in some fungal clades, it has been suggested that the FLO was present earlier in the fungal evolutionary lineage (441,457). Salichos and Rokas (457) report that FWD1 and FRH are the ancestral progenitors of the circadian clock and that, over evolutionary time, the White Collar Complex proteins were first gained (when the basidiomycetes diverged), followed by FRQ as the most recent addition in the Ascomycetes. Indeed, FRQ is not present in many early-branching fungi (Basidiomycetes, Schizosaccharomycetes, Eurotiomycetes, and Saccharomycetes), and the presence of FRQ in the Dothiodiomycetes, Leotiomyces, and Sordariomycetes (of which *N. crassa* and *M. oryzae* are members) suggests that the fully fledged FWO was gained shortly after the Eurotiomycetes diverged (457). Importantly, once present, FRQ seems to be well conserved (441,457).

Brody (441) reports that the 'modern' FRQ observed in fungi today evolved earlier than Salichos and Rokas' report, around the time of Basidiomycota divergence, as there is evidence of FRQ motifs in Basidiomycetes, Zoopagomycota, and Mucoromycotina. Further, Brody (441) suggests that the conservation of FRQ motifs across a diverse set of organisms (fungi, plants, animals etc.) indicates that the foundations of FRQ were present much earlier than originally thought. The Saccharomycetes also show a loss of White

Collar proteins, but high conservation of FRH, suggesting a fitness increase associated with FRH and FRQ (457). Indeed, as discussed earlier, it is unsurprising that the species with a FRQ homologue also show high conservation of FRH, given FRH's role in FRQ stability (195).

Interestingly, FWD1 is not as well conserved as FRH, despite being one of the earliest members of the circadian system, and was lost in the Microsporidia, but this may be because FWD1 is not essential for circadian function, only removal of hyperphosphorylated FRQ (see 6.1.1). Altogether, it seems that (functional) FLO machinery was present prior to the evolution of the FWO, but that the FWO provided significant benefits once present and thus is comparatively well conserved (101,178,190,212,228,233,434,438,441,457,459,549).

6.1.4 FRQ functions in plant-fungal pathogenesis

As mentioned previously, the importance of the circadian clock is becoming increasingly recognised in plant-fungal pathogenesis (see chapters 1, 4 and 5), where time of day, the rhythmic expression of genes, and the activity of their products can have a profound effect on both the pathogen and host organism (for particularly noteworthy articles, see (101–103,122,144,177,228,257,259,460,577)). Importantly, as of 2014, *N. crassa* has been shown to be a facultative phytopathogen towards Scots pine, allowing for numerous relevant parallels to be drawn between the model clock species and plant pathogenic fungi (484). Despite its dogmatic position in the circadian rhythmicity of *N. crassa* and fungal research in general, the specific role of FRQ in pathogenicity is considerably less studied (Table 6.1).

In *Botrytis cinerea*, for example, Hevia and colleagues (117) observed circadian rhythmicity in the BcFRQ protein (*B. cinerea* FRQ) using a luciferase reporter construct. Upon deletion of the *frq* gene, *B. cinerea* displays altered and nutrient-dependent conidiation phenotypes – under potato dextrose agar (PDA) culture, the *B. cinerea* Δ *frq* strain produced only sclerotia and microconidia (which cannot infect their host) under LD conditions, and thus (indirectly) displays reduced pathogenicity; whereas under complete media (CM) culture, macroconidia (which are capable of infection) production was restored (117). This is unsurprising, considering FRQ's reported role in nutritional sensation (213,574). Further, the Δ *frq* macroconidia generated presented wild type-like lesions and, surprisingly, increased infection severity in *Arabidopsis*, suggesting that FRQ is unessential for pathogenesis and may reduce pathogenicity depending on time of day (117). Hevia and colleagues (117) subsequently generated an FRQ overexpression strain, which did not favour night-time infections in contrast to the wild type, further implying that FRQ is responsible for the rhythmic gating of virulence in *B. cinerea*. Supportingly, the Δ *frq* strain did not show any significant difference between dawn and dusk infection severity (117). Concurrently, the FRQ overexpression strain showed a significant reduction of virulence, regardless of time of day, implicating FRQ in downregulating pathogenesis, at dawn especially (117). Indeed, based on the FRQ::LUC reporter strain, FRQ levels are low at dusk and high near dawn (117).

FRQ's role in *Verticillium dahliae*, however, paints a different picture, as *Vdfrq* shows no light regulation or circadian expression under both LD and DD conditions, potentially due to altered FRQ-FRH interaction, as *VdFRQ* amino acid sequences showed low sequence conservation at this site, which would consequently reduce FRQ stability and FFC formation (see 6.1.2) (434). After mutation and subsequent disruption of FRQ in *V.*

dahliae, growth rates are reduced, perhaps as a result of the altered regulation of metabolism, transport, and redox homeostasis, all of which are controlled in a circadian manner (and, by proxy, FRQ) in *N. crassa* (434). Further, the differences in growth rate between the Δ frq and wild type *V. dahliae* strains were nutritionally dependent, in a similar fashion to *B. cinerea*, where growth rates were reduced relative to the wild type under prune lactose yeast agar (PLYA) culture, but not minimal media (MM) or basal modified medium (BMM), again implicating FRQ in nutritional sensation, independently of clock function (213,434,574). Δ frq strains also retained conidial banding, again suggesting that this phenotype is a FLO, as observed in *N. crassa* (178,184,191,210,485,509).

FRQ in *V. dahliae* does, however, regulate photoreceptor, transcription factor, and secondary metabolite gene expression, and thus has a role in environmental sensation beyond nutritional status (434). Fascinatingly, the Δ frq mutants showed a significant downregulation of both *wc1* and *wc2* in both light and dark, relative to the wild type (434). This suggests that while VdFRQ may not show circadian rhythmicity, it may maintain its (cytoplasmic) function in WC1 post-translational upregulation and *wc2* transcript stabilisation, reminiscent of *N. crassa* FRQ (161,178,193,195,221,235,236,527). It would, therefore, be of interest to determine if the *V. dahliae* FRQ perhaps has reduced WCC repression activity, perhaps through its interaction with CK1 or FRH, as mentioned above. Altered interaction with CK1 is unlikely to be the case, however, as Cascant-Lopez and colleagues (434) show that VdFRQ has high homology to its *N. crassa* counterpart at the FRQ-CK1 interaction domains (FCD), with only a single amino acid difference at position 418. An alternative explanation arises from the observations presented by Cascant-Lopez (434), whereby the expression of *vvd*

after light exposure in the Δ frq strain is significantly higher than the wild type; as mentioned above (6.1.3.2), VVD sequesters photoactivated WCC, preventing its continuous PLRE-based upregulation of FRQ, while FRQ also represses the activity of VVD in the nucleus, so when FRQ is absent, VVD will be present to a higher degree (178,181,205,209,228,231,234). However, VVD does not repress the transcription of either member of the WCC, and instead stabilises the protein complex, increasing its half-life, and so does not sufficiently explain why WC1 and WC2 levels are low in the Δ frq strains (207,214). Cascant-Lopez and colleagues (434), then suppose that functional *V. dahliae* FRQ represses vvd transcription. Finally, (434) VdFRQ's role in pathogenesis toward Arabidopsis and strawberry plants was observed, showing altered pathogenicity in a strain-dependent manner: Δ frq mutants from a moderately virulent background (Δ frq_12253) showed a significant reduction in virulence, but those from a highly virulent isolate (Δ frq_12008) did not, suggesting that frq can be important, but not essential, for pathogenesis.

For *M. oryzae* FRQ specifically, there have been a limited number of studies performed (101,258,259), all of which point towards a role of this circadian gene in the outcome of disease. Similarly to *N. crassa*, in a fwd1 knockout strain (which subsequently leads to increased levels of hyperphosphorylated FRQ, see above), *M. oryzae* did not display diurnal conidial banding under LD conditions (259), which again implicates either FWD1 as having a role beyond clearing hyperphosphorylated FRQ from the circadian system, or (cytoplasmic) hyperphosphorylated FRQ as having a role in conidiation and conidial banding, both of which are inextricably linked in the wild type circadian system (235,259,533). Further, both the wild type and FWD1 mutant displayed diurnal (LD) and circadian (DD) regulation of FRQ expression, showing (molecular) circadian rhythmicity in

M. oryzae and solidifying FWD1 as a non-essential circadian-related gene (259). Altogether, FWD1, while not essential for the circadian regulation of FRQ expression in *M. oryzae*, is needed for the degradation of FRQ as well as diurnal and circadian conidial banding, and suggests that phosphorylation status (and thus circadian function) of FRQ does not affect conidial banding: it is solely the abundance of cytoplasmic FRQ, regardless of phosphorylation status (235,259,533). The FWD1 mutant strain also displayed reduced *frq* transcript levels upon light induction, which perhaps suggests that an abundance of FRQ (independent of phosphorylation status) may repress PLRE-based induction of *frq* transcription by the WCC, and as such, may present a tertiary feedback loop in the circadian system (259). Indeed, the WCC has been implicated in light perception and circadian rhythmicity in *M. oryzae* (see 5.1.2, and (82,101)). Further phenotypic traits in the FWD1 mutant included reduced growth rates, conidiation, conidial germination, appressorial formation, and, importantly, virulence (259). It is difficult to disentangle whether the non-functional FWD1 or build-up of (hyperphosphorylated) FRQ, or indeed both, is responsible for the presented phenotypes from these results, however.

To address the roles of FWD1 and FRQ in these traits, Shi and colleagues (259) subsequently generated an FRQ knockout strain by deleting the latter half of the 'gene' (see 6.2.1.1 for this contentious topic). The FRQ mutant also displayed slowed growth, reduced conidiation, delayed conidial germination, decreased appressorial formation, and reduced virulence, essentially phenocopying the *fwd1* mutant. In this way, an abundance of (hyperphosphorylated) FRQ or a loss of FRQ function present the same outcome, and thus the phosphorylation status or excessive presence/absence of FRQ, may ultimately dictate the aforementioned traits in *M. oryzae* (259). Whilst this result seems somewhat counterintuitive, as mentioned above, FRQ functions both in the

positive and negative arm of the circadian system, where an overabundance or scarcity of clock components can present similar phenotypes (see table 6.1 and (117,183,184,191,192,200,213,221,225,258,259,408,434,437,439,485,502,509,529,578)). It should be noted that Shi and colleagues (259) grew their *M. oryzae* strains and rice seedlings under a 16/8 h LD photoperiod at 25 C but did not specify timing of inoculation or synchronisation of photoperiod, which may have affected infection severity.

Park and Lee (258) also reported an FRQ C-terminal deletion mutant, generated using their novel bidirectional genetics (BiG) platform (see also 6.2.1.1). This work predominantly focussed on vegetative growth, pigmentation, and asexual and sexual reproductive phenotypes of the prospective mutants, since the mutagenesis and screening strategy was the main focus, rather than circadian rhythmicity. However, their FRQ mutant strain presented conidiophore elongation defects, with smaller and more compact conidia as result (258). In contrast to Shi and colleagues, Park and Lee reported no significant effect of FRQ mutation on growth rate, conidial germination, or appressorium formation, and thus the C terminal is likely unessential for FRQ function in these traits in *M. oryzae* (258,259). Park and Lee also made no mention of conidial banding or circadian (dys)function in their FRQ mutant. Interestingly, Park and Lee also did not report on the FRQ mutant's pathogenicity (unlike the others reported in the same article). Finally, Kim and colleagues (101), whilst not directly mutating the *M. oryzae* FRQ, did show that *frq* transcription is light activated and dependent on the WCC (WC-1, specifically), further implicating a functional FRQ in the circadian clock of *M. oryzae*.

Based on experimental work (Chapters 4 and 5), bioinformatic analyses, and literature review (throughout), *M. oryzae* has been shown to have a functional circadian clock,

whose rhythmic and diurnal conidial banding is absolutely dependent on the White Collar Complex (WC-2, specifically). Further, since WC2 (see Chapter 5) and FRQ has been reported to play a role in pathogenesis and virulence-related traits (82,101,258,259), there is likely an ultimate role of circadian entrainment and FRQ in the growth, development, virulence, and fitness in *M. oryzae*. This chapter, therefore, describes FRQ in *M. oryzae* and determines its function under a range of light cycles in growth, conidiation and conidial development, and pathogenicity towards both host- and non-host plants.

6.2 Results

6.2.1 Finding the *M. oryzae* FRQ gene

6.2.1.1 MGG_17345 and MGG_17344 map to either end of the *N. crassa* FRQ gene

To identify an *M. oryzae* FRQ orthologue, a BlastP was initially carried out against the model fungal clock species, *N. crassa*. FRQ FASTA files from NCBI were uploaded and mapped against the *M. oryzae* genome. Accordingly, BlastP results showed two *M. oryzae* predicted proteins (MGG_17345 and MGG_17344) with homology to either end of the *N. crassa* FRQ; MGG_17345 was located at the N terminal and MGG_17344 the C terminal, suggesting a misannotation of the *M. oryzae* genome. In support of this, Park and Lee (2013) created a FRQ knockout by insertion of a HPH knockout construct conferring hygromycin resistance into the MGG_17344 (C-terminal) section of *M. oryzae* FRQ, however they do not mention the fact that FRQ maps well to the MGG_17345 'gene'. Further, Deng and colleagues (84) say that the *M. oryzae* frq gene ID is MGG_009036, which does not correspond to FRQ and instead codes for Alpha-L-arabinofuranosidase, however their primers used for RT-PCR (5'-

GCTATCGACCTCTCGGACACGGG-3' forward and 5'- ACGGAGCGTAGCCTCGAGCTCT-3' reverse) bind very close to the start of the MGG_17345 gene (N-terminal) and 147 bases downstream of MGG_17345, respectively (84). According to Deng (84), this transcript oscillated in a circadian manner, suggesting that while they successfully amplified part of FRQ, they misnamed it as MGG_009036 in their paper. Likewise, Kim and colleagues (101) used primers present upstream of, and on MGG_17345. Finally, Shi and colleagues (259) created an FRQ deletion construct, and their primer pairs used to generate the gene knockout vectors targeted the entirety of MGG_17344 to ~1kb downstream of MGG_17344 (MoFRQ DownF and DownR; 1085bp) and ~1kb downstream of MGG_17345 to the end of MGG_17344 (MoFRQ UpF and MoFRQ UpR; 1360bp), respectively). This deletion would remove approximately half of the full MGG_17345 – MGG_17344 genomic sequence and, if MGG_17345 codes for an FRQ-independent product, it may still be (semi-) functional, as MGG_17345 was not deleted by this construct. Together, it seems that the true *M. oryzae* FRQ gene contains MGG_17345, MGG_17344, and the section between the two.

6.2.1.2 Predicting the *M. oryzae* FRQ sequence

To further confirm MGG_17345 – MGG_17344 as the complete *M. oryzae* FRQ gene, the entire genomic DNA sequence between 17345 and 17344 was submitted to the NCBI ORFfinder, which generated potential open reading frames, one which spanned the entirety of 17345 (potentially coding for 123 amino acids, highlighted ORF1 on Fig. 6.4), and a second which mapped to the majority of the 'intergenic' region between 17345 and 17344, including the entirety of 17344 (potentially coding for 888 AAs, ORF4 on Fig. 6.4), and between these two open reading frames is a small potential intron of 52bp (Fig. 6.4 shows all potential ORFs between MGG_17345 and 17344). It is possible that the

translating ribosomes may bypass this gap between the two ORFs in a similar manner to that reported by Herr, where a fusion occurred between two ORFs (50 nt apart) of the bacteriophage T4 gene 60 (579), or stop codon readthrough may occur, where the ribosome miscodes at a stop codon (580). Alternatively, this sequence could be further misannotation. Regardless, when independently submitted to Pfam MotifFinder (a protein family database comparison tool) and InterPro, the putative amino acid sequences from both MGG_17345 and MGG_17344 ORFs showed FRQ protein family hits and circadian rhythm Gene Ontology (GO) terms (581,582). For MGG_17344 amino acid sequences, the long ORF was truncated to only include the sequence from MGG_17344 and FRQ motifs were still recognised. Interestingly, these two ORFs may correspond to L- and S-FRQ (see 6.1.3.5), as in *N. crassa*, there are two initiation sites separated by a small intron that result in a 989 amino acid (L-FRQ) and 898 amino acid (S-FRQ) polypeptides (178,518,531,549), so the two *M. oryzae* open reading frames (123 AA and 888AAs) together may correspond to the full length FRQ (1011 AAs).

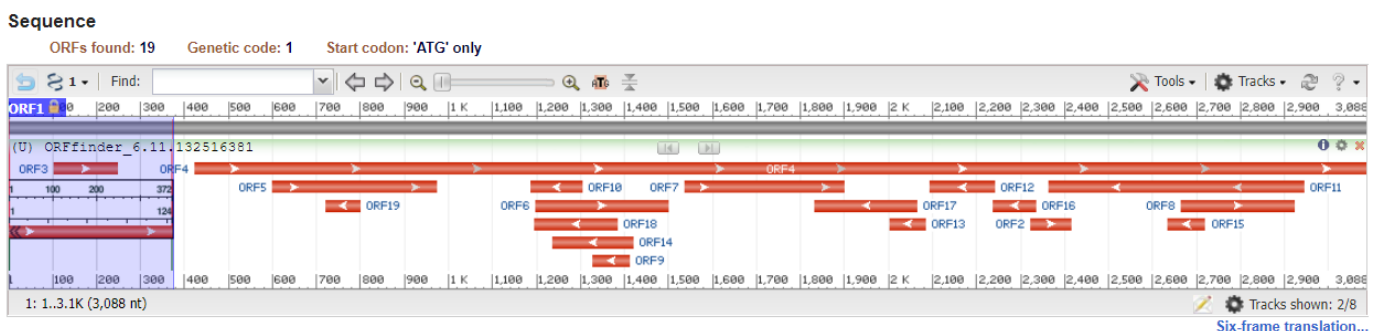


Figure 6.4: Predicted MGG_17345 – MGG_17344 open reading frames. An open reading frame prediction tool (ORF finder) showing potential ORFs in the proposed *M. oryzae* FRQ.

Assuming that these two ORFs were FRQ protein-coding, the putative amino acid sequences from them were submitted to a BlastP. BlastP results showed good homology to several known fungal FRQ protein sequences, including *N. crassa* (Table 6.3).

Interestingly, the potential protein sequence showed high homology to entomopathogenic, phytopathogenic, and plant-interacting species of the Sordariomycete class (of which *M. oryzae* and *N. crassa* are members) (table 6.3).

Table 6.3: MGG 17345-17344 ORF 1 + 4 predicted protein homology to sordariomycete FRQ

Species	% cover	% identity	Notes	Relevant reference(s)
<i>Neurospora crassa</i>	84	45.06	Model clock species, facultative plant pathogen	(484,531)
<i>Hirsutella minnesotensis</i>	98	42	Soil-borne, entomopathogenic to nematodes	(232,583,584)
<i>Diaporthe helianth</i>	86	45.47	Phytopathogenic; causes phomopsis stem canker of sunflower. Spread by wind and dew-drop	(585)
<i>Pochonia chlamydosporia</i>	98	41.42	Soil-borne and entomopathogenic to nematodes and endophytic to plant hosts	(586)
<i>Botrytis cinerea</i>	72	33.77	Phytopathogenic; grey mould of several fruit species	(117)
<i>Verticillium dahliae</i>	78	38.74	Phytopathogenic; causes verticillium wilt in several plant species	(434)
<i>Plectosphaerella cucumerina</i>	71	44.2	Phytopathogenic; causes potato wilt	(587)
<i>Annulohyphoxylon maeteangense</i>	70	42.5	Endophytic and saprotrophic to plant material	(588)
<i>Metarhizium robertsii</i>	63	45.84	Soil-borne and entomopathogenic to nematodes; endophytic to plant hosts	(589)
<i>Trichoderma parareesei</i>	73	45.18	Plant symbiont; used as a biocontrol agent against phytopathogenic fungi	(590)
<i>Daldinia bambusicola</i>	74	41.61	Endophytic; produces antimicrobial volatile organic compounds (VOCs)	(591)
<i>Beauveria bassiana</i>	74	41.2	Entomopathogenic; broad host range	(232)

6.2.1.3 The predicted *M. oryzae* FRQ sequence contains numerous phosphorylation sites

Next, under the assumption that this MGG_17345-17344 ORF1 + ORF4 contained the putative FRQ amino acid sequence, the sequence was submitted to several different prediction tools to determine (predicted) functional similarity to the well-described *N. crassa* FRQ. Firstly, FRQ is a protein that becomes increasingly phosphorylated throughout the circadian day, so requires several phosphorylation sites for kinase activity, including CK1, Protein kinase C, cAMP-dependent protein kinase A, and CKII (178,195,531). The MGG_17345-173544 putative amino acid sequence was submitted to YinOYang (Ver. 1.2; (592)), NetPhos (Ver. 3.1; (593)), and KinasePhos (Ver 3.0; (594)), all of which predicted high phosphorylation potential (Fig. 6.5). YinOYang locates potential O-(beta)-GlcNAc acceptors (a modification highly associated with phosphorylation) based on human genome training data; 115 potential sites were predicted, suggesting that the potential FRQ protein can become highly phosphorylated and post-translationally modified (Fig. 6.5). NetPhos 3.1 predicted 179 phospho-kinase sites (Fig. 6.5) and KinasePhos 3.0 (594) predicted 75 potential AGC_PKA kinase family sites, again suggesting high phosphorylation potential. *N. crassa* FRQ is known to contain at least 80 confirmed phosphorylation sites, and mutations in these sites can both increase and decrease period length depending on their location (181,193,195).

Lewis and colleagues (531) reported that *N. crassa* FRQ contains two phosphorylation sites for cAMP-dependent protein kinase A (RRXS) near the N-terminus, of which there is one (RRNS) present on the predicted *M. oryzae* sequence. Myhits Motifscan (595) also predicted many N-glycosylation, cAMP and cGMP-dependent protein kinase, Casein kinase II, protein kinase C, and Tyrosine kinase phosphorylation sites, agreeing with the

expected FRQ phosphorylation capability. Interestingly, Myhits Motifscan also identified FRQ protein family motifs, further suggesting that the predicted MGG_17345 – MGG_17344 ORF 1 + ORF 4 amino acid sequence contains FRQ (Fig. 6.5).

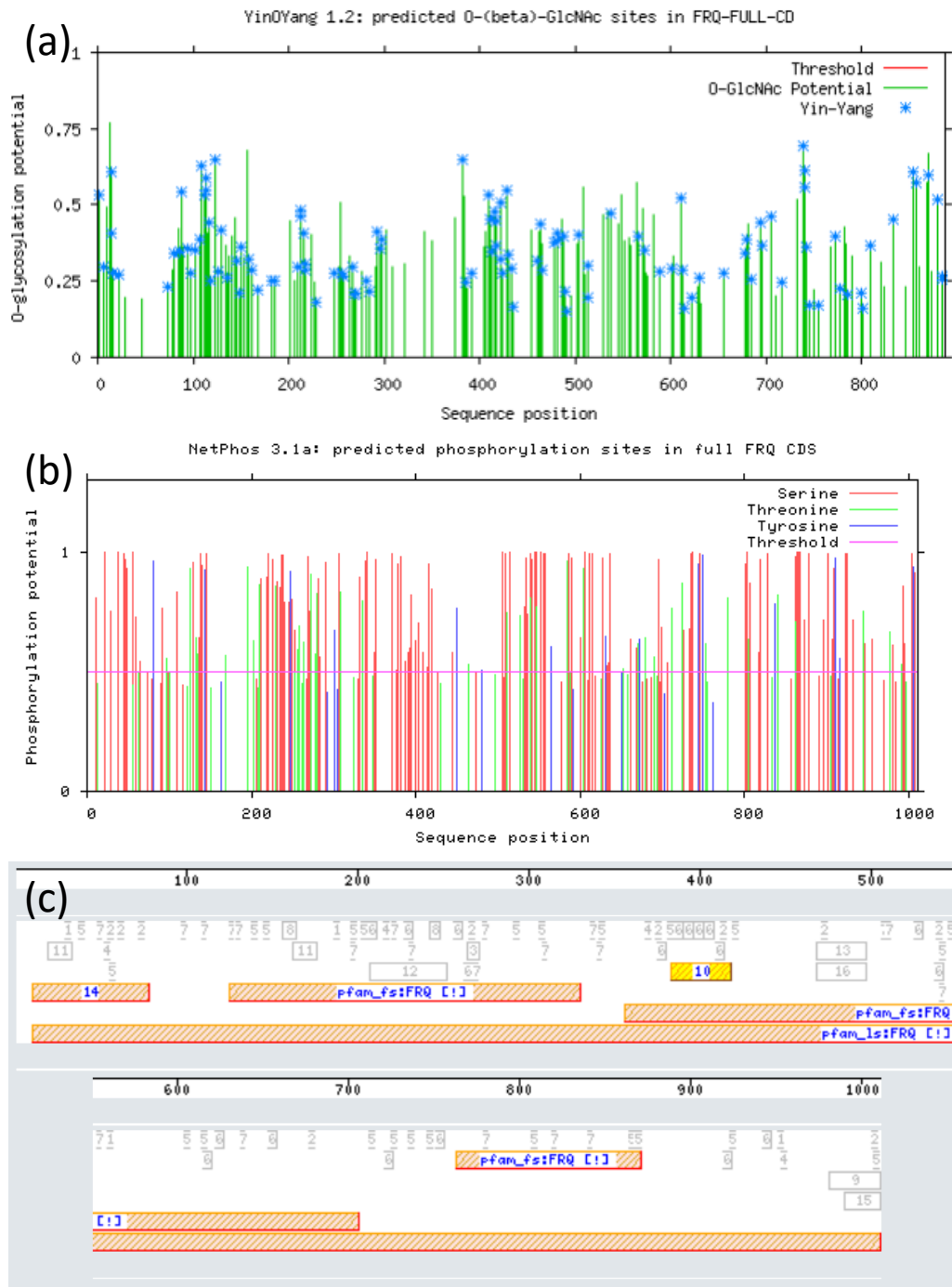


Figure 6.5: The predicted *M. oryzae* FRQ is likely to have a high capacity for phosphorylation. The MGG_17345 – MGG_17344 predicted amino acid sequence was submitted to phosphorylation site prediction webtools (a) YinOYang, (b) NetPhos 3, and (c) MyHits Motifscan.

6.2.1.4 *M. oryzae* FRQ contains PEST domains for ubiquitination

PEST domains are regions rich in proline (P), glutamic acid (E), serine (S) and threonine (T), commonly flanked by positively charged residues, and act as a signal motif for ubiquitin-mediated protein turnover (531,596). *N. crassa* FRQ contains PEST domains, which can become increasingly phosphorylated throughout the circadian day (178), and are required for phosphorylation- and ubiquitination-mediated turnover of FRQ. Lewis and colleagues (531) compared *Neurospora* and *Sordaria* FRQ proteins and discovered two highly conserved PEST regions. The *M. oryzae* potential FRQ AA sequence shows at least 2 PEST domains (based on EMBOSS ePESTfind (597) with a threshold score of ≥ 5). Two of the predicted *M. oryzae* PEST domains map to MGG_17344 in very close proximity to one another and so may actually be one continuous motif, and one is present in the region between MGG_17345 and 17344, close to the beginning of MGG_17344, suggesting that the C-terminal of *M. oryzae* is enriched for PEST sequences. This C-terminal enrichment of PEST and phosphorylation sites is common to FRQ described in the literature and is reported to have a role in FRQ protein stability (178,221). It is interesting that there are no high scoring predicted PEST domains present at the N-terminal of the potential amino acid sequence in *M. oryzae*, as it has been shown that *N. crassa* FRQ becomes increasingly phosphorylated at the N-terminus and PEST domains late in the day (178). There are, however, three predicted PEST motifs that have scores just below the threshold and are located towards the N terminus (amino acid positions 68-88, 131-144, and 242-270), and thus may have some function (Fig. 6.6).

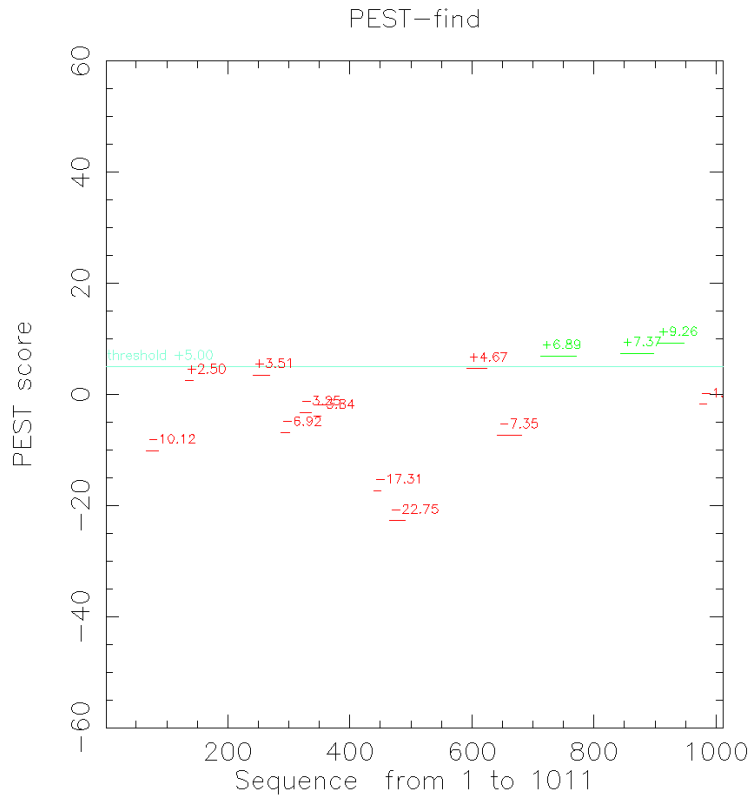


Figure 6.6: The *M. oryzae* predicted amino acid sequence shows a C-terminal enrichment of PEST domains. Based on EMBOSS ePESTfind, there are at least 2 potential PEST domains above the prediction threshold in the *M. oryzae* FRQ.

6.2.1.5 *M. oryzae* FRQ contains a coiled-coil domain for FRQ dimerization

Prior to entering the nucleus, *N. crassa* FRQ dimerises and interacts with FRH (which stabilises FRQ and prevents its degradation) and CK1 to form the FFC. FRQ-FRQ interaction is facilitated by a 30 AA coiled-coil domain located near the FRQ N-terminus (178,510). Incidentally, Cheng and colleagues reported that the coiled-coil domain is the most conserved region of FRQ across fungi, and that deletion of this structure can lead to arrhythmic conidiation (510). The potential *M. oryzae* FRQ amino acid sequence was submitted to Waggawagga (598) and DeepCoil (599), two coiled-coil prediction tools. Both tools predicted a high likelihood of a Coiled-coil domain present at approximately 150 AAs downstream of the MGG_17345 ORF1 start site (approximately 20 AAs into ORF4), close to the N-terminal (Fig. 6.7) and commensurate with the *N. crassa* FRQ. This result was also confirmed using MESSA (600), where a single coiled coil site was present at AA 140 – 168.

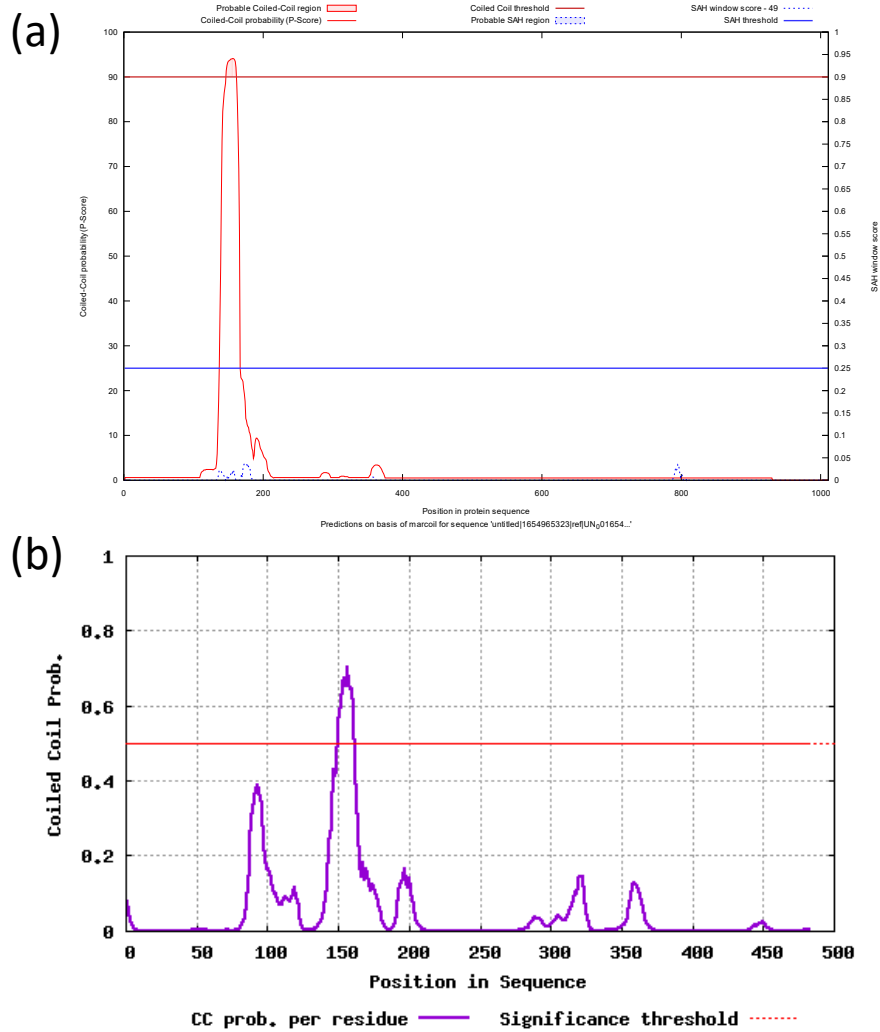


Figure 6.7: The *M. oryzae* predicted FRQ AA sequence contains an N-terminally located coiled-coil domain according to (a) Waggawagga and (b) DeepCoil.

6.2.1.6 *M. oryzae* FRQ contains motifs indicative of nuclear and cytoplasmic localisation

FRQ also requires nuclear localization signals (NLSs) to facilitate entry into the nucleus as part of the FFC (195,224,434,601). The predicted *M. oryzae* FRQ AA sequence was submitted to cNLS mapper, a nuclear localization signal prediction webtool (602). Since FRQ is present and active in both the nucleus and the cytoplasm depending on time of day, a low cut-off score was applied to the amino acid sequence; scores of 1-2 are predicted to be cytoplasm-localised, 3-5 nuclear and cytoplasmic-localised, 7-8 partially nuclear-localised, and ≥ 8 exclusively nuclear-localised. Unsurprisingly, the predicted *M. oryzae* amino acid sequence shows regions indicative of both nuclear and cytoplasmic localization, suggesting that the protein can move into and out of the nucleus (Fig. 6.8).

The nuclear localization signals with high cNLS scores seem to be isolated to the centre of the polypeptide sequence (Fig. 6.8). This is of particular interest, as phosphorylation (which occurs in 'clusters' throughout the circadian day) preferentially acts on the central region of *N. crassa* FRQ (178). Phosphorylation is known to have both an enhancing or inhibitory effect on nuclear activity (195,603), so rapid and preferential phosphorylation in the central region close to the FRQ NLS may either aid or abate FRQ's journey to the nucleus. Hypothetically, if phosphorylation of the FRQ NLS aided in its access to the nucleus, then it would be expected that hyperphosphorylated FRQ would be enriched in the nucleus compared to the cytoplasm, and since phosphorylation occurs over time, there would be a significant time delay between FRQ protein synthesis and FRQ nuclear shipment, as progressive phosphorylation occurs.

Alternatively, if phosphorylation reduced FRQ access to (or removed it from) the nucleus, hypophosphorylated FRQ would rapidly move into the nucleus early in the circadian day

to perform its function in the negative arm of the clock and repress its own transcription via the WCC. The remaining cytoplasmic FRQ would then be phosphorylated primarily at the central region containing the NLS, thus reducing the shipment of FRQ to the nucleus, allowing for the circadian cycle to begin anew. This is the more likely scenario of the two, as newly synthesised, hypophosphorylated FRQ is rapidly localised to the nucleus early in the circadian day, and low levels of hypophosphorylated FRQ are found in the nucleus, acting in the negative feedback loop of the clock (221). Further, upon deletion of a *N. crassa* FRQ NLS, Schafmeier and colleagues (221) showed increased levels of hyperphosphorylated cytoplasmic FRQ.

In additional support of FRQ phosphorylation of the central NLS preventing its entry into the nucleus, point mutations within the FRQ-CK1 interaction domain resulted in hypophosphorylation of FRQ throughout the circadian day, but did not cause a significant increase in nuclear-localised FRQ, suggesting that as phosphorylation of cytoplasmic FRQ continues throughout the day, it may become increasingly unable to enter the nucleus (195). Concurrently, this mutation suggested that entry of FRQ into the nucleus is not solely dependent on FRH or FRQ phosphorylation status, as nuclear abundance of FRQ did not increase, and so perhaps a different member of the FFC, such as FRH, is rate-limiting (195). It has also been shown that as FRQ becomes increasingly phosphorylated, it is less able to interact with WC2 and thus unable to interfere with WCC function and subsequently repress of FRQ transcription (195).

Phosphorylation state and structure of FRQ are also closely tied; in its hypophosphorylated state, FRQ is in a closed conformation and becomes increasingly opened upon phosphorylation due to a change in overall charge, where the

phosphorylated sites repel one another (178). As FRQ opens, a degradation signal is also exposed, leading to protein turnover (178). Together, FRQ structure, function and localisation are potentially linked to the phosphorylation status, and the proximity of NLSs to phosphorylation sites likely has an effect on FRQ localisation.

(a)

Predicted NLSs in query sequence	
MQRMPKAIIDLSDTGHPLRRSPPRQVASKGKKAHNASPGDRDDESGSSGR	50
LRRNSTDESNETGHSDPRQWFNQSNQNPSTYDMNNMEGKFSSLLIFLTSRT	100
RMADQALGSSRLAVLSKDVRIEMTNKPSLRPTVTQSSADEYRSVIDDL	150
TIENRLKEELRRYKQFGTDLMRKDKLFEIKVHGLPGKKKRELEATLRDF	200
ASTLEGSTDTSSGAKKPSKSGKFKSSGGATSKHASSSSNSRPVDSAYAS	250
MSTDPGTGTATGTGNSSGKSTGRATHSNSKSAHQKVESYLEDIPEGL	300
YPRYLSMTEKDKQKLVVRRLEQLFTGEMSGPSIGTTDRSSSKAEPMTGGS	350
FSKGKEAAREAQIQVKDKKRSRDNGSSNSQSNQDGGSGGSGSGHGGGS	400
GGSGGGSGGGNGSRSHGSSQDLQASEQRPTRLDLDPPRIQVPSENMEY	450
IRHLGMVPPALQAGTKANPINVSMADAGWVYMNLLCNLAQLHIINVPAF	500
IRAAVSSKSTKFLSPDGQKIRWRGGTDGTRFSSDSGNTSSRERSSTDED	550
DSSDKSGSPGKRRKYPDEPARAVHVKLVRENTSRSTSVHYKPMFVQQP	600
SFETSGEESSSPSGLEESNFGNRTSGWGYSGSGSPRKRRIIDGAIIV	650
YTGAPFCTDLSGDPGDISPATYMASANMTQSHDMPNSDATIHRTWSGSSL	700
PYRPFNNPKNTRIEAPNGVGLDDTSDDFMADVSSDSEDEMEWESDEEY	750
GTPTLLCLEAYLGGVQPEDHFLVEVITHRRRDRQDKNEDEPRPRFRER	800
SDSTTASVMERIKLLKASSPRPVRPVRQSLARTKMIYKTVRLNRLDPVE	850
LPPAASFVPPFSTSSSDSDIDESDLLESEEGQDAELCGPLSFIPPSIGRP	900
SLFRTESSLYPDSAYPEGQDLQSDDEEAESDDVGILQIGGTGNSKNK	950
PGKKSVMNRQQGLDMHLRSLVRRPQTDISNGPSKQPDPARTQSSVATAGR	1000
AESGYNSSLED	1011

Predicted monopartite NLS		
Pos.	Sequence	Score
26	VASKGKKAHNA	2
185	LPGKKKRELE	4
186	PGKKKRELE	2
557	GSPGKRRKYP	10
558	SPGKRRKYPD	3
559	PGKRRKYPDD	12
635	GSSPRKRRIID	17.5
637	SPRKRRIIDG	15

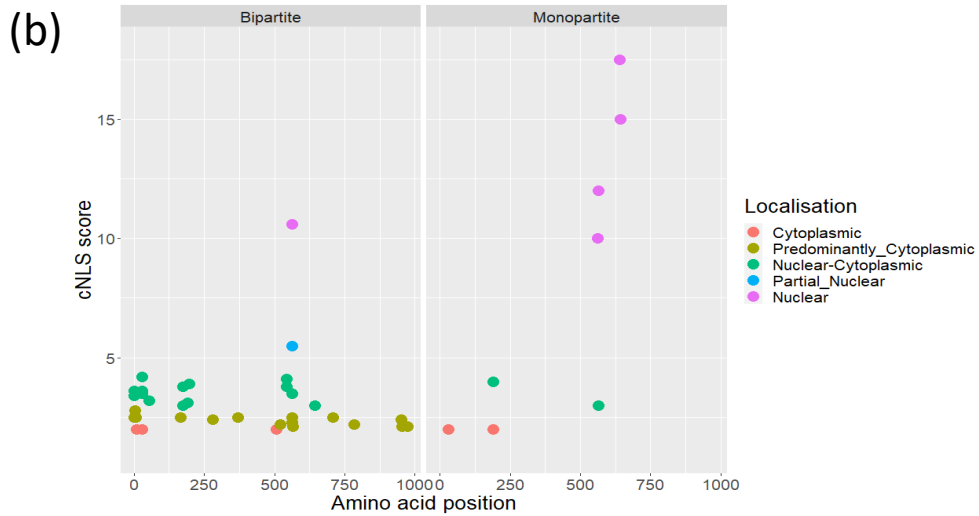


Figure 6.8: The predicted *M. oryzae* FRQ protein has motifs indicative of nuclear and cytoplasmic localisation. (a) cNLS mapper analysis of mono-/bipartite cellular localisation motifs, and (b) AA sequence position of the localisation motifs, showing an enrichment of nuclear localisation signals in the centre of *M. oryzae* FRQ.

6.2.1.7 The predicted *M. oryzae* FRQ shows intrinsically disordered motifs

N. crassa FRQ is known to be an intrinsically disordered protein (IDP), where it has no inherent, fixed structure (178,181,190). PredictProtein (604), PSIPRED (605), and MESSA (Meta Server for Sequence Analysis (600)) all show that the predicted *M. oryzae* FRQ amino acid sequence is highly disordered (Fig. 6.9), further implicating MGG_17345 and MGG_17344 as the FRQ gene.

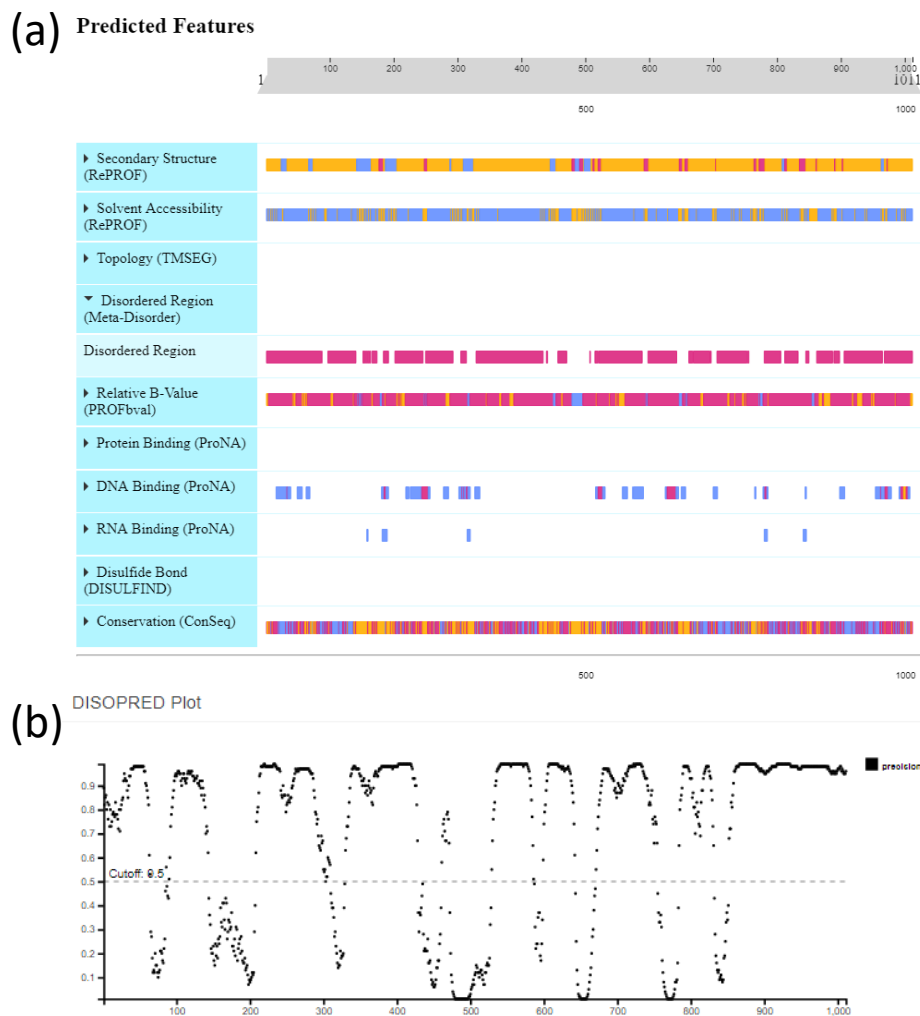


Figure 6.9: *M. oryzae* FRQ is likely a disordered protein. Output disorder prediction graphs for the *M. oryzae* FRQ from (a) PredictProtein, and (b) PsiPred

6.2.1.8 *M. oryzae* predicted FRQ shows conservation of the FRQ-FRH interaction domain

In *N. crassa*, the FRQ-FRH interaction domain (FFD) is located at residues 728 – 797 (195,200). Accordingly, the *N. crassa* FRQ and potential *M. oryzae* FRQ AA sequences were submitted to Emboss stretcher (a protein alignment webtool): the *N. crassa* sequence aligned to the *M. oryzae* FRQ sequence at AA sites 728 – 805 (albeit with some gaps), further suggesting that the predicted FRQ sequence acts in a similar manner to that observed in *N. crassa* (Fig. 6.10). The alignment further showed 43.3% identity, 56.3% similarity, and 33.6% gaps.

6.2.1.9 *M. oryzae* FRQ contains several (S/T)PXX sites, suggesting transcriptional regulation capability

SPXX and TPXX motifs are associated with transcription factors and DNA-binding, and the *N. crassa* FRQ contains six absolutely conserved (S/T)PXX sites (531,606,607). The predicted *M. oryzae* FRQ amino acid sequence contains 9 SPXX and 2 TPXX sites (11 (S/T)PXX total). Both of the TPXX sites are located in the region between MGG_17345 and 17344; 5 SPXX sites are in this same region, and 3 SPXX sites are located in MGG_17345, suggesting either an enrichment of these motifs in the N-terminal region of the polypeptide, or a deterioration of (S/T)PXX sites in the C-terminus MGG_17345.

Altogether, given the consistency of amino acid sequence, motifs, and predicted structure/function of the MGG_17345 – 17344 ORF1 + ORF4, it is likely that at least one of the isoforms of the *M. oryzae* FRQ protein consists of a transcript from MGG_17345 (123 AAs) followed by a peptide sequence that starts at the 3' end of MGG_17345 and runs up to and includes MGG_17344.

6.2.2 Generating an FRQ mutant in *M. oryzae*

In a similar manner to the WC2 mutant generation, sgRNA and donor oligos were designed to create a premature termination codon in the MGG_17345 gene (for full details see 2.10 – 2.17 and (269)). MGG_17345 was targeted in part due to its confirmed light and time of day-dependent transcription (84,101). Whilst the sequence between MGG_17345 and MGG_17344 is likely to contain a large open reading frame that could be prematurely interrupted (see above), this has not been confirmed experimentally, so edits in the region between MGG_17345 and MGG_17344 were avoided. The introduction of a premature termination codon (PTC) downstream in MGG_17344 (as

opposed to e.g., a large deletion) may allow for functional FRQ, as only the end of the protein would be truncated, so MGG_17345 was targeted. Further, in the more likely event that the double stranded DNA break was repaired by non-homologous end joining rather than homology-directed repair, indels could create a frameshift, which would have a more deleterious effect if they occurred closer to the transcriptional start site (TSS). MGG_17345 indels may also alter and potentially halt alternative splicing in *M. oryzae* FRQ, therefore increasing the likelihood of *M. oryzae* producing either L- or S-FRQ (if present, see above).

Potential MGG_17345 target sequences were determined using E-CRISP, and a sequence approximately halfway through was selected for DNA cleavage and editing (Fig. 6.11, 'MGG_17345_12_0'). A codon ~23 bp upstream of the putative Cas9 cut site was selected that required a single base edit to create a premature termination codon (GAG, Glutamic acid, to TAG, STOP). Compatible primers were selected using Primer3web centred around the edit site and donor sequence. 80 bp double-stranded donor sequences (with the edited codon highlighted) and diagnostic primers are shown in Table 6.4.

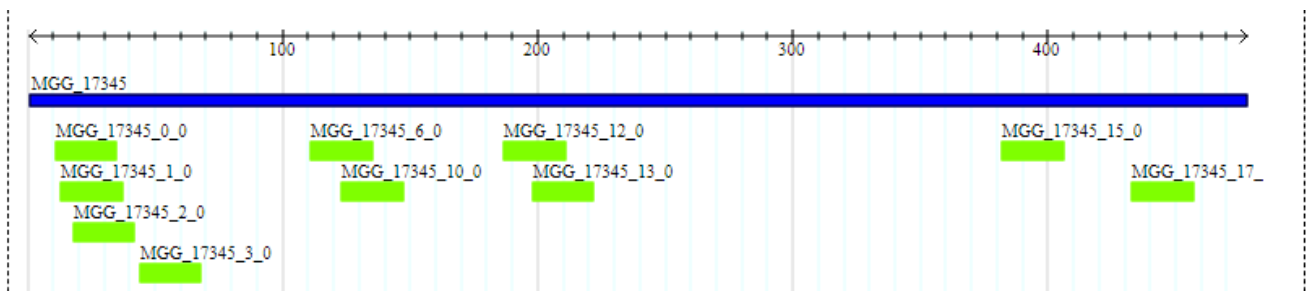


Figure 6.11: Potential MGG_17345 Cas9 target sequences. E-Crisp predicted Cas9 target sites on the *M. oryzae* FRQ (MGG_17345).

Table 6.4: Δ FRQ donor DNA and diagnostic primers

Δ FRQ donor template top strand (5'-3')	GAATTCGACGGACGAGAGCAACT <u>TAG</u> ACCGGTCACAGCGA CCCTAGGCAATGGTTTAACCAGTCCAACCAAAACCCAGC
Δ FRQ donor template bottom strand (5'-3')	GCTGGGGTTTTGGTTGGACTGGTTAAACCATTGCCTAGGG TCGCTGTGACCGGT <u>CTA</u> GTTGCTCTCGTCCGTCGAATTCTTC
FRQ diagnostic forward primer (5'-3')	CCCAAAGCTATCGACCTCTC
FRQ diagnostic reverse primer (5'-3')	CTGGGGTTTTGGTTGGACTG

This change from GAG to TAG would also remove the presence of a recognition site for the restriction enzyme BsmI (GTCTC), which could be used for screening (based on restriction mapper virtual digests). A 224 bp amplicon was generated by the MGG_17345 diagnostic primers which, upon BsmI digestion, should yield a 163 bp and 63 bp fragment in the unedited amplicons.

No transformants were located that were unsuccessfully cut by BsmI, suggesting a very low HDR efficiency for the MGG_17345 target sequence. However, one amplicon showed a large (~45 bp) insertion (Fig. 6.12). Insertions of this size are unheard of for NHEJ-mediated mutation and potentially suggested micro-homology mediated end joining or partial homology directed repair (608). This insertion mutant was subsequently Sanger sequenced (Eurofins Sanger sequencing), confirming a large 47bp insertion.

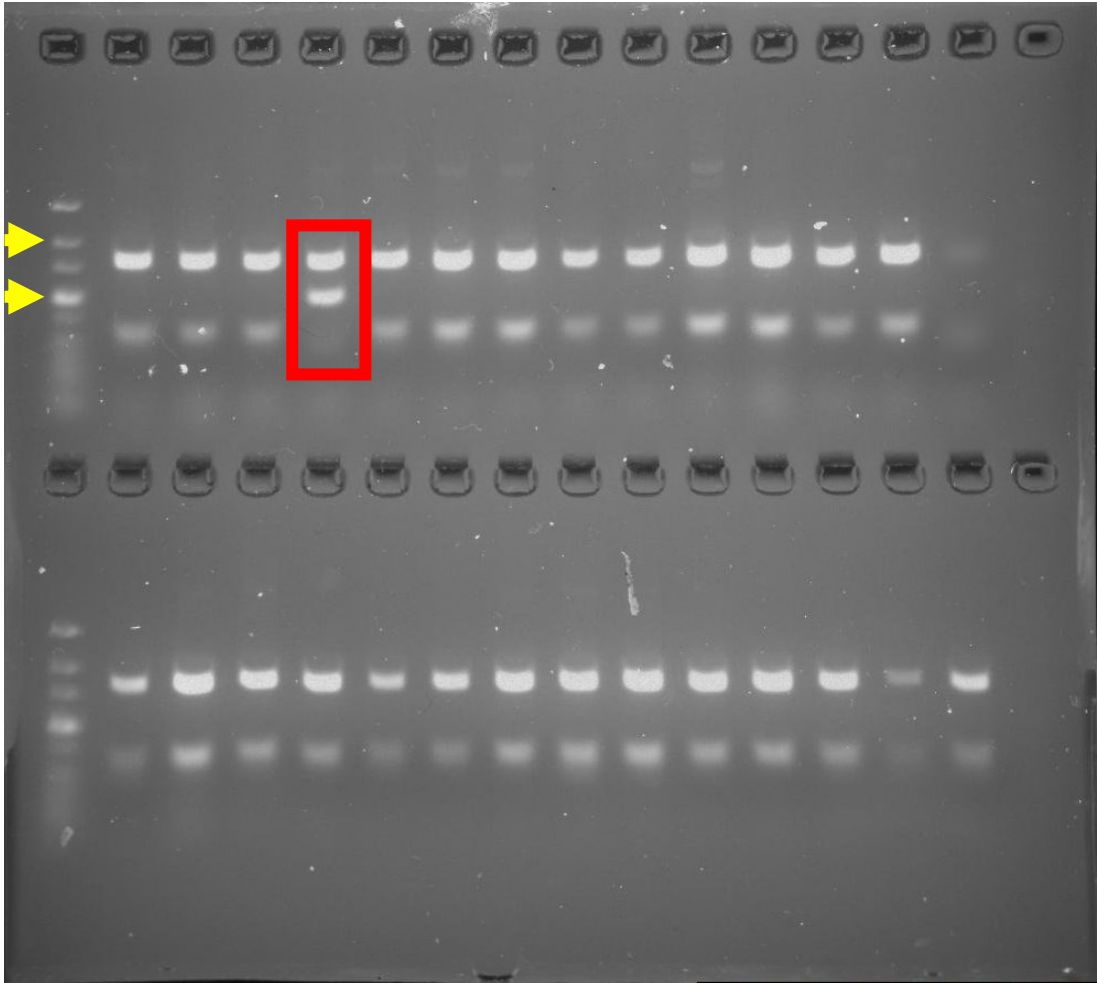


Figure 6.12: MGG_17345-targeting Cas9 mutation facilitated a large insertion. Post-digestion MGG_17345 amplicons (expected sizes: 163 bp and 63 bp) on a 3% Agarose gel with an ultra-low range ladder. Yellow arrowheads denote 100 and 200 bp, with the band between being 150 bp. The red box shows the large insertional MGG_17345 mutant, which is also cut by BsmAI.

Fascinatingly, upon manual inspection of the sequence, the 47 bp insertion was identical to the donor DNA. The sequence directly upstream of the integrated donor DNA was identical to the wild type, but the last 3 bp of the target sequence and the PAM site were absent (Fig. 6.13). Together, the homologous donor DNA insertion and wild type sequence both being present in the mutant suggests that Cas9 successfully caused a double strand break at the expected location (3 bp upstream of the target sequence PAM), but only partial homology-directed repair occurred downstream of the cut. In support of successful targeted Cas9 cutting, the final 3 bp and the PAM site is missing from the upstream wild-type repeat (CAA-TGG), which is the exact expected cut location (609). The insertion, therefore, likely occurred directly adjacent to the expected host genome cut site and was not facilitated by NHEJ.

It is likely that the 3' homology arm successfully bound and integrated into the host genome, introducing the donor sequence, which includes the GAG – TAG edit. However, based on this sequence information, the 5' homology arm upstream of the edit site did not successfully integrate, causing a repetition instead of a replacement (Fig. 6.13). Since the only difference between the donor and wild type sequence is the GAG – TAG edit, the integrated downstream sequence is identical to the wild type. If the donor sequence was not inserted and instead a spontaneous wild type gene repetition occurred, then after BsmAI digestion there would be two fragments identical to the wild type, with an additional short fragment created as a result of the additional BsmAI site introduced. This is not the case, since two fragments remained after BsmAI digestion, one of which was larger than the wild type (Fig. 6.12).

While the donor DNA was (partially) successful in its integration, rather than creating a premature termination codon as designed, the 47 bp insertion instead caused a frameshift mutation. Fortunately, this frameshift also introduced two TAG (stop) codons shortly downstream of the integration site, in frame to the transcriptional start site of MGG_17345, and thus is likely to ultimately display a similar outcome to that which was originally designed for HDR, where a prematurely truncated gene product is formed. However, if the FRQ protein produced in this mutant is still (semi-) functional, it is possible that FRQ is N-terminally truncated (due to the premature termination codon in MGG_17345), or that L- or S-FRQ (if present in *M. oryzae*) is preferentially produced due to a change in alternative splicing. Alternatively, this mutation could introduce additional phosphorylation sites, which could facilitate a faster cycling of the circadian system (161,181,558). Figure 6.13 shows the annotated sequence of the FRQ insertional mutant (purple) compared to the wild type (red). Due to a lack of other HDR mutants, this

MGG_17345 insertional mutant (henceforth known as FRQ^{NIN}, short for FRQ N-terminal-insertion) was used for subsequent experiments.

6.2.3 FRQ^{NIN} maintains conidial banding, but has an altered period

6.2.3.1 FRQ^{NIN} shows conidial banding, but its latency period prior to banding is lengthened

In contrast to WC2 (see 5.2.2.1), the insertional FRQ mutant displayed conidial banding after a period of entrainment (Fig. 6.14), implicating this rhythmic output as a WC-FLO, like in *N. crassa* (see 6.16). Banding was not observed after 12 d of growth in constant light or darkness, a phenotype common to the wild type. Interestingly though, the latency period prior to conidial banding of the FRQ^{NIN} mutant was lengthened by approximately 4 d, giving rise to an average latency period of 10 d, reminiscent of the delayed conidiation phenotype observed by Tong and colleague's FRQ1/2 knockout in *B. bassiana* (232). This phenotype was partially restored in the GFP complementation, where the average latency period was reduced to 8-9 days (2 days longer than the wild type). It is important to note that the addition of a GFP tag at the C-terminal of FRQ may cause a conformational shape change in the protein.

To determine if a lack of conidial banding metabolite(s) was responsible for the increased FRQ^{NIN} latency period, FRQ^{NIN} colonies were cultured in liquid CM to produce FRQ^{NIN} SM (see 2.1 and 2.4). Wild type guy11 strains were then subsequently cultured on both wild type SM (SM) and FRQ^{NIN} SM (frq-SM), both of which were effective in reducing the latency period by ~2 d (Fig. 6.14). FRQ^{NIN} colonies were then grown on wild type SM plates, and the banding period was reduced to approximately 6 d, which is typical of the wild type grown on CM plates with no supplementary spent media (Fig. 6.14). Taken

together, FRQ^{NIN} may produce the metabolite(s) at wild type levels but is likely to be less sensitive to it. In support of this, as seen in the wild type (see 4.2.4), relatively high concentrations are needed to activate the early banding phenotype. However, once this concentration threshold is surpassed, the latency period is reduced by ~ 2 d. Further, as mentioned above, FRQ (in both *M. oryzae* and other fungal species) has been implicated in roles beyond clock function, including nutritional sensitivity (213,434,574).

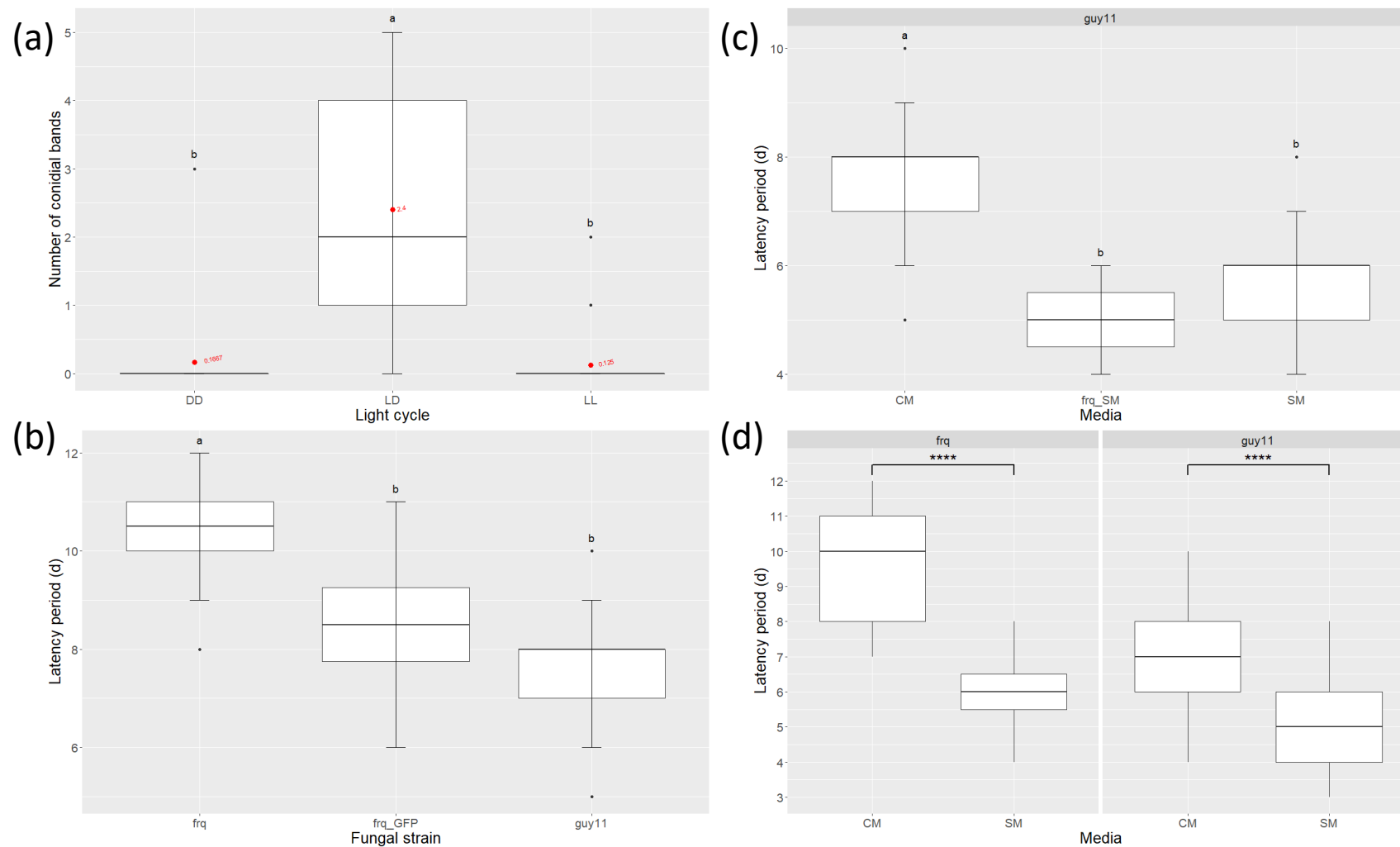


Figure 6.14: FRQ plays a role in the conidial banding latency period. (a) FRQ^{NIN} maintains its conidial banding and requires light dark cycles for entrainment, reminiscent of the wild type (n = 18 DD, n = 15 LD, n = 24 LL), but (b) the latency period prior to conidial banding is elongated in FRQ^{NIN} and (partially) rescued upon complementation (n = 10 frq, n = 12 frq::GFP, n = 23 wild type guy11). (c) FRQ^{NIN} still produces to the conidial banding metabolite(s) (n = 23 CM, n = 3 frq-SM, n = 17 SM), but (d) is less sensitive to it. (n = 10 frq SM, n = 6 frq CM, n = 23 guy11 CM, n = 17 guy11 SM). Letters describe statistically significant differences between groups (p < 0.05, Tukey's HSD), bars with stars atop denote statistically significant differences (p < 0.05, ANOVA), red points and text show the mean values for each group.

6.2.3.2 FRQ^{NIN} displays circadian conidial banding, but its period is shortened under constant light

The *M. oryzae* FRQ^{NIN} mutant also showed no significant difference in the number of conidial bands produced after 14 d of growth in LD conditions, or 10 d of LD entrainment followed by 4 d of constant light or darkness (LD-DD and LD-LL, respectively), which suggests that the FRQ^{NIN} mutant maintains a circadian rhythm in conidial banding (Fig. 6.15). However, upon transfer to constant light after LD entrainment, the calculated FRQ^{NIN} period (see 3.2.1) falls to ~16 h, suggesting that the insertion gives rise to a shorter, light-dependent period (Fig. 6.15). Additionally, if the FRQ^{NIN} period is ~16 h in constant light and continues robustly in free running conditions, there should be approximately 6 bands produced after 96 h (4 d in constant conditions). Considering that after 14 d of growth under LD, LD-DD, and LD-LL, FRQ^{NIN} colonies showed 3-4 bands on average, then the FRQ^{NIN} mutant must lose its rhythmicity after 3-4 circadian cycles (of ~16 h) in constant light (Fig. 6.15). In comparison to the wild type, the FRQ^{NIN} mutant displays a faster but non-significant alteration of calculated period under LD or LD-DD conditions, but the period is much shorter under LD-LL conditions, perhaps suggesting altered photoadaptation, phosphorylation capacity/status, or reduced alternative splicing, all of which can give rise to significantly shortened periods (116,161,178,181,192,195,198,201,207,209,210,214,225,227,409,513,517,540,548).

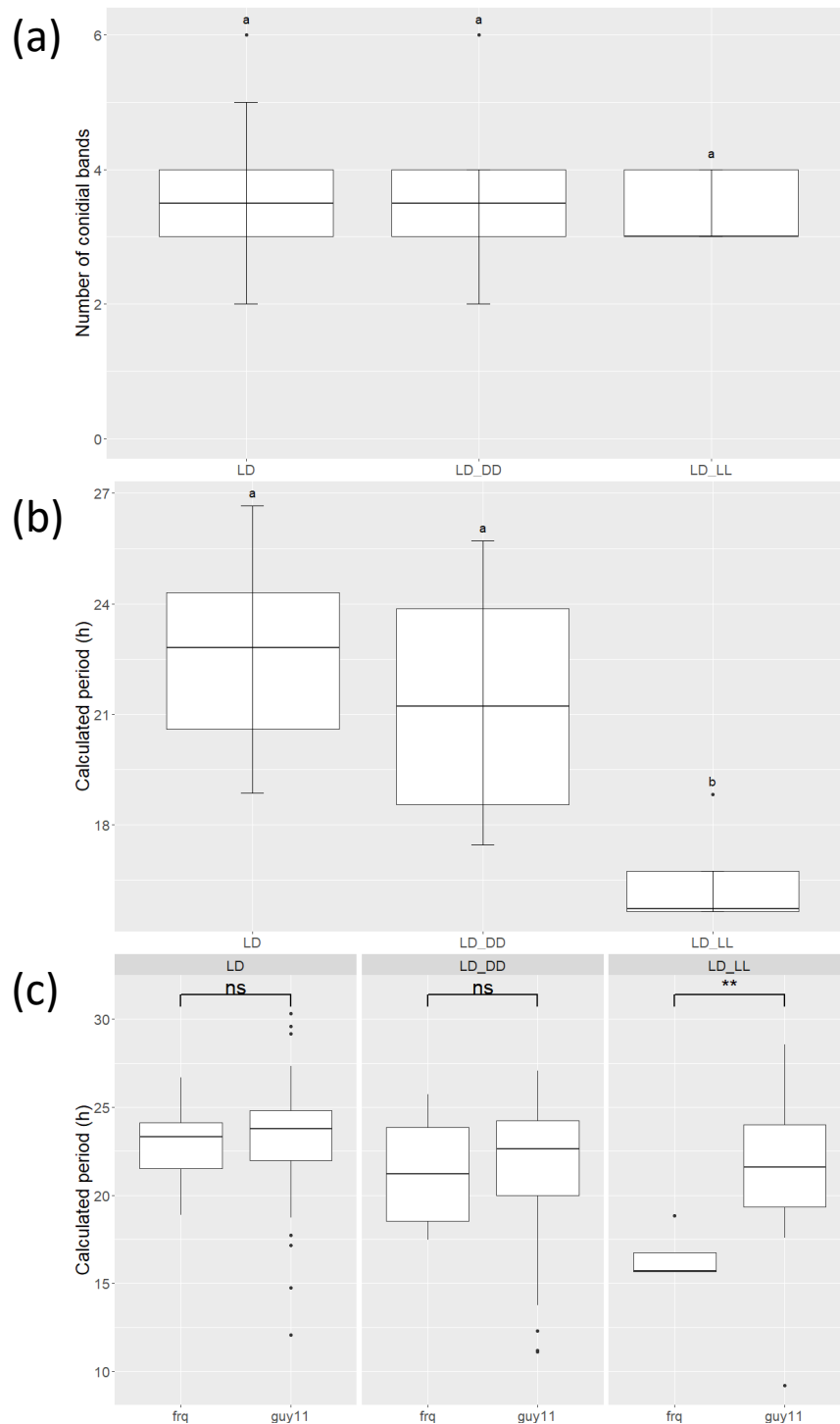


Figure 6.15: FRQ plays a role in the circadian periodicity of *M. oryzae*. (a) FRQ^{NIN} continues to display conidial banding for a number of circadian cycles upon transfer to constant dark or light (n = 10 LD, n = 6 LD-DD, n = 6 LD-LL), but (b, c) periodicity is significantly reduced under prolonged light exposure (n = 10 frq LD, n = 23 guy11 LD, n = 6 frq LD-DD, n = 14 guy11 LD-DD, n = 6 frq LD-LL, n = 13 guy11 LD-LL). Letters describe statistically significant differences between groups (p < 0.05, Tukey's HSD), bars with stars atop denote statistically significant differences (p < 0.05, ANOVA).

6.2.4 FRQ^{NIN} shows environmentally-dependent vegetative growth differences

In a similar manner to the wild type, light-dark cycles reduce the average growth rate compared to constant dark or light-grown conditions; FRQ^{NIN} grows quickest under constant light (similarly to WC2), followed by constant dark (Fig. 6.16). LD and LD-LL conditions show the slowest growth like the WC2 mutant, suggesting that the WCC-FFC circadian machinery plays a role in photoadaptation to light and/or dark in *M. oryzae*. Compared to the wild type, FRQ^{NIN} shows a decreased growth rate under LD cycling conditions, but an increased growth rate under constant light; there are no significant differences under DD, LD-DD or LD-LL, which further implicates FRQ in a photoadaptive role and as such, the FRQ^{NIN} mutant may still sense the dark (Fig. 6.16). Finally, in a similar fashion to the WC2::GFP complementation mutant, FRQ::GFP displays a reduced growth rate compared to both the wild type and FRQ^{NIN}, which could be a result of increased resource allocation to produce GFP, or an altered protein conformation (Fig. 6.16).

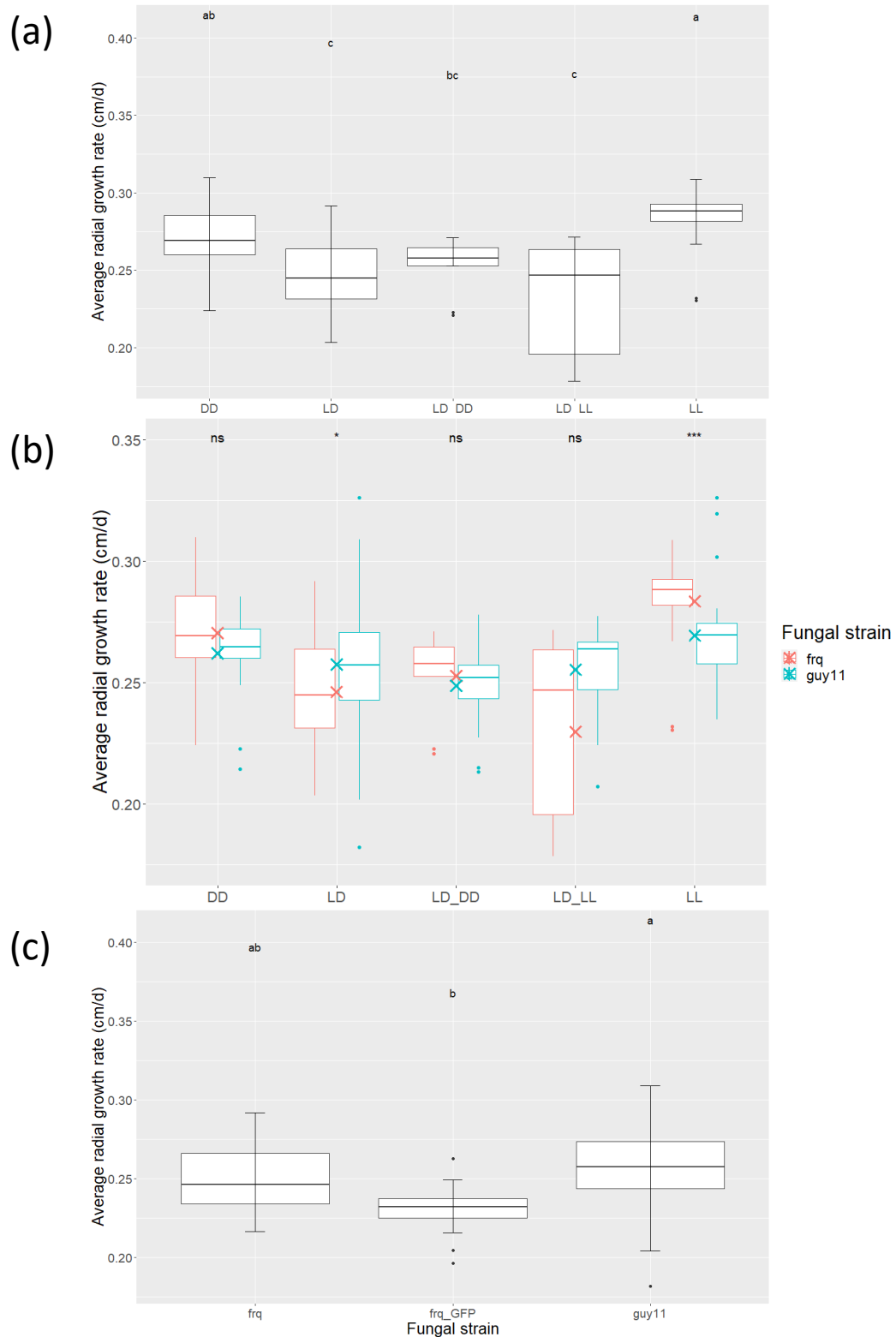


Figure 6.16: FRQ^{NIN} shows light-dependent altered vegetative growth rates. (a) Like the wild type, FRQ^{NIN} grows fastest under constant conditions, (b) FRQ^{NIN} grows slower than the wild type under LD and faster under LL conditions, (c) FRQ::GFP complementation does not rescue the reduced growth rate observed under LD conditions in FRQ^{NIN}, suggesting altered function or additional resource expenditure due to GFP. (n = 18 FRQ^{NIN} DD, n = 10 FRQ^{NIN} LD, n = 10 LD-DD FRQ^{NIN}, n = 10 FRQ^{NIN} LD-LL, n = 24 FRQ^{NIN} LL, n = 16 guy11 DD, n = 23 guy11 LD, n = 15 guy11 LD-DD, n = 13 guy11 LD-LL, n = 19 guy11 LL, n = 12 FRQ::GFP LD). Letters describe statistically significant differences between groups (p < 0.05, Tukey's HSD), Bars with stars atop denote statistically significant differences (p < 0.05, ANOVA), and crosses mean values.

6.2.5 FRQ^{NIN} mutation affects conidiation and conidial development

6.2.5.1 FRQ^{NIN} mutation causes a profound reduction in conidiation

Compared to the wild type, the FRQ^{NIN} mutant produces an order of magnitude fewer conidia under all light treatments, and very few colonies produced more than 100,000 conidia per ml, to the extent that several colonies had to be harvested and pooled for most experiments (Fig. 6.17). Interestingly, FRQ^{NIN} displays an additional light-dependent repression in conidiation, where light under any circumstances (LD, LD-DD, LD-LL and LL) reduces conidiation compared to constant dark-grown colonies (Fig. 6.17). However, even under constant darkness, FRQ^{NIN} mutant colonies vary rarely produce more than 1×10^6 conidia per ml (Fig. 6.17), and in the wild type, LD conditions are most conducive for conidiation, not constant darkness.

Again, harvest time (dawn or dusk) had little effect on conidiation, further suggesting that it takes longer than 12 h to produce conidia. Because of this massive reduction in conidiation, many experiments could not be performed after growth under LD-DD, LD-LL, and LL conditions. The FRQ::GFP complementation partially restores the conidial reduction, to levels similar to the wild type.

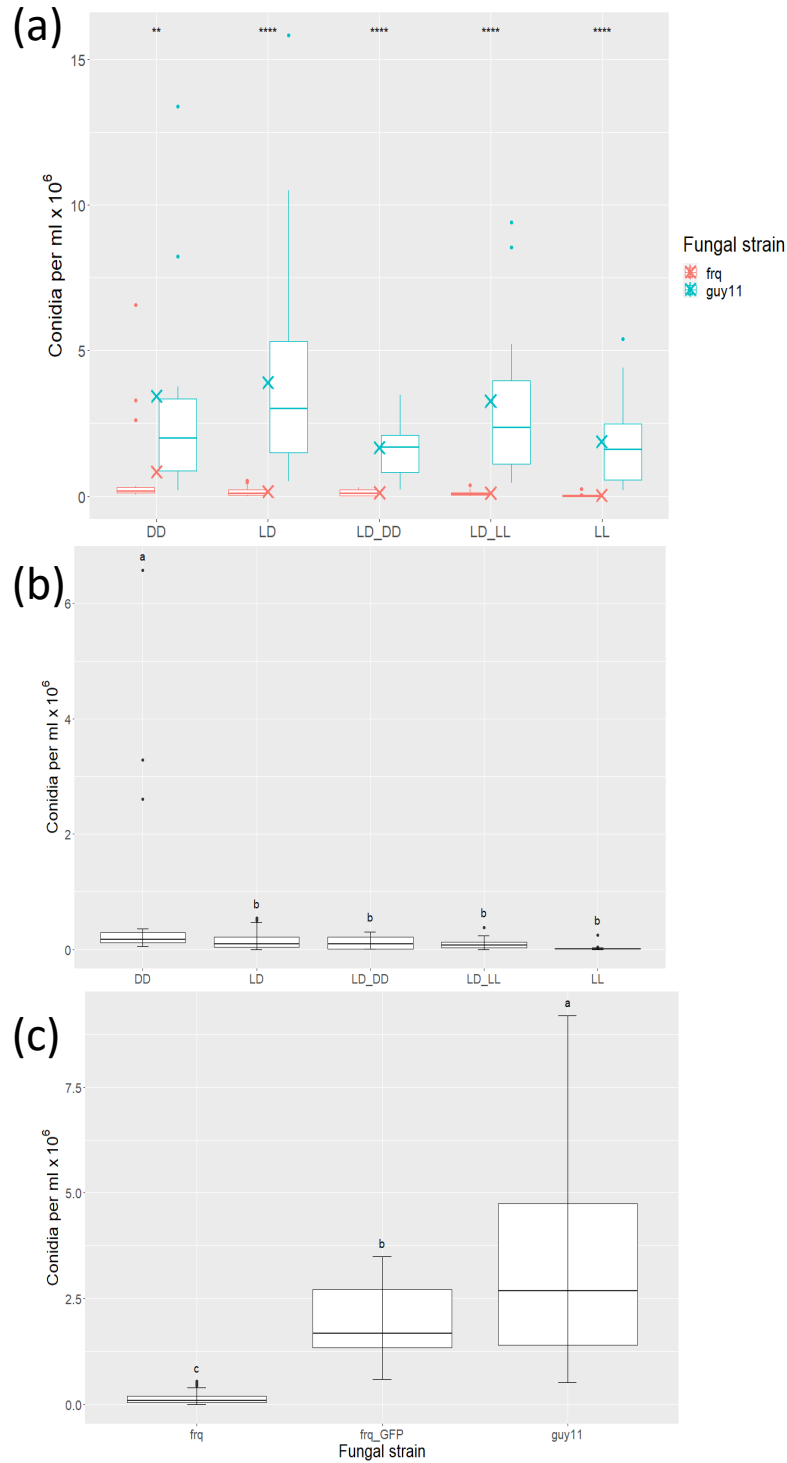


Figure 6.17: FRQ plays an important role in conidiation. (a) FRQ^{NIN} produces far fewer conidia than the wild type, regardless of environmental light conditions ($n = 24$ DD FRQ^{NIN} , $n = 15$ DD *guy11*, $n = 81$ LD FRQ^{NIN} , $n = 68$ LD *guy11*, $n = 19$ LD-DD FRQ^{NIN} , $n = 17$ LD-DD *guy11*, $n = 15$ LD-LL FRQ^{NIN} , $n = 18$ LD-LL *guy11*, $n = 25$ LL FRQ^{NIN} , $n = 16$ LL *guy11*), (b) FRQ^{NIN} shows light-dependent conidiation repression, where light under any circumstances (LD, LD-DD, LD-LL, and LL) represses conidial production ($n = 24$ DD, $n = 81$ LD, $n = 10$ LD-DD, $n = 15$ LD-LL, $n = 25$ LL), and (c) $FRQ::GFP$ complementation partially rescues the conidial defects ($n = 72$ FRQ^{NIN} , $n = 8$ $FRQ::GFP$, $n = 56$ *guy11*). Letters describe statistically significant differences between groups ($p < 0.05$, Tukey's HSD), Bars with stars atop denote statistically significant differences ($p < 0.05$, ANOVA), and crosses indicate mean values.

6.2.5.2 The FRQ^{NIN} mutant conidia are less likely to germinate

Due to the reduced conidiation phenotype, it was difficult to harvest sufficient quantities of conidia for conidial development assays, and as such only LD and DD conditions are presented. FRQ^{NIN} conidia display a reduced germination rate under both DD and LD conditions (Fig. 6.18). Considering that there is no significant difference between DD and LD germination rates in FRQ^{NIN} this reduced germination phenotype could mean that the FRQ^{NIN} mutation causes an overall reduction in germination, or that FRQ^{NIN} mutant conidia are hypersensitive to the constant light and increased temperature as a result of the imaging system (discussed in previous chapters). Ideally, this experiment would be repeated under constant darkness, but this would mean that different conidia would be observed at each subsequent time point.

Interestingly, despite the reduced germination, by 8 HPI, there were no significant differences in appressorial formation between the wild type and FRQ^{NIN} conidia (Fig. 6.18). Further, FRQ^{NIN} retains its dark-entrained reduction in appressorial development, similar to the wild type (Fig. 6.18). This suggests that those conidia that do germinate are as, if not more, likely to develop appressoria than the wild type by 8 HPI and thus may develop slightly quicker, perhaps as result of faster cycling of the clock machinery, since FRQ^{NIN} displays a shorter period under prolonged light exposure, which it would experience under the imaging setup.

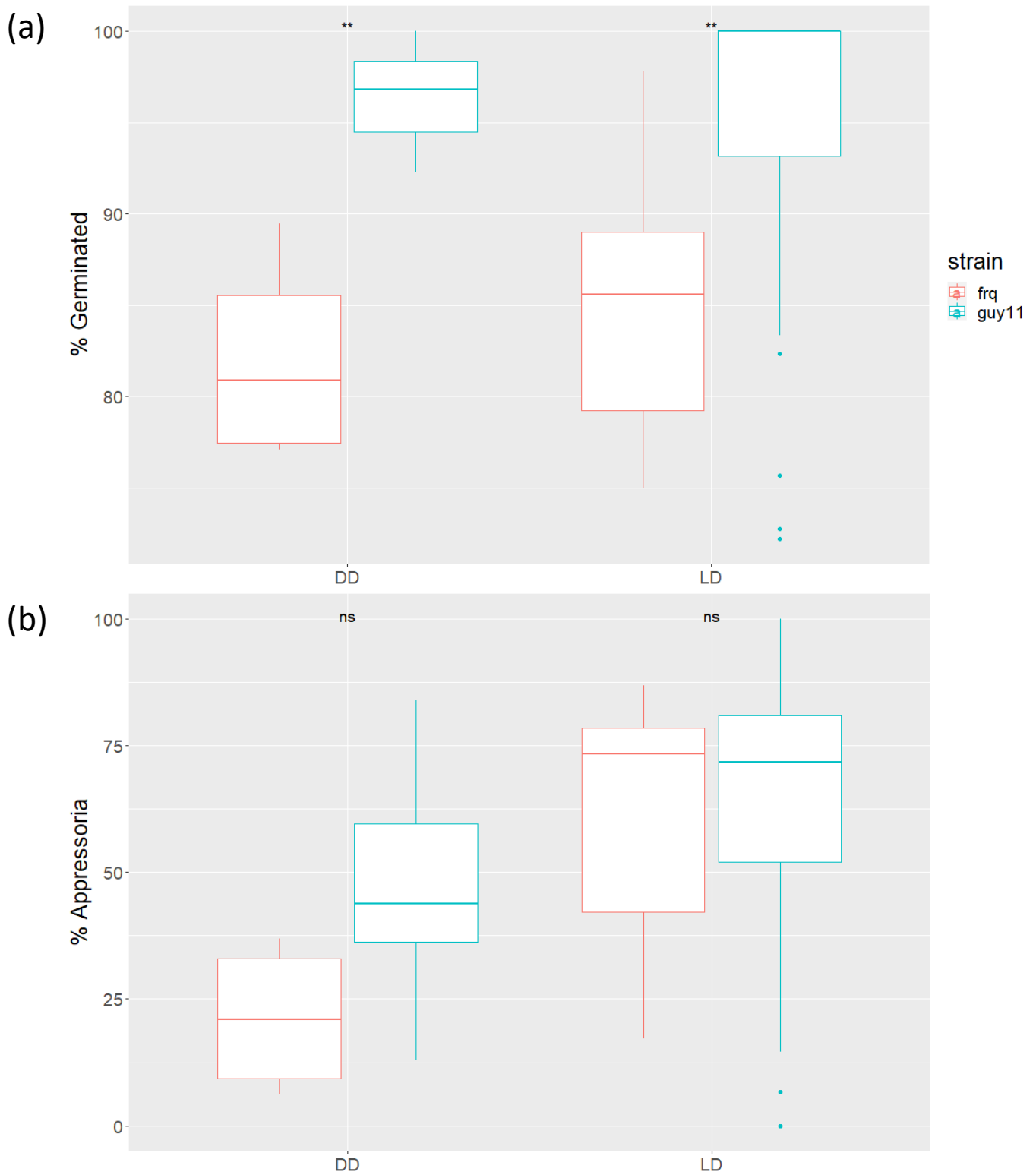


Figure 6.18: FRQ^{NIN} conidia are less likely to germinate, but those that do are more likely to produce appressoria. (a) By 8 hours post inoculation, fewer FRQ^{NIN} conidia germinated compared to the wild type under both DD and LD pre-harvest entrainment conditions, however (b) there were no significant differences between the wild type and FRQ^{NIN} by 8 HPI in terms of appressorial development, and so those FRQ^{NIN} conidia that do germinate are more likely to produce appressoria or produce them faster than the wild type. n = 3 *guy11* DD, n = 21 *guy11* LD, n = 3 FRQ^{NIN} DD, n = 3 LD FRQ^{NIN}. Stars represent increasing statistical significance (ANOVA). 'ns' denotes no significant difference between groups (p > 0.05).

6.2.5.3 FRQ^{NIN} produces smaller conidia

FRQ^{NIN} conidial adherence is not altered compared to the wild type, further suggesting that circadian machinery has little effect on spore tip mucilage production (data not shown). The conidia remaining after agitation are again larger on average than those measured before agitation (Fig. 6.19) in a similar fashion to the wild type. However, the FRQ^{NIN} conidia are smaller than the wild type both prior to and after agitation (Fig. 6.19). Since WC2 conidia are also smaller than the wild type but germinate and develop faster, a decrease in conidial size (and potentially resources) is unlikely to be the cause of an increased developmental rate. The consistent reduction in conidial size in both WC2 and FRQ mutation does, however, implicate the circadian machinery in conidial size.

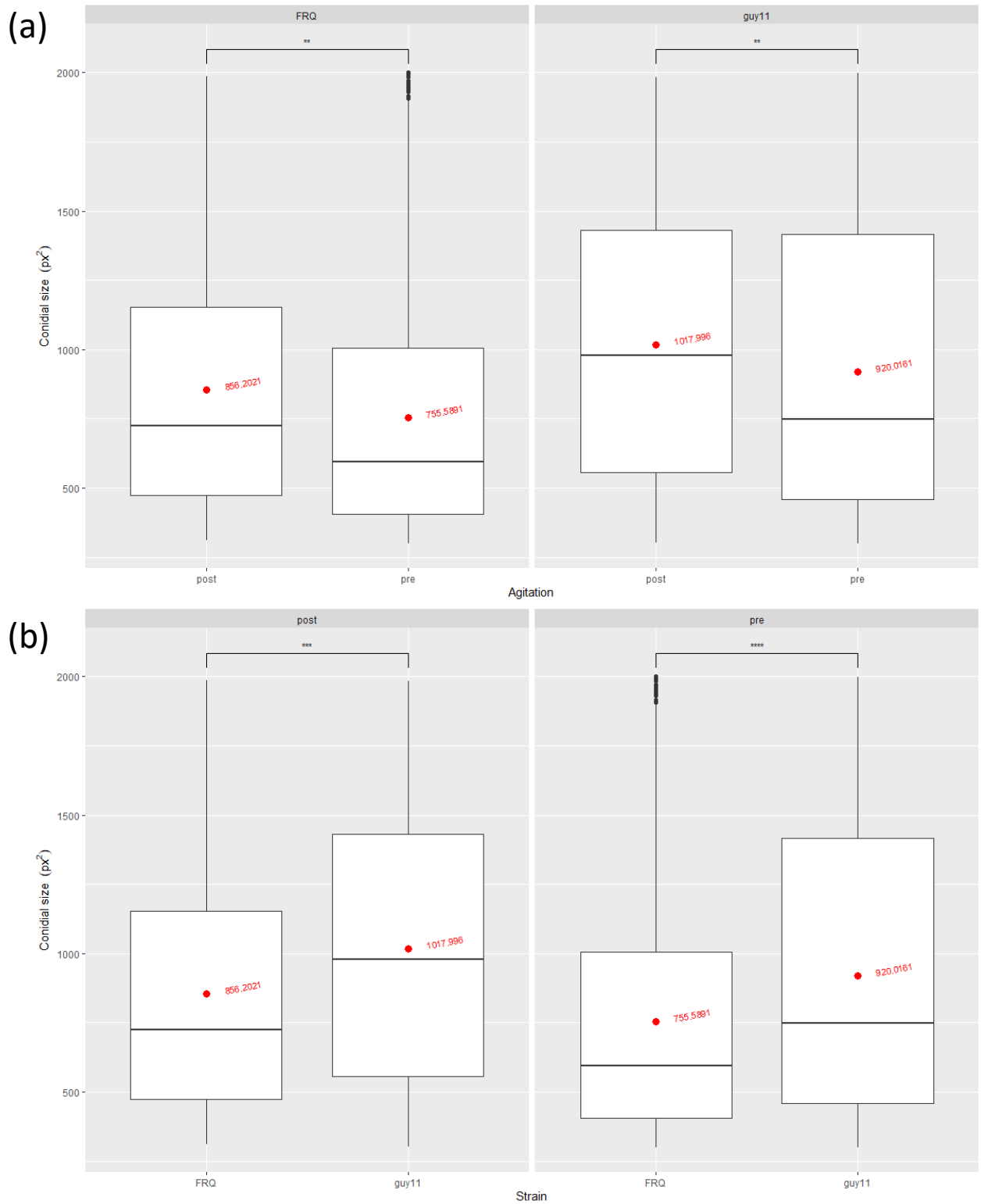


Figure 6.19: Circadian machinery plays a role in conidial size. (a) Similarly to the wild type, FRQ^{NIN} shows a distinct separation of conidial size prior to and after agitation, again suggesting that larger conidia adhere to hydrophobic surfaces better, and that *M. oryzae* conidial size may have a functional role. However, (b) the conidia in FRQ^{NIN} are smaller than the wild type, both prior to and after agitation. (n = 3 per treatment, at least 100 conidia counted per treatment). Stars represent increasing statistical significance (ANOVA, p < 0.05). Red points and text show the mean values for each group.

6.2.5.4 FRQ^{NIN} appressoria generate higher turgor pressure

Again, it was difficult to generate sufficient conidial concentrations for cytorrhysis experiments in FRQ^{NIN}, and as such only DD, LD, and LD-DD conditions were used. Pre-harvest light conditions had little effect on appressorial collapse as there were no significant differences, where ~50% and ~70% of the appressoria had collapsed under 1 M and 2 M glycerol concentrations, regardless of light treatment (Fig. 6.20). However, under LD conditions, FRQ^{NIN} mutants consistently showed a reduction in cytorrhysis compared to the wild type, where ~75% of wild type appressoria had collapsed by 1 M and above, approximately 20% more than the mutant (Fig. 6.20). This suggests that the FRQ^{NIN} mutant may generate a higher appressorial turgor pressure or that they are increasingly melanised and thus better equipped to prevent loss of turgor.

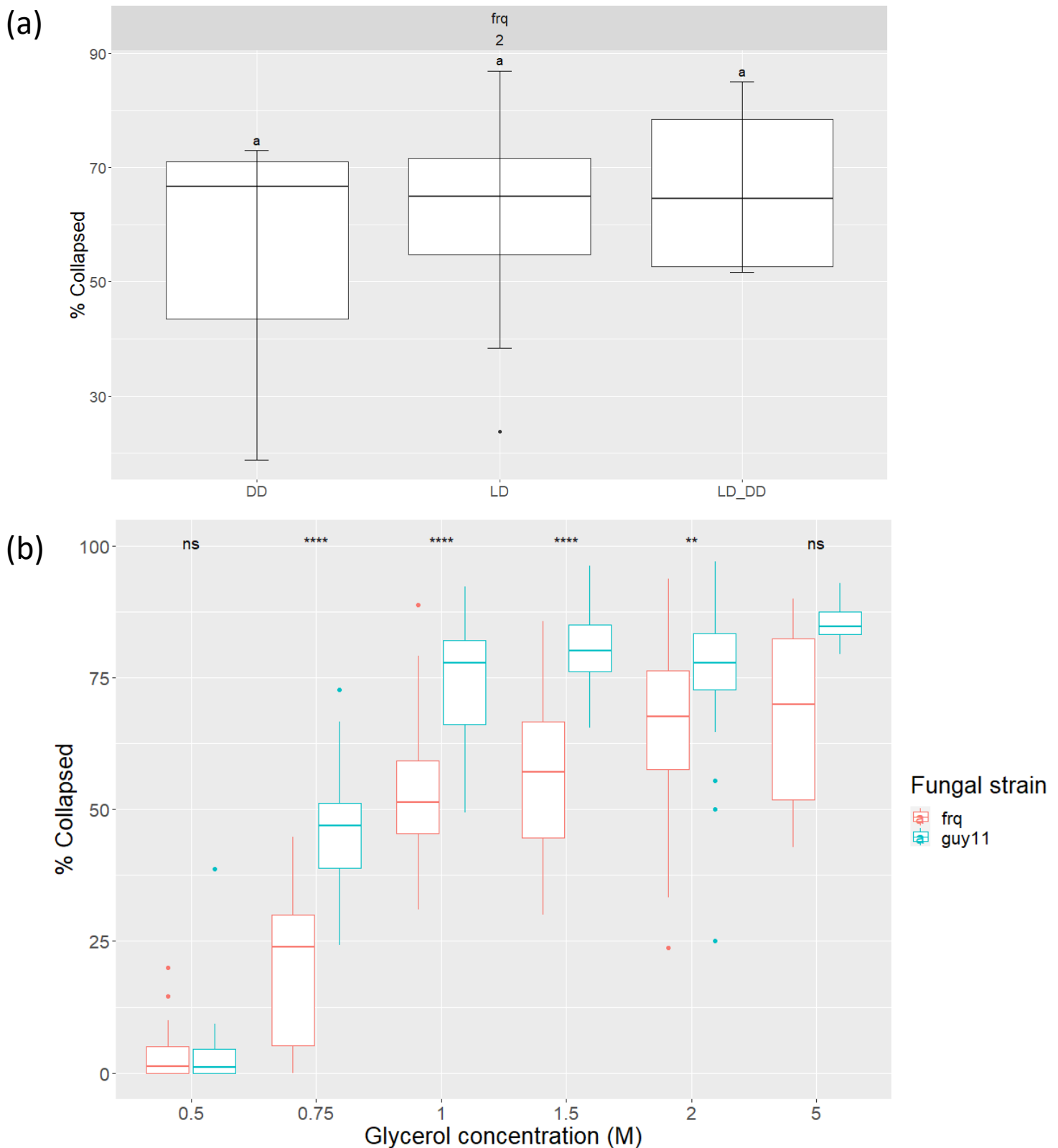


Figure 6.20: FRQ^{NIN} generates higher appressorial turgor pressure or appressoria are more resistant to osmotic stress. (a) Pre-harvest entrainment conditions had little effect on appressorial cytorrhysis in FRQ^{NIN} (n = 3 DD, n = 12 LD, n = 3 LD-DD), but (b) FRQ^{NIN} consistently showed reduced appressorial collapse compared to the wild type under a range of glycerol concentrations, suggesting FRQ^{NIN} appressoria generate higher turgor pressure or are more resistant to collapse (n = 11 FRQ^{NIN} , n = 12 $guy11$ [0.5 M], n = 5 FRQ^{NIN} , n = 5 $guy11$ [0.75 M], n = 11 FRQ^{NIN} , n = 12 $guy11$ [1 M], n = 8 FRQ^{NIN} , n = 12 $guy11$ [1.5 M], n = 12 FRQ^{NIN} , n = 12 $guy11$ [2 M], n = 3 FRQ^{NIN} , n = 3 $guy11$ [5 M]). Letters describe statistically significant differences between groups (p < 0.05, Tukey's HSD), Bars with stars atop denote statistically significant differences (p < 0.05, ANOVA).

6.2.6 Penetration and early *in planta* cell-cell movement is not affected by FRQ^{NIN} mutation

Wild type rice leaf sheath inoculations showed a slight, but insignificant increase in appressorial penetration compared to FRQ^{NIN} by 24 HPI, in a stark contrast to the reduced penetration phenotype observed in the WC2 mutant (Fig. 6.21). Approximately 5% of penetrated and invasive hyphae showed *in planta* cell to cell movement in the mutant FRQ^{NIN}, FRQ::GFP complement, and wild type by 24 HPI, suggesting that the FRQ^{NIN} mutation does not play a role in early-infection virulence under LD conditions (Fig. 6.21).

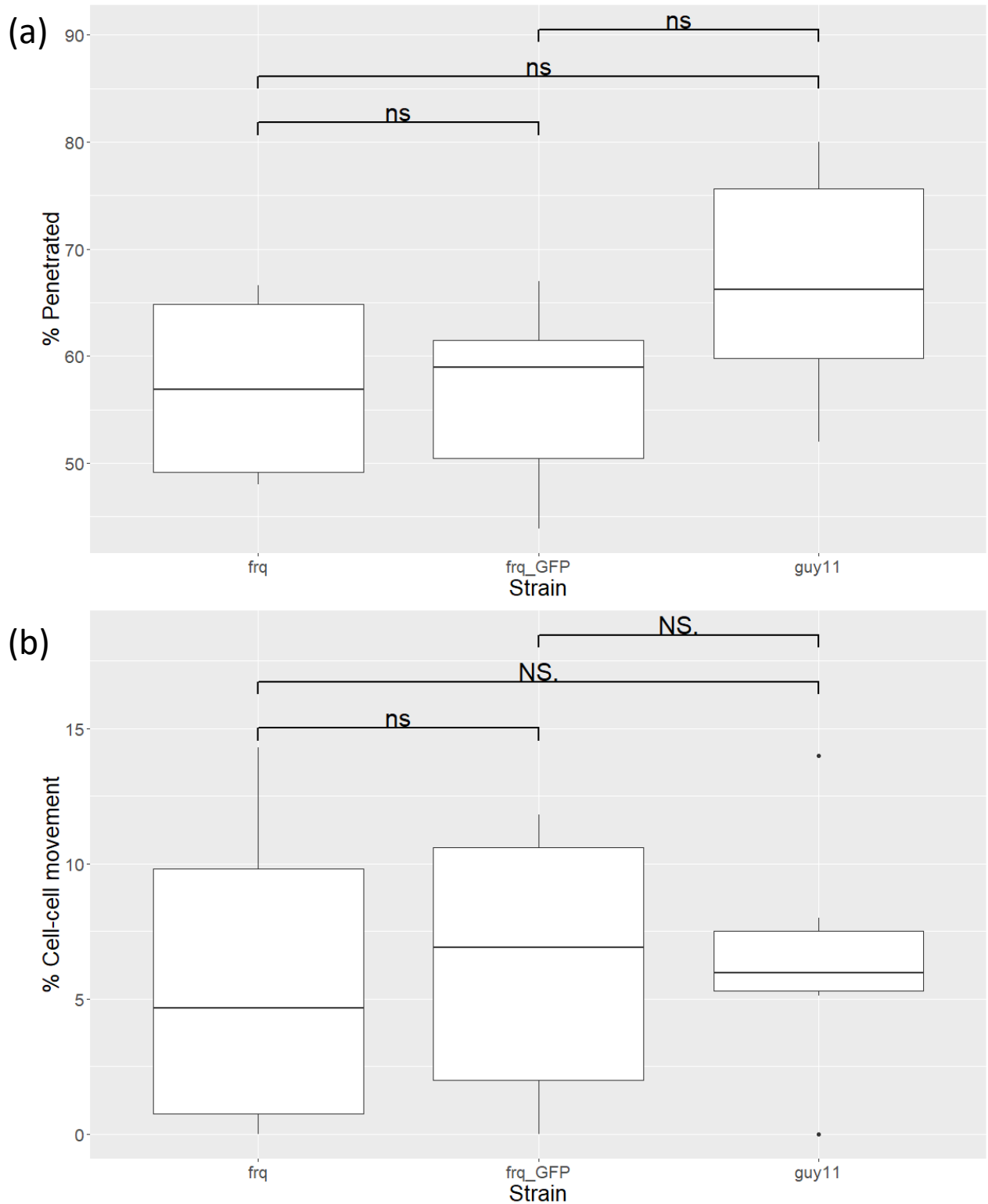


Figure 6.21: FRQ^{NIN} does not show altered penetration or cell-cell movement 24 hours post-inoculation. There are no significant differences between wild type, FRQ^{NIN}, or FRQ::GFP complementation strains in terms of (a) penetration or (b) *in planta* cell-cell movement (n = 6 per strain, at least 100 conidia were counted per sample). Bars with stars atop denote statistically significant differences (p < 0.05, ANOVA).

No significant differences were observed at 48 HPI either (Fig. 6.22), further implying that the FRQ^{NIN} mutation plays little role in early virulence; ~90% of appressoria observed had facilitated plant cuticle penetration in FRQ^{NIN}, FRQ::GFP complement, and wild type, and ~75% or more invasive hyphae displayed cell-cell movement (Fig. 6.22). Interestingly, by 48 HPI, FRQ^{NIN} shows a slightly elevated (although insignificant) number of invasive hyphae constrained to the primary penetrated cell compared to the wild type or complementation mutant (Fig. 6.22), a phenotype reminiscent of the WC2 mutant (discussed in 5.2.6).

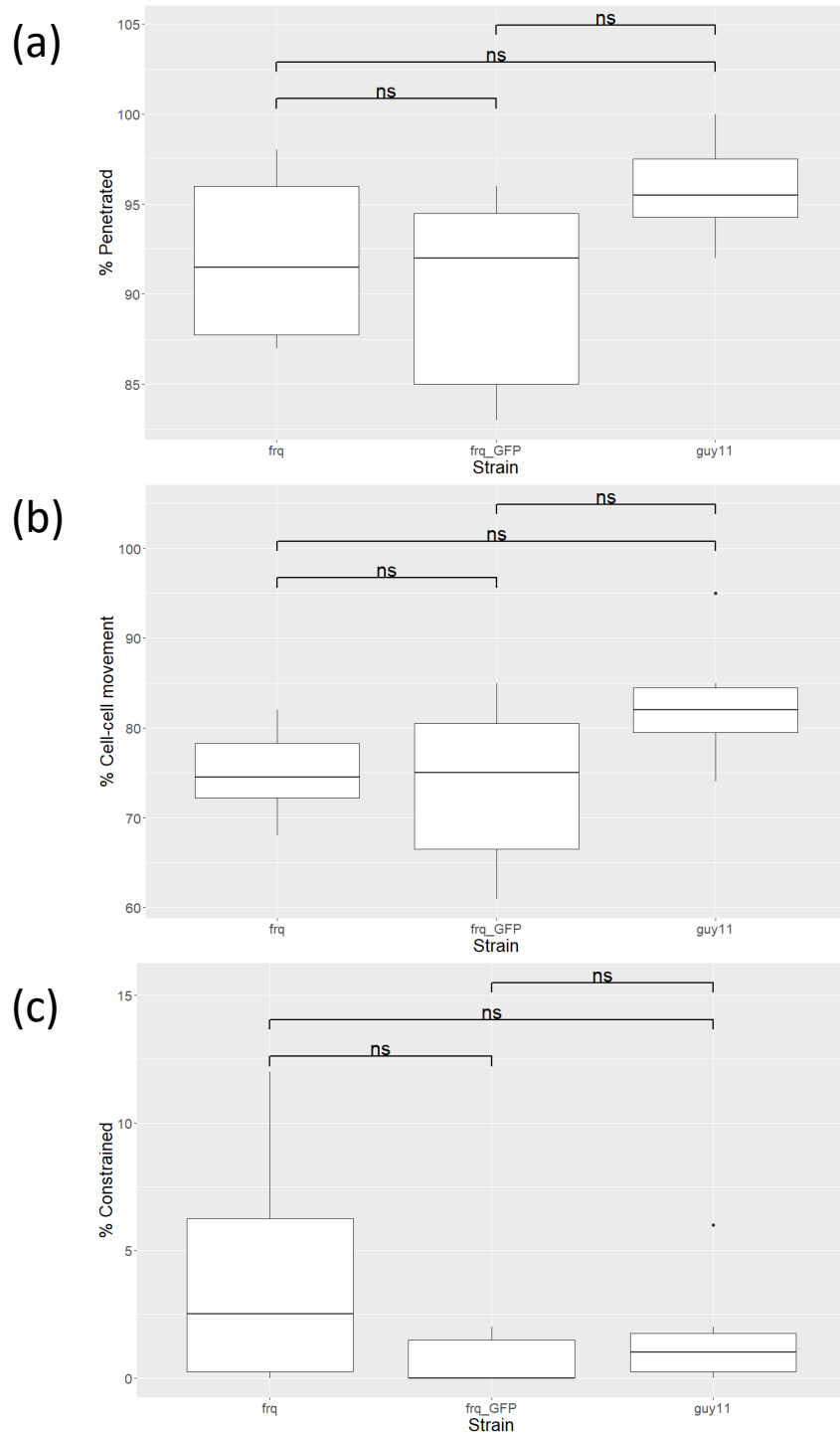


Figure 6.22: FRQ^{NIN} strains show no significant difference in penetration and cell-cell movement 48 hours post-inoculation. FRQ^{NIN} strains did not show significantly altered (a) penetration, or (b) *in planta* cell-cell movement, and (c) were not constrained to the primary cell, like in the WC2 mutant (n = 6 per strain, at least 50 conidia were counted per sample). Bars with stars atop denote statistically significant differences (p < 0.05, ANOVA).

6.2.7 Asynchronous FRQ^{NIN} inoculations reduce rice-specific virulence

6.2.7.1 Antiphase-entrained FRQ^{NIN} is less virulent than the wild type in rice at dawn (subjective dusk)

Again, insufficient conidial quantities were a significant issue for FRQ^{NIN} plant inoculations, and as such inoculations were only carried out after constant dark, in phase LD, or antiphase DL pre-inoculation treatments, since other conditions (LD-DD, LD-LL, and LL) rarely produced enough conidia for spray inoculations.

At dusk, FRQ^{NIN} and wild type infections showed no significant difference in lesion region area under any pre-inoculation light treatment (DD, DL, and LD), again suggesting that the rice clock may be more important than the fungal clock at dusk (Fig. 6.23). At dawn, wild type lesions were larger than FRQ^{NIN} after DD pre-treatment, and smaller under antiphase conditions, implying that FRQ^{NIN} may be more virulent at its subjective dusk (Fig. 6.23). However, under DL conditions at dawn (fungal subjective dusk), FRQ^{NIN} mutants show significantly fewer lesions than the wild type, which disagrees with its increased dusk virulence (Fig. 6.23). The reduced DL FRQ^{NIN} lesion density but increased DL FRQ^{NIN} lesion size at dawn may instead be a result of reduced competition from nearby invasive hyphae, and as such shows a negative correlation between lesion density and lesion size, similar to the WC2 mutant (see 5.2.7 – 5.2.8). In support of this, there were no significant differences between FRQ^{NIN} and the wild type for lesion coverage per leaf at dawn or dusk, except under DL conditions at dawn, where FRQ^{NIN} lesions covered a significantly lower proportion of the inoculated leaves (Fig. 6.23).

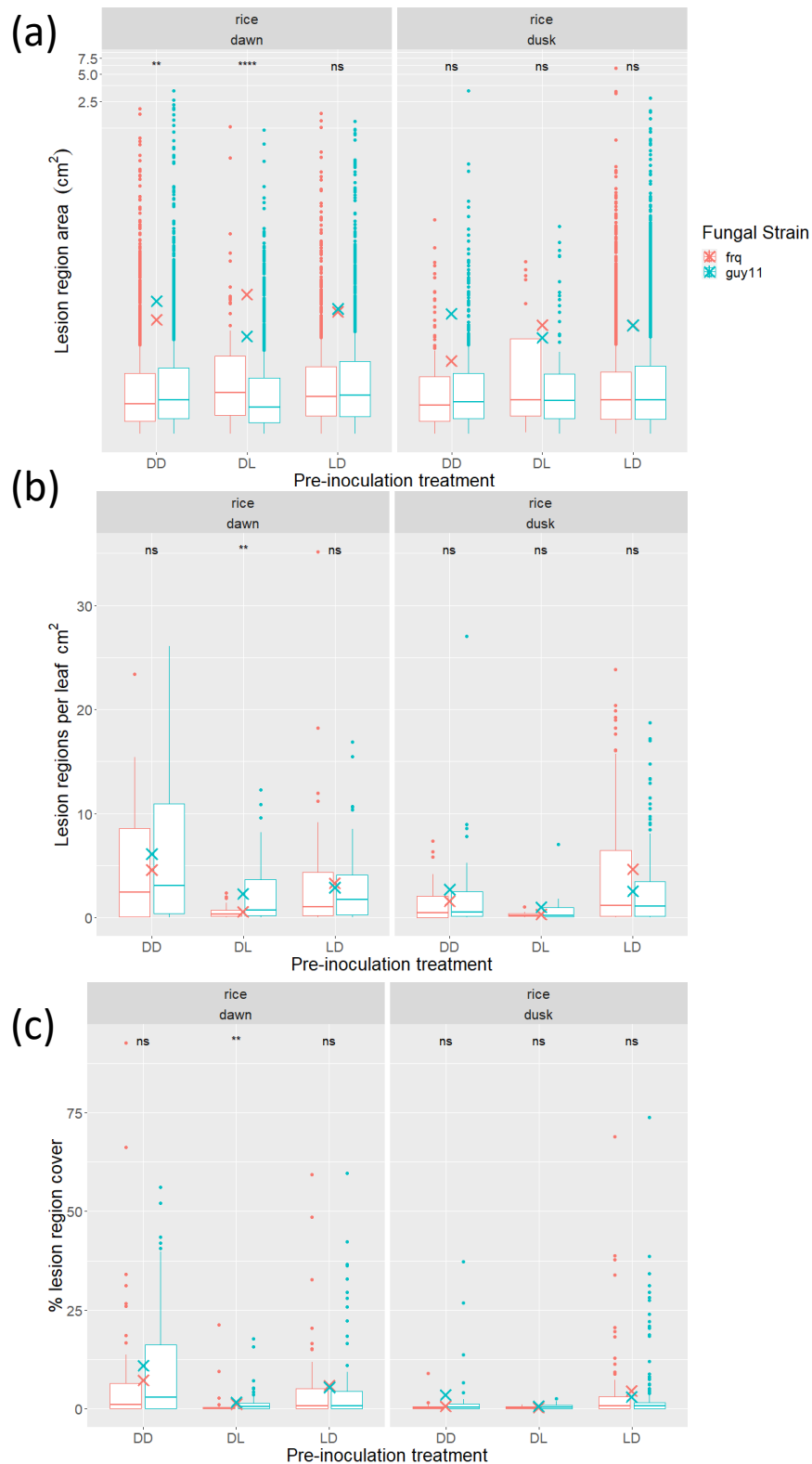


Figure 6.23: The FRQ^{NIN} strain is less pathogenic than the wild type after antiphase entrainment at dawn towards rice. (a) FRQ^{NIN} produces smaller lesions after DD entrainment, but larger lesions after DL entrainment at dawn (n = 2358 lesions *guy11*/ 1924 FRQ^{NIN} DD dawn, n = 601 *guy11*/ 235 FRQ^{NIN} DD dusk, n = 1303 *guy11*/ 138 FRQ^{NIN} DL dawn, n = 93 *guy11*/ 20 FRQ^{NIN} DL dusk, n = 1565 *guy11*/ 1094 FRQ^{NIN} LD dawn, n = 6098 *guy11*/ 3479 FRQ^{NIN} LD dusk). (b) Under DL entrainment, however, the FRQ^{NIN} strain gave rise to lower leaf lesion densities, and (c) FRQ^{NIN} mutation does not affect leaf lesion coverage, except after DL entrainment at dawn, where FRQ^{NIN} disease severity is reduced compared to the wild type (n = 55 leaves *guy11*/ 59 FRQ^{NIN} DD dawn, n = 28 *guy11*/ 22 FRQ^{NIN} DD dusk, n = 63 *guy11*/ 31 FRQ^{NIN} DL dawn, n = 12 *guy11*/ 9 FRQ^{NIN} DL dusk, n = 87 *guy11*/ 58 FRQ^{NIN} LD dawn, n = 224 *guy11*/ 84 FRQ^{NIN} LD dusk). Stars represent increasing statistical significance (Dunn's test, p < 0.05), and crosses represent mean values.

6.2.7.2 Constant darkness-entrained colonies favour dawn inoculations in FRQ^{NIN}

For rice-FRQ^{NIN} inoculations, constant dark and antiphase pre-treated FRQ^{NIN} mutants did not show any significant difference in lesion size between dawn and dusk, whereas under synchronous LD conditions, FRQ^{NIN} showed larger lesions at dawn, similar to the wild type (Fig. 6.24). Contrastingly, FRQ^{NIN} LD and DL inoculations did not show a time of day-dependent outcome in lesion density, whereas constant dark pre-treated FRQ^{NIN} colonies showed increased numbers of lesions at dawn (6.24). LD and DL inoculations also showed no time-of-day effect on leaf coverage, and constant dark-grown colonies showed an increased coverage at dawn (Fig. 6.24), a phenotype also observed in the wild type (see 4.2.6)

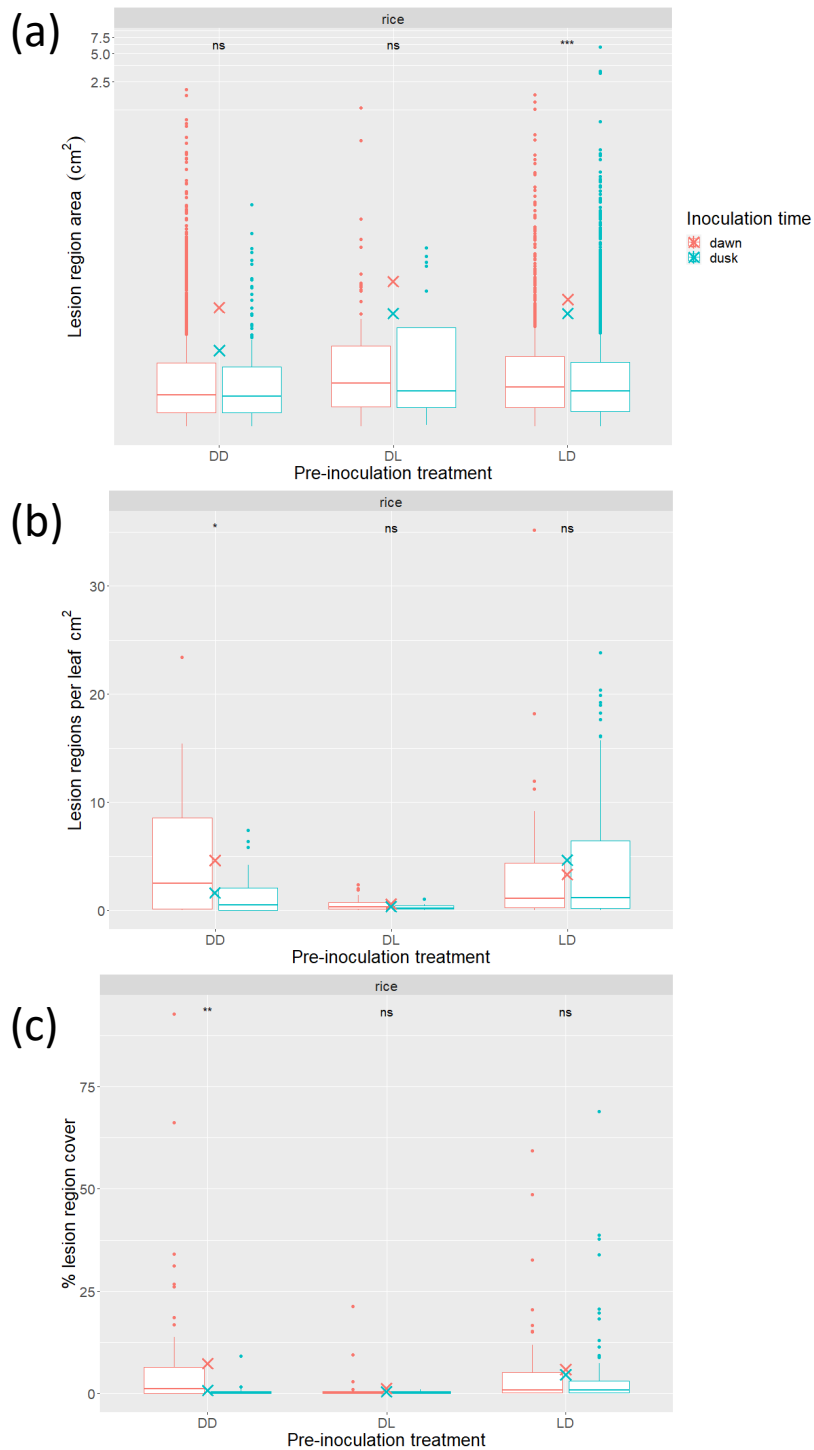


Figure 6.24: Prolonged darkness-entrained FRQ^{NIN} strains prefer dawn in rice inoculations. (a) Synchronous entrainment of FRQ^{NIN} and rice gave rise to larger lesions at dawn (n = 1924 lesions DD dawn/ 235 dusk, n = 138 DL dawn/ 20 dusk, n = 1094 LD dawn/ 3479 dusk), (b) DD-entrained FRQ^{NIN} showed an increased dawn lesion density, and (c) DD-entrained FRQ^{NIN} strains also showed an increased leaf coverage at dawn. (n = 59 leaves DD dawn/ 22 dusk, n = 31 leaves DL dawn/ 9 dusk, n = 58 LD dawn/ 84 dusk). Stars represent increasing statistical significance (Dunn's test, p < 0.05), and crosses mean values.

6.2.7.3 Pre-inoculation treatment affects FRQ^{NIN} virulence in rice

When comparing pre-inoculation treatment effects on FRQ^{NIN} virulence, DD, DL, and LD inoculations gave rise to larger lesion regions at dawn, again suggesting the plant clock may be more important than the fungal clock: dusk inoculations showed a reduced deviation from the mean (possibly because of the reduced number of lesions) (Fig. 6.25).

Antiphase treatments showed a significant decrease in lesion density at dawn, but treatment seems to have less of an effect on lesion density compared to the wild type (Fig. 6.25). Antiphase pre-treatment also gave rise to a reduced lesion coverage at both dawn and dusk (along with dusk DD inoculations), suggesting that the FRQ^{NIN} mutant cannot compensate for asynchrony with the plant host as well as the wild type (Fig. 6.25).

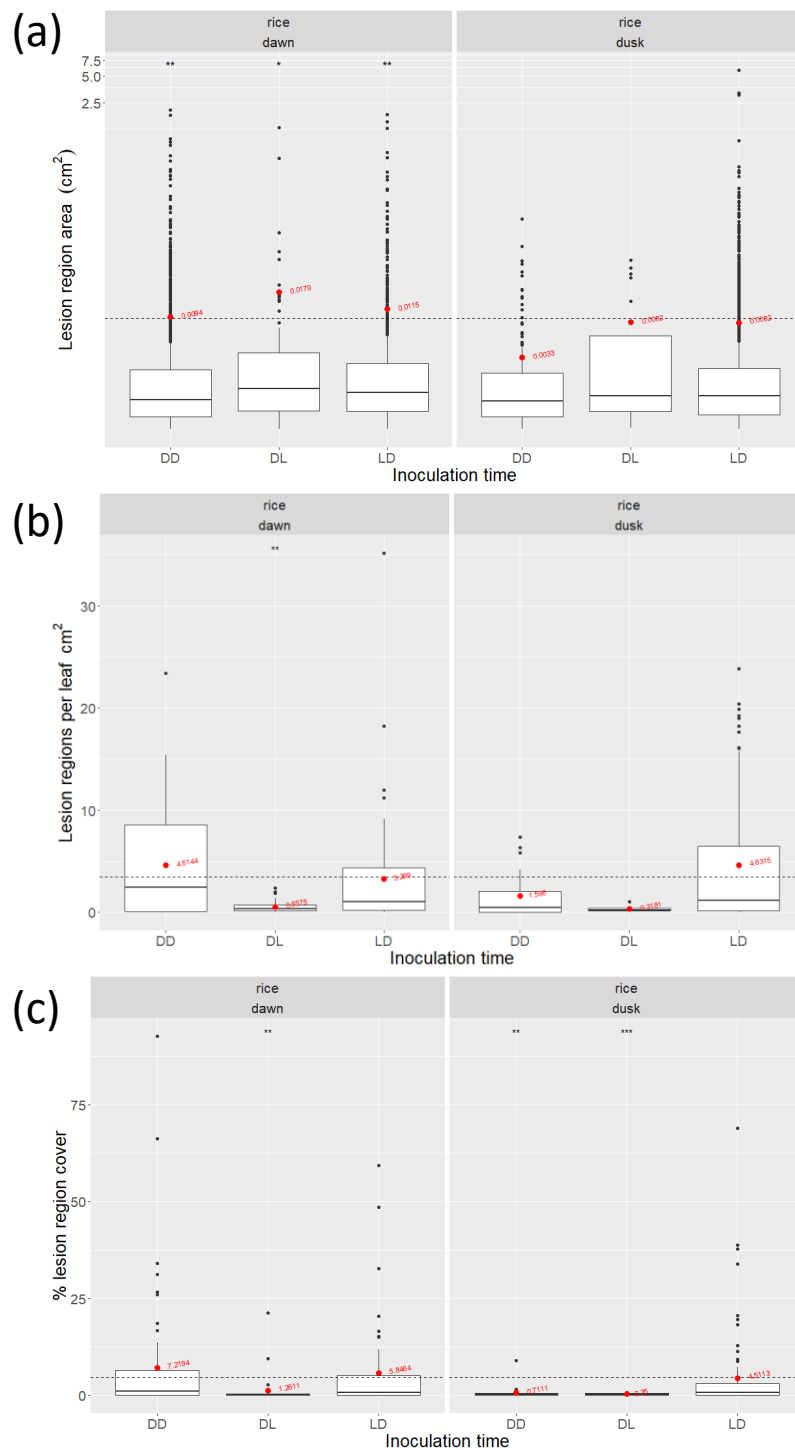


Figure 6.25: Pre-inoculation treatment plays a role in dawn virulence in FRQ^{NIN} mutants. (a) FRQ^{NIN} lesions are larger at rice subjective dawn (n = 1924 lesions DD dawn/ 235 dusk, n = 138 DL dawn/ 20 dusk, n = 1094 LD dawn/ 3479 dusk), (b) antiphase-entrained FRQ^{NIN} infections give rise to lower lesion densities in rice, (c) asynchronous entrainment conditions reduces infection severity in FRQ^{NIN} (n = 59 leaves DD dawn/ 22 dusk, n = 31 leaves DL dawn/ 9 dusk, n = 58 LD dawn/ 84 dusk). Stars represent increasing statistical significance (Dunn's test, p < 0.05), and red dots/text denotes mean values for each group.

6.2.8 FRQ^{NIN} and non-host interactions

6.2.8.1 Antiphase-entrained FRQ^{NIN} inoculations reduce barley-specific virulence

In non-host barley interactions, FRQ^{NIN} displays smaller lesions at dawn after antiphase entrainment (subjective dusk) and at dusk after in phase entrainment, suggesting that FRQ^{NIN} has partially lost its dusk virulence in barley (Fig. 6.26). The median lesion size in DL dawn inoculations is higher in FRQ^{NIN}, but this is likely due to the reduced lesion density, as no other treatments saw a difference in lesion density between the wild type and FRQ^{NIN} mutant (Fig. 6.26). This result agrees with the wild type-like penetration and cell-cell movement in FRQ^{NIN} under LD conditions. FRQ^{NIN} also showed a decrease in leaf coverage compared to the wild type under antiphase conditions at dawn only, further suggesting that antiphase conditions negatively impact FRQ^{NIN} to a greater degree than the wild type (Fig. 6.26).

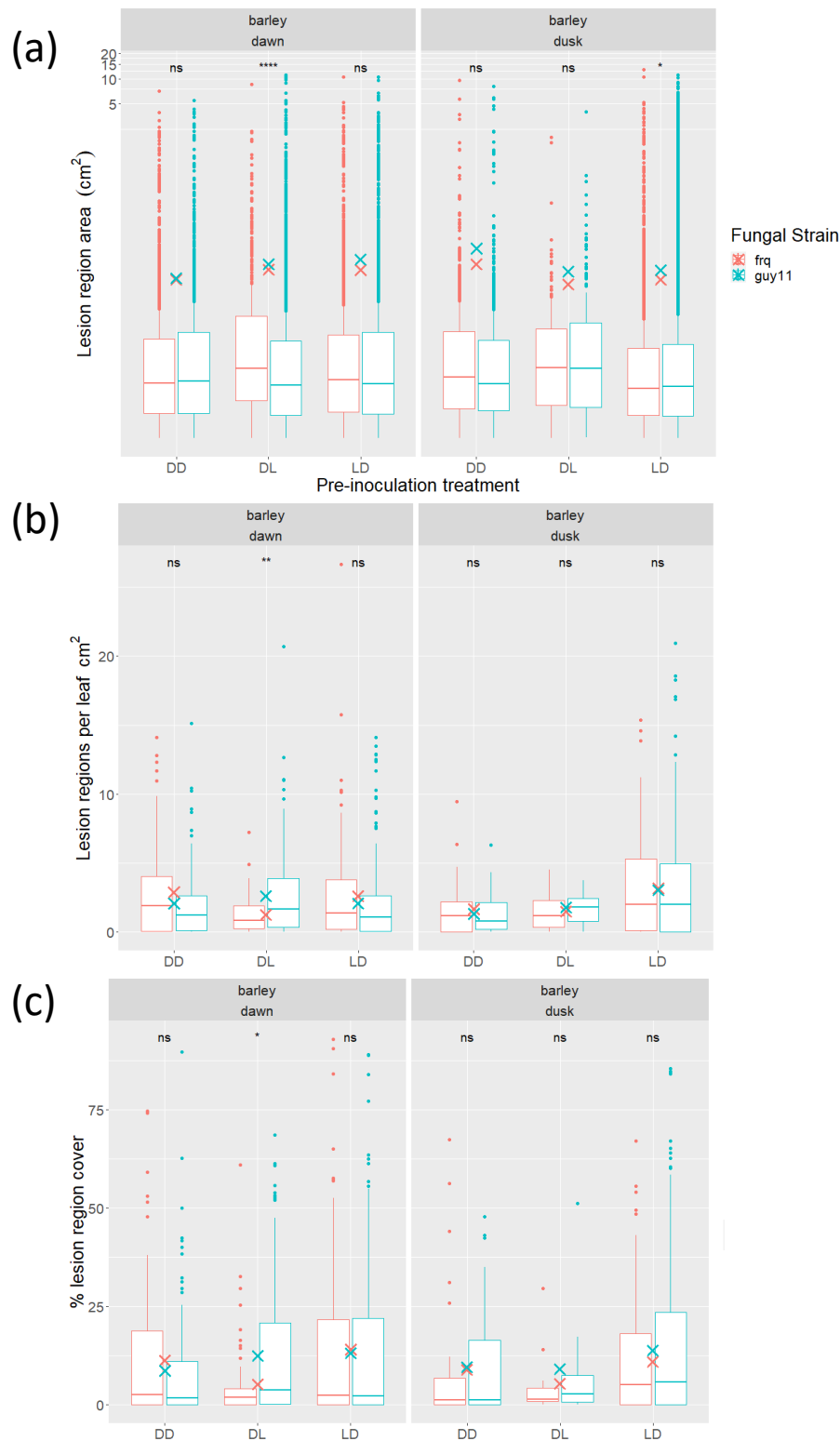


Figure 6.26: *FRQ^{NIN}* mutants display reduced antiphase-entrained pathogenicity. (a) *FRQ^{NIN}* produces smaller lesions than the wild type at dawn after DL entrainment and at dusk after LD entrainment, suggesting reduced (subjective) dusk pathogenicity (n = 2100 lesions DL guy11/ 2113 *FRQ^{NIN}* DD dawn, n = 508 guy11/ 623 *FRQ^{NIN}* DD dusk, n = 4183 guy11/ 746 *FRQ^{NIN}* DL dawn, n = 172 guy11/ 167 *FRQ^{NIN}* DL dusk, n = 3276 guy11/ 2546 *FRQ^{NIN}* LD dawn, n = 11215 guy11/ 3898 *FRQ^{NIN}* LD dusk). Antiphase entrainment also displays (b) lower lesion densities and (c) lower lesion coverage at dawn/ subjective dusk (n = 97 leaves guy11/ 93 *FRQ^{NIN}* DD dawn, n = 39 guy11/ 32 *FRQ^{NIN}* DD dusk, n = 151 guy11/ 62 *FRQ^{NIN}* DL dawn, n = 10 guy11/ 11 *FRQ^{NIN}* DL dusk, n = 196 guy11/ 113 *FRQ^{NIN}* LD dawn, n = 374 guy11/ 118 *FRQ^{NIN}* LD dusk). Stars represent increasing statistical significance (Dunn's test, p < 0.05), and crosses represent mean values.

6.2.8.2 FRQ^{NIN} does not display time of day-dependent non-host virulence

In barley inoculations, LD-entrained FRQ^{NIN} infections showed increased lesion sizes at dawn, whereas DD-entrained infections displayed increased sizes at dusk – antiphase entrainment showed no significant difference in lesion size between dawn and dusk (Fig. 6.27). However, inoculation time had no effect on FRQ^{NIN} lesion density after constant darkness, in-phase, or antiphase pre-inoculation entrainment, suggesting that FRQ^{NIN} may have lost its gating of penetration or early cell-cell movement timing in non-host interactions (Fig. 6.27). In further support of this, FRQ^{NIN} leaf coverage shows no significant difference between dawn and dusk under any pre-inoculation treatments (Fig. 6.27).

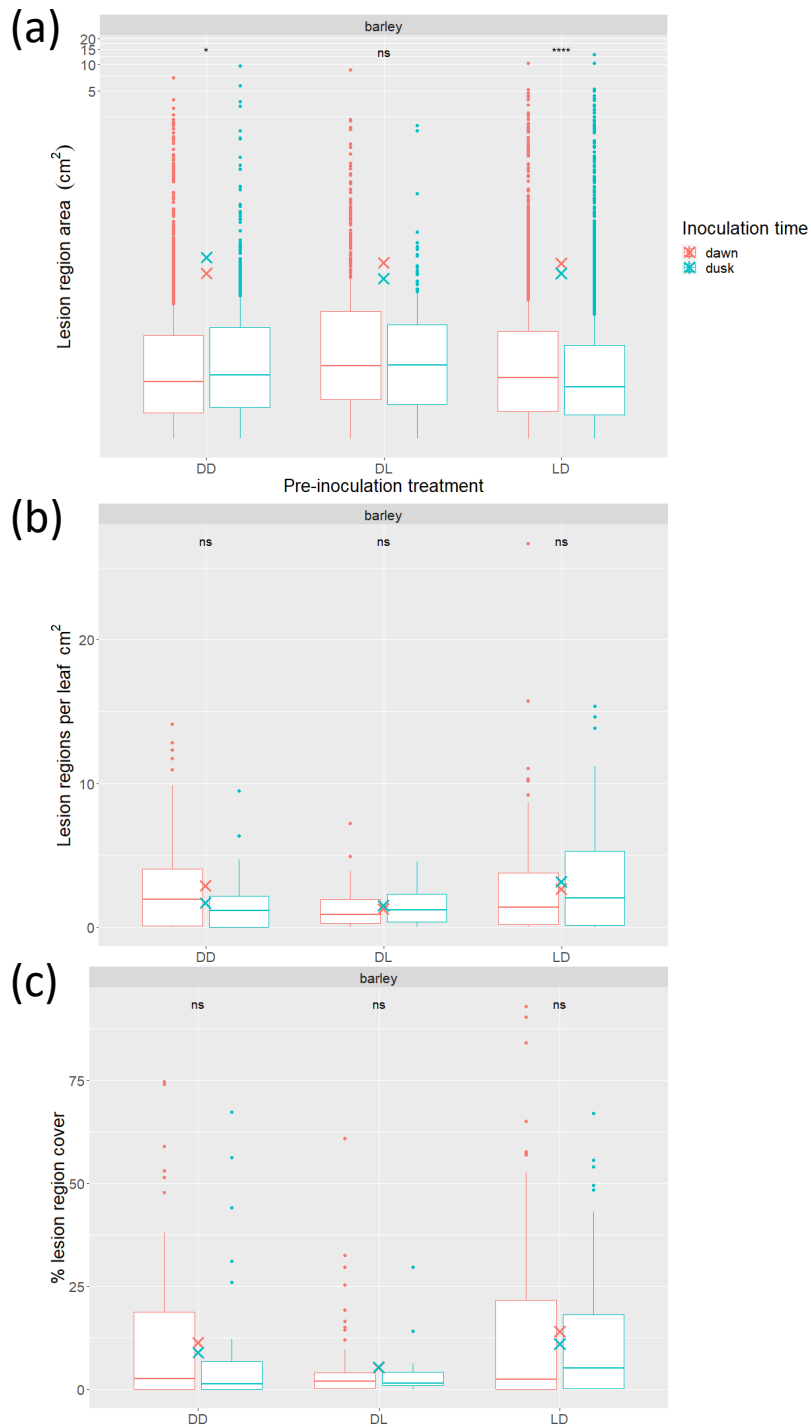


Figure 6.27: Pre-inoculation entrainment has little effect on time of day-dependent infection severity in FRQ^{NIN}-barley inoculations. (a) DD and LD-entrained FRQ^{NIN} inoculations gave rise to smaller and larger lesions at dawn and dusk, respectively (n = 2113 lesions DD dawn/ 623 dusk, n = 746 DL dawn/ 167 dusk, n = 2546 LD dawn/ 3898 dusk). Pre-inoculation entrainment had no effect between dawn and dusk inoculations in terms of (b) lesion density and (c) lesion coverage (n = 93 leaves DD dawn/ 32 dusk, n = 62 DL dawn/11 dusk, n = 113 LD dawn/ 118 dusk). Stars represent increasing statistical significance (Dunn's test, p < 0.05), and crosses mean values.

6.2.8.3 Antiphase entrainment reduces dawn pathogenicity in FRQ^{NIN}

Compared to the base mean, DD-entrained FRQ^{NIN} lesions are smaller at dawn and larger at dusk, whereas antiphase lesions are larger in dawn inoculations (subjective dusk) and smaller at dusk (subjective dawn) (Fig. 6.28). LD-entrained FRQ^{NIN} lesion area did not deviate from the base mean, suggesting FRQ^{NIN} may be more virulent at dusk towards barley in a similar manner to the wild type (Fig. 6.28). In contrast to pre-inoculation light conditions affecting lesion size, light conditions had no significant effect on lesion density in barley at both dawn and dusk; no treatments deviated significantly from the base mean. In a similar manner to rice inoculations, antiphase pre-entrainment conditions showed a reduction in lesion coverage at dawn compared to other treatments, further showing that asynchrony with the plant has an increasingly negative effect on FRQ^{NIN} pathogenicity.

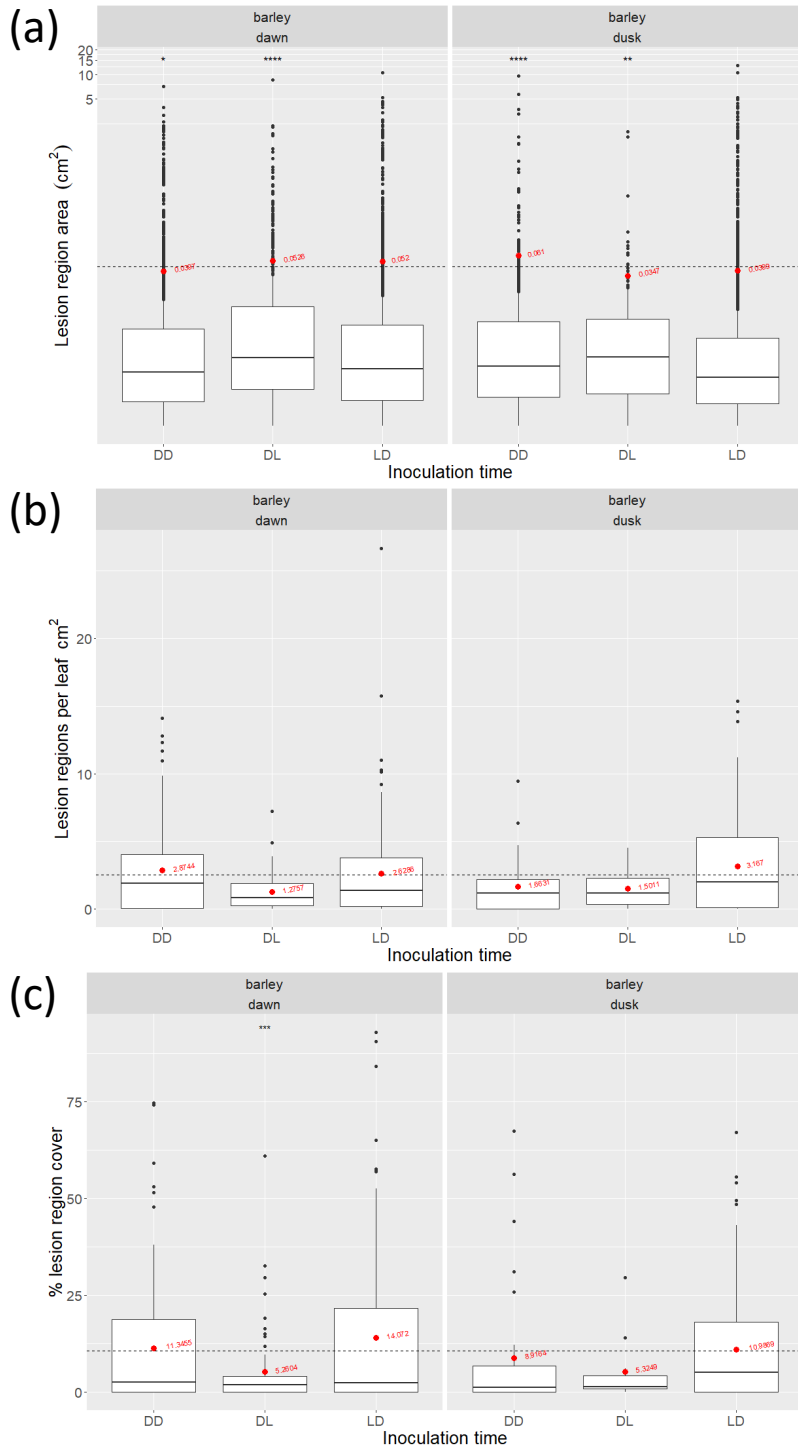


Figure 6.28: Antiphase entrainment to the host in *FRQ^{NIN}* reduces disease severity. (a) DD entrainment gives rise to smaller lesions at dawn and larger lesions at dusk, whereas antiphase DL entrainment causes larger lesions at dawn and smaller lesions at dusk ($n = 2113$ lesions DD dawn/ 623 dusk, $n = 746$ DL dawn/ 167 dusk, $n = 2546$ LD dawn/ 3898 dusk), (b) pre-inoculation entrainment has no effect on lesion density, regardless of inoculation timing, and (c) DL entrainment causes reduced lesion coverage at dawn (subjective dusk) in *FRQ^{NIN}* ($n = 93$ leaves DD dawn/ 32 dusk, $n = 62$ DL dawn/11 dusk, $n = 113$ LD dawn/ 118 dusk). Stars represent increasing statistical significance (Dunn's test, $p < 0.05$), and red dots/text denotes mean values for each group.

6.2.9 FRQ^{NIN} maintains optimal leaf size in rice infections

When ignoring time of day effects, FRQ^{NIN} shows similar, although dampened lesion density profiles in rice and barley, with slightly lower maximal lesion densities (Fig. 6.29). In rice, FRQ^{NIN} lesion density decreases as leaf area increases, unlike in the wild type, where the highest lesion densities are in the smallest leaves and those between 10-15 cm². The density profile observed in barley is similar to the wild type, and displays near-identical preferences for leaf areas ~10 cm².

When accounting for time of day, however, FRQ^{NIN} lesion density show wild-type like lesion density profiles at dawn in barley and dusk in rice which, incidentally, are the times of day when those respective plants are least susceptible to infection (disease severity is highest at dawn in rice and at dusk for barley in wild type infections), perhaps suggesting that FRQ gates virulence in *M. oryzae* or aids in the interpretation of plant-derived signals (Fig. 6.29). At dawn in rice, FRQ^{NIN} lesion density decreases near-linearly as leaf area increases, unlike the wild type which shows highest densities in the smallest leaves and those above 10 cm². Interestingly, FRQ expression and subsequent protein levels are highest in the circadian morning, so perhaps FRQ represses virulence early in the day, and therefore has little effect in the circadian evening, when FRQ levels are lower, which would explain the wild type-like profile seen in dusk inoculations.

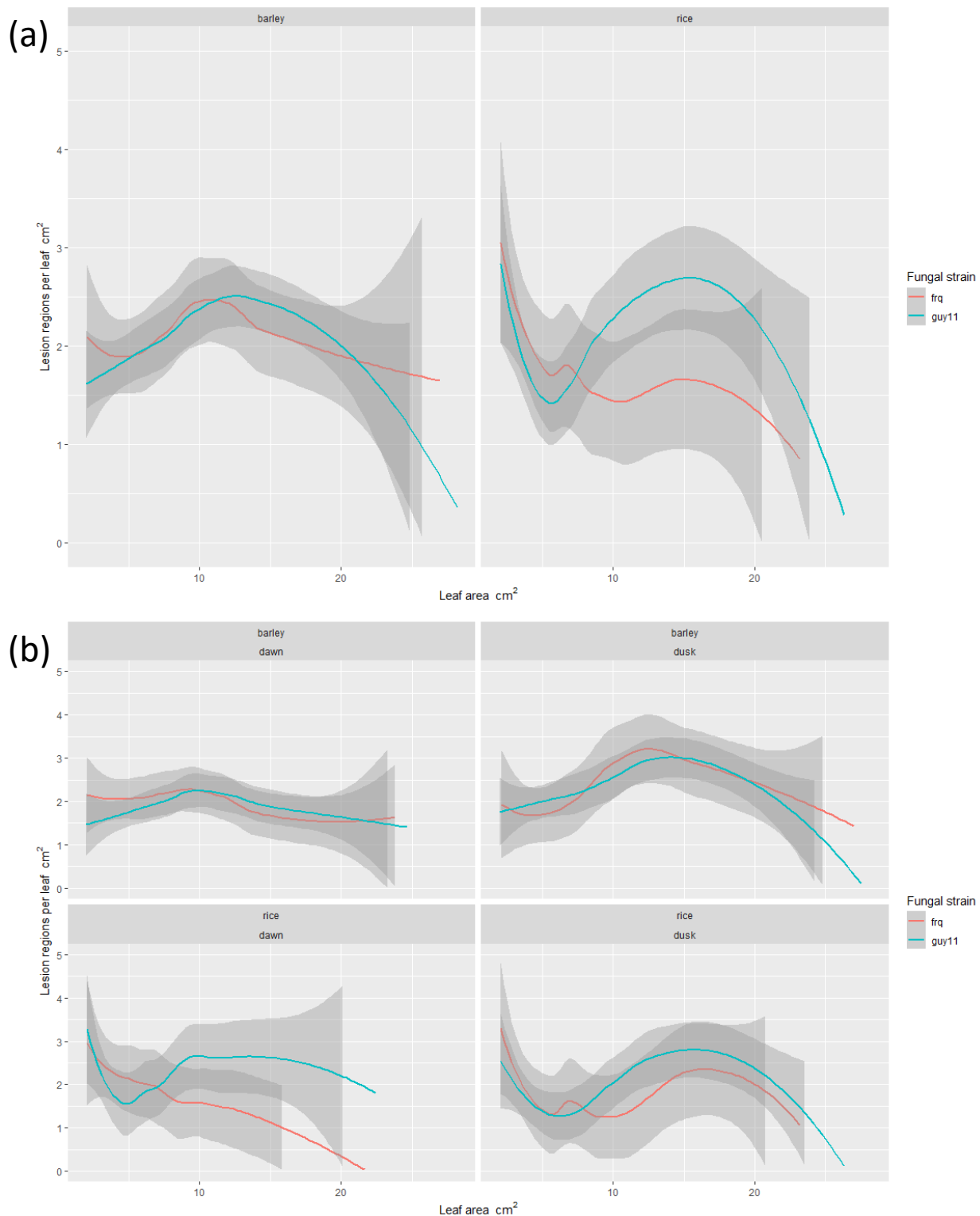


Figure 6.29: FRQ^{NIN} plays a role in host-dependent dawn virulence. (a) FRQ^{NIN}-barley infections do not display any leaf area-dependent lesion densities when inoculation timing is ignored, and FRQ^{NIN} lesion densities in rice decrease as leaf area increases. However, (b) when accounting for inoculation timing, FRQ^{NIN} lesion densities follow a similar profile as the wild type at dawn in barley and dusk in rice (sub-optimal infection timings). In contrast to the wild type, FRQ^{NIN}-rice infections show a near-linear decrease in densities at dawn and show a higher lesion density than the wild type in 10-15 cm² ('adolescent') leaves in barley at dusk (n = 444 leaves guy11 / 268 FRQ^{NIN} barley dawn, n = 423 guy11 / 161 FRQ^{NIN} barley dusk, n = 205 guy11 / 148 FRQ^{NIN} rice dawn, n = 264 guy11 / 115 FRQ^{NIN} rice dusk). Data displayed using Loess smoothed conditional means, grey shading denotes standard error.

6.2.10 Δ WC2 mutation has a more severe impact on pathogenicity than FRQ^{NIN}

6.2.10.1 Δ WC2 is less pathogenic than FRQ^{NIN} in rice inoculations after LD entrainment

Compared to FRQ^{NIN}, WC2 produces larger lesions after synchronous LD entrainment with the rice plant host at both dawn and dusk, but there were no differences between the mutants after antiphase and constant darkness entrainment (Fig. 6.30). Further, FRQ^{NIN} and WC2 mutants display no difference in lesion density in rice, except at dusk after LD entrainment, where WC2 produces fewer lesions per leaf cm² (Fig. 6.30). Together, these results again suggest that lesion density and average lesion size are negatively correlated and that WC2 may have lost its dusk virulence (Fig. 6.30). In support of this, FRQ^{NIN} lesions cover a greater proportion of infected leaves at dusk after LD entrainment only, despite the (on average) larger WC2 lesions observed at this time (Fig. 6.30). There were no significant differences observed in terms of lesion size, density, or cover under DD and DL entrainment conditions at dawn or dusk, suggesting that mutations in both WC2 and FRQ negatively affect virulence.

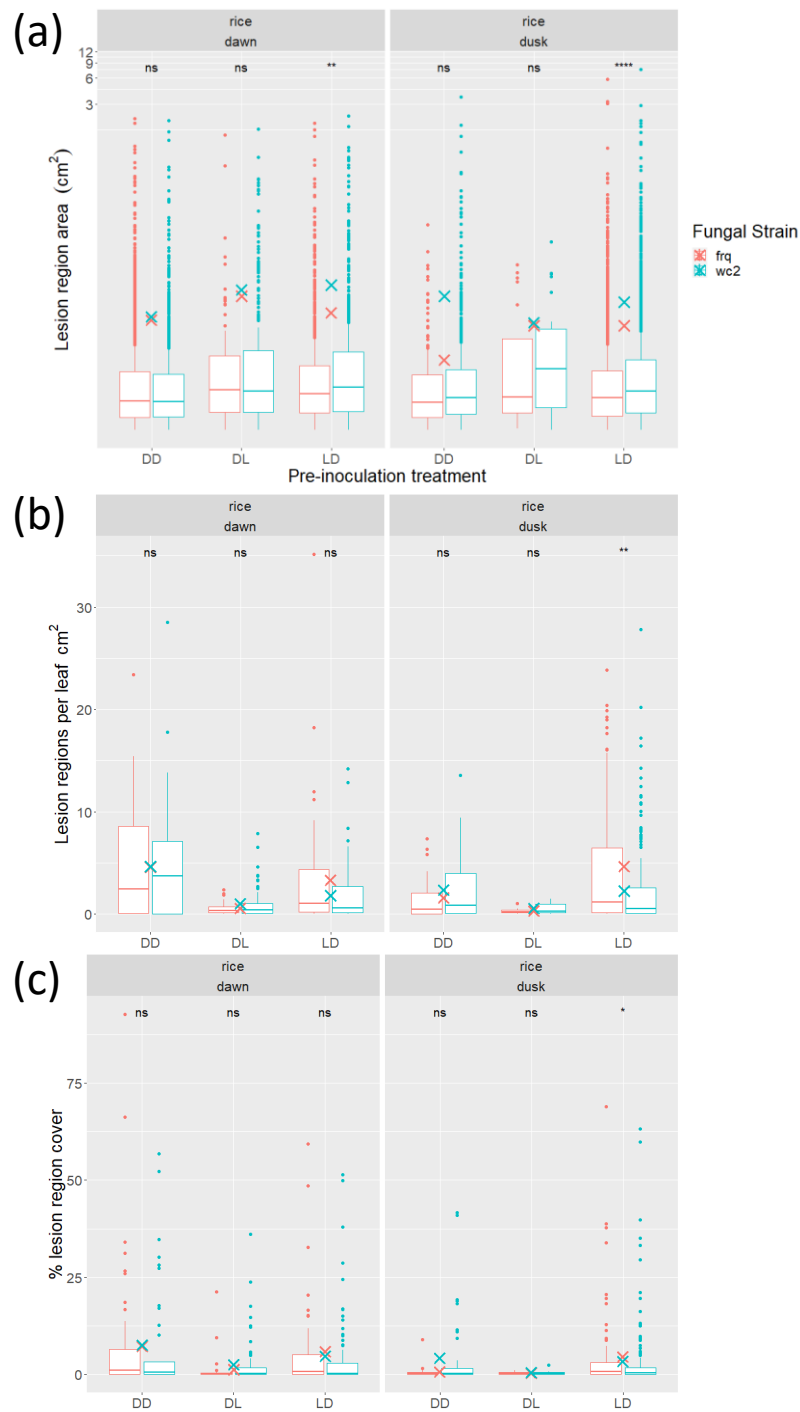


Figure 6.30: The $\Delta WC2$ mutants are less pathogenic than FRQ^{NIN} towards rice. (a) FRQ^{NIN} produces smaller lesions than $\Delta WC2$ at in rice infections after LD entrainment (n = 1094 lesions $\Delta WC2$ / 1924 FRQ^{NIN} DD dawn, n = 697 $\Delta WC2$ / 235 FRQ^{NIN} DD dusk, n = 358 $\Delta WC2$ / 138 FRQ^{NIN} DL dawn, n = 29 $\Delta WC2$ / 20 FRQ^{NIN} DL dusk, n = 624 $\Delta WC2$ / 1094 FRQ^{NIN} LD dawn, n = 2749 $\Delta WC2$ / 3479 FRQ^{NIN} LD dusk). However (b) FRQ^{NIN} produces more lesions at dusk after LD entrainment and (c) covers a greater proportion of leaves (n = 41 leaves $\Delta WC2$ / 59 FRQ^{NIN} DD dawn, n = 45 $\Delta WC2$ / 22 FRQ^{NIN} DD dusk, n = 63 $\Delta WC2$ / 31 FRQ^{NIN} DL dawn, n = 9 $\Delta WC2$ / 9 FRQ^{NIN} DL dusk, n = 83 $\Delta WC2$ / 58 FRQ^{NIN} LD dawn, n = 177 $\Delta WC2$ / 84 FRQ^{NIN} LD dusk). Stars represent increasing statistical significance (Dunn's test, p < 0.05), and crosses mean values.

6.2.10.2 Δ WC2 is less pathogenic than FRQ^{NIN} towards barley under all pre-inoculation treatments and times, except after antiphase entrainment at dawn

In non-host barley inoculations, WC2 again shows a reduction in pathogenicity compared to FRQ^{NIN} (Fig. 6.31). WC2 mutants gave rise to smaller lesions than FRQ^{NIN} after LD entrainment at both dawn and dusk and at dawn after DL treatments (subjective dusk). Interestingly, WC2 gave rise to larger lesions than FRQ^{NIN} after constant dark pre-inoculation entrainment, but the median area is lower than FRQ^{NIN} at both dawn and dusk, likely as a result of their decreased lesion density (Fig. 6.31). In agreement with the penetration defects seen in WC2 rice leaf sheathe inoculations, WC2 mutants gave rise to reduced lesion densities compared to FRQ^{NIN} after DD and LD pre-inoculations at dawn and dusk, and fewer lesions at dusk after antiphase entrainment (subjective dawn) (Fig. 6.31). There were no observed differences in lesion density between FRQ^{NIN} and WC2 at dawn after antiphase entrainment (subjective dusk), suggesting that the circadian clock may gate dusk virulence (Fig. 6.31).

This reduced WC2 pathogenicity under all inoculations and times except antiphase-entrained dawn infections in barley is also seen in terms of percent leaf coverage, again suggesting that lesion density (or pathogenic load), not lesion size, is the main determinant in disease severity in both host rice and non-host barley infections (Fig. 6.31). In this way, under ecologically relevant conditions, where conidial densities and pathogenic load is not controlled for (here, all plants were inoculated with the same volume and concentration of conidial inoculum), the wild type would be most pathogenic, followed by WC2 and finally FRQ^{NIN}. Even though WC2 conidia are less virulent than FRQ^{NIN} under most conditions, the number of conidia produced per colony in FRQ^{NIN} are

~5% of the wild type and ~10% of WC2 and so would show fewer infections if spread naturally by wind and dewdrop.

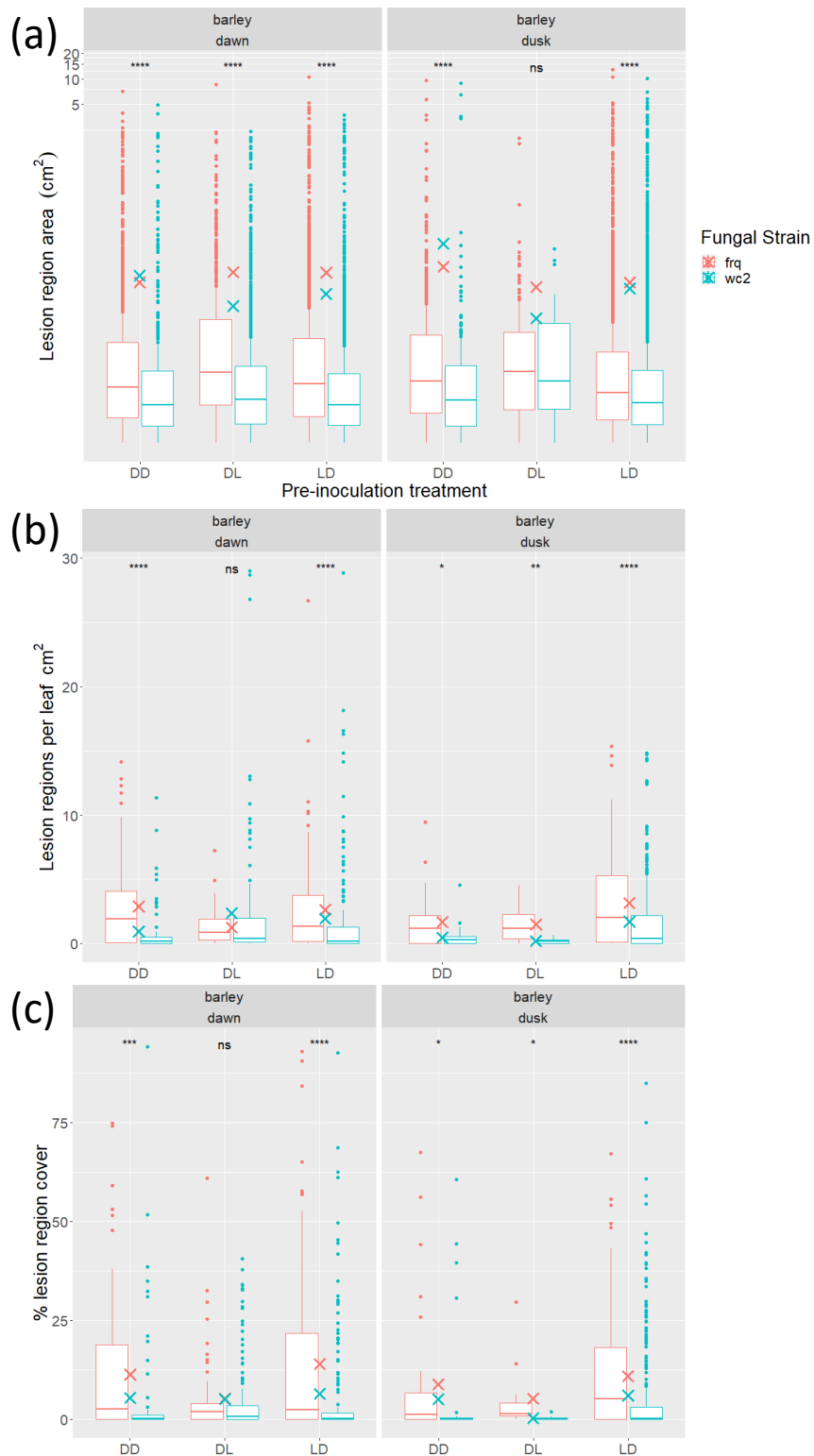


Figure 6.31: *FRQ^{NIN}* mutant strains are more virulent than their *WC2* counterpart towards barley. (a) *WC2* lesions are larger after DD entrainment at dawn and dusk, but smaller after LD entrainment, and after DL entrainment at dawn ($n = 567$ lesions $\Delta WC2$ / 2113 *FRQ^{NIN}* DD dawn, $n = 206$ $\Delta WC2$ / 623 *FRQ^{NIN}* DD dusk, $n = 1991$ $\Delta WC2$ / 746 *FRQ^{NIN}* DL dawn, $n = 24$ $\Delta WC2$ / 167 *FRQ^{NIN}* DL dusk, $n = 2371$ $\Delta WC2$ / 2546 *FRQ^{NIN}* LD dawn, $n = 5236$ $\Delta WC2$ / 3898 *FRQ^{NIN}* LD dusk). *FRQ^{NIN}* causes higher lesion densities (b) and lesion coverage (c) than *WC2* after all pre-inoculation entrainment conditions at both dawn and dusk, except after DL entrainment, where there is no significant difference between the strains ($n = 70$ leaves $\Delta WC2$ / 93 *FRQ^{NIN}* DD dawn, $n = 35$ $\Delta WC2$ / 32 *FRQ^{NIN}* DD dusk, $n = 119$ $\Delta WC2$ / 62 *FRQ^{NIN}* DL dawn, $n = 13$ $\Delta WC2$ / 11 *FRQ^{NIN}* DL dusk, $n = 158$ $\Delta WC2$ / 113 *FRQ^{NIN}* LD dawn, $n = 279$ $\Delta WC2$ / 118 *FRQ^{NIN}* LD dusk). Stars represent increasing statistical significance (Dunn's test, $p < 0.05$), and crosses mean values.

6.3 Discussion

This chapter has shown that, based on literature review, bioinformatic analyses, and experimental work, the *M. oryzae* FRQ gene occupies both MGG_17345 and MGG_17344, and that mutation to MGG_17345 can produce phenotypes indicative of FRQ dysfunction. Based on this presented work, it is difficult to determine if a true FRQ knockout/null strain has been generated in FRQ^{NIN} due to the unexpected large, semi-homology directed repair-mediated insertion and frameshift. Instead, the results obtained here may be the result of (a) a true FRQ knockout, (b) reduced/non-existent alternative splicing of FRQ, producing a higher L:S-FRQ ratio or only L-FRQ, (c) the insertion gives rise to increased phosphorylation site(s) on the FRQ mutant protein, facilitating a faster cycling and/or increased (cytoplasmic) hyperphosphorylated FRQ, or (d) an N-terminally truncated FRQ. Any of these outcomes could sufficiently explain the reported phenotypes presented in FRQ^{NIN}. Table 6.5 recontextualises Table 6.1 regarding the FRQ mutant phenotypes presented in FRQ^{NIN}, reiterating that FRQ^{NIN} is a likely a null, alternative splicing (L-FRQ), or increased phosphorylation mutant. To further determine the type of mutation presented in FRQ^{NIN}, qRT-PCR primers have been designed (using NCBI primer blast) targeting MGG_17345, which can be used in conjunction with published primers from other *M. oryzae* FRQ work targeting the region downstream of MGG_17345 (84,258,259). These experiments have not yet been performed, and thus are not covered here.

Table 6.5: Common and divergent phenotypes between a range of reported FRQ mutants and FRQ^{NIN} (green represents common phenotypes, red divergent, yellow potential, and white/NA are untested)

Species	Mutation	growth	conidiation	germination	appressoria	virulence	temperature entrainment	light sensitivity	diurnal conidial banding	circadian conidial banding	osmotic stress response	nutritional sensation	period
<i>M. oryzae</i>	C-terminal deletion	slowed	reduced	delayed	decreased	reduced	NA	NA	NA	NA	NA	NA	NA
<i>M. oryzae</i>	C-terminal insertional KO	no change	NA	no change	no change	NA	NA	NA	NA	NA	NA	NA	NA
<i>N. crassa</i>	Null	slowed	reduced	NA	NA	NA	No	altered	conditional	conditional	increased but arrhythmic	altered	shortened
<i>N. crassa</i>	coiled-coil domain deletion	NA	NA	NA	NA	NA	NA	NA	no	no	NA	NA	arrhythmic

<i>N. crassa</i>	phosphorylation site mutagenesis	NA	NA	NA	NA	NA	NA	NA	NA	NA	NA	NA	site-dependent
<i>N. crassa</i>	C-terminal deletion	NA	NA	NA	NA	NA	NA	insensitive	conditional	no	NA	NA	NA
<i>N. crassa</i>	PEST phosphorylation site change	NA	NA	NA	NA	NA	NA	NA	no	no	NA	NA	NA
<i>N. crassa</i>	PEST domain deletion	NA	NA	NA	NA	NA	NA	NA	no	no	NA	NA	NA
<i>N. crassa</i>	qrf elimination	NA	NA	NA	NA	NA	high temperatures only	yes	yes	high temperatures only	NA	NA	longer
<i>N. crassa</i>	C-terminal point mutation	NA	NA	NA	NA	NA	NA	NA	NA	NA	NA	NA	shortened
<i>N. crassa</i>	constitutive expression	NA	NA	NA	NA	NA	NA	yes	yes	no	NA	NA	arrhythmic

<i>N. crassa</i>	S85 and/or S87 substitution	NA	NA	NA	NA	NA	NA	yes	yes	no	NA	NA	arrhythmic
<i>N. crassa</i>	C-terminal phosphorylation site substitution	NA	NA	NA	NA	NA	NA	yes	yes	yes	NA	NA	shortened
<i>N. crassa</i>	codon optimisation	NA	NA	NA	NA	NA	NA	yes	no	no	NA	NA	arrhythmic
<i>N. crassa</i>	L-FRQ only	NA	NA	NA	NA	NA	NA	yes	yes	yes	NA	NA	shortened
<i>N. crassa</i>	S-FRQ only	NA	NA	NA	NA	NA	low temperatures only	yes	yes	yes	NA	NA	longer
<i>B. cinerea</i>	Overexpression	NA	NA	NA	NA	reduced	NA	no	no	no	NA	NA	arrhythmic
<i>B. cinerea</i>	Null	NA	reduced	increased aggressiveness	no change	increased aggressiveness	NA	altered	no	no	NA	altered	arrhythmic
<i>V. dahliae</i>	null	slowed	NA	NA	NA	reduced (isolate-	yes	yes	yes	No (wild type-like)	NA	altered	arrhythmic (no change)

						dependen t)							
<i>B. bassiana</i>	FRQ1 deletion	no change	delayed, reduced	NA	NA	NA	NA	yes	no	no	NA	NA	arrhythmic (no change)
<i>B. bassiana</i>	FRQ2 deletion	no change	delayed, reduced	NA	NA	NA	NA	yes	no	no	NA	NA	arrhythmic (no change)

Here, FRQ^{NIN} has been shown to maintain photosensitivity and conidial banding, albeit with a significantly shortened and light-dependent period. If a true FRQ-null mutant has been generated, which is a possibility, this implicates *M. oryzae* conidial banding as a WC-FLO (White Collar Complex-dependent FRQ-less oscillator), since conidial banding is observed and maintained under constant conditions in FRQ^{NIN} but is entirely arrested under both diurnal and constant conditions in the Δ WC2 strain (see 5.2.2.1). This is unsurprising, considering FRQ null strains have been consistently reported to be ‘conditionally rhythmic’, whereas WCC mutants commonly present a more severe effect on the circadian system, and as such, the *N. crassa* conidial banding phenotype has been suggested to be a WC-FLO (117,161,177,178,181,183,184,184,191,192,195,199,200,202,203,210,213,227,234,379,408,434,437,439,476,485,502,507–509,518,528,530,578). Concurrently, if the WCC is non-functional, then frq transcription and subsequent translation would be significantly reduced, which should mirror (some of) the phenotypes (such as conidial banding or conidiation) of an FRQ null strain (181,184,192,227). Since this is not the case for conidial banding, it is possible that FRQ is (a) not essential for conidial banding in *M. oryzae*, (b) conidial banding is a slave oscillator to the FWO, reverting back to its inherent WC-FLO period when FRQ is inactive, or (c) the phosphorylation status of FRQ is not a determinant in conidial banding, rather its abundance and (cytoplasmic) concentration, which, in the wild type, is partially dependent on phosphorylation status, since FWD1 acts to clear hyperphosphorylated FRQ from the cytoplasm (161,178,181,183,184,189,191,193,195,210,229,235,259,485,509). In this way, FRQ may act to inhibit conidiation during the daylight hours, when it is highly abundant and active in both the nucleus and the cytoplasm, prior to complete inactivation of WCC-mediated

frq transcription and phosphorylation-dependent degradation of FRQ protein. When FRQ levels eventually fall towards the end of the circadian day due to a lack of WCC-based transcription and FWD1-mediated turnover, conidiation can begin again, forming the next dark conidial band at the end of the circadian day, prior to dawn. A differentiation must be made here between the timing of conidiation/conidial banding, and the degree of conidiation, since FRQ^{NIN} still displays this phenotype, but its conidiation capacity is severely reduced.

It is particularly interesting that the periodicity of FRQ^{NIN} is significantly reduced after transfer to constant light, but not constant darkness. This perhaps suggests that the photoadaptive capability and/or PLRE-based WCC activation is altered in FRQ^{NIN}, both of which could serve to reduce the period in a light-dependent manner. The FRQ^{NIN} mutant may also present a reduced ability to inhibit VVD activity, and thus would indirectly increase VVD-WCC formation, effectively preventing PLRE activation of frq (192,201,227,434). Alternatively, if FRQ^{NIN} has reduced positive arm activity, this would cause reduced levels of WCC because of altered FRQ-mediated WC1 post-translational stabilisation and wc2 transcriptional upregulation, and the resulting reduction in functional WCC levels could cause the clock to cycle faster under prolonged light exposure(178,181,201).

As reported previously, FRQ likely plays a role in nutritional sensation and signalling (117,213,434,574). Indeed, in the *M. oryzae* FRQ^{NIN} strain presented here, the latency period prior to conidial banding is significantly increased, but this mutant has been shown to produce wild type-like levels of the conidial banding metabolite(s), which suggests altered, but not complete, insensitivity. This phenotype is somewhat reminiscent of Tong

and colleagues' (232) report, where non-functional FRQ1/2 mutants in *B. bassiana* showed delayed conidiation, so perhaps there is a common nutrient or nutritional signal-dependent phenotype between the two fungal pathogens. Deng and colleagues (84) also showed that deletion of the *M. oryzae* rhythmic gene TWILIGHT (TWL, as mentioned in previous chapters) causes altered nutritional utilisation and redox homeostasis, and significantly reduced conidiation and pathogenicity. Wild type *twl* transcription also shows a similar but phase-advanced expression pattern compared to *frq*, instead peaking just prior to dawn and dusk (hence its appropriate name) (84). Further, Deng and colleagues showed that wild-type *M. oryzae* utilises rice- (host) derived nutrients significantly better than barley- (non-host) derived nutrients, where colonies produced over twice as many conidia on rice extract media compared to barley extract media. This observation was maintained in the TWL mutant, but to a reduced extent, suggesting that TWL is not absolutely essential for nutritional preference (84). Many of the aforementioned phenotypes are similar to those presented in FRQ^{NIN}, suggesting that FRQ may regulate TWL or vice versa, perhaps alongside the WCC. Deng and colleagues subsequently showed that TWL is unlikely to be a core component of the clock and instead is a clock-controlled gene, and therefore likely to be regulated by FWO in a circadian manner.

The most striking phenotype presented by FRQ^{NIN} is the profound reduction in conidiation, to the point at which many conidia-dependent experiments could not be performed. Under all entraining conditions, FRQ^{NIN} produces almost an order of magnitude fewer conidia per colony than the wild type, despite showing only a mildly decreased growth rate under some entrainment conditions, which suggests that conidiation is not dependent on vegetative growth rates in *M. oryzae*. Further, constant

dark entrained FRQ^{NIN} strains produce more conidia than any other treatment, implying that FRQ^{NIN} conidiation is hypersensitive to light under any circumstances (LD, LD-DD, LD-LL, LL), perhaps through altered VVD or WCC regulation. A reduction in conidiation, whilst not necessarily impacting virulence and pathogenicity directly, should significantly reduce rice blast propagation in the wild due to a decreased pathogenic load, as fewer conidia should cause fewer penetrations and subsequent infections. Indeed, as reported throughout (chapters 4, 5, and 6), lesion density, not lesion size, is the main determinant of disease severity, and thus more conidia should give rise to a more severe disease outcome.

Interestingly, whilst FRQ^{NIN} conidia are less likely to germinate (a phenotype reminiscent of Shi and colleagues (259) and Park and Lee's (258) studies on *M. oryzae* FRQ and FWD1), possibly due to reduced conidial size (and, by proxy, resources), they are as, if not more, likely to produce appressoria compared to the wild type within a given time frame (8 h here). Indeed, Hevia and colleagues (117) reported an increased 'aggressiveness' in *B. cinerea* FRQ null conidia, which suggested that FRQ inhibits conidial germination (and perhaps subsequent virulence) at certain times of day, until disease-conducive environmental conditions are met (117,258,259). A similar phenomenon might be presented here, as FRQ^{NIN} may no longer be able to repress virulence traits, thereby causing increased conidial developmental rates and an 'always virulent' phenotype. Δ WC2 (which is seemingly light insensitive) also displays faster conidial developmental rates, as does the constant light-entrained wild type, which could phenocopy the FRQ sensitivity, since conidial development assays are performed under constant light (see 2.6). Likewise, Kim and Lee and colleagues' WC1 null mutant, which (like WC2 dysfunction) also reduces FRQ transcription, shows a loss of light-dependent disease

repression, further implicating the circadian clock and light in the negative gating of virulence during the (circadian) day (82,101).

FRQ^{NIN} appressoria were shown to be more resistant to cytorrhysis and thus likely produced higher appressorial turgor pressure, which can be used to penetrate the host plant cuticle. Supportingly, the clock is known to control osmotic stress responses in a wide range of species (101,113,139,151,152), including in *N. crassa*, where altered clock function, specifically *frq* knockouts, can increase the osmotic stress response, suggesting that the core clock component(s) inhibits osmotic stress response gene(s) in a rhythmic manner (184,192,439). However, Kim and colleagues (101) reported that WC1 mutation had little effect on osmotic stress responses in *M. oryzae*, which instead implicates FRQ as having an extra-circadian and repressive role in conidial germination, development, and appressorial stability. Despite FRQ having extra-circadian function, FRQ itself is a rhythmic and circadian gene, so any processes influenced by FRQ subsequently become circadian themselves, and thus can be described as slave oscillators.

Altogether, the *M. oryzae* FRQ may serve to inhibit virulence in a daytime-dependent manner which, incidentally, is when FRQ protein levels are at their highest in *N. crassa* and *M. oryzae* (178,181,192,201,212,221,225,437). In support of this, FRQ^{NIN} shows no significant defects in host plant penetration or cell-cell movement after LD entrainment, further suggesting that FRQ is not essential for virulence. However, asynchronicity with the plant consistently reduces virulence in FRQ^{NIN}, suggesting reduced interpretation of host-derived temporal signals. If FRQ does temporally gate and inhibit pathogenesis, from an evolutionary standpoint it would be beneficial to be constantly virulent at all times of day at a basal level or by 'default', which upon gain of function of temporal inhibitors of

virulence would restrict virulence to disease-conducive times of day only, acting to reduce resource expenditure, as virulence-related products would undoubtedly be energetically expensive. As mentioned above (6.1.3.8), FRQ is potentially the most recent addition to the clock over an evolutionary timescale (441,457). It would, therefore, be interesting to determine if the conservation of FRQ is particularly enriched or conserved in the opportunistic (plant) fungal pathogens that (unlike *M. oryzae* or *B. cinerea*) are less able to infect their host outside of disease-conducive times of day, such as when the stomata are open.

M. oryzae also seems to display host- (rice) and non-host (barley) differences in time-of-day effects and disease severity, similar to the wild type (4.2.6) and reminiscent of Deng and colleagues' study (84) with rice vs barley extract (see above). Circadian mutation can subsequently alter pathogenicity in a (seemingly) host species-dependent manner, similar to that observed by Cascant-Lopez and Ruiz-Roldan (84,434,456). Likewise, *M. oryzae* displays behaviour indicative of necrotrophic (as opposed to hemibiotrophic) pathogenesis in *Arabidopsis* infections, where the pathogen does not utilise 3 genes essential for rice pathogenesis, showing a diversity of infection mechanisms depending on the host species (480). As mentioned in previous chapters, however, the differences in time of day-dependent disease outcomes between species may be a result of altered susceptibility or defence regulation in the plant host as opposed to *M. oryzae* virulence.

Summarily, whilst FRQ^{NIN} predominantly displays wild type-like virulence and pathogenicity towards rice (and to a lesser extent towards barley), the *M. oryzae* FRQ may indirectly determine pathogenicity by inducing conidiation, and likely represses

virulence-related traits (including conidial and appressorial development, osmotic regulation, and nutritional sensation/acquisition) in a daylight-dependent manner.

7 General discussion

7.1 Context

Circadian clocks are found almost ubiquitously in biological organisms, including plants and their pathogens; recent evidence shows plant defence to be gated in a circadian manner, allowing plants to coordinate gene expression and metabolism to anticipate attack (77,103,111,117,121,136,152,158,159,253,388,419,456,460,489,490,493).

Likewise, the circadian clock in phytopathogenic fungi is important in disease outcome, where dysfunction of clock components can alter fitness- and pathogenesis-related traits, including growth rates, asexual and sexual reproduction, conidiation, germination and development, and even virulence directly (82,84,101,103,108,116,117,119,212,215,232,258,259,392,412,413,430,434,448,456,460,467,473).

M. oryzae has repeatedly been shown to display diurnal and circadian phenotypes, most strikingly rhythmic conidiation, where translucent, hyaline and vegetative growth occurs during the daytime, and dark, melanised growth associated with conidiation occurs at night

(82,101,104,108,110,177,180,181,192,194,198,215,259,371,448,452,479,503,508,515,610). The circadian clock and blue light are closely tied, as a core clock protein, WC1, functions as a blue light photoreceptor; and the accessory circadian protein, VVD (which is responsible for the photoadaptation of the clock) senses and responds to blue light (82,101,101,108,116,118,119,178,181,184,198,201,205,207–210,214,215,225,232,234,259,370,392,409,413,434,448,458,479,513,540,610,611).

In the model clock fungus, *N. crassa* (a fellow member of the Sordariomycetes), this diurnal banding pattern can continue to occur in free running, constant conditions, where one banding cycle (hyaline growth followed by carotenised, orange growth) occurs approximately every 24 h and, as such, is a circadian phenotype (161,178,181,183,192,198). Conidial banding can be arrested in *N. crassa* when core components of the circadian clock are rendered dysfunctional through genetic techniques (177,184,199,202,227,234,379,437,485,502,507,508,511,512,518).

It has been shown in the literature, with bioinformatic analyses, and experimentally (herein) that *M. oryzae* likely possesses all the necessary and accessory genes responsible for a circadian clock (Chapters 4, 5, and 6, and (82,84,101,258,259)). There has been previous convincing evidence towards *M. oryzae* displaying circadian gene regulation, such as that shown in TWL (84), and FRQ (259), but to date no study has been performed on the role of time of day, entrainment, and how core clock mutation affects *M. oryzae* growth, development, and virulence. Other work has addressed facets of these in isolation, but not in its entirety (82,84,101,258,259).

7.2 Study aims

This study, therefore, sought to determine how timing, entrainment, and circadian function ultimately affects the pathogenicity of *M. oryzae* and, to a lesser extent, the time of day-dependence of susceptibility in host- and non-host plants toward rice blast disease. To address these topics, several novel image analysis-based toolkits were developed (Chapter 3) to assess pre- and post-inoculation behaviour of *M. oryzae* and its ability to cause disease in plants, and mainly focussed on (a) the *ex-planta* growth on petri dishes and its diurnal/circadian behaviour, (b) conidiation and conidial development, and

(c) disease severity as a result of rice blast infection. These tools, alongside CRISPR-based mutation of the *M. oryzae* core clock components, WC2 and FRQ, facilitated some progress toward addressing the aforementioned agriculturally relevant issues.

7.3 Key findings

7.3.1 *M. oryzae* has a functional, nutritionally compensated circadian conidial banding phenotype

Firstly, circadian function was studied in *M. oryzae*, where it displays a conidial banding phenotype indicative of a nutritionally compensated circadian rhythm. Here, *M. oryzae* was grown under constant darkness or light (DD, and LL, respectively) for several days, where no obvious banding occurred under any circumstances, unlike entrainment to 12 h light/dark cycles (LD). After a sufficient period of entrainment under LD conditions (usually 10 d throughout this work), however, *M. oryzae* could be moved to constant conditions (LD-DD or LD-LL) and still display conidial banding with a period of approximately 24 h and thus, was likely a circadian rhythm.

One of the key facets of circadian rhythmicity is the nutritional and/or temperature compensation in these oscillations, where the periodicity should be maintained under a range of different, but physiologically relevant conditions (174,181,183,196,228,257,404,459,476,485). *M. oryzae* was therefore submitted to constant conditions after entrainment to LD whilst grown on minimal media (MM), complete media (CM), and CM supplemented with spent media from shaking culture of *M. oryzae* (SM). Conidial banding again continued to occur with a period of ~ 24 h, indicative of a functional circadian clock.

7.3.2 WC2 is necessary for conidial banding

Upon disruption of the core clock gene, WC2, in *M. oryzae*, conidial banding was completely arrested under all experimental conditions, even LD. WC2 is therefore absolutely essential for conidial banding and the rhythmic differentiation of growth types. It is important to consider here that whilst the WC2 mutant lost all conidial banding, it does not necessarily mean that Δ WC2 has lost all clock function: conidial banding is merely a readout of the circadian clock. Likewise, there are several examples where core clock knockout mutants still exhibit circadian regulation of gene expression, but WC2 has been suggested to be the key determinant in the canonical circadian system in fungi (216,227,437). Indeed, circadian rhythmicity has repeatedly been shown to have a level of redundancy, with WC-FLOs and FLOs (175,181,183–185,188,189,191,192,196,210,213,457,485,509,513).

7.3.3 FRQ is not required for conidial banding, but affects the period of the clock

In agreement with this circadian redundancy, upon mutation of the *M. oryzae* FRQ (MGG_17345 – 17344) gene, diurnal and circadian conidial banding was maintained, in spite of other severe phenotypes. These results therefore imply that the core clock gene FRQ may not be necessary for conidial banding in *M. oryzae* and it may instead be a WC-FLO (as is the case in *N. crassa*). However, as discussed in 6.2.2, the semi-HDR mediated insertional mutation of FRQ^{NIN} may not have generated a true null strain, and thus the FRQ mutant may still produce (semi-) functional protein. This insertional mutation did give rise to phenotype(s) indicative of FRQ dysfunction, though: FRQ^{NIN} displays a significant reduction in the circadian period (the amount of time taken to complete one cycle of the clock), in a light-dependent manner, where upon transfer to constant light, its period was significantly reduced, but maintained at approximately 24 h in constant

darkness. Concurrently, the period of the wild type was also shortened under constant light, but the extent of this shortening in FRQ^{NIN} was more severe, where FRQ^{NIN}'s cycle is approximately 5 h shorter than the wild type under the same conditions. This reduced periodicity has been observed previously upon FRQ mutation (161,178,181,193,195,203,221,527,530), which implicates conidial banding as a slave WC-FLO, where conidial banding is absolutely dependent on WCC function, and reverts to its inherent and light-dependent period when FRQ is absent or dysfunctional (178,181,183,184,191,210,485,509).

7.3.4 Conidiation, conidial banding, and conidial development is controlled by nutritional status and secreted metabolite(s)

Interestingly, even though the circadian rhythm was maintained on differing media, the latency period, i.e., the number of days prior to the overt conidial banding pattern, was significantly altered, where minimal media increased the latency period, and SM (where the nutrients are at least in excess) reduced the latency period consistently. Further, double concentrated media (2x CM, where all the nutrient concentrations were doubled) did not significantly alter the latency period. Together, these results suggested that, as opposed to an abundance or lack of nutrients, some sort of metabolite or secreted product is responsible for the latency period, and that there may be a minimum threshold of biomass/growth/population density of *M. oryzae* required to produce this metabolite to sufficient levels. The spent media could be autoclaved, stored for long periods of time, diffuse through cellophane, and filtered through 10 kD pores but still maintain its efficacy, so is unlikely to be protein-based and may be a small molecule(s). Further, since the spent media was effective in a dose-dependent manner, it may serve as a quorum sensing molecule(s) (612–617).

The colonies cultured on this spent media also showed increased growth rates, perhaps as a result of the reduced latency period (*M. oryzae* colonies were shown to have an increased growth rate post-conidial banding), and so it may cause colonies that are present in regions with high population densities (indicated by relatively high concentrations of the spent media metabolite(s)) to spread out further in order to locate regions with lower population densities and, therefore, potential available nutrients. In support of its role in competitive inhibition, culture on SM also decreased conidiation in the wild type despite its increased growth rate. Further, conidial germination and appressorial development was almost completely arrested when conidia were resuspended in SM instead of water. This might provide an additional element of competitive inhibition, where if conidia land in an area with high population densities, the relatively high concentration of the metabolite(s) would prevent new colonies from forming in the area. Altogether, the 'mystery metabolite(s)' serves to reduce the latency period, increase vegetative growth, suppress conidiation, and arrest conidial germination and development, and thus is an excellent target for a novel fungicide(s).

7.3.5 FRQ and WC2 have roles in nutritional sensation

Whilst the focus on spent media and the latency period is seemingly tangential, circadian machinery has been shown to be (at least partly) responsible for nutritional sensation, including in *M. oryzae* (82,84,116,117,161,177,181,183,189,191,210,212,257,413,509). In this study alone, the $\Delta WC2$ mutant generated did not show conidial banding under any conditions, even when cultured on SM. $\Delta WC2$ was shown to produce the conidial banding metabolite, but was completely insensitive to it, since the wild type *guy11* showed the decreased latency period when cultured on WC2-SM. Likewise, the FRQ^{NIN} insertional mutant generated in this work still displays conidial banding, but its latency period is

significantly increased, usually by at least 2 d, reminiscent of the wild type when grown on MM. Upon culture on wild type SM, FRQ^{NIN}'s latency period was reduced by 2 d, similar to the wild type. However, since the concentration of the conidial banding metabolite is unlikely to decrease in the media and, if anything, should increase, it is instead suggested that FRQ^{NIN} displays reduced sensitivity to the metabolite(s). These results complement those generated by Deng, Lee, and Kim and colleagues, where *M. oryzae* TWL mutants showed reduced (light and species-dependent) nutritional sensitivity to plant-derived nutrients, and WC1 was expressed differentially depending on nutritional composition (CM, CM without nitrogen or carbon, minimal media, CM supplemented with H₂O₂ as an oxidative stress, or CM supplemented with NaCl as an osmotic stress) (82,84,101).

7.3.6 Circadian entrainment and function plays a role in vegetative growth

As well as affecting conidial banding, differing entrainment conditions and circadian mutation also impacted colony growth rates. Overall, constant conditions (LL and DD) increased growth rates relative to colonies grown under LD conditions. However, after the latency period had elapsed and conidial banding began to occur, the average daily growth rates of colonies entrained under LD conditions (including LD-DD and LD-LL) grew significantly faster, implicating the clock in the rhythmic gating of vegetative growth and asexual development. Accordingly, the transcription of anabolic and catabolic functions in *N. crassa* is controlled in a rhythmic fashion, where (subjective) dawn predominantly upregulates catabolic genes, and (subjective) dusk upregulates anabolic genes (417): CSP1 (which controls ergosterol synthesis and membranous lipid composition) is activated by the WCC in a morning-specific manner (219,220), haem biosynthesis is regulated by the WCC in *C. neoformans* (467), WC1 mutation in *F. oxysporum* causes impaired carotenogenesis (456), and WC1 mediates secondary metabolism in *C. militaris*

(430), amongst several other examples (84,101,116,177,181,188,198,204,215,231,240,377,392,434,474,513,618). Upon circadian mutation, WC2 and FRQ both maintained increased average growth rates under constant conditions, which was particularly surprising for WC2, considering its lack of conidial banding and suggests maintained light/dark perception (or that light-dark cycles initially slow the growth of wild type *M. oryzae*). Additionally, in comparison to the wild type, WC2 showed a reduced growth rate under constant darkness, LD, and LD-LL entrainment, and FRQ showed a reduced growth rate under LD only, but an increased growth rate compared to the wild type under LL (perhaps because of the almost complete lack of conidiation facilitating greater resources to be redirected toward vegetative growth). Together, the two clock components likely play a role in light/dark adaptation in *M. oryzae*.

7.3.7 The circadian clock functions in conidiation

Circadian entrainment and its subsequent dysfunction has also been consistently shown, both in the literature and herein, to play a role in conidiation and sporulation of several fungal species (82,84,101,108,116,117,119,232,259,392,430,452,456,505,506,619). In *M. oryzae*, specifically, light quality, intensity, and circadian dysfunction has been shown to affect conidiation, conidial release, morphology, and development (82,101,258,259). In the experiments performed in this work, harvest time (dawn or dusk) had no significant effect on conidial production under any pre-harvest entraining conditions or in circadian mutants, which suggests that it takes more than 12 h to produce mature conidia, regardless of the entraining environment. However, pre-harvest entraining conditions did have a significant effect on conidiation, where 12 h L/D was most conducive for conidiation in both the wild type and WC2 mutant, which is unsurprising given that this

treatment most closely resembles the natural environment that *M. oryzae* has evolved under. Interestingly, pre-harvest entrainment conditions had a smaller effect on conidiation in $\Delta WC2$ and FRQ^{NIN} compared to the wild type, where $\Delta WC2$ produced the fewest conidia after prolonged exposure to darkness (DD or LD-DD entrainment) perhaps suggesting reduced dark adaptation, (82,101), and FRQ^{NIN} showed hypersensitivity to light, where conidiation was significantly reduced after light exposure under any conditions (LD, LD-DD, LD-LL, and LL), implying a loss of light adaptation (116,413). The dampened effect of pre-harvest treatment in the circadian mutants could be the result of reduced plasticity and response to different environments.

Whilst pre-harvest entrainment conditions altered conidiation within each strain, circadian mutation also caused a reduction in conidiation (under most conditions) compared to the wild type. $\Delta WC2$ produced fewer conidia after DD, LD, and LD-DD entrainment, but produced wild type-like levels of conidia after entrainment under LD-LL and LL, again implicating a loss of dark adaptation (or erroneous and constant 'perception' of light). FRQ^{NIN} , on the other hand, produced almost an order of magnitude fewer conidia than the wild type, under all pre-harvest entraining conditions, and thus the clock components WC2 (which activates FRQ in a time of day-dependent manner) and FRQ, especially, have a profound role in conidiation in *M. oryzae*. The reduced conidiation phenotype shown in FRQ^{NIN} complements Shi and colleagues' results, where they reported that their ' Δfrq ' mutants produced ~10x fewer conidia than the wild type and FRQ-complement strain (259).

7.3.8 Pre-harvest entrainment and the circadian clock influences conidial development

Time of day had little effect on conidial germination and subsequent development, which was surprising, considering its role in virulence in several pathosystems. However, conidia have limited available resources and are unlikely to move after their initial dispersal, in part due to the production of spore tip mucilage, which is not significantly altered by time of day. In this way, conidia are 'terminal', and their consistent germination and development, regardless of time of day, may be a reflection of this – they have no other option but to germinate and develop in the hopes of successful infection. However, circadian mutants display altered conidial developmental rates, where $\Delta WC2$ conidia germinated and developed quicker than the wild under most entraining conditions, except after LD-LL and LL entrainment, again suggesting that $\Delta WC2$ are presenting a phenotype similar to constant light perception. FRQ^{NIN} also showed decreased conidial germination (as did Shi and colleagues), but those that did germinate developed faster than the wild type (this phenomenon was not discussed by Shi and colleagues) (259). This quickened development, common to the circadian mutants, could be the result of the reduced conidial sizes observed in both FRQ^{NIN} and $\Delta WC2$. Alternatively, these data might suggest differential and tissue type-dependent clock function in *M. oryzae*, where the clock might not function in determining the time of day in conidia (or it may be irrelevant) but may instead be utilised for determining the amount of time that has passed, where slowing the conidial developmental rate, as in the wild type, might allow for optimal timing of infection. Supportingly, *M. oryzae* conidial *wc1* transcript levels have been shown to be approximately 4-fold higher than their hyphal counterpart (101). Kim and colleagues subsequently suggested that WC1 may play a role in conidia-specific functions,

so it may be possible that the *M. oryzae* circadian machinery has a tissue-specific function.

7.3.9 The circadian clock affects early-stage pathogenicity

Appressoria typically generate an enormous amount of turgor pressure in order to penetrate the host plant cuticle (523,620). As is the case in other conidial phenotypes, time of day had no significant impact on appressorial turgor pressure, again suggesting that once conidia are produced, they tend to germinate and develop in a similar fashion. However, circadian mutants show altered appressorial turgor pressure, both compared to the wild type, and between pre-harvest treatments. $\Delta WC2$ appressoria, for example collapse at a higher rate compared to the wild type and thus likely produce a lower turgor pressure, which may lead to reduced penetration of the plant cuticle. $\Delta WC2$ colonies grown under constant conditions (DD and LL) also showed a decrease in appressorial collapse compared to those grown under LD, LD-DD, and LD-LL, which may further implicate WC2 in photoadaptation. FRQ^{NIN} , on the other hand, showed no difference in appressorial collapse between colonies grown under DD, LD, or LD-DD (LD-LL and LL were not tested because of the exceptionally low conidia produced under these conditions). Additionally, FRQ^{NIN} consistently showed reduced appressorial collapse compared to the wild type under a range of different glycerol concentrations (0.5 – 5 M), perhaps suggesting that FRQ serves to reduce or inhibit the accumulation of solutes in the appressoria. Alternatively, the increased developmental rate of FRQ conidia may have allowed FRQ to accumulate more solutes and/or increase the melanisation of the appressoria (which can act as a protective barrier against cytorrhysis) in the same period of time. This hypothesis would not explain the reduced turgor pressure in the faster-developing $\Delta WC2$ conidia, though.

Accordingly, FRQ^{NIN} did not show any significant differences from the wild type in terms of penetration and *in planta* cell-to-cell movement in the early stages of pathogenesis. Δ WC2, on the other hand, was less able to penetrate the plant cuticle, had reduced cell-to-cell movement, and its invasive hyphae were often constrained to the primary infected cell. These results may be due to the reduced turgor pressure generated as a result of WC2 dysfunction. This reduced pathogenesis phenotype was similar to that reported by Deng and colleagues in their TWL mutant, which is a clock-controlled gene (and displays similar expression timing to WCC activity), and therefore may be directly influenced by WC2 (84).

7.3.10 Timing, entrainment, and circadian function influences disease severity in host- and non-host *M. oryzae*-plant interactions

Finally, inoculation timing, pre-inoculation entrainment, and circadian dysfunction were shown to affect disease outcome, seemingly in a species-dependent manner. Generally, more severe disease outcomes were observed at dawn in the host, short-day rice, and at dusk in the non-host, long-day barley, and, as such, implicates the plant clock as the key determinant in the outcome of infection. However, if inoculation occurred after a period of darkness (i.e., dawn in LD-entrained colonies, or after DD entrainment), infection severity was typically more severe at dawn, whereas prolonged exposure to light (LL and LD-LL) generally favoured dusk inoculation, implicating the *M. oryzae* clock in pathogenicity and conidial priming. In the Δ WC2 strain, however, time of day had little effect on disease severity, except after prolonged light exposure, where dusk-favoured infections were maintained, further implicating WC2's role in environmental sensation and photoadaptation. FRQ^{NIN} also displayed a reduced time of day effect on pathogenicity but maintained its dawn-favoured infection severity after DD entrainment (it is important

to consider that FRQ^{NIN} could not consistently produce sufficient conidia after LD-LL and LL entrainment, so the effect of prolonged light exposure was not tested). Additionally, pre-inoculation entrainment of wild type *M. oryzae* generally had a greater effect on disease severity when inoculation occurred at times when the plants were most susceptible (dawn for rice and dusk for barley).

Asynchronicity with the plant generally inhibits virulence; antiphase-entrained *M. oryzae* shows reduced lesion coverage in rice, regardless of time of day in the wild type, and prolonged light exposure inhibits dawn pathogenicity in both rice and barley. The effect of asynchronicity with the plant on disease outcome was further amplified in the circadian mutants, where antiphase-entrained FRQ^{NIN} had particularly reduced virulence. Prolonged light exposure also inhibits Δ WC2 pathogenicity at dawn. LD-LL and LL entrainment could not be tested FRQ^{NIN}, but based on the other light hypersensitivity phenotypes, it would likely have a profound effect on virulence. Indeed, a significant reduction in conidiation indirectly reduces pathogenicity because of decreased inoculum. Together, perhaps a functional circadian system increases the plasticity of virulence based on current environmental conditions, a phenotype that is seemingly lost or dampened upon circadian disruption

When comparing the wild type to the circadian mutants in terms of virulence at different times of day, and under a range of pre-inoculation conditions, Δ WC2 showed fewer lesions than the wild type at dawn under DL, LD, and LL conditions in rice. And in barley infections, Δ WC2 produced both fewer lesions and a lower leaf coverage under all entraining conditions at both dawn and dusk. This suggests that the *M. oryzae* circadian clock may be either (a) more important in non-host, long-day plants such as barley, or (b)

M. oryzae is able to utilise host-derived rice signals to re-entrain its circadian clock, in a manner reminiscent to Deng and colleagues' study, where growth of *M. oryzae* Δ TWL mutants on rice extract media rescued the reduced conidiation phenotype to a far greater extent than that grown on barley extract media (84). Further, Deng and colleagues showed that rice extract media from plants grown under light were better able to restore this phenotype than those grown under darkness, suggesting that light- and potentially circadian-dependent nutrition of the host plant can affect pathogenesis and circadian-related traits in *M. oryzae* (84). This observation may also be the result of increased nutrients as a result of photosynthesis, which would not occur in the dark (the paper made no comment on how/if nutrition was controlled for). FRQ^{NIN} , on the other hand, showed little deviation from the wild type in terms of pathogenicity towards both rice and barley, except after antiphasic entrainment at dawn, where virulence was significantly decreased, which perhaps suggests a reduced re-entrainment capability. Altogether, there seems to be a complex interaction between *M. oryzae* and the plant it is invading, perhaps on a species-by-species basis, which is influenced by (subjective) time of day, pre-inoculation environmental conditions, and circadian function. All of these experiments were, out of necessity, performed under light, however: images cannot be captured without light, and conidia cannot be harvested, nor plants inoculated without sight. Performing these experiments under true darkness would certainly be worthwhile, if not experimentally difficult (as noted in chapter 4).

7.4 The role of the circadian clock in rice blast disease

A hypothesis for the general role of the circadian clock in *M. oryzae* pathogenesis is therefore presented: prior to infection and when growing *ex planta*, the clock serves to repress conidiation during the light hours of the day (specifically when blue light is in high

relative abundance), and gates vegetative growth in a temporal manner. This gating of conidial banding is chiefly controlled by the WCC, but FRQ is largely responsible for conidiation, perhaps amplifying the effects of the WCC. The circadian clock then functions in the conidia as a stopwatch, whereby the amount of time elapsed (perhaps after dispersal, sensation of hydrophobic surfaces, or altered relative abundances of certain wavelengths of light) is measured to fine tune conidial germination, development, and subsequent appressorial production to facilitate optimal timing of penetration into the host cuticle. Once inside the plant, the *M. oryzae* clock may utilise host-derived rice signals to ensure synchronisation with the plant, perhaps through the clock-controlled TWL (84). In non-host barley interactions, since *M. oryzae* is less able to utilise or make sense of the plant-derived temporal signals, it instead relies more heavily on its endogenous clock, and as such, pre-inoculation entrainment and circadian dysfunction gives rise to a greater reduction in pathogenicity and ultimate disease severity. Synchronisation with the plant could facilitate increased disease severity, as *M. oryzae* may produce plant immune system inhibitors at specific times and regulate stress responses to times when these stresses, such as the plant ROS burst, are most likely to occur. Altogether, this work has begun to address the complex interaction between time of day, environmental entrainment, and the circadian clock (all of which are inextricably linked) in the rice blast pathosystem, from a pathogen-centric view.

7.5 Future research

This work has made some headway into determining the role of entrainment and circadian function in the outcome of the economically important rice blast pathosystem, but several questions remain, and avenues not sufficiently explored. Experiments involving (time course) transcriptomics, (relative) protein abundance and localisation

(either through fluorescently-tagged strains or western blot), metabolomics, and genetic manipulation should be utilised for further work. Some questions and topics that should be addressed as a follow-up on the work presented here include:

- How expression of core clock and clock-controlled genes are influenced by time of day, pre-inoculation entrainment, and tissue type, both *in-* and *ex-planta*
- Whether the abundance, localisation, and phosphorylation status of FRQ (and other core clock proteins) are altered throughout the day in *M. oryzae* to further confirm circadian function
- Using the GFP-tagged complementation mutants, study the rhythmic expression and localisation of core clock components, and how entraining conditions can alter them; this could be performed microscopically or with anti-GFP antibodies for use in western blots
- Determine the effects of relative intensities of different wavelengths of light and the role of specific photoreceptors; is green light as important in phytopathogenic fungi as the conservation of the photoreceptor suggests?
- How does temperature influence the *M. oryzae* circadian machinery?
- Further elucidate the composition and function of the mystery metabolite.
- Perform pathogenicity experiments in plant clock mutants; a LUX ARRHYTHMO (LUX) luciferase reporter line has been generated in collaboration with the National Institute of Agricultural Botany (NIAB), and the design for a CRISPR-mediated LUX knockout has been completed.
- Determine the role of the plant/pathogen circadian clock in susceptibility and virulence, respectively, in a wider range of host- and non-host, and short- and long-day plants.

8 References

1. United Nations, Department of Economic and Social Affairs, Population Division. World population prospects 2022: summary of results [Internet]. 2022 [cited 2022 Aug 16]. Available from: https://www.un.org/development/desa/pd/sites/www.un.org.development.desa.pd/files/wpp2022_summary_of_results.pdf
2. Food and Agriculture Organisation of the United Nations. Report of the world food summit 1996 part 1. In Rome; 1996.
3. FAO. Rice market monitor. 2018.
4. FAO, WFP. Monitoring food security in countries with conflict situations. 2018. Report No.: 3.
5. Research Institute (IFPRI) IFP. 2017 Global Food Policy Report [Internet]. Washington, DC: International Food Policy Research Institute; 2017 [cited 2022 Jun 30]. Available from: <https://ebrary.ifpri.org/digital/collection/p15738coll2/id/131085>
6. Breisinger C, Ecker O, Tan JFT. How Do We Break the Links? 2015;12.
7. Ritchie H, Roser M. Agricultural Production. Our World Data [Internet]. 2020 Mar 5 [cited 2022 Aug 22]; Available from: <https://ourworldindata.org/agricultural-production>
8. A. Lusigi. Africa and the Russia-Ukraine conflict: Seizing the opportunity in the crisis | Africa Renewal [Internet]. un.org. 2022 [cited 2022 Aug 22]. Available from: <https://www.un.org/africarenewal/magazine/africa-and-russia-ukraine-conflict-seizing-opportunity-crisis>
9. Chakraborty S, Newton AC. Climate change, plant diseases and food security: an overview: Climate change and food security. *Plant Pathol.* 2011 Feb;60(1):2–14.
10. FAO. FAO food outlook october 2016. Rome: Food and Agriculture Organization of the United Nations; 2016.
11. Schmidhuber J, Tubiello FN. Global food security under climate change. *Proc Natl Acad Sci.* 2007 Dec 11;104(50):19703–8.
12. Castejón-Muñoz M. The effect of temperature and relative humidity on the airborne concentration of *Pyricularia oryzae* spores and the development of rice blast in southern Spain. *Span J Agric Res.* 2008;9.
13. FAO. Special event on impact of climate change, pests and diseases on food security and poverty reduction. In 2005.
14. Evans N, Baierl A, Semenov MA, Gladders P, Fitt BDL. Range and severity of a plant disease increased by global warming. *J R Soc Interface.* 2008 May 6;5(22):525–31.
15. Strange RN, Scott PR. Plant Disease: A Threat to Global Food Security. *Annu Rev Phytopathol.* 2005 Sep 1;43(1):83–116.

16. Fry WE, Birch PRJ, Judelson HS, Grünwald NJ, Danies G, Everts KL, et al. Five Reasons to Consider *Phytophthora infestans* a Reemerging Pathogen. *Phytopathology*®. 2015 Jul;105(7):966–81.
17. Goss EM, Tabima JF, Cooke DEL, Restrepo S, Fry WE, Forbes GA, et al. The Irish potato famine pathogen *Phytophthora infestans* originated in central Mexico rather than the Andes. *Proc Natl Acad Sci*. 2014 Jun 17;111(24):8791–6.
18. Nowicki M, Foolad MR, Nowakowska M, Kozik EU. Potato and Tomato Late Blight Caused by *Phytophthora infestans* : An Overview of Pathology and Resistance Breeding. *Plant Dis*. 2012 Jan;96(1):4–17.
19. Newton AC. Exploitation of Diversity within Crops—the Key to Disease Tolerance? *Front Plant Sci* [Internet]. 2016 May 20 [cited 2022 Jun 30];7. Available from: <http://journal.frontiersin.org/Article/10.3389/fpls.2016.00665/abstract>
20. Zhu Y, Chen H, Fan J, Wang Y, Li Y, Chen J, et al. Genetic diversity and disease control in rice. *Nature*. 2000 Aug;406(6797):718–22.
21. Kumar MK, Veerabhadraswamy AL. Kumar, M.K., & Veerabhadraswamy, A.L. (2014). Appraise a combination of fungicides against blast and sheath blight diseases of paddy (*Oryza sativa* L.). *Journal of Experimental Biology and Agricultural Sciences*, 2, 49-57. *J Exp Biol Agric Sci*. 2014;2:49–57.
22. Nalley L, Tsiboe F, Durand-Morat A, Shew A, Thoma G. Economic and Environmental Impact of Rice Blast Pathogen (*Magnaporthe oryzae*) Alleviation in the United States. Wang Z, editor. *PLOS ONE*. 2016 Dec 1;11(12):e0167295.
23. Hashim I, Mamiro DP, Mabagala RB, Tefera T. Smallholder Farmers' Knowledge, Perception and Management of Rice Blast Disease in Upland Rice Production in Tanzania. *J Agric Sci*. 2018 Jun 8;10(7):137.
24. Hahn M. The rising threat of fungicide resistance in plant pathogenic fungi: Botrytis as a case study. *J Chem Biol*. 2014 Oct;7(4):133–41.
25. WHO. Antibiotic resistance [Internet]. World Health Organisation. 2020 [cited 2022 Aug 22]. Available from: <https://www.who.int/news-room/fact-sheets/detail/antibiotic-resistance>
26. Singh KP, Kumari P, Rai PK. Current Status of the Disease-Resistant Gene(s)/QTLs, and Strategies for Improvement in Brassica juncea. *Front Plant Sci*. 2021 Mar 3;12:617405.
27. Karpyn AE, Riser D, Tracy T, Wang R, Shen Y. The changing landscape of food deserts. 2020;12.
28. FAO. Economics and the international year of rice. 2004.
29. Pandey S, Byerlee D, Dawe D, Dobermann A, Mohanty S, Rozelle S, et al. Rice in the global economy: strategic research and policy issues for food security. International Rice Research Institute; 2010 p. 487.
30. Swain DK, Rawade YA, Mohanty UC. Climate Impact Analysis and Adaptations for Sustainable Rice Production System. In: *Climate Vulnerability* [Internet]. Elsevier; 2013

[cited 2022 Jun 30]. p. 25–35. Available from:
<https://linkinghub.elsevier.com/retrieve/pii/B9780123847034002069>

31. Yuchengco AT. Request for the inclusion of an additional item in the agenda of the fifty-seventh session (UN General Assembly International Year of Rice). United Nations; 2002.
32. IRRI, Mohanty S. Rice today: trends in global rice consumption. 2013.
33. Muthayya S, Sugimoto JD, Montgomery S, Maberly GF. An overview of global rice production, supply, trade, and consumption: Global rice production, consumption, and trade. *Ann N Y Acad Sci*. 2014 Sep;1324(1):7–14.
34. IRRI. Asia society / IRRI task force outlines strategy to combat hunger in Asai.pdf. 2018.
35. African Development Bank. New rice for africa (NERICA) dissemination project: increasing domestic production improving food security. 2014.
36. Gnanamanickam SS. Rice and Its Importance to Human Life. In: *Biological Control of Rice Diseases* [Internet]. Dordrecht: Springer Netherlands; 2009 [cited 2022 Jun 30]. p. 1–11. Available from: http://link.springer.com/10.1007/978-90-481-2465-7_1
37. GRiSP. Rice almanac: source book for the most important economic activities on Earth. Fourth Edition. Los Baños, Philippines: IRRI; 2013. 283 p.
38. Dawe D. The changing structure of the world rice market, 1950–2000. *Food Policy*. 2002 Aug;27(4):355–70.
39. FAO. Rice and human nutrition. 2004.
40. Dasgupta S, Hossain MdM, Huq M, Wheeler D. Climate change and soil salinity: The case of coastal Bangladesh. *Ambio*. 2015 Dec;44(8):815–26.
41. Leff B, Ramankutty N, Foley JA. Geographic distribution of major crops across the world: GLOBAL CROP DISTRIBUTION. *Glob Biogeochem Cycles*. 2004 Mar;18(1):n/a-n/a.
42. Brown AHD, Hodgkin T. Indicators of Genetic Diversity, Genetic Erosion, and Genetic Vulnerability for Plant Genetic Resources. In: Ahuja MR, Jain SM, editors. *Genetic Diversity and Erosion in Plants* [Internet]. Cham: Springer International Publishing; 2015 [cited 2022 Aug 22]. p. 25–53. (Sustainable Development and Biodiversity; vol. 7). Available from: http://link.springer.com/10.1007/978-3-319-25637-5_2
43. McDonald BA, Stukenbrock EH. Rapid emergence of pathogens in agro-ecosystems: global threats to agricultural sustainability and food security. *Philos Trans R Soc B Biol Sci*. 2016 Dec 5;371(1709):20160026.
44. Mondal D, Ghosh A, Roy D, Kumar A, Bera S, Ghosh R, et al. Yield loss assessment of rice (*Oryza Sativa* L.) due to different biotic stresses under system of rice intensification (SRI). *J Entomol Zool Stud*. 2017;7.
45. Schuck S, Weinhold A, Luu VT, Baldwin IT. Isolating Fungal Pathogens from a Dynamic Disease Outbreak in a Native Plant Population to Establish Plant-Pathogen Bioassays for the Ecological Model Plant *Nicotiana attenuata*. Mittapalli O, editor. *PLoS ONE*. 2014 Jul 18;9(7):e102915.

46. Bevitori R, Ghini R. Rice Blast Disease in Climate Change Times. *Rice Res Open Access* [Internet]. 2014 [cited 2022 Jun 30];03(01). Available from: <http://esciencecentral.org/journals/rice-blast-disease-in-climate-change-times-2375-4338.1000e111.php?aid=38022>
47. Cheng C, Gao X, Feng B, Sheen J, Shan L, He P. Plant immune response to pathogens differs with changing temperatures. *Nat Commun*. 2013 Dec;4(1):2530.
48. Deutsch CA, Tewksbury JJ, Tigchelaar M, Battisti DS, Merrill SC, Huey RB, et al. Increase in crop losses to insect pests in a warming climate. *Science*. 2018 Aug 31;361(6405):916–9.
49. Prakash A, Rao J, Mukherjee A, Berliner J, Pokhare S, Adak T, et al. Climate change: impact on crop pests. Cuttack: Applied Zoologists Research Association (AZRA), Central Rice Research Institute; 2014.
50. Scherm H, Sutherst RW, Harrington R, Ingram JSI. Global networking for assessment of impacts of global change on plant pests. *Environ Pollut*. 2000 Jun;108(3):333–41.
51. Luo Y. Risk analysis of yield losses caused by rice leaf blast associated with temperature changes above and below for five Asian countries. *Agric Ecosyst Environ*. 1998 Apr;68(3):197–205.
52. Luo Y, TeBeest DO, Teng PS, Fabellar NG. Simulation Studies on Risk Analysis of Rice Leaf Blast Epidemics Associated with Global Climate Change in Several Asian Countries. *J Biogeogr*. 1995 Jul;22(4/5):673.
53. Potrykus I. Golden Rice and Beyond. *Plant Physiol*. 2001 Mar 1;125(3):1157–61.
54. Potrykus I. Nutritionally Enhanced Rice to Combat Malnutrition Disorders of the Poor. *Nutr Rev*. 2003 Jun 1;61(suppl_6):S101–4.
55. Dean R, Van Kan JAL, Pretorius ZA, Hammond-Kosack KE, Di Pietro A, Spanu PD, et al. The Top 10 fungal pathogens in molecular plant pathology: Top 10 fungal pathogens. *Mol Plant Pathol*. 2012 May;13(4):414–30.
56. Ou SH. Rice diseases. 2nd ed. Kew, Surrey, UK: Commonwealth Mycological Institute; 1985. 380 p.
57. Khang CH, Valent B. *Magnaporthe oryzae* and Rice Blast Disease. 2017;14.
58. Martin-Urdiroz M, Oses-Ruiz M, Ryder LS, Talbot NJ. Investigating the biology of plant infection by the rice blast fungus *Magnaporthe oryzae*. *Fungal Genet Biol*. 2016 May;90:61–8.
59. Valent B, Khang CH. Recent advances in rice blast effector research. *Curr Opin Plant Biol*. 2010 Aug 1;13(4):434–41.
60. Kim CK. Epidemiology of Rice Blast Disease in Korea. In: *Major Fungal Diseases of Rice* [Internet]. Dordrecht: Springer Netherlands; 2001 [cited 2022 Aug 22]. p. 119–29. Available from: http://link.springer.com/10.1007/978-94-017-2157-8_9

61. Collard BCY, Mackill DJ. Marker-assisted selection: an approach for precision plant breeding in the twenty-first century. *Philos Trans R Soc B Biol Sci.* 2008 Feb 12;363(1491):557–72.
62. Sosnowski MR, Fletcher JD, Daly AM, Rodoni BC, Viljanen-Rollinson SLH. Techniques for the treatment, removal and disposal of host material during programmes for plant pathogen eradication. *Plant Pathol.* 2009 Aug;58(4):621–35.
63. Saleh D, Milazzo J, Adreit H, Fournier E, Tharreau D. South-East Asia is the center of origin, diversity and dispersion of the rice blast fungus, *Magnaporthe oryzae*. *New Phytol.* 2014 Mar;201(4):1440–56.
64. Karavolias NG, Horner W, Abugu MN, Evanega SN. Application of Gene Editing for Climate Change in Agriculture. *Front Sustain Food Syst.* 2021 Sep 7;5:685801.
65. Li X, Pan L, Bi D, Tian X, Li L, Xu Z, et al. Generation of Marker-Free Transgenic Rice Resistant to Rice Blast Disease Using Ac/Ds Transposon-Mediated Transgene Reintegration System. *Front Plant Sci.* 2021 Apr 20;12:644437.
66. Tyagi S, Kesiraju K, Saakre M, Rathinam M, Raman V, Pattanayak D, et al. Genome Editing for Resistance to Insect Pests: An Emerging Tool for Crop Improvement. *ACS Omega.* 2020 Aug 25;5(33):20674–83.
67. Wang F, Wang C, Liu P, Lei C, Hao W, Gao Y, et al. Enhanced Rice Blast Resistance by CRISPR/Cas9-Targeted Mutagenesis of the ERF Transcription Factor Gene OsERF922. Wilson RA, editor. *PLOS ONE.* 2016 Apr 26;11(4):e0154027.
68. Yang Y, Xu C, Shen Z, Yan C. Crop Quality Improvement Through Genome Editing Strategy. *Front Genome Ed.* 2022 Jan 31;3:819687.
69. Zhang Y, Massel K, Godwin ID, Gao C. Applications and potential of genome editing in crop improvement. *Genome Biol.* 2018 Dec;19(1):210.
70. Abdullah M, Okemo P, Furtado A, Henry R. Potential of Genome Editing to Capture Diversity From Australian Wild Rice Relatives. *Front Genome Ed.* 2022 Apr 27;4:875243.
71. Bandyopadhyay A, Kancharla N, Javalkote VS, Dasgupta S, Brutnell TP. CRISPR-Cas12a (Cpf1): A Versatile Tool in the Plant Genome Editing Tool Box for Agricultural Advancement. *Front Plant Sci.* 2020 Nov 2;11:584151.
72. Khan H, McDonald MC, Williams SJ, Solomon PS. Assessing the efficacy of CRISPR/Cas9 genome editing in the wheat pathogen *Parastagonospora nodorum*. *Fungal Biol Biotechnol.* 2020 Dec;7(1):4.
73. Li JF, Norville JE, Aach J, McCormack M, Zhang D, Bush J, et al. Multiplex and homologous recombination-mediated genome editing in *Arabidopsis* and *Nicotiana benthamiana* using guide RNA and Cas9. *Nat Biotechnol.* 2013 Aug;31(8):688–91.
74. Xia X, Cheng X, Li R, Yao J, Li Z, Cheng Y. Advances in application of genome editing in tomato and recent development of genome editing technology. *Theor Appl Genet.* 2021 Sep;134(9):2727–47.
75. FAO. Rice market Monitor December 2017. 2017.

76. FAO. rice price update (December 2017). 2017.
77. Parker D, Beckmann M, Enot DP, Overy DP, Rios ZC, Gilbert M, et al. Rice blast infection of *Brachypodium distachyon* as a model system to study dynamic host/pathogen interactions. *Nat Protoc.* 2008 Mar;3(3):435–45.
78. Talbot NJ. Having a blast: exploring the pathogenicity of *Magnaporthe grisea*. 1995;8.
79. Talbot NJ, Ebbole DJ, Hamer JE. Identification and characterization of MPG1, a gene involved in pathogenicity from the rice blast fungus *Magnaporthe grisea*. *Plant Cell.* 1993 Nov;5(11):1575–90.
80. CABI. *Magnaporthe oryzae* (rice blast disease) [Internet]. CABI; 2021. Available from: <https://www.cabi.org/isc/datasheet/46103>
81. Koeck M, Hardham AR, Dodds PN. The role of effectors of biotrophic and hemibiotrophic fungi in infection: Effectors of biotrophic fungi. *Cell Microbiol.* 2011 Dec;13(12):1849–57.
82. Lee K, Singh P, Chung WC, Ash J, Kim TS, Hang L, et al. Light regulation of asexual development in the rice blast fungus, *Magnaporthe oryzae*. *Fungal Genet Biol.* 2006 Oct;43(10):694–706.
83. Marcel S, Sawers R, Oakeley E, Angliker H, Paszkowski U. Tissue-Adapted Invasion Strategies of the Rice Blast Fungus *Magnaporthe oryzae*. *Plant Cell.* 2010 Oct 27;22(9):3177–87.
84. Deng YZ, Qu Z, Naqvi NI. Twilight, a Novel Circadian-Regulated Gene, Integrates Phototropism with Nutrient and Redox Homeostasis during Fungal Development. Guo HS, editor. *PLOS Pathog.* 2015 Jun 23;11(6):e1004972.
85. Wilson RA, Talbot NJ. Under pressure: investigating the biology of plant infection by *Magnaporthe oryzae*. *Nat Rev Microbiol.* 2009 Mar;7(3):185–95.
86. Momany M, Talbot NJ. Septins Focus Cellular Growth for Host Infection by Pathogenic Fungi. *Front Cell Dev Biol* [Internet]. 2017 Apr 5 [cited 2022 Jun 30];5. Available from: <http://journal.frontiersin.org/article/10.3389/fcell.2017.00033/full>
87. Wang ZY, Jenkinson JM, Holcombe LJ, Soanes DM, Veneault-Fourrey C, Bhambra GK, et al. The molecular biology of appressorium turgor generation by the rice blast fungus *Magnaporthe grisea*. *Biochem Soc Trans.* 2005 Apr 1;33(2):384–8.
88. Kim S, Park J, Park SY, Mitchell TK, Lee YH. Identification and analysis of in planta expressed genes of *Magnaporthe oryzae*. *BMC Genomics* [Internet]. 2010 Dec [cited 2022 Jun 30];11(1). Available from: <https://bmcgenomics.biomedcentral.com/articles/10.1186/1471-2164-11-104>
89. Fernandez J, Orth K. Rise of a Cereal Killer: The Biology of *Magnaporthe oryzae* Biotrophic Growth. *Trends Microbiol.* 2018 Jul;26(7):582–97.
90. Asibi AE, Chai Q, Coulter JA. Rice Blast: A Disease with Implications for Global Food Security. *Agronomy.* 2019 Aug 15;9(8):451.

91. Faulkner C, Robatzek S. Plants and pathogens: putting infection strategies and defence mechanisms on the map. *Curr Opin Plant Biol.* 2012 Dec;15(6):699–707.
92. Mentlak TA, Kombrink A, Shinya T, Ryder LS, Otomo I, Saitoh H, et al. Effector-Mediated Suppression of Chitin-Triggered Immunity by *Magnaporthe oryzae* Is Necessary for Rice Blast Disease. *Plant Cell.* 2012 Feb 28;24(1):322–35.
93. Kankanala P, Czymmek K, Valent B. Roles for Rice Membrane Dynamics and Plasmodesmata during Biotrophic Invasion by the Blast Fungus. *Plant Cell.* 2007 Mar 26;19(2):706–24.
94. Sakulkoo W, Osés-Ruiz M, Oliveira Garcia E, Soanes DM, Littlejohn GR, Hacker C, et al. A single fungal MAP kinase controls plant cell-to-cell invasion by the rice blast fungus. *Science.* 2018 Mar 23;359(6382):1399–403.
95. Giraldo MC, Dagdas YF, Gupta YK, Mentlak TA, Yi M, Martinez-Rocha AL, et al. Two distinct secretion systems facilitate tissue invasion by the rice blast fungus *Magnaporthe oryzae*. *Nat Commun [Internet].* 2013 Oct [cited 2022 Jun 30];4(1). Available from: <http://www.nature.com/articles/ncomms2996>
96. Khang CH, Berruyer R, Giraldo MC, Kankanala P, Park SY, Czymmek K, et al. Translocation of *Magnaporthe oryzae* Effectors into Rice Cells and Their Subsequent Cell-to-Cell Movement. *Plant Cell.* 2010 Jun 4;22(4):1388–403.
97. Jones K, Khang CH. Visualizing the Movement of *Magnaporthe oryzae* Effector Proteins in Rice Cells During Infection. In: Ma W, Wolpert T, editors. *Plant Pathogenic Fungi and Oomycetes [Internet].* New York, NY: Springer New York; 2018 [cited 2022 Jun 30]. p. 103–17. Available from: http://link.springer.com/10.1007/978-1-4939-8724-5_9
98. Saunders DGO, Aves SJ, Talbot NJ. Cell Cycle–Mediated Regulation of Plant Infection by the Rice Blast Fungus. *Plant Cell.* 2010 Mar 25;22(2):497–507.
99. Sweigard JA, Carroll AM, Kang S, Farrall L, Chumley FG, Valent B. Identification, cloning, and characterization of PWL2, a gene for host species specificity in the rice blast fungus. *Plant Cell.* 1995 Aug;7(8):1221–33.
100. Zhang S, Xu JR. Effectors and Effector Delivery in *Magnaporthe oryzae*. Heitman J, editor. *PLoS Pathog.* 2014 Jan 2;10(1):e1003826.
101. Kim S, Singh P, Park J, Park S, Friedman A, Zheng T, et al. Genetic and molecular characterization of a blue light photoreceptor MGWC-1 in *Magnaporthe oryzae*. *Fungal Genet Biol.* 2011 Apr;48(4):400–7.
102. de Leone MJ, Hernando CE, Romanowski A, Careno DA, Soverna AF, Sun H, et al. Bacterial Infection Disrupts Clock Gene Expression to Attenuate Immune Responses. *Curr Biol.* 2020 May;30(9):1740-1747.e6.
103. de Leone MJ, Hernando CE, Mora-García S, Yanovsky MJ. It’s a matter of time: the role of transcriptional regulation in the circadian clock-pathogen crosstalk in plants. *Transcription.* 2020 Aug 7;11(3–4):100–16.
104. Schumacher J. How light affects the life of *Botrytis*. *Fungal Genet Biol.* 2017 Sep;106:26–41.

105. Horsfall JG, Cowling EB, editors. Plant disease: an advanced treatise. New York: Academic Press; 1977. 5 p.
106. Abuelsoud W, Cortleven A, Schmülling T. Photoperiod stress induces an oxidative burst-like response and is associated with increased apoplastic peroxidase and decreased catalase activities. *J Plant Physiol.* 2020 Oct;253:153252.
107. Cagnola JI, Cerdan PD, Pacin M, Andrade A, Rodriguez MV, Zurbriggen MD, et al. Long-day photoperiod enhances jasmonic acid-related plant defense. *Plant Physiol.* 2018 Aug 1;pp.00443.2018.
108. Cohrs KC, Schumacher J. The Two Cryptochrome/Photolyase Family Proteins Fulfill Distinct Roles in DNA Photorepair and Regulation of Conidiation in the Gray Mold Fungus *Botrytis cinerea*. Master ER, editor. *Appl Environ Microbiol.* 2017 Sep;83(17):e00812-17.
109. Cortleven A, Roeber VM, Frank M, Bertels J, Lortzing V, Beemster G, et al. The transcriptomic landscape of the photoperiodic stress response in *Arabidopsis thaliana* resembles the response to pathogen infection. 2021;37.
110. Flaherty JE, Dunkle LD. Identification and expression analysis of regulatory genes induced during conidiation in *Exserohilum turcicum*. *Fungal Genet Biol.* 2005 May;42(5):471–81.
111. Kim H, Ridenour JB, Dunkle LD, Bluhm BH. Regulation of Stomatal Tropism and Infection by Light in *Cercospora zeaе-maydis*: Evidence for Coordinated Host/Pathogen Responses to Photoperiod? He S, editor. *PLoS Pathog.* 2011 Jul 28;7(7):e1002113.
112. Liversage J, Coetzee MPA, Bluhm BH, Berger DK, Crampton BG. LOVE across kingdoms: Blue light perception vital for growth and development in plant–fungal interactions. *Fungal Biol Rev.* 2018 Mar;32(2):86–103.
113. Roeber VM, Schmülling T, Cortleven A. The Photoperiod: Handling and Causing Stress in Plants. *Front Plant Sci* [Internet]. 2022 Jan 25 [cited 2022 Jun 30];12. Available from: <https://www.frontiersin.org/articles/10.3389/fpls.2021.781988/full>
114. Wang H, Jiang YP, Yu HJ, Xia XJ, Shi K, Zhou YH, et al. Light quality affects incidence of powdery mildew, expression of defence-related genes and associated metabolism in cucumber plants. *Eur J Plant Pathol.* 2010 May;127(1):125–35.
115. Yang YX, Wang MM, Yin YL, Onac E, Zhou GF, Peng S, et al. RNA-seq analysis reveals the role of red light in resistance against *Pseudomonas syringae* pv. tomato DC3000 in tomato plants. *BMC Genomics* [Internet]. 2015 Dec [cited 2022 Jun 30];16(1). Available from: <https://bmcbgenomics.biomedcentral.com/articles/10.1186/s12864-015-1228-7>
116. Canessa P, Schumacher J, Hevia MA, Tudzynski P, Larrondo LF. Assessing the Effects of Light on Differentiation and Virulence of the Plant Pathogen *Botrytis cinerea*: Characterization of the White Collar Complex. Freitag M, editor. *PLoS ONE.* 2013 Dec 31;8(12):e84223.
117. Hevia MA, Canessa P, Müller-Esparza H, Larrondo LF. A circadian oscillator in the fungus *Botrytis cinerea* regulates virulence when infecting *Arabidopsis thaliana*. *Proc Natl Acad Sci.* 2015 Jul 14;112(28):8744–9.

118. Idnurm A, Heitman J. Photosensing Fungi: Phytochrome in the Spotlight. *Curr Biol*. 2005 Oct;15(20):R829–32.
119. Schumacher J, Simon A, Cohrs KC, Viaud M, Tudzynski P. The Transcription Factor BcLTF1 Regulates Virulence and Light Responses in the Necrotrophic Plant Pathogen *Botrytis cinerea*. Dunlap JC, editor. *PLoS Genet*. 2014 Jan 9;10(1):e1004040.
120. Ingle RA, Stoker C, Stone W, Adams N, Smith R, Grant M, et al. Jasmonate signalling drives time-of-day differences in susceptibility of *Arabidopsis* to the fungal pathogen *Botrytis cinerea*. *Plant J*. 2015 Dec;84(5):937–48.
121. McClung CR. Defence at dawn. *Nature*. 2011 Feb;470(7332):44–5.
122. Roden LC, Ingle RA. Lights, Rhythms, Infection: The Role of Light and the Circadian Clock in Determining the Outcome of Plant–Pathogen Interactions. *Plant Cell*. 2009 Sep;21(9):2546–52.
123. Bigeard J, Colcombet J, Hirt H. Signaling Mechanisms in Pattern-Triggered Immunity (PTI). *Mol Plant*. 2015 Apr;8(4):521–39.
124. Jones JDG, Dangl JL. The plant immune system. *Nature*. 2006 Nov;444(7117):323–9.
125. Nishad R, Ahmed T, Rahman VJ, Kareem A. Modulation of Plant Defense System in Response to Microbial Interactions. *Front Microbiol*. 2020 Jul 3;11:1298.
126. Spoel SH, Dong X. How do plants achieve immunity? Defence without specialized immune cells. *Nat Rev Immunol*. 2012 Feb;12(2):89–100.
127. Choi HW, Klessig DF. DAMPs, MAMPs, and NAMPs in plant innate immunity. *BMC Plant Biol*. 2016 Dec;16(1):232.
128. Zhou JM, Zhang Y. Plant Immunity: Danger Perception and Signaling. *Cell*. 2020 May;181(5):978–89.
129. de Torres Zabala M, Littlejohn G, Jayaraman S, Studholme D, Bailey T, Lawson T, et al. Chloroplasts play a central role in plant defence and are targeted by pathogen effectors. *Nat Plants*. 2015 Jun;1(6):15074.
130. Köster P, DeFalco TA, Zipfel C. Ca²⁺ signals in plant immunity. *EMBO J* [Internet]. 2022 Jun 14 [cited 2022 Aug 14];41(12). Available from: <https://onlinelibrary.wiley.com/doi/10.15252/emboj.2022110741>
131. Lecourieux D, Ranjeva R, Pugin A. Calcium in plant defence-signalling pathways. *New Phytol*. 2006 Jul;171(2):249–69.
132. Wang Y, Li X, Fan B, Zhu C, Chen Z. Regulation and Function of Defense-Related Callose Deposition in Plants. *Int J Mol Sci*. 2021 Feb 27;22(5):2393.
133. Li P, Lu YJ, Chen H, Day B. The Lifecycle of the Plant Immune System. *Crit Rev Plant Sci*. 2020 Jan 2;39(1):72–100.
134. Vallad GE, Goodman RM. Systemic Acquired Resistance and Induced Systemic Resistance in Conventional Agriculture. *Crop Sci*. 2004 Nov;44(6):1920–34.

135. Bechtold U, Karpinski S, Mullineaux PM. The influence of the light environment and photosynthesis on oxidative signalling responses in plant-biotrophic pathogen interactions. *Plant Cell Environ.* 2005 Aug;28(8):1046–55.
136. Bolouri Moghaddam MR, Van den Ende W. Sweet immunity in the plant circadian regulatory network. *J Exp Bot.* 2013 Apr;64(6):1439–49.
137. Cerrudo I, Keller MM, Cargnel MD, Demkura PV, de Wit M, Patitucci MS, et al. Low Red/Far-Red Ratios Reduce Arabidopsis Resistance to *Botrytis cinerea* and Jasmonate Responses via a COI1-JAZ10-Dependent, Salicylic Acid-Independent Mechanism. *Plant Physiol.* 2012 Apr 2;158(4):2042–52.
138. Chandra-Shekara AC, Gupte M, Navarre D, Raina S, Raina R, Klessig D, et al. Light-dependent hypersensitive response and resistance signaling against Turnip Crinkle Virus in Arabidopsis. *Plant J.* 2006 Feb;45(3):320–34.
139. Creux N, Harmer S. Circadian Rhythms in Plants. *Cold Spring Harb Perspect Biol.* 2019 Sep;11(9):a034611.
140. Evrard A, Ndatimana T, Eulgem T. FORCA, a promoter element that responds to crosstalk between defense and light signaling. *BMC Plant Biol* [Internet]. 2009 Dec [cited 2022 Jun 30];9(1). Available from: <https://bmcplantbiol.biomedcentral.com/articles/10.1186/1471-2229-9-2>
141. Griebel T, Zeier J. Light Regulation and Daytime Dependency of Inducible Plant Defenses in Arabidopsis: Phytochrome Signaling Controls Systemic Acquired Resistance Rather Than Local Defense. *Plant Physiol.* 2008 Jun;147(2):790–801.
142. Hua J. Modulation of plant immunity by light, circadian rhythm, and temperature. *Curr Opin Plant Biol.* 2013 Aug;16(4):406–13.
143. Kim J, Kim HS, Choi SH, Jang JY, Jeong MJ, Lee S. The Importance of the Circadian Clock in Regulating Plant Metabolism. *Int J Mol Sci.* 2017 Dec 11;18(12):2680.
144. Kim MG, Macoy DM, Lee JY, Cha JY, Kim WY. Interactions between Plant Immunity, Temperature, Light, and Circadian Rhythm. 2021;9:14.
145. Kim SG, Yon F, Gaquerel E, Gulati J, Baldwin IT. Tissue Specific Diurnal Rhythms of Metabolites and Their Regulation during Herbivore Attack in a Native Tobacco, *Nicotiana attenuata*. Kliebenstein DJ, editor. *PLoS ONE.* 2011 Oct 18;6(10):e26214.
146. Li R, Llorca LC, Schuman MC, Wang Y, Wang L, Joo Y, et al. ZEITLUPE in the Roots of Wild Tobacco Regulates Jasmonate-Mediated Nicotine Biosynthesis and Resistance to a Generalist Herbivore. *Plant Physiol.* 2018 Jun;177(2):833–46.
147. Li Z, Bonaldi K, Uribe F, Pruneda-Paz JL. A Localized *Pseudomonas syringae* Infection Triggers Systemic Clock Responses in Arabidopsis. *Curr Biol.* 2018 Feb;28(4):630-639.e4.
148. Lu H, McClung CR, Zhang C. Tick Tock: Circadian Regulation of Plant Innate Immunity. *Annu Rev Phytopathol.* 2017 Aug 4;55(1):287–311.
149. Macioszek VK, Sobczak M, Skoczowski A, Oliwa J, Michlewska S, Gapińska M, et al. The Effect of Photoperiod on Necrosis Development, Photosynthetic Efficiency and 'Green

- Islands' Formation in *Brassica juncea* Infected with *Alternaria brassicicola*. *Int J Mol Sci*. 2021 Aug 5;22(16):8435.
150. Meng L, Van Labeke MC, Höfte M. Timing of light quality affects susceptibility to *Botrytis cinerea* in strawberry leaves. *J Photochem Photobiol B*. 2020 Oct;211:111988.
 151. Sanchez SE, Kay SA. The Plant Circadian Clock: From a Simple Timekeeper to a Complex Developmental Manager. *Cold Spring Harb Perspect Biol*. 2016 Dec;8(12):a027748.
 152. Seo PJ, Mas P. STRESSing the role of the plant circadian clock. *Trends Plant Sci*. 2015 Apr;20(4):230–7.
 153. Spoel SH, Dong X. Making Sense of Hormone Crosstalk during Plant Immune Responses. *Cell Host Microbe*. 2008 Jun;3(6):348–51.
 154. Wang Y, Bao Z, Zhu Y, Hua J. Analysis of Temperature Modulation of Plant Defense Against Biotrophic Microbes. *Mol Plant-Microbe Interactions*[®]. 2009 May;22(5):498–506.
 155. de Wit M, Spoel SH, Sanchez-Perez GF, Gommers CMM, Pieterse CMJ, Voosenek LACJ, et al. Perception of low red:far-red ratio compromises both salicylic acid- and jasmonic acid-dependent pathogen defences in *Arabidopsis*. *Plant J*. 2013 Jul;75(1):90–103.
 156. Wu L, Yang HQ. CRYPTOCHROME 1 Is Implicated in Promoting R Protein-Mediated Plant Resistance to *Pseudomonas syringae* in *Arabidopsis*. *Mol Plant*. 2010 May;3(3):539–48.
 157. Zeier J, Pink B, Mueller MartinJ, Berger S. Light conditions influence specific defence responses in incompatible plant?pathogen interactions: uncoupling systemic resistance from salicylic acid and PR-1 accumulation. *Planta* [Internet]. 2004 Aug [cited 2022 Jun 30];219(4). Available from: <http://link.springer.com/10.1007/s00425-004-1272-z>
 158. Zhang C, Xie Q, Anderson RG, Ng G, Seitz NC, Peterson T, et al. Crosstalk between the Circadian Clock and Innate Immunity in *Arabidopsis*. Ausubel FM, editor. *PLoS Pathog*. 2013 Jun 6;9(6):e1003370.
 159. Zhang C, Gao M, Seitz NC, Angel W, Hallworth A, Wiratan L, et al. LUX ARRHYTHMO mediates crosstalk between the circadian clock and defense in *Arabidopsis*. *Nat Commun* [Internet]. 2019 Dec [cited 2022 Jun 30];10(1). Available from: <http://www.nature.com/articles/s41467-019-10485-6>
 160. Zhang J, Ren Z, Zhou Y, Ma Z, Ma Y, Hou D, et al. NPR1 and Redox Rhythmx: Connections, between Circadian Clock and Plant Immunity. *Int J Mol Sci*. 2019 Mar 10;20(5):1211.
 161. Baker CL, Loros JJ, Dunlap JC. The circadian clock of *Neurospora crassa*. *FEMS Microbiol Rev*. 2012 Jan;36(1):95–110.
 162. Deng W, Clausen J, Boden S, Oliver SN, Casao MC, Ford B, et al. Dawn and Dusk Set States of the Circadian Oscillator in Sprouting Barley (*Hordeum vulgare*) Seedlings. Wang T, editor. *PLOS ONE*. 2015 Jun 11;10(6):e0129781.
 163. Goodspeed D, Chehab EW, Min-Venditti A, Braam J, Covington MF. *Arabidopsis* synchronizes jasmonate-mediated defense with insect circadian behavior. *Proc Natl Acad Sci*. 2012 Mar 20;109(12):4674–7.

164. Aschoff J, editor. Biological Rhythms [Internet]. Boston, MA: Springer US; 1981 [cited 2022 Aug 16]. Available from: <http://link.springer.com/10.1007/978-1-4615-6552-9>
165. Mancuso S, Shabala S, editors. Rhythms in plants: phenomenology, mechanisms, and adaptive significance. Berlin ; New York: Springer; 2007. 361 p.
166. Acebrón JA, Bonilla LL, Pérez Vicente CJ, Ritort F, Spigler R. The Kuramoto model: A simple paradigm for synchronization phenomena. *Rev Mod Phys*. 2005 Apr 7;77(1):137–85.
167. Bodenstein C, Heiland I, Schuster S. Temperature compensation and entrainment in circadian rhythms. *Phys Biol*. 2012 Jun 1;9(3):036011.
168. Liu Y, Bell-Pedersen D. Circadian Rhythms in *Neurospora crassa* and Other Filamentous Fungi. *Eukaryot Cell*. 2006 Aug;5(8):1184–93.
169. McClung CR. Plant Circadian Rhythms. *Plant Cell*. 2006 Apr;18(4):792–803.
170. Ananthasubramaniam B, Diernfellner A, Brunner M, Herzog H. Ultradian Rhythms in the Transcriptome of *Neurospora crassa*. *iScience*. 2018 Nov;9:475–86.
171. Bell-Pedersen D, Garceau N, Loros JJ. Circadian rhythms in fungi. *J Genet*. 1996 Dec;75(3):387–401.
172. Más P, Yanovsky MJ. Time for circadian rhythms: plants get synchronized. *Curr Opin Plant Biol*. 2009 Oct;12(5):574–9.
173. Wang W, Barnaby JY, Tada Y, Li H, Tör M, Caldelari D, et al. Timing of plant immune responses by a central circadian regulator. *Nature*. 2011 Feb;470(7332):110–4.
174. Oliveira AG, Stevani CV, Waldenmaier HE, Viviani V, Emerson JM, Loros JJ, et al. Circadian Control Sheds Light on Fungal Bioluminescence. *Curr Biol*. 2015 Mar;25(7):964–8.
175. de Paula RM, Lewis ZA, Greene AV, Seo KS, Morgan LW, Vitalini MW, et al. Two Circadian Timing Circuits in *Neurospora crassa* Cells Share Components and Regulate Distinct Rhythmic Processes. *J Biol Rhythms*. 2006 Jun;21(3):159–68.
176. Filichkin SA, Breton G, Priest HD, Dharmawardhana P, Jaiswal P, Fox SE, et al. Global Profiling of Rice and Poplar Transcriptomes Highlights Key Conserved Circadian-Controlled Pathways and cis-Regulatory Modules. Blazquez MA, editor. *PLoS ONE*. 2011 Jun 9;6(6):e16907.
177. Hevia MA, Canessa P, Larrondo LF. Circadian clocks and the regulation of virulence in fungi: Getting up to speed. *Semin Cell Dev Biol*. 2016 Sep;57:147–55.
178. Hurley J, Loros JJ, Dunlap JC. Dissecting the Mechanisms of the Clock in *Neurospora*. In: *Methods in Enzymology* [Internet]. Elsevier; 2015 [cited 2022 Jun 30]. p. 29–52. Available from: <https://linkinghub.elsevier.com/retrieve/pii/S007668791400010X>
179. Pruneda-Paz JL, Kay SA. An expanding universe of circadian networks in higher plants. *Trends Plant Sci*. 2010 May;15(5):259–65.

180. Meng L, Mestdagh H, Ameye M, Audenaert K, Höfte M, Van Labeke MC. Phenotypic Variation of *Botrytis cinerea* Isolates Is Influenced by Spectral Light Quality. *Front Plant Sci.* 2020 Aug 13;11:1233.
181. Dunlap JC, Loros JJ. Making Time: Conservation of Biological Clocks from Fungi to Animals. Heitman J, Gow NAR, editors. *Microbiol Spectr.* 2017 May 19;5(3):5.3.05.
182. Panter PE, Muranaka T, Cuitun-Coronado D, Graham CA, Yochikawa A, Kudoh H, et al. Circadian Regulation of the Plant Transcriptome Under Natural Conditions. *Front Genet* [Internet]. 2019 Nov 29 [cited 2022 Jun 30];10. Available from: <https://www.frontiersin.org/article/10.3389/fgene.2019.01239/full>
183. Pogue AM, Price-Lloyd N, Bell-Pedersen D, Heintzen C, Loros JJ, Dunlap JC. Assignment of an essential role for the *Neurospora frequency* gene in circadian entrainment to temperature cycles. *Proc Natl Acad Sci.* 2005 Feb 8;102(6):2210–5.
184. Yoshida Y, Iigusa H, Wang N, Hasunuma K. Cross-Talk between the Cellular Redox State and the Circadian System in *Neurospora*. Yamazaki S, editor. *PLoS ONE.* 2011 Dec 2;6(12):e28227.
185. Adhvaryu K, Firoozi G, Motavaze K, Lakin-Thomas P. PRD-1, a Component of the Circadian System of *Neurospora crassa*, Is a Member of the DEAD-box RNA Helicase Family. *J Biol Rhythms.* 2016 Jun;31(3):258–71.
186. Baker CL, Dunlap JC. Circadian rhythms: Phosphorylating the CLOCK. *Cell Cycle.* 2010 Jan 15;9(2):227–32.
187. Larrondo LF, Olivares-Yañez C, Baker CL, Loros JJ, Dunlap JC. Decoupling circadian clock protein turnover from circadian period determination. *Science* [Internet]. 2015 Jan 30 [cited 2022 Jun 30];347(6221). Available from: <https://www.science.org/doi/10.1126/science.1257277>
188. Correa A, Lewis ZA, Greene AV, March IJ, Gomer RH, Bell-Pedersen D. Multiple oscillators regulate circadian gene expression in *Neurospora*. *Proc Natl Acad Sci.* 2003 Nov 11;100(23):13597–602.
189. Dunlap JC, Loros JJ. The *Neurospora* Circadian System. *J Biol Rhythms.* 2004 Oct;19(5):414–24.
190. Hurley JM, Loros JJ, Dunlap JC. Circadian Oscillators: Around the Transcription–Translation Feedback Loop and on to Output. *Trends Biochem Sci.* 2016 Oct;41(10):834–46.
191. Lakin-Thomas PL, Brody S. Circadian Rhythms in Microorganisms: New Complexities. *Annu Rev Microbiol.* 2004 Oct 1;58(1):489–519.
192. Vitalini MW, de Paula RM, Park WD, Bell-Pedersen D. The Rhythms of Life: Circadian Output Pathways in *Neurospora*. *J Biol Rhythms.* 2006 Dec;21(6):432–44.
193. Baker CL, Kettenbach AN, Loros JJ, Gerber SA, Dunlap JC. Quantitative Proteomics Reveals a Dynamic Interactome and Phase-Specific Phosphorylation in the *Neurospora* Circadian Clock. *Mol Cell.* 2009 May;34(3):354–63.

194. Bluhm BH, Burnham AM, Dunkle LD. A circadian rhythm regulating hyphal melanization in *Cercospora kikuchii*. *Mycologia*. 2010 Nov;102(6):1221–8.
195. Cha J, Yuan H, Liu Y. Regulation of the Activity and Cellular Localization of the Circadian Clock Protein FRQ. *J Biol Chem*. 2011 Apr;286(13):11469–78.
196. Cha J, Zhou M, Liu Y. Mechanism of the *Neurospora* Circadian Clock, a FREQUENCY-centric View. *Biochemistry*. 2015 Jan 20;54(2):150–6.
197. Chen CH, Dunlap JC, Loros JJ. *Neurospora* illuminates fungal photoreception. *Fungal Genet Biol*. 2010 Nov;47(11):922–9.
198. Chen CH, DeMay BS, Gladfelter AS, Dunlap JC, Loros JJ. Physical interaction between VIVID and white collar complex regulates photoadaptation in *Neurospora*. *Proc Natl Acad Sci*. 2010 Sep 21;107(38):16715–20.
199. Cheng P, Yang Y, Wang L, He Q, Liu Y. WHITE COLLAR-1, a Multifunctional *Neurospora* Protein Involved in the Circadian Feedback Loops, Light Sensing, and Transcription Repression of *wc-2*. *J Biol Chem*. 2003 Feb;278(6):3801–8.
200. Cheng P, He Q, Wang L, Liu Y. Regulation of the *Neurospora* circadian clock by an RNA helicase. *Genes Dev*. 2005 Jan 15;19(2):234–41.
201. Cockrell AL, Pirlo RK, Babson DM, Cusick KD, Soto CM, Petersen ER, et al. Suppressing the *Neurospora crassa* circadian clock while maintaining light responsiveness in continuous stirred tank reactors. *Sci Rep*. 2015 Sep;5(1):10691.
202. Denault DL. WC-2 mediates WC-1-FRQ interaction within the PAS protein-linked circadian feedback loop of *Neurospora*. *EMBO J*. 2001 Jan 15;20(1):109–17.
203. Diernfellner A, Colot HV, Dintsis O, Loros JJ, Dunlap JC, Brunner M. Long and short isoforms of *Neurospora* clock protein FRQ support temperature-compensated circadian rhythms. *FEBS Lett*. 2007 Dec 22;581(30):5759–64.
204. Dong W, Tang X, Yu Y, Nilsen R, Kim R, Griffith J, et al. Systems Biology of the Clock in *Neurospora crassa*. *Provent NJ*, editor. *PLoS ONE*. 2008 Aug 29;3(8):e3105.
205. Froehlich AC, Liu Y, Loros JJ, Dunlap JC. White Collar-1, a Circadian Blue Light Photoreceptor, Binding to the *frequency* Promoter. *Science*. 2002 Aug 2;297(5582):815–9.
206. Froehlich AC, Loros JJ, Dunlap JC. Rhythmic binding of a WHITE COLLAR-containing complex to the *frequency* promoter is inhibited by FREQUENCY. *Proc Natl Acad Sci*. 2003 May 13;100(10):5914–9.
207. Gin E, Diernfellner ACR, Brunner M, Höfer T. The *Neurospora* photoreceptor VIVID exerts negative and positive control on light sensing to achieve adaptation. *Mol Syst Biol*. 2013 Jan;9(1):667.
208. He Q, Liu Y. Molecular mechanism of light responses in *Neurospora* : from light-induced transcription to photoadaptation. *Genes Dev*. 2005 Dec 1;19(23):2888–99.

209. Hunt SM, Thompson S, Elvin M, Heintzen C. VIVID interacts with the WHITE COLLAR complex and FREQUENCY-interacting RNA helicase to alter light and clock responses in *Neurospora*. *Proc Natl Acad Sci*. 2010 Sep 21;107(38):16709–14.
210. Lakin-Thomas PL, Bell-Pedersen D, Brody S. The Genetics of Circadian Rhythms in *Neurospora*. In: *Advances in Genetics* [Internet]. Elsevier; 2011 [cited 2022 Jun 30]. p. 55–103. Available from: <https://linkinghub.elsevier.com/retrieve/pii/B9780123876904000039>
211. Lee K, Dunlap JC, Loros JJ. Roles for WHITE COLLAR-1 in Circadian and General Photoperception in *Neurospora crassa*. *Genetics*. 2003 Jan 1;163(1):103–14.
212. Lee SJ, Morse D, Hijri M. Holobiont chronobiology: mycorrhiza may be a key to linking aboveground and underground rhythms. *Mycorrhiza*. 2019 Oct;29(5):403–12.
213. Li S, Motavaze K, Kafes E, Suntharalingam S, Lakin-Thomas P. A New Mutation Affecting FRQ-Less Rhythms in the Circadian System of *Neurospora crassa*. Bell-Pederson D, editor. *PLoS Genet*. 2011 Jun 23;7(6):e1002151.
214. Malzahn E, Ciprianidis S, Káldi K, Schafmeier T, Brunner M. Photoadaptation in *Neurospora* by Competitive Interaction of Activating and Inhibitory LOV Domains. *Cell*. 2010 Sep;142(5):762–72.
215. McCorison CB, Goodwin SB. The wheat pathogen *Zymoseptoria tritici* senses and responds to different wavelengths of light. *BMC Genomics* [Internet]. 2020 Dec [cited 2022 Jun 30];21(1). Available from: <https://bmcgenomics.biomedcentral.com/articles/10.1186/s12864-020-06899-y>
216. Neiss A, Schafmeier T, Brunner M. Transcriptional regulation and function of the *Neurospora* clock gene *white collar 2* and its isoforms. *EMBO Rep*. 2008 Aug;9(8):788–94.
217. Nowrousian M, Duffield GE, Loros JJ, Dunlap JC. The *frequency* Gene Is Required for Temperature-Dependent Regulation of Many Clock-Controlled Genes in *Neurospora crassa*. *Genetics*. 2003 Jul 1;164(3):923–33.
218. Nsa IY, Karunarathna N, Liu X, Huang H, Boettger B, Bell-Pedersen D. A Novel Cryptochrome-Dependent Oscillator in *Neurospora crassa*. *Genetics*. 2015 Jan 1;199(1):233–45.
219. Sancar G, Sancar C, Brügger B, Ha N, Sachsenheimer T, Gin E, et al. A Global Circadian Repressor Controls Antiphase Expression of Metabolic Genes in *Neurospora*. *Mol Cell*. 2011 Dec;44(5):687–97.
220. Sancar G, Sancar C, Brunner M. Metabolic compensation of the *Neurospora* clock by a glucose-dependent feedback of the circadian repressor CSP1 on the core oscillator. *Genes Dev*. 2012 Nov 1;26(21):2435–42.
221. Schafmeier T, Káldi K, Diernfellner A, Mohr C, Brunner M. Phosphorylation-dependent maturation of *Neurospora* circadian clock protein from a nuclear repressor toward a cytoplasmic activator. *Genes Dev*. 2006 Feb 1;20(3):297–306.

222. Shi M, Collett M, Loros JJ, Dunlap JC. FRQ-Interacting RNA Helicase Mediates Negative and Positive Feedback in the *Neurospora* Circadian Clock. *Genetics*. 2010 Feb 1;184(2):351–61.
223. Smith KM, Sancar G, Dekhang R, Sullivan CM, Li S, Tag AG, et al. Transcription Factors in Light and Circadian Clock Signaling Networks Revealed by Genomewide Mapping of Direct Targets for *Neurospora* White Collar Complex. *Eukaryot Cell*. 2010 Oct;9(10):1549–56.
224. Wang B, Kettenbach AN, Gerber SA, Loros JJ, Dunlap JC. *Neurospora* WC-1 Recruits SWI/SNF to Remodel frequency and Initiate a Circadian Cycle. Kramer A, editor. *PLoS Genet*. 2014 Sep 25;10(9):e1004599.
225. Young MW, Kay SA. Time zones: a comparative genetics of circadian clocks. *Nat Rev Genet*. 2001 Sep;2(9):702–15.
226. Zhang L, Wan Y, Huang G, Wang D, Yu X, Huang G, et al. The exosome controls alternative splicing by mediating the gene expression and assembly of the spliceosome complex. *Sci Rep [Internet]*. 2015 Oct [cited 2022 Jun 30];5(1). Available from: <http://www.nature.com/articles/srep13403>
227. Collett MA, Garceau N, Dunlap JC, Loros JJ. Light and Clock Expression of the *Neurospora* Clock Gene *frequency* Is Differentially Driven by but Dependent on WHITE COLLAR-2. *Genetics*. 2002 Jan 1;160(1):149–58.
228. Costantini C, Renga G, Sellitto F, Borghi M, Stincardini C, Pariano M, et al. Microbes in the Era of Circadian Medicine. *Front Cell Infect Microbiol [Internet]*. 2020 Feb 5 [cited 2022 Jun 30];10. Available from: <https://www.frontiersin.org/article/10.3389/fcimb.2020.00030/full>
229. Dunlap JC. Proteins in the *Neurospora* Circadian Clockworks. *J Biol Chem*. 2006 Sep;281(39):28489–93.
230. Dunlap JC, Loros JJ. How fungi keep time: circadian system in *Neurospora* and other fungi. *Curr Opin Microbiol*. 2006 Dec;9(6):579–87.
231. Hurley JM, Dasgupta A, Emerson JM, Zhou X, Ringelberg CS, Knabe N, et al. Analysis of clock-regulated genes in *Neurospora* reveals widespread posttranscriptional control of metabolic potential. *Proc Natl Acad Sci*. 2014 Dec 2;111(48):16995–7002.
232. Tong SM, Wang DY, Cai Q, Ying SH, Feng MG. Opposite Nuclear Dynamics of Two FRH-Dominated Frequency Proteins Orchestrate Non-Rhythmic Conidiation in *Beauveria bassiana*. *Cells*. 2020 Mar 5;9(3):626.
233. Upadhyay A, Brunner M, Herzog H. An Inactivation Switch Enables Rhythms in a *Neurospora* Clock Model. *Int J Mol Sci*. 2019 Jun 19;20(12):2985.
234. Wang B, Zhou X, Loros JJ, Dunlap JC. Alternative Use of DNA Binding Domains by the *Neurospora* White Collar Complex Dictates Circadian Regulation and Light Responses. *Mol Cell Biol*. 2016 Mar;36(5):781–93.

235. He Q. FWD1-mediated degradation of FREQUENCY in *Neurospora* establishes a conserved mechanism for circadian clock regulation. *EMBO J.* 2003 Sep 1;22(17):4421–30.
236. Querfurth C, Diernfellner ACR, Gin E, Malzahn E, Höfer T, Brunner M. Circadian Conformational Change of the *Neurospora* Clock Protein FREQUENCY Triggered by Clustered Hyperphosphorylation of a Basic Domain. *Mol Cell.* 2011 Sep;43(5):713–22.
237. Bell-Pedersen D. Understanding Circadian Rhythmicity in *Neurospora crassa*: From Behavior to Genes and Back Again. *Fungal Genet Biol.* 2000 Feb;29(1):1–18.
238. Smolen P, Baxter DA, Byrne JH. Modeling Circadian Oscillations with Interlocking Positive and Negative Feedback Loops. *J Neurosci.* 2001 Sep 1;21(17):6644–56.
239. Faure S, Turner AS, Gruszka D, Christodoulou V, Davis SJ, von Korff M, et al. Mutation at the circadian clock gene *EARLY MATURITY 8* adapts domesticated barley (*Hordeum vulgare*) to short growing seasons. *Proc Natl Acad Sci.* 2012 May 22;109(21):8328–33.
240. Rodriguez-Romero J, Hedtke M, Kastner C, Müller S, Fischer R. Fungi, Hidden in Soil or Up in the Air: Light Makes a Difference. *Annu Rev Microbiol.* 2010 Oct 13;64(1):585–610.
241. Eisenman HC, Casadevall A. Synthesis and assembly of fungal melanin. *Appl Microbiol Biotechnol.* 2012 Feb;93(3):931–40.
242. Bendix C, Marshall CM, Harmon FG. Circadian Clock Genes Universally Control Key Agricultural Traits. *Mol Plant.* 2015 Aug;8(8):1135–52.
243. Bhardwaj V, Meier S, Petersen LN, Ingle RA, Roden LC. Defence Responses of *Arabidopsis thaliana* to Infection by *Pseudomonas syringae* Are Regulated by the Circadian Clock. Hazen SP, editor. *PLoS ONE.* 2011 Oct 31;6(10):e26968.
244. Curtis AM, Bellet MM, Sassone-Corsi P, O’Neill LAJ. Circadian Clock Proteins and Immunity. *Immunity.* 2014 Feb;40(2):178–86.
245. De Caluwé J, Xiao Q, Hermans C, Verbruggen N, Leloup JC, Gonze D. A Compact Model for the Complex Plant Circadian Clock. *Front Plant Sci* [Internet]. 2016 Feb 5 [cited 2022 Jun 30];7. Available from: <http://journal.frontiersin.org/Article/10.3389/fpls.2016.00074/abstract>
246. Goodspeed D, Liu JD, Chehab EW, Sheng Z, Francisco M, Kliebenstein DJ, et al. Postharvest Circadian Entrainment Enhances Crop Pest Resistance and Phytochemical Cycling. *Curr Biol.* 2013 Jul;23(13):1235–41.
247. Hosseini-Moghaddam MS, Soltani J. An investigation on the effects of photoperiod, aging and culture media on vegetative growth and sporulation of rice blast pathogen *Pyricularia oryzae*. 2013;3(2):10.
248. Izawa T. Physiological significance of the plant circadian clock in natural field conditions: Physiological significance of circadian clock. *Plant Cell Environ.* 2012 Oct;35(10):1729–41.
249. Nitschke S, Cortleven A, Iven T, Feussner I, Havaux M, Riefler M, et al. Circadian Stress Regimes Affect the Circadian Clock and Cause Jasmonic Acid-Dependent Cell Death in Cytokinin-Deficient *Arabidopsis* Plants. *Plant Cell.* 2016 Jun 27;tpc.00016.2016.

250. Robertson FC, Skeffington AW, Gardner MJ, Webb AAR. Interactions between circadian and hormonal signalling in plants. *Plant Mol Biol.* 2009 Mar;69(4):419–27.
251. Scholz SS, Schmidt-Heck W, Guthke R, Furch ACU, Reichelt M, Gershenzon J, et al. *Verticillium dahliae*-*Arabidopsis* Interaction Causes Changes in Gene Expression Profiles and Jasmonate Levels on Different Time Scales. *Front Microbiol.* 2018 Feb 13;9:217.
252. Sugiyama N, Izawa T, Oikawa T, Shimamoto K. Light regulation of circadian clock-controlled gene expression in rice: Rice circadian clock. *Plant J.* 2001 Dec 23;26(6):607–15.
253. Yamauchi Y, Makihara M, Ishikawa A. Leaf age and time of inoculation contribute to nonhost resistance to *Pyricularia oryzae* in *Arabidopsis thaliana*. *Plant Biotechnol.* 2017;34(4):207–10.
254. Zhang Y, Wang Y, Wei H, Li N, Tian W, Chong K, et al. Circadian Evening Complex Represses Jasmonate-Induced Leaf Senescence in *Arabidopsis*. *Mol Plant.* 2018 Feb;11(2):326–37.
255. Hassidim M, Dakhiya Y, Turjeman A, Hussien D, Shor E, Anidjar A, et al. *CIRCADIAN CLOCK ASSOCIATED1 (CCA1)* and the Circadian Control of Stomatal Aperture. *Plant Physiol.* 2017 Dec;175(4):1864–77.
256. Castro-Longoria E, Brody S, Bartnicki-García S. Kinetics of circadian band development in *Neurospora crassa*. *Fungal Genet Biol.* 2007 Jul;44(7):672–81.
257. Larrondo LF, Canessa P. The Clock Keeps on Ticking: Emerging Roles for Circadian Regulation in the Control of Fungal Physiology and Pathogenesis. In: Rodrigues ML, editor. *Fungal Physiology and Immunopathogenesis* [Internet]. Cham: Springer International Publishing; 2018 [cited 2022 Jun 30]. p. 121–56. Available from: http://link.springer.com/10.1007/82_2018_143
258. Park J, Lee YH. Bidirectional-Genetics Platform, a Dual-Purpose Mutagenesis Strategy for Filamentous Fungi. *Eukaryot Cell.* 2013 Nov;12(11):1547–53.
259. Shi H, Chen N, Zhu X, Liang S, Li L, Wang J, et al. F-box proteins MoFwd1, MoCdc4 and MoFbx15 regulate development and pathogenicity in the rice blast fungus *Magnaporthe oryzae*. *Environ Microbiol.* 2019 Aug;21(8):3027–45.
260. Koga H, Dohi K, Mori M. Abscisic acid and low temperatures suppress the whole plant-specific resistance reaction of rice plants to the infection of *Magnaporthe grisea*. *Physiol Mol Plant Pathol.* 2004 Jul;65(1):3–9.
261. Bell-Pedersen D, Shinohara ML, Loros JJ, Dunlap JC. Circadian clock-controlled genes isolated from *Neurospora crassa* are late night- to early morning-specific. *Proc Natl Acad Sci.* 1996 Nov 12;93(23):13096–101.
262. Li J, Liu YH, Zhang Y, Chen C, Yu X, Yu SW. Drought stress modulates diurnal oscillations of circadian clock and drought-responsive genes in *Oryza sativa* L. *Yi Chuan Hered.* 2017 Sep 20;39(9):837–46.
263. Schindelin J, Arganda-Carreras I, Frise E, Kaynig V, Longair M, Pietzsch T, et al. Fiji: an open-source platform for biological-image analysis. *Nat Methods.* 2012 Jul;9(7):676–82.

264. Stanley MS, Callow ME, Perry R, Alberte RS, Smith R, Callow JA. Inhibition of Fungal Spore Adhesion by Zosteric Acid as the Basis for a Novel, Nontoxic Crop Protection Technology. *Phytopathology*[®]. 2002 Apr;92(4):378–83.
265. Sharkey JP, Foo DCW, Kabla A, Baumberg JJ, Bowman RW. A one-piece 3D printed flexure translation stage for open-source microscopy. *Rev Sci Instrum*. 2016 Feb;87(2):025104.
266. Oliveira-Garcia E, Valent B. Characterizing the Secretion Systems of *Magnaporthe oryzae*. In: Jacob S, editor. *Magnaporthe oryzae* [Internet]. New York, NY: Springer US; 2021 [cited 2022 Aug 23]. p. 69–77. (Methods in Molecular Biology; vol. 2356). Available from: https://link.springer.com/10.1007/978-1-0716-1613-0_5
267. Murchie EH, Lawson T. Chlorophyll fluorescence analysis: a guide to good practice and understanding some new applications. *J Exp Bot*. 2013 Oct;64(13):3983–98.
268. Nouri H, Anderson S, Sutton P, Beecham S, Nagler P, Jarchow CJ, et al. NDVI, scale invariance and the modifiable areal unit problem: An assessment of vegetation in the Adelaide Parklands. *Sci Total Environ*. 2017 Apr;584–585:11–8.
269. Foster AJ, Martin-Urdiroz M, Yan X, Wright HS, Soanes DM, Talbot NJ. CRISPR-Cas9 ribonucleoprotein-mediated co-editing and counterselection in the rice blast fungus. *Sci Rep*. 2018 Dec;8(1):14355.
270. Heigwer F, Kerr G, Boutros M. E-CRISP: fast CRISPR target site identification. *Nat Methods*. 2014 Feb;11(2):122–3.
271. NEB. EnGen sgRNA Designer [Internet]. [cited 2022 Dec 19]. Available from: <https://sgrna.neb.com/#!/sgrna>
272. Blaiklock P. RestrictionMapper version 3 [Internet]. [cited 2022 Dec 19]. Available from: <https://restrictionmapper.org/>
273. Untergasser A, Cutcutache I, Koressaar T, Ye J, Faircloth BC, Remm M, et al. Primer3—new capabilities and interfaces. *Nucleic Acids Res*. 2012 Aug;40(15):e115.
274. Jia Y, Wamishe YA, Zhou B. An expedited method for isolation of DNA for PCR from *Magnaporthe oryzae* stored on filter paper. *Crop J*. 2014 Oct;2(5):267–71.
275. Mendiburu F de. agricolae: Statistical Procedures for Agricultural Research [Internet]. 2021 [cited 2022 Dec 29]. Available from: <https://CRAN.R-project.org/package=agricolae>
276. Robinson D, Hayes A, Couch [aut S, cre, RStudio, Patil I, et al. broom: Convert Statistical Objects into Tidy Tibbles [Internet]. 2022 [cited 2022 Dec 29]. Available from: <https://CRAN.R-project.org/package=broom>
277. Wickham H, François R, Henry L, Müller K, RStudio. dplyr: A Grammar of Data Manipulation [Internet]. 2022 [cited 2022 Dec 29]. Available from: <https://CRAN.R-project.org/package=dplyr>
278. Wickham H, Chang W, Henry L, Pedersen TL, Takahashi K, Wilke C, et al. ggplot2: Create Elegant Data Visualisations Using the Grammar of Graphics [Internet]. 2022 [cited 2022 Dec 29]. Available from: <https://CRAN.R-project.org/package=ggplot2>

279. Aphalo PJ, Slowikowski K, Mouksassi S. ggpmisc: Miscellaneous Extensions to 'ggplot2' [Internet]. 2022 [cited 2022 Dec 29]. Available from: <https://CRAN.R-project.org/package=ggpmisc>
280. Kassambara A. ggpubr: 'ggplot2' Based Publication Ready Plots [Internet]. 2022 [cited 2022 Dec 29]. Available from: <https://CRAN.R-project.org/package=ggpubr>
281. Iannone R, Cheng J, Schloerke B, Hughes E, Seo J, RStudio. gt: Easily Create Presentation-Ready Display Tables [Internet]. 2022 [cited 2022 Dec 29]. Available from: <https://CRAN.R-project.org/package=gt>
282. Gordon M, Gragg S, Konings P. htmlTable: Advanced Tables for Markdown/HTML [Internet]. 2022 [cited 2022 Dec 29]. Available from: <https://CRAN.R-project.org/package=htmlTable>
283. Zhu [aut H, cre, Travison T, Tsai T, Beasley W, Xie Y, et al. kableExtra: Construct Complex Table with 'kable' and Pipe Syntax [Internet]. 2021 [cited 2022 Dec 29]. Available from: <https://CRAN.R-project.org/package=kableExtra>
284. Ooms [aut J, cre. magick: Advanced Graphics and Image-Processing in R [Internet]. 2021 [cited 2022 Dec 29]. Available from: <https://CRAN.R-project.org/package=magick>
285. Wickham H, Bryan J, attribution) Rs (Copyright holder of all R code and all C code without explicit copyright, code) MK (Author of included R, code) KV (Author of included libxls, code) CL (Author of included libxls, et al. readxl: Read Excel Files [Internet]. 2022 [cited 2022 Dec 29]. Available from: <https://CRAN.R-project.org/package=readxl>
286. Kassambara A. rstatix: Pipe-Friendly Framework for Basic Statistical Tests [Internet]. 2022 [cited 2022 Dec 29]. Available from: <https://CRAN.R-project.org/package=rstatix>
287. Wickham H, Seidel D, RStudio. scales: Scale Functions for Visualization [Internet]. 2022 [cited 2022 Dec 29]. Available from: <https://CRAN.R-project.org/package=scales>
288. Wickham H, Girlich M, RStudio. tidyr: Tidy Messy Data [Internet]. 2022 [cited 2022 Dec 29]. Available from: <https://CRAN.R-project.org/package=tidyr>
289. Wickham H, RStudio. tidyverse: Easily Install and Load the 'Tidyverse' [Internet]. 2022 [cited 2022 Dec 29]. Available from: <https://CRAN.R-project.org/package=tidyverse>
290. Bock CH, Poole GH, Parker PE, Gottwald TR. Plant Disease Severity Estimated Visually, by Digital Photography and Image Analysis, and by Hyperspectral Imaging. *Crit Rev Plant Sci*. 2010 Mar 10;29(2):59–107.
291. Hughes A, Askew K, Scotson CP, Williams K, Sauze C, Corke F, et al. Non-destructive, high-content analysis of wheat grain traits using X-ray micro computed tomography. *Plant Methods*. 2017 Dec;13(1):76.
292. Kashyap Y, Sharma T, Shahnawaz S. Analysis of Plant Diseases with Detection using Image Processing Methods. *Int J Comput Appl*. 2017 May 17;166(7):28–31.
293. Li L, Zhang Q, Huang D. A Review of Imaging Techniques for Plant Phenotyping. *Sensors*. 2014 Oct 24;14(11):20078–111.

294. Muskat LC, Kerkhoff Y, Humbert P, Nattkemper TW, Eilenberg J, Patel AV. Image analysis-based quantification of fungal sporulation by automatic conidia counting and gray value correlation. *MethodsX*. 2021;8:101218.
295. Mutka AM, Bart RS. Image-based phenotyping of plant disease symptoms. *Front Plant Sci* [Internet]. 2015 Jan 5 [cited 2022 Jun 30];5. Available from: <http://journal.frontiersin.org/article/10.3389/fpls.2014.00734/abstract>
296. Mutka AM, Fentress SJ, Sher JW, Berry JC, Pretz C, Nusinow DA, et al. Quantitative, image-based phenotyping methods provide insight into spatial and temporal dimensions of plant disease. *Plant Physiol*. 2016 Jul 21;pp.00984.2016.
297. Pujari JD, Yakkundimath R, Byadgi AS. Image Processing Based Detection of Fungal Diseases in Plants. *Procedia Comput Sci*. 2015;46:1802–8.
298. Singh V, Misra AK. Detection of plant leaf diseases using image segmentation and soft computing techniques. *Inf Process Agric*. 2017 Mar;4(1):41–9.
299. Wang C, Yang Y, Yuan X, Xu Q, Feng Y, Yu H, et al. Genome-wide association study of blast resistance in indica rice. *BMC Plant Biol*. 2014 Dec;14(1):311.
300. Wang G, Sun Y, Wang J. Automatic Image-Based Plant Disease Severity Estimation Using Deep Learning. *Comput Intell Neurosci*. 2017;2017:1–8.
301. Williams D, Britten A, McCallum S, Jones H, Aitkenhead M, Karley A, et al. A method for automatic segmentation and splitting of hyperspectral images of raspberry plants collected in field conditions. *Plant Methods*. 2017 Dec;13(1):74.
302. Cheng HD, Jiang XH, Sun Y, Wang J. Color image segmentation: advances and prospects. *Pattern Recognit*. 2001 Dec;34(12):2259–81.
303. Cairns TC, Feurstein C, Zheng X, Zheng P, Sun J, Meyer V. A quantitative image analysis pipeline for the characterization of filamentous fungal morphologies as a tool to uncover targets for morphology engineering: a case study using *aplD* in *Aspergillus niger*. *Biotechnol Biofuels* [Internet]. 2019 Dec [cited 2022 Jun 30];12(1). Available from: <https://biotechnologyforbiofuels.biomedcentral.com/articles/10.1186/s13068-019-1473-0>
304. Sibiya M, Sumbwanyambe M. An Algorithm for Severity Estimation of Plant Leaf Diseases by the Use of Colour Threshold Image Segmentation and Fuzzy Logic Inference: A Proposed Algorithm to Update a “Leaf Doctor” Application. *AgriEngineering*. 2019 May 1;1(2):205–19.
305. Valle B, Simonneau T, Boulord R, Sourd F, Frisson T, Ryckewaert M, et al. PYM: a new, affordable, image-based method using a Raspberry Pi to phenotype plant leaf area in a wide diversity of environments. *Plant Methods* [Internet]. 2017 Dec [cited 2022 Jun 30];13(1). Available from: <https://plantmethods.biomedcentral.com/articles/10.1186/s13007-017-0248-5>
306. Chen W, Li W, Dong X, Pei J. A Review of Biological Image Analysis. *Curr Bioinforma*. 2018 Jul 3;13(4):337–43.

307. Das Choudhury S, Samal A, Awada T. Leveraging Image Analysis for High-Throughput Plant Phenotyping. *Front Plant Sci* [Internet]. 2019 Apr 24 [cited 2022 Jun 30];10. Available from: <https://www.frontiersin.org/article/10.3389/fpls.2019.00508/full>
308. Hartmann A, Czauderna T, Hoffmann R, Stein N, Schreiber F. HTPPheno: An image analysis pipeline for high-throughput plant phenotyping. *BMC Bioinformatics* [Internet]. 2011 Dec [cited 2022 Jun 30];12(1). Available from: <https://bmcbioinformatics.biomedcentral.com/articles/10.1186/1471-2105-12-148>
309. Kherlopian AR, Song T, Duan Q, Neimark MA, Po MJ, Gohagan JK, et al. A review of imaging techniques for systems biology. *BMC Syst Biol* [Internet]. 2008 Dec [cited 2022 Jun 30];2(1). Available from: <https://bmcsystbiol.biomedcentral.com/articles/10.1186/1752-0509-2-74>
310. Knecht AC, Campbell MT, Caprez A, Swanson DR, Walia H. Image Harvest: an open-source platform for high-throughput plant image processing and analysis. *J Exp Bot*. 2016 May;67(11):3587–99.
311. Lowe A, Harrison N, French AP. Hyperspectral image analysis techniques for the detection and classification of the early onset of plant disease and stress. *Plant Methods* [Internet]. 2017 Dec [cited 2022 Jun 30];13(1). Available from: <http://plantmethods.biomedcentral.com/articles/10.1186/s13007-017-0233-z>
312. Moller B, Chen H, Schmidt T, Zieschank A, Patzak R, Turke M, et al. rhizoTrak: A flexible open source Fiji plugin for user-friendly manual annotation of time-series images from minirhizotrons. 2019;19.
313. Vasseur F, Bresson J, Wang G, Schwab R, Weigel D. Image-based methods for phenotyping growth dynamics and fitness components in *Arabidopsis thaliana*. *Plant Methods* [Internet]. 2018 Dec [cited 2022 Jun 30];14(1). Available from: <https://plantmethods.biomedcentral.com/articles/10.1186/s13007-018-0331-6>
314. Rzanny M, Seeland M, Wäldchen J, Mäder P. Acquiring and preprocessing leaf images for automated plant identification: understanding the tradeoff between effort and information gain. *Plant Methods*. 2017 Dec;13(1):97.
315. Gonzalez RC, Woods RE. *Digital image processing*. New York, NY: Pearson; 2018. 1168 p.
316. Jurio A, Pagola M, Galar M, Lopez-Molina C, Paternain D. A Comparison Study of Different Color Spaces in Clustering Based Image Segmentation. In: Hüllermeier E, Kruse R, Hoffmann F, editors. *Information Processing and Management of Uncertainty in Knowledge-Based Systems Applications* [Internet]. Berlin, Heidelberg: Springer Berlin Heidelberg; 2010 [cited 2022 Aug 24]. p. 532–41. (Communications in Computer and Information Science; vol. 81). Available from: http://link.springer.com/10.1007/978-3-642-14058-7_55
317. M L. *Image processing #1: Contours and Areas* [Internet]. Medium. 2021 [cited 2022 Aug 24]. Available from: <https://economyoftime.net/image-processing-1-contours-and-areas-c50a586c6675>
318. Stutz D, Hermans A, Leibe B. Superpixels: An evaluation of the state-of-the-art. *Comput Vis Image Underst*. 2018 Jan;166:1–27.

319. Bernas T, Zarebski M, Cook RR, Dobrucki JW, Cook PR. Minimizing photobleaching during confocal microscopy of fluorescent probes bound to chromatin: role of anoxia and photon flux. *J Microsc.* 2004 Sep;215(Pt 3):281–96.
320. Bianconi F, Bello R, Fernández A, González E. On Comparing Colour Spaces From a Performance Perspective: Application to Automated Classification of Polished Natural Stones. In: Murino V, Puppo E, Sona D, Cristani M, Sansone C, editors. *New Trends in Image Analysis and Processing -- ICIAP 2015 Workshops*. Cham: Springer International Publishing; 2015. p. 71–8. (Lecture Notes in Computer Science).
321. Ford A, Roberts A. Colour Space Conversions [Internet]. BBC; 1998. Available from: <http://poynton.ca/PDFs/coloureq.pdf>
322. Papagianni M. Characterization of Fungal Morphology using Digital Image Analysis Techniques. *J Microb Biochem Technol* [Internet]. 2014 [cited 2022 Jun 30];06(04). Available from: <https://www.omicsonline.org/open-access/characterization-of-fungal-morphology-using-digital-image-analysis-techniques-1948-5948.1000142.php?aid=25456>
323. Pridmore TP, French AP, Pound MP. What lies beneath: underlying assumptions in bioimage analysis. *Trends Plant Sci.* 2012 Dec;17(12):688–92.
324. Vidal-Diez de Ulzurrun G, Huang TY, Chang CW, Lin HC, Hsueh YP. Fungal feature tracker (FFT): A tool for quantitatively characterizing the morphology and growth of filamentous fungi. Poiset T, editor. *PLOS Comput Biol.* 2019 Oct 31;15(10):e1007428.
325. Yang W, Guo Z, Huang C, Duan L, Chen G, Jiang N, et al. Combining high-throughput phenotyping and genome-wide association studies to reveal natural genetic variation in rice. *Nat Commun* [Internet]. 2014 Dec [cited 2022 Jun 30];5(1). Available from: <http://www.nature.com/articles/ncomms6087>
326. Sandmann M, Grosch R, Graefe J. The Use of Features from Fluorescence, Thermography, and NDVI Imaging to Detect Biotic Stress in Lettuce. *Plant Dis.* 2018 Jun;102(6):1101–7.
327. Shihan MH, Novo SG, Le Marchand SJ, Wang Y, Duncan MK. A simple method for quantitating confocal fluorescent images. *Biochem Biophys Rep.* 2021 Mar;25:100916.
328. Brunk M, Sputh S, Doose S, van de Linde S, Terpitz U. HyphaTracker: An ImageJ toolbox for time-resolved analysis of spore germination in filamentous fungi. *Sci Rep* [Internet]. 2018 Dec [cited 2022 Jun 30];8(1). Available from: <http://www.nature.com/articles/s41598-017-19103-1>
329. Kahu SY, Raut RB, Bhurchandi KM. Review and evaluation of color spaces for image/video compression. *Color Res Appl.* 2019;44(1):8–33.
330. French A, Pridmore T, Lowe A, Pound M. *Image Analysis Methods for Biologists* (University of Nottingham Future Learn course). Online presented at; 2018; Online.
331. Sun G, Jia X, Geng T. Plant Diseases Recognition Based on Image Processing Technology. *J Electr Comput Eng.* 2018;2018:1–7.
332. Awty-Carroll D, Clifton-Brown J, Robson P. Using k-NN to analyse images of diverse germination phenotypes and detect single seed germination in *Miscanthus sinensis*. *Plant*

- Methods [Internet]. 2018 Dec [cited 2022 Jun 30];14(1). Available from: <https://plantmethods.biomedcentral.com/articles/10.1186/s13007-018-0272-0>
333. Jayakody H, Liu S, Whitty M, Petrie P. Microscope image based fully automated stomata detection and pore measurement method for grapevines. *Plant Methods* [Internet]. 2017 Dec [cited 2022 Jun 30];13(1). Available from: <http://plantmethods.biomedcentral.com/articles/10.1186/s13007-017-0244-9>
334. Pérez-Bueno ML, Pineda M, Cabeza FM, Barón M. Multicolor Fluorescence Imaging as a Candidate for Disease Detection in Plant Phenotyping. *Front Plant Sci* [Internet]. 2016 Dec 2 [cited 2022 Jun 30];7. Available from: <http://journal.frontiersin.org/article/10.3389/fpls.2016.01790/full>
335. Easlon HM, Bloom AJ. Easy Leaf Area: Automated digital image analysis for rapid and accurate measurement of leaf area. *Appl Plant Sci*. 2014 Jul;2(7):1400033.
336. Getman-Pickering ZL, Campbell A, Aflitto N, Grele A, Davis JK, Uguine TA. LeafByte: A mobile application that measures leaf area and herbivory quickly and accurately. *Methods Ecol Evol*. 2020;11(2):215–21.
337. Weight C, Parnham D, Waites R. TECHNICAL ADVANCE: LeafAnalyser: a computational method for rapid and large-scale analyses of leaf shape variation: Computational analysis of leaf shape variation. *Plant J*. 2007 Oct 5;53(3):578–86.
338. Tessmer OL, Jiao Y, Cruz JA, Kramer DM, Chen J. Functional approach to high-throughput plant growth analysis. *BMC Syst Biol*. 2013 Dec;7(S6):S17.
339. Bresson J, Bieker S, Riester L, Doll J, Zentgraf U. A guideline for leaf senescence analyses: from quantification to physiological and molecular investigations. *J Exp Bot*. 2018 Feb 12;69(4):769–86.
340. Walter A, Schurr U. Dynamics of Leaf and Root Growth: Endogenous Control versus Environmental Impact. *Ann Bot*. 2005 May 1;95(6):891–900.
341. Walter A, Scharr H, Gilmer F, Zierer R, Nagel KA, Ernst M, et al. Dynamics of seedling growth acclimation towards altered light conditions can be quantified via GROWSCREEN: a setup and procedure designed for rapid optical phenotyping of different plant species. *New Phytol*. 2007 Apr;174(2):447–55.
342. Price CA, Symonova O, Mileyko Y, Hilley T, Weitz JS. Leaf Extraction and Analysis Framework Graphical User Interface: Segmenting and Analyzing the Structure of Leaf Veins and Areoles. *Plant Physiol*. 2011 Jan 3;155(1):236–45.
343. Backhaus A, Kuwabara A, Bauch M, Monk N, Sanguinetti G, Fleming A. LEAFPROCESSOR : a new leaf phenotyping tool using contour bending energy and shape cluster analysis. *New Phytol*. 2010 Jul;187(1):251–61.
344. Remmler L, Rolland-Lagan AG. Computational Method for Quantifying Growth Patterns at the Adaxial Leaf Surface in Three Dimensions. *Plant Physiol*. 2012 May;159(1):27–39.
345. Rousseau C, Belin E, Bove E, Rousseau D, Fabre F, Berruyer R, et al. High throughput quantitative phenotyping of plant resistance using chlorophyll fluorescence image analysis. *Plant Methods*. 2013 Dec;9(1):17.

346. Ferreira T, Rasband W. ImageJ User Guide. :198.
347. Mutterer J, Rasband W. ImageJ Macro Language Programmer's Reference Guide v1.46d. :45.
348. NIH. macro 'Get Time' [Internet]. imageJ. [cited 2022 Sep 7]. Available from: <https://imagej.nih.gov/ij/macros/GetDateAndTime.txt>
349. NIH. Wait For User Macro Demo [Internet]. imagej.nih.gov. [cited 2022 Sep 7]. Available from: <https://imagej.nih.gov/ij/macros/WaitForUserDemo.txt>
350. ImageJ User Guide - IJ 1.46r [Internet]. [cited 2022 Sep 7]. Available from: <https://imagej.nih.gov/ij/docs/guide/146.html>
351. Enhance Local Contrast (CLAHE) [Internet]. ImageJ Wiki. [cited 2022 Sep 7]. Available from: <https://imagej.github.io/plugins/clahe>
352. Pethybridge SJ, Nelson SC. Leaf Doctor: A New Portable Application for Quantifying Plant Disease Severity. *Plant Dis*. 2015 Oct;99(10):1310–6.
353. Kankaanpää P, Paavolainen L, Tiitta S, Karjalainen M, Päivärinne J, Nieminen J, et al. BioImageXD: an open, general-purpose and high-throughput image-processing platform. *Nat Methods*. 2012 Jul;9(7):683–9.
354. Federici F, Dupuy L, Laplaze L, Heisler M, Haseloff J. Integrated genetic and computation methods for in planta cytometry. *Nat Methods*. 2012 May;9(5):483–5.
355. Machado BB, Orue JPM, Arruda MS, Santos CV, Sarath DS, Goncalves WN, et al. BioLeaf: A professional mobile application to measure foliar damage caused by insect herbivory. *Comput Electron Agric*. 2016 Nov;129:44–55.
356. Varma V, Osuri AM. Black Spot: a platform for automated and rapid estimation of leaf area from scanned images. *Plant Ecol*. 2013 Dec;214(12):1529–34.
357. Bakr EM. A new software for measuring leaf area, and area damaged by *Tetranychus urticae* Koch. *J Appl Entomol*. 2005 Apr;129(3):173–5.
358. Ubbens J, Cieslak M, Prusinkiewicz P, Stavness I. The use of plant models in deep learning: an application to leaf counting in rosette plants. *Plant Methods* [Internet]. 2018 Dec [cited 2022 Jun 30];14(1). Available from: <https://plantmethods.biomedcentral.com/articles/10.1186/s13007-018-0273-z>
359. Henriksson J, Hench J, Tong YG, Johansson A, Johansson D, Bürglin TR. Endrov: an integrated platform for image analysis. *Nat Methods*. 2013 Jun;10(6):454–6.
360. Bylesjö M, Segura V, Soolanayakanahally RY, Rae AM, Trygg J, Gustafsson P, et al. LAMINA: a tool for rapid quantification of leaf size and shape parameters. *BMC Plant Biol*. 2008;8(1):82.
361. Dornbusch T, Andrieu B. Lamina2Shape—An image processing tool for an explicit description of lamina shape tested on winter wheat (*Triticum aestivum* L.). *Comput Electron Agric*. 2010 Jan;70(1):217–24.

362. Ispiryan R, Grigoriev I, zu Castell W, Schäffner AR. A segmentation procedure using colour features applied to images of *Arabidopsis thaliana*. *Funct Plant Biol.* 2013;40(10):1065.
363. Müller-Linow M, Pinto-Espinosa F, Scharr H, Rascher U. The leaf angle distribution of natural plant populations: assessing the canopy with a novel software tool. *Plant Methods.* 2015;11(1):11.
364. Novotný P, Suk T. Leaf recognition of woody species in Central Europe. *Biosyst Eng.* 2013 Aug;115(4):444–52.
365. Kumar N, Belhumeur PN, Biswas A, Jacobs DW, Kress WJ, Lopez IC, et al. Leafsnap: A Computer Vision System for Automatic Plant Species Identification. In: Fitzgibbon A, Lazebnik S, Perona P, Sato Y, Schmid C, editors. *Computer Vision – ECCV 2012* [Internet]. Berlin, Heidelberg: Springer Berlin Heidelberg; 2012 [cited 2022 Aug 14]. p. 502–16. (Lecture Notes in Computer Science; vol. 7573). Available from: http://link.springer.com/10.1007/978-3-642-33709-3_36
366. Anderson C, Rosas-Anderson P. Leafscan [Internet]. Leafscan; 2017. Available from: <https://itunes.apple.com/app/id1254892230>.
367. Maloof JN, Nozue K, Mumbach MR, Palmer CM. LeafJ: An ImageJ Plugin for Semi-automated Leaf Shape Measurement. *J Vis Exp.* 2013 Jan 21;(71):50028.
368. Plantix. Plantix | Best Agriculture App [Internet]. [cited 2022 Aug 24]. Available from: <https://plantix.net/en/>
369. Delta-t. WinDIAS Leaf Area Meter - Leaf Area Measurement System - Size of Leaf [Internet]. [cited 2022 Aug 24]. Available from: <https://delta-t.co.uk/product/wd3/>
370. Franco DL, Canessa P, Bellora N, Risau-Gusman S, Olivares-Yañez C, Pérez-Lara R, et al. Spontaneous circadian rhythms in a cold-adapted natural isolate of *Aureobasidium pullulans*. *Sci Rep* [Internet]. 2017 Dec [cited 2022 Jun 30];7(1). Available from: <http://www.nature.com/articles/s41598-017-14085-6>
371. Fuller KK, Ringelberg CS, Loros JJ, Dunlap JC. The Fungal Pathogen *Aspergillus fumigatus* Regulates Growth, Metabolism, and Stress Resistance in Response to Light. Heitman J, editor. *mBio* [Internet]. 2013 May [cited 2022 Jun 30];4(2). Available from: <https://journals.asm.org/doi/10.1128/mBio.00142-13>
372. Shi Z, Christian D, Leung H. Interactions Between Spore Morphogenetic Mutations Affect Cell Types, Sporulation, and Pathogenesis in *Magnaporthe grisea*. *Mol Plant-Microbe Interactions*®. 1998 Mar;11(3):199–207.
373. Zhang S, Liang M, Naqvi NI, Lin C, Qian W, Zhang LH, et al. Phototrophy and starvation-based induction of autophagy upon removal of Gcn5-catalyzed acetylation of Atg7 in *Magnaporthe oryzae*. *Autophagy.* 2017 Aug 3;13(8):1318–30.
374. Rui O, Hahn M. The Slr2-type MAP kinase Bmp3 of *Botrytis cinerea* is required for normal saprotrophic growth, conidiation, plant surface sensing and host tissue colonization. *Mol Plant Pathol.* 2007 Mar;8(2):173–84.
375. Sargent ML, Kaltenborn SH. Effects of Medium Composition and Carbon Dioxide on Circadian Conidiation in *Neurospora*. *Plant Physiol.* 1972 Jul 1;50(1):171–5.

376. Schmoll M, Franchi L, Kubicek CP. Envoy, a PAS/LOV Domain Protein of *Hypocrea jecorina* (Anamorph *Trichoderma reesei*), Modulates Cellulase Gene Transcription in Response to Light. *Eukaryot Cell*. 2005 Dec;4(12):1998–2007.
377. Tisch D, Schmoll M. Light regulation of metabolic pathways in fungi. *Appl Microbiol Biotechnol*. 2010 Feb;85(5):1259–77.
378. Ma H, Zhang L, Yu X, Wan Y, Wang D, Shi W, et al. Regulation of the *Neurospora* Circadian Clock by the Spliceosome Component PRP5. *G3 GenesGenomesGenetics*. 2019 Nov 1;9(11):3653–61.
379. Gooch VD, Freeman L, Lakin-Thomas PL. Time-Lapse Analysis of the Circadian Rhythms of Conidiation and Growth Rate in *Neurospora*. *J Biol Rhythms*. 2004 Dec;19(6):493–503.
380. Nguyen TH, Kandel M, Shakir HM, Best-Popescu C, Arikath J, Do MN, et al. Halo-free Phase Contrast Microscopy. *Sci Rep*. 2017 Apr;7(1):44034.
381. Liu XH, Zhuang FL, Lu JP, Lin FC. Identification and molecular cloning Moplaa gene, a homologue of Homo sapiens PLAA, in *Magnaporthe oryzae*. *Microbiol Res*. 2011 Dec;167(1):8–13.
382. Ryder LS, Talbot NJ. Regulation of appressorium development in pathogenic fungi. *Curr Opin Plant Biol*. 2015 Aug;26:8–13.
383. Zhang H, Tang W, Liu K, Huang Q, Zhang X, Yan X, et al. Eight RGS and RGS-like Proteins Orchestrate Growth, Differentiation, and Pathogenicity of *Magnaporthe oryzae*. *Howlett BJ, editor. PLoS Pathog*. 2011 Dec 29;7(12):e1002450.
384. Aver'yanov AA, Lapikova VP, Pasechnik TD, Abramova OS, Gaivoronskaya LM, Kuznetsov VV, et al. Pre-illumination of rice blast conidia induces tolerance to subsequent oxidative stress. *Fungal Biol*. 2014 Aug;118(8):743–53.
385. Collins JT, Knapper J, Stirling J, Mduda J, Mayagaya V, Mwakajinga GA, et al. Robotic microscopy for everyone: the OpenFlexure Microscope. 2020;10.
386. 9. API - The PiCamera Class — Picamera 1.13 Documentation [Internet]. [cited 2022 Sep 7]. Available from: https://picamera.readthedocs.io/en/release-1.13/api_camera.html
387. Motion - Open source security camera software [Internet]. Motion. [cited 2022 Aug 29]. Available from: <https://motion-project.github.io/>
388. Rathinavel S, Sundararajan KS. Chronopathological Aspects of Disease Incidence in Rice (*Oryza sativa* L.). *Chronobiol Int*. 2003 Jan;20(1):81–96.
389. Sunder S, Singh R, Agarwal R. Brown spot of rice: an overview. *Indian Phytopathol*. 2014;16.
390. Chen X, Jia Y, Wu BM. Evaluation of Rice Responses to the Blast Fungus *Magnaporthe oryzae* at Different Growth Stages. *Plant Dis*. 2019 Jan;103(1):132–6.
391. R. Sujatha, S. Kumar, G. U. Akhil. Leaf disease detection using image processing. *JCHPS*. 2017;10(1):670–2.

392. Tiley AMM, Lawless C, Pilo P, Karki SJ, Lu J, Long Z, et al. The *Zymoseptoria tritici* white collar-1 gene, *ZtWco-1*, is required for development and virulence on wheat. *Fungal Genet Biol.* 2022 Jul;161:103715.
393. Valent B, Farrall L, Chumley FG. *Magnaporthe grisea* genes for pathogenicity and virulence identified through a series of backcrosses. *Genetics.* 1991 Jan;127(1):87–101.
394. Zhang R, Zheng F, Wei S, Zhang S, Li G, Cao P, et al. Evolution of Disease Defense Genes and Their Regulators in Plants. *Int J Mol Sci.* 2019 Jan 15;20(2):335.
395. Stewart EL, McDonald BA. Measuring Quantitative Virulence in the Wheat Pathogen *Zymoseptoria tritici* Using High-Throughput Automated Image Analysis. *Phytopathology*®. 2014 Sep;104(9):985–92.
396. Stewart EL, Hagerty CH, Mikaberidze A, Mundt CC, Zhong Z, McDonald BA. An Improved Method for Measuring Quantitative Resistance to the Wheat Pathogen *Zymoseptoria tritici* Using High-Throughput Automated Image Analysis. *Phytopathology*®. 2016 Jul;106(7):782–8.
397. GitHub - shapely/shapely: Manipulation and analysis of geometric objects [Internet]. [cited 2022 Dec 19]. Available from: <https://github.com/shapely/shapely>
398. Odenbach D, Breth B, Thines E, Weber RWS, Anke H, Foster AJ. The transcription factor Con7p is a central regulator of infection-related morphogenesis in the rice blast fungus *Magnaporthe grisea*: Con7p regulates morphogenesis in *Magnaporthe grisea*. *Mol Microbiol.* 2007 Mar 23;64(2):293–307.
399. Shi X, Long Y, He F, Zhang C, Wang R, Zhang T, et al. The fungal pathogen *Magnaporthe oryzae* suppresses innate immunity by modulating a host potassium channel. Wang Y, editor. *PLOS Pathog.* 2018 Jan 31;14(1):e1006878.
400. McCloy RA, Rogers S, Caldon CE, Lorca T, Castro A, Burgess A. Partial inhibition of Cdk1 in G2 phase overrides the SAC and decouples mitotic events. *Cell Cycle.* 2014 May 1;13(9):1400–12.
401. Jakic B, Buszko M, Cappellano G, Wick G. Elevated sodium leads to the increased expression of HSP60 and induces apoptosis in HUVECs. *PLoS ONE.* 2017 Jun 12;12(6):e0179383.
402. Rogers AM, Egan MJ. Autophagy machinery promotes the chaperone-mediated formation and compartmentalization of protein aggregates during appressorium development by the rice blast fungus. Weis K, editor. *Mol Biol Cell.* 2020 Oct 1;31(21):2298–305.
403. Covington MF, Harmer SL. The Circadian Clock Regulates Auxin Signaling and Responses in *Arabidopsis*. Weigel D, editor. *PLoS Biol.* 2007 Aug 7;5(8):e222.
404. Yerushalmi S, Green RM. Evidence for the adaptive significance of circadian rhythms. *Ecol Lett.* 2009 Sep;12(9):970–81.
405. Zhao S, Zhang Q, Liu M, Zhou H, Ma C, Wang P. Regulation of Plant Responses to Salt Stress. *Int J Mol Sci.* 2021 Apr 28;22(9):4609.

406. Belden WJ, Lewis ZA, Selker EU, Loros JJ, Dunlap JC. CHD1 Remodels Chromatin and Influences Transient DNA Methylation at the Clock Gene frequency. Takahashi JS, editor. *PLoS Genet*. 2011 Jul 21;7(7):e1002166.
407. Hughes ME, Abruzzi KC, Allada R, Anafi R, Arpat AB, Asher G, et al. Guidelines for Genome-Scale Analysis of Biological Rhythms. *J Biol Rhythms*. 2017 Oct;32(5):380–93.
408. Roenneberg T, Dragovic Z, Meroow M. Demasking biological oscillators: Properties and principles of entrainment exemplified by the *Neurospora* circadian clock. *Proc Natl Acad Sci*. 2005 May 24;102(21):7742–7.
409. Shrode LB, Lewis ZA, White LD, Bell-Pedersen D, Ebbole DJ. vvd Is Required for Light Adaptation of Conidiation-Specific Genes of *Neurospora crassa*, but Not Circadian Conidiation. *Fungal Genet Biol*. 2001 Apr;32(3):169–81.
410. Wang ZY, Tobin EM. Constitutive Expression of the CIRCADIAN CLOCK ASSOCIATED 1 (CCA1) Gene Disrupts Circadian Rhythms and Suppresses Its Own Expression. *Cell*. 1998 Jun;93(7):1207–17.
411. Blackman BK. Changing Responses to Changing Seasons: Natural Variation in the Plasticity of Flowering Time. *Plant Physiol*. 2017 Jan;173(1):16–26.
412. Idnurm A, Crosson S. The Photobiology of Microbial Pathogenesis. Madhani HD, editor. *PLoS Pathog*. 2009 Nov 26;5(11):e1000470.
413. Yoshida Y, Maeda T, Lee B, Hasunuma K. Conidiation rhythm and light entrainment in superoxide dismutase mutant in *Neurospora crassa*. *Mol Genet Genomics*. 2008 Feb;279(2):193–202.
414. Xie XZ, Xue YJ, Zhou JJ, Zhang B, Chang H, Takano M. Phytochromes Regulate SA and JA Signaling Pathways in Rice and Are Required for Developmentally Controlled Resistance to *Magnaporthe grisea*. *Mol Plant*. 2011 Jul;4(4):688–96.
415. Herrera-Estrella A, Horwitz BA. Looking through the eyes of fungi: molecular genetics of photoreception: Looking through the eyes of fungi. *Mol Microbiol*. 2007 Mar 16;64(1):5–15.
416. Loros JJ, Dunlap JC, Larrondo LF, Shi M, Belden WJ, Gooch VD, et al. Circadian Output, Input, and Intracellular Oscillators: Insights into the Circadian Systems of Single Cells. *Cold Spring Harb Symp Quant Biol*. 2007 Jan;72(1):201–14.
417. Sancar C, Sancar G, Ha N, Cesbron F, Brunner M. Dawn- and dusk-phased circadian transcription rhythms coordinate anabolic and catabolic functions in *Neurospora*. *BMC Biol*. 2015 Dec;13(1):17.
418. Bieszke JA, Braun EL, Bean LE, Kang S, Natvig DO, Borkovich KA. The *nop-1* gene of *Neurospora crassa* encodes a seven transmembrane helix retinal-binding protein homologous to archaeal rhodopsins. *Proc Natl Acad Sci*. 1999 Jul 6;96(14):8034–9.
419. Butt GR, Qayyum ZA, Jones MA. Plant Defence Mechanisms Are Modulated by the Circadian System. *Biology*. 2020 Dec 9;9(12):454.

420. Lyu X, Shen C, Fu Y, Xie J, Jiang D, Li G, et al. The Microbial Opsin Homolog Sop1 is involved in *Sclerotinia sclerotiorum* Development and Environmental Stress Response. *Front Microbiol* [Internet]. 2016 Jan 7 [cited 2022 Jun 30];6. Available from: <http://journal.frontiersin.org/Article/10.3389/fmicb.2015.01504/abstract>
421. Samach A, Gover A. Photoperiodism: The consistent use of CONSTANS. *Curr Biol*. 2001 Aug;11(16):R651–4.
422. Santamaría-Hernando S, Rodríguez-Herva JJ, Martínez-García PM, Río-Álvarez I, González-Melendi P, Zamorano J, et al. *Pseudomonas syringae* pv. tomato exploits light signals to optimize virulence and colonization of leaves. *Environ Microbiol*. 2018 Dec;20(12):4261–80.
423. Kotilainen T, Aphalo Pj, Brelsford Cc, Böök H, Devraj S, Heikkilä A, et al. Patterns in the spectral composition of sunlight and biologically meaningful spectral photon ratios as affected by atmospheric factors. *Agric For Meteorol*. 2020 Sep;291:108041.
424. Chiang C, Olsen JE, Basler D, Bånkestad D, Hoch G. Latitude and Weather Influences on Sun Light Quality and the Relationship to Tree Growth. *Forests*. 2019 Jul 24;10(8):610.
425. Goldberg B, Klein WH. Variations in the spectral distribution of daylight at various geographical locations on the earth's surface. *Sol Energy*. 1977;19(1):3–13.
426. Hughes JE, Morgan DC, Bonington S. Photoperiodic time signals during twilight. 1984;10.
427. Lee DW, Downum KR. The spectral distribution of biologically active solar radiation at Miami, Florida, USA. *Int J Biometeorol*. 1991;35(1):48–54.
428. Sellaro R, Smith RW, Legris M, Fleck C, Casal JJ. Phytochrome B dynamics departs from photoequilibrium in the field: phyB dynamics in the field. *Plant Cell Environ*. 2019 Feb;42(2):606–17.
429. Zoratti L, Jaakola L, Häggman H, Giongo L. Modification of Sunlight Radiation through Colored Photo-Selective Nets Affects Anthocyanin Profile in *Vaccinium* spp. Berries. Xu C, editor. *PLOS ONE*. 2015 Aug 19;10(8):e0135935.
430. Yang T, Guo M, Yang H, Guo S, Dong C. The blue-light receptor CmWC-1 mediates fruit body development and secondary metabolism in *Cordyceps militaris*. *Appl Microbiol Biotechnol*. 2016 Jan;100(2):743–55.
431. World Health Organization. Global solar UV index: a practical guide : a joint recommendation of World Health Organization, World Meteorological Organization, United Nations Environment Programme, International Commission on Non-Ionizing Radiation Protection. WHO: Geneva; 2002.
432. Yokawa K, Kagenishi T, Baluška F. UV-B Induced Generation of Reactive Oxygen Species Promotes Formation of BFA-Induced Compartments in Cells of *Arabidopsis* Root Apices. *Front Plant Sci* [Internet]. 2016 Jan 13 [cited 2022 Aug 16];6. Available from: <http://journal.frontiersin.org/Article/10.3389/fpls.2015.01162/abstract>
433. Nitschke S, Cortleven A, Schmülling T. Novel Stress in Plants by Altering the Photoperiod. *Trends Plant Sci*. 2017 Nov;22(11):913–6.

434. Cascant-Lopez E, Crosthwaite SK, Johnson LJ, Harrison RJ. No Evidence That Homologs of Key Circadian Clock Genes Direct Circadian Programs of Development or mRNA Abundance in *Verticillium dahliae*. *Front Microbiol* [Internet]. 2020 Aug 28 [cited 2022 Jun 30];11. Available from: <https://www.frontiersin.org/article/10.3389/fmicb.2020.01977/full>
435. Konagaya K, Al Riza DF, Nie S, Yoneda M, Hirata T, Takahashi N, et al. Monitoring mature tomato (red stage) quality during storage using ultraviolet-induced visible fluorescence image. *Postharvest Biol Technol*. 2020 Feb;160:111031.
436. Mizuno T, Nomoto Y, Oka H, Kitayama M, Takeuchi A, Tsubouchi M, et al. Ambient Temperature Signal Feeds into the Circadian Clock Transcriptional Circuitry Through the EC Night-Time Repressor in *Arabidopsis thaliana*. *Plant Cell Physiol*. 2014 May;55(5):958–76.
437. Crosthwaite SK, Dunlap JC, Loros JJ. *Neurospora wc-1* and *wc-2* : Transcription, Photoresponses, and the Origins of Circadian Rhythmicity. *Science*. 1997 May 2;276(5313):763–9.
438. Lee SJ, Kong M, Morse D, Hijri M. Expression of putative circadian clock components in the arbuscular mycorrhizal fungus *Rhizoglyphus irregularis*. *Mycorrhiza*. 2018 Aug;28(5–6):523–34.
439. Vitalini MW, de Paula RM, Goldsmith CS, Jones CA, Borkovich KA, Bell-Pedersen D. Circadian rhythmicity mediated by temporal regulation of the activity of p38 MAPK. *Proc Natl Acad Sci*. 2007 Nov 13;104(46):18223–8.
440. Austin B, Lowne née. An Endogenous Rhythm of Spore Discharge in *Sordaria fimicola*. *Ann Bot*. 1968 Apr;32(2):262–78.
441. Brody S. Circadian Rhythms in Fungi: Structure/Function/Evolution of Some Clock Components. *J Biol Rhythms*. 2019 Aug;34(4):364–79.
442. Carreras-Villaseñor N, Sánchez-Arreguín JA, Herrera-Estrella AH. Trichoderma: sensing the environment for survival and dispersal. *Microbiology*. 2012 Jan 1;158(1):3–16.
443. Corrochano LM. Fungal photobiology: a synopsis. *IMA Fungus*. 2011 Jun;2(1):25–8.
444. Edgar RS, Green EW, Zhao Y, van Ooijen G, Olmedo M, Qin X, et al. Peroxiredoxins are conserved markers of circadian rhythms. *Nature*. 2012 May 24;485(7399):459–64.
445. Eelderink-Chen Z, Mazzotta G, Sturre M, Bosman J, Roenneberg T, Meroow M. A circadian clock in *Saccharomyces cerevisiae*. *Proc Natl Acad Sci*. 2010 Feb 2;107(5):2043–7.
446. Fustin JM, Ye S, Rakers C, Kaneko K, Fukumoto K, Yamano M, et al. Methylation deficiency disrupts biological rhythms from bacteria to humans. *Commun Biol* [Internet]. 2020 Dec [cited 2022 Jun 30];3(1). Available from: <http://www.nature.com/articles/s42003-020-0942-0>
447. Greene AV, Keller N, Haas H, Bell-Pedersen D. A Circadian Oscillator in *Aspergillus* spp . Regulates Daily Development and Gene Expression. *Eukaryot Cell*. 2003 Apr;2(2):231–7.

448. Idnurm A, Heitman J. Light Controls Growth and Development via a Conserved Pathway in the Fungal Kingdom. Chory J, editor. PLoS Biol. 2005 Mar 15;3(4):e95.
449. McClung CR. Comes a time. Curr Opin Plant Biol. 2008 Oct;11(5):514–20.
450. Millar AJ. A Suite of Photoreceptors Entrain the Plant Circadian Clock. J Biol Rhythms. 2003 Jun;18(3):217–26.
451. Purschwitz J, Müller S, Kastner C, Fischer R. Seeing the rainbow: light sensing in fungi. Curr Opin Microbiol. 2006 Dec;9(6):566–71.
452. Purschwitz J, Müller S, Kastner C, Schöser M, Haas H, Espeso EA, et al. Functional and Physical Interaction of Blue- and Red-Light Sensors in *Aspergillus nidulans*. Curr Biol. 2008 Feb;18(4):255–9.
453. Roenneberg T, Merrow M. Life before the Clock: Modeling Circadian Evolution. J Biol Rhythms. 2002 Dec;17(6):495–505.
454. Roenneberg T, Daan S, Merrow M. The Art of Entrainment. J Biol Rhythms. 2003 Jun;18(3):183–94.
455. Ruger-Herreros C, Corrochano LM. Conidiation in *Neurospora crassa*: vegetative reproduction by a model fungus. Int Microbiol. 2020 Jan;23(1):97–105.
456. Ruiz-Roldán MC, Garre V, Guarro J, Mariné M, Roncero MIG. Role of the White Collar 1 Photoreceptor in Carotenogenesis, UV Resistance, Hydrophobicity, and Virulence of *Fusarium oxysporum*. Eukaryot Cell. 2008 Jul;7(7):1227–30.
457. Salichos L, Rokas A. The diversity and evolution of circadian clock proteins in fungi. Mycologia. 2010 Mar;102(2):269–78.
458. Sanz C, Rodríguez-Romero J, Idnurm A, Christie JM, Heitman J, Corrochano LM, et al. *Phycomyces* MADB interacts with MADA to form the primary photoreceptor complex for fungal phototropism. Proc Natl Acad Sci. 2009 Apr 28;106(17):7095–100.
459. Traeger S, Nowrousian M. Analysis of Circadian Rhythms in the Basal Filamentous Ascomycete *Pyronema confluens*. G3 GenesGenomesGenetics. 2015 Oct 1;5(10):2061–71.
460. Shimizu S, Yamauchi Y, Ishikawa A. Photoperiod Following Inoculation of Arabidopsis with *Pyricularia oryzae* (syn. *Magnaporthe oryzae*) Influences on the Plant–Pathogen Interaction. Int J Mol Sci. 2021 May 8;22(9):5004.
461. Goodspeed D, Chehab EW, Covington MF, Braam J. Circadian control of jasmonates and salicylates: The clock role in plant defense. Plant Signal Behav. 2013 Feb;8(2):e23123.
462. Soanes DM, Richards TA, Talbot NJ. Insights from Sequencing Fungal and Oomycete Genomes: What Can We Learn about Plant Disease and the Evolution of Pathogenicity? Plant Cell. 2007 Nov;19(11):3318–26.
463. Endo M, Shimizu H, Nohales MA, Araki T, Kay SA. Tissue-specific clocks in Arabidopsis show asymmetric coupling. Nature. 2014 Nov 20;515(7527):419–22.

464. James AB, Monreal JA, Nimmo GA, Kelly CL, Herzyk P, Jenkins GI, et al. The circadian clock in *Arabidopsis* roots is a simplified slave version of the clock in shoots. *Science*. 2008 Dec 19;322(5909):1832–5.
465. Para A, Farré EM, Imaizumi T, Pruneda-Paz JL, Harmon FG, Kay SA. PRR3 Is a Vascular Regulator of TOC1 Stability in the *Arabidopsis* Circadian Clock. *Plant Cell*. 2007 Dec 31;19(11):3462–73.
466. Dunlap JC. Genetic and Molecular Analysis of Circadian Rhythms. *Annu Rev Genet*. 1996 Dec;30(1):579–601.
467. Idnurm A, Heitman J. Ferrochelatase is a conserved downstream target of the blue light-sensing White collar complex in fungi. *Microbiology*. 2010 Aug 1;156(8):2393–407.
468. Schafmeier T, Diernfellner A, Schäfer A, Dintsis O, Neiss A, Brunner M. Circadian activity and abundance rhythms of the *Neurospora* clock transcription factor WCC associated with rapid nucleo–cytoplasmic shuttling. *Genes Dev*. 2008 Dec 15;22(24):3397–402.
469. Ford B, Deng W, Clausen J, Oliver S, Boden S, Hemming M, et al. Barley (*Hordeum vulgare*) circadian clock genes can respond rapidly to temperature in an *EARLY FLOWERING 3*-dependent manner. *J Exp Bot*. 2016 Oct 1;67(18):5517–28.
470. BLAST: Basic Local Alignment Search Tool [Internet]. [cited 2022 Dec 19]. Available from: <https://blast.ncbi.nlm.nih.gov/Blast.cgi>
471. Ensembl Fungi [Internet]. [cited 2022 Dec 19]. Available from: <https://fungi.ensembl.org/index.html>
472. Yates AD, Allen J, Amode RM, Azov AG, Barba M, Becerra A, et al. Ensembl Genomes 2022: an expanding genome resource for non-vertebrates. *Nucleic Acids Res*. 2022 Jan 7;50(D1):D996–1003.
473. Adam A, Deimel S, Pardo-Medina J, García-Martínez J, Konte T, Limón M, et al. Protein Activity of the *Fusarium fujikuroi* Rhodopsins CarO and OpsA and Their Relation to Fungus–Plant Interaction. *Int J Mol Sci*. 2018 Jan 11;19(1):215.
474. Bieszke JA, Li L, Borkovich KA. The fungal opsin gene *nop-1* is negatively-regulated by a component of the blue light sensing pathway and influences conidiation-specific gene expression in *Neurospora crassa*. *Curr Genet*. 2007 Sep;52(3–4):149–57.
475. Elvin M, Loros JJ, Dunlap JC, Heintzen C. The PAS/LOV protein VIVID supports a rapidly dampened daytime oscillator that facilitates entrainment of the *Neurospora* circadian clock. *Genes Dev*. 2005 Nov 1;19(21):2593–605.
476. Collett MA, Dunlap JC, Loros JJ. Circadian Clock-Specific Roles for the Light Response Protein WHITE COLLAR-2. *Mol Cell Biol*. 2001 Apr 15;21(8):2619–28.
477. Hatakeyama R, Nakahama T, Higuchi Y, Kitamoto K. Light Represses Conidiation in Koji Mold *Aspergillus oryzae*. *Biosci Biotechnol Biochem*. 2007 Aug 23;71(8):1844–9.
478. Schumacher J, Pradier JM, Simon A, Traeger S, Moraga J, Collado IG, et al. Natural Variation in the VELVET Gene *bcvel1* Affects Virulence and Light-Dependent Differentiation in *Botrytis cinerea*. Harris S, editor. *PLoS ONE*. 2012 Oct 31;7(10):e47840.

479. Yoshida Y, Hasunuma K. Reactive Oxygen Species Affect Photomorphogenesis in *Neurospora crassa*. *J Biol Chem*. 2004 Feb;279(8):6986–93.
480. Park JY, Jin J, Lee YW, Kang S, Lee YH. Rice Blast Fungus (*Magnaporthe oryzae*) Infects *Arabidopsis* via a Mechanism Distinct from That Required for the Infection of Rice. *Plant Physiol*. 2009 Jan 6;149(1):474–86.
481. Blumenstein A, Vienken K, Tasler R, Purschwitz J, Veith D, Frankenberg-Dinkel N, et al. The *Aspergillus nidulans* Phytochrome FphA Represses Sexual Development in Red Light. *Curr Biol*. 2005 Oct;15(20):1833–8.
482. Idnurm A. Light Sensing in *Aspergillus fumigatus* Highlights the Case for Establishing New Models for Fungal Photobiology. *mBio* [Internet]. 2013 Jul [cited 2022 Jun 30];4(3). Available from: <https://journals.asm.org/doi/10.1128/mBio.00260-13>
483. Röhrig J, Kastner C, Fischer R. Light inhibits spore germination through phytochrome in *Aspergillus nidulans*. *Curr Genet*. 2013 May;59(1–2):55–62.
484. Kuo HC, Hui S, Choi J, Asiegbo FO, Valkonen JPT, Lee YH. Secret lifestyles of *Neurospora crassa*. *Sci Rep* [Internet]. 2015 May [cited 2022 Jun 30];4(1). Available from: <http://www.nature.com/articles/srep05135>
485. Granshaw T, Tsukamoto M, Brody S. Circadian Rhythms in *Neurospora Crassa*: Farnesol or Geraniol Allow Expression of Rhythmicity in the Otherwise Arrhythmic Strains frq 10, wc-1, and wc-2. *J Biol Rhythms*. 2003 Aug;18(4):287–96.
486. Matheis S, Yemelin A, Scheps D, Andresen K, Jacob S, Thines E, et al. Functions of the *Magnaporthe oryzae* Flb3p and Flb4p transcription factors in the regulation of conidiation. *Microbiol Res*. 2017 Mar;196:106–17.
487. Hirschie Johnson C, Elliott JA, Foster R. Entrainment of Circadian Programs. *Chronobiol Int*. 2003 Jan;20(5):741–74.
488. Jiang CJ, Shimono M, Sugano S, Kojima M, Yazawa K, Yoshida R, et al. Abscisic Acid Interacts Antagonistically with Salicylic Acid Signaling Pathway in Rice–*Magnaporthe grisea* Interaction. *Mol Plant-Microbe Interactions*®. 2010 Jun;23(6):791–8.
489. Cecchini E, Geri C, Love AJ, Coupland G, Covey SN, Milner JJ. Mutations that delay flowering in *Arabidopsis* de-couple symptom response from cauliflower mosaic virus accumulation during infection. *Mol Plant Pathol*. 2002 Mar;3(2):81–90.
490. Sarris PF, Duxbury Z, Huh SU, Ma Y, Segonzac C, Sklenar J, et al. A Plant Immune Receptor Detects Pathogen Effectors that Target WRKY Transcription Factors. *Cell*. 2015 May;161(5):1089–100.
491. O. Windram, P. Madhou, S. Mchattie, C. Hill, R. Hickman, E. Cooke, et al. *Arabidopsis* Defense against *Botrytis cinerea*: Chronology and Regulation Deciphered by High-Resolution Temporal Transcriptomic Analysis. *Plant Cell*. 2012 Oct 24;24(9):3530–57.
492. Nishiura A, Kitagawa S, Matsumura M, Kazama Y, Abe T, Mizuno N, et al. An early-flowering einkorn wheat mutant with deletions of PHYTOCLOCK 1/LUX ARRHYTHMO and VERNALIZATION 2 exhibits a high level of VERNALIZATION 1 expression induced by vernalization. *J Plant Physiol*. 2018 Mar;222:28–38.

493. Izawa T. Daylength Measurements by Rice Plants in Photoperiodic Short-Day Flowering. In: International Review of Cytology [Internet]. Elsevier; 2007 [cited 2022 Jun 30]. p. 191–222. Available from: <https://linkinghub.elsevier.com/retrieve/pii/S0074769607560067>
494. Murakami M, Tago Y, Yamashino T, Mizuno T. Comparative Overviews of Clock-Associated Genes of *Arabidopsis thaliana* and *Oryza sativa*. *Plant Cell Physiol.* 2007 Jan;48(1):110–21.
495. Islam SZ, Honda Y, Arase S. Light-induced Resistance of Broad Bean against *Botrytis cinerea*. *J Phytopathol.* 1998 Oct;146(10):479–85.
496. Islam SZ, Babadoost M, Honda Y. Effect of Red Light Treatment of Seedlings of Pepper, Pumpkin, and Tomato on the Occurrence of *Phytophthora Damping-off*. *HortScience.* 2002 Jul;37(4):678–81.
497. Rahman MZ, Honda Y, Arase S. Red-Light-Induced Resistance in Broad Bean (*Vicia faba* L.) to Leaf Spot Disease Caused by *Alternaria tenuissima*. *J Phytopathol.* 2003 Feb;151(2):86–91.
498. Doehlemann G, Hemetsberger C. Apoplastic immunity and its suppression by filamentous plant pathogens. *New Phytol.* 2013 Jun;198(4):1001–16.
499. Egan MJ, Talbot NJ. Genomes, free radicals and plant cell invasion: recent developments in plant pathogenic fungi. *Curr Opin Plant Biol.* 2008 Aug;11(4):367–72.
500. Egan MJ, Wang ZY, Jones MA, Smirnov N, Talbot NJ. Generation of reactive oxygen species by fungal NADPH oxidases is required for rice blast disease. *Proc Natl Acad Sci.* 2007 Jul 10;104(28):11772–7.
501. Cheng P, Yang Y, Gardner KH, Liu Y. PAS Domain-Mediated WC-1/WC-2 Interaction Is Essential for Maintaining the Steady-State Level of WC-1 and the Function of Both Proteins in Circadian Clock and Light Responses of *Neurospora*. *Mol Cell Biol.* 2002 Jan 15;22(2):517–24.
502. Mellow M. Circadian regulation of the light input pathway in *Neurospora crassa*. *EMBO J.* 2001 Feb 1;20(3):307–15.
503. Schwerdtfeger C, Linden H. Localization and light-dependent phosphorylation of white collar 1 and 2, the two central components of blue light signaling in *Neurospora crassa*: Blue light signal transduction in *N. crassa*. *Eur J Biochem.* 2000 Jan;267(2):414–22.
504. Morgan LW, Greene AV, Bell-Pedersen D. Circadian and light-induced expression of luciferase in *Neurospora crassa*. *Fungal Genet Biol.* 2003 Apr;38(3):327–32.
505. Ballario P, Vittorioso P, Magrelli A, Talora C, Cabibbo A, Macino G. White collar-1, a central regulator of blue light responses in *Neurospora*, is a zinc finger protein. *EMBO J.* 1996 Apr;15(7):1650–7.
506. Bayram Ö, Krappmann S, Ni M, Bok JW, Helmstaedt K, Valerius O, et al. VelB/VeA/LaeA Complex Coordinates Light Signal with Fungal Development and Secondary Metabolism. *Science.* 2008 Jun 13;320(5882):1504–6.

507. Filippovich SYu, Bachurina GP, Kritsky MS. Effect of 5-Azacytidine on the Light-Sensitive Formation of Sexual and Asexual Reproductive Structures in *wc-1* and *wc-2* Mutants of *Neurospora crassa*. *Appl Biochem Microbiol*. 2004 Jul;40(4):398–403.
508. Lauter FR, Yamashiro CT, Yanofsky C. Light stimulation of conidiation in *Neurospora crassa*: Studies with the wild-type strain and mutants *wc-1*, *wc-2* and *acon-2*. *J Photochem Photobiol B*. 1997 Feb;37(3):203–11.
509. Lakin-Thomas PL, Brody S. Circadian rhythms in *Neurospora crassa* : Lipid deficiencies restore robust rhythmicity to null *frequency* and *white-collar* mutants. *Proc Natl Acad Sci*. 2000 Jan 4;97(1):256–61.
510. Cheng P. Coiled-coil domain-mediated FRQ-FRQ interaction is essential for its circadian clock function in *Neurospora*. *EMBO J*. 2001 Jan 15;20(1):101–8.
511. Dragovic Z. Light reception and circadian behavior in ‘blind’ and ‘clock-less’ mutants of *Neurospora crassa*. *EMBO J*. 2002 Jul 15;21(14):3643–51.
512. Sun G, Zhou Z, Liu X, Gai K, Liu Q, Cha J, et al. Suppression of WHITE COLLAR-independent frequency Transcription by Histone H3 Lysine 36 Methyltransferase SET-2 Is Necessary for Clock Function in *Neurospora*. *J Biol Chem*. 2016 May;291(21):11055–63.
513. Schneider K, Perrino S, Oelhafen K, Li S, Zatzepin A, Lakin-Thomas P, et al. Rhythmic Conidiation in Constant Light in *Vivid* Mutants of *Neurospora crassa*. *Genetics*. 2009 Mar 1;181(3):917–31.
514. Brenna A, Grimaldi B, Filetici P, Ballario P. Physical association of the WC-1 photoreceptor and the histone acetyltransferase NGF-1 is required for blue light signal transduction in *Neurospora crassa*. *Tansey WP, editor. Mol Biol Cell*. 2012 Oct;23(19):3863–72.
515. He Q, Cheng P, Yang Y, Wang L, Gardner KH, Liu Y. White Collar-1, a DNA Binding Transcription Factor and a Light Sensor. *Science*. 2002 Aug 2;297(5582):840–3.
516. Crosthwaite SK, Loros JJ, Dunlap JC. Light-induced resetting of a circadian clock is mediated by a rapid increase in frequency transcript. *Cell*. 1995 Jun;81(7):1003–12.
517. Dasgupta A, Chen CH, Lee C, Gladfelter AS, Dunlap JC, Loros JJ. Biological Significance of Photoreceptor Photocycle Length: VIVID Photocycle Governs the Dynamic VIVID-White Collar Complex Pool Mediating Photo-adaptation and Response to Changes in Light Intensity. *Crane B, editor. PLOS Genet*. 2015 May 15;11(5):e1005215.
518. Cheng P, Yang Y, Liu Y. Interlocked feedback loops contribute to the robustness of the *Neurospora* circadian clock. *Proc Natl Acad Sci*. 2001 Jun 19;98(13):7408–13.
519. Kotzabasis K, Navakoudis E, Vakalounakis DJ. Photobiological Control of Crop Production and Plant Diseases. *Z Für Naturforschung C*. 2008 Feb 1;63(1–2):113–23.
520. Schumacher J, Simon A, Cohrs KC, Traeger S, Porquier A, Dalmais B, et al. The VELVET Complex in the Gray Mold Fungus *Botrytis cinerea* : Impact of BcLAE1 on Differentiation, Secondary Metabolism, and Virulence. *Mol Plant-Microbe Interactions®*. 2015 Jun;28(6):659–74.

521. TAN KK. Blue-light Inhibition of Sporulation in *Botrytis cinerea*. *Microbiology*. 1974;82(1):191–200.
522. Cheng P, He Q, Yang Y, Wang L, Liu Y. Functional conservation of light, oxygen, or voltage domains in light sensing. *Proc Natl Acad Sci*. 2003 May 13;100(10):5938–43.
523. Howard RJ, Ferrari MA, Roach DH, Money NP. Penetration of hard substrates by a fungus employing enormous turgor pressures. *Proc Natl Acad Sci*. 1991 Dec 15;88(24):11281–4.
524. Chumley FG. Genetic Analysis of Melanin-Deficient, Nonpathogenic Mutants of *Magnaporthe grisea*. *Mol Plant Microbe Interact*. 1990;3(3):135.
525. Corwin JA, Copeland D, Feusier J, Subedy A, Eshbaugh R, Palmer C, et al. The Quantitative Basis of the Arabidopsis Innate Immune System to Endemic Pathogens Depends on Pathogen Genetics. Koenig D, editor. *PLOS Genet*. 2016 Feb 11;12(2):e1005789.
526. Kramer C, Loros JJ, Dunlap JC, Crosthwaite SK. Role for antisense RNA in regulating circadian clock function in *Neurospora crassa*. *Nature*. 2003 Feb;421(6926):948–52.
527. Zhou M, Guo J, Cha J, Chae M, Chen S, Barral JM, et al. Non-optimal codon usage affects expression, structure and function of clock protein FRQ. *Nature*. 2013 Mar;495(7439):111–5.
528. Xue Z, Ye Q, Anson SR, Yang J, Xiao G, Kowbel D, et al. Transcriptional interference by antisense RNA is required for circadian clock function. *Nature*. 2014 Oct 30;514(7524):650–3.
529. Mellow MW, Garceau NY, Dunlap JC. Dissection of a circadian oscillation into discrete domains. *Proc Natl Acad Sci*. 1997 Apr 15;94(8):3877–82.
530. Liu Y, Garceau NY, Loros JJ, Dunlap JC. Thermally Regulated Translational Control of FRQ Mediates Aspects of Temperature Responses in the *Neurospora* Circadian Clock. *Cell*. 1997 May;89(3):477–86.
531. Lewis MT, Morgan LW, Feldman JF. Analysis of frequency (*frq*) clock gene homologs: evidence for a helix-turn-helix transcription factor. *Mol Gen Genet MGG*. 1997 Jan;253(4):401–14.
532. Tang CT, Li S, Long C, Cha J, Huang G, Li L, et al. Setting the pace of the *Neurospora* circadian clock by multiple independent FRQ phosphorylation events. *Proc Natl Acad Sci*. 2009 Jun 30;106(26):10722–7.
533. Liu X, Chen A, Caicedo-Casso A, Cui G, Du M, He Q, et al. FRQ-CK1 interaction determines the period of circadian rhythms in *Neurospora*. *Nat Commun*. 2019 Dec;10(1):4352.
534. Cha J, Chang SS, Huang G, Cheng P, Liu Y. Control of WHITE COLLAR localization by phosphorylation is a critical step in the circadian negative feedback process. *EMBO J*. 2008 Dec 17;27(24):3246–55.
535. Klemz S, Wallach T, Korge S, Rosing M, Klemz R, Maier B, et al. Protein phosphatase 4 controls circadian clock dynamics by modulating CLOCK/BMAL1 activity. *Genes Dev*. 2021 Aug 1;35(15–16):1161–74.

536. Mehra A, Shi M, Baker CL, Colot HV, Loros JJ, Dunlap JC. A Role for Casein Kinase 2 in the Mechanism Underlying Circadian Temperature Compensation. *Cell*. 2009 May;137(4):749–60.
537. Mehra A, Baker CL, Loros JJ, Dunlap JC. Post-translational modifications in circadian rhythms. *Trends Biochem Sci*. 2009 Oct;34(10):483–90.
538. Yang Y, Cheng P, Zhi G, Liu Y. Identification of a Calcium/Calmodulin-dependent Protein Kinase That Phosphorylates the *Neurospora* Circadian Clock Protein FREQUENCY. *J Biol Chem*. 2001 Nov;276(44):41064–72.
539. Yang Y, Cheng P, Liu Y. Regulation of the *Neurospora* circadian clock by casein kinase II. *Genes Dev*. 2002 Apr 15;16(8):994–1006.
540. Heintzen C, Loros JJ, Dunlap JC. The PAS Protein VIVID Defines a Clock-Associated Feedback Loop that Represses Light Input, Modulates Gating, and Regulates Clock Resetting. *Cell*. 2001 Feb;104(3):453–64.
541. Putker M, Wong DCS, Seinkmane E, Rzechorzek NM, Zeng A, Hoyle NP, et al. CRYPTOCHROMES confer robustness, not rhythmicity, to circadian timekeeping. *EMBO J* [Internet]. 2021 Apr [cited 2022 Jun 30];40(7). Available from: <https://onlinelibrary.wiley.com/doi/10.15252/embj.2020106745>
542. Huber MD, Gerace L. The size-wise nucleus: nuclear volume control in eukaryotes. *J Cell Biol*. 2007 Nov 19;179(4):583–4.
543. Jorgensen P, Edgington NP, Schneider BL, Rupeš I, Tyers M, Fitcher B. The Size of the Nucleus Increases as Yeast Cells Grow. Cohen-Fix O, editor. *Mol Biol Cell*. 2007 Sep;18(9):3523–32.
544. Diernfellner ACR, Querfurth C, Salazar C, Höfer T, Brunner M. Phosphorylation modulates rapid nucleocytoplasmic shuttling and cytoplasmic accumulation of *Neurospora* clock protein FRQ on a circadian time scale. *Genes Dev*. 2009 Sep 15;23(18):2192–200.
545. Guo J, Liu Y. Molecular mechanism of the *Neurospora* circadian oscillator. *Protein Cell*. 2010 Apr;1(4):331–41.
546. Guo J, Cheng P, Liu Y. Functional Significance of FRH in Regulating the Phosphorylation and Stability of *Neurospora* Circadian Clock Protein FRQ. *J Biol Chem*. 2010 Apr;285(15):11508–15.
547. Loros JJ, Dunlap JC. Genetic and Molecular Analysis of Circadian Rhythms in *Neurospora*. *Annu Rev Physiol*. 2001 Mar;63(1):757–94.
548. Grimaldi B, Coiro P, Filetici P, Berge E, Dobosy JR, Freitag M, et al. The *Neurospora crassa* White Collar-1 dependent Blue Light Response Requires Acetylation of Histone H3 Lysine 14 by NGF-1□D. *Mol Biol Cell*. 2006;17:8.
549. Colot HV, Loros JJ, Dunlap JC. Temperature-modulated Alternative Splicing and Promoter Use in the Circadian Clock Gene frequency□D. *Mol Biol Cell*. 2005;16:9.

550. Belden WJ, Loros JJ, Dunlap JC. Execution of the Circadian Negative Feedback Loop in *Neurospora* Requires the ATP-Dependent Chromatin-Remodeling Enzyme CLOCKSWITCH. *Mol Cell*. 2007 Feb;25(4):587–600.
551. Huang C, Zhu B. Roles of H3K36-specific histone methyltransferases in transcription: antagonizing silencing and safeguarding transcription fidelity. *Biophys Rep*. 2018 Aug;4(4):170–7.
552. Dziembowski A, Lorentzen E, Conti E, Séraphin B. A single subunit, Dis3, is essentially responsible for yeast exosome core activity. *Nat Struct Mol Biol*. 2007 Jan;14(1):15–22.
553. Liu Q, Greimann JC, Lima CD. Reconstitution, Activities, and Structure of the Eukaryotic RNA Exosome. *Cell*. 2006 Dec;127(6):1223–37.
554. Noguchi E, Hayashi N, Azuma Y, Seki T, Nakamura M, Nakashima N, et al. Dis3, implicated in mitotic control, binds directly to Ran and enhances the GEF activity of RCC1. *EMBO J*. 1996 Oct;15(20):5595–605.
555. Will CL, Luhrmann R. Spliceosome Structure and Function. *Cold Spring Harb Perspect Biol*. 2011 Jul 1;3(7):a003707–a003707.
556. Loros JJ, Feldman JF. Loss of Temperature Compensation of Circadian Period Length in the *frq-9* Mutant of *Neurospora crassa*. *J Biol Rhythms*. 1986 Sep;1(3):187–98.
557. Black DL. Mechanisms of Alternative Pre-Messenger RNA Splicing. *Annu Rev Biochem*. 2003 Jun;72(1):291–336.
558. Pearlman SM, Serber Z, Ferrell JE. A Mechanism for the Evolution of Phosphorylation Sites. *Cell*. 2011 Nov;147(4):934–46.
559. Kulkarni SD, Zhou F, Sen ND, Zhang H, Hinnebusch AG, Lorsch JR. Temperature-dependent regulation of upstream open reading frame translation in *S. cerevisiae*. *BMC Biol*. 2019 Dec;17(1):101.
560. Sidaway-Lee K, Costa MJ, Rand DA, Finkenstadt B, Penfield S. Direct measurement of transcription rates reveals multiple mechanisms for configuration of the *Arabidopsis* ambient temperature response. *Genome Biol*. 2014;15(3):R45.
561. Wigge PA, Guillaume-Schoepfer D, Jaeger KE, Geng F, Doccua FG, Costa A, et al. Ribosomes act as cryosensors in plants [Internet]. *Plant Biology*; 2020 Dec [cited 2022 Aug 14]. Available from: <http://biorxiv.org/lookup/doi/10.1101/2020.12.07.414789>
562. Mao Y, Liu H, Liu Y, Tao S. Deciphering the rules by which dynamics of mRNA secondary structure affect translation efficiency in *Saccharomyces cerevisiae*. *Nucleic Acids Res*. 2014 Apr;42(8):4813–22.
563. Plotkin JB, Kudla G. Synonymous but not the same: the causes and consequences of codon bias. *Nat Rev Genet*. 2011 Jan;12(1):32–42.
564. Zhou Z, Dang Y, Zhou M, Li L, Yu C hung, Fu J, et al. Codon usage is an important determinant of gene expression levels largely through its effects on transcription. *Proc Natl Acad Sci* [Internet]. 2016 Oct 11 [cited 2022 Jun 30];113(41). Available from: <https://pnas.org/doi/full/10.1073/pnas.1606724113>

565. Le Nouën C, McCarty T, Yang L, Brown M, Wimmer E, Collins PL, et al. Rescue of codon-pair deoptimized respiratory syncytial virus by the emergence of genomes with very large internal deletions that complemented replication. *Proc Natl Acad Sci*. 2021 Mar 30;118(13):e2020969118.
566. Giménez-Roig J, Núñez-Manchón E, Alemany R, Villanueva E, Fillat C. Codon Usage and Adenovirus Fitness: Implications for Vaccine Development. *Front Microbiol*. 2021 Feb 10;12:633946.
567. Groenke N, Trimpert J, Merz S, Conradie AM, Wyler E, Zhang H, et al. Mechanism of Virus Attenuation by Codon Pair Deoptimization. *Cell Rep*. 2020 Apr;31(4):107586.
568. de Smit MH, van Duin J. Secondary structure of the ribosome binding site determines translational efficiency: a quantitative analysis. *Proc Natl Acad Sci*. 1990 Oct;87(19):7668–72.
569. Tulloch F, Atkinson NJ, Evans DJ, Ryan MD, Simmonds P. RNA virus attenuation by codon pair deoptimisation is an artefact of increases in CpG/UpA dinucleotide frequencies. *eLife*. 2014 Dec 9;3:e04531.
570. Dror V, Winston F. The Swi/Snf Chromatin Remodeling Complex Is Required for Ribosomal DNA and Telomeric Silencing in *Saccharomyces cerevisiae*. *Mol Cell Biol*. 2004 Sep 15;24(18):8227–35.
571. Laurent BC, Treich I, Carlson M. The yeast SNF2/SWI2 protein has DNA-stimulated ATPase activity required for transcriptional activation. *Genes Dev*. 1993 Apr;7(4):583–91.
572. Li S, Lakin-Thomas P. Effects of *prd* Circadian Clock Mutations on FRQ-Less Rhythms in *Neurospora*. *J Biol Rhythms*. 2010 Apr;25(2):71–80.
573. Yang Y, He Q, Cheng P, Wrage P, Yarden O, Liu Y. Distinct roles for PP1 and PP2A in the *Neurospora* circadian clock. *Genes Dev*. 2004 Feb 1;18(3):255–60.
574. Ratnayake L, Adhvaryu KK, Kafes E, Motavaze K, Lakin-Thomas P. A component of the TOR (Target Of Rapamycin) nutrient-sensing pathway plays a role in circadian rhythmicity in *Neurospora crassa*. *PLoS Genet*. 2018 Jun;14(6):e1007457.
575. Kippert F, Lloyd D. A temperature-compensated ultradian clock ticks in *Schizosaccharomyces pombe*. *Microbiology*. 1995 Apr 1;141(4):883–90.
576. Kashiwa T, Suzuki T. High-quality genome assembly of the soybean fungal pathogen *Cercospora kikuchii*. Todd R, editor. *G3 GenesGenomesGenetics*. 2021 Sep 27;11(10):jkab277.
577. Westwood ML, O'Donnell AJ, de Bekker C, Lively CM, Zuk M, Reece SE. The evolutionary ecology of circadian rhythms in infection. *Nat Ecol Evol*. 2019 Apr;3(4):552–60.
578. Lakin-Thomas PL. Circadian clock genes *frequency* and *white collar-1* are not essential for entrainment to temperature cycles in *Neurospora crassa*. *Proc Natl Acad Sci*. 2006 Mar 21;103(12):4469–74.
579. Herr AJ. One protein from two open reading frames: mechanism of a 50 nt translational bypass. *EMBO J*. 2000 Jun 1;19(11):2671–80.

580. Wangen JR, Green R. Stop codon context influences genome-wide stimulation of termination codon readthrough by aminoglycosides. *eLife* [Internet]. 2020 Jan 23 [cited 2022 Jun 30];9. Available from: <https://elifesciences.org/articles/52611>
581. Blum M, Chang HY, Chuguransky S, Grego T, Kandasaamy S, Mitchell A, et al. The InterPro protein families and domains database: 20 years on. *Nucleic Acids Res.* 2021 Jan 8;49(D1):D344–54.
582. Finn RD, Bateman A, Clements J, Coggill P, Eberhardt RY, Eddy SR, et al. Pfam: the protein families database. *Nucleic Acids Res.* 2014 Jan;42(D1):D222–30.
583. Chen S, Liu XZ, Chen FJ. *Hirsutella minnesotensis* sp. nov., a New Pathogen of the Soybean Cyst Nematode. *Mycologia.* 2000 Sep;92(5):819.
584. Qu J, Zou X, Cao W, Xu Z, Liang Z. Two new species of *Hirsutella* (Ophiocordycipitaceae, Sordariomycetes) that are parasitic on lepidopteran insects from China. *MycoKeys.* 2021 Aug 9;82:81–96.
585. Thompson SM, Tan YP, Young AJ, Neate SM, Aitken EAB, Shivas RG. Stem cankers on sunflower (*Helianthus annuus*) in Australia reveal a complex of pathogenic *Diaporthe* (*Phomopsis*) species. *Persoonia - Mol Phylogeny Evol Fungi.* 2011 Dec 31;27(1):80–9.
586. Manzanilla-Lopez RH, Esteves I, Finetti-Sialer MM, Hirsch PR, Ward E, Devonshire J, et al. *Pochonia chlamydosporia*: Advances and Challenges to Improve Its Performance as a Biological Control Agent of Sedentary Endo-parasitic Nematodes. *J Nematol.* 2013;45(1):1–7.
587. Pétriacq P, Stassen JHM, Ton J. Spore Density Determines Infection Strategy by the Plant Pathogenic Fungus *Plectosphaerella cucumerina*. *Plant Physiol.* 2016 Apr;170(4):2325–39.
588. Franco MEE, Wisecaver JH, Arnold AE, Ju Y, Slot JC, Ahrendt S, et al. Ecological generalism drives hyperdiversity of secondary metabolite gene clusters in xylarialean endophytes. *New Phytol.* 2022 Feb;233(3):1317–30.
589. Peng H, Zhang YL, Ying SH, Feng MG. The Essential and the Nonessential Roles of Four Clock Elements in the Circadian Rhythm of *Metarhizium robertsii*. *J Fungi.* 2022 May 25;8(6):558.
590. Rubio MB, Quijada NM, Pérez E, Domínguez S, Monte E, Hermosa R. Identifying Beneficial Qualities of *Trichoderma parareesei* for Plants. *Appl Environ Microbiol.* 2014 Mar 15;80(6):1864–73.
591. Pandey A, Banerjee D. *Daldinia bambusicola* Ch4/11 an Endophytic Fungus Producing Volatile Organic Compounds Having Antimicrobial and Olio Chemical Potential. 2014;9.
592. Gupta R, Brunak S. Prediction of glycosylation across the human proteome and the correlation to protein function. *Pac Symp Biocomput Pac Symp Biocomput.* 2002;310–22.
593. Blom N, Sicheritz-Pontén T, Gupta R, Gammeltoft S, Brunak S. Prediction of post-translational glycosylation and phosphorylation of proteins from the amino acid sequence. *PROTEOMICS.* 2004 Jun;4(6):1633–49.

594. Ma R, Li S, Li W, Yao L, Huang HD, Lee TY. KinasePhos 3.0: Redesign and expansion of the prediction on kinase-specific phosphorylation sites. *Genomics Proteomics Bioinformatics*. 2022 Jun 30;S1672-0229(22)00081-X.
595. Pagni M, Ioannidis V, Cerutti L, Zahn-Zabal M, Jongeneel CV, Hau J, et al. MyHits: improvements to an interactive resource for analyzing protein sequences. *Nucleic Acids Res*. 2007 Jul;35(Web Server issue):W433–7.
596. Meyer RD, Srinivasan S, Singh AJ, Mahoney JE, Gharahassanlou KR, Rahimi N. PEST Motif Serine and Tyrosine Phosphorylation Controls Vascular Endothelial Growth Factor Receptor 2 Stability and Downregulation. *Mol Cell Biol*. 2011 May 15;31(10):2010–25.
597. EMBOSS: epestfind manual [Internet]. [cited 2023 Mar 7]. Available from: <https://emboss.bioinformatics.nl/cgi-bin/emboss/help/epestfind>
598. Simm D, Hatje K, Kollmar M. Waggawagga: comparative visualization of coiled-coil predictions and detection of stable single α -helices (SAH domains). *Bioinformatics*. 2015 Mar 1;31(5):767–9.
599. Ludwiczak J, Winski A, Szczepaniak K, Alva V, Dunin-Horkawicz S. DeepCoil—a fast and accurate prediction of coiled-coil domains in protein sequences. Hancock J, editor. *Bioinformatics*. 2019 Aug 15;35(16):2790–5.
600. Cong Q, Grishin NV. MESSA: MEta-Server for protein Sequence Analysis. *BMC Biol* [Internet]. 2012 Dec [cited 2022 Jun 30];10(1). Available from: <https://bmcbiol.biomedcentral.com/articles/10.1186/1741-7007-10-82>
601. Luo C. Nuclear localization is required for function of the essential clock protein FRQ. *EMBO J*. 1998 Mar 2;17(5):1228–35.
602. Kosugi S, Hasebe M, Tomita M, Yanagawa H. Systematic identification of cell cycle-dependent yeast nucleocytoplasmic shuttling proteins by prediction of composite motifs. *Proc Natl Acad Sci*. 2009 Jun 23;106(25):10171–6.
603. Nardozzi JD, Lott K, Cingolani G. Phosphorylation meets nuclear import: a review. *Cell Commun Signal* [Internet]. 2010 Dec [cited 2022 Jun 30];8(1). Available from: <https://biosignaling.biomedcentral.com/articles/10.1186/1478-811X-8-32>
604. Bernhofer M, Dallago C, Karl T, Satagopam V, Heinzinger M, Littmann M, et al. PredictProtein - Predicting Protein Structure and Function for 29 Years. *Nucleic Acids Res*. 2021 Jul 2;49(W1):W535–40.
605. Buchan DWA, Jones DT. The PSIPRED Protein Analysis Workbench: 20 years on. *Nucleic Acids Res*. 2019 Jul 2;47(W1):W402–7.
606. Suzuki M. SPXX, a frequent sequence motif in gene regulatory proteins. *J Mol Biol*. 1989 May;207(1):61–84.
607. Suzuki M, Yagi N. Structure of the SPXX motif. *Proc R Soc Lond B Biol Sci*. 1991 Dec 23;246(1317):231–5.
608. Zhang C, Meng X, Wei X, Lu L. Highly efficient CRISPR mutagenesis by microhomology-mediated end joining in *Aspergillus fumigatus*. *Fungal Genet Biol*. 2016 Jan;86:47–57.

609. Shi X, Shou J, Mehryar MM, Li J, Wang L, Zhang M, et al. Cas9 has no exonuclease activity resulting in staggered cleavage with overhangs and predictable di- and tri-nucleotide CRISPR insertions without template donor. *Cell Discov* [Internet]. 2019 Dec [cited 2022 Jun 30];5(1). Available from: <http://www.nature.com/articles/s41421-019-0120-z>
610. Linden H, Ballario P, Macino G. Blue Light Regulation in *Neurospora crassa*. *Fungal Genet Biol*. 1997 Dec;22(3):141–50.
611. Michael TP, Park S, Kim TS, Booth J, Byer A, Sun Q, et al. Simple Sequence Repeats Provide a Substrate for Phenotypic Variation in the *Neurospora crassa* Circadian Clock. Redfield R, editor. *PLoS ONE*. 2007 Aug 29;2(8):e795.
612. Albuquerque P, Casadevall A. Quorum sensing in fungi – a review. *Med Mycol*. 2012 May;50(4):337–45.
613. Barriuso J, Hogan DA, Keshavarz T, Martínez MJ. Role of quorum sensing and chemical communication in fungal biotechnology and pathogenesis. *FEMS Microbiol Rev*. 2018 Sep 1;42(5):627–38.
614. Deep A, Chaudhary U, Gupta V. Quorum sensing and Bacterial Pathogenicity: From Molecules to Disease. *J Lab Physicians*. 2011 Jan;3(01):004–11.
615. de Kievit TR, Iglewski BH. Bacterial Quorum Sensing in Pathogenic Relationships. Portnoy DA, editor. *Infect Immun*. 2000 Sep;68(9):4839–49.
616. Mehmood A, Liu G, Wang X, Meng G, Wang C, Liu Y. Fungal Quorum-Sensing Molecules and Inhibitors with Potential Antifungal Activity: A Review. *Molecules*. 2019 May 21;24(10):1950.
617. Pena RT, Blasco L, Ambroa A, González-Pedrajo B, Fernández-García L, López M, et al. Relationship Between Quorum Sensing and Secretion Systems. *Front Microbiol*. 2019 Jun 7;10:1100.
618. Linden H. White collar 2, a partner in blue-light signal transduction, controlling expression of light-regulated genes in *Neurospora crassa*. *EMBO J*. 1997 Jan 1;16(1):98–109.
619. Bayram Ö, Krappmann S, Seiler S, Vogt N, Braus GH. *Neurospora crassa* ve-1 affects asexual conidiation. *Fungal Genet Biol*. 2008 Feb;45(2):127–38.
620. Dulal N, Rogers A, Wang Y, Egan M. Dynamic assembly of a higher-order septin structure during appressorium morphogenesis by the rice blast fungus. *Fungal Genet Biol*. 2020 Jul;140:103385.

9 Supplementary material

9.1 Fiji macro code

9.1.1 Colony area and conidial banding

```
setBackgroundcolor(255, 255, 255); // set the background colour to white
run("Set Scale...", "distance=0 global"); // remove scale from any previous image
run("Set Measurements...", "area centroid center perimeter fit shape feret's display add
redirect=None decimal=3");
run("Select None");
run("Clear Results"); // clears the results table from any previous analysis
roiManager("reset"); // reset the roiManager from any previous analysis
print("\\Clear"); // clears the log from any previous analysis
Table.showRowIndex(true);
//getdateandtime macro:
MonthNames
newArray("Jan","Feb","Mar","Apr","May","Jun","Jul","Aug","Sep","Oct","Nov","Dec");
DayNames = newArray("Sun", "Mon","Tue","Wed","Thu","Fri","Sat");
getDateAndTime(year, month, dayOfWeek, dayOfMonth, hour, minute, second, msec);
TimeString = "Date: "+DayNames[dayOfWeek]+" ";
if (dayOfMonth<10) {TimeString = TimeString+"0";}
TimeString = TimeString+dayOfMonth+"-"+MonthNames[month]+"-"+year+"\nTime: ";
if (hour<10) {TimeString = TimeString+"0";}
TimeString = TimeString+hour+":.";
if (minute<10) {TimeString = TimeString+"0";}
TimeString = TimeString+minute+":.";
if (second<10) {TimeString = TimeString+"0";}
TimeString = TimeString+second;
print("analysis start date/time:");
print(TimeString);
originalName = getTitle(); //retains the file name
input_folder = File.directory(); //retains input folder
print("input folder: "+input_folder);
output_folder = input_folder+"banding_analysis_output/"; //sets output folder
original_width = getWidth();
original_height = getHeight();
original_image_area = (original_width * original_height);
print("original width: "+original_width);
print("original height: "+original_height);
print("original image area: "+original_image_area);
min_plate_area = (original_image_area * 0.1); //plate must occupy at least 10% of the image
print("minimum plate area: "+min_plate_area);
File.makeDirectory(output_folder); //locates or creates an output folder if not already present
//output_folder = input_folder+"banding_analysis_output/"
print("output folder: "+output_folder);
print("image title: "+originalName);
selectWindow(originalName);
//manually select plate
run("Duplicate...", "title=[find plate]");
```

```

setTool(0);
waitForUser("draw a box around the petri dish and press okay");
run("Crop");
//get plate parameters and set scale
plate_width = getWidth();
print(originalName+" plate width: "+plate_width);
plate_height = getHeight();
print(originalName+" plate height: "+plate_height);
plate_width_centre = plate_width/2;
print(originalName+" plate width centre: "+plate_width_centre);
plate_height_centre = plate_height/2;
print(originalName+" plate height centre: "+plate_height_centre);
plate_diam = (plate_width + plate_height)/2;
print(originalName+" plate diameter: "+plate_diam);
plate_radius = plate_diam/2;
print(originalName+" plate radius: "+plate_radius);
pixels_per_cm = (plate_diam/9);
print(originalName+" pixels per cm: "+pixels_per_cm);
pixels_per_mm = pixels_per_cm/10;
print(originalName+" pixels per mm: "+pixels_per_mm);
run("Set Scale...", "distance="+plate_diam+" known=9 pixel=1 unit=cm global");
selectWindow("find plate");
run("Select All");
run("Invert");//inverts image for thresholding and plotting
//threshold for colony
selectWindow("find plate");
//clear edges of plate from image (prevents counting the plate as a particle);
plate_clear_x = getWidth()*0.1;
plate_clear_y = getHeight()*0.1;
plate_clear_width = getWidth()*0.8;
plate_clear_height = getHeight()*0.8;
makeRectangle(plate_clear_x, plate_clear_y, plate_clear_width, plate_clear_height);
setBackground(0, 0, 0);// set the background colour to black
setBackground(255, 255, 255);// set the background colour to white
run("Select All");
run("Duplicate...", "title=[colony centre]");
//manual threshold version below:
run("Color Threshold...");
beep();
waitForUser("Manual thresholding step", "move the sliders for HSB to cover the colony
perimeter, press 'select' in the threshold window, then okay in this box");
//automated version below: comment out from "min=newArray(3)" to "run("Create selection")"
/*
//colour thresholding can depend on lighting and colony conditions - MAY NEED TO BE ADJUSTED!
min=newArray(3);
max=newArray(3);
filter=newArray(3);
a=getTitle();
run("HSB Stack");
run("Convert Stack to Images");
selectWindow("Hue");

```

```

rename("0");
selectWindow("Saturation");
rename("1");
selectWindow("Brightness");
rename("2");
min[0]=0;
max[0]=255;
filter[0]="pass";
min[1]=0;
max[1]=200;
//max[1]=245;
filter[1]="pass";
min[2]=10;
max[2]=245;
filter[2]="pass";
for (i=0;i<3;i++){
  selectWindow(""+i);
  setThreshold(min[i], max[i]);
  run("Convert to Mask");
  if (filter[i]=="stop") run("Invert");
}
imageCalculator("AND create", "0","1");
imageCalculator("AND create", "Result of 0","2");
for (i=0;i<3;i++){
  selectWindow(""+i);
  close();
}
selectWindow("Result of 0");
close();
selectWindow("Result of Result of 0");
rename(a);
// Colour Thresholding-----
run("Create Selection");
*/
run("Make Binary");
run("Select None");
run("Dilate");
run("Dilate");
run("Close-");
//run("Fill Holes");
run("Erode");
run("Erode");
run("Fill Holes");
run("Analyze Particles...", "size=5-62 circularity=0.10-1.00 display include summarize
add");//selects particle between 5 and 62cm2 (petri dish area ~63.6cm2)
//find colony centre
roiManager("select", 0);
roiManager("measure");
for (a = 0; a < nResults(); a++) {
  radius = sqrt((getResult('Area', a))/PI);
  diameter = (2*radius);

```

```

setResult("Circular Radius", a, radius);
setResult("Circular Diameter", a, diameter);
}
updateResults();
//print parameters
//colony_centreX = getResult("XM")*pixels_per_cm;
colony_centreX = getResult("X")*pixels_per_cm;
print(originalName+" colony centre x coordinate: "+colony_centreX);
//colony_centreY = getResult("YM")*pixels_per_cm;
colony_centreY = getResult("Y")*pixels_per_cm;
print(originalName+" colony centre y coordinate: "+colony_centreY);
print(originalName+" colony centre coordinates: ("+colony_centreX+","+colony_centreY+")
(x,y)");
colony_diameter = getResult("Feret");
print(originalName+" colony diameter: "+colony_diameter+" (cm)");
colony_diameter_px = colony_diameter*pixels_per_cm;
print(originalName+" colony diameter: "+colony_diameter_px+" (px)");
colony_radius = colony_diameter/2;
print(originalName+" colony radius: "+colony_radius+" (cm)");
colony_radius_px = colony_radius*pixels_per_cm;
print(originalName+" colony radius: "+colony_radius_px+" (px)");
selectWindow("find plate");
//calculate colony x and y offset
offx = (plate_width_centre - colony_centreX);
print(originalName+" colony centre x offset: "+offx);
offy = (plate_height_centre - colony_centreY);
print(originalName+" colony centre y offset: "+offy);
print(originalName+" colony centre x,y offset: ("+offx+","+offy+") (x,y)");
run("Enhance Local Contrast (CLAHE)", "blocksize="+pixels_per_mm+" histogram=255
maximum=100 mask=*None* fast_(less_accurate)");
run("Gaussian Blur...", "sigma=0.05 scaled");
//move colony centre to image centre
run("Translate...", "x="+offx+ " y="+offy+" interpolation=Bilinear");
//log new centre values
selectWindow("find plate");
new_centre_x = getWidth()/2;
print(originalName+" new centre x: "+new_centre_x);
new_centre_y = getHeight()/2;
print(originalName+" new centre y: "+new_centre_y);
print(originalName+" new centre x,y: ("+new_centre_x+","+new_centre_y+") (x,y)");
roiManager("reset");
run("Select None");
//set rotation angle and number of rotations (rotations must be a whole number)
//angle = 5;
angle = 30;
print("rotational angle: "+angle);
//rotations = 30/angle;
rotations = 360/angle;
print("number of rotations: "+rotations);
saveAs("Results", output_folder+originalName+" colony statistics table.csv");
run("Clear Results");

```

```

//create tables and plots
//Plot.create(originalName+" - Rotational Segment Intensities", "colony radius (cm)", "Inverted
Pixel Intensity");
Plot.create(originalName+" - Rotational Segment Intensities", "percent colony radius", "Inverted
Pixel Intensity");
Plot.setFormatFlags("11001100111111");
Plot.setLimits(0, 100, 0, 255);
//loop: create rectangle segment at colony (image) centre, with length = radius (4.5cm) and
height 10px
//get x points and y pixel intensity of segment 1
//add x points and y pixel intensity of segment 1 to results table
//adds y pixel intensity of segment 1 to rotational segment intensities plot
//repeat for segment 2 for n rotations
//line_length = new_centre_x+colony_radius_px;
for(segment = 0; segment < rotations; segment++){
    makeRectangle(new_centre_x, new_centre_y, colony_radius_px, 10);
    run("Plot Profile");
    Plot.getValues(x_position, y_intensity);
    close();
    selectWindow("find plate");
    run("Select None");
    run("Rotate... ", "angle="+angle+" grid=1 interpolation=Bilinear");
    Table.setColumn("x_position", x_position);
    results_length = nResults;
    for(percent = 0; percent < results_length; percent++) {
        value = getResult("x_position", percent);
        P_colony_radius = (value/colony_radius)*100;
        setResult("percent_colony_radius", percent, P_colony_radius);
    }
    updateResults();
    Table.setColumn("segment_intensity_"+segment+1, y_intensity);
    percent_colony_radius_array = Table.getColumn("percent_colony_radius");
    Plot.add("line", percent_colony_radius_array, y_intensity);
}
updateResults();
result_length = nResults;
print("number of results: "+result_length);
for(x_row = 0; x_row < result_length; x_row++){
    sum_row = 0;
    for(column = 1; column < rotations+1; column++){
        sum_row_int = getResult("segment_intensity_"+column, x_row);
        sum_row = sum_row + sum_row_int;
        setResult("Sum_segment_intensity", x_row, sum_row);
    }
    mean_row = sum_row/rotations;
    setResult("mean_segment_intensity", x_row, mean_row);
}
updateResults();
mean_values_array = Table.getColumn("mean_segment_intensity");
Plot.add("Circle", percent_colony_radius_array, mean_values_array);
Plot.show();

```

```

all_lines_plot = getTitle();
print("all lines plot title: "+all_lines_plot);
Plot.makeHighResolution(all_lines_plot+"high res plot",4.0,"disable");
///SAVE HIGH RES PLOT TO INPUT_FOLDER+ORIGINALNAME+"ALL_LINES_PLOT"+.PNG
saveAs("PNG", output_folder+all_lines_plot);
close();
//new plot showing just mean values
Plot.create(originalName+" - Mean Rotational Segment Intensities", "percent colony radius",
"Inverted Pixel Intensity");
Plot.setFormatFlags("11001100111111");
Plot.setLimits(0, 100, 0, 255);
Plot.add("line", percent_colony_radius_array, mean_values_array);
Plot.show();
mean_line_plot = getTitle();
print("mean line plot title: "+mean_line_plot);
Plot.makeHighResolution(all_lines_plot+"high res plot",4.0,"disable");
saveAs("PNG", output_folder+mean_line_plot);
close();
//////////standard deviation
for(x_row = 0; x_row < result_length; x_row++){
    sum_sq_diff = 0;
    for(column = 1; column < rotations+1; column++){
        sq_diff = Math.sqrt((getResult("segment_intensity_"+column, x_row))-
(getResult("mean_segment_intensity", x_row)));
        setResult("square_difference_to_mean_"+column, x_row, sq_diff);
        sum_sq_diff_int = getResult("square_difference_to_mean_"+column,
x_row);
        sum_sq_diff = sum_sq_diff + sum_sq_diff_int;
    }
    setResult("sum of square differences to mean", x_row, sum_sq_diff);
    sum_sq_diff_n_1 = (getResult("sum of square differences to mean", x_row)/(rotations-
1));
    setResult("(sum sq diff to mean)/variance", x_row, sum_sq_diff_n_1);
    standard_deviation = Math.sqrt(getResult("(sum sq diff to mean)/variance", x_row));
    setResult("standard deviation", x_row, standard_deviation);
    standard_error_of_mean = ((getResult("standard deviation",
x_row))/(Math.sqrt(rotations)));
    setResult("standard error of mean (SEM)", x_row, standard_error_of_mean);
}
updateResults();
Plot.create(originalName+" - Rotational Segment Intensities - STANDARD DEVIATION", "percent
colony radius", "Inverted Pixel Intensity");
Plot.setFormatFlags("11001100111111");
Plot.setLimits(0, 100, 0, 255);
Plot.add("line", percent_colony_radius_array, mean_values_array);
Plot.add("error", Table.getColumn("standard deviation", "Results"));
Plot.show();
standard_deviation_plot = getTitle();
print("Standard deviation line plot title: "+standard_deviation_plot);
Plot.makeHighResolution(standard_deviation_plot+"high res plot",4.0,"disable");
saveAs("PNG", output_folder+standard_deviation_plot);

```

```

close();
Plot.create(originalName+" - Rotational Segment Intensities - SEM", "percent colony radius",
"Inverted Pixel Intensity");
Plot.setFormatFlags("11001100111111");
Plot.setLimits(0, 100, 0, 255);
Plot.add("line", percent_colony_radius_array, mean_values_array);
Plot.add("error", Table.getColumn("standard error of mean (SEM)", "Results"));
Plot.show();
SEM_plot = getTitle();
print("SEM line plot title: "+SEM_plot);
Plot.makeHighResolution(SEM_plot+"high res plot",4.0,"disable");
saveAs("PNG", output_folder+SEM_plot);
close();
//save results table as a csv
saveAs("Results", output_folder+originalName+" results table.csv");
selectWindow("Log");
saveAs("text", output_folder+originalName+" log info.txt");
print("colony statistics results table file name: "+originalName+"colony statistics table.csv");
print("rotational segments results table file name: "+originalName+"rotational segments results
table.csv");
print("log file name: "+originalName+" log info.txt");

```

9.1.2 Conidial counts

```

setBatchMode(true);
roiManager("Reset");//resets the roiManager if previous images have been run
setTool("rectangle");
originalName = getTitle();//calls the input image title
//crops to the central portion of the image, reducing the 'halo' effect
var A = getWidth()/4;
var B = getHeight()/4;
var C = getWidth()/2;
var D = getHeight()/2;
makeRectangle(A, B, C, D);
run("Duplicate...", "title=spore_count_-_ "+originalName);//duplicates the image to work on
setForegroundColor(0, 0, 255);// sets foreground colour to blue
run("Set Scale...", "distance=0 known=0 pixel=1 unit=pixel global");//removes scale
rename("spore_count_-_ "+originalName);//renames image to working image
run("Duplicate...", "title=original_spore_image_-_ "+originalName);//duplicates the image to
work on
var y = getTitle();
selectWindow("spore_count_-_ "+originalName);
run("8-bit");//converts the working image to 8-bit
run("Subtract Background...", "rolling=50 light stack");//removes the background
run("Minimum...", "radius=2");//applies minimum pixel intensity threshold to better segment
conidia from bright background
setThreshold(0, 225);//thresholds the image to ignore the bright background
run("Convert to Mask", "method=Default background=Light calculate");//creates a binary image
of the thresholded image
run("Fill Holes", "stack");//makes a solid particle for the spores
run("Erode");//erodes the binary image twice to remove any noise
run("Dilate");//dilates the binary image by the same amount to (roughly) recreate their size

```

```

run("Watershed", "stack");//makes a solid particle for the spores
run("Set Measurements...", "area mean standard min centroid perimeter shape display add
redirect=[&y] decimal=3");//redirects the analysis and count to the original image
run("Analyze Particles...", "size=200-2000 circularity=0.60-0.85 show=Overlay display exclude
include summarize add");// analyses number of spores based on pixel size. You may need to edit
this based on your image size/pixel density
selectWindow("original_spore_image_-_" +originalName);
roiManager("draw");//draws the outline of the spores from the roiManager onto the spore count
image
saveAs("jpg", "OUTPUT/FILE/PATH/" + originalName + "- annotated conidia");//saves the
annotated conidia to the user-defined file path
close();
selectWindow("spore_count_-_" +originalName);
close();
selectWindow(originalName);
run("Open Next");//opens the next image in the input folder
run("Select None");

```

9.1.3 Appressorial cytorrhysis location

```

roiManager("Reset");//resets the roiManager if previous images have been run
originalName = getTitle();
input_folder = File.directory();
output_folder = input_folder+"cytorrhysis appressoria output";
File.makeDirectory(output_folder);
run("Select None");
var A = getWidth()/4;
var B = getHeight()/4;
var C = getWidth()/2;
var D = getHeight()/2;
makeRectangle(A, B, C, D);
run("Duplicate...", "title=spore_count_-_" +originalName);//duplicates the image to work on
setForegroundColor(0, 0, 255);// sets foreground colour to blue
run("Set Scale...", "distance=0 known=0 pixel=1 unit=pixel global");//removes scale
rename("spore_count_-_" +originalName);//renames image to working image
run("Duplicate...", "title=original_spore_image_-_" +originalName);//duplicates the image to
work on
var y = getTitle();
selectWindow("spore_count_-_" +originalName);
run("8-bit");//converts the working image to 8-bit
run("Subtract Background...", "rolling=50 light stack");//removes the background
run("Minimum...", "radius=2");//uses a minimum pixel value filter to increase the contrast of the
spores against the background (https://imagej.nih.gov/ij/docs/menus/process.html - minimum)
//setThreshold(0, 235);//thresholds the image to ignore the bright background
setThreshold(0, 225);//thresholds the image to ignore the bright background
run("Convert to Mask", "method=Default background=Light calculate");//creates a binary image
of the thresholded image
run("Dilate");//dilates the binary image by the same amount to (roughly) recreate their size
run("Erode");//erodes the binary image twice to remove any noise
run("Close-");

```

```

run("Fill Holes", "stack");//makes a solid particle for the spores
run("Watershed", "stack");//makes a solid particle for the spores
//run("Outline", "stack");//outlines the spores
run("Set Measurements...", "area mean standard min centroid perimeter shape display add
redirect=[&y] decimal=3");//redirects the analysis and count to the original image
run("Analyze Particles...", "size=1000-3000 circularity=0.7-1.00 show=Overlay display exclude
include summarize add");// analyses number of spores based on pixel size. You may need to edit
this based on your image size.
selectWindow("original_spore_image_-_" +originalName);
roiManager("draw");//draws the outline of the spores from the roiManager onto the spore count
image
saveAs("PNG", output_folder+"/"+originalName+"annotated appressoria");
saveAs("Results", output_folder+"/"+originalName+" appressoria finder results.csv");

```

9.1.4 Leaf segmentation and pre-processing

```

//use BATCH PROCESS//
setBatchMode(true);//sets batch mode on - saves time and does not actively open images
roiManager("reset");//resets roi manager
run("Select None");//resets selection
originalName = getTitle(); //retains the file name
rename("original image") //renames image
run("Select None");
var W = getWidth();//gets image width
var H = getHeight();//gets image height
run("Canvas Size...", "width=6800 height=9360 position=Top-Left");//sets image size
run("Size...", "width=6800 height=9360 depth=1 interpolation=None");//sets image size
run("Set Scale...", "distance=315 known=1 pixel=1 unit=cm global");//sets the image scale
(change for your needs)
run("Set Measurements...", "area mean min display add redirect=None decimal=3");//resets
redirecting image
setBackground(0, 0, 0);//sets background colour to black
run("Select All");//selects everythin in the image
run("Duplicate...", "title=[working image]");//duplicates to create a working image
run("Select None");//resets selection
run("Canvas Size...", "width=6800 height=9360 position=Top-Left");//sets image size
run("Size...", "width=6800 height=9360 depth=1 interpolation=None");//sets image size
makeRectangle(3400, 0, 3600, 4900);//creates a rectangle around the calibration card
run("Clear", "slice");//clears the calibration card from the image to prevent colour interference
run("Select None");//resets selection
run("Canvas Size...", "width=6800 height=9360 position=Top-Left");//sets image size
run("Size...", "width=6800 height=9360 depth=1 interpolation=None");//sets image size
run("Select All");//selects everything in the image
run("Duplicate...", "title=[cropped leaves]");//duplicates the image for thresholding
run("Color Threshold...");//colour thresholding
// Color Thresholder 2.0.0-rc-68/1.52e
// Autogenerated macro, single images only! ****to select leaf area**** may need to change
based on imaging setup
min=newArray(3);
max=newArray(3);

```

```

filter=newArray(3);
a=getTitle();
run("HSB Stack");
run("Convert Stack to Images");
selectWindow("Hue");
rename("0"); //renames hue to 0
selectWindow("Saturation");
rename("1"); //renames saturation to 1
selectWindow("Brightness");
rename("2"); //renames brightness to 2
min[0]=0;
max[0]=255; //sets hue (edit as necessary)
filter[0]="pass";
min[1]=50; //sets saturation (edit as necessary)
max[1]=255;
filter[1]="pass";
min[2]=40; //sets brightness (edit as necessary)
max[2]=255;
filter[2]="pass";
for (i=0;i<3;i++){
  selectWindow(""+i);
  setThreshold(min[i], max[i]);
  run("Convert to Mask");
  if (filter[i]=="stop") run("Invert");
}
imageCalculator("AND create", "0","1");
imageCalculator("AND create", "Result of 0","2");
for (i=0;i<3;i++){
  selectWindow(""+i);
  close();
}
selectWindow("Result of 0");
close();
selectWindow("Result of Result of 0");
rename(a);
// Colour Thresholding-----
run("Make Binary");//creates a binary image of the thresholded area
run("Fill Holes");//fills any gaps in the binary image
run("Analyze Particles...", "size=0.1-10000.00 display include add");//analyses the individual
'particles' (leaves)
selectWindow("working image");//moves back to the non-binary image
rename(originalName+"- individual leaf");//renames the image "&file_name& - individual leaf"
run("Select None");//resets selection
selectWindow("cropped leaves");//moves back to the binary image
run("Close");//closes the binary image
//BELOW USES THE ROI MANAGER TO SELECT EACH INDIVIDUAL LEAF, DUPLICATE IT, AND SAVE
IT AS AN INDIVIDUAL FILE - CHOOSE FILE DESTINATION BELOW
selectWindow(originalName+"- individual leaf");//moves back to the non-binary image
for (u=000; u<roiManager("count"); ++u) {
  run("Duplicate...", "title=crop");
  roiManager("Select", u);
}

```

```

        run("Crop");
        saveAs("tiff", "FILE/PATH/HERE/" + "individual leaf - " + originalName + " - " + (u+001));
        close();
        selectWindow(originalName+"- individual leaf");
    }
    close();//closes the active image except for the original file, ready to move onto the next image
    in the folder.
    selectWindow("original image");

```

9.1.5 Chlorophyll fluorescence

```

//reset parameters
setBackground(255, 255, 255);
roiManager("Reset");//resets any previous information
run("Set Scale...", "distance=0 known=0 unit=pixel");//resets scale measurements
run("Set Measurements...", "area mean min display add redirect=None decimal=3");//resets the
redirect
//select NDVI image
waitForUser("Click on the NDVI image, then press ok");
run("Select None");
//retain NDVI image title
var NDVI = getTitle();
//select FvFm image
waitForUser("Click on the FvFm image, then press ok");
run("Select None");
//retain FvFm image title
var FvFm = getTitle();
//draw a leaf around the NDVI leaf
selectWindow(NDVI);
setTool("rectangle");
waitForUser("draw a box around the leaf of interest on the NDVI image, then press ok");
//duplicate that selection on NDVI leaf - NDVI working image
run("Duplicate...", "title=[NDVI working image]");
//apply selection to FvFm image
selectWindow(FvFm);
run("Restore Selection");
//duplicate that selection on FvFm leaf - FvFm working image
run("Duplicate...", "title=[FvFm working image]");
//duplicate NDVI working image twice;
selectWindow("NDVI working image")
//
background removal threshold
run("Duplicate...", "title=[NDVI background removal threshold]");
//
background removed
run("Duplicate...", "title=[NDVI background removed]");
//threshold background removal threshold image
selectWindow("NDVI background removal threshold");
run("Color Threshold...");//thresholds for the leaves to remove the background
// Color Thresholder 2.0.0-rc-69/1.52p
// Autogenerated macro, single images only!
min=newArray(3);

```

```

max=newArray(3);
filter=newArray(3);
a=getTitle();
run("HSB Stack");
run("Convert Stack to Images");
selectWindow("Hue");
rename("0");
selectWindow("Saturation");
rename("1");
selectWindow("Brightness");
rename("2");
min[0]=0;
max[0]=255;
filter[0]="pass";
min[1]=0;
max[1]=125;
filter[1]="pass";
min[2]=10;
max[2]=255;
filter[2]="pass";
for (i=0;i<3;i++){
  selectWindow(""+i);
  setThreshold(min[i], max[i]);
  run("Convert to Mask");
  if (filter[i]=="stop") run("Invert");
}
imageCalculator("AND create", "0","1");
imageCalculator("AND create", "Result of 0","2");
for (i=0;i<3;i++){
  selectWindow(""+i);
  close();
}
selectWindow("Result of 0");
close();
selectWindow("Result of Result of 0");
rename(a);
// Colour Thresholding-----
run("Make Binary");
//create selection of background
run("Create Selection");
//apply selection to background removal image
selectWindow("NDVI background removed");
run("Restore Selection");
//clear selection of background
run("Clear", "slice");
//apply selection to FvFm working image
selectWindow("FvFm working image");
run("Restore Selection");
//clear selection of background
run("Clear", "slice");
//select none of NDVI background removal image

```

```

selectWindow("NDVI background removed");
run("Select None");
//get image dimensions
var x = getWidth();
var y = getHeight();
//duplicate 4x
//          NDVI leaf area threshold
run("Duplicate...", "title=[NDVI leaf area threshold]");
//          NDVI leaf area
run("Duplicate...", "title=[NDVI leaf area]");
//          NDVI healthy area threshold
run("Duplicate...", "title=[NDVI healthy area threshold]");
//          NDVI unhealthy area threshold
run("Duplicate...", "title=[NDVI unhealthy area threshold]");
//create drawing for NDVI
newImage("NDVI drawing", "RGB white", x, y, 1);
//select FvFm image without background
selectWindow("FvFm working image");
run("Select None");
//duplicate 4x
//          FvFm leaf area threshold
run("Duplicate...", "title=[FvFm leaf area threshold]");
//          FvFm leaf area
run("Duplicate...", "title=[FvFm leaf area]");
//          FvFm healthy area threshold
run("Duplicate...", "title=[FvFm healthy area threshold]");
//          FvFm unhealthy area threshold
run("Duplicate...", "title=[FvFm unhealthy area threshold]");
//create drawing for FvFm
newImage("FvFm drawing", "RGB white", x, y, 1);
selectWindow("NDVI leaf area threshold");
//threshold NDVI leaf area threshold
run("Color Threshold...");//thresholds for the leaves to remove the background
// Color Thresholder 2.0.0-rc-69/1.52p
// Autogenerated macro, single images only!
min=newArray(3);
max=newArray(3);
filter=newArray(3);
a=getTitle();
run("HSB Stack");
run("Convert Stack to Images");
selectWindow("Hue");
rename("0");
selectWindow("Saturation");
rename("1");
selectWindow("Brightness");
rename("2");
min[0]=0;
max[0]=255;
filter[0]="pass";
min[1]=10;

```

```

max[1]=255;
filter[1]="pass";
min[2]=10;
max[2]=255;
filter[2]="pass";
for (i=0;i<3;i++){
  selectWindow(""+i);
  setThreshold(min[i], max[i]);
  run("Convert to Mask");
  if (filter[i]=="stop") run("Invert");
}
imageCalculator("AND create", "0","1");
imageCalculator("AND create", "Result of 0","2");
for (i=0;i<3;i++){
  selectWindow(""+i);
  close();
}
selectWindow("Result of 0");
close();
selectWindow("Result of Result of 0");
rename(a);
// Colour Thresholding-----
//create binary image
run("Make Binary");
//create selection
run("Create Selection");
//restore selection in FvFm drawing (to visualise dead tissue)
selectWindow("FvFm drawing");
run("Restore Selection");
//threshold NDVI healthy leaf area threshold
selectWindow("NDVI healthy area threshold");
run("Color Threshold...");//thresholds for the leaves to remove the background
// Color Thresholder 2.0.0-rc-69/1.52p
// Autogenerated macro, single images only!
min=newArray(3);
max=newArray(3);
filter=newArray(3);
a=getTitle();
run("HSB Stack");
run("Convert Stack to Images");
selectWindow("Hue");
rename("0");
selectWindow("Saturation");
rename("1");
selectWindow("Brightness");
rename("2");
min[0]=0;
max[0]=72;
filter[0]="pass";
min[1]=10;
max[1]=255;

```

```

filter[1]="pass";
min[2]=10;
max[2]=255;
filter[2]="pass";
for (i=0;i<3;i++){
  selectWindow(""+i);
  setThreshold(min[i], max[i]);
  run("Convert to Mask");
  if (filter[i]=="stop") run("Invert");
}
imageCalculator("AND create", "0","1");
imageCalculator("AND create", "Result of 0","2");
for (i=0;i<3;i++){
  selectWindow(""+i);
  close();
}
selectWindow("Result of 0");
close();
selectWindow("Result of Result of 0");
rename(a);
// Colour Thresholding-----
//create binary image
run("Make Binary");
//create selection
run("Create Selection");
//threshold NDVI unhealthy leaf area threshold
selectWindow("NDVI unhealthy area threshold");
run("Color Threshold...");//thresholds for the leaves to remove the background
// Color Thresholder 2.0.0-rc-69/1.52p
// Autogenerated macro, single images only!
min=newArray(3);
max=newArray(3);
filter=newArray(3);
a=getTitle();
run("HSB Stack");
run("Convert Stack to Images");
selectWindow("Hue");
rename("0");
selectWindow("Saturation");
rename("1");
selectWindow("Brightness");
rename("2");
min[0]=73;
max[0]=255;
filter[0]="pass";
min[1]=10;
max[1]=255;
filter[1]="pass";
min[2]=10;
max[2]=255;
filter[2]="pass";

```

```

for (i=0;i<3;i++){
  selectWindow(""+i);
  setThreshold(min[i], max[i]);
  run("Convert to Mask");
  if (filter[i]=="stop") run("Invert");
}
imageCalculator("AND create", "0", "1");
imageCalculator("AND create", "Result of 0", "2");
for (i=0;i<3;i++){
  selectWindow(""+i);
  close();
}
selectWindow("Result of 0");
close();
selectWindow("Result of Result of 0");
rename(a);
// Colour Thresholding-----
//create binary image
run("Make Binary");
//create selection
run("Create Selection");
//threshold FvFm leaf area threshold
selectWindow("FvFm leaf area threshold");
run("Color Threshold...");//thresholds for the leaves to remove the background
// Color Thresholder 2.0.0-rc-69/1.52p
// Autogenerated macro, single images only!
min=newArray(3);
max=newArray(3);
filter=newArray(3);
a=getTitle();
run("HSB Stack");
run("Convert Stack to Images");
selectWindow("Hue");
rename("0");
selectWindow("Saturation");
rename("1");
selectWindow("Brightness");
rename("2");
min[0]=0;
max[0]=255;
filter[0]="pass";
min[1]=10;
max[1]=255;
filter[1]="pass";
min[2]=10;
max[2]=255;
filter[2]="pass";
for (i=0;i<3;i++){
  selectWindow(""+i);
  setThreshold(min[i], max[i]);
  run("Convert to Mask");
}

```

```

    if (filter[i]=="stop") run("Invert");
}
imageCalculator("AND create", "0","1");
imageCalculator("AND create", "Result of 0","2");
for (i=0;i<3;i++){
    selectWindow(""+i);
    close();
}
selectWindow("Result of 0");
close();
selectWindow("Result of Result of 0");
rename(a);
// Colour Thresholding-----
//create binary image
run("Make Binary");
//create selection
run("Create Selection");
//threshold FvFm healthy area threshold
selectWindow("FvFm healthy area threshold");
run("Color Threshold...");//thresholds for the leaves to remove the background
// Color Thresholder 2.0.0-rc-69/1.52p
// Autogenerated macro, single images only!
min=newArray(3);
max=newArray(3);
filter=newArray(3);
a=getTitle();
run("HSB Stack");
run("Convert Stack to Images");
selectWindow("Hue");
rename("0");
selectWindow("Saturation");
rename("1");
selectWindow("Brightness");
rename("2");
min[0]=0;
max[0]=13;
filter[0]="pass";
min[1]=10;
max[1]=255;
filter[1]="pass";
min[2]=10;
max[2]=255;
filter[2]="pass";
for (i=0;i<3;i++){
    selectWindow(""+i);
    setThreshold(min[i], max[i]);
    run("Convert to Mask");
    if (filter[i]=="stop") run("Invert");
}
imageCalculator("AND create", "0","1");
imageCalculator("AND create", "Result of 0","2");

```

```

for (i=0;i<3;i++){
  selectWindow(""+i);
  close();
}
selectWindow("Result of 0");
close();
selectWindow("Result of Result of 0");
rename(a);
// Colour Thresholding-----
//create binary image
run("Make Binary");
//create selection
run("Create Selection");
//threshold FvFm unhealthy leaf area threshold
selectWindow("FvFm unhealthy area threshold");
run("Color Threshold...");//thresholds for the leaves to remove the background
// Color Thresholder 2.0.0-rc-69/1.52p
// Autogenerated macro, single images only!
min=newArray(3);
max=newArray(3);
filter=newArray(3);
a=getTitle();
run("HSB Stack");
run("Convert Stack to Images");
selectWindow("Hue");
rename("0");
selectWindow("Saturation");
rename("1");
selectWindow("Brightness");
rename("2");
min[0]=14;
max[0]=255;
filter[0]="pass";
min[1]=10;
max[1]=255;
filter[1]="pass";
min[2]=10;
max[2]=255;
filter[2]="pass";
for (i=0;i<3;i++){
  selectWindow(""+i);
  setThreshold(min[i], max[i]);
  run("Convert to Mask");
  if (filter[i]=="stop") run("Invert");
}
imageCalculator("AND create", "0","1");
imageCalculator("AND create", "Result of 0","2");
for (i=0;i<3;i++){
  selectWindow(""+i);
  close();
}

```

```

selectWindow("Result of 0");
close();
selectWindow("Result of Result of 0");
rename(a);
// Colour Thresholding-----
//create binary image
run("Make Binary");
//create selection
run("Create Selection");
//drawings
selectWindow("NDVI leaf area threshold");//NDVI leaf area in green filled
run("Create Selection");
run("Measure");
selectWindow("NDVI drawing");
setForegroundColor(0, 255, 0);
run("Restore Selection");
run("Fill", "Slice");
selectWindow("FvFm drawing");//FvFm leaf area on NDVI image in black filled
setForegroundColor(0, 0, 0);
run("Restore Selection");
run("Fill", "Slice");
selectWindow("NDVI healthy area threshold");//NDVI healthy area in red filled
run("Create Selection");
run("Measure");
selectWindow("NDVI drawing");
setForegroundColor(255, 0, 0);
run("Restore Selection");
run("Fill", "Slice");
selectWindow("NDVI unhealthy area threshold");//NDVI unhealthy area in blue drawn
run("Create Selection");
run("Measure");
selectWindow("NDVI drawing");
setForegroundColor(0, 0, 255);
run("Restore Selection");
run("Draw", "Slice");
selectWindow("FvFm leaf area threshold");//FvFm leaf area in green filled
run("Create Selection");
run("Measure");
selectWindow("FvFm drawing");
setForegroundColor(0, 255, 0);
run("Restore Selection");
run("Fill", "Slice");
selectWindow("FvFm healthy area threshold");//FvFm healthy area in red filled
run("Create Selection");
run("Measure");
selectWindow("FvFm drawing");
setForegroundColor(255, 0, 0);
run("Restore Selection");
run("Fill", "Slice");
selectWindow("FvFm unhealthy area threshold");//FvFm unhealthy area in blue drawn
run("Create Selection");

```

```

run("Measure");
selectWindow("FvFm drawing");
setForegroundColor(0, 0, 255);
run("Restore Selection");
run("Draw", "Slice");
selectWindow("NDVI working image");
close();
selectWindow("FvFm working image");
close();
selectWindow("NDVI background removed");
close();
selectWindow("NDVI background removal threshold");
//close();
selectWindow("NDVI leaf area");
close();
selectWindow("FvFm leaf area");
close();
selectWindow("NDVI leaf area threshold");
close();
selectWindow("NDVI healthy area threshold");
close();
selectWindow("NDVI unhealthy area threshold");
close();
selectWindow("FvFm leaf area threshold");
close();
selectWindow("FvFm healthy area threshold");
close();
selectWindow("FvFm unhealthy area threshold");
close();
NDVI_leaf = getResult("Area", 0);
NDVI_healthy = getResult("Area", 1);
NDVI_unhealthy = getResult("Area", 2);
FvFm_leaf = getResult("Area", 3);
FvFm_healthy = getResult("Area", 4);
FvFm_unhealthy = getResult("Area", 5);
dead_tissue = NDVI_leaf - FvFm_leaf;
P_dead = (dead_tissue / NDVI_leaf) * 100;
P_NDVI_healthy = (NDVI_healthy / NDVI_leaf) * 100;
P_NDVI_unhealthy = (NDVI_unhealthy / NDVI_leaf) * 100;
P_FvFm_healthy = (FvFm_healthy / NDVI_leaf) * 100;
P_FvFm_unhealthy = (FvFm_unhealthy / NDVI_leaf) * 100;
setResult("Label", 6, "Dead tissue (NDVI - FvFm)");
setResult("Area", 6, dead_tissue);
setResult("Label", 7, "Percent dead tissue");
setResult("Area", 7, P_dead);
setResult("Label", 8, "Percent healthy tissue (NDVI)");
setResult("Area", 8, P_NDVI_healthy);
setResult("Label", 9, "Percent unhealthy tissue (NDVI)");
setResult("Area", 9, P_NDVI_unhealthy);
setResult("Label", 10, "Percent healthy tissue (FvFm)");
setResult("Area", 10, P_FvFm_healthy);

```

```
setResult("Label", 11, "Percent unhealthy tissue (FvFm)");
setResult("Area", 11, P_FvFm_unhealthy);
```

9.1.6 Confocal ratiometric and intensity analysis

```
/*import settings: view stack: hyperstack
 * data organisation: open individually
 * colour: default
 * autoscale: yes
 */
run("Set Measurements...", "area mean display add redirect=None decimal=3");
run("Clear Results");
originalName = getTitle();
getVoxelSize(width, height, depth, unit);
print("width: "+width);
print("height: "+height);
print("depth: "+depth);
run("Set Scale...", "distance=0 known=0 unit=pixel");
waitForUser("select the brightfield channel");
run("Duplicate...", "title=brightfield_channel duplicate channels=2");
run("16-bit");
waitForUser("select the GFP channel");
run("Duplicate...", "title=GFP_channel duplicate channels=1");
run("16-bit");
waitForUser("scroll to the first slice of the section you want to analyse");
slice_1 = getSliceNumber();
print("slice 1: "+slice_1);
waitForUser("scroll to the final slice of the section you want to analyse");
final_slice = getSliceNumber();
print("Final slice: "+final_slice);
n_slices = final_slice - slice_1;
slice_mid = (slice_1 + final_slice)/2;
print("slices analysed: "+n_slices);
selectWindow("brightfield_channel");
setSlice(slice_1);
setTool(0);
waitForUser("Draw a box in the vacuole of the cell");
getSelectionBounds(x_vac, y_vac, width_vac, height_vac);
vac_area = width_vac * height_vac;
print("Vacuole selection area: "+vac_area);
selectWindow("GFP_channel");
setSlice(slice_mid);
waitForUser("draw a box in the nucleus of the cell");
getSelectionBounds(x_nuc, y_nuc, width_nuc, height_nuc);
selectWindow("brightfield_channel");
setSlice(slice_mid);
waitForUser("draw a box in the cytoplasm of the cell");
getSelectionBounds(x_cyt, y_cyt, width_cyt, height_cyt);
selectWindow("GFP_channel");
setSlice(slice_1);
```

```

////////////////////////////////////vacuolar
for (a = 1; a <= n_slices; a++) {
    setSlice(a);
    makeRectangle(x_vac, y_vac, width_vac, height_vac);
    run("Measure");
}
sum_grey_vac = 0
for(vac = 0; vac < n_slices; vac++) {
    vac_int = getResult("Mean", vac);
    sum_grey_vac = sum_grey_vac + vac_int;
}
setResult("Label", nResults, "sum slice vacuolar grey value");
setResult("Mean", nResults-1, sum_grey_vac);
mean_grey_vac = sum_grey_vac/n_slices;
setResult("Label", nResults, "mean vacuolar grey value");
setResult("Mean", nResults-1, mean_grey_vac);
run("Clear Results");
////////////////////////////////////nuclear
setSlice(slice_1);
for (b = 1; b <= n_slices; b++) {
    setSlice(b);
    makeRectangle(x_nuc, y_nuc, width_nuc, height_nuc);
    run("Measure");
}

sum_grey_nuc = 0
for(nuc = 0; nuc < n_slices; nuc++) {
    nuc_int = getResult("Mean", nuc);
    sum_grey_nuc = sum_grey_nuc + nuc_int;
}
setResult("Label", nResults, "sum slice nuclear grey value");
setResult("Mean", nResults-1, sum_grey_nuc);
mean_grey_nuc = sum_grey_nuc/n_slices;
setResult("Label", nResults, "mean nuclear grey value");
setResult("Mean", nResults-1, mean_grey_nuc);
run("Clear Results");
////////////////////////////////////cytoplasmic
setSlice(slice_1);
for (c = 1; c <= n_slices; c++) {
    setSlice(c);
    makeRectangle(x_cyt, y_cyt, width_cyt, height_cyt);
    run("Measure");
}
sum_grey_cyt = 0
for(cyt = 0; cyt < n_slices; cyt++) {
    cyt_int = getResult("Mean", cyt);
    sum_grey_cyt = sum_grey_cyt + cyt_int;
}
setResult("Label", nResults, "sum slice cytoplasmic grey value");
setResult("Mean", nResults-1, sum_grey_cyt);
mean_grey_cyt = sum_grey_cyt/n_slices;

```

```

setResult("Label", nResults, "mean cytoplasmic grey value");
setResult("Mean", nResults-1, mean_grey_cyt);
run("Clear Results");
///set results
setResult("Label", nResults, "vacuolar");
setResult("Mean grey value", nResults-1, mean_grey_vac);
setResult("Label", nResults, "nuclear");
setResult("Mean grey value", nResults-1, mean_grey_nuc);
setResult("Label", nResults, "cytoplasmic");
setResult("Mean grey value", nResults-1, mean_grey_cyt);
///ratio calculations
nuc_vac = getResult("Mean grey value", 1) - getResult("Mean grey value", 0);
setResult("Label", nResults, "nuclear - vacuolar");
setResult("Mean grey value", nResults-1, nuc_vac);
cyt_vac = getResult("Mean grey value", 2) - getResult("Mean grey value", 0);
setResult("Label", nResults, "cytoplasmic - vacuolar");
setResult("Mean grey value", nResults-1, cyt_vac);
nuc_cyt_ratio = nuc_vac / cyt_vac;
setResult("Label", nResults, "nuclear:cytoplasmic");
setResult("Mean grey value", nResults-1, nuc_cyt_ratio);
var_sum = ((nuc_vac - cyt_vac)/((nuc_vac + cyt_vac)/2));
setResult("Label", nResults, "(nuclear-cytoplasmic variance)/((nuclear+cytoplasmic)/2)");
setResult("Mean grey value", nResults-1, var_sum);
selectWindow("brightfield_channel");
close();
selectWindow("GFP_channel");
close();
selectWindow(originalName);

```

9.2 Automated conidial development time course acquisition

```

from picamera import PiCamera
from time import sleep
camera = PiCamera()
camera.resolution = (1920, 1080)
camera.framerate = 50
camera.start_preview(fullscreen=False, window = (0, 100, 1080, 1080)) ##x,y,quality
sleep(2)
for filename in camera.capture_continuous('/FILE/PATH/HERE/Timepoint{counter:001d}.jpg'):
    print('Captured %s' % filename)
    sleep(1800) #wait 30 min

```